DESIGN OF LIQUID CRYSTAL DIMERS AND TRIMERS– SYNTHESIS AND CHARACTERIZATION OF NOVEL SYSTEMS CONTAINING BENT-CORE AND CALAMITIC MESOGENIC UNITS

DISSERTATION

zur Erlangung des Doktorgrades der Naturwissenschaften
(Dr. rer. nat.)

der

Naturwissenschaftlichen Fakultät II
Chemie, Physik und Mathematik

der Martin-Luther-Universität
Halle-Wittenberg

vorgelegt von

Frau Maria Gabriela Tamba
geboren am 02.08.1979 in Bacau

Gutachter:

1. Prof. Dr. W. Weißflog
2. Prof. Dr. R. Zentel

Halle (Saale), den 29.09.2014

Contents

1 Introduction **1**

1.1 Liquid crystals, a short introduction 1

1.2 Molecular shape and liquid crystal phases........ 2

1.3 Bent-shaped mesogens........ 3

  1.3.1 General considerations........ 3

  1.3.2 Structure of banana-shaped mesogens 5

  1.3.3 Mesophases of banana-shaped mesogens........ 7

1.4 Liquid crystal oligomers: dimeric and trimeric mesogens........ 13

1.5 Binary mixtures of banana-shaped and calamitic mesogens........ 18

2 Objectives of this thesis **19**

3 Synthesis **22**

3.1 ‘*Banana-calamit’* dimers **1** – **30** of **type I**........ 22

  3.1.1 General aspects 22

  3.1.2 Dimer series **1** – **6**........ 24

  3.1.3 Dimer series **7** – **12**........ 26

  3.1.4 Dimer series **13 – 19**........ 29

  3.1.5 Dimers **20** – **24**........ 33

  3.1.6 Dimer series **25**........ 34

  3.1.7 Dimer series **26**........ 35

  3.1.8 Dimer series **27**........ 35

  3.1.9 Dimer series **28** and **29**........ 36

  3.1.10 Dimer series **30**........ 37

3.2 ‘*Banana-calamit*’ dimers **31** and **32** of **type II**........ 38

3.3 ‘*Calamit – banana – calamit*’ trimers **33** – **36** of **type I**........ 39

3.4 ‘*Banana – calamit – banana*’ trimers **37** and **38** of **type II**........ 41

  3.4.1 Trimer series **37**........ 41

  3.4.2 Trimer series **38**........ 42

4 Experimental techniques **43**

4.1 Polarising optical microscopy........ 43

4.2 Calorimetric studies........ 43

4.3 X-ray diffraction measurements 44

4.4 Electro-optical studies 46

5 Mesophase behaviour of ‘*banana - calamit*’ dimers of type I **48**

5.1 Effect of the length of the spacer *m* on the mesophase behaviour of dimer series **1** – **6**........ 49

  5.1.1 The dimer series **1**........ 49

    5.1.1.1 The rectangular columnar Col_r phase of dimer **1b** with $m = 3$ 53

5.1.1.2 The nematic and columnar phases of dimers **1** with *m* = 5 - 10 55

5.1.1.3 The oblique columnar $\mathrm{Col_{ob}P_{FE}}$ phase of dimer **1i** with *m* = 11 62

5.1.1.4 The nematic and smectic $\mathrm{SmC_c}$ phases of dimer **1j** with *m* = 12........... 65

5.1.2 The dimer series **2** – **6**... 67

5.1.2.1 The smectic $\mathrm{SmC_sP_{FE}}$ phase of dimer **2b**... 70

5.1.2.2 The mesophase behaviour of dimer series **3**.. 72

5.1.2.3 The mesophase behaviour of dimer series **4**.. 72

5.1.2.4 The smectic polymorphism of dimers **5** 75

5.1.2.5 The smectic $\mathrm{SmXP_{AF}}$ phase of dimer **6a** 84

5.1.2.6 The rectangular columnar $\mathrm{Col_rP_{AF}}$ phase of dimer **6b**........................... 88

5.2 Effect of the length of the terminal chain *p* attached to the calamitic mesogenic unit on the mesophase behaviour of dimer series **1** – **6** 90

5.3 Effect of the length of the terminal chain *n* attached to the bent-core mesogenic unit on the mesophase behaviour of dimer series **1** – **6** 92

5.4 Effect of the type of the groups *X*, *Y* linking the spacer to the bent-core mesogenic unit and the calamitic moiety on the mesophase behaviour of dimer series **7 – 12** 93

5.4.1 Substitution of the *ether* group in position *X* by the *carboxyl* group in dimer series **7 – 9** 95

5.4.2 Substitution of the *ether* group in position *X* by the *oxycarbonyl* group in dimer series **10 – 11** 95

5.4.2.1 Occurrence of a polar crystalline $\mathrm{Cr^*P_{FE}}$ phase for dimers **10** 95

5.4.2.2 Electro-optical switching behaviour of $\mathrm{SmC_aP_{AF}}$ phases of dimer **11a** .. 97

5.4.3 Substitution of the *ether* group in position *Y* by the *carboxyl* group: Occurrence of a polar crystalline $\mathrm{Cr^*P_{AF}}$ phase for dimer **12** 100

5.5 Variations of the bent-core mesogenic unit of dimers **13** - **28**.. 102

5.5.1 Variation of the direction of the *ester* linking groups *E* in the bent-core mesogenic unit of dimer series **13 – 19**.. 102

5.5.1.1 Occurrence of a N - $\mathrm{N_X}$ phase transition for dimer **13b**......................... 105

5.5.1.2 The mesophase behaviour of dimers **15a - d**... 107

5.5.1.3 The undulated smectic $\mathrm{USmC_aP_{AF}}$ phase of dimer **16a**......................... 109

5.5.1.4 Field-induced enhancement of the transition temperature between the polar and non-polar smectic phases of dimer **17a**............................ 112

5.5.1.5 The mesophase behaviour of dimer **18**.. 114

5.5.1.6 The mesophase behaviour of dimer **19**.. 114

5.5.2 Variations of the direction of the *ester* linking groups *E* and the type of the group *X* linking the spacer to the bent-core mesogenic unit of dimers **20 - 24**........ 116

5.5.2.1 The mesophase behaviour of dimers **20 - 22** 117

5.5.2.2 The mesophase behaviour of dimers **23** and **24**: Smectic polymorphism of dimer **24** 118

5.5.3 Effect of a *cyano*- group terminally attached to the bent-core unit on the mesophase behaviour: Occurrence of a N - $\mathrm{N_X}$ phase transition for dimer **25c** 119

5.5.4 Effect of the lateral substituents *chlorine*- and *methyl*- at the bent-core mesogenic unit on the mesophase behaviour of dimer series **26** and **27**.................. 122

5.5.5 Effect of the number of aromatic rings in the bent-core unit of dimer series **28**...... 124

5.6 Variation of the molecular structure of the calamitic unit of dimer series **29** and **30** 125

5.6.1 Introduction of a *biphenylene* unit in the calamitic moiety of dimer series **29** 126

5.6.2 Introduction of a *bis-azobenzene* unit in the calamitic moiety of dimer series **30** ... 127

5.7 Electro-optical characterization of the nematic phase of dimer **15b**....................................... 131

5.7.1 Studies on the elastic properties... 132

5.7.1.1 Uniform FRÉEDERICKSZ transition 132

5.7.1.2 BROCHARD-LEGER walls 134

5.7.2 Longitudinal and normal electroconvection rolls above the splay FRÉEDERICKSZ transition 136

5.7.2.1 Model for an instability leading to a novel type of electroconvection patterns 137

5.7.2.2 Measurements of the anisotropies 138

5.7.2.3 Longitudinal electroconvection rolls above the splay FRÉEDERICKSZ transition... 139

5.7.3 Field-induced texture transitions by means of an electric field............................... 140

5.7.3.1 Electro-optical experiments in planar cells.. 140

5.7.3.2 Electro-optical experiments in homeotropic cells 142

6 Mesophase behaviour of ‘*banana - calamit*’ dimers of type II 144

6.1 The mesophase behaviour of dimers **31** and **32**.. 144

6.1.1 Dimers **31** bearing the *spacer-calamit* unit in the *5*-position on the central *resorcinol* fragment of the bent-core moiety... 146

6.1.2 Dimers **32** bearing the *spacer-calamit* unit in the *4*-position on the central *resorcinol* fragment of the bent-core moiety... 146

6.2 The effect of the linking position of the mesogenic units on the mesophase behaviour of the analogous dimers of **types I** and **II**.. 150

7 Mesophase behaviour of ‘*calamit – banana – calamit*’ trimers 151

7.1 Trimers **33** containing a *resorcinol* fragment in central position of the bent-core moiety....... 153

7.2 Trimers **34** containing an *isophthalic acid* unit in central position of the bent-core moiety.... 154

7.3 Trimers **35** bearing long terminal chains *p* 154

7.4 Trimer **36** containing a seven-ring bent-core unit... 157

8 Mesophase behaviour of ‘*banana – calamit – banana*’ trimers 159

8.1 Trimers **37** containing *phenylene* and *biphenylene* units 159

8.2 Trimers **38** containing an *azobenzene* unit.. 162

9 Summary 165

10 Experimental Section 176

10.1 General aspects 176

10.2 Starting materials.. 177

10.3 General procedures 178

10.3.1 WILLIAMSON etherification 178
10.3.2 MITSUNOBU etherification 179
10.3.3 STEGLICH esterification 179
10.3.4 Esterification via acid chlorides 179
10.3.5 Oxidation with sodium chlorite 180
10.3.6 Deprotection of benzylether and benzylesters by means of hydrogenolysis 181
10.3.7 Alkaline hydrolysis of benzyl substituted benzoates 181
10.4 Synthesis of compound **1a** 182

References **183**

Appendix

Symbols and abbreviations

Chemical materials

Ar	Aromatic
n-Bu	*n*-Butyl
Bu_4NI	Tetrabutylammonium iodide
Bn	Benzyl
Bz	Benzoyl
DCC	*N*,*N*′-Dicyclohexylcarbodiimide
DEAD	Diethyl azodicarboxylate
DMAP	4-Dimethylaminopyridine
DMF	Dimethylformamide
DMSO	Dimethyl sulfoxide
Et	Ethyl
Et_2O	Diethyl ether
EtOAc	Ethyl acetate
EtOH	Ethanol
Me	Methyl
MeOH	Methanol
Pd/C	Palladium on activated charcoal
PE	Petrolether
Ph	Phenyl
PPh_3	Triphenylphosphine
$O{=}PPh_3$	Triphenylphosphine oxide
TEA	Triethylamine
THF	Tetrahydrofuran

Differential scanning calorimetry

ΔH	Transition enthalpy
C_p	Heat capacity
DSC	Differential scanning calorimetry
H	Enthalpy

Electro-optical investigations

τ	Switching time
a.c.	Alternative current
AF	Antiferroelectric
d.c.	Direct current
E	Electric field or electric field strength
E_{th}	Threshold field
f	Frequency
FE	Ferroelectric
ITO	Indium tin oxide
K	Franck elastic constant
P_S	Spontaneous polarization
U	Voltage
U_{th}	Threshold voltage
V_{pp}	Peak-to-peak voltage

Nuclear magnetic resonance spectroscopy

δ	Chemical shift
Ar-H	Aromatic hydrogen

br s	Broad singlet
d	Doublet
dd	Doubled doublet
J	Coupling constant
m	Complex multiplet
m/z	Mass/charge
NMR	Nuclear magnetic resonance
q	Quartet
quint	Quintett
ppm	Parts per million
rel. int.	Relative intensity
s	Singlet
t	Triplet

Phase Name

b	Biaxial
B_1– B_7	Designation of '*banana mesophases*' suggested in the workshop *Banana-Shaped Liquid Crystals: 'Chirality by Achiral Molecules'* held in Berlin in December 1997
B_3, B_4	Higher ordered mesophases or soft crystalline phases
c	Intercalated
CB, CB_2	Possible designation for B_2 mesophase
CG	Mesophase with C_1 symmetry and one polarization vector
Col_h	Hexagonal columnar mesophase
Col_{ob}	Oblique columnar mesophase
Col_r	Rectangular columnar mesophase
Col_x	Columnar mesophase with unknown structure
C_P	Mesophase with C_{2v} symmetry and one polarization vector
Cr	Crystalline phase
Cub	Cubic mesophase
I	Isotropic liquid phase
LC	Liquid crystal or Liquid crystalline
M	Mesophase with unknown structure
N	Nematic mesophase
N_b	Biaxial nematic mesophase
P	Mesophase with polar order
P_{AF}	Antiferroelectric polar order
P_{FE}	Ferroelectric polar order
SmA	Smectic A mesophase, untilted smectic mesophase without in-plane order
$\mathrm{Sm}\tilde{\mathrm{A}}$	Modulated smectic mesophase (the layers are broken into ribbons)
SmA_b	Biaxial orthogonal smectic A mesophase
SmAP	Mesophase with C_{2v} symmetry and one polarization vector
SmC	Smectic C mesophase, tilted smectic mesophase without in-plane order
$\mathrm{Sm}\tilde{\mathrm{C}}$	Modulated smectic C mesophase (the layers are broken into ribbons)
SmC*	Chiral smectic C mesophase
SmC_a	Smectic C phase with anticlinic organization (alternating tilt-direction)
SmC_aP_{AF}	Antiferroelectric SmCP mesophase in which the interface arrangement of the molecules is anticlinic
SmC_aP_{FE}	Ferroelectric SmCP mesophase in which the interface arrangement of the molecules is anticlinic
SmC_c	Intercalated smectic C mesophase
SmC_G	Mesophase with C_1 symmetry and one polarization vector, double tilted smectic mesophase
$SmCP_{AF}$	SmC mesophase with antiferroelectric polar order
$SmCP_{AF}$[*]	SmC mesophase with chiral superstructure and antiferroelectric polar

	order
$SmCP_{FE}$	SmC mesophase with ferroelectric polar order
SmC_s	Smectic C mesophase with synclinic organization (uniform tilt-direction)
SmC_sP_{AF}	Antiferroelectric SmCP mesophase in which the interface arrangement of the molecules is synclinic
SmC_sP_{FE}	Ferroelectric SmCP mesophase in which the interface arrangement of the molecules is synclinic
SmX	Smectic mesophase with unknown structure
USm	Undulated (sinusoidal deformed) smectic mesophase
$U^{m}Sm$	Modulated undulated smectic mesophase
$USmC_aP_{AF}$	Undulated smectic mesophase with an homogeneously chiral anticlinic antiferroelectric organisation
$USmC_sP_{AF}$	Synclinic antiferroelectric organisation between the layers and alternation of the tilt direction along the layers
[*]	Mesophase with supramolecular chirality, characterised by the spontaneous formation of a conglomerate of domains of opposite chirality sense whereby the molecules themselves are configurational achiral or racemic

Polarising optical microscopy

A	Analyser
P	Polariser
POM	Polarising optical microscopy
s	Singularities

X-ray diffraction methode

θ	Tilt angle
λ	Wavelength
χ	Azimuthal angle of the 2D scattering
τ	Average tilt angle
a, b, γ	Lattice parameters
d	Layer spacing
h, k, l	MILLER indices
L	Length of molecule
L_{eff}	Effective length of molecule
L_{calc}	Calculated length of molecule
XRD	X-ray diffraction
2D	Two dimensional
3D	Three dimensional

Others

α	Bending angle between the wings of the bent-core mesogen
Comp.	Signature of the compound
IUPAC	International union of pure and applied chemistry
m	Length of the spacer connecting the bent-core unit and the calamitic moiety
n	Length of the terminal chain attached to the bent-core moiety
$\mathbf{n}$	Vector along the long molecular axis of the molecule
$\mathbf{n_0}$	Orientation of the initial director
p	Length of the terminal chain attached to the calamitic moiety
T	Temperature
TLC	Thin layer chromatography

1 Introduction

1.1 Liquid crystals, a short introduction

The Austrian botanist REINITZER is credited with discovering of the ***liquid crystal*** phase in 1888,[1] a state of matter in which the degree of molecular order is intermediate between the three dimensional, long-range positional and orientational order found in solid crystals and the absence of long-range order found in isotropic liquids, gases, and amorphous solids.[2,3] The compounds in the liquid crystal state are called ***liquid crystals*** (LC) and their phases are called ***mesophases***, or ***mesomorphic phases*** (from Greek, *mésos*: middle; *mesomorphic*: intermediate form). The breakdown of the three dimensional superstructure of a solid occurs in a stepwise manner when a solid melts via one or more LC phases, as shown in Figure 1.1 for materials constituted of calamitic molecules.[2,4,5]

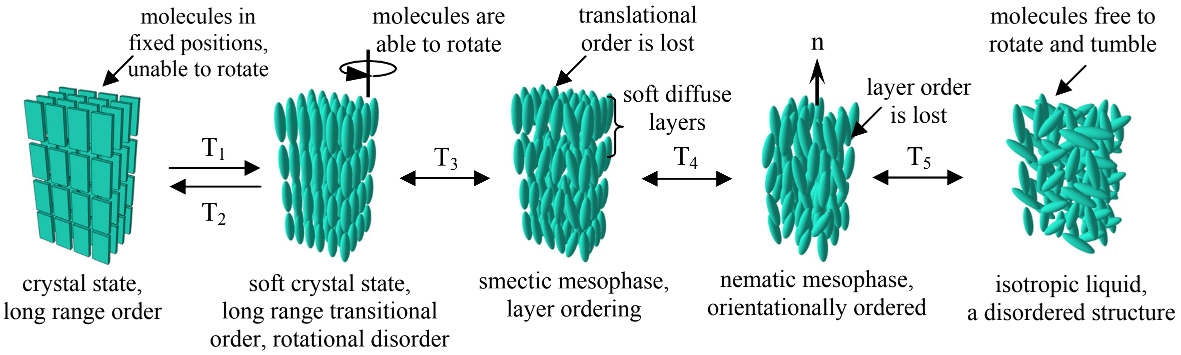
molecules in fixed positions, unable to rotate
molecules are able to rotate
translational order is lost
soft diffuse layers
n
layer order is lost
molecules free to rotate and tumble
T_1
T_2
T_3
T_4
T_5
crystal state, long range order
soft crystal state, long range transitional order, rotational disorder
smectic mesophase, layer ordering
nematic mesophase, orientationally ordered
isotropic liquid, a disordered structure

Figure 1.1: The melting process of a calamitic LC material; pictorial representation according to references.[2,5]

Liquid crystals can be divided into ***thermotropic*** and ***lyotropic*** mesogens. Compounds that form mesophases as a function of temperature are thermotropic liquid crystals. Transitions between the various thermotropic liquid crystal mesophases invariably occur at defined temperatures and with little hysteresis observed between heating and cooling cycles. If the liquid crystalline mesophase is induced (in a certain temperature interval) by the concentration in a solvent they are called lyotropic liquid crystals. A great number of materials have been found to be thermotropic or lyotropic liquid crystals, and some of them exhibit both types of behaviour (amphotropic liquid crystals).[6] LC behaviour is omnipresent in biological systems,[7,8] such as peptides, DNA, phospholipids, steroids and carbohydrates,[9] many proteins and cell membranes. Solutions of soap and various related detergents, as well as the tobacco mosaic virus are other well-known LC examples.

Due to the orientational order of the molecules in their LC phases, these mesogens exhibit anisotropic properties, i.e. the physical properties of the LCs material depend on the direction in which they are measured. That is, various physical properties, such as dielectric constant, refractive index, magnetic susceptibility, conductivity, and viscosity, have different values in the direction parallel and perpendicular to the molecular axis. The anisotropic nature of LCs is responsible for the unique optical properties exploited by scientists and engineers in a variety of applications. The ease of controlling their bulk orientation by surface alignment, in conjunction with their anisotropic physical properties enable reorientation of the molecular axis by applying a voltage, which is the basis of many applications of LC diplays.

In conclusion, the LC state combines the properties of a liquid (e.g. flow, ability to form droplets) and a crystalline solid (e.g. anisotropy of some physical properties) which gives rise to materials with anisotropic physical properties, switchable under the influence of external stimuli. This thesis only deals with thermotropic liquid crystals.

1.2 Molecular shape and liquid crystal phases

A major pathway to modify the phase structures,[10] and to achieve a significant increase in the complexity of soft self-assembly in LC phases is the modification of the molecular shape,[11] combined with the tendency of segregation of incompatible fragments into different compartments, the geometric frustration and space filling effects, as well as the chirality of LC systems.[12]

A pronounced anisotropy in the shapes and interactions of molecules or molecular aggregates is usually necessary for the formation of LC mesophases. The non-covalent interactions have a great effect on a material’s liquid crystallinity. Thermotropic LCs were formerly classified into two main groups according to their structural character: calamitic (rod-like) and discotic (disc-like) mesogens. There are other mesogens related to these main mesogenic categories with properties associated or very different from those of classical rod or disc-shaped mesogens, i.e. the *bent-core molecules* (called also *banana-shaped LC*, *boomerang-shaped LC*, *bow-shaped LC*), pyramidic mesogens (bowl-shaped and cone-shaped), polycatenary mesogens (biforked and phasmidic), sanidic mesogens (board-like molecules), wedge-shaped molecules, oligomeric LCs (dimers and trimers), dendrimers,[13] etc. Figure 1.2 depicts the schematic shapes of some mesogens. Many of these compounds form *classical* nematic and smectic phases, while others present deviations from the conventional layer thickness (double layers, interpenetrating layers) or form cubic and/or columnar phases

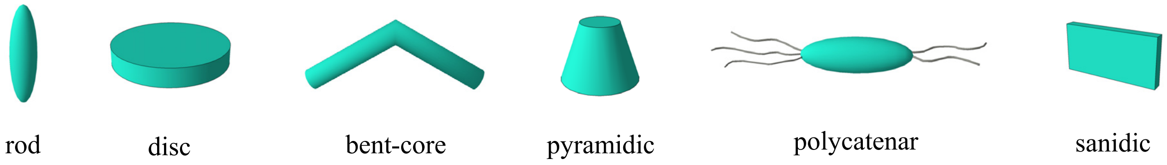

Figure 1.2: Different shapes of mesogens.

Depending on the degree of positional order, different thermotropic LC phases can be distinguished. The least ordered phase is the **nematic** phase (N, see Fig. 1.3a), where the molecules have exclusively long-range orientational order, i.e. the molecules tend to align themselves parallel to each other with their long axis parallel to a preferential direction $\boldsymbol{n}$. In the biaxial nematic phase (N_b, Fig. 1.3e) there is an additional correlation of the molecules perpendicular to the director, i.e. N_b has two minor directors labelled $\boldsymbol{l}$ and $\boldsymbol{m}$, which are both perpendicular to the major director $\boldsymbol{n}$ and mutually perpendicular to each other.[14,15,16] More ordered phases can be formed if incompatible parts of the molecules are segregated into subspaces (e.g. segregation of flexible aliphatic chains from rigid aromatic parts) giving rise to long-range positional order in one, two or three dimensions. In the case of rod-like molecules, layer structures could be formed (**smectic** phases, Sm, see Fig. 1.3 b-d),[17] while the discotic molecules prefer an organisation in columns (**columnar** phases, Col)[18] (Fig. 1.3f). Additional modes of structural organisation in LC systems are bicontinuous 3D phases and 3D ordered arrays of closed aggregates,[19] which often represent cubic mesophases.[20] However, it should be pointed out that these are general considerations and a specific shape of the molecules is not exactly related to the type of mesophase formed and can lead to an additional orientational order within layers, columns and 3D structures, enhancing the level of complexity of the self organised system. In addition, the molecular shape is not only defined by the chemical structure, but also by the molecular dynamics.

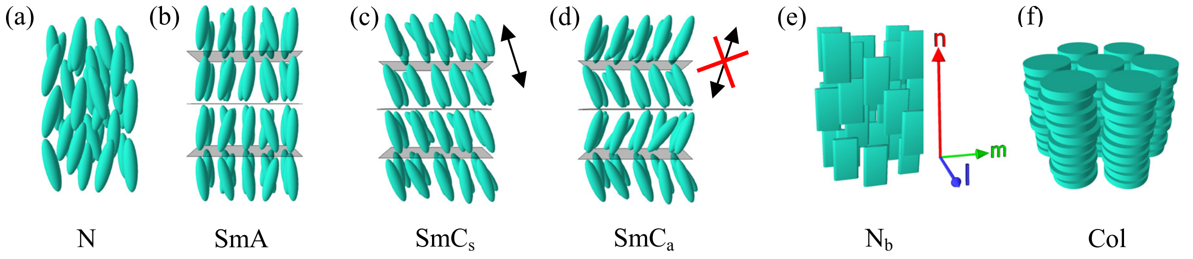

Figure 1.3: Schematic representation of types of LC phases (a-d) formed by rod-like molecules: (a) uniaxial nematic N phase; (b) SmA phase; (c) SmC$_s$ phase with synclinic (identical) tilt direction in adjacent layers; (d) SmC$_a$ phase with anticlinic (opposite) tilt direction in adjacent layers. The arrows indicate the out-of-plane interlayer fluctuations which can easily take place in SmC$_s$ phases and are hindered in SmC$_a$ phases of calamitic mesogens; (e) biaxial nematic N$_b$ phase; ***n*** is larger than ***m*** or ***l*** to denote the major director; (f) columnar Col phase of discotic molecules.

In this thesis the nomenclature recommended by IUPAC in 2001 for definitions of basic terms relating to low-molar-mass and polymer LCs by BARON *et al.*[3] was used. In the following sub-chapter we will focus on the bent-shaped molecules.

1.3 Bent-shaped mesogens

1.3.1 General considerations

The synthesis of bent-shaped LCs molecules has been first reported by VORLÄNDER in 1929 (see Fig. 1.4a)[21]. The molecules with shapes deviating from a rod, such as bent shape have been considered to be 'bad' molecules for forming LC phases and therefore their mesomorphic behaviour was not investigated till later. The current immense interest in these materials was triggered by investigations of NIORI *et al.* in 1996 on a banana-shaped SCHIFF's base derivative (1,3-phenylene bis[4-(4-*n*-alkoxyphenyliminomethyl)benzoates].[22] They were the first to report on smectic phases of achiral molecules incorporating a bent-shaped rigid core which show polar order and chiral superstructures in their LC mesophases.[23] The definition of banana (bent, bow) mesogens by IUPAC[3] recommends that they are 'constituted of bent or so-called banana-shaped molecules in which two mesogenic groups are linked through a semi-rigid group in such a way as not to be collinear'.

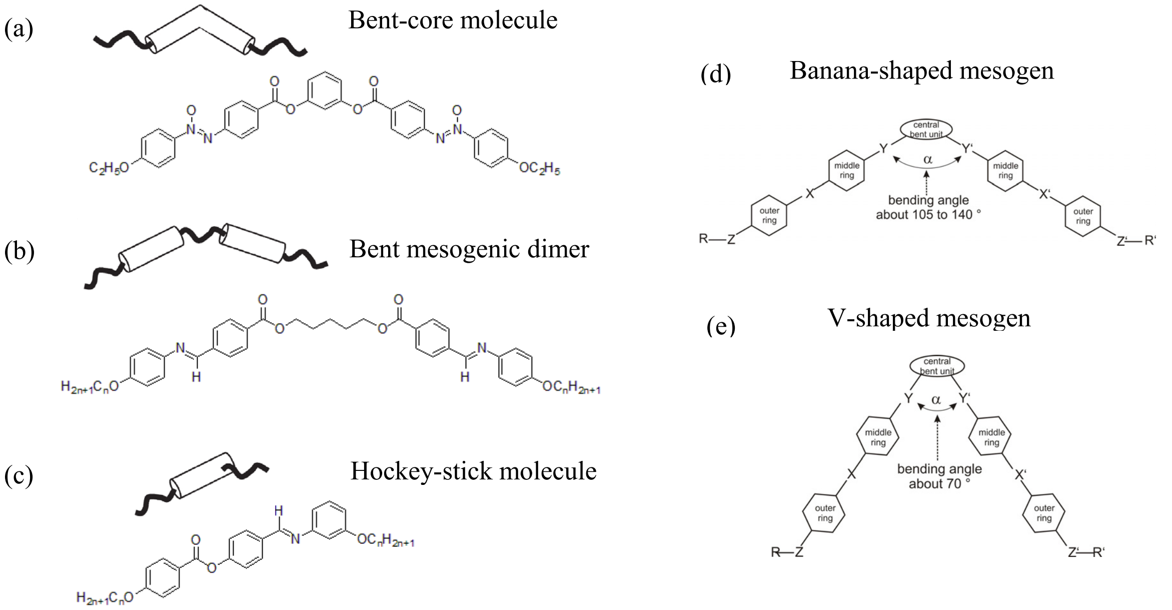

(a) Bent-core molecule

(b) Bent mesogenic dimer

(c) Hockey-stick molecule

(d) Banana-shaped mesogen

(e) V-shaped mesogen

Figure 1.4: (a-c) The three types of bent-shaped mesogens.[24] The general template of the structures of (d) banana-shaped mesogens and (e) V-shaped mesogens.

The molecules with a bent shape (Fig. 1.4) can be classified in three main categories: ***bent-core mesogens***, ***bent mesogenic dimers*** and ***hockey-stick molecules***. The first category is constituted by the ***bent-core molecules*** which include a rather rigid central bent unit such as the 1,3-disubstituted *benzene* ring[25] (Fig. 1.4a), a 1,3'-disubstituted *biphenyl* fragment[26] or 2,7-disubstituted naphthalene rings, etc. The second category is constituted of ***bent mesogenic dimers*** composed of two rod-like mesogenic units connected by an *odd* numbered and flexible non-cyclic spacer (Fig. 1.4b).[27] In some cases, these mesogens possess similar polar mesophases to those found for the bent-core mesogens. In the case of such molecules connected through 'one linking unit' like *methylene*, *carbonyl*, *ether* and *thioether* units it was found that the compounds exhibit smectic phases, however, the results do not clarify if there are '*banana phases*'. The molecules with very short linking units (e.g. CH_2, CO, S, O,[28] CH_2OOC,[29] etc.) can be regarded as borderline cases between these two structural types. PELZ *et al*. synthesized asymmetric twins with *methyleneoxycarbonyl* spacer.[29] The third category is formed by ***hockey-stick molecules***, e.g. where an *alkyl* chain is attached to the *meta*-position at one end of a rod-like segment (Fig. 1.4c).[30] In the following we will focus on the field of bent-core mesogens.

The ***bent-core molecules*** are the molecules incorporating a bent in the rather rigid aromatic part and can be broadly classified into two categories: ***banana-shaped*** and ***V-shaped molecules***. The attachment of two mesogenic units in the 1,2-positions gives V-shaped molecules (Fig. 1.4e, the bending angle α between the mesogenic segments attached to the central benzene nucleus is ~70°),[31] whereas a linkage in the 1,3-positions[32] result in the formation of the banana-shaped mesogens (Fig. 1.4d, the bending angle α is ~105 - 140°). The mesomorphic behaviour of these two classes of bent-core molecules is different. The V-shaped molecules form mesophases similar to those shown by classical calamitic LCs.[31,33] The banana-shaped compounds show new smectic phases including two-dimensional phases, which are not comparable to or miscible with the phases formed by calamitic LCs.[34,35]

1.3.2 Structure of banana-shaped mesogens

The molecular structure and intermolecular interactions in the banana-shaped molecules plays a major role in the occurrence of polarity and chirality in the mesophases of these compounds. Various designs of the bent-core compounds were investigated in order to understand the relationship between molecular structure and mesomorphic properties; some latest reviews are the ones from TSCHIERSKE *et al.*,[24] TAKEZOE *et al.*[36] and EREMIN *et al.*[37]

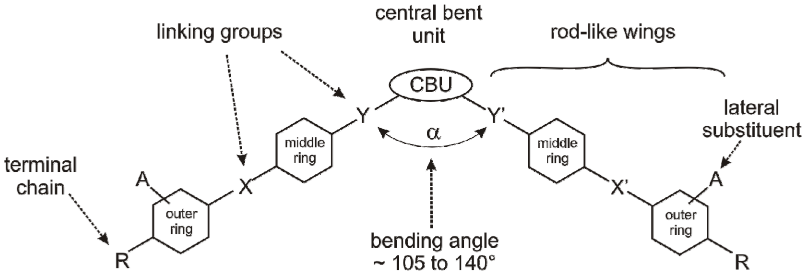

Figure 1.5: The general template of the molecular structures of banana-shaped mesogens.

In the banana-shaped molecules, the *central unit*, together with the outer and middle rings are connected by the *linking groups* (X, X', Y, Y') to form the *bent core* (see Fig. 1.5). The *bending angle α* (the opening angle between the two rod-like wings) is about 105 to 140° in order to show the typical properties of banana-shaped mesogens (layer polarity)[38] and it can result e.g. from 1,3-*phenylene* central ring or a 1,3'-disubstituted *biphenyl* fragment, and 2,7-disubstituted *naphthalene* or 2,6-disubstituted *pyridine* rings.[24] SCHRÖDER *et al.* presented bent-core LCs with *benzoylpiperazine* and *benzoylpiperidine* central moiety.[39] The general tendency is that increasing the size of the rigid bent unit results in increasing of the transition temperatures and leads to a stabilisation of columnar phases. For such compounds longer terminal chains are required to suppress the columnar phases and to obtain polar smectic phases. There are only a few compounds incorporating non-aromatic (alicyclic or heteroalicyclic) units in the rigid segments, for example six-membered rings such as *piperazines*[39] and *tetrahydropyranes*,[40] *cyclohexanes*.[41] Modification of the bending angle *α* is achieved by incorporation of substituents at the central unit, close to the linking groups Y, Y' (see Fig. 1.5)[32,38] or by using five membered heterocycles instead of six-membered rings.[40,42] 1,3,4-*Oxadiazole* derivatives,[43] 1,3-*oxazoles*,[16] and 1,2,4-*oxadiazoles*[42] are examples of 5-membered aromatic rings, which, due to their larger bending angle are at the borderline between bent-core and calamitic mesogens.

The most used *linking units* X, Y in the bent-core molecules are the *ester* groups (popular due to the enhanced chemical stability)[26] and the SCHIFF's base groups[44,45] (i.e. *azomethine* units) which have a broader variety of polymorphic mesophases than the corresponding *ester* compounds. Also double bonds, triple bonds and CH_2O linkages, *azobenzene* units (photo-responsive materials)[46,47] etc., were used. Generally, a certain degree of flexibility of the bent core has to be maintained in order to allow the organisation in LC phases and to prevent crystallisation. The dramatic effect of the direction of the linking units X, X', Y and Y' upon the LC properties was the subjects of different studies.[48,49] The length of the bent-core unit and the bending angle α of the central unit are most important for the formation of polar ordered mesophases.

Regarding the size of the bent-core mesogens, it seems that the minimum number of rings required for obtaining LC phases is between four [27] and five.[32,50] Usually, three-ring molecules with a 1,3-*phenylene* unit are not able to form mesophases. This statement is only true, however, if the interaction forces are dominated by the molecular shape. If hydrogen bonds or microsegregation effects dominate, the molecular shape and the mesophase behaviour are not so clearly related. Some examples are the bent phasmidic molecules bearing three *alkyloxy* chains at both terminal *phenyl* rings and *amido* group containing mesogens.[51,52] Furthermore, the strong tendency towards microsegregation is well-known for molecules bearing *perfluoroalkyl* chains[53] which exhibit smectic phases up to high temperatures. Recently, WEISSFLOG *et al.* had reported on the mesophase behaviour of three-ring bent-core bis(4-subst.-phenyl) 2-methyl-iso-phthalates exhibiting N, SmA and SmC phases, which can be understood by the extended bending angle caused by the lateral *methyl* group.[54] These materials are considered to be at the boundary between calamitic liquid crystals and banana-shaped liquid crystals and therefore of high interest. KANG *et al.*[55] presented a four-ring compound with an oxadiazole central core which forms a nematic phase, a SmC phase and an optically isotropic phase with randomly distributed domains of opposite handedness which exhibits an antiferroelectric response. In 2009, WEISSFLOG *et al.* reported on the unusual mesophase behaviour of substituted *N-benzoylpiperazine* mesogens containing three *phenyl* rings together with a *piperazine* moiety which exhibit non-polar SmA and SmC phases.[56] For these materials a polar structure can be induced by applying an electric field. More recently, chiral ordered B_1 and B_7 phases, which are typical for banana-shaped liquid crystals, have been observed on four-ring asymmetric *salicylideneimine* derivatives by DEB *et al.*.[57] Six[35,58] and seven[59,60] aromatic rings in banana-shaped mesogens are also known and the mesophase stability seems to increase upon increasing the number of rings.[61] In some cases six-ring compounds form conventional smectic phases in addition to '*banana-phases*'.[62]

Another interesting aspect to observe is the impact on the thermotropic properties of bent-shaped molecules on the introduction of lateral substituents (*fluorine*,[63] *chlorine*,[64] *methyl*,[65] *methoxy*,[66] *cyano*,[67] *nitro*,[61] *bromine*[68] or a combination of different substituents[61,69]) in the wings or in the central part of a these compounds.[24] In general, melting points are lowered upon introduction of lateral substituents. Bulky substituents can suppress the LC properties completely and sometimes pronounced changes in switching behaviour can be observed upon introduction of small polar substituents.[70] The variation of the terminal *alkyloxy* chain or fluorination of the terminal chain can also have a remarkable effect on the mesomorphic properties of bent-shaped molecules. Despite their achiral molecular structure, bent-core molecules can form chiral mesophase domains due to two symmetry-breaking events. However, bent-core compounds with chiral carbon atoms in the terminal tails have also been studied. In these cases the transition temperatures are lowered[71] and ferroelectricity is induced.[72] Some more exotic bent-core LCs have also been studied, e.g. polycatenar bent-shaped mesogens[73], hydrogen-bonded bent-shaped mesogens[74] and bent-core mesogens incorporated in dendritic systems.[75]

1.3.3 Mesophases of banana-shaped mesogens

In this sub-chapter, an introduction in the complexity of the mesophases of bent-core mesogens is given. Two nomenclatures are used for the ordering of the rich variety of mesophases of various symmetries formed by the bent-core mesogens. The first one is based on the nomenclature of conventional liquid crystals. A subscription behind the phase symbol notes the interface arrangement of the molecules from layer to layer, i.e. for the uniform tilt-direction (synclinic organization) the subscript ***s***, e.g. $\mathrm{SmC_s}$, or for alternating tilt-direction (anticlinic organization) the subscript ***a***, e.g. $\mathrm{SmC_a}$ (see Fig. 1.3c and d, in chapter 1.2). Additionally, the letter ***P*** indicates if the mesophase is a polar phase. There may be a subscription behind it describing the switching behaviour. The subscription ***AF*** stands for antiferroelectric and ***FE*** for ferroelectric mesophases. The ferroelectric structure is characterized by a parallel direction of the polar order in adjacent layers, whereas the corresponding structure with an antiparallel organization is designated as antiferroelectric. The FE state represents a macroscopic polar structure whereas the AF structure is macroscopic apolar and therefore more stable than the FE states. Thus, $\mathrm{SmC_sP_{FE}}$ describes a mesophase where the long axes of the bent-shaped molecules are tilted with respect to the layer normal, from layer to layer parallel with each other, showing ferroelectric switching behaviour in electric field. It is well known that the synclinic tilt is usually preferred due to the dynamics in the LC phases, which include out-of-plane interlayer fluctuations. However, the anticlinic arrangement can be favoured enthalpically by steric and polar interactions at the interlayer interfaces.[76,77]

The other nomenclature is the one suggested at the workshop on '*Banana-shaped Liquid Crystals: Chirality by Achiral Molecules*', held in Berlin in 1997, where seven mesogenic phases were identified and simply designated as $\mathbf{B_n}$, B_1–B_7.[32] (B_8 phase was added later). '**B**' stands for bent, banana, bow, or boomerang. The subscript '**n**' corresponds to the sequence of discovery of the different phases. Based on the textural features and preliminary X-ray results, however, this nomenclature does not cover the whole spectra of banana mesophases known nowadays, i.e. several new phases and sub-phases have been recently discovered.

The bent shaped structure favors a steric packing of the molecules in which the 'bows' point in the same direction, giving rise to a layer with a uniform polar vector and therefore to a polar order along the direction of molecular bows. The important requirement for polar switching is that the packing is relatively strong but not too strong. The dipole moments which are parallel to the layer planes (along the C_2 symmetry axis) sum up, leading to a polarisation (P_S) of each layer (SmCP and SmAP phases). This results in monodomains with a finite residual spontaneous macroscopic electric polarisation P_S (volume density of the molecular dipoles). Hence the sterically induced alignment of the molecular bows of achiral mesogens gives rise to a polar superstructure. The axis of polarisation is in most cases parallel to the layers. The magnitude of the polarisation found for the bent-shaped molecules is remarkably higher than that measured for the polar calamitic compounds.[24,32,36]

If the bent molecules in the smectic layers are tilted with respect to the layer normal, the layers become chiral although the individual molecules are achiral.[78,79] That means that the combination of director tilt and polarity leads to chirality in the bent-shaped molecule. On the other hand, in calamitic polar mesogens the combination of director tilt and chirality gives polarity. To escape from a macroscopic polar order in the bulk, bent-shaped molecules promote the formation of antiferroelectric phases. These antiferroelectric phases can be switched into the ferroelectric state after applying a sufficiently strong electric field. This new way to achieve macroscopic polar order[80] and chirality has immediately attracted rapidly growing interest both among theoreticians and experimentalists. From 1996 to early 2014 several thousands of bent core molecules exhibiting mesomorphic properties have been synthesized. More than a few times the phase assignment of compounds in the past proved to be incomplete due to renewed insights or improved experimental techniques. The early developments in this field were reviewed in 1999[32] and reviews over some special aspects have also appeared during recent years.[24,36,50]

The orientation of a bent-core molecule can be defined by two directors: one director ***n*** along the long molecular axis and another director ***p*** in the direction of the bow. Due to packing constrains, bent-core molecules tend to segregate into planes, with their polar axis defined by ***p*** aligned along a common direction. Since the layer normal ***k*** defines a direction independently of ***n*** and ***p*** a variety of mesophases with different symmetries may result.[81] The polar axis can be controlled by application of an electric field due to the existence of an electric polarisation, i.e. the mesophase is switchable. Bent-core achiral mesogens can form phases in which the symmetry is spontaneously broken. For the case of smectic liquid crystals formed by bent-shaped molecules different possible arrangements have been proposed by Brand *et al.*[79] The so-called '*minimal banana smectics*' possess one polarisation vector and corresponding arrangements and symmetries are sketched in Figure 1.6.

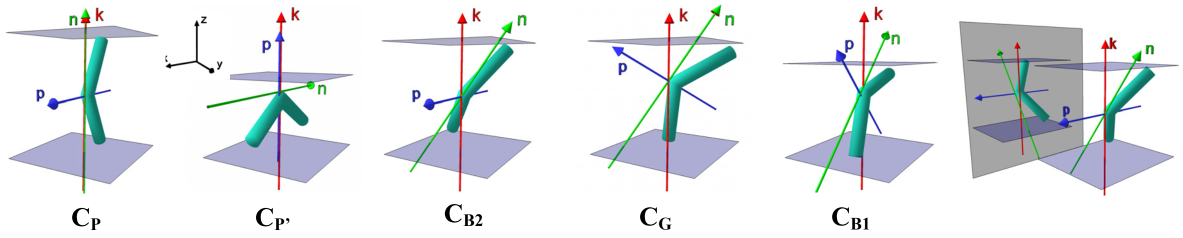

C_P $C_{P'}$ C_{B2} C_G C_{B1}

(a) (b) (c) (d) (e) (f)

Figure 1.6: (a-e) Possible arrangements of molecules in smectic layers and (f) structural chirality of the SmCP phase according to Brand *et al.*[79]

A phase with C_{2v} symmetry is called C_P (Fig. 1.6a) or ***SmAP phase***. There, the bent molecules are arranged orthogonally in smectic layers which combined with the close packing requirement results in a polar order along the direction of molecular bows, i.e. a spontaneous macroscopic polarisation. This is the key difference between the SmAP phase and the SmA phase, where there is no preferred direction perpendicular to the layer normal. Eremin *et al*[82] reported for the first time the observation of a SmAP phase in low-molecular bent-shaped compounds. Link *et al*[83] reported about a similar SmAP phase found in achiral side-chain polymers.

The most common phase is the one with C_2 symmetry, also designated as C_{B2} (see Fig. 1.6c) or ***B_2 phase*** or ***SmCP phase***. The structure of the phase consists of smectic layers with tilted molecules. The polar order is in the direction perpendicular to the layer normal. The polar direction in adjacent layers is antiparallel in the ***SmCP$_{AF}$ phase***, and resp. parallel in the ***SmCP$_{FE}$ phase.*** The polar and chiral layer structures arise from two symmetry-breaking events: the existence of a polar axis C_2 and the tilt of the molecular long-axis from the layer normal (SmC-like).[50] It is important here to realize that the chirality in the B_2 phase does not arise from a superhelical organization like in the SmC* phase, although the symmetry in both cases is C_2. On the other hand, it was suggested that some bent-core molecules may exist in chiral conformational states and are chiral only on average.[84] In the SmCP configuration the layer normal, the tilt direction and the polar axis define a chiral system which is either right-handed or left-handed as shown in Figure 1.7b. Variation of either polarisation direction (indicated by crosses or dots in circles) or of the tilt direction changes the chirality sense of the layer (indicated by red (-) vs. blue (+) colour, this colour code will be used throughout this work).[78] Including the synclinic and anticlinic arrangement of the layers, there are four possible combinations of the layers (see Fig. 1.7a). In SmC_aP_{AF} and SmC_sP_{FE} structures, all the layers of a macroscopic domain have the same chirality sense. These phase structures are homogeneous chiral and occur in both enantiomeric forms (as conglomerates). In the SmC_sP_{AF} and SmC_aP_{FE} structures there are equal numbers of layers with (+) and (-) chirality and hence these superstructures are racemic on a macroscopic scale.[78]

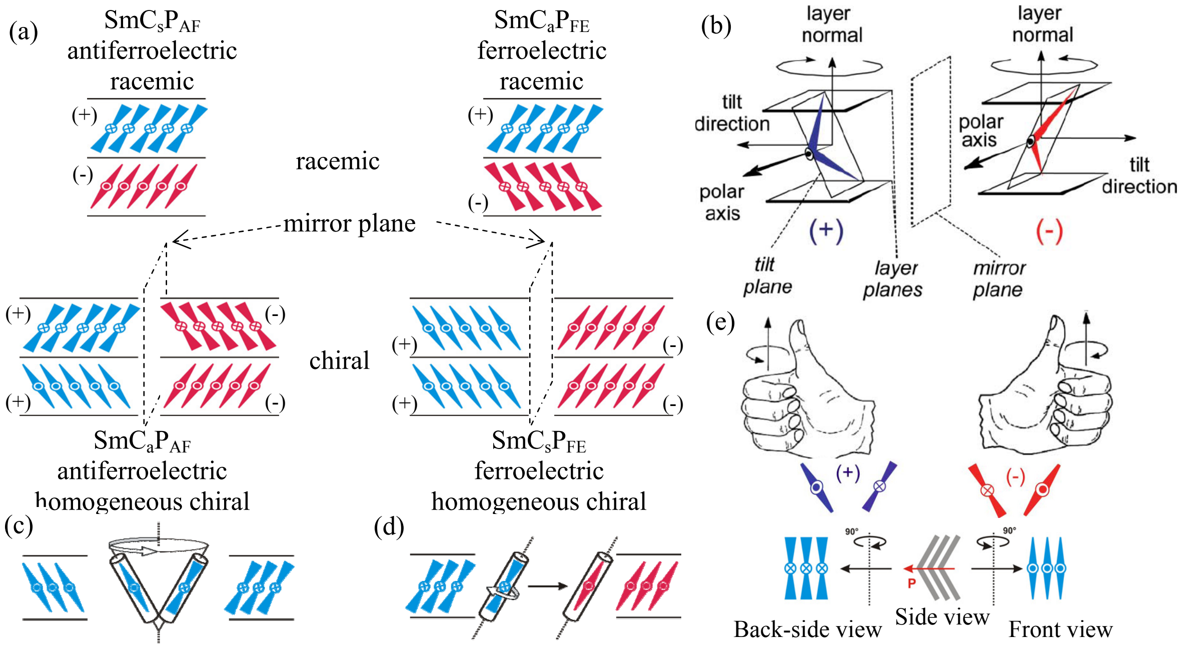
(a)
SmCsPAF
antiferroelectric
racemic
SmCaPFE
ferroelectric
racemic
(+)
(-)
racemic
mirror plane
chiral
SmCaPAF
antiferroelectric
homogeneous chiral
SmCsPFE
ferroelectric
homogeneous chiral
(b)
layer normal
tilt direction
polar axis
(+)
(-)
tilt plane
layer planes
mirror plane
(c)
(d)
(e)
90°
P
Back-side view
Side view
Front view

Figure 1.7: (a) The supramolecular arrangements resulting from the combination of the different tilt directions and polar directions; (b) origin of the superstructural chirality within the smectic phases of bent-core molecules; (c,d) schematic representation of the polar switching process: (c) by a fast collective rotation around a tilt cone; (d) by a rotation of the molecules around the long axis; (e) bent-core molecules: side view, back-side and front view; pictorial representation according to TSCHIERSKE *et al.*[24]

An extended review of the topic of chirality and its measure can be found in ref.[12,85,86] In most cases the ground state is antiferroelectric and by applying an electric field along the layers one can switch to the ferroelectric state. The chirality of the layers usually remains conserved. The switching process between the AF and FE states of these tilted phases usually occurs by a fast collective rotation around a tilt cone (see Fig. 1.7c). This switching process simultaneously reverses polar direction as well as tilt direction. This can be observed optically between crossed polarisers by a rotation of the dark extinction brushes, occurring in circular domains. Both AF ground states are energetically very similar. The formation of either SmC_aP_{AF} or SmC_sP_{AF} structures strongly depends on the chemical structure of the material and the experimental conditions (surfaces, applied fields,[87] history of the sample, etc.). Very often both SmC_aP_{AF} or SmC_sP_{AF} structures coexist in one sample. The second switching process can be realized by a rotation of the molecules around the long axis, where the polarisation reversal takes place (Fig. 1.7d). The AF organization is macroscopic apolar and therefore more stable than the FE state. In the case of the bent-shaped mesogens, the AF structure is additionally stabilised by the possibility of out-of-plane interlayer fluctuations. The AF state represents an arrangement with synclinic interlayer interfaces, i.e. the *alkyl* chains are aligned parallel at the interlayer interfaces (Fig. 1.8). This synclinicity easily allows interlayer fluctuations and is therefore entropically favoured as shown in Figure 1.8. On the other hand, in the FE ground state the similar bending direction of the molecules in adjacent layers leads to anticlinic interlayer interfaces. It means that these interlayer fluctuations are hindered in the FE state, which is entropically unfavourable (Fig. 1.8). Remarkably, this entropic effect upon the bulk phase structure in the mesophases of bent-shaped molecules is in contradiction with the one found for the SmC_s and SmC_a phases of calamitic mesogens (Fig. 1.3c and d). Therefore, in most polar smectic phases of bent- shaped mesogens the ground state is AF. The FE state can be induced by alignment applying an electric field, since there is only a small energy barrier between the AF and the FE states. A classical switching current response obtained for the AF phase of a bent-core compound under a triangular-wave field is characterized by the occurrence of two repolarisation peaks in each half period of the applied voltage, whereas for the FE phase only a peak could be detected. The values of the P_S in the SmCP phases are in the range between 300–1000 nC cm^{-2}. This value is much larger than those observed for SmC^*_{FE} and SmC^*_{AF} phases of chiral calamitic molecules (5–200 nC cm^{-2}).[12]

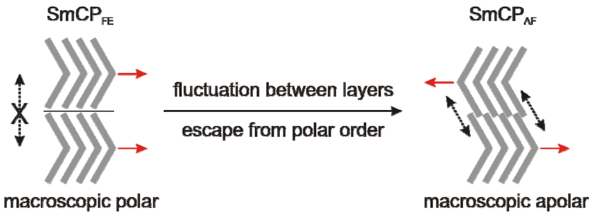

Figure 1.8: Interlayer fluctuations of the molecules between the adjacent layers.[88]

This new way to macroscopic polar order and chirality immediately have attracted rapidly growing interest both among theoreticians and experimentalists, mainly because of the ability of these bent molecules to originate LC mesophases that exhibit spontaneous polarisation (P_S) in the absence of chiral groups in their molecular structure. Initially, the ferroelectricity[89] and antiferroelectricity[90] were discovered in chiral compounds exhibiting tilted smectic phases long before the field of bent-core molecules started attracting such a high interest. In 1974 MEYER[91] hypothesized that ferroelectricity could exist in a chiral smectic C (SmC*) LC phase made from chiral molecules using symmetry arguments. It was thought that molecular chirality was needed to reduce the symmetry of a material and produce a polar superstructure. MEYER's arguments was that the simultaneous presence of the molecular chirality and director tilt would lead to a polar order, because chirality breaks inversion symmetry, a condition needed for polar order. On the other side, CLARK's arguments were that the symmetry of bent-shaped LC phases is sometimes broken as a result of simultaneous director tilt and polar order perpendicular to the director.[78] Hence, astonishing LC phases can exist and (anti)ferroelectricity is sometimes observed,[32] a property previously only found for chiral compounds. The bent-core mesogens are the first ferroelectric and antiferroelectric LCs realized without introducing molecular chirality. Spontaneous chiral deracemization at microscopic and macroscopic levels occurs and is controllable. Moreover, achiral bent-core molecules enhance system chirality. As a result, the interplay between polarity and chirality provides chiral nonlinear optic effects. The P_S is usually determined in electro-optical switching experiments: under applied periodic rectangular or triangular waveforms.

The ***B_5 phase*** shows many similarities with the SmCP phase (B_2). The electro-optical response, textural features and the symmetry are almost identical. A B_2-B_5 transition is accompanied by a sharpening of the X-ray pattern in the wide angle region and increasing viscosity.[32,92] The key difference to the SmCP phase is that the B_5 phase possesses an in-plane density modulation which can be described by a rectangular two-dimensional network.[32,92] Since the B_5 phase is relatively rare it has not been studied in much detail and probably could be regarded as a candidate to an analogue to hexatic phases of calamitic mesogens.

Other phase structures are formed by the partial collapse of the layers which leads to ribbon-like segments organising in such a way that the bend directions of the molecules in adjacent ribbons are antiparallel. This organization results in an efficient escape from macroscopic polar order. The new-formed mesophases are characterised by a 2D lattice resulting from the positional ordering of these ribbons. These mesophases can be regarded as modulated polar smectic phases (Sm$\tilde{A}$P or Sm$\tilde{C}$P) or alternatively as columnar phases built up by ribbons with an orientational correlation of the molecules in adjacent ribbons. The molecules within the ribbons can be either tilted (columnar oblique phase, ***Col_{ob}***, Fig. 1.9 c) or non-tilted (columnar rectangular phase, ***Col_r***, Fig. 1.9 a, b). This type of mesophases is often abbreviated as ***B_1 phase***. In general, these columnar phases do not show any switching behaviour.[93] It is usually observed in compounds with relatively short terminal (*alkyl*) chains. The Col_r phase consists of a rectangular packing of ribbons, i.e. infinite ribbon-like segments of smectic layers. The polarisation directions of the ribbons are cancelling along the C_2 axis. The two-dimensional lattice is in the plane of the polar direction, i.e. the polarisation direction is perpendicular to the columns. TAKANISHI *et al*.[27] reported on bent mesogenic dimers where the polarisation direction in the columnar phases should be perpendicular to the 2D lattice, i.e. the polarisation direction should be along the columns with an antiparallel packing of adjacent columns. SZYDLOWSKA *et al*.[94] also reported such columnar phases and assigned them as B_{1rev} (Figure 1.9 b). In some cases, below this orthogonal phase an additional oblique columnar (Col_{ob}) phase was observed, where the molecules have a synclinic tilt (designated as $B1_{rev,tilted}$).[94,95] Recently, it was shown that the B_1 phase can exhibit several sub-phases which sometimes show switching properties,[94] a 3-D modulated phase structure[94] or a tilted structure.[29]

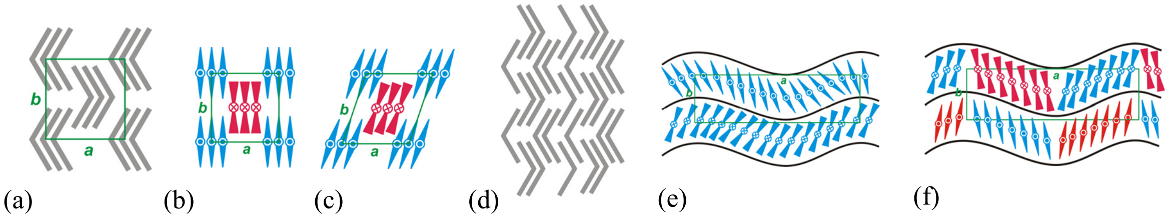

(a) (b) (c) (d) (e) (f)

Figure 1.9: Schematic representation of organisation of molecules in: (a) B_1 phase (Col_r phase); (b) B_{1rev} phase (Col_rP_{AF} phase); (c) Col_{ob} phase; (d) B_6 phase (Sm_c, intercalated smectic phase); (e,f) models of undulated (sinusoidal deformed) smectic phase USmCP: (e) $USmC_aP_{AF}$ phase; (f) $USmC_sP_{AF}$ phase.

Smectic phase with an intercalated layer structures (designated as ***B_6 phases***) are formed if the size of the ribbons or slabs is very small and there is no positional correlation between them, i.e. no 2D-lattice is present (see Fig. 1.9 d). Such intercalated layer structures $\mathrm{SmA_c}$ or $\mathrm{SmC_c}$ phases (the subscript '**c**' is recommended to describe intercalated phases[3,96]) are characterised by a layer distance comparable or smaller than half the molecular length. The B_6 phase[97] is typically exhibited by bent-shaped mesogens with very short terminal tails. It occurs rarely and in contrast to the SmCP phase, it does not show electro-optical switching.[32,98]

The formation of ***undulated*** and ***modulated layers*** and columnar phases in the case of calamitic systems can be the consequence of a frustration of the layer organisation as a result of a mismatch of the area required by rigid cores and *alkyl* chains at the aromatic–aliphatic interfaces[99] as well as the polar effects[100] in the layer structure. In the case of bent-shaped molecules, the situation is more complex due to the competition of the order parameters (density modulation, tilt and polarisation) and the presence of the polar vector parallel to the layer planes. Additionally, the polar vector can have a component perpendicular to the layers (***SmCG phases***). In the undulated structures the layers are sinusoidal deformed (***USmA***, ***USmC,*** Fig. 1.9 e, f.), whereas in the modulated layers structures (e.g. ribbon phases, Col, SmÃ, SmX̃) the smectic layers are broken into discrete ribbons. In the $\mathrm{USmC_aP_{AF}}$ structure (see Fig. 1.9 e) the tilt direction can change from layer to layer (anticlinic tilt would lead to a homogeneous chiral structure). In the $\mathrm{USmC_sP_{AF}}$ structure the correlation between the undulated layers is synclinic, but the tilt direction changes along the undulated layers. This structure would be racemic, but requires additional defects in the layers (positions where the tilt direction changes, see Fig. 1.9 f) which are unfavourable if there is a significant tilt.

The assignment of the ***B_7 phase*** is used for a wide range of different mesophases, which all exhibit characteristic textural features, i.e. helical filaments, checkerboard textures or banana-leaf shaped domains.[24,36,101] COLEMAN *et al.*[102] combined several techniques to conclude that the B_7 mesophase is a fluid polar smectic liquid crystal. In this phase local splay prevails in the form of periodic supermolecular-scale polarisation modulation stripes coupled to layer undulation waves.[102] The precise structure of these mesophases is not clear to date. Therefore, the less specific descriptor B_7 should still be used and this assignment should be used exclusively for B_7 type mesophases which show the medium angle scattering in the X-ray diffraction pattern. Remarkably, mostly all the compounds which form this type of B_7 phases have highly polar substituents (e.g. -CN, -NO_2) at the central *benzene* ring of the bent unit.

B_7 - like mesophases (***B_7' phases***) are modulated-undulated fluid smectic phases, which are often assigned also as B_7 phases because of the typical textures with helical filaments. The key difference is the diffraction pattern characterised by the absence of medium angle reflections and the simple layer structure with satellites of weak intensity behind the layer reflections, suggesting an undulated, i.e. sinusoidal deformed, layer structure without order in the layers. This type of mesophases typically shows FE or AF switching and it can be observed for molecules with quite different molecular structures (e.g.[102]).

The ***B_3 phases*** are considered soft crystalline phases (high ordered mesophases). This phase is a tilted lamellar crystalline phase that does not exhibit switching behaviour. This phase should possess SHG activity,[103] also in the absence of an applied field, indicating spontaneous polar ordering.

The ***B_4 phases*** are high ordered mesophases (soft crystalline phases), i.e. a helical twisted layer structure with semicrystalline ordering of the layers, large optical rotation and light scattering suggesting a strongly chiral local structure. This phase is formed by spontaneously self-assembling helical nanofilaments, the morphology of which is driven by a tendency for local saddle splay deformation of the semicrystalline layers.[104] Usually, the B_4 phase is formed as a low temperature phase in compounds exhibiting B_2 phases,[105] although B_4-B_7 transitions also have been observed.[106]

'New' banana phases with a two-layer structure made of ***SmCG layers*** was been reported by BEDEL *et al.*[107] The smectic phase with triclinic symmetry, i.e. the lowest symmetry, was predicted by DE GENNES[108] and was named smectic *CG* phase, where *G* stands for generalized (see Fig. 1.6). The Sm*CG* phase is characterized by two tilt directions with respect to the layer normal, tilt of the molecular plane (clinic) and tilt of the molecular kink directions (leaning). A complete overview on the recent developments in the field of banana-shaped LCs and its phases was given by REDDY *et al.*[24]

1.4 Liquid crystal oligomers: dimeric and trimeric mesogens

By definition the ***liquid crystal oligomers*** are mesogens constituted of molecules composed of two or more semi-rigid mesogenic units interconnected *via* flexible spacers, most commonly *alkyl* chains. Some extensive reviews on the relationship between molecular structure and liquid crystalline behaviour in the LC oligomers are given by IMRIE *et al.*[109,110] The major interest in the linear LC oligomers was initially focused on their ability to act as model compounds for semi-flexible main chain liquid crystalline polymers.[111] However, the studies are recently strongly concentrated on their own mesomorphic behaviour, which is quite different to that found for the conventional corresponding low molar mass liquid crystals.

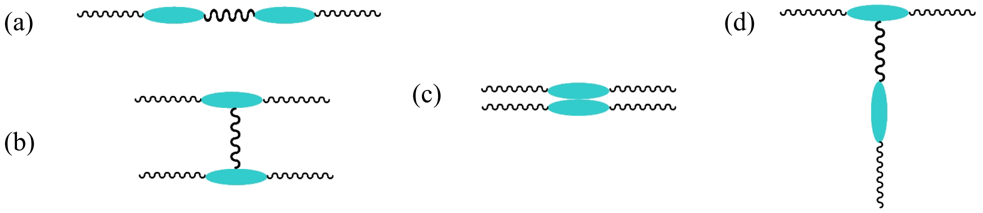

Figure 1.10: Structures of few examples of different types of LC dimers: (a) linear dimer; (b) H-shaped dimer *(laterally-connected* or *ligated twin mesogen*); (c) fused twin mesogen; and (d) T-shaped dimer.

The simplest LC oligomers are the ***liquid crystal dimers*** (also known as *mesogenic dimers* or *twin mesogens*) in which two LC units are linked *via* a single flexible spacer. Dimers can be distinguished by their connection topology. A few examples are schematically represented in the Figure 1.10. LC dimeric systems containing identical mesogenic units are assigned as being *symmetric dimers*, e.g.[112], while *non-symmetric dimers* consist of two different mesogenic groups, e.g.[113] Although the most widely used spacer in dimers is an *alkyl* chain, other types of spacer including, for example, *malonates*,[114] branched *alkyl* chains[34] and *siloxanes*[115] have been used.

A liquid-crystal dimer with flexible hydrocarbon chains having an *odd* number of carbon atoms , i.e an *odd* - parity of the single units in the spacer, is called an *odd-membered liquid crystal dimer*, while one with hydrocarbon chains having an *even* number of carbon atoms, i.e. an *even* - parity of the single units in spacer, is assigned as an *even-membered liquid crystal* *dimer*. The thermal behaviour of dimers is quite different from that of conventional low molar mass mesogens; in particular, their transitional properties exhibit a pronounced alternation on varying the number and parity of *methylene* groups in the spacer.[111]

On varying the length and parity of the spacer, strong *odd-even* effects are usually observed in the transitional properties of the dimeric LCs.[116] These effects are reminiscent of that observed for the polymeric systems.[117] These *odd-even* effects are most often attributed to the dependence of the molecular shape on the number of units linking the two mesogenic moieties, and by considering the spacer to exist in its all-*trans* conformation, see (Fig. 1.11). The *odd* membered dimers tend to assume a bent shape conformation with the two mesogens tilted with respect to each other. An *even* membered dimer has a zig-zag shape in which the mesogenic units are anti-parallel and are more likely to lie parallel to each other (Fig. 1.11).[118] As a result, the *odd*-numbered spacers have a stronger tendency to form SmC-like phases while *even*-numbered analogues form SmA phases.[116,119] However, this simplistic interpretation of the transitional properties of dimers has completely neglected the flexibility of the spacer. A more realistic interpretation of the dependence of the transitional properties on the length and parity of the spacer must include a wide range of conformations and not solely the all-*trans* arrangement.[120] In 1999, some more striking properties of dimers with a flexible *alkylene* spacer were discovered.[121,122] Some compounds with an *odd* number of flexible units between the two mesogens adopt a bent conformation resulting in LC phases with electro-optical switching properties.

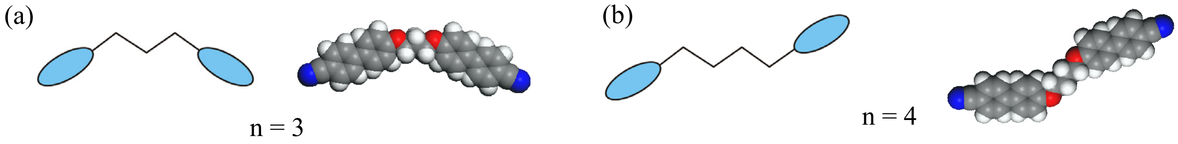

Figure 1.11: Molecular shape of dimeric molecules with (a) an *odd* and (b) an *even* number of flexible units between the two mesogens.

For many dimers, composed of monomers that form smectic phases, it was found that the smectic phase behaviour was suppressed.[117] On the other hand, it is known that dimers with long terminal tails promote smectic behaviour.[123] Some series of compounds even exhibit a rich polymorphism of smectic phases.[124] A simple relationship between the occurrence of smectic behaviour and the molecular structure of *symmetric dimers* was deduced from studies on the α,ω-bis(4-*n*-alkylanilinebenzylidene-4'-oxy)alkane series (as named in literature[124]). To obtain smectic properties the length of the terminal tails must be greater than half the length of the spacer.[124] For different ratio between the lengths of the terminal chains and the spacer length nematic behaviour was observed for these systems. In this case a simple monolayer structure was present which is thought to be stabilized by the microphase segregation into three regions.

Non-symmetric dimers, in which two different mesogenic groups are linked through a flexible spacer, have also been described extensively in literature.[125,126] In general, the different mesogenic units have been chosen because they are known to exhibit a specific favourable molecular interaction, i.e. the linking of electron rich and electron deficient mesogenic groups. Interestingly, there are numerous reports in the literature where such a particular non-symmetric dimer structure was chosen, in part, because binary mixtures of conventional low molar mass LCs containing these mesogenic units were know to exhibit unusual phase behaviour. For example, a binary mixture of two nematogens could show smectic behaviour, the so-called induced smectic phases.[127] In addition, the phase behaviour of the corresponding symmetric dimers was known, allowing the behaviour of the non-symmetric dimers to be compared with it.[124,128] These non-symmetric dimers tend to arrange in intercalated (Fig. 1.12c) or interdigitated (Fig. 1.12d) smectic organizations.[113] The intercalated arrangement is stabilized by the increase in entropy gained from the homogeneously mixed mesogenic units (non-specific interactions). Another possible stabilizing factor is the electrostatic quadrupolar interaction between the different mesogens having quadrupole moments of opposite sign.[129] In some cases however also symmetric dimers are known to exhibit intercalated mesophases (Fig. 1.12b).[116]

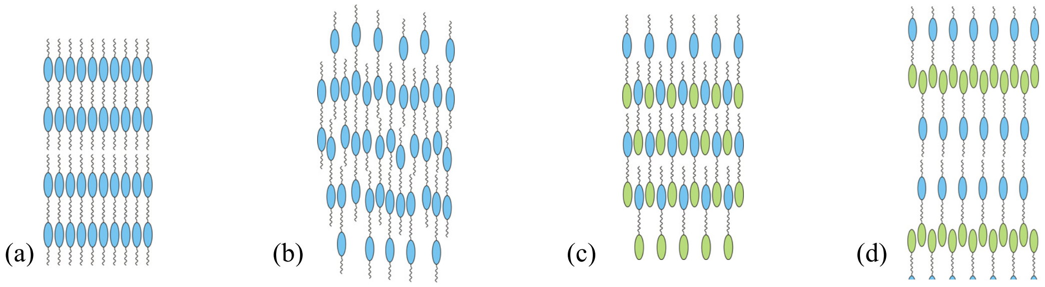

Figure 1.12: Schematic representation of the molecular organisation for (a, b) symmetric dimer LCs in: (a) the monolayer and (b) the intercalated SmA phases; (c, d) non-symmetric dimer LCs in: (c) the intercalated and (d) the interdigitated SmA phases.[110,116]

Another structural feature which has been varied in the dimeric architecture is the type of linking group between the hydrocarbon spacer and mesogenic units including ethers,[112] esters,[130] thioesters,[131] and thioethers.[132] These molecules continue to attract considerable research attention with recent studies including: the role of the spacer in determining liquid crystal behaviour,[133] dimers linked in a linear fashion,[110] laterally connected dimers,[134] dimers containing bent-core mesogenic units,[135] cholesteryl-containing dimers,[136] dimers containing rod- and disc-shaped mesogenic units and their potential to exhibit the biaxial nematic phase,[137] non-symmetric dimers containing both a bent-core and calamitic mesogenic units,[138,139,140] hydrogen-bonded dimers,[141] phase behaviour in bent *odd*-membered dimers;[142] the flexoelectric properties of dimers,[143] and light-emitting dimers.[144]

The first report on symmetric '*banana – banana*' dimers consisting of two rigid bent-core mesogenic units linked *via* a flexible *alkyl* spacer containing *dimethylsiloxane* units in the centre was made by DANTLGRABER *et. al.*[88] This study showed that the number of *dimethylsiloxane* units of the spacer determines the ferroelectric or antiferroelectric nature of the SmCP phase, i.e. the *odd*-membered dimers show ferroelectric switching, whereas the *even*-membered dimers show antiferroelectric switching. This particular spacer was found to lower the transition temperatures of the mesogens and facilitate the easy switching characteristics from antiferroelectric to surface-stabilized ferroelectric states of the SmCP phase. Similar behaviour has been reported for other bent-core mesogenic dimers.[145] On variations of the terminal chain and also the two *alkyl* spacers linking the mesogenic units to the central *siloxane* core it was found that no *odd–even* effect was observed on phase type on varying the parity of the *alkyl* spacers.[135] KOSATA *et al.*[146] made a comparative study on the mesomorphic properties of symmetrical dimers in which two bent-core moieties are connected by *alkyl*, *tetraethylene glycol* or *siloxane* containing spacers. Those containing wholly *alkyl* spacers were not mesogenic, while those with tetraethylene glycol spacers exhibited columnar mesophases and those with siloxane containing spacers exhibited a $\mathrm{SmCP_{FE}}$ mesophase. The chemical nature of the spacer plays an important role in determining the phase behaviour of these dimers. Remarkably, it was observed that the ground-state structure of the SmCP phase can be changed on going from a monomeric to a dimeric system.[146] SADASHIVA and co-workers [147] reported the synthesis of several mesogenic dimers composed of bent-core molecules possessing an *alkylene* spacer of varying parity. A ferroelectric switchable polar oblique columnar phase was established for these dimers. SADASHIVA's group[148] reported recently also on symmetrical bent-core dimers (with a 5-hydroxyisophthalic acid central unit) connected at the apex positions by *alkylene* spacers. Remarkably, these dimers exhibit a first order phase transition SmA-SmA' phase. This transition has been attributed to conformational changes in the chains. Notably, the change in the parity of the spacer does not change the phase behaviour of these dimers.[147,148] This observation is in contrast to the dramatic *odd–even* effect observed as the parity of the spacer is varied for several series of dimers derived from calamitic mesogenic segments. These results indicate that the dimers composed of bent-core mesogens themselves are of significant interest in their own right because their phase behaviour seems to be different from the monomeric systems. However, the clear understanding of the correlation between the overall molecular structure and mesomorphic properties of dimeric systems is still at the beginning.

Non-symmetric dimers containing both a bent-core and calamitic *cyanobiphenyl-* group have been first reported by YELAMAGGAD and co-workers.[138,149,150] The dimer containing a *hexamethylene* spacer exhibited biaxial nematic, $\mathrm{N_b}$, and biaxial smectic A, $\mathrm{SmA_b}$, and a further unidentified mesophase. The biaxial nature of this nematic phase could not be proved by further studies. The nematic phases formed by bent-core mesogens are of great interest for theoretical and practical reasons, e.g. due to their chiral nature and exceptional electro-optical features.[151] In 2012 WANG *et al.*[152] gave an account of some further dimers containing *cyanobiphenyl* unit with a bent-core unit with or without a second cyano group at the central *phenyl* ring exhibiting nematic phase and higher ordered phases. The lower temperature of one of these compounds was found to be also $\mathrm{SmA_b}$ phase. The $\mathrm{SmA_b}$ phase in this system is of special interest as a candidate for improving and expanding the utility of LC displays due to the fast switching rates.[153,154,155] Moreover, the presence of a high temperature N phase can facilitate the alignment to a defect-free smectic structure, i.e. opening new ways to LCD technologies. The formation of the N phase above the biaxial SmA phase in these systems is a possible pathway to the formation of the biaxial N phase in similar systems containing bent-shaped and calamitic mesogens. Furthermore, *cyanobiphenyl* group was connected to three- and four-ring bent-core fragments to create nematic materials.[156,157] SHANKER *et al.* reported on calamitic fragments other than *cyanobiphenyl* connected in lateral or terminal version to five-ring bent-core moieties which exhibited phase sequences with uniaxial N and additional Col or Sm phases.[158] YELAMAGGAD's group reported also on structurally frustrated mesophases obtained over a wide thermal interval in dimers covalently joining a bent-core mesogen to cholesterol through a flexible spacer.[140] Notably, some of these dimeric designs lead to polar smectic LCs and new phase sequences originating from the interplay between the shape anisotropy of the two mesogenic units as well as the parity and length of the flexible spacer. *Even*-membered dimers exhibited blue phases over a long temperature range, chiral nematic and then either columnar or tilted smectic phases. The *odd*-membered dimers exhibited only a columnar phase, indicating a strong dependence of packing on the parity of the flexible spacer for such dimers.

One of the major issues in the development of LC dimers, especially non-symmetrical dimers, was the search for ***biaxiality*** in the nematic LC systems. Banana-shaped compounds appear to be appropriate candidates for formation of non-polar and polar biaxial nematic phases.[159] Despite the prediction of the existence of the biaxial nematic N_b phase on the basis of molecular field calculations in 1970,[160] the first claim to be found was in a complex lyotropic system in 1980,[161] and later on in a low-molar-mass thermotropic LC system in 1986.[162] Numerous studies claiming the observation of the N_b phases were proved by means of deuterium NMR spectroscopy to be uniaxial phases.[163] Meanwhile, simulations on bent-shaped molecules indicated that the N_b phases could be stable in such molecular systems.[164] Evidence for the biaxiality of a N phase composed of bent - shaped oxadiazole molecules has been provided.[15,16] The first N_b phase above the biaxial SmA_b phase was reported by YELAMAGGAD *et al*. for a non-symmetric banana–rod system.[165] However, experimental confirmation is not as sufficient as for the oxadiazole molecule, i.e. the assignment of the mesophases was conducted only by means of optical measurements (i.e. conoscopy).

A ***liquid crystal trimer*** consists of molecules containing three mesogenic units interconnected via two flexible spacers. These structural components may be assembled in a number of various ways to give, for example: linear trimers,[166] trimers in which one or more mesogenic units are connected in a lateral position,[167] cyclic trimers,[168] star-shaped trimers,[169] trimers containing rod-like and disc-like mesogenic moieties.[168] Examples of some of these molecular architectures are shown schematically in Figure 1.13. These systems can be broadly classified into three groups depending upon the chemical nature of the mesogenic segments they possess: symmetric (with all the mesogenic units identical), mixed (in which two of the mesogens are identical), and non-symmetric. The non-symmetry may be introduced in various ways, e.g. using *alkyl* chains of non-identical lengths,[170] different terminal groups or some combination of all these variations.[171] The structure - property relationships in higher oligomers such as molecular assemblages in dendrimers, tetrapodes, non-linear discotic and rod-disc oligomers, U-shaped, Y-shaped, λ-shaped, S-shaped and other non-linear oligomers[172] are not the subject of this work.

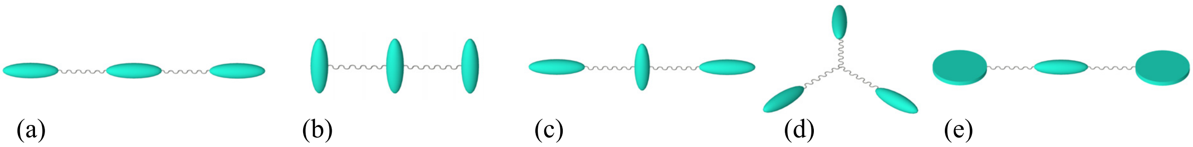

Figure 1.13:Molecular architectures of a selection of LCs trimers: (a) linear trimers; (b,c) trimers laterally connected; (d) star-shaped trimers; (e) trimers containing rod-like and disc-like mesogenic moieties.

The different molecular architecture has been exploited to address issues in a range of quite different areas and has given rise to potential applications for these new materials. In this work, only trimers in which the bent-core and calamitic mesogenic units are linked essentially in a linear fashion will be considered.

The first examples of mesomorphic linear trimers consisting of bent-core and rod-like anisotropic segments have been reported by YELAMAGGAD *et al.*,[173] in an exploratory attempt to realize molecules capable of stabilizing optically biaxial mesophases. All of the trimers exhibit an enantiotropic uniaxial nematic phase.

1.5 Binary mixtures of banana-shaped and calamitic mesogens

The binary mixtures of banana-shaped and calamitic mesogens can also result in new mesophases with interesting properties. GORECKA *et al.*[174] reported on the emergence and/or stabilization of the anticlinic ordering produced by doping calamitic synclinic or non-tilted smectic phases with banana-shaped molecules at low concentrations. It was reported that the doping effect is not effective for bent-core molecules with a *thiophene* ring as central unit (large bending angle of about 154°). Furthermore, the induction effect of an anticlinic phase is surely a steric effect and the anticlinic order is easily imagined to be formed in the smectic phase by assuming that calamitic parts align parallel to one of the wings of the bent-core compounds (see Fig. 1.14).[36] Such entropy-driven induction of anticlinic ordering was demonstrated by MONTE-CARLO simulation.[175] By doping a calamitic SmA host with a low concentration (3%) of bent-core molecules with an overall length twice that of calamitic molecules, an anticlinic order is induced, provided that the bending angle is 100 –150°. The simulation results are consistent with those experiments conducted by GORECKA *et al.*[175] but do not give any evidence of the induced biaxial SmA phase reported by PRATIBHA *et al.*[176] There are two reports of phase diagrams in binary mixtures consisting of bent-core molecules and calamitic polar rigid molecules.[177,178] PRATIBHA *et al.*[178] used a bent-core molecule forming a B_2 phase, and resp., a calamitic molecule 8OCB (4-cyano-4’-octyloxybiphenyl) which possesses a N–SmA phase sequence. By mixing them, B_2 and N are stabilized near 0 and 100% 8OCB, respectively. The induction of B_1 is observed at an intermediate mixing ratio. Totally different phase behaviour was found by TAKANISHI *et al.*[179] who used mixtures of a bent-shaped molecule P-8-OPIMB (1,3-phenylene bis[4-(4-*n*-octyloxyphenyliminomethyl) benzoates]) which exhibits a phase sequence B_2–B_3–B_4, and resp. the calamitic molecule 5CB (4-Cyano-4'-pentylbiphenyl) which possesses a N phase. The B_2 and B_3 phases are destabilized and disappear at 20wt% 5CB, and only the B_4 phase is stabilized. The distinctive feature in the mixtures presented in ref.[179] is the growth in size of segregated chiral domains. In studies of different mixtures with a non-polar flexible molecule such as *n*-hexadecane, the X-ray diffraction studies show a 3 Å increase in layer thickness, indicating that the flexible molecules are located between the smectic layers of the bent-core molecules.[179,180]

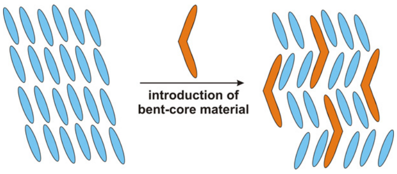

Figure 1.14: Schematic representation of the effect of introduction of banana-shaped molecules into synclinic smectic phase composed of calamitic mesogens. Pictorial representation according to TAKEZOE *et. al.*[36]

There are several reports in the literature of studies of binary mixtures of banana-shaped and calamitic compounds from our working group by SCHRÖDER *et al.*,[181,182] the latest report is directly related to this work (but not presented here for the sake of brevity).[183] The covalently connected dimer and trimer structures presented in this work were chosen, in part because binary mixtures of conventional low molar mass LCs containing these mesogenic units were know to exhibit unusual phase behaviour.

2 Objectives of this thesis

The aim of the research described in this thesis is to design, synthesize and characterize novel mesogenic dimers and trimers in which at least one mesogenic unit possesses a banana-shaped (bent-core) mesogen whereas the other is a calamitic moiety of different size. This work is an attempt to better understand the impact of molecular design on the mesomorphic behaviour of these new LC systems and the factors that could influence their potential application in switchable cells. The combinations of bent-core and calamitic mesogenic units in the dimers and trimers under discussion should clarify whether and to what extent the mesophase behaviour of the monomers can be modified. Another question to answer is if there is a '*competition*' of the contribution of the calamitic and bent-core moieties on the mesomorphic behaviour of the oligomeric systems, i.e. to clarify whether this combination can lead to polymorphism variants with '*banana phases*'(columnar and polar smectic phases), as well as mesophases typical for calamitic compounds (N, SmA, SmC phases). A further point of interest is whether the nematic, SmA or SmC phases formed by these novel oligomeric systems would exhibit the properties of calamitic mesogens, or perhaps the features of the phases formed by corresponding monomeric bent-core mesogens. The main target when designing these LCs systems was to identify novel chemically stable compounds with switchable enantiotropic mesophases that exhibit a wide range of temperature (as near to room temperature as possible) with potential use in display devices.

The general formula of the novel non-symmetrical '***banana – calamit***' dimers (**type I** and **type II**), symmetrical '***calamit - banana – calamit'*** trimers (**type I**) and '***banana – calamit – banana***' trimers (**type II**) are depicted in Figure 2.1.

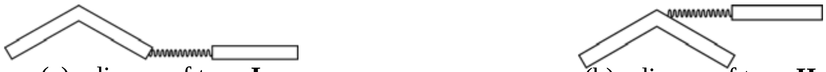

(a) dimers of type **I**

(b) dimers of type **II**

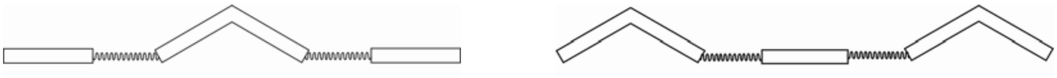

(c) trimers of type **I**

(d) trimers of type **II**

Figure 2.1: General formula of the synthesized compounds.

After the description of the synthetic pathway of the target materials in chapter **3**, in chapter **4** follows a brief introduction of the experimental techniques used for physical characterization of the liquid crystal phases. The rest of the chapters is dedicated to the description of the mesophase behaviour of the target oligomeric systems.

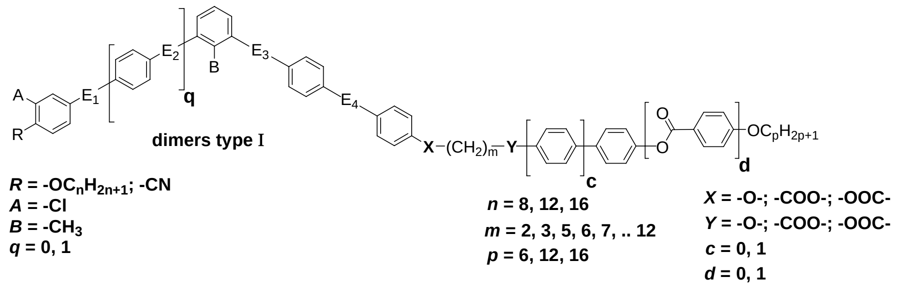

Figure 2.2: General formula of ***terminally – terminally*** connected '*banana-calamit*' dimers of **type I**.

In chapter **5** we focus on the structure – property relationship in ***terminally – terminally T – T*** connected '***banana-calamit***' dimers of **type I** (see Fig. 2.1a and Fig. 2.2). We used bent-core mesogens consisting of five or six aromatic rings, connected by *ester* linking groups ***E_1 – E_4***. The influence of the variation of the length of the terminal chain ***n*** and ***p*** attached to the bent-core moiety and calamitic part, as well as the influence of the variation of the length and parity of the flexible spacer ***m*** is studied in the chapters 5.1, 5.2 and 5.3. The influence of the nature of connecting groups ***X*** and ***Y*** (–COO-, -OOC- and –O-) linking the hydrocarbon spacer with the two mesogenic moieties on the mesophase behaviour was studied in different dimer series in chapter 5.4. In chapter 5.5, the focus is on the influence of several variations of the bent-core mesogenic unit, i.e. the direction of the ester linking groups ***E_1 – E_4*** in the bent-core fragment, the polarity of the terminal group ***R***, the lateral substitution ***A***, ***B*** and enhancing the number of aromatic rings. Simultaneously, changes of the mesomorphic properties induced by varying the spacer length *m* and the length of the terminal chains *n* and *p* attached to the mesogenic units are considered. In chapter 5.6 we describe several new systems of **type I**, with three-ring calamitic mesogenic units incorporating *biphenylene* fragments and *bis-azobenzene* segments. In chapter 5.7 details of characterization of nematic phases of dimeric systems under study by means of electro-optical studies are given.

In chapter **6** we concentrate on the variation of the linking position of the *spacer - calamit* unit on the central *resorcinol* fragment of the bent-core moiety, i.e. in a ***laterally – terminally L – T*** fashion in the '***banana-calamit***' dimers of **type II**, (see Fig. 2.1b and Fig. 2.3). The mesophase behaviour of these new dimers was compared with those previously found for *terminally - terminally* linked dimers. These variations are studied also in correlation with modification of the length of the flexible spacer *m*.

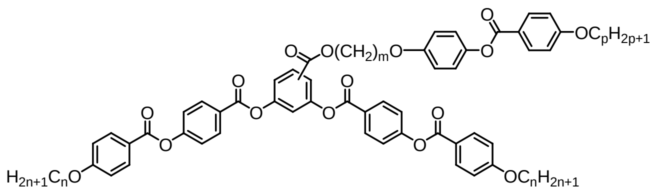

Figure 2.3: General formula of '*banana-calamit*' dimers (**type II**), ***laterally – terminally*** connected in the *5* – position (assigned as **L – *5* - T**) and, respectively, in the *4* - position (**L – *4* - T**) of the central *resorcinol* unit.

In chapter **7** our interest is focused on the study of the structure-property relationships of the '***calamit – banana - calamit***' trimers of **type I** containing two identical calamitic mesogenic units connected *via* two spacers to a bent-core moiety in a linear fashion (Fig. 2.1c and Fig. 2.4). The influence of the variation of the molecular structure on the mesomorphic properties of these systems is studied also in correlation with changes of length of spacer *m*, terminal chain attached to the calamitic part *p*, as well as the direction of the ester connecting groups ***Z***, ***W*** and the number of aromatic rings on the bent unit ***q***.

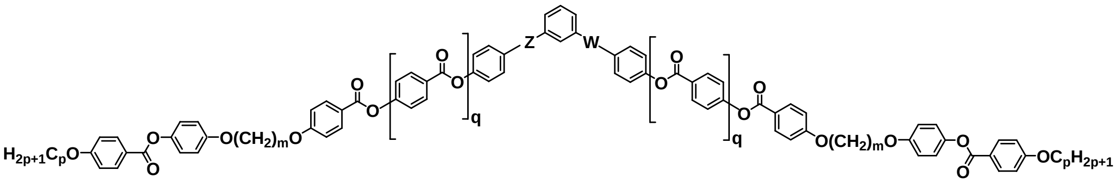

Figure 2.4: General formula of *'calamit – banana - calamit'* trimers (**type I**).

The trimeric systems of **type II**, ***'banana - calamit – banana'*** trimers containing two identical bent-core units connected *via* two equal spacers to a calamitic mesogenic moiety in a linear fashion (Fig. 2.1d and Fig. 2.5) are the subject of chapter **8**. The role of the introduction of *phenylene* and *biphenylene* fragments (***r*** = 0, 1, see Fig. 2.5a), as well as of the *azobenzene* segments (Fig. 2.5b) as calamitic moiety on the mesomorphic behaviour of these trimers was studied. Simultaneously, changes of the mesomorphic properties induced by varying the spacer length *m* were considered.

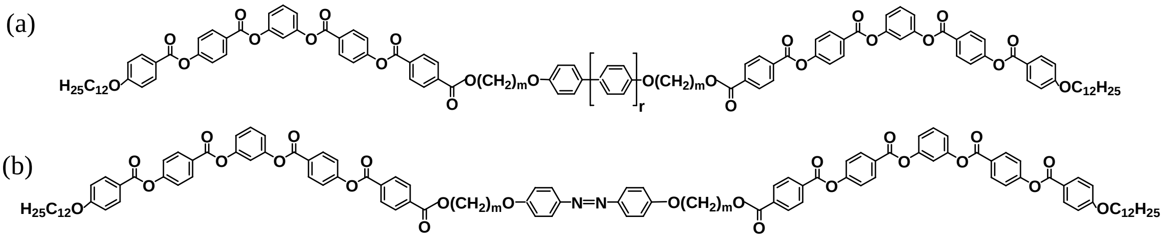

Figure 2.5: General formula of *'banana - calamit – banana'* trimers (**type II**) containing (a) *phenylene* and *biphenylene* fragments and (b) *azobenzene* segments.

3 Synthesis

In the first two parts of this chapter the synthetic pathway to the non-symmetrical '*banana-calamit*' dimers of **type I** (series **1 – 30**, ***terminal–terminal*** linking) and of **type II** (series **31 – 32**, ***lateral–terminal*** linking) will be described. Next, the synthesis of the symmetrical trimers of **type I** ('*calamit – banana – calamit'* trimer series **33 – 36**, ***terminal–terminal*** linking) and resp. of **type II** ('*banana– calamit – banana'* trimer series **37 – 38**, ***terminal–terminal*** linking) will be presented. The experimental procedures to prepare the compounds under discussion are given together with the analytical data in the Experimental Section (chapter 10) and Appendix. The structure and purity of the compounds were proved by ^{1}H and ^{13}C NMR-spectroscopy and elemental analysis.[i]

3.1 '*Banana-calamit'* dimers 1 – 30 of type I

3.1.1 General aspects

The compounds under study consist of a five-ring[ii] or six-ring bent-core moiety and a two-ring or three-ring calamitic unit. The mesogenic parts are connected by an aliphatic spacer in a *terminal – terminal* fashion. Both terminal hydrocarbon chains attached to the bent-core moiety and the calamitic unit are linked to the aromatic rings by *ether* groups. The hydrocarbon spacers are linked to the aromatic rings by *ether* and/or *ester* groups. Furthermore, all *phenyl* rings in the bent-core unit are connected to each other by *carboxylic* groups.

A general example of synthetic strategy to obtain non-symmetrical dimers of **type I** is outlined in Schemes 3.1. The strategically crucial point was to find the best linking position in the final reaction step which allowed us an effective purification, because the solubility and chromatographic properties of the intermediates and final products are relatively similar. The best way to prepare the compounds under discussion is the connection of a bent-core fragment and a *spacer - calamit* moiety both ω-functionalized. To synthesise these compounds well-known reactions in organic chemistry have been used: esterifications, etherifications, oxidations and deprotection reactions.

---

[i] The compounds presented in this work are labelled with Arabic numbers from **1** to **38**, followed by a letter from **a** to **d** to differentiate between different members of the same homologues series. ***n*** is the number of the carbon atoms in the terminal hydrocarbon chain attached to the bent-core segment; ***m*** is the length of the hydrocarbon chain spacer connecting the mesogenic units; ***p*** is the length of the terminal hydrocarbon chain attached to the calamitic segment of the molecules. For the labelling of the intermediate compounds the letter '**i**' was used. In the associated brackets the value of the corresponding varied lengths of ***n***, ***m*** and ***p*** are given.

[ii] The terms 'five-ring' and 'six-ring' are used in this work for compounds consisting of five and six aromatic rings, respectively.

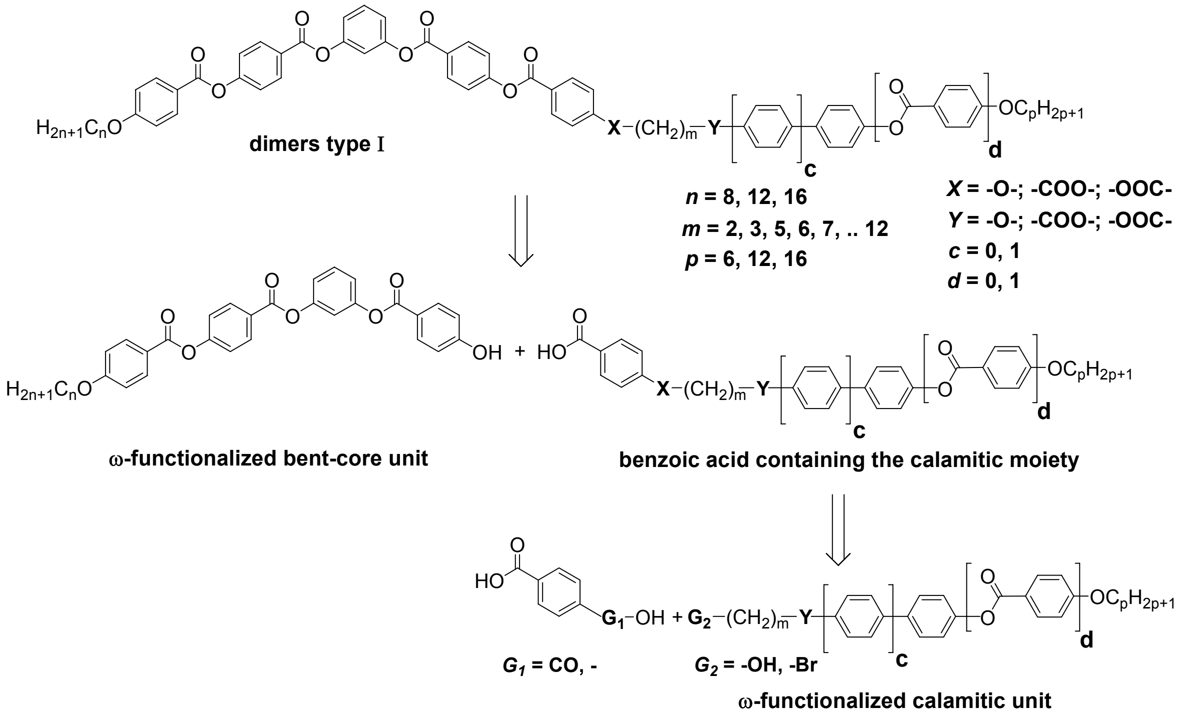

Scheme 3.1: Example of a retrosynthetic approach to the synthesis of dimers of **type I**.

Some general considerations on the different reactions types used in this work are given:

1) The esterification reactions of phenolic parts with fragments containing benzoic acids were mainly conducted by means of *N,N'*-dicyclohexylcarbodiimide (DCC) as a coupling reagent in the presence of 4-dimethylaminopyridine (DMAP) as catalyst in dichloromethane (CH_2Cl_2) by STEGLICH method[184] (or using tetrahydrofuran (THF) as solvent for less soluble benzoic acid derivatives). In parallel, there were several attempts to conduct this type of esterification reaction using the acid chloride method especially for the less soluble benzoic acids and / or the acid chloride available in our laboratory. The benzoic acids were converted to the corresponding acid chloride by means of thionyl chloride ($SOCl_2$)[58] or oxalyl chloride $(COCl)_2$[146] in CH_2Cl_2. The crude acid chlorides was dissolved in toluene, resp. CH_2Cl_2 and reacted further with the corresponding phenol in presence of pyridine or DMAP as catalyst. The difference in yield for the most of the esterification reactions is not significant between the two methods (70 to 80 %), however the DCC mediated reaction produced higher yield in some cases and takes shorter time. Isolation and purification of the end product was achieved by repeated column chromatography and crystallisation for both methods and were equally time-consuming. In all the schemes presented later on in this work only the most productive method is presented.
2) The etherification reactions in this work were performed using three different methods. The WILLIAMSON reactions were conducted under well-known conditions using phenols and *n*-alkyl halides, α,ω–halogen alkanes by means of potassium carbonate (K_2CO_3) or caesium carbonate (Cs_2CO_3) as base[185] in acetone, acetonitrile or butan-2-one under reflux or in dimethylformamide (DMF) at 70 - 80 °C, in presence of potassium iodide (KI) or tetrabutylammonium iodide (Bu_4NI) as catalyst. The purity of the resulting intermediate using butan-2-one as solvent is higher than that of the intermediates

resulting from the reaction in DMF at higher temperatures. However, longer reaction times are necessary for the reaction with butan-2-one as solvent. The same intermediates have been obtained by the MITSUNOBU reactions[186] in high yields and good quality. The MITSUNOBU reactions were conducted using *n*-alkanols, phenols or diols with triphenylphosphine (PPh_3) and diethyl azodicarboxylate (DEAD) in absolute THF at room temperature.[187] The reactions after MITSUNOBU produced higher yield in some cases than the considerably cheaper modified WILLIAMSON etherifications, i.e. 60% in MITSUNOBU reactions vs. 50% in WILLIAMSON reactions for three-ring calamitic moieties connected to the spacer part, for instance, and takes shorter time (2 days vs. 1 week). However, the purification is more time-consuming in the case of MITSUNOBU reaction intermediates because the removal of the triphenylphosphine oxide ($O{=}PPh_3$) derived from PPh_3 requires column chromatography. For the third etherification method sodium hydride (NaH, 60% in oil) was used to form the corresponding sodium phenolate, which can react with ω-halogen substituted alcohol in DMF at 110 – 120 °C. Due to the modest reactivity of the chloro-compound used for this reactions the yields were relatively low (20 - 30 %).

3) A PINNICK/LINDGREN[188,189] modified method on oxidation of aldehyde groups to carboxylic acids was performed using sodium chlorite ($NaClO_2$) as oxidizing agent in presence of sodium dihydrogenphosphate dihydrate ($NaH_2PO_4{\cdot}2H_2O$) and resorcinol in THF and H_2O at room temperature. The yields of these reactions were high (> 90 %).
4) The deprotection reactions of benzyl ethers and benzyl esters, i.e. the hydrogenolytic debenzylation of the -OH groups succeeded by means of hydrogen in ethyl acetate with 5 % Pd catalyst on carbon[190] or by means of ammonium formate and 5 % Pd catalyst on carbon in acetone.[191] The yields of these reactions were high (80 – 90 %).

3.1.2 Dimer series 1 – 6

In this section, the synthesis of dimers **1** will be discussed, as a representative example for the synthetic strategy to obtain dimers series **1** – **6**. The dimer series **1** contains 10 homologous compounds, thus being the series with the largest range of spacer chain lengths (m = 2, 3, 5-12 *methylene* units). The compounds **1** have a constant length of the alkyloxy chain attached to the bent-core unit (n = 12) and to the calamitic part (p = 6). The compounds **1** represent dimers of **type I** with a five-ring bent-core moiety and a calamitic hexyloxybenzoyloxyphenyl unit. The bent-core unit possesses a central *resorcinol* moiety, the ester linking groups within one wing of the bent-core moiety having the same direction. This is the ***reference structure*** for the bent-core unit in this thesis assigned as $\mathbf{E_0}$. If not otherwise indicated, data refer to an $\mathbf{E_0}$ structure for the bent-core moieties in the following sections of this thesis. The mesophase behaviour of compounds **1** - **6** is described in chapters 5.1-5.3.

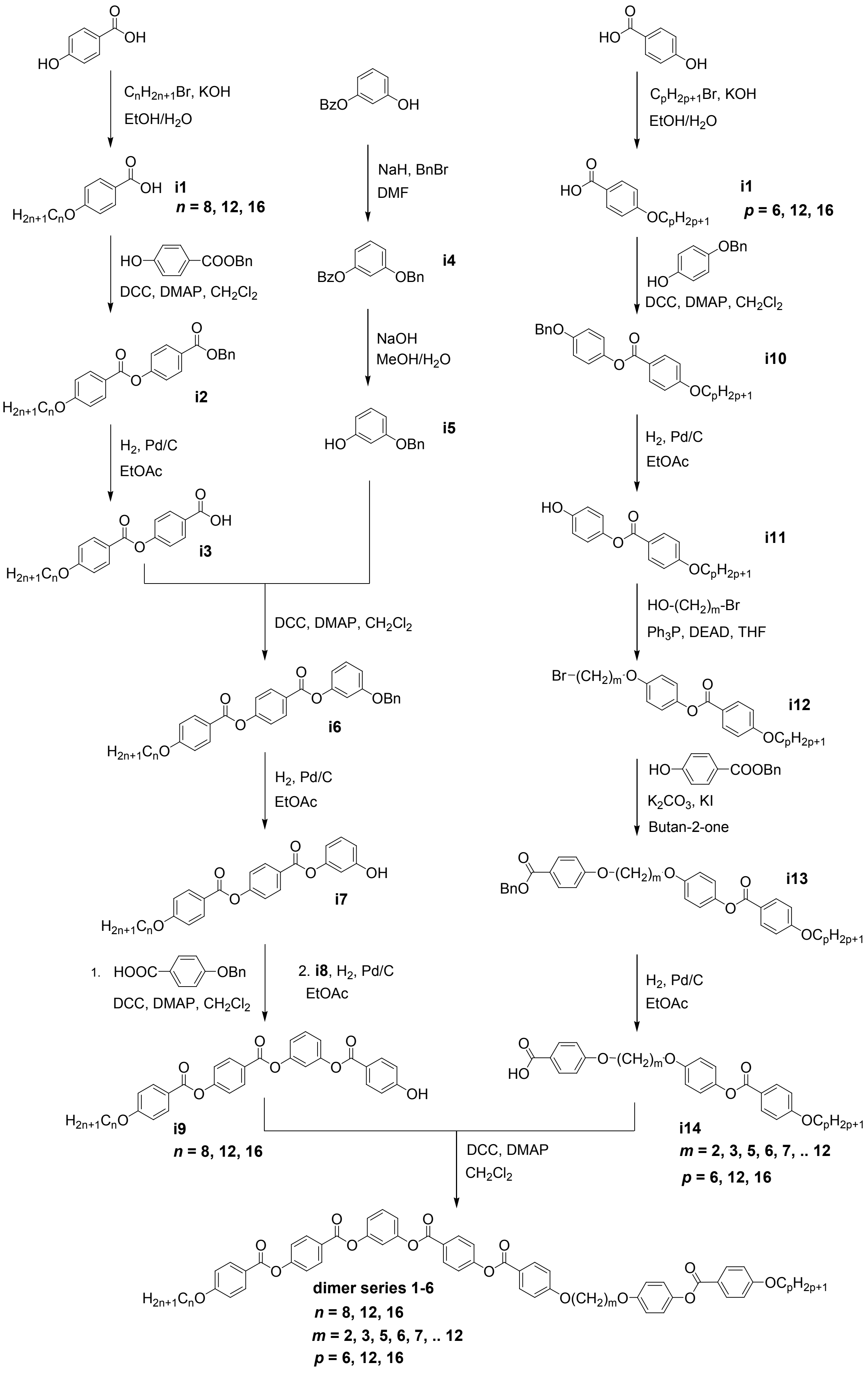
O
OH
HO
C$_n$H$_{2n+1}$Br, KOH
EtOH/H$_2$O
BzO
OH
O
HO
OH
C$_p$H$_{2p+1}$Br, KOH
EtOH/H$_2$O
O
OH
i1
n = 8, 12, 16
H$_{2n+1}$C$_n$O
NaH, BnBr
DMF
O
HO
i1
OC$_p$H$_{2p+1}$
p = 6, 12, 16
HO–⌬–COOBn
DCC, DMAP, CH$_2$Cl$_2$
BzO
OBn
i4
OBn
HO
DCC, DMAP, CH$_2$Cl$_2$
O
OBn
O
O
i2
H$_{2n+1}$C$_n$O
NaOH
MeOH/H$_2$O
BnO
O
O
i10
OC$_p$H$_{2p+1}$
H$_2$, Pd/C
EtOAc
HO
OBn
i5
H$_2$, Pd/C
EtOAc
O
OH
O
O
i3
H$_{2n+1}$C$_n$O
HO
O
O
i11
OC$_p$H$_{2p+1}$
DCC, DMAP, CH$_2$Cl$_2$
HO-(CH$_2$)$_m$-Br
Ph$_3$P, DEAD, THF
O
O
O
OBn
i6
H$_{2n+1}$C$_n$O
Br–(CH$_2$)$_m$-O
O
O
i12
OC$_p$H$_{2p+1}$
H$_2$, Pd/C
EtOAc
HO–⌬–COOBn
K$_2$CO$_3$, KI
Butan-2-one
O
O
O
OH
i7
H$_{2n+1}$C$_n$O
O
BnO
O–(CH$_2$)$_m$-O
O
O
i13
OC$_p$H$_{2p+1}$
1. HOOC–⌬–OBn
DCC, DMAP, CH$_2$Cl$_2$
2. i8, H$_2$, Pd/C
EtOAc
H$_2$, Pd/C
EtOAc
O
O
O
O
O
OH
H$_{2n+1}$C$_n$O
i9
n = 8, 12, 16
O
HO
O–(CH$_2$)$_m$-O
O
O
i14
OC$_p$H$_{2p+1}$
m = 2, 3, 5, 6, 7, .. 12
p = 6, 12, 16
DCC, DMAP
CH$_2$Cl$_2$
O
O
O
O
O
O
O
O
H$_{2n+1}$C$_n$O
dimer series 1-6
n = 8, 12, 16
m = 2, 3, 5, 6, 7, .. 12
p = 6, 12, 16
O(CH$_2$)$_m$O
O
OC$_p$H$_{2p+1}$

Scheme 3.2: Synthesis of compounds **1** – **6**.

The synthetic strategy to obtain the '*banana-calamit'* dimer series **1**–**6** is outlined in Scheme 3.2. The final step of the synthesis of target molecules **1** was the esterification of the four-ring phenolic bent-core moiety **i9** (*n* = 8, 12, 16) with the benzoic acid containing the calamitic unit **i14** (*m* = 2, 3, 5, .. 12). The synthetic approach to prepare the ω-functionalized phenolic bent-core moieties **i9** is outlined on the left side of Scheme 3.2. The 4-*n*-alkyloxybenzoic acids **i1** were obtained in a modified WILLIAMSON etherification with the corresponding alkyl bromides in presence of KOH in EtOH/H_2O under reflux. The benzoic acids **i1** were esterified with the benzyl 4-hydroxybenzoate using the STEGLICH method in presence of DCC/DMAP to give the intermediates **i2**, followed by deprotection of the benzylated intermediate by means of hydrogenolysis in the presence of 5% Pd/C to result the 4-(4-*n*-alkyloxybenzoyloxy)benzoic acids **i3**.[192] The 3-benzyloxyphenol **i5** was prepared by etherification of commercially available resorcinol monobenzoate with benzyl bromide in presence of NaH in DMF, followed by saponification of the 3-benzyloxyphenyl benzoate **i4** in EtOH and NaOH. The phenolic three-ring compounds **i7**, 3-hydroxyphenyl 4-[4-(4-*n*-alkyloxybenzoyloxy)]benzoates, was synthesized by esterification of 3-benzyloxyphenol (**i5**) with the two-ring benzoic acids **i3** in presence of DCC/DMAP and further deprotection of the intermediates **i6** by means of hydrogenolysis in the presence of 5% Pd/C.[193,58] The synthesis of the four-ring bent-core moieties **i9**, 3-(4-hydroxybenzoyloxy)phenyl 4-(4-alkyloxybenzoyloxy)-benzoates, bearing a phenolic group in a terminal position is based on the STEGLICH esterification of the three-ring phenols **i7** with 4-(benzyloxy)benzoic acid in presence of DCC/DMAP, followed by a hydrogenolytic debenzylation of the intermediates **i8** by means of hydrogen in the presence of Pd/C. The phenolic four-ring compounds **i9** was reported by MURTHY *et al.*[193,194]

The synthetic approach to prepare the benzoic acids **i14** containing the calamitic moiety and the spacer part is given on the right side of the Scheme 3.2. The two-ring phenols **i11**, 4-hydroxyphenyl 4-*n*-alkyloxybenzoates were synthesised as shown in the reaction pathway.[192] The bromo-compounds **i12**, 4-(ω-bromoalkyloxy) phenyl 4-alkyloxybenzoates were synthesized by means of MITSUNOBU etherification of phenols **i11** and ω-bromoalkanols with PPh_3/DEAD in THF. The 4-{ω-[4-(4-alkyloxybenzoyloxy)phenyloxy]alkyloxy}benzoic acids (**i14**) containing the calamitic moiety connected to the spacer were synthesized by WILLIAMSON etherification of bromo-compounds **i12** with benzyl 4-hydroxybenzoates, in presence of K_2CO_3/KI in butan-2-one and following benzyl deprotection. The benzoic acid **i14** with *m* = 6 and *p* = 6 was already reported by us.[195] The final compounds **1** were prepared by the STEGLICH esterification of the phenolic four-ring bent-core moieties **i9** (*n* = 8, 12, 16) with the benzoic acids **i14** (*m* = 2, 3, 5, 6, 7,.. 12).

3.1.3 Dimer series 7 – 12

In order to study the influence of the groups ***X*** and ***Y*** connecting the spacer with the two different mesogenic moieties on the mesophase behaviour dimers **7** – **12** were synthesized. The mesophase behaviour of these compounds is described in chapter 5.4.

The synthetic pathway to obtain the series **7** – **9** (connecting groups ***X*** = –COO- and ***Y*** = –O- and *m* = 6, 11) is outlined in Scheme 3.3. The first step was to append hydrocarbon chains bearing a terminal hydroxyl function to 4-hydroxyphenyl 4-*n*-alkyloxybenzoates **i11** via a

WILLIAMSON etherification with a ω-bromoalkanol in presence of K_2CO_3/KI in DMF. The resulted 4-(ω-hydroxyalkyloxy)phenyl 4-alkyloxybenzoates **i15** were esterified with the 4-formylbenzoic acid in the presence of DCC/DMAP to give the aldehyde intermediates **i16** which were further oxidized by means of $NaClO_2$ to give 4-{ω-[4-(4-alkyloxybenzoyloxy)-phenyloxy]alkyloxycarbonyl}benzoic acids (**i17**). Similar substituted *n*-alkanols **i15** and benzoic acids **i17** were already reported by us.[195] The target molecules **7** – **9** were obtained by DCC-esterification reaction of these benzoic acid **i17** with the four-ring bent-core phenols **i9** reported in section 3.1.2.

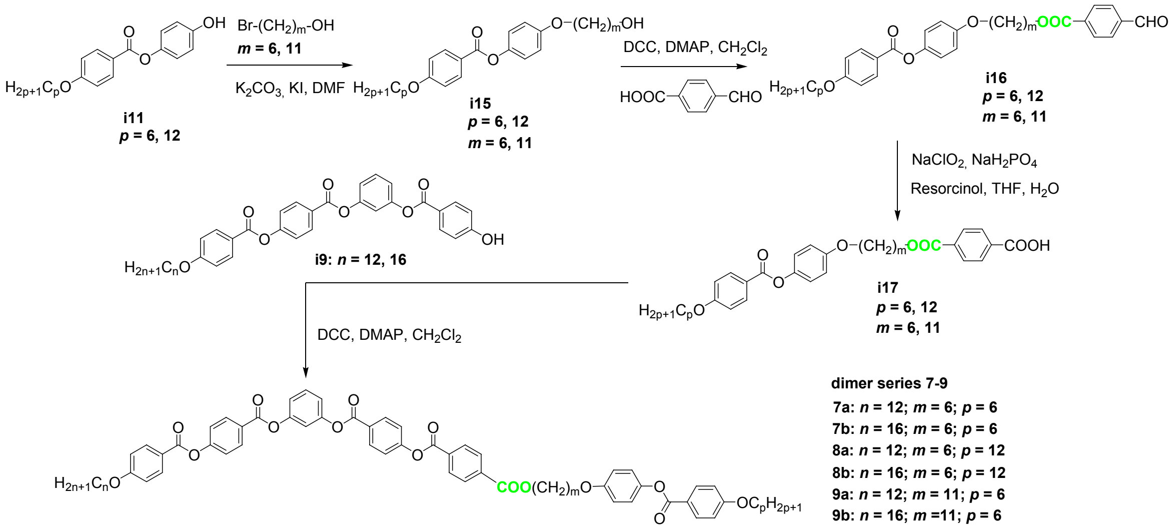
Br-(CH2)m-OH
m = 6, 11
K2CO3, KI, DMF
i11
p = 6, 12
i15
p = 6, 12
m = 6, 11
DCC, DMAP, CH2Cl2
HOOC–C6H4–CHO
i16
p = 6, 12
m = 6, 11
NaClO2, NaH2PO4
Resorcinol, THF, H2O
i9: n = 12, 16
i17
p = 6, 12
m = 6, 11
DCC, DMAP, CH2Cl2
dimer series 7-9
7a: n = 12; m = 6; p = 6
7b: n = 16; m = 6; p = 6
8a: n = 12; m = 6; p = 12
8b: n = 16; m = 6; p = 12
9a: n = 12; m = 11; p = 6
9b: n = 16; m =11; p = 6

Scheme 3.3: Synthesis of compounds **7** – **9**.

The strategy to obtain the series **10** – **11** which differ from compounds **7** – **9** by the direction of one connecting group (***X*** = –OOC-, ***Y*** = –O- and *m* = 5) is given in Scheme 3.4. The benzoic acids **i20** containing the calamitic parts were synthesised using the following pathway. The 6-bromohexanoyl chloride was reacted with the benzyl 4-hydroxybenzoate in presence of TEA/DMAP in toluene to give compound **i18**. Similar to the procedure previously described for compounds **i15**, the ω-bromo–functionalized ester **i18** was further etherified in a WILLIAMSON reaction and followed by deprotection by means of hydrogenolysis to result the 4-{ω-[4-(4-alkyloxybenzoyloxy)phenyloxy]alkylcarbonyloxy} benzoic acids **i20**. The last step was the esterification reaction of the 3-(4-hydroxybenzoyloxy)phenyl 4-(4-alkyloxybenzoyl-oxy)benzoates (**i9**) with the benzoic acids containing the calamitic unit **i20.**

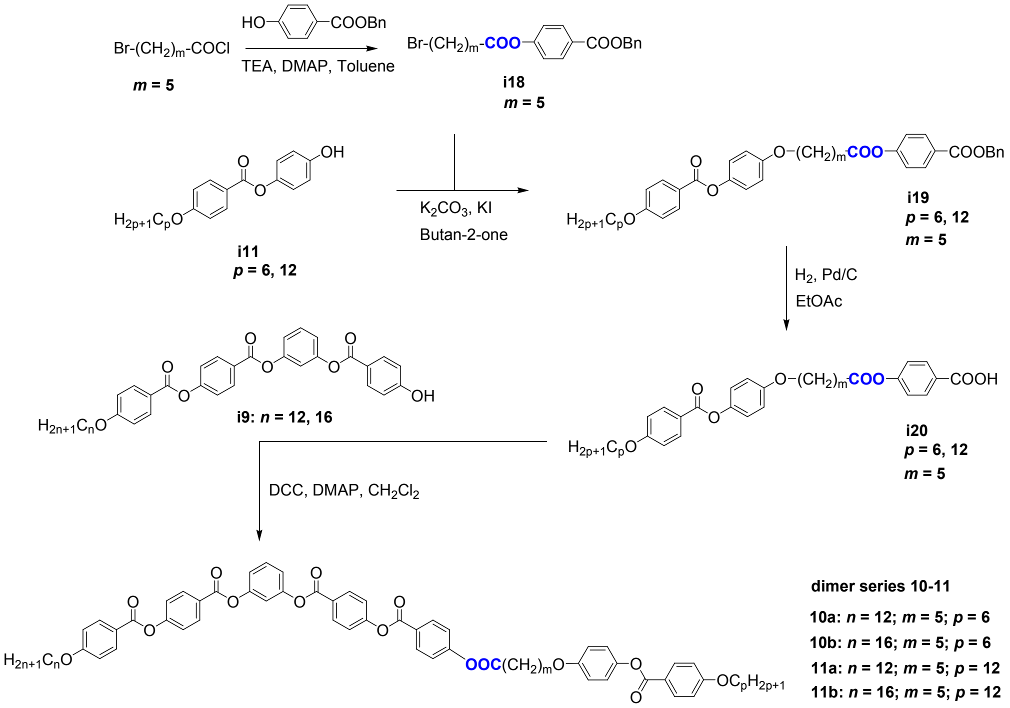
Br-(CH2)m-COCl
m = 5
HO–C6H4–COOBn
TEA, DMAP, Toluene
Br-(CH2)m-COO–C6H4–COOBn
i18
m = 5
H2p+1CpO
OH
i11
p = 6, 12
K2CO3, KI
Butan-2-one
O–(CH2)mCOO
COOBn
i19
p = 6, 12
m = 5
H2, Pd/C
EtOAc
H2n+1CnO
OH
i9: n = 12, 16
COOH
i20
p = 6, 12
m = 5
DCC, DMAP, CH2Cl2
OOC(CH2)mO
OCpH2p+1
dimer series 10-11
10a: n = 12; m = 5; p = 6
10b: n = 16; m = 5; p = 6
11a: n = 12; m = 5; p = 12
11b: n = 16; m = 5; p = 12

Scheme 3.4: Synthesis of compounds **10** – **11**.

The synthesis of compound **12** ($m = 15$) with an inversed position of the connecting groups between the spacer and the two mesogenic units, i.e. ***X*** = –O- and ***Y*** = –COO-, is presented in Scheme 3.5. The first step was the reaction of phenol **i11** with 16-bromohexadecanoic acid in presence of DCC/DMAP. The bromo-functionalized compound **i21** was etherified in a WILLIAMSON reaction in presence of K_2CO_3/KI with the benzyl 4-hydroxybenzoate and further deprotection of benzyl benzoate **i22** by means of hydrogenolysis with Pd catalyst results the benzoic acid (**i23**). The final compound **12** was prepared by the esterification of the four-ring bent-core phenol **i9** with the 4-substituted benzoic acid containing the calamitic part, **i23**.

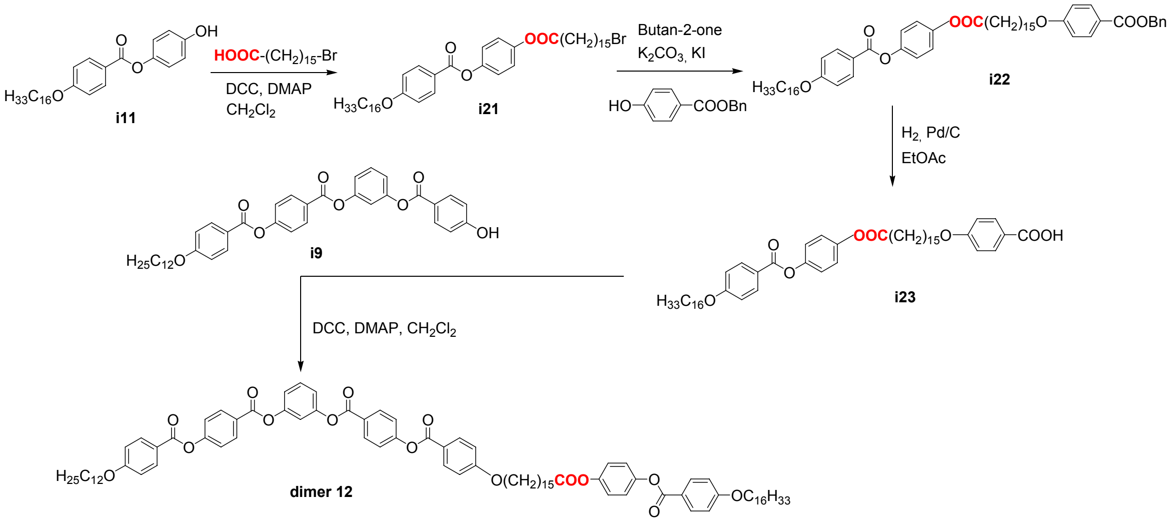
H33C16O
OH
i11
HOOC-(CH2)15-Br
DCC, DMAP
CH2Cl2
OOC(CH2)15Br
i21
Butan-2-one
K2CO3, KI
HO–C6H4–COOBn
OOC(CH2)15O
COOBn
i22
H2, Pd/C
EtOAc
H25C12O
OH
i9
COOH
i23
DCC, DMAP, CH2Cl2
O(CH2)15COO
OC16H33
dimer 12

Scheme 3.5: Synthesis of compound **12**.

3.1.4 Dimer series 13 – 19[196]

In order to study the influence of the direction of the ester linking groups ***E*** connecting the five *phenyl* rings of the bent-core unit on the mesophase behaviour of dimer **type I**, compounds **13** – **19** were synthesised. The direction of each of the four ester groups ***E*** between the *phenyl* rings of the bent-core unit has been inverted with respect to the position of the ester linking groups in the ***reference structure*** **E_0** used in the dimers **1** – **12**. Since for each group of isomers the direction of only one ester group has been changed, the inversion of the first, second, third and fourth one is assigned as **E_1**, **E_2**, **E_3** and **E_4**, respectively (see general formula in the Fig. 3.1 and an example explaining the abbreviation system for the *E* groups in Fig. 5.64, chapter 5.5.1). The mesophase behaviour of dimers **13** – **19** is described in chapter 5.5.1 and these results were already published by our research group.[196]

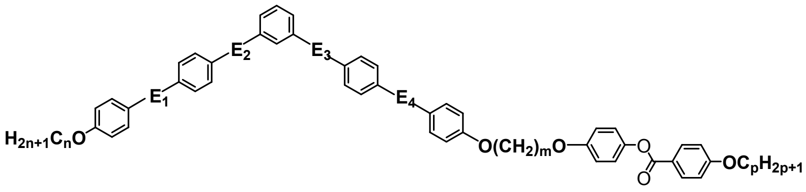

Figure 3.1: General formula of dimers **13** – **19**.

Dimers 15a and 16a with an inverse carboxylic group in E_1-position

The synthetic strategy to obtain the dimers **15a** and **16a** which possess an **E_1** structure (with an inversion of the first ester connecting group **E_1** with respect to the **E_0** structure) is described in Scheme 3.6. The 4-*n*-dodecyloxyphenol **i25** was esterified with the 4-formylbenzoic acid to give the aldehyde intermediate **i26** which was further oxidized by means of $NaClO_2/NaH_2PO_4$ to give 4-(4-*n*-dodecyloxy-phenyloxycarbonyl)benzoic acid **i27**. Its esterification with 3-benzyloxyphenol **i5** and further deprotection of the benzylether intermediate **i28** results in the three-ring phenol **i29**. The substituted phenol **i29** was reported by our research group.[192] The synthesis of the four-ring bent-core moiety **i31**, 3-(4-hydroxybenzoyloxy)phenyl 4-(4-*n*-dodecylphenyloxycarbonyl)-benzoate, bearing a phenolic group in a terminal position is based on the STEGLICH esterification of phenol **i29** with benzyl 4-hydroxybenzoic acid followed by a hydrogenolytic debenzylation of the benzoate **i30**. The final compounds **15a** and **16a** were prepared by the STEGLICH esterification of the phenolic four-ring bent-core moiety **i31** with the 4-{ω-[4-(4-hexyloxybenzoyloxy)phenyloxy]alkyloxy}benzoic acid (**i14**, *m* = 6, 11).[196]

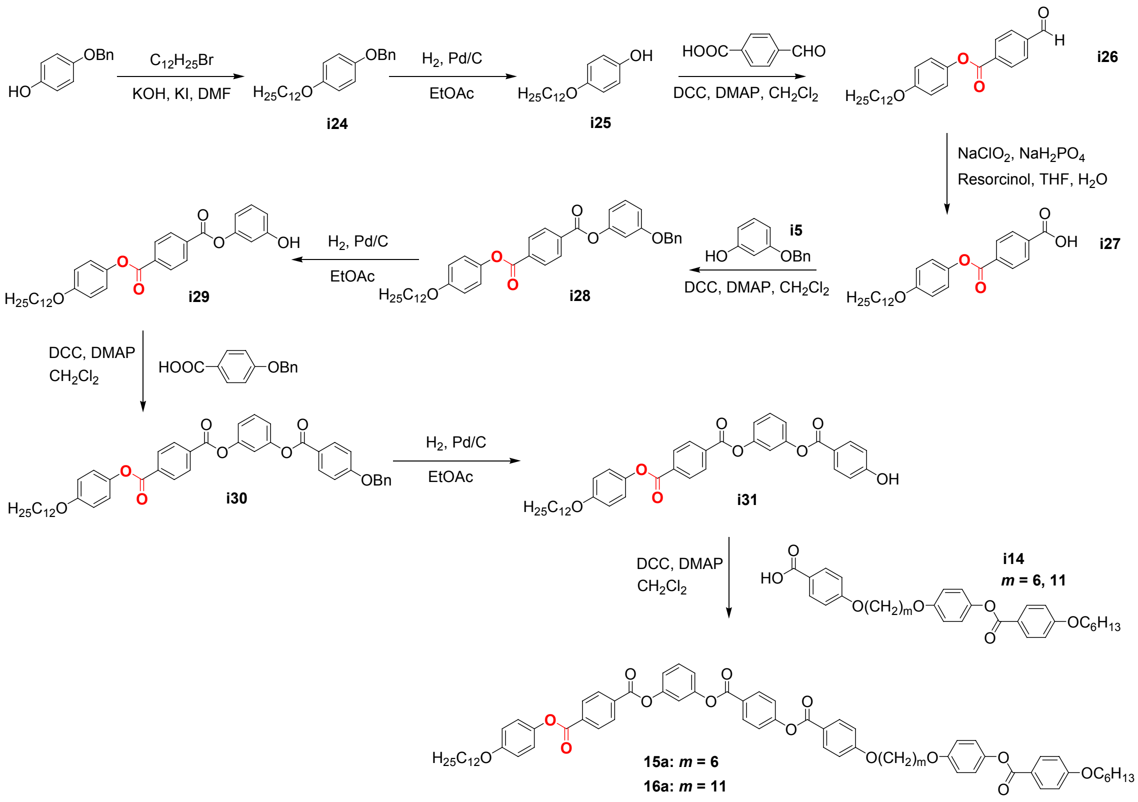
C12H25Br
KOH, KI, DMF
i24
H2, Pd/C
EtOAc
i25
HOOC–C6H4–CHO
DCC, DMAP, CH2Cl2
i26
NaClO2, NaH2PO4
Resorcinol, THF, H2O
i27
i5
DCC, DMAP, CH2Cl2
i28
H2, Pd/C
EtOAc
i29
DCC, DMAP
CH2Cl2
HOOC–C6H4–OBn
i30
H2, Pd/C
EtOAc
i31
DCC, DMAP
CH2Cl2
i14
m = 6, 11
15a: m = 6
16a: m = 11

Scheme 3.6: Synthesis of compounds **15a** and **16a**.

Dimers 13a, 14, 15b, 16b, 17a, 18 and 19 with an inverse carboxylic group in E$_2$-position

The synthetic pathway to obtain the dimers of series **13** to **19** which possess an **E$_2$**-structure (with an inversion of the second ester connecting group **E$_2$** with respect to the **E$_0$** structure) is outlined in Scheme 3.7. The 4-hydroxyphenyl 4-*n*-alkyloxybenzoates **i33**[192] were synthesised in analogy to the phenols **i11**. The esterification of the commercially available 3-hydroxybenzaldehyde with 4-benzyloxybenzoic acid results in 3-formylphenyl 4-benzyloxybenzoate **i34** which was further oxidized by means of $NaClO_2$/NaH_2PO_4 to give 3-[4-benzyloxy(benzoyloxy)]benzoic acid **i35**. Its reaction with the two-ring phenols **i33** and further deprotection of the benzyl group resulted in the four-ring phenols **i37**.[196] The esterification reactions of these four-ring bent-core units **i37** bearing a phenolic group in a terminal position with the calamitic moieties 4-{ω-[4-(4-alkyloxybenzoyloxy)phenyloxy]alkyloxy}benzoic acids **i14** (*m* = 3, 6, 11; *p* = 6, 12) yielded the final products **13a, 14, 15b, 16b, 17a, 18** and **19**.[196]

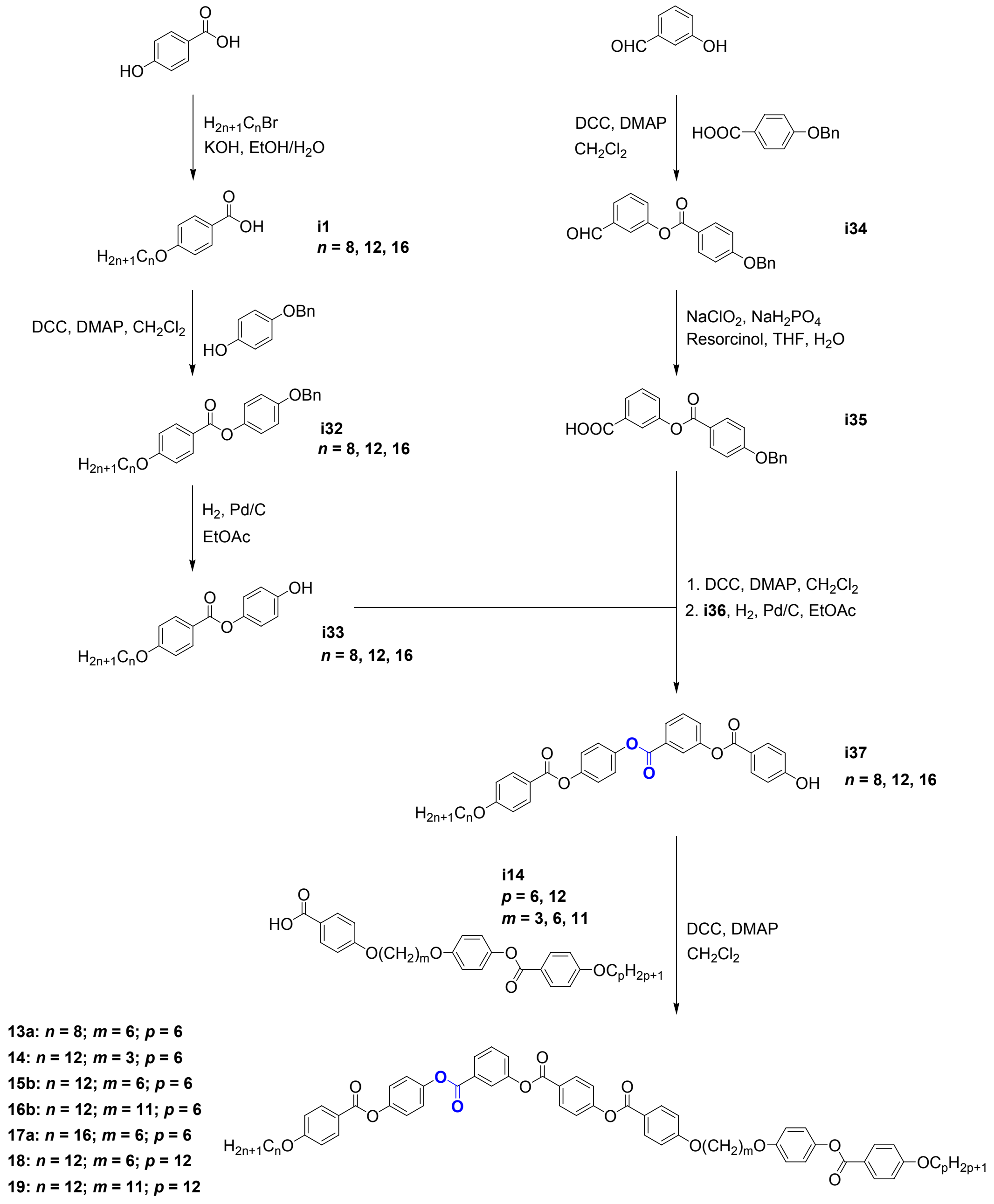
$H_{2n+1}C_nBr$
KOH, EtOH/H_2O
i1
n = 8, 12, 16
DCC, DMAP, CH_2Cl_2
i32
n = 8, 12, 16
H_2, Pd/C
EtOAc
i33
n = 8, 12, 16
DCC, DMAP
CH_2Cl_2
i34
$NaClO_2$, NaH_2PO_4
Resorcinol, THF, H_2O
i35
1. DCC, DMAP, CH_2Cl_2
2. i36, H_2, Pd/C, EtOAc
i37
n = 8, 12, 16
i14
p = 6, 12
m = 3, 6, 11
DCC, DMAP
CH_2Cl_2
13a: n = 8; m = 6; p = 6
14: n = 12; m = 3; p = 6
15b: n = 12; m = 6; p = 6
16b: n = 12; m = 11; p = 6
17a: n = 16; m = 6; p = 6
18: n = 12; m = 6; p = 12
19: n = 12; m = 11; p = 12

Scheme 3.7: Synthesis of compounds **13a, 14, 15b, 16b, 17a, 18** and **19**.

Dimers 13b, 15c and 17b with an inverse carboxylic group in E_3-position

The synthetic pathway to obtain the dimers **13b, 15c** and **17b** which possess an inversion of the third ester connecting group $\mathbf{E_3}$ with respect to the $\mathbf{E_0}$ structure is given in Scheme 3.8. 3-Hydroxybenzaldehyde was esterified with 4-(4-*n*-alkyloxybenzoyloxy)benzoic acids **i3** (*n* = 8, 12, 16) in presence of DCC/DMAP to give the benzaldehydes **i38**, which were oxidized using $NaClO_2$ to give 3-[4-(4-*n*-alkyloxybenzoyloxy)benzoyloxy]benzoic acids **i39**. The three-ring benzoic acids **i39** were esterified with 4-(benzyloxy)phenol and hydrogenolytic deprotection of the benzyl-protected compounds **i40** result in the formation of phenols **i41**, 3-(4-hydroxyphenoxycarbonyl)phenyl 4-(4-*n*-alkyloxybenzoyloxy)benzoates. The final compounds

13b, 15c and **17b** were prepared by the STEGLICH esterification of the four-ring bent-core phenols **i41** with the benzoic acids **i14** bearing the calamitic moiety.[196]

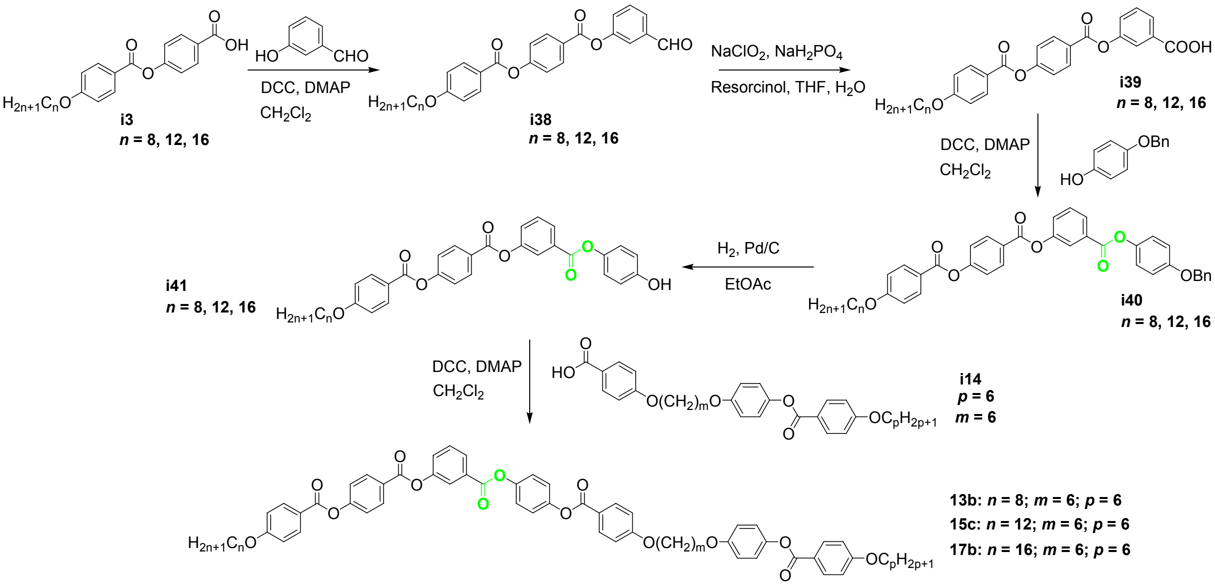

DCC, DMAP
CH_2Cl_2
$NaClO_2$, NaH_2PO_4
Resorcinol, THF, H_2O
DCC, DMAP
CH_2Cl_2
H_2, Pd/C
EtOAc
DCC, DMAP
CH_2Cl_2
i3
n = 8, 12, 16
i38
n = 8, 12, 16
i39
n = 8, 12, 16
i40
n = 8, 12, 16
i41
n = 8, 12, 16
i14
p = 6
m = 6
13b: n = 8; m = 6; p = 6
15c: n = 12; m = 6; p = 6
17b: n = 16; m = 6; p = 6

Scheme 3.8: Synthesis of compounds **13b, 15c** and **17b**.

Dimer 15d with an inverse carboxylic group in E_4-position

The dimer **15d** with an inversion of the fourth ester connecting group $\mathbf{E_4}$ with respect to the $\mathbf{E_0}$ structure was prepared according to Scheme 3.9. The phenolic three-ring compound **i7** was esterified with the commercially available 4-formylbenzoic acid to give the 3-(4-formylbenzoyloxy)phenyl [4-(4-*n*-dodecyloxybenzoyloxy)benzoate] **i42**. The aldehyde intermediate **i42** was oxidized using $NaClO_2$ to result 4-{3-[4-(4-*n*-dodecyloxy-benzoyloxy)-benzoyloxy]phenoxycarbonyl}benzoic acid **i43**.[146] The bromo-compound **i12**, 4-(ω-bromohexyloxy)phenyl 4-hexyloxybenzoate, was etherified via a WILLIAMSON method with 4-benzyloxyphenol in presence of K_2CO_3/KI in butan-2-one. The deprotection of the intermediate **i44** by means of hydrogen results in the phenol **i45** bearing the calamitic unit. The three-ring phenol **i45** was esterified in presence of DCC/DMAP with the four-ring bent-core moiety **i43** bearing a carboxylic group in a terminal position to give the dimer **15d**.[196]

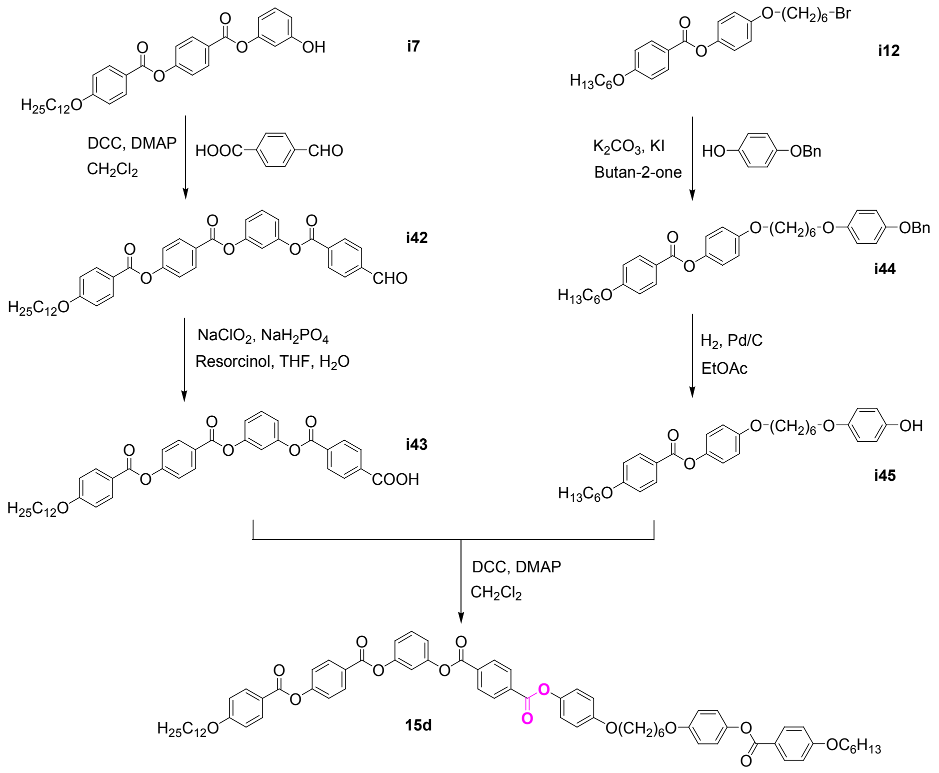
i7
DCC, DMAP
CH2Cl2
HOOC–C6H4–CHO
i42
NaClO2, NaH2PO4
Resorcinol, THF, H2O
i43
i12
K2CO3, KI
Butan-2-one
HO–C6H4–OBn
i44
H2, Pd/C
EtOAc
i45
DCC, DMAP
CH2Cl2
15d

Scheme 3.9: Synthesis of compound **15d**.

3.1.5 Dimers 20 – 24

In this chapter the synthetic pathway for compounds **20** – **24** (n = 12; m = 5, 6, 11; p = 6, 12) will be presented. These dimers possess different directions of the group ***X*** connecting the bent-core moiety with the spacer unit (-COO-/-OOC-), while the second group is ***Y*** = –O-, and the direction of the second ester linking group $\mathbf{E_2}$ is reversed with respect to the ***reference structure*** $\mathbf{E_0}$ of the bent-core unit (see chapters 5.5.1 and 5.5.2). Their mesophase behaviour is described in chapter 5.5.2**.**

The target molecules **20**, **21** and **22** (n = 12; m = 6, 11; p = 6, 12) have been synthesized from the four-ring bent-core unit bearing a phenolic group in a terminal position **i37** and the calamitic moiety 4-{ω-[4-(4-alkyloxybenzoyloxy)phenyloxy]alkyloxycarbonyl}benzoic acid (**i17**, m = 6, 11; p = 6, 12) by an acylation reaction using the carbodiimide method (Scheme 3.10).

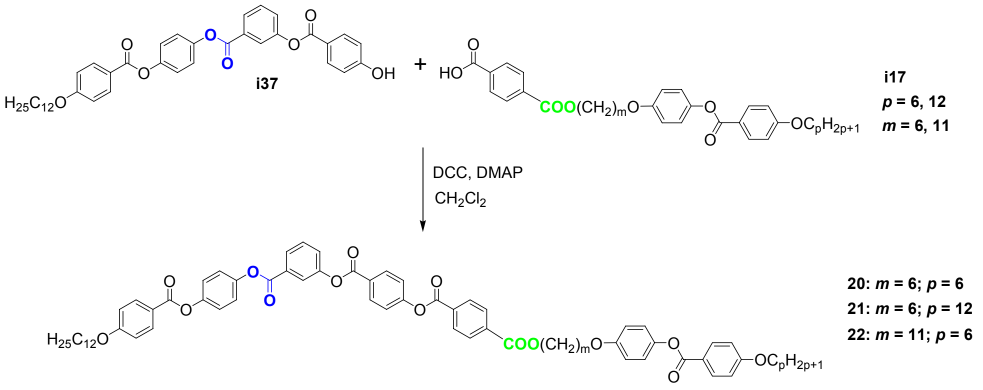
i37
+
i17
p = 6, 12
m = 6, 11
DCC, DMAP
CH2Cl2
20: m = 6; p = 6
21: m = 6; p = 12
22: m = 11; p = 6

Scheme 3.10: Synthesis of compounds **20**, **21** and **22**.

The final compounds **23** and **24** (n = 12; m = 5; p = 6, 12) have been prepared from the four-ring phenol **i37** and the benzoic acids containing the calamitic moieties connected to the spacer unit, **i20**, 4-{ω-[4-(4-alkyloxybenzoyloxy)phenyloxy]hexanoyloxy}benzoic acids (m = 5; p = 6, 12) by an esterification reaction using the carbodiimide method (Scheme 3.11).

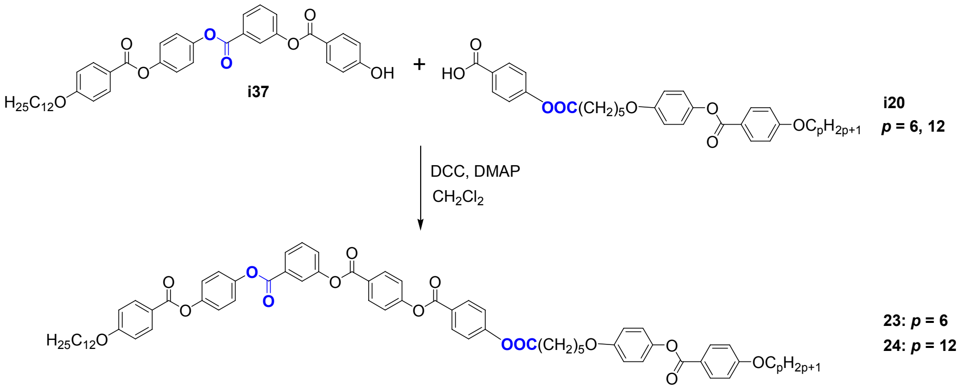

$H_{25}C_{12}O$
i37
OH
+
HO
$OOC(CH_2)_5O$
OC_pH_{2p+1}
i20
p = 6, 12
DCC, DMAP
CH_2Cl_2
23: p = 6
24: p = 12

Scheme 3.11: Synthesis of compounds **23** and **24**.

3.1.6 Dimer series 25[197]

The dimers **25** (m = 3, 6, 11; p = 6; $\mathbf{E_2}$) were prepared in order to study the influence of the polar terminal *cyano*- group attached to the bent-core unit on the mesophase behaviour. The strategy to obtain the dimers **25** is outlined in Scheme 3.12 and is analogue to that described in Scheme 3.7, however now starting with the 4-cyanobenzoic acid. The four-ring phenol **i49**, 4-(4-cyanobenzoyloxy)phenyl 3-(4-hydroxybenzoyloxy)benzoate synthesised by deprotection of the corresponding benzyl-protected compound **i48** was esterified with the substituted benzoic acids **i14** bearing the calamitic moiety to give the target compounds **25**. The mesophase behaviour of these compounds is described in chapter 5.5.3 and these results were already published by our research group.[197]

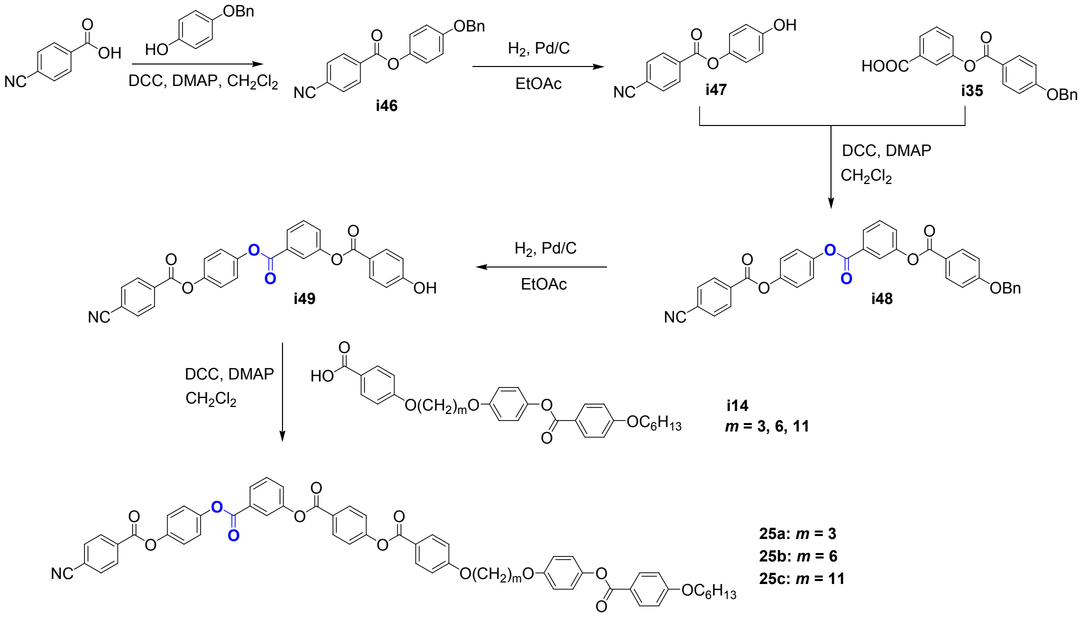

NC
OH
HO
OBn
DCC, DMAP, CH_2Cl_2
i46
H_2, Pd/C
EtOAc
i47
HOOC
i35
DCC, DMAP
CH_2Cl_2
i49
i48
DCC, DMAP
CH_2Cl_2
$O(CH_2)_mO$
OC_6H_{13}
i14
m = 3, 6, 11
25a: m = 3
25b: m = 6
25c: m = 11

Scheme 3.12: Synthesis of compounds **25**.

3.1.7 Dimer series 26[197]

In order to study the effect of lateral substitution by *chlorine* in 3-position at the outer ring of the bent-core unit on the mesophase behaviour, dimer series **26** (*n* = 12; *m* = 3, 6, 11; *p* = 6) was prepared as shown in Scheme 3.13. The general reaction pathway is analogue to that sketched in Scheme 3.2, however now starting with 3-chloro-4-hydroxybenzoic acid. The mesophase behaviour of these compounds is described in chapter 5.5.4 and these results were already published by our research group.[197]

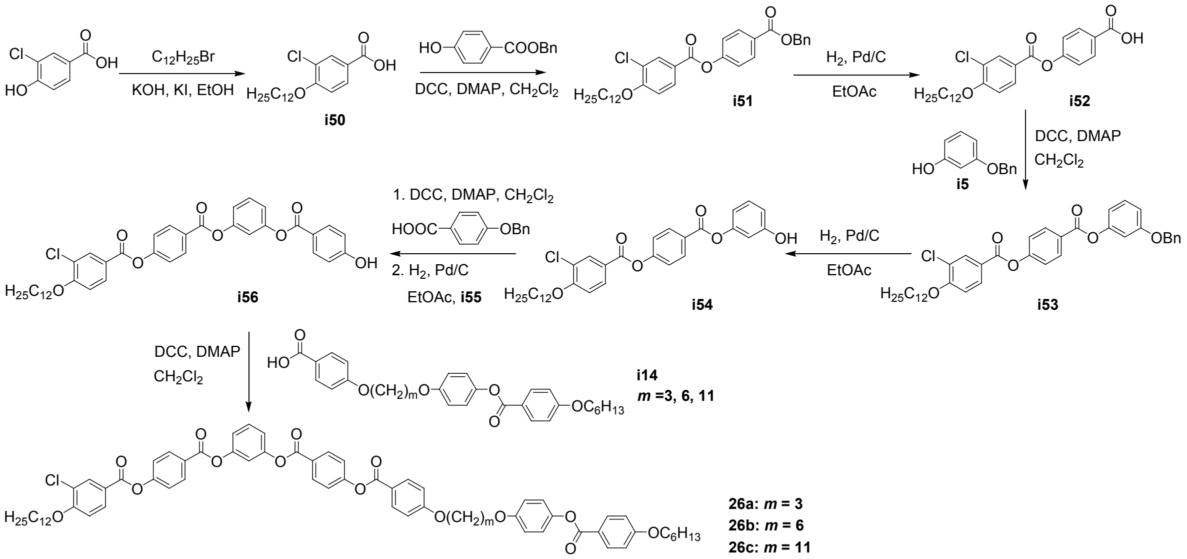

Scheme 3.13: Synthesis of compounds **26**.

3.1.8 Dimer series 27[197]

Compounds **27** (*n* = 12; *m* = 3, 6, 11; *p* = 6) contain a lateral *methyl*- group in the 2-position of the central ring of the bent-core unit. The synthetic way is outlined in Scheme 3.14. The 4-(4-*n*-dodecyloxybenzoyloxy)benzoic acid **i3** was converted to the corresponding acid chloride by means of $(COCl)_2$ and pyridine in CH_2Cl_2 under reflux. The crude acid chloride was reacted with a 5-fold excess of 2-methylresorcinol in presence of pyridine in toluene. The monosubstituted resorcinol derivative **i58** was synthesized according to a procedure reported in the literature by ACHTEN *et al.*[58] The three-ring phenol 3-hydroxy-2-methylphenyl 4-[4-(4-*n*-dodecyloxybenzoyloxy)]benzoate (**i58**) was esterified with 4-benzyloxybenzoic acid, and further deprotection of the intermediate **i59** by means of hydrogen results in 3-(4-hydroxy-benzoyloxy-2-methylphenyl) 4-(4-*n*-dodecyloxybenzoyloxy)benzoate **i60**. Its esterification with the calamitic moieties 4-{ω-[4-(4-alkyloxybenzoyloxy)phenyloxy]-alkyloxy}benzoic acids (**i14**, *m* = 3, 6, 11; *p* = 6) in presence of DCC/DMAP yielded the target compounds **27**. Their mesophase behaviour is described in chapter 5.5.4 and these results were already published by our research group.[197]

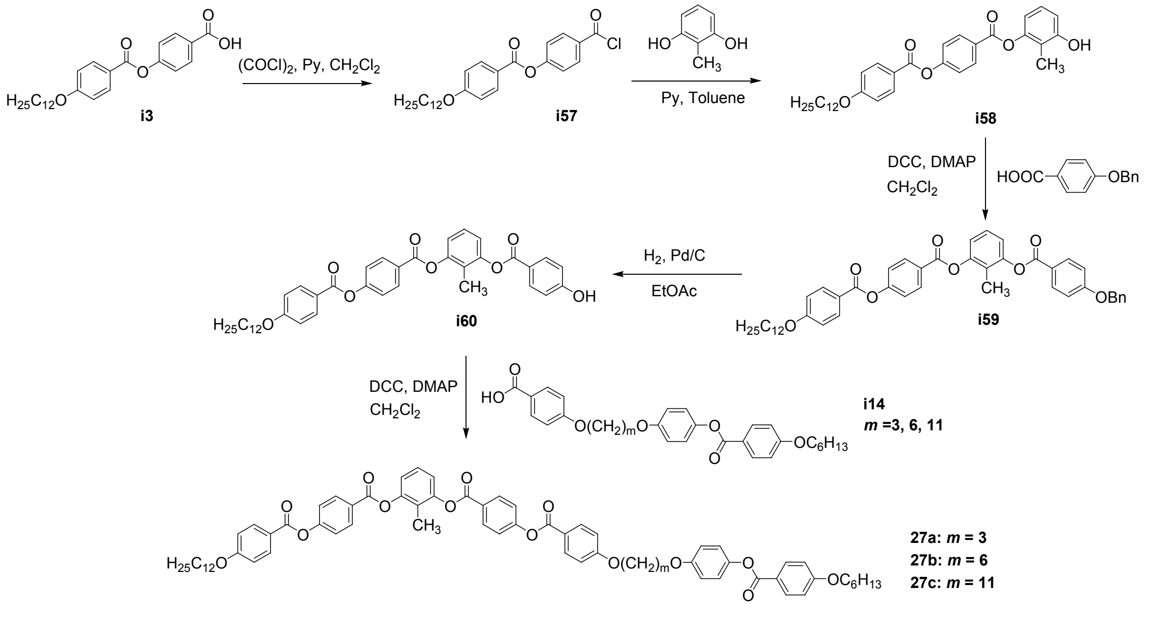

Scheme 3.14: Synthesis of compounds **27**.

3.1.9 Dimer series 28[197] and 29[195]

The number of aromatic rings in the bent-core mesogenic unit of dimer series **28** was increased to six (n = 12; m = 6, 11; p = 6). The synthetic pathway is outlined in Scheme 3.15. The esterification of the 4-(4-*n*-dodecyloxybenzoyloxy)benzoic acid **i3** with the benzyl 4-hydroxybenzoate and hydrogenolytic deprotection of the benzyl-protected compounds **i61** result in the formation of 4-[4-(4-*n*-dodecyloxybenzoyloxy)benzoyloxy]benzoic acid (**i62**). **i62** was esterified with 3-benzyloxyphenol (**i5**) and on further deprotection of the intermediate **i63** by means of hydrogenolysis to result 3-hydroxyphenyl 4-[4-(4-*n*-dodecyloxybenzoyloxy)-benzoyloxy] benzoate **i64.** The four-ring phenol **i64** was esterified with the 4-(benzyloxy)-benzoic acid and the benzyl ether **i65** was deprotected to result the five-ring phenol **i66.**[146].The target molecules **28** have been synthesized from the five-ring phenolic bent-core unit **i66** and the calamitic moieties 4-{ω-[4-(4-alkyloxybenzoyloxy)phenyloxy]-alkyloxy}benzoic acids (**i14**, m = 6, 11; p = 6) by an esterification using DCC/DMAP. The mesophase behaviour of compounds **28** is described in chapter 5.5.5 and these results were already published by our research group.[197]

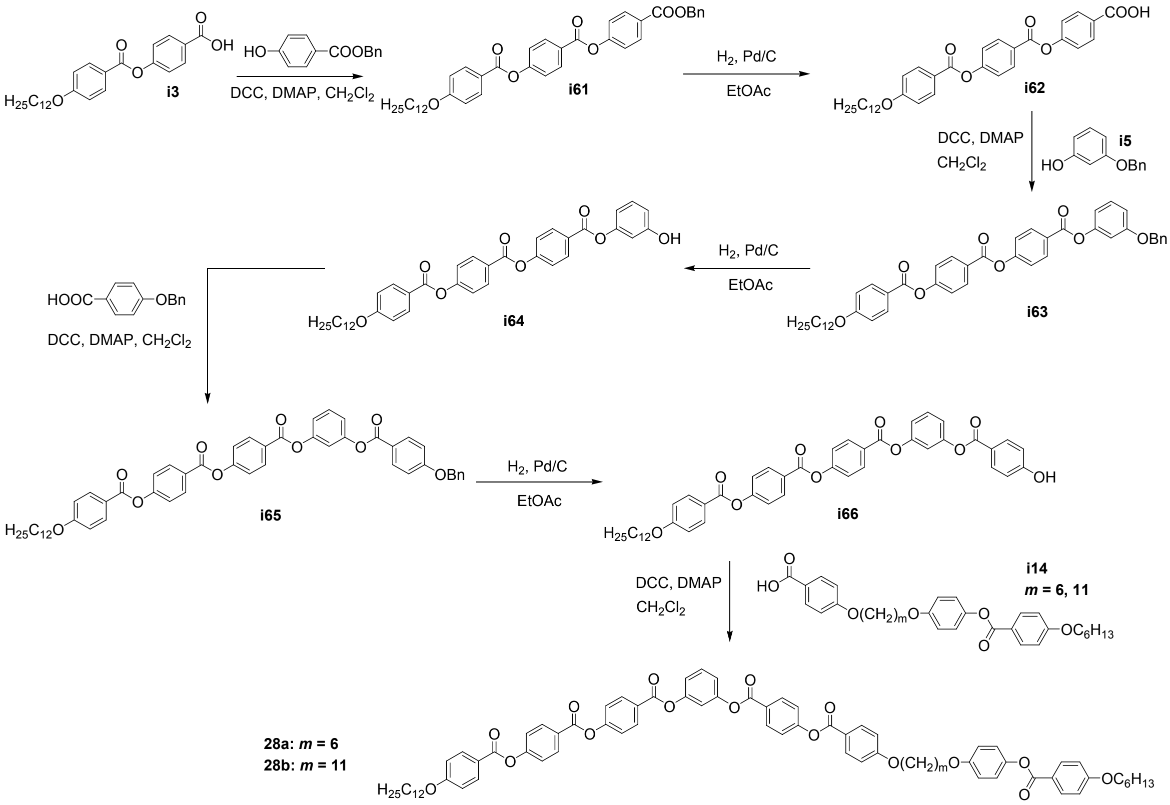

Scheme 3.15: Synthesis of compounds **28**.

Structural variations on the calamitic part of the dimers led to compounds **29**, which have been synthesised in collaboration with B. KOSATA described elsewhere.[146] Their mesophase behaviour is discussed in chapter 5.6.1.

3.1.10 Dimer series 30[198]

The linking of a five-ring bent-core mesogen with a calamitic *bis-azobenzene* moiety by means of flexible spacers results in non-symmetrical dimers **30** (n = 12; m = 2, 4, 6). As shown in Scheme 3.16, the 4-formylbenzoic acid was reacted with benzylbromide in presence of K_2CO_3/KI in DMF to result benzyl 4-formylbenzoate **i67**, which was oxidized by means of $NaClO_2$/NaH_2PO_4 to give 4-(benzyloxycarbonyl)benzoic acid (**i68**). Its esterification with the four-ring phenol **i9**, followed by deprotection of the benzyl ester intermediate **i69** results in the *n*-dodecyloxy substituted five-ring bent-core benzoic acid, 4-(4-{3-[4-(4-*n*-dodecyloxybenzoyl-oxy)benzoyloxy]phenoxycarbonyl}phenoxycarbonyl)benzoic acid (**i70**). Synthesis and properties of 4-(ω-hydroxyalkyloxy)bisazobenzenes having different alkylene spacer have been described by RÖTZ *et al.*[199] and the materials were available in our laboratory. The target compounds **30** have been synthesized from the five-ring bent-core acid **i70** and the calamitic *azo*-moieties (with m = 2, 4, 6) by STEGLICH esterification. The mesophase behaviour of dimers **30** is described in chapter 5.6.2 and these results were already published by our research group.[198]

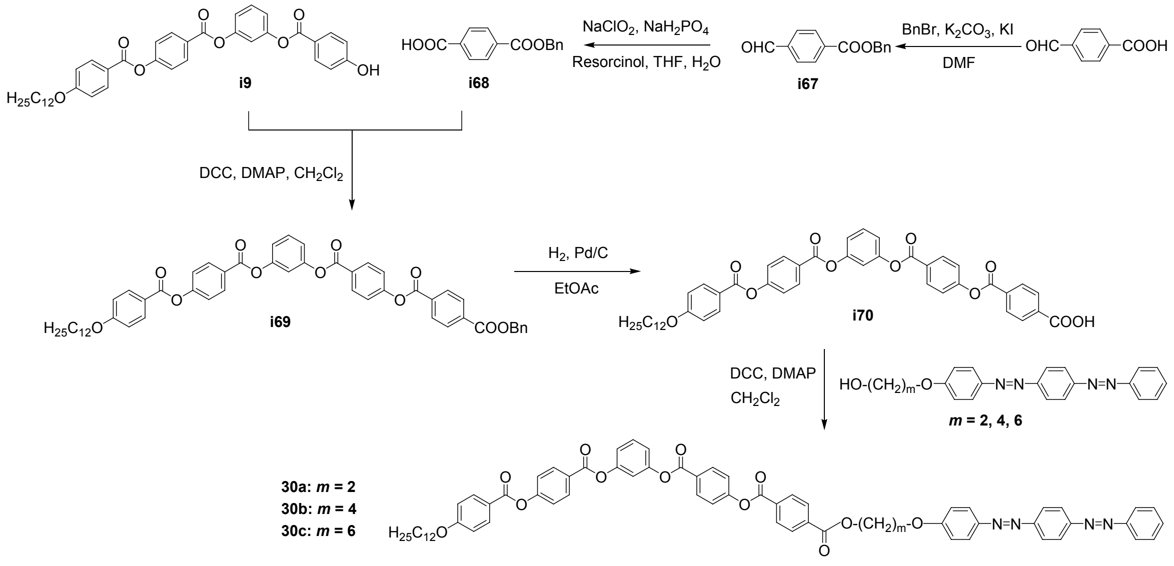
NaClO$_2$, NaH$_2$PO$_4$
Resorcinol, THF, H$_2$O
BnBr, K$_2$CO$_3$, KI
DMF
HOOC–C$_6$H$_4$–COOBn
OHC–C$_6$H$_4$–COOBn
OHC–C$_6$H$_4$–COOH
i9
i68
i67
DCC, DMAP, CH$_2$Cl$_2$
H$_2$, Pd/C
EtOAc
i69
i70
DCC, DMAP
CH$_2$Cl$_2$
HO-(CH$_2$)$_m$-O–C$_6$H$_4$–N=N–C$_6$H$_4$–N=N–C$_6$H$_5$
m = 2, 4, 6
30a: m = 2
30b: m = 4
30c: m = 6

Scheme 3.16: Synthesis of compounds **30**.

3.2 '*Banana-calamit*' dimers 31 and 32 of type II

In order to study the influence of the position to connect the calamitic moiety to the bent-core mesogenic unit dimers of **type II** were synthesised. The compounds **31** are dimers of **type II** connected ***laterally - terminally*** in the *5*-position on the central *resorcinol* fragment of the bent-core moiety (here assigned as **L – *5* – T**, see Scheme 3.17 and Table 6.1, chapter 6.1), whereas the compounds **32** are connected in a similar way in the *4*-position (**L – *4* – T**). The synthetic strategy to obtain the dimers **31** and **32** is outlined in Scheme 3.17. The methyl 3,5-dihydroxybenzoate and resp. methyl 2,4-dihydroxybenzoate were etherified with benzyl bromide in presence of K_2CO_3/Bu_4NI in butan-2-one. The resulting methyl 3,5-dibenzyloxybenzoate and resp. 2,4-substituted ester **i71** were saponified with KOH in EtOH/H_2O to result the 3,5-dibenzyloxybenzoic acid and resp. 2,4-dibenzyloxybenzoic acid **i72**. The WILLIAMSON etherification of the 4-hydroxyphenyl 4-*n*-hexyloxy-benzoate (**i11**) with ω-bromo-*n*-alkanols in presence of K_2CO_3/KI in DMF result in 4-(ω-hydroxyalkyloxy)phenyl 4-hexyloxybenzoates **i73**. The alcohols **i73** were esterified with the benzoic acids **i72** and further deprotection of the benzyl ether intermediates **i74** by means of hydrogenolysis result in resorcinols **i75** (ω-[4-(4-hexyloxybenzoyloxy)phenoxy]alkyl 3,5-dihydroxybenzoate, and resp. 2,4- dihydroxybenzoate). The final compounds **31** and **32** were prepared by the STEGLICH esterification of the substituted *resorcinols* **i75** (*m*=6, 11) with 4-(4-*n*-dodecyloxybenzoyloxy)benzoic acid **i3.** The mesophase behaviour of dimer series **31** and **32** is described in chapter 6.

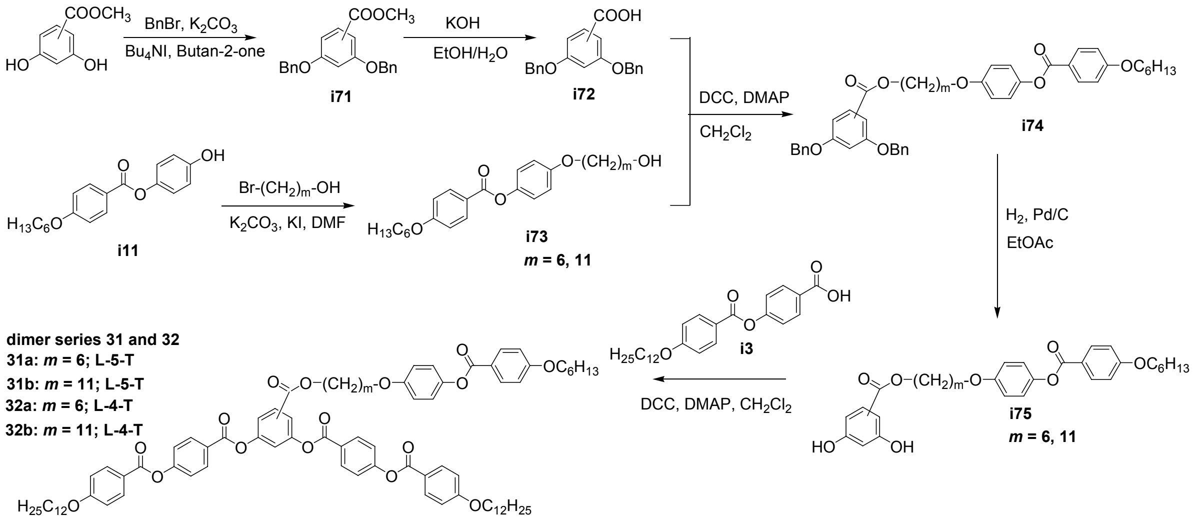
COOCH3
HO
OH
BnBr, K2CO3
Bu4NI, Butan-2-one
BnO
OBn
i71
KOH
EtOH/H2O
COOH
i72
DCC, DMAP
CH2Cl2
O-(CH2)m-O
OC6H13
i74
H2, Pd/C
EtOAc
H13C6O
OH
i11
Br-(CH2)m-OH
K2CO3, KI, DMF
O-(CH2)m-OH
i73
m = 6, 11
H25C12O
i3
DCC, DMAP, CH2Cl2
i75
m = 6, 11
dimer series 31 and 32
31a: m = 6; L-5-T
31b: m = 11; L-5-T
32a: m = 6; L-4-T
32b: m = 11; L-4-T
OC12H25

Scheme 3.17: Synthesis of dimer series **31** and **32**, connected ***laterally - terminally*** in the *5*- and resp. *4*-position on the central *resorcinol* fragment of the bent-core moiety (here assigned as **L – *5* - T** and **L – *4* - T**).

3.3 '*Calamit – banana – calamit*' trimers 33 – 36 of type I

Symmetric trimers **33 – 36** *'calamit – banana - calamit'* of **type I** containing two identical calamitic mesogenic units connected *via* two equal flexible spacers through ether groups to a bent-core unit in a linear fashion (***terminally – terminally*** connection) were synthesised. The used five- or seven-ring bent-core moieties were derived from *resorcinol* for trimers **33**, **35a** and **36** or from *isophthalic acid* for trimers **34** and **35b**. The mesophase behaviour of these compounds is described in chapter 7.

The pathway to prepare the trimers **33a**, **33b**, **33c** (*m* = 3, 6, 11; *p* = 6) and **35a** (*m* = 11; *p* = 16) is outlined in Scheme 3.18. The 1,3-phenylen bis(4-hydroxybenzoate) **i77** was prepared by esterification of resorcinol with the 4-benzyloxybenzoic acid, followed by a deprotection of the 1,3-phenylen bis(4-benzyloxybenzoate) **i76**. Esterification of the resorcinol derivative **i77** with the benzoic acids containing the calamitic moieties **i14** (*m* = 3, 6, 11; *p* = 6, 16) in presence of DCC/DMAP yielded the target trimers **33a, 33b, 33c** and **35a**.

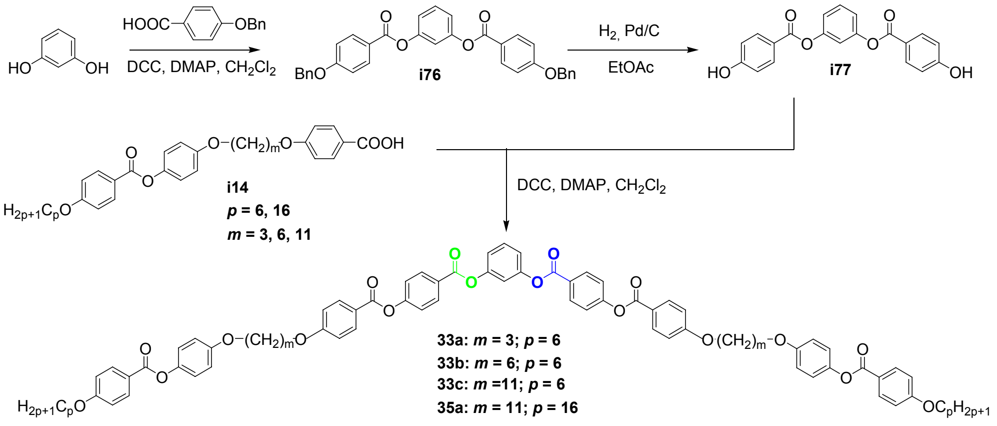
HO
OH
HOOC
OBn
DCC, DMAP, CH2Cl2
BnO
i76
H2, Pd/C
EtOAc
i77
O-(CH2)mO
COOH
H2p+1CpO
i14
p = 6, 16
m = 3, 6, 11
DCC, DMAP, CH2Cl2
33a: m = 3; p = 6
33b: m = 6; p = 6
33c: m =11; p = 6
35a: m = 11; p = 16
O(CH2)m-O
OCpH2p+1

Scheme 3.18: Synthesis of compounds **33a, 33b, 33c** and **35a**.

The trimers **34a**, **34b**, **34c** (m = 3, 6, 11; p = 6) and **35b** (m = 11; p = 16) were synthesised as shown in Scheme 3.19. The bis(4-hydroxyphenyl) isophthalate **i79** was prepared by esterification of isophthalic acid with the 4-benzyloxyphenol and deprotection of the benzyl-protected compound **i78** by means of hydrogen in the presence of Pd/C. Esterification of the *isophthalic acid* derivative **i79** with the ω-carboxyl-substituted calamitic moieties **i14** (m = 3, 6, 11; p = 6, 16) in presence of DCC/DMAP yielded the trimers **34a**, **34b**, **34c** and **35b**.

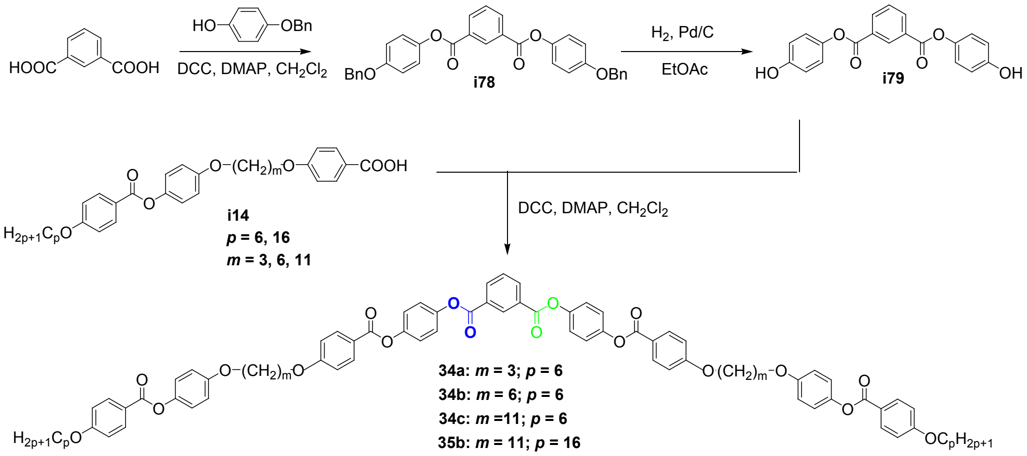
HOOC
COOH
HO
OBn
DCC, DMAP, CH₂Cl₂
BnO
i78
OBn
H₂, Pd/C
EtOAc
HO
i79
OH
O-(CH₂)ₘO
COOH
H₂ₚ₊₁CₚO
i14
p = 6, 16
m = 3, 6, 11
DCC, DMAP, CH₂Cl₂
O-(CH₂)ₘO
O(CH₂)ₘ-O
H₂ₚ₊₁CₚO
OCₚH₂ₚ₊₁
34a: m = 3; p = 6
34b: m = 6; p = 6
34c: m =11; p = 6
35b: m = 11; p = 16

Scheme 3.19: Synthesis of compounds **34a**, **34b**, **34c** and **35b**.

The synthesis of trimer **36** (m = 6; p = 6) which contains a seven-ring bent-core unit is outlined in Scheme 3.20. The esterification of the 4-{ω-[4-(4-hexyloxybenzoyloxy)-phenyloxy]hexyloxy}benzoic acid **i14** (m = 6; p = 6) with 4-hydroxybenzaldehyde gave the aldehyde **i68,** which was oxidized by means of $NaClO_2/NaH_2PO_4$ to result ω-carboxyl-substituted calamitic moiety **i81** (m = 6; p = 6). Esterification of the 1,3-phenylene bis(4-hydroxybenzoate) **i77** with the benzoic acid containing the calamitic moiety **i81** in presence of DCC/DMAP yielded the target trimer **36**.

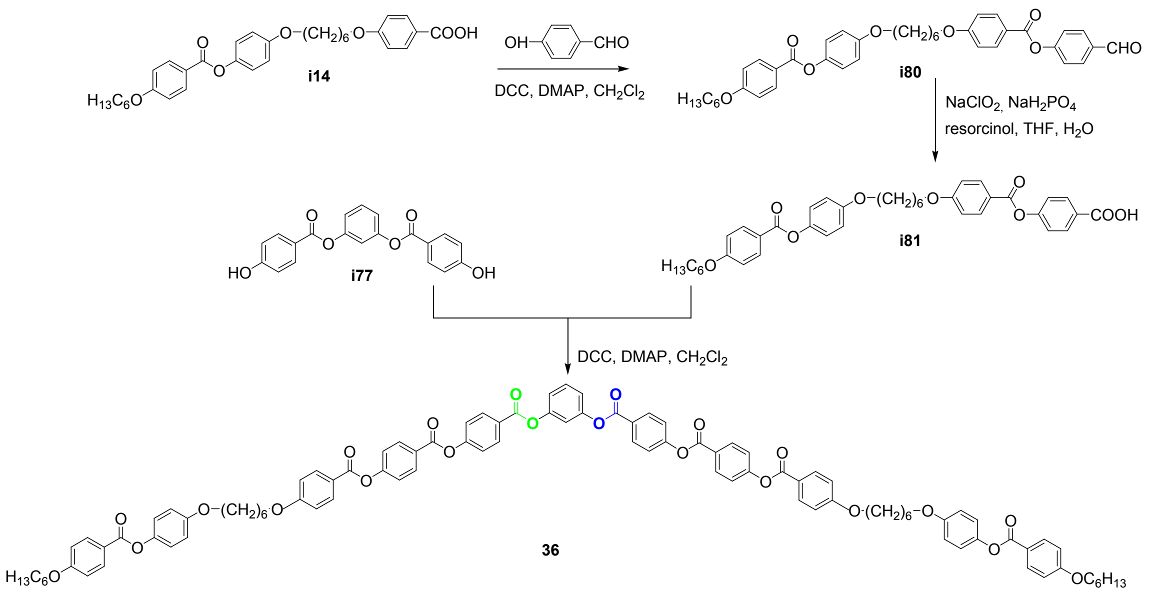
O-(CH₂)₆O
COOH
H₁₃C₆O
i14
OH
CHO
DCC, DMAP, CH₂Cl₂
O-(CH₂)₆O
CHO
H₁₃C₆O
i80
NaClO₂, NaH₂PO₄
resorcinol, THF, H₂O
HO
i77
OH
O-(CH₂)₆O
COOH
H₁₃C₆O
i81
DCC, DMAP, CH₂Cl₂
O-(CH₂)₆O
O(CH₂)₆-O
H₁₃C₆O
OC₆H₁₃
36

Scheme 3.20: Synthesis of compound **36**.

3.4 '*Banana – calamit – banana*' trimers 37 and 38 of type II

Symmetric trimers '*banana-calamit-banana'* of **type II** containing two identical bent-core mesogenic segments connected through two equal flexible spacer units in a linear *end - to – end* manner to a calamitic structural unit consisting of a 1,4-disubstituted *benzene* unit (trimer **37a**), 4,4'-*biphenylene* fragment (trimers **37b** and **37c**) and 4,4′-*azobenzenes* segment (trimers **38**) were synthesised. The mesophase behaviour of these compounds is described in chapter 8.

3.4.1 Trimer series 37

The synthetic strategy to obtain the trimer **37a** (*n* = 12; *m* = 4) containing a 1,4-disubstituted benzene is outlined in Scheme 3.21. Due to the symmetrical structure of these trimers, their preparation can be described in a simple way. Esterification of the *n*-dodecyloxy substituted five-ring bent-core benzoic acid **i70** with 4,4′-bis(4-hydroxybutyloxy)benzene (available in our laboratory) in presence of DCC/DMAP yielded the trimer **37a**.

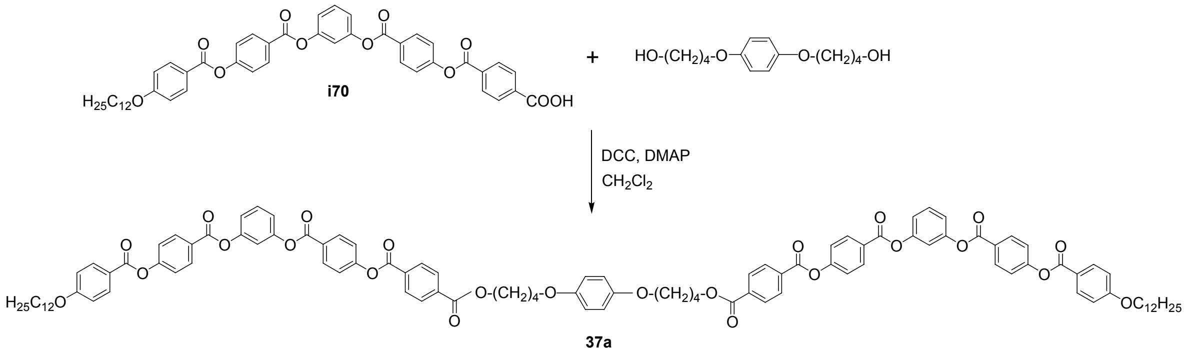
H25C12O
i70
COOH
+
HO-(CH2)4-O
O-(CH2)4-OH
DCC, DMAP
CH2Cl2
H25C12O
O-(CH2)4-O
O-(CH2)4-O
OC12H25
37a

Scheme 3.21: Synthesis of compound **37a**.

The trimers **37b** and **37c** (*n* = 12; *m* = 4, 11) containing a 4,4'-disubstituted *biphenylene* unit as a calamitic structural unit were obtained analogue to the trimer **37a**. The esterification of the *n*-dodecyloxy substituted five-ring bent-core benzoic acid **i70** with 4,4′-bis(ω-hydroxyalkyloxy)biphenyl (*m* = 4, 11; available in our laboratory) in presence of DCC/DMAP yielded the trimers **37b** and **37c** (see Scheme 3.22). Their mesophase behaviour is described in chapter 8.1.

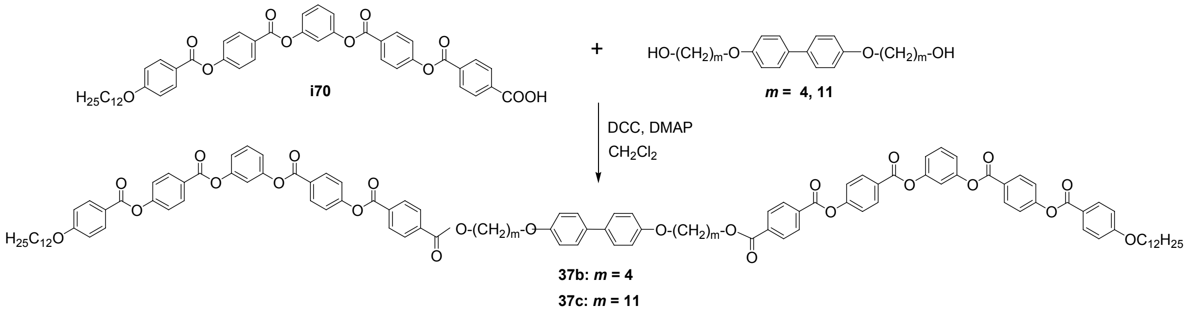
H25C12O
i70
COOH
+
HO-(CH2)m-O
O-(CH2)m-OH
m = 4, 11
DCC, DMAP
CH2Cl2
H25C12O
O-(CH2)m-O
O-(CH2)m-O
OC12H25
37b: m = 4
37c: m = 11

Scheme 3.22: Synthesis of compounds **37b** and **37c**.

3.4.2 Trimer series 38[198]

The compounds **38** contain a 4,4′-bis(ω-hydroxyalkyloxy)azobenzenes moiety (*m* = 2, 4, 5, 6) which serves as bridge between two five-ring bent-core moieties. The trimers **38** were synthesized according to a similar strategy as that used for compounds **37**: the *n*-dodecyloxy substituted five-ring bent-core benzoic acid **i70** was esterified with the 4,4′-bis(ω-hydroxyalkyloxy)azobenzenes to obtain the target trimers (see Scheme 3.23). The 4,4′-bis(ω-hydroxyalkyloxy)azobenzenes (*m* = 2, 4, 5, 6; available in our laboratory) have been described by RÖTZ et al.[200] The mesophase behaviour of these trimers is described in chapter 8.2 and these results were already published by our research group.[198]

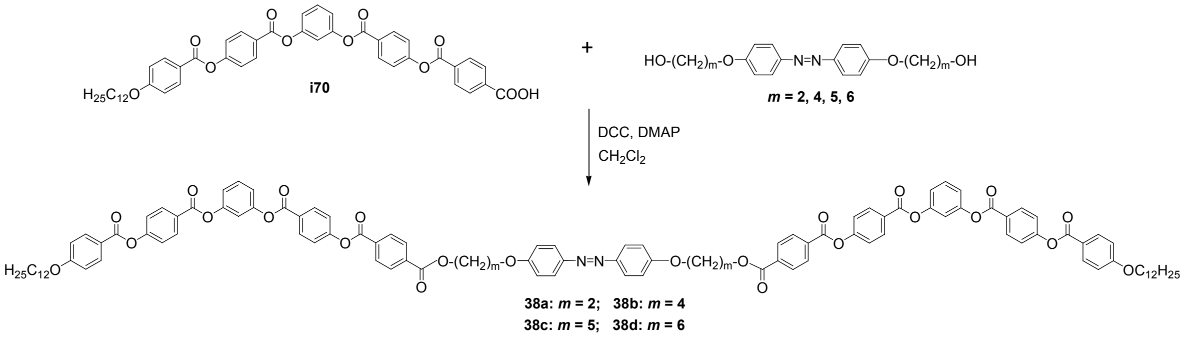
H25C12O
i70
COOH
+
HO-(CH2)m-O
N=N
O-(CH2)m-OH
m = 2, 4, 5, 6
DCC, DMAP
CH2Cl2
O-(CH2)m-O
N=N
O-(CH2)m-O
OC12H25
38a: m = 2; 38b: m = 4
38c: m = 5; 38d: m = 6

Scheme 3.23: Synthesis of compounds **38**.

4

Experimental techniques

The assignment of the LC mesophases of the oligomeric system under study is based on combined results of polarising optical microscopy (POM), differential scanning calorimetry (DSC), electro-optical investigations and X-ray diffraction experiments (XRD). Together these methods build a picture of the structure and properties of the LC phases.

4.1 Polarising optical microscopy

Most of the liquid crystals are found to be birefringent due to their anisotropic nature. The polarizing optical microscopy (POM) method can be used as a method to determine phase transition temperatures and phase types by textural analysis of the temperature dependant behaviour of samples between crossed polarisers. Characteristic textures and defect structures, which change when passing a phase transition, give hints of the phase type. The birefringence and the defects of a liquid crystal are responsible for the colours and the patterns seen in a polarising microscope wherein light first passes through a polariser, then through the liquid crystal sample, and finally through a second polariser. The second polariser (also known as the analyser) is orientated at 90° to the first polariser, in such a called crossed polarisers position. Because of the crossed polarisers no light reaches the observer's eyes unless the liquid crystal changes the polarisation state of the light. The difference in the intensity of light passing through the second polariser is dependent on director orientation, birefringence and sample thickness. For a planar/homogenous aligned liquid crystal sample (i.e. if the director is parallel to the substrates), when a sample is illuminated with white light, areas of darkness occur when the director is parallel to the polarisers. The optical textures were observed using a polarising microscope *Nikon* Labophot-2A (*Nikon*, Japan) equipped with a *Linkam* hot stage and an automatic temperature controller (THMS 610, *Linkam* TP 92, UK). The photographs of the textural investigations were registered with a *Nikon* Coolpix 5400 – digital camera (*Nikon*, Japan).

4.2 Calorimetric studies

The occurrence of a phase transition is related to a change in the ordering of the molecules. These order changes may be positional, translational or orientational. Any change in ordering posses an associated change in enthalpy, entropy and volume. The phase transitions between the liquid crystalline state are in most cases first order, with a few exceptions. The enthalpy changes are relatively small in the order of a few kJ mol^{-1}. A first order phase transition involves a spontaneous change in enthalpy, entropy and volume at the transition, whereas a second order phase transition is associated with a gradual change in these properties.[2] The measurements of the temperature dependence of the heat capacity C_p and/or the enthalpy ΔH helps the characterization of the thermal behaviour of the liquid crystal phases. The most common calorimetric technique used to study liquid crystals is differential scanning calorimetry (DSC). DSC is a thermo - analytical technique in which the difference in the amount of heat required to increase the temperature of a sample and reference is measured as a function of temperature. The sample and the reference are heated at the same rate over a defined temperature range. The reference sample should have a well-defined heat capacity over the range of temperatures to be scanned. As phase transitions occur in the sample the sample furnace must supply more or less heat flow to maintain the same temperature as the reference sample. Melting processes are endothermic and so more heat flow is required to maintain the sample temperature, whereas crystallisation processes are exothermic and so less heat flow is required. The advantages of this method are in the high sensitivity for detecting the enthalpy changes, very small sample size required and the overall rapid and convenient operation. However, DSC is not well suited to making detailed quantitative measurements near liquid crystal phase transitions. The disadvantage of DSC measurements is the difficulty to distinguish first- and second-order transitions. Although slower rates can be used, DSC machines work best for fairly rapid scans and require minimum scan rates of 0.1 K/min. A quantitative distinction between first and second order transitions could be found by making a series of measurements at different scan rates with further extrapolating of the transition enthalpy to rate zero. Strongly first order transition does not exhibit dependence of the latent heat on the cooling / heating rate. Whereas the enthalpy H shows almost linear dependence in case of the second or weakly first order transitions. Usually, for the results presented in this work, the measurements were conducted with a rate of 5 K/min and 10 K/min using the experimental set-up *Perkin Elmer* DSC Pyris 1 (*Perkin Elmer*, *Inc*., USA).

4.3 X-ray diffraction measurements

X-ray diffraction (XRD) is a very powerful technique in the field of liquid crystals which perform a key role in the identification of LC phases and in the study of LC phase transitions. The analyses of X-ray diffraction patterns provide information about the layer distances or lattice parameters and the relative orientation and spatial orientational distribution of the molecules.

X-ray diffraction arises from elastic scattering of radiation by electrons. The angles at which X-rays are scattered depend on the distance between centres of mass within the LC material. The basic equation of X-ray diffraction is the BRAGG law. This law states that X-rays reflected from adjacent atomic planes separated by a distance d of a crystal interfere constructively when the path difference between them is an integer multiple of the wavelength λ, i.e.

$$n\lambda = 2d_{hkl} \sin\theta \qquad \text{(eq. 1)}$$

Here n, an integer, is the order of the reflection. The reflected rays make an angle of 2θ with the direction of the incident beam. X-ray ‘reflection’ is present only when the planes are aligned at the correct angle to satisfy the BRAGG condition. There is no reflection at other angles and for this reason it is called X-ray diffraction. It means, the determination of the BRAGG angle(s) can be related to the inter-planar distance or lattice constant.

In the case of liquid crystals the crystalline lattice is not observed, instead the scattering is formed from the centres of mass of adjacent molecules. Nematic liquid crystals are an orientationally ordered fluid and the lack of ordering produces broad, less intense reflections, in both the wide and small angle regions for nematic materials. Smectic phases exhibit both orientational as well as positional ordering in one dimension, therefore their XRD patterns display sharp reflections in the small angle region associated with layer spacing, but diffuse scattering in the wide angle region associated with intermolecular distances. Columnar phases show an additional positional ordering in a second dimension and the XRD analysis shows a 2D lattice.

LC materials are multidomain, and so the Bragg conditions are satisfied for all values of n and all possible diffraction peaks are observed. In unaligned samples, domains are orientated with all angles of θ. The Bragg reflections are averaged out if monitored with an area detector as a circle. In the X-ray pattern of well-oriented monodomains the layer reflections are located on the meridian whereas the diffuse scattering maxima in the wide angle region, indicating the absence of in-plane order, are observed perpendicular to this (SmA) or at certain angle (SmC). This is observed by the formation of arcs for diffuse scattering peaks and as intense spots for Bragg peaks. Bragg's law predicts the direction of any diffracted ray, but no information can be obtained with respect to the intensity of the scattered beam. The relative position of the diffuse outer maxima with respect to the preferred axis (meridian of the pattern) can be determined by a χ-scan. From this follows the determination of the tilt of the molecules within the smectic layers. XRD measurements on non-oriented samples were done with a Guinier film camera as well as a Guinier goniometer (*Huber* Diffraktionstechnik GmbH, Germany). Quartz-monochromatized CuK_α radiation (Cu-$\mathrm{K}_{\alpha1}$-radiation; $\lambda = 0.154056$ nm) was used; the incident X-ray beam was perpendicular to the glass capillaries.

Oriented samples were obtained by long annealing of a drop of the liquid crystal on a glass plate after very slow cooling of the isotropic liquid (see Fig. 4.1b). In this case the smectic layers could be aligned parallel to the substrates and the incident X-ray beam was parallel to the smectic layers (see Fig. 4.1a).

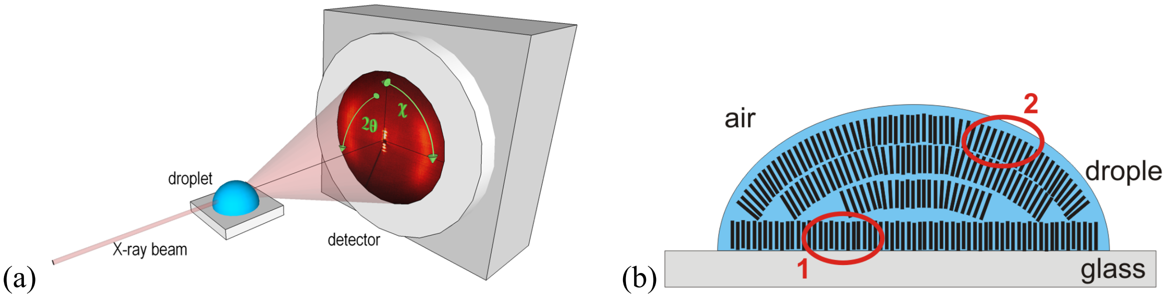

Figure 4.1: (a) Scheme of the X-ray setup with the 2D detector. (b) Schematic representation of the observed preferred orientation of the molecules in the droplet sample at the boundary surface between the (1) glass / LC and (2) air / LC.

The samples for the 2D XRD measurements can also prepared by sealing the sample in glass capillaries (with an outside diameter of 0.8 mm to 1 mm and wall thickness of 0.01 mm, manufactured by the *Hilgenberg GmbH*, Germany). Alignment was achieved in thin capillaries under a magnetic field ($B \approx 1$ T) with samples in a temperature controlled furnace, using Ni filtered and pin hole collimated CuK_α radiation (Cu-K_α-radiation; $\lambda = 0.15418$ nm); the incident

X-ray beam was perpendicular to the glass capillaries. The substances had to be heated, for orientation, into the isotropic liquid during the sample preparation for the X-ray investigations. However, measurements on cooling and on heating could be conducted. Two-dimensional patterns for aligned samples were recorded with a two-dimensional detector (*HI-Star, Siemens AG*, Germany).

4.4 Electro-optical studies

The symmetry of banana-shaped LC phases is sometimes broken as a result of simultaneous director tilt and polar order perpendicular to the director.[78] Hence astonishing LC phases that exhibit spontaneous polarisation (P_S) in the absence of chiral groups in their molecular structure and (anti)ferroelectricity are sometimes observed.[32] P_S is usually determined in electro - optical switching experiments: under applied periodic rectangular or triangular waveforms. The switching of the P_S induces a transient electric current peak in each half period of the driving field.[201] The ability of the ferroelectric LCs to switch the direction of optical axes under the influence of external electric field is one of the most studied features.

For the ferroelectric phase the macroscopic polarisation does not linearly depend on the external field, i.e. it presents a hysteresis-like behaviour (Fig. 4.2a). The macroscopic polarisation is saturated in the limit of large fields ($E > E_{th}$). The macroscopic polarisation remains non-zero in the absence of the external field. In this case two stable states are allowed; with spontaneous polarisation 'up' ($+P_S$) and 'down' ($-P_S$). The switching between these states appears on applying of the field above a certain threshold E_{th}. The rate of the switching is characterised by the switching time τ.

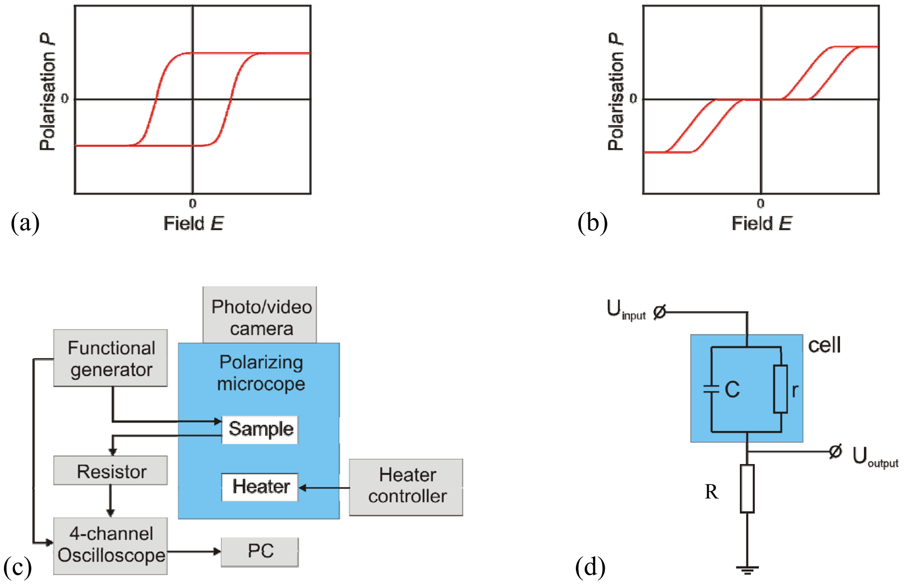

Figure 4.2: (a) One-loop ferroelectric hysteresis curve; (b) two-loop anti-ferroelectric hysteresis curve; (c) the block scheme of the electro-optic setup; (d) the electrical scheme: C and r are the internal capacitance and resistance of the LC cell. R is the external resistor.

For the anti-ferroelectric mesophases the situation is different, i.e. the macroscopic polarisation in the absence of external field is zero. A transition into the ferroelectric state can be induced on application of a field E ($E > E_{th}$). The field-dependent macroscopic polarisation shows a typical anti-ferroelectric two-loop hysteresis curve (Fig. 4.2b). The measurements of the P_S can be conducted on application of electric field to a capacitor filled with the liquid crystalline sample. Mainly triangular-wave voltage was employed in polarisation measurements. The reorientation of the macroscopic polarisation in the sample induces a current impulse through the capacitor when the applied voltage over the capacitor exceeds a threshold voltage U_{th}. $U_{th} = E_{th}$ x d, where d is the distance between the capacitor plates. The value of this switching polarisation is:

$$P_{sw} = \frac{1}{S} \int_{over\, the\, pulse} I(t)dt \qquad \text{(eq. 2)}$$

where S is the area of the capacitor. In the ferroelectric material there is only one transition with the threshold E_{th} between the FE+ and FE- states. In means that one peak in half a period of the applied voltage represents the current response. In the antiferroelectric phases there are two transitions: AFE -> FE with E_{th1} and the inversed FE -> AFE transition with E_{th2}. These transitions provide two current impulses per half a period. The switching times can be extracted from the current response curves for the step-like shape of the external field. It is important to note that throughout this thesis P_{AF} and P_{FE} are used to describe the experimentally determined switching behaviour of a polar mesophase (P_{AF}: two peaks, tristable; P_{FE} only one peak, bistable).

For the results presented in this thesis, the compounds under study were loaded into commercial liquid crystal cells (*E.H.C. Co*., Japan) with gaps of 2 μm to 25 μm. These cells had 1 cm^2 indium tin oxide (ITO) electrodes coated with and without a rubbed polyimide layer to induce planar alignment. The cells were mounted in the heating stage of the polarising microscope and a voltage of variable shape was applied to the electrodes (8116 A, *Hewlett-Packard*, USA). The measurements of the switching polarisation were made employing the triangular-wave voltage method.[202] The switching polarisation was measured by integration of the repolarisation current. The scheme of the experimental set-up is shown in Figure 4.2 c, d. The following devices were used in the experimental set-up: oscilloscope (*Hewlett Packard*, HP 54601A, USA); functional generator (*Keithley*, 3910, USA); amplifier (*Krohn-Hite*, KH 7500, USA); resistors (*Time Electronics*, Model 800, UK); polarising microscope (*Leica* DMRXP); digital camera (*Nikon* Coolpix 4500, Japan); heating stage (*Mettler-Toledo*, FP900, Switzerland).

5 Mesophase behaviour of '*banana-calamit*' dimers of type I

In the chapter 5 we focus on the structure-properties relationship of ***terminally - terminally*** connected non-symmetric '*banana-calamit*' liquid crystal dimers containing bent-core mesogenic units and calamitic moieties (dimers of **type I**; see Figure 5.1 and 5.2).

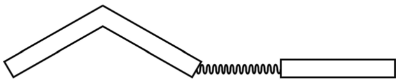

Figure 5.1: General formula of non-symmetric dimers **type I** series under study.

We used bent-core mesogens consisting of five or six aromatic rings, connected by ester linking groups ***E₁* – *E₄***. The spacer is a *hydrocarbon* chain which is connected on the mesogenic units through different ether and ester groups ***X***, ***Y*** of different directions. The influence of the variation of the length of the terminal chain attached to the bent-core moiety and to the calamitic part, as well as the influence of the length and parity of the flexible spacer is studied in the chapters 5.1, 5.2 and 5.3.

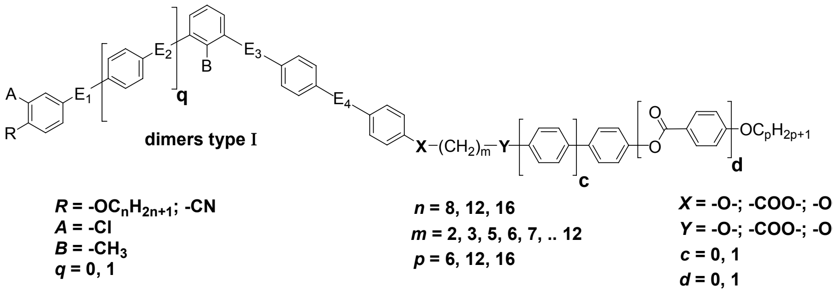

Figure 5.2: General formula of non-symmetric dimers **type I** series under study.

The effect of the connecting groups ***X*** and ***Y*** (–COO-, -OOC- and –O-) on the mesophase behaviour was studied in different dimer series in chapter 5.4. In chapter 5.5, the focus is on several variations of the bent-core mesogenic unit on the mesophase behaviour of '*banana-calamit*' dimers. The variation of the direction of the ester linking groups ***E₁* – *E₄*** in the bent-core unit and the impact on the mesomorphic properties was studied in chapter 5.5.1. The results of these investigations are combined with a study of the influence of the type and direction of the connecting groups ***X*** and ***Y*** in chapter 5.5.2. Afterwards, the variation of the polarity of the terminal group ***R***, lateral substitution and enhancing the number of aromatic rings (chapter 5.5.3, 5.5.4 and 5.5.5, resp.) is discussed. Simultaneously, changes of the mesomorphic properties induced by varying the length of the spacer and of the terminal chains attached to the mesogenic units are considered. In chapter 5.6 we describe several new dimer systems of **type I**, with three-ring calamitic mesogenic units incorporating *biphenylene* units and *bis-azobenzene* segments. In chapter 5.7 we describe in detail the electro-optical characterization of nematic phases of some dimeric systems.

In this chapter you will find an account of several novelties concerning the phase behaviour of these substances:

- the combinations lead to compounds exhibiting polymorphism variants with phases typical for bent-core molecules ($SmCP_A$, Col) as well as mesophases characteristic for calamitic compounds (N, SmA),
- appearance of new phase sequences with non-polar and polar phases of special interest: nematic-columnar and nematic-smectic,
- an unusual *odd-even* effect: the appearance of the nematic phase only for the even-membered dimers; intermediate spacer lengths (n = 6-10) show both nematic and columnar phases while for the longer member (n = 12) nematic and smectic (SmC_c/ B_6) phases are observed,
- these nematic phases exhibit special properties, e.g. field-induced biaxiality, special electro-convection pattern and high flexoelectricity, as well as possible field induced transitions into smectic-like phases,
- the occurrence of a N – N_X phase transition characterised by a low transition enthalpy,
- the existence of a SmC_s – SmC_a phase transition characterised by a small transition enthalpy,
- some examples of rich polymorphism of polar switchable phases typical for bent-core mesogens,
- the appearance of new intercalated smectic phases.

5.1 Effect of the length of the spacer *m* on the mesophase behaviour of dimer series 1 -6

5.1.1 The dimer series 1

The dimer series **1** contains 10 homologous compounds, thus being the series with the largest range of spacer chain lengths (*m* = 2, 3, 5-12 methylene units). The compounds **1** have a constant length of the *alkyloxy* chain attached to the bent-core unit (*n* = 12) and to the calamitic part (*p* = 6). Thus, for the series of dimers **1** the influence of the length of the aliphatic spacer upon the mesomorphic properties will be scanned. The compounds **1** represent dimers of **type I** with a five-ring bent-core moiety and a calamitic hexyloxybenzoyloxyphenyl unit. The bent-core unit possesses a central *resorcinol* unit, the ester linking groups within one wing having the same direction. This is the ***reference structure*** for the bent-core unit in this thesis assigned as $\mathbf{E_0}$. If not otherwise indicated, data refer to an $\mathbf{E_0}$ structure for the bent-core moieties in the following sections of this thesis.

All compounds **1** exhibit liquid crystalline behaviour. The mesophase types, transition temperatures together with the associated transition enthalpies and lattice parameters for series **1** are given in Table 5.1. Nearly all compounds exhibit columnar mesophases (several in combination with a nematic phase). The exceptions are the early member **1a** (*m* = 2), which exhibits only a monotropic nematic phase and the longest member **1j** (*m* = 12), which shows nematic and smectic behaviour. Almost all exhibited mesophases are monotropic, except the member with **1i** (*m* = 11), which shows an enantiotropic Col_{ob} phase.

Table 5.1: Transition temperatures [°C], mesophase types, transition enthalpy values [kJ/mol], layer spacing *d* [nm], tilt angle τ of the molecules [°] with respect to the layer normal in SmC phases and with respect to the normal to *a* in Col phases, lattice parameters (*a*, *b*, *γ*) and P_S values of dimer series **1**.[a]

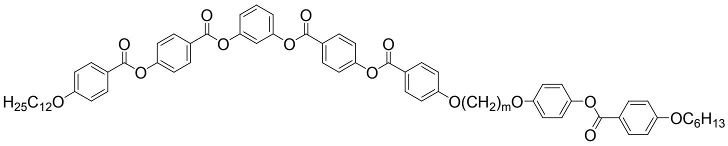

Comp.	*m*	Transitions temperatures [°C] Δ*H* [kJ·mol^{-1}]	Phase type	Lattice parameters					P_S *nC/cm*^{2}
				d [nm]	τ [°]	*a* [nm]	*b* [nm]	γ [°]	
1a	2	Cr 178 (N 163) I *72.8* -[b]	N						
1b	3	Cr 150 (Col$_r$P$_{AF}$ 127) I *65.7* *24.0*	Col$_r$P$_{AF}$		11	7.57	5.51	90.0	350
1c	5	Cr 137 (Col$_{ob}$P$_{AF}$ 132) I *64.4* *24.8*	Col$_{ob}$P$_{AF}$		42	3.55	4.65	91.5	370
1d	6	Cr 148.5 (Col$_x$ 125.5 N 145.5) I *61.2* *13.1* *1.3*	N Col$_x$[c]		-[c]	-[c]	-[c]	-[c]	-[c]
1e	7	Cr 147 (Col$_{ob}$P$_{AF}$ 132) I *74.1* *24.5*	Col$_{ob}$P$_{AF}$		40	3.55	4.74	94.4	390
1f	8	Cr 141 (Col$_x$ 124 N 136) I *78.9* *0.06* *2.5*	N Col$_x$ [c]		-[c]	-[c]	-[c]	-[c]	-[c]
1g	9	Cr 136 (Col$_{ob}$P$_{AF}$ 130) I *84.4* *25.7*	Col$_{ob}$P$_{AF}$		43	3.38	4.79	100.3	400
1h	10	Cr 130 (Col$_{ob}$P$_{AF}$ 116 N 129) I *98.6* *12.4* *3.3*	N Col$_{ob}$P$_{AF}$		50	3.30	4.89	108.3	410
1i	11	Cr 121 Col$_{ob}$P$_{FE}$ 132.5 I *58.8* *25.3*	Col$_{ob}$P$_{FE}$		44	3.20	5.00	110.0	380
1j	12	Cr 135 (SmC$_c$P$_{AF}$ 121 N 125) I *101.1* *12.4* *2.5*	N SmC$_c$P$_{AF}$	2.28	24				300

[a] Transition temperatures (°C) and enthalpy values [kJ/mol] of dimer series **1** were taken from the second DSC heating scans (10 Kmin^{-1}); values in parentheses indicate monotropic mesophases, in this case the transition temperatures and enthalpy values were taken from the first DSC cooling scans and the transition temperatures were checked by polarising microscopy; [b] the transition is not detectable on DSC and the transition temperature value is determined by polarising microscopy; [c] could not be determined due to rapid crystallization of the sample.

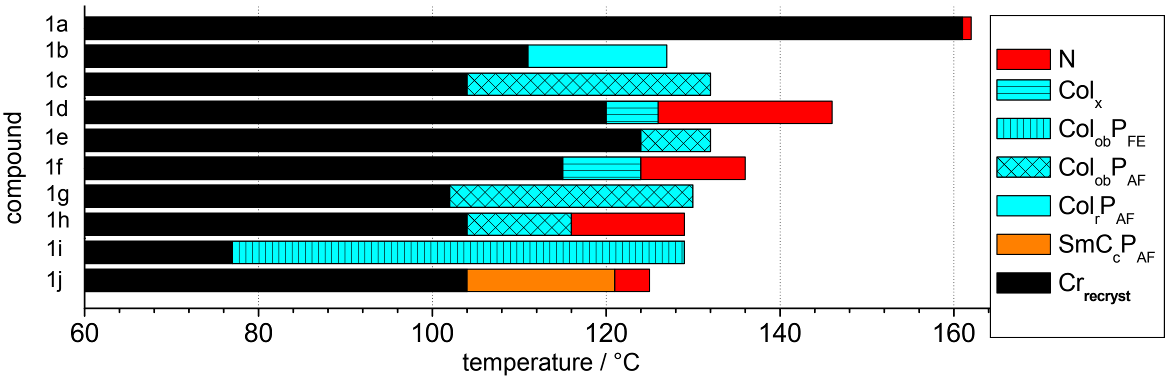

Figure 5.3: Transition temperatures (°C) of dimer series **1**, taken from the first DSC cooling scans (10 Kmin^{-1}).

The shortest member of the series **1a** ($m = 2$) exhibits exclusively nematic behaviour while the homologue with $m = 3$, **1b**, only columnar behaviour. The next homologues with *even*-numbered spacer lengths ($m = 6, 8, 10$) give rise to both nematic and columnar phases while for the longer member **1j** ($m = 12$) nematic and smectic (SmC_c) phases are observed. Thus, increasing spacer length appeared to promote smectic over columnar behaviour. The *odd*-numbered dimers exhibit exclusively columnar phases, however of different types.

The Col_x phases described in the Table 5.1 and Figure 5.3 are columnar phases which are unidentified because of their fast crystallization immediately after formation. Here and in the following, the generic name Col_x is assigned to all columnar phases which could not be fully investigated. This means that Col_x phases of different compounds can have different optical or structural features.

A dependence of the I-N, I-Col, N-Col and N-SmC_c transition temperatures on the number of methylene units, m, in the flexible spacer for the dimer series **1** was established (Fig. 5.4). A general tendency of a clear alternation of the isotropic–LC transition temperatures with increasing number m of methylene units in the flexible spacer was found. The *even* members exhibit the higher values. For spacer lengths $m = 10$ and higher the effect has been extinguished. It should be mentioned that strictly speaking the direct comparison of the transition temperatures of different phases is not appropriate because of the very different structural changes which accompanied these transitions.

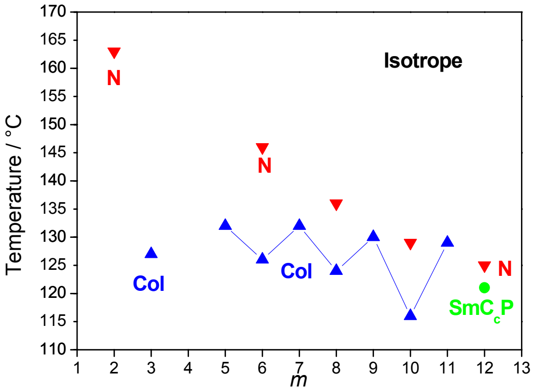

Figure 5.4: Dependence of the transition temperatures on the number of methylene units, ***m***, in the flexible spacer for the dimer series **1**; ▲ I–Col and N–Col transitions, ▼ I– N transitions and ● N–SmC_c transition; values are taken from the first cooling DSC scans.

A second type of alternation is attributed to the I-Col and N-Col transition temperatures (blue line). Using this aspect the *odd*-numbered homologues show the higher transition temperatures. It seems that for the *even* members the increase of the number of methylene units in the spacer is associated with a continuous decrease of the Col-N transition temperatures. The alternation of the transition temperatures but also of the phase type in dependence of the spacer length is highly unusual, especially in the combination of type nematic and columnar phases. On the other hand, looking at the I-N transition temperatures one can observe a monotone decrease of the values on increasing the spacer length from 163 °C ($m = 2$) to 125 °C ($m = 12$). Interestingly, we could observe the nematic phase only for the *even*-membered dimers. The enthalpy values for the I–N transition were found to be in the range of about 1.3 to 3.3 $kJ \cdot mol^{-1}$, whereas generally for the nematic to the low temperature mesophases (Col or SmC_c phases) transitions values of about 12 to 13 $kJ \cdot mol^{-1}$ were found. An exception is compound **1f** ($m = 8$) which exhibits a very small N - Col_x transition enthalpy (0.06 $kJ \cdot mol^{-1}$).

Table 5.2: X-ray diffraction data from aligned samples of the Col_rP_{AF} and $Col_{ob}P_{AF}$ phases of compounds **1** and an estimate of the number of molecules in the cross section of the ribbons within the corresponding Col phases.

Comp.	m	T [°C]	Phase type	Parameter[a] [nm]	$V_{mol,cr}$[b] [nm^3]	$V_{mol,is}$[c] [nm^3]	V_{cell}[d] [nm^3]	$n_{cell,cr}$[e]	$n_{cell,is}$[f]	$n_{cell,LC}$[g]
1b	3	124	Col_rP_{AF}	$a = 7.57$ $b = 5.51$	1.475	1.877	21.69	14.70	11.55	13.13
1c	5	124	$Col_{ob}P_{AF}$	$a = 3.55$ $b = 4.65$ $\gamma = 91.5$	1.525	1.941	8.58	5.60	4.40	5.00
1e	7	127	$Col_{ob}P_{AF}$	$a = 3.55$ $b = 4.74$ $\gamma = 94.4$	1.575	2.004	8.72	5.54	4.35	4.95
1g	9	126	$Col_{ob}P_{AF}$	$a = 3.38$ $b = 4.79$ $\gamma = 100.3$	1.624	2.067	8.28	5.10	4.11	4.55
1h	10	114	$Col_{ob}P_{AF}$	$a = 3.30$ $b = 4.89$ $\gamma = 108.3$	1.649	2.098	7.97	4.80	3.77	4.29
1i	11	125	$Col_{ob}P_{FE}$	$a = 3.20$ $b = 5.00$ $\gamma = 110.0$	1.674	2.130	7.82	4.67	3.67	4.17

[a] Lattice parameter with an error of the calculated parameters in the order of 0.1 nm; [b] $V_{mol,cr}$ = molecular volume in the crystal calculated using crystal volume increments,[203] average packing coefficient in the crystal $k = 0.7$ according to Kitaigorodski;[204] [c] $V_{mol,is}$ = molecular volume in the isotropic liquid, average packing coefficient $k = 0.55$; [d] V_{cell} = unit cell volume obtained from the lattice parameters and assuming a height of $h = 0.52$ nm (assuming a stacking in bend direction of molecules with a bend angle of 120°) calculated according to $V_{cell} = a \times b \times 0.52$ nm [nm^3] for the Col_r phase and $V_{cell} = a \times b \times \sin\gamma \times 0.52$ nm [nm^3] for the Col_{ob} phases; n_{cell} = number of molecules in a unit cell with crystal-like density (cr) according to [e] $n_{cell,cr} = V_{cell}/V_{mol,cr}$, with liquid-like density (is) according to [f] $n_{cell,is} = n_{cell,cr} \cdot 0.55/0.7$, and in the LC phase [g] $n_{cell,LC}$ estimated as the intermediate between that in the crystalline and the liquid phase.

Another interesting point is the structure-property relationship on varying the length of the spacer resulting in different columnar phases. The lattice parameters of the columnar phases depend on the length of the flexible spacer (only the Col_{ob} phases are compared, see Table 5.2). On increasing the spacer length the parameter a of the Col_{ob} phases is slightly decreasing, while parameter b and the oblique angle (γ) are slightly increasing. The number of the molecules in the unit cell in the Col_{ob} phases is also slightly decreasing with increasing spacer length. The correlation of a and n_{cell} speaks for the molecules being packed along a in one ribbon (b is associated to the molecular length). In the following the physical properties of the dimer series **1** will be discussed in detail in the subchapters 5.1.1.1 to 5.1.1.4, excepting the dimer **1a** which exhibits a monotropic nematic phase only.

5.1.1.1 The rectangular columnar Col$_r$ phase of dimer 1b with $m = 3$

The dimer **1b** shows the typical textural features of the so-called B_1 phase (Col$_r$). On cooling from the isotropic liquid a dendritic growth of the texture could be observed. On further cooling the dendritic aggregates transform into a mosaic-like texture with banana-leaf like and focal conic regions (see Fig. 5.5).

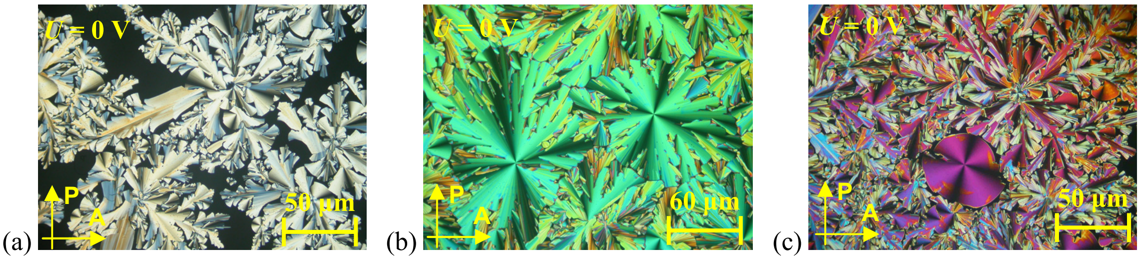

Figure 5.5: The optical photomicrographs of the Col$_r$ phase of compound **1b** at $U = 0$ V: (a) at 127 °C, during dendritic growing from the isotropic liquid; (b,c) at 125 °C, mosaic texture with focal conic regions.

In the case of compound **1b** this mesophase is monotropic, however X-ray investigations were able to be performed. By very slow cooling of a drop of the isotropic liquid on a glass plate we obtained well-developed domains of the mesophase. The X-ray diffraction pattern is characterized by a diffuse scattering in the wide angle region and sharp BRAGG-reflections in the small angle region (Fig. 5.6a,b). The small-angle reflections can be indexed to a centred two-dimensional rectangular lattice, with the lattice parameters $a = 7.57$ nm and $b = 5.51$ nm (Fig. 5.7). From the χ-scan of the wide angle region a tilt angle of the molecules with respect to the a-axes of the real lattice of 79° could be estimated (Fig. 5.6c). The intensity is corrected by subtracting the scattering of the isotropic sample to enhance the effect of the anisotropy of the outer diffuse scattering in the liquid-crystalline phase. The distribution of the diffuse scattering suggests a synclinic tilt of the molecules.

The interpretation of the small-angle BRAGG-reflections as resulting from a two-dimensional rectangular lattice is illustrated in Figure 5.7. It shows the reciprocal lattice with the indices of the observed reflections: $a = 7.57$ nm; $b = 5.51$ nm (observed only for indices hk with $h + k = 2n$). The position of the maximum of the outer diffuse scattering indicates a tilt of the long molecular axes with respect to the b-axis of the 2D lattice of 11° (see Table 5.2).

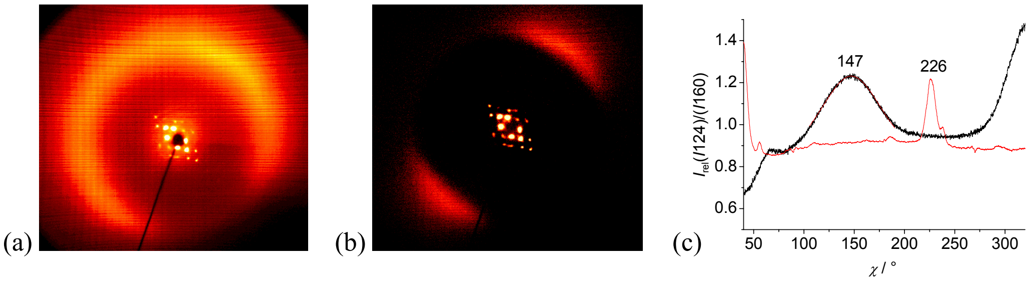

Figure 5.6: XRD pattern of a surface-aligned sample of the Col$_r$ phase of compound **1b** at 124 °C on cooling: (a) original scattering, (b) the same XRD pattern, but the intensity of the isotropic liquid is subtracted (suggesting a synclinic tilt of the molecules), (c) distribution of the wide-angle scattering along χ (black line) with maximum at 147° [$I_{rel} = I(124\ °C) / I(160\ °C, I)$] in comparison with the χ-position of the 0k-reflections (red line) with a maximum at 226° (estimated tilt angle of the molecules with respect to the a-axes of the real lattice: 79°).

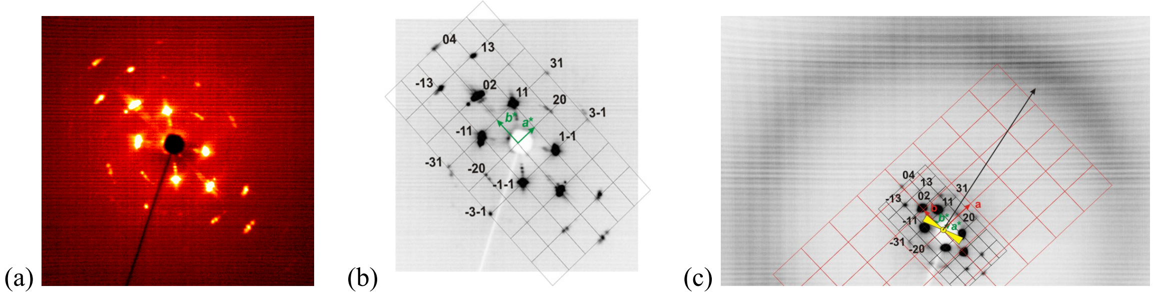

Figure 5.7: (a-c) 2D XRD pattern for a surface-aligned sample of compound **1b** in the small angle region of the Col_r phase at 124 °C: (a) original pattern and (b) reciprocal lattice with *hk* values for the observed reflections; (c) position of the maximum of the diffuse scattering (black arrow) with respect to the reciprocal 2D lattice (black) and orientation of the molecules in the corresponding real lattice (red, arbitrary size).

On applying a triangular-wave electric field above a relatively high threshold voltage of 25 V μm^{-1} the columnar phase is switchable, i.e. two polarisation current peaks per half period were recorded which indicates an AF ground state ($P_S = 350$ nC cm^{-2}, Fig. 5.8e).

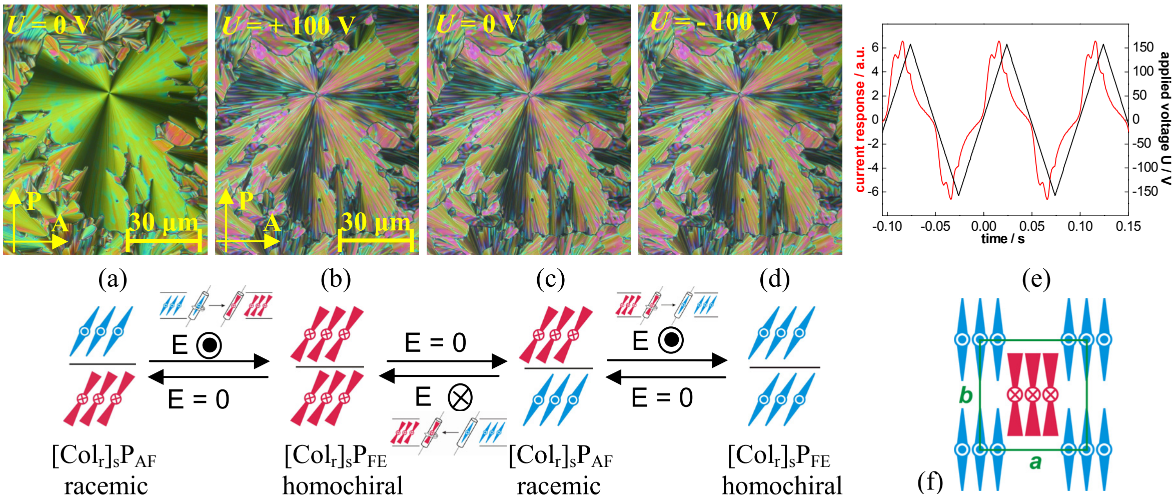

Figure 5.8: Electro-optical investigations of the Col_rP_{AF} phase of compound **1b** under a d.c. electric field at 124 °C; textures observed between crossed polarisers in the same region of the sample in a 6 µm polyimide-coated ITO cell; (a) $U = 0$ V, before starting the experiment; (b,d) $U = \pm 100$ V; (c) $U = 0$ V; (e) AF switching current response obtained by applying a triangular-wave voltage ($U = 377$ V_{pp}, $f = 3$ Hz, $R = 5$ kΩ, $T = 122$ °C, $P_S = 350$ nC cm^{-2}); (a-d, down) proposed models of the organization of the molecules in the ribbons in the FE states and (a,c) in the AF ground-state, considering one column as a fragment of a smectic layer; (f) model of the Col_rP_{AF} phase.

In the circular domains obtained by cooling without field, the extinction crosses are always inclined with respect to the directions of polariser and analyser, indicating a synclinic organization of the molecules in the ground-state structure (Fig. 5.8a). The positions of the circular domains do not change on reversal or removal of the field, only a change in the birefringence could be observed which is independent of the polarity of the applied field (Fig. 5.8b-d). This indicates that the synclinic organization of the ground-state structure is not significantly changed by the field and confirms that the switching process takes place by a collective rotation around the long molecular axis (change of the polar direction without changing the tilt direction of the molecules, see Fig. 5.8). Furthermore, the proposed models of the organization of the molecules in the FE states ($[\mathrm{Col_r}]_s\mathrm{P_{FE}}$) and AF states ($[\mathrm{Col_r}]_s\mathrm{P_{AF}}$) of the $\mathrm{Col_rP_{AF}}$ phase are shown.

The molecules are organized in ribbons with alternating polar directions along *a* in the ground-state structure. The size of the crystallographic cell of the $\mathrm{Col_rP_{AF}}$ phase, seems to be sufficiently large (about 13 molecules per cross-section) to consider one column as a fragment of a smectic layer. This is the reason why in this work the proposed models of the AF switching of the molecules in the ribbons are illustrated as reorganization of the molecules in a smectic layer organization, if not otherwise stated. This means in this case the switching is illustrated as for a $\mathrm{SmC_sP_{AF}}$ phase. The field-induced reorganization of the molecules in ribbon phases takes place by collective rotation around the long axis because the inter-ribbon interfaces hinder rotation on a cone. The steric hindrance arising from interactions between columns boundaries do not limit the collective rotation around the long molecular axis. It follows from X-ray investigations and electro-optical measurements that this phase is a $\mathrm{Col_r}$ phase which is synclinic and AF, i.e. a $[\mathrm{Col_r}]_s\mathrm{P_{AF}}$ phase.

5.1.1.2 The nematic and columnar phases of dimers 1 with *m* = 5 - 10

All compounds of the series **1** with *m* = 5-10 exhibit columnar phases. The *even*-membered dimers exhibit additionally nematic phases (see Table 5.1 and Figure 5.3).

As a representative example the mesophase behaviour of compound **1h** with *m* = 10 will be discussed in more detail. This compound exhibits two monotropic mesophases. The high-temperature phase could be easily identified as a nematic phase by its characteristic texture. The nematic phase occurred with striking nematic droplets (with director fluctuations, flickering) emanating from the dark background (Fig. 5.9a). Depending on the boundary conditions, on further cooling the nematic phase displays a uniform planar texture, schlieren (Fig. 5.9b) or a marbled texture (Fig. 5.9c).

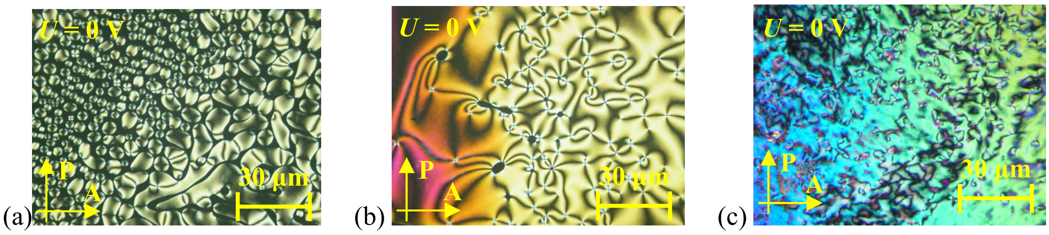

Figure 5.9 The optical photomicrographs of the nematic phase of compound **1h** at *U* = 0 V: (a) nematic droplets at 129 °C during growing from the isotropic state; (b) at 128.5 °C, on further cooling the nematic droplets transforms into a schlieren texture; (c) schlieren threaded- marbled patterns.

The nematic phase of compound **1h** is a monotropic mesophase which exists in a temperature range of 12 K and displays some unusual optical and electro-optical properties. Over the whole temperature range of the nematic phase chiral domains of opposite handedness can be observed although the molecules are achiral (for some examples in literature see ref.[64,205]). Starting from the crossed position of the polarisers and rotating one polariser clockwise by a small angle (5–15°) dark and light domains become visible. Rotating the polariser anticlockwise by the same angle causes the effect to be reversed, i.e. the previously dark domains now appear light and *vice versa*. The textures of the nematic phase of compound **1h** at 127 °C, as obtained between crossed polarisers (Fig. 5.10a) and slightly decrossed polarisers (Fig. 5.10b,c) showing chiral ((+) and (–)) domains are below presented. The brightness of the (+) and (–) domains is reversed by changing the direction of the polarisers. These domains can be seen also by illuminating the sample with circularly polarised light in the reflection mode of the microscope.

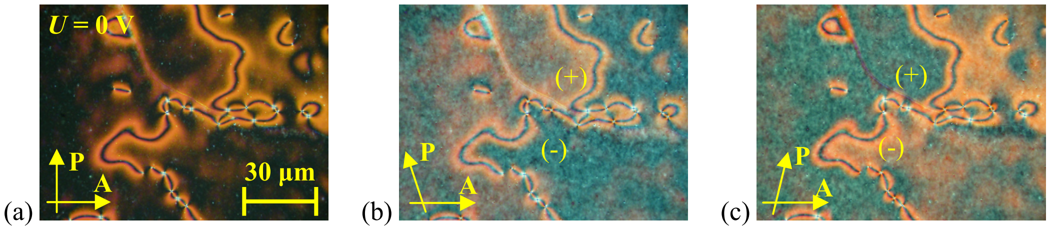

Figure 5.10: The optical photomicrograph of the nematic phase of compound **1h** at 127 °C in a 5µm non-coated ITO cell, at $U = 0$ V observed between crossed polarisers (a), and by rotating one polariser by +15° (b) and by -15° (c) from the crossed position (showing chiral (+) and (–) domains).

The spontaneous formation of regions with opposite handedness in the nematic phase is obviously the result of bend–twist deformations which are promoted by the bent shape of the molecules, as already reported in the literature.[64,205,206] The pitch of the twisted domains is clearly larger than the sample thickness, so that the texture corresponds to a nematic phase. The occurrence of spontaneous twisted regions in nematic phases is also seen in computer simulations of bent molecules.[207] We observed that domains of opposite handedness are formed with equal probability. Notably, these domains occur in random places of the sandwich cell and can be altered by mechanical stress or by temperature change.

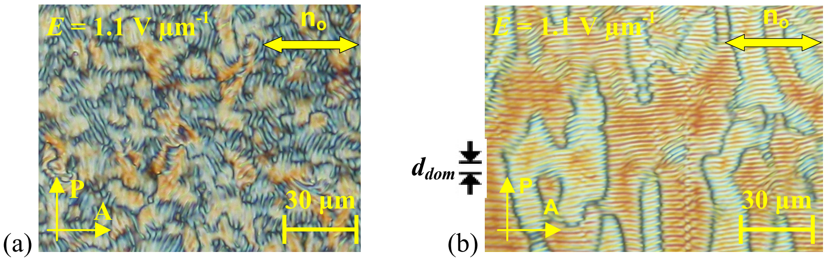

Figure 5.11: Textures of nematic phase of compound **1h** observed between crossed polarisers: (a-b) domain patterns in the nematic phase at 127 °C by application of an a.c. field; the electric field strength is $E = 1.1$ V μm^{-1} (22 Hz); sample thickness: 6 µm; period of the domains, d_{dom}: 6 µm; the black arrows in (b) mark the period of the domains equal to the cell thickness, 6 µm; the orientation of the initial director $\mathbf{n_o}$ is marked.

Remarkably, the nematic phase of these dimeric compounds shows unusual electro-optical behaviour on applying an electric field,[195] as illustrated for example, for compound **1h** (Fig. 5.11). By application of a relatively low a.c. field (1.0 V μm^{-1}; 22 Hz) fluctuating domains appear. These domains are WILLIAMS–KAPUSTIN domains, since the period of the domains, d_{dom}, corresponds to the cell thickness (6 µm), see Figure 5.11.

On applying higher fields (3 V μm^{-1}; 20 Hz) to the planar oriented nematic phase in a 6 µm polyimide-coated cell, domains with equidistant stripes parallel to the original direction of the director $\mathbf{n_o}$ appear (Fig. 5.12a). The period of these domains was found to be 10 µm which is clearly greater than the sample thickness. On further increasing the voltage the domain period decreases, i.e. 8 µm at 5 Vμm^{-1} (Fig. 5.12b), 6 µm at 9 Vμm^{-1} (Fig. 5.12c). With increasing voltage above 12 Vμm^{-1} the domain pattern is completely changed to a myelin-like texture with fine equidistant stripes (Fig. 5.12d). The period of these equidistant stripes within the domains decreases with increasing voltage to 19 Vμm^{-1}. On application of a relatively high d.c. field (25 V µm^{-1}) the stripes disappear and an optical texture results which is reminiscent of a smectic fan-shaped texture (Fig. 5.12e,f). This field-induced fan-shaped texture is observed in the whole existence region of the nematic phase. However, during the electro-optical experiments no polar switching was detected. If the electric field is removed, the smectic-like texture disappears and the texture of the planar oriented nematic phase reappears. Similar electro-optical behaviour has been reported for the nematic phase of different bent-core compounds.[64,205,208]

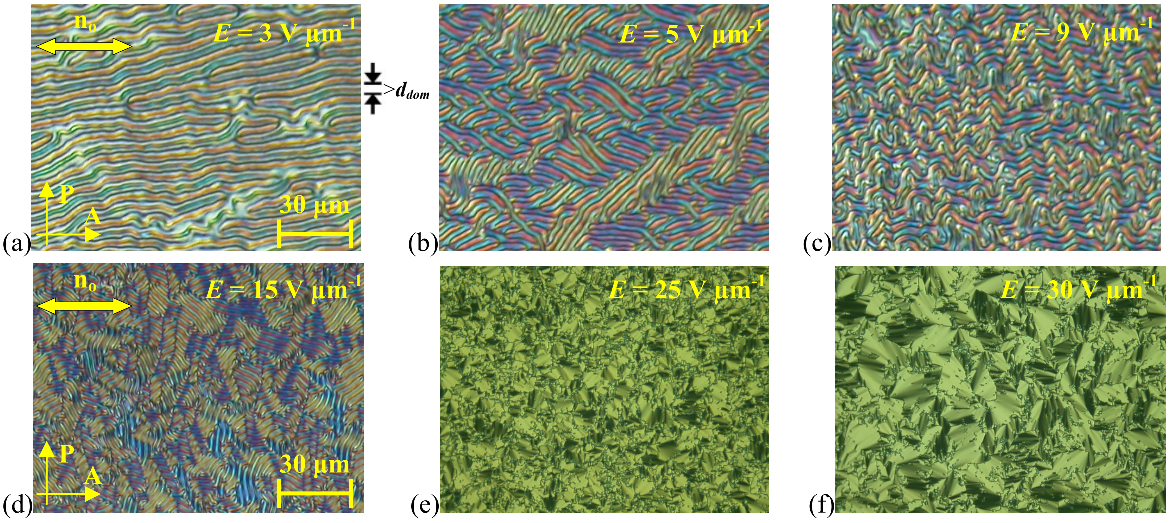

Figure 5.12: Field-induced texture changes of the nematic phase of compound **1h** at 127 °C, observed between crossed polarisers in the same region of a 6 µm polyimide-coated ITO cell, by application of an electric field with the strength E: (a) 3 Vμm^{-1} (20 Hz); (b) 5 Vμm^{-1}; (c) 9 Vμm^{-1}; (d) 15 Vμm^{-1}; (e) 25 Vμm^{-1}; (f) 30 Vμm^{-1}; the black arrows in (a) mark the period of the domains which was found to be 10 µm and is clearly greater than the cell thickness 6 µm; the orientation of the initial director $\mathbf{n_o}$ is marked.

Although the field-induced formation of a smectic phase cannot be excluded, it is more probable that the originally partially twisted sample is deformed by the electric field in such a way that a fan-shaped texture is built up which is also characteristic of a cholesteric phase, but we have no explanation for the mechanism by which such fan-shaped texture can be generated. Further X-ray investigations of the field induced structures are in progress. Similar electro-optical behaviour has been found for all nematic phases of the dimer series **1** and further discussion on special properties of the nematic phases under electric field will follow in the chapter 5.5. In order to clarify the structural features of the nematic phase, X-ray measurements were performed by applying a magnetic field of about 1T. The results confirm the presence of a nematic phase and the existence of cybotactic groups is clearly proven on the base of well-oriented samples. The X-ray pattern shows a diffuse dumb-bell-like scattering maximum in the small angle region, and a diffuse wide angle scattering located around the equator (Fig. 5.13a,b). The diffuse, small-angle scattering in the nematic phase can be attributed to cybotactic groups representing fluctuating arrays of molecules with a short-range order of the same type as the long-range order in the low-temperature Col$_{ob}$ phase.

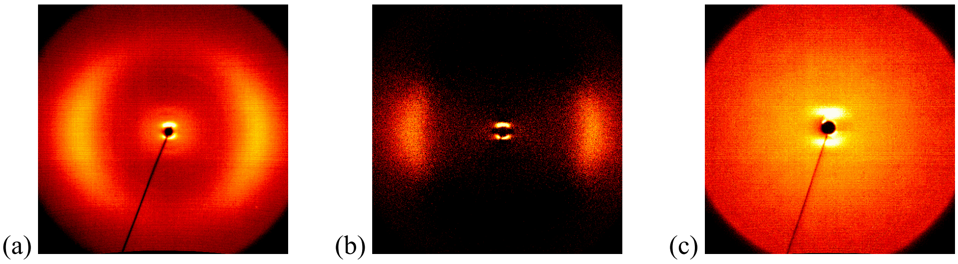

Figure 5.13: The XRD patterns of an aligned sample of the nematic phase of compound **1h** at 125 °C: (a) original XRD pattern; (b) the same XRD pattern, but the intensity of the isotropic liquid is subtracted; (c) scattering in the small angle region.

On further cooling of the nematic phase the dimers **1d** and **1f** (m = 6 and 8) exhibit monotropic columnar phases Col$_x$, which crystallize immediately after formation (only textural investigation were possible). The dimers with spacer length m = 5, 7, 9 and 10 form also monotropic columnar phases, but in this case structural investigations could be performed. On cooling from the isotropic liquid or from the nematic phase a dendritic growth of the texture could be observed (Fig. 5.14 a,b). On further cooling the dendritic aggregates transform into a mosaic-like texture, characteristic for a Col$_r$ phase; also high birefringent and low birefringent banana-leaf like regions and focal conic regions could be observed (Fig. 5.14c).

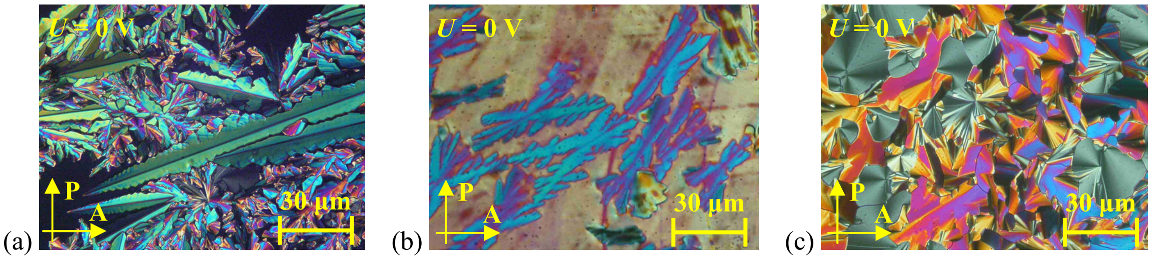

Figure 5.14: Textures of the Col$_{ob}$ phases of the dimers **1** with m = 5, 7, 9, 10 at U = 0 V: (a) growth of the dendritic domains of compound **1c** on cooling from the isotropic liquid; (b) growth of the dendritic domains of compound **1h** on cooling from the nematic phase (light domains represent nematic phase); (c) the mosaic texture with focal conic regions (compound **1g**).

Well-developed domains of the mesophase of compound **1g** (m = 9) could be obtained by very slow cooling of a drop of the isotropic liquid on a glass plate. The X-ray diffraction pattern is characterized by a diffuse scattering in the wide angle region and sharp BRAGG-reflections in the small angle region (Fig. 5.15a,b). From the χ-scan (Fig. 5.15d) of the wide angle region we could estimate a tilt angle of the molecules with respect to the a-axis of the real lattice of 47°. The distribution of the diffuse scattering in the wide angle region suggests a synclinic tilt of the molecules.

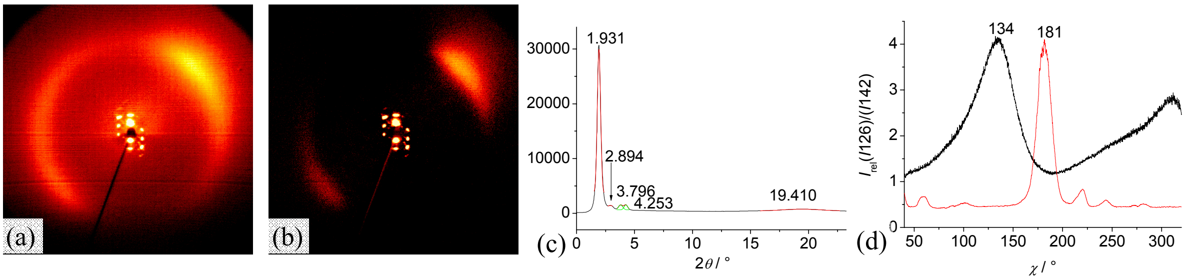

Figure 5.15: XRD patterns of a surface-aligned sample of the $\mathrm{Col_{ob}}$ phase of compound **1g** at 126 °C: (a) original pattern; (b) the same XRD pattern, but the intensity of the isotropic liquid is subtracted; (c) θ-scan of the diffraction pattern with the d-values; (d) distribution of the wide-angle scattering along χ (black line) with maximum at 134° [$I_{rel} = I(126\ °C) / I(142\ °C, I)$] in comparison with the χ-position of the $0k$-reflections (red line) with a maximum at 181° (estimated tilt angle of the molecules with respect to the a-axes of the real lattice: 47°).

The small-angle reflections can be indexed to a two-dimensional oblique lattice, with the lattice parameters $a = 3.38$ nm, $b = 4.79$ nm and $\gamma = 100.3°$ (Fig. 5.16a,b). The orientation of the molecules in the real lattice is shown in Figure 5.16c.

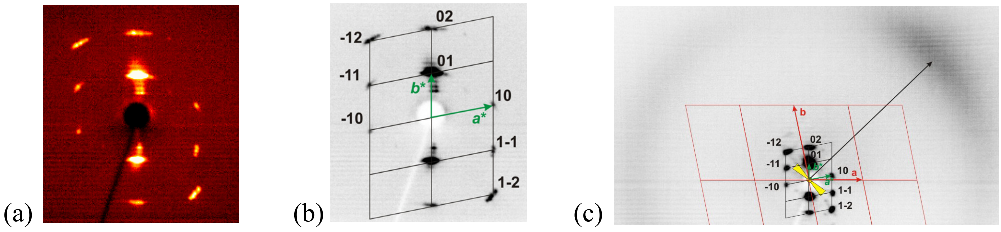

Figure 5.16: (a, b) XRD pattern of a surface-aligned sample of the $\mathrm{Col_{ob}}$ phase of compound **1g** in the small angle region at 126 °C: (a) original pattern; (b) reciprocal lattice with hk values for the observed reflections; (c) position of the maximum of the diffuse scattering (black arrow) with respect to the reciprocal 2D lattice (black) and orientation of the molecules in the corresponding real lattice (red, arbitrary size).

On applying a triangular-wave field above 15 Vμm^{-1} the $\mathrm{Col_{ob}}$ phase of compound **1g** shows an electro-optical switching. The current response indicates an antiferroelectric ground state, i.e. two polarisation current peaks per half period were recorded. The value of the spontaneous polarisation was found to be 400 nC cm^{-2} (Fig. 5.17d). Applying an electric field to the virgin banana-leaf like texture of compound **1g** with high birefringent and low birefringent regions, the stripes within the texture disappear and the birefringence (and therefore the interference colour) is changing. The texture is transformed under a triangular wave electric field into a smooth texture which is independent of the polarity of the applied field and does not relaxes after removal of the electric field (Fig. 5.17b,c). This confirms that the switching process takes place by a collective rotation around the long molecular axis, which changes the polar direction without changing the tilt direction of the molecules.

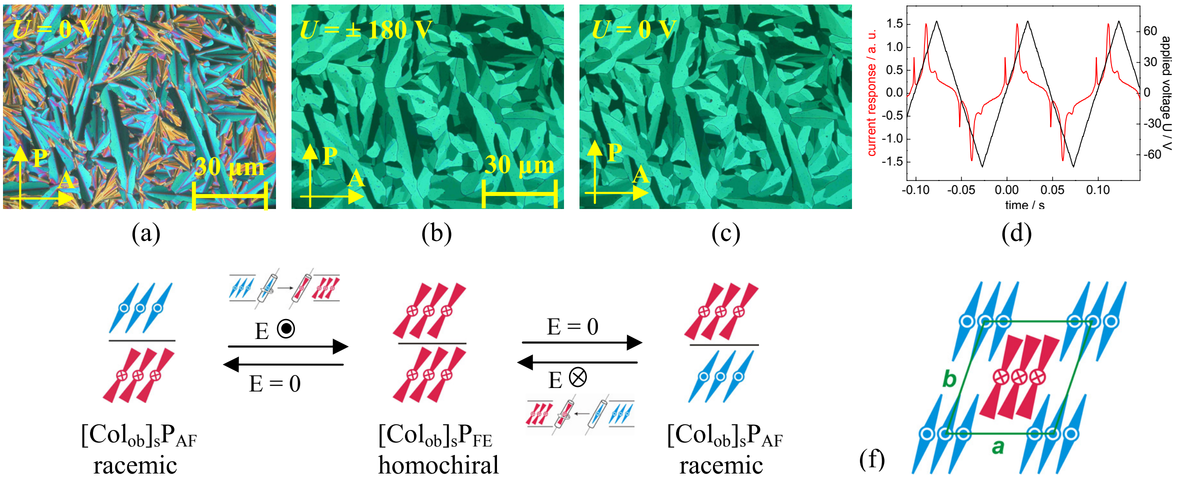

Figure 5.17: Electro-optical investigations of the switching process of the $\mathrm{Col_{ob}P_{AF}}$ phase of compound **1g**; textures observed between crossed polarisers in the same region of the sample in a 5 µm non-coated ITO cell at 126 °C; (a) $U = 0$ V, before starting the experiment and (b) under a d.c. field ($U = \pm 180$ V); (c) $U = 0$ V; (a-c, down) proposed models of organization of the molecules in the ribbons in the FE state (b) and in the AF ground-state (a,c), considering one column as a fragment of a smectic layer; (d) AF switching current response obtained by applying a triangular-wave voltage ($U = 140\ \mathrm{V_{pp}}$, $f = 5$ Hz, $R = 5$ kΩ, $T = 126$ °C, $P_S = 400\ \mathrm{nC\ cm^{-2}}$); (f) model of the $\mathrm{Col_{ob}P_{AF}}$ phase.

ORTEGA *et al.*[209] and KIRCHHOFF [210] postulated possible molecular orientations for the two main domain types in the B_1 texture. The banana-leaf domains have the molecular dipoles pointing perpendicular to the glass plates, aligned with the field, and the other, higher birefringence areas have the dipoles parallel with the glass surfaces. By applying fields about 15 $\mathrm{V\mu m^{-1}}$ the brighter domains are destroyed as the molecules are forced to rotate and line up with the electric field. This effect can be seen quite clearly in Figure 5.17b. On removal of the field the field-induced texture remains (Fig. 5.17c). In Figure 5.17 the proposed models of the organization of the molecules in the FE state ($\mathrm{[Col_{ob}]_sP_{FE}}$) and AF states ($\mathrm{[Col_{ob}]_sP_{AF}}$) of the $\mathrm{Col_{ob}P_{AF}}$ phase of compound **1g** are shown. The molecules are organized in ribbons with a reversal of the polar direction along direction *b* in the ground-state structure. The size of the crystallographic cell of the $\mathrm{Col_{ob}P_{AF}}$ phase, seems to be sufficiently large (about 5 molecules per cross-section) to consider one column as a fragment of a smectic phase layer, as already discussed for the $\mathrm{[Col_r]_sP_{AF}}$ phase of compound **1b** in Figure 5.8. On the basis of these experimental observations, the mesophase of the compound **1g** has been designated as the $\mathrm{Col_{ob}}$ phase which is synclinic and AF, i.e. a $\mathrm{[Col_{ob}]_sP_{AF}}$ phase.

Since the molecular conformation of compound **1g** is unknown, the construction of an appropriate model for the organization of the molecules in this $\mathrm{Col_{ob}P_{AF}}$ phase is very difficult and has to be a speculative one. Based on the special features of the molecular structure of the $\mathrm{Col_{ob}P_{AF}}$ phase of compound **1g** following assumptions were made:[195] (a) the bent-core and calamitic moieties of the molecule are sufficiently de-coupled by the spacer, (b) the moieties of different shape and flexibility (bent-core, rod-like core and aliphatic chains) tend to separate from each other, (c) the molecules accept an irregular up and down orientation and it is assumed that both directions of the polar axes of the bent-core parts - up and down - exist; (d) the aliphatic parts are able to interdigitate. Using these assumptions a general structural model for the $\mathrm{Col_{ob}}$ phases of dimers **1** has been derived by us (see Fig. 5.18).[195] For the $\mathrm{Col_{ob}P_{AF}}$

phase of compound **1g** the lattice parameter *b* corresponds to the length of the dimer obtained from CPK models considering the observed tilt angle of about 43° of the mesogenic units. This general model is in agreement with the results of dielectric measurements which show that the dynamic of the bent and the calamitic units are nearly independent from each other.[195]

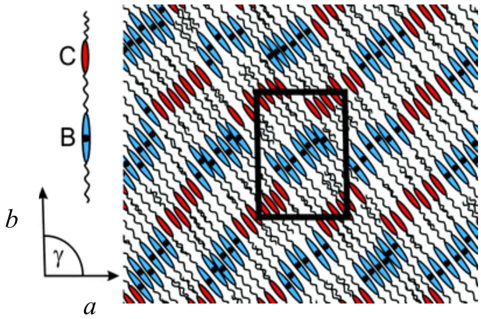

Figure 5.18: A general model proposed for the Col_{ob} phase of this type of '*banana–calamit*' dimers.[195] C: calamitic moiety; B: bent-core; the dots inside the bent-cores represent the polar axes of the bent-core parts being perpendicular to the paper plane. The angle γ deviates from 90° with 4° - 22°. It is assumed that both directions of the polar axes of the bent-core parts - up and down - exist.

TSCHIERSKE *et al.*[211] proposed a model for the organization of the molecules in the $\mathrm{Col}_{ob}\mathrm{P}_{AF}$ phase of some bent-core molecules. There are some general assumptions which can be made also for the $\mathrm{Col}_{ob}\mathrm{P}_{AF}$ phases formed by the '*banana-calamit*' dimers in this thesis, but because of the high flexibility of the molecules, any model for their packing is highly speculative. There are two principally different organizations which can lead to antiferroelectricity in the ribbon phases. Either the polar direction changes along the direction *b* between the modulated layers (see Fig. 5.19a), or the antipolar order is realized within the modulated layers from ribbon to ribbon (*i.e.*, along the direction *a* and *b*), as shown in Figure 5.19d.

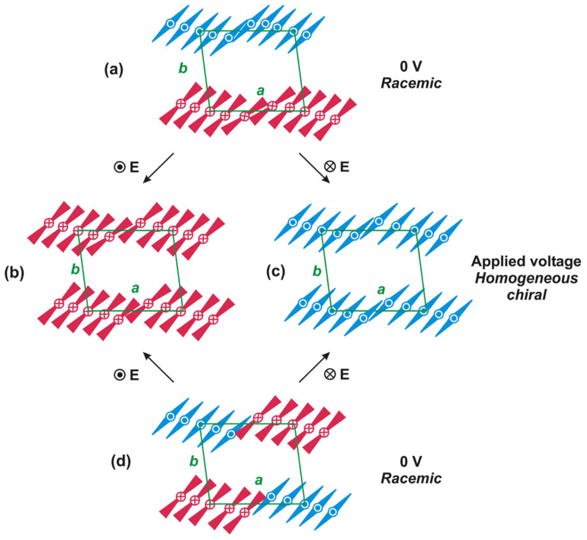

Figure 5.19: Proposed model for the organization of the molecules in the $\mathrm{Col}_{ob}\mathrm{P}_{AF}$ phase (a) AF organization with alternation of the polar direction between the modulated layers; (b) FE organization; (c) FE organization with opposite polarity and chirality; (d) AF organization with alternation of the polar direction from ribbon to ribbon within the modulated layers. The number of molecules in the ribbons and the tilt direction of the molecules with respect to *b* were arbitrarily chosen. The molecules could also be organized more parallel to *b*. This proposed model for the organization of the molecules in the $\mathrm{Col}_{ob}\mathrm{P}_{FE}$ phase has been already described by TSCHIERSKE *et al.*[211]

The ribbon structure can be achieved when there is an overlapping of about one half of the rigid bent cores at the interfaces between adjacent ribbons (Fig. 5.19), which means that the inter-ribbon interfaces of the AF arrangements (Fig. 5.19a,d) become different. Only the reversal of the polar directions within the modulated layers (along direction *a*, as in Fig. 5.19d) allows a parallel packing of the rod-like wings of the aromatic cores at the interfaces between the ribbons. This enables a continuous packing of the rod-like wings in adjacent ribbons and therefore this organization seems to be favourable. If the polar direction in adjacent ribbons would be synpolar (FE, see Fig. 5.19b,c), then the rod-like wings would not be parallel at these interfaces and therefore an unfavourable packing results at these interfaces. It can be concluded that in the $\mathrm{Col_{ob}P_{AF}}$ phases the polar direction changes within the modulated layers from ribbon to ribbon, as shown in Figure 5.19d. This also means that a FE organization, which requires a uniform polar order along direction *a* (Fig. 5.19b,c) is less favourable than the AF structure (Fig. 5.19d). Therefore, the switching of the AF ground state into the FE state requires significant energy and the threshold voltage for this switching process becomes much higher than in the smectic phases. Hence, the AF switching is the result of the steric frustration arising from very large *alkyl* chains, leading to the formation of unfavourable inter-ribbon interfaces ($\mathrm{Col_{ob}P_{AF}}$ phases).

5.1.1.3 The oblique columnar $\mathrm{Col_{ob}P_{FE}}$ phase of dimer 1i with $m = 11$

Dimer **1i** is the only compound in series **1** which exhibits an enantiotropic columnar mesophase. The texture of the Col phase of dimer **1i** is similar to the textures of the $\mathrm{Col_r}$ or $\mathrm{Col_{ob}}$ phases presented above. On cooling from the isotropic liquid a dendritic growth of the texture could be observed (Fig. 5.20a). On further cooling the dendritic aggregates transform into a texture with banana-leaf like regions and mosaic-like texture with high birefringent and very low birefringent regions (Fig. 5.20b,c).

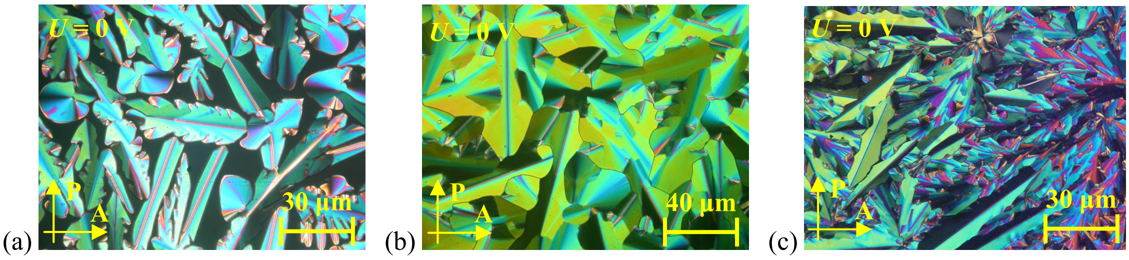

Figure 5.20: Textures of the $\mathrm{Col_{ob}}$ phase of compound **1i** at $U = 0$ V: (a) at 129 °C; (b,c) at 117 °C.

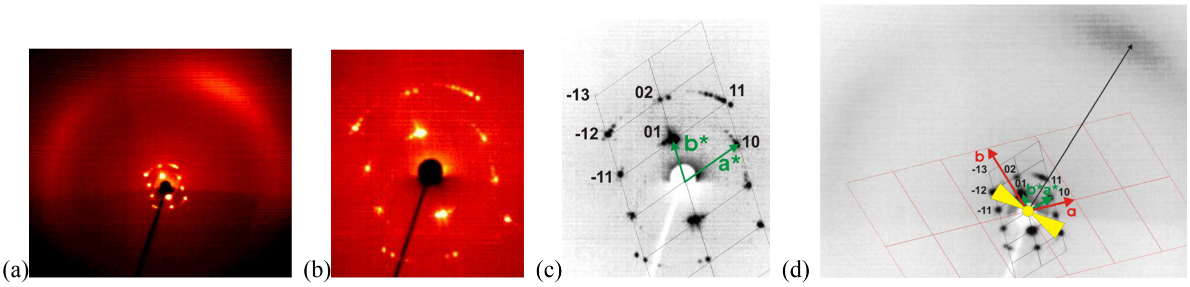

Figure 5.21: XRD patterns of a surface-aligned sample of $\mathrm{Col_{ob}}$ phase of compound **1i** at 125 °C: (a) original pattern (the higher intensity at the top right suggests a synclinic tilt of the molecules within the $\mathrm{Col_{ob}}$ phase); (b) original small-angle pattern; (c) reciprocal lattice with *hk* values for the observed reflections; (d) position of the maximum of the diffuse scattering (black arrow) with respect to reciprocal 2D lattice (black) and orientation of the molecules in the real lattice (red).

The X-ray diffraction pattern of a surface-aligned sample in the $\mathrm{Col_{ob}}$ phase of compound **1i** is characterized by a diffuse scattering in the wide angle region and sharp BRAGG-reflections in the small angle region (Fig. 5.21a-c). From the χ-scan of the wide angle region a synclinic tilt of the molecules is evident with a tilt angle of 46° with respect to the *a*-axes of the real lattice.

The interpretation of the small-angle BRAGG-reflections as resulting from a two-dimensional oblique lattice (a = 3.20 nm; b = 5.00 nm and γ = 110°) is shown in Figure 5.21c. The orientation of the molecules in the real lattice is shown in Figure 5.21d.

The Col_{ob} phase of compound **1i** shows an electro-optical switching on application of a relatively high threshold electric field of about 25 $V\mu m^{-1}$. Under an electric field the birefringence (and therefore the interference colour) is decreasing and the stripes within the texture disappear. The switched states are independent of the polarity of the external applied electric field (Fig. 5.22b). Indeed, in the circular domains, where the extinction brushes are inclined with respect to the crossed position of the polarisers, the position of the extinction crosses does not change, neither on terminating the field nor on reversing the field (Fig. 5.22b,c). These observations suggest that the chirality of the layers switches by collective rotation of molecules around their long axes on reversing the applied field. This switching is accompanied by a current response with only one sharp current peak in the half period of a triangular wave voltage (Fig. 5.22d), also at low frequencies (down to 0.1 Hz) indicating a FE ground state (Ps = 380 nC cm^{-2}). This single peak is a first indication of a FE switching process, but this is not a clear proof of ferroelectricity. If the relaxation to the AF ground state would be too slow, then the two polarisation current peaks of an AF switching can coalesce to only one peak. Therefore, it was proposed to use a modified triangular wave field, where a delay is introduced at zero voltage. Also under these conditions, using non-coated ITO cells, independent of the temperature and cell thickness (5, 10 μm), only one peak is observed in the modified triangular wave field (Fig. 5.22e). This indicates that a bistable switching takes place, and that switching always occurs after zero-voltage crossing of the applied field.

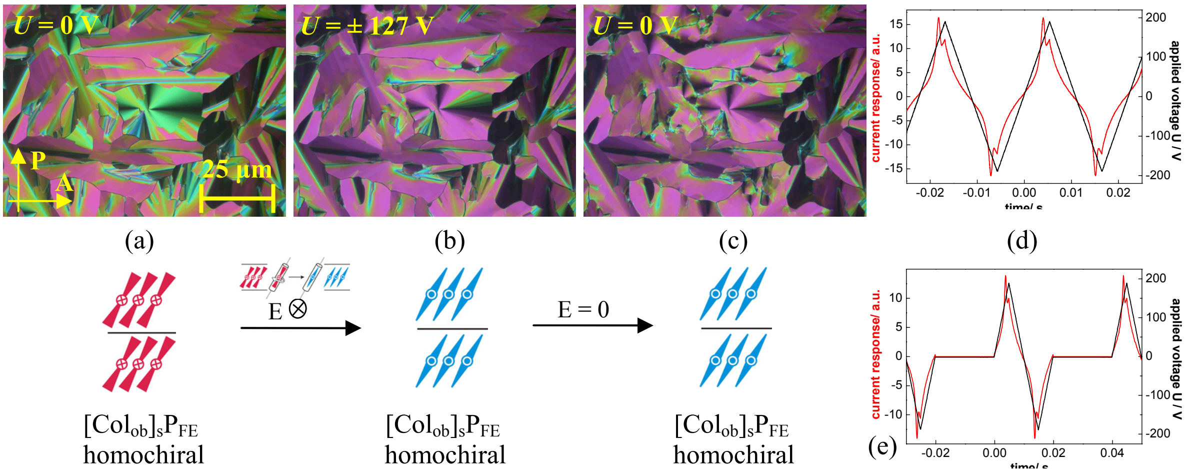

Figure 5.22: Electro-optical investigations of the $Col_{ob}P_{FE}$ phase of compound **1i** under a d.c. electric field in a 6 μm polyimide-coated ITO cell at 125 °C; textures observed between crossed polarisers in the same region of the sample at (a) U = 0 V, before starting the experiment; (b) U = ± 127 V; (c) U = 0 V; (a-c, down) models of the organization of the molecules in the FE states, considering one column as a fragment of a smectic layer; (d,e) FE switching current response obtained by applying (d) a simple and (e) a modified triangular-wave field (U = 380 V_{pp}, f = 5 Hz, R = 5 kΩ, T = 125 °C; P_S = 380 nC cm^{-2}).

The proposed models of the organization of the molecules in the FE states ($[Col_{ob}]_sP_{FE}$) of the $Col_{ob}P_{FE}$ phase are shown in Figure 5.22. In the ground-state the molecules are organized in ribbons with alternating polar direction along direction a. The size of the crystallographic cell of the $\mathrm{Col_{ob}P_{FE}}$ phase, seems to be sufficiently large (about 4 molecules per cross-section) to consider one column as a fragment of a smectic layer. It follows from X-ray investigations and electro-optical measurements that this phase is a $\mathrm{Col_{ob}}$ phase which is synclinic and FE, $\mathrm{[Col_{ob}]_sP_{FE}}$ phase.

Since the molecular conformation of this '*banana-calamit*' compound is unknown and a lot of different shapes can be assumed, the construction of an appropriate model for the organization of the molecules in the $\mathrm{Col_{ob}P_{FE}}$ phase is very difficult and has to be a speculative one. Based on the special features of the molecular structure we made the assumptions that the parameter *a* should correspond to the width of the ribbons, whereas *b* is associated with the thickness of the ribbons. The molecules are tilted with respect to the *a* axes of the real lattice (tilt angle 46°). The first assumption is that a splay of polarisation is involved in the stabilization of the 2D lattice.[102] A splay-modulated arrangement of ribbons, as shown in Figure 5.23, with an overall synclinic correlation between adjacent ribbons ($\mathrm{SmC_sP_{FE}}$–like along direction *b* and an AF organization along direction *a* seems to be the most reasonable structure for the $\mathrm{Col_{ob}P_{FE}}$ phase of compound **1i.** In the $\mathrm{Col_{ob}P_{FE}}$ phase of compound **1i** the splay seems to be relatively weak, as it can be removed under an electric field, leading to a FE switching smectic phase. Also, the formation of an oblique lattice instead of a rectangular one is in line with a relatively weak splay of polarisation. The proposed model for the organization of the molecules in the $\mathrm{Col_{ob}P_{FE}}$ phase, shown in Figure 5.23, is already described by KEITH *et al.* in reference.[212] The molecules are organized in ribbons with a reversal of the polar direction along direction *a* in the proposed ground-state structure (Fig. 5.23a). The field-induced reorganization of the molecules in ribbon phases usually takes place by collective rotation around the long axis because the inter-ribbon interfaces hinder rotation on a cone. This reorganization would lead to a synpolar (FE) ribbon structure where the synclinic tilt of the molecules is retained.

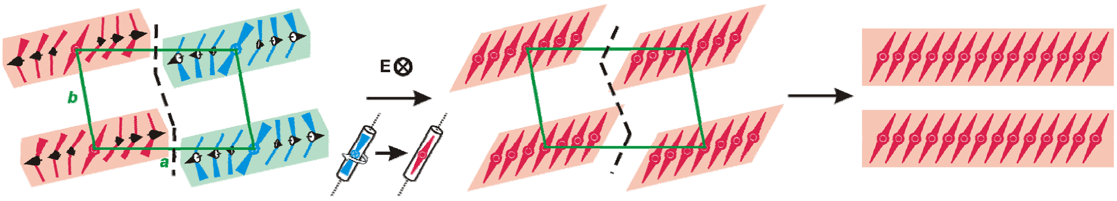

(a) (b) (c)

Figure 5.23: (a) Proposed model of ground-state organization in the $\mathrm{Col_{ob}P_{FE}}$ phase with polarisation splay between adjacent ribbons; (b) the field-induced synpolar ribbon structure is unstable due to the unfavorable interfaces between the ribbons (broken line); (c) the field-induced non-modulated smectic phase without unfavorable interfaces between the ribbons is formed instead ($\mathrm{SmC_sP_{FE}}$–like phase). This proposed model for the organization of the molecules in the $\mathrm{Col_{ob}P_{FE}}$ phase is already described in reference.[212]

However, there would be unfavourable steric interactions at the interfaces between the ribbons (Fig. 5.23b) in such a modulated smectic phase with a synpolar organization of the molecules in adjacent ribbons (along direction *b*). Because of this unfavourable steric interactions, these interfaces are unstable and a non-modulated smectic phase without these interfaces is formed instead (Fig. 5.23c). Practically, a field-induced transition to a synclinic and synpolar smectic phase ($\mathrm{SmC_sP_{FE}}$) takes place. Such field-induced transitions were reported previously also for other polarisation-modulated smectic phases (for $\mathrm{B_7}$-type phases,[213] some examples of field-induced Col to Sm transitions.[102,209,214]). The high threshold voltage (25 $\mathrm{V\mu m^{-1}}$) required for FE switching and the relatively high polarisation value (P_S = 380 nC cm^{-2}) are strong arguments that a field-induced change of the mesophase structure takes place over the switching process. The construction of an appropriate model for the organization of the molecules in the $Col_{ob}P_{FE}$ phase is very difficult and this model of the organization of the molecules is just a speculative one.

5.1.1.4 The nematic and smectic SmC$_c$ phases of dimer 1j with *m* = 12

Compound **1j** (*m* = 12) exhibits two monotropic mesophases. The high-temperature phase could be easily identified as a nematic phase by its characteristic texture. The nematic phase shows over the whole temperature range chiral domains of opposite handedness, as already described in the chapter 5.1.1.2.[64,205] The brightness of the (+) and (–) domains (corresponding to the optically active domains in the Fig. 5.24a-c) is reversed by changing the direction of the polarisers.

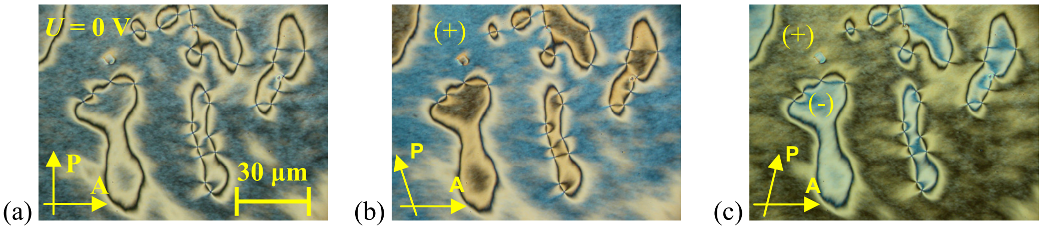

Figure 5.24: Textures of nematic phase of compound **1j** at 124 °C in a 5µm non-coated ITO cell at *U* = 0 V observed in the same region of the sample (a) between crossed polarisers and by rotating one polariser by 15° (b) clockwise and (c) anticlockwise from the crossed position.

On further cooling the schlieren texture turned into fans with features characteristic of N-to-SmA or N-to-SmC transition. This new liquid-crystalline phase separates from the nematic phase in the form of *batônnets* (Fig. 5.25a) which then coalesce and form a fan-shaped texture (Fig. 5.25b). It was impossible to obtain a homeotropic texture either by shearing or by surface treatment, which implies a phase with tilted molecules, which can be characterised as a SmC$_c$ phase. Shearing this specimen led to a grey, schlieren-like texture with singularities of $s = \pm1$ and $s = \pm1/2$ (Fig. 5.25c) which have also been observed in SmCP$_{AF}$, intercalated SmC phases of mesogenic twins or the B$_6$ phase of bent-core mesogens.[3,47,96,116,118,122,215] The occurrence of such singularities is attributed to an opposite tilt direction of the mesogenic groups between adjacent layers.

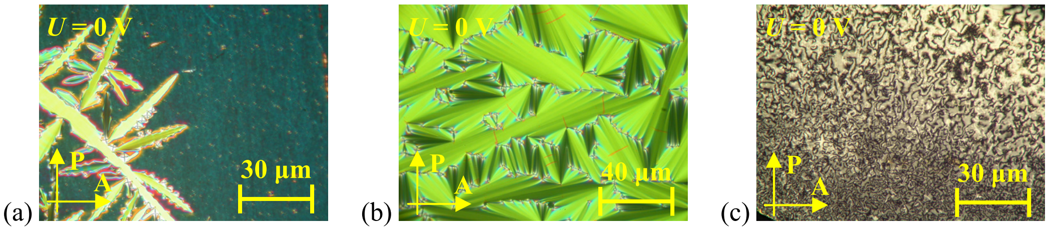

Figure 5.25: Textures of SmC$_c$ phase of compound **1j**: (a,b) in a 6 µm polyimide-coated ITO cell at *U* = 0 V (a) at 121 °C on growing from the N phase (the dark blue domains represent N phase regions) and (b) at 119 °C; (c) schlieren texture at 119 °C between two untreated glass slides obtained after shearing the sample.

X-ray measurements on the two mesophases of the compound **1j** were performed by applying a magnetic field of about 1 T. For the nematic phase the results confirm the absence of a layer structure, but the existence of cybotactic smectic groups is clearly proven on the base of well-oriented samples. The X-ray pattern shows a diffuse dumb-bell like scattering maximum in the small angle region and a diffuse wide angle scattering located around the equator, see Figure 5.26a,b. The diffuse, small-angle scattering in the nematic phase can be attributed to cybotactic groups of the SmC-type representing fluctuating arrays of molecules with a short-range order of the same type as the long-range order in the low-temperature $\mathrm{SmC_c}$ phase. The X-ray diffraction pattern of the low-temperature mesophase of compound **1j** (Fig. 5.26c-e) is characterized by a diffuse scattering in the wide angle region and sharp equidistant BRAGG-reflections in the small angle region. Only one layer reflection corresponding to a periodicity smaller than half the molecular length appears in the small-angle region (d = 2.28 nm). This periodicity strongly indicates an intercalated structure like B_6 / $\mathrm{SmC_c}$ phase. The molecular length (L = 6.7 nm) is measured from CPK models (from $\mathrm{MM_2}$-optimized models, using Chem3D, Cambridge software corporation), for fully extended chains, and assuming a zigzag shape for compounds with *even*-membered spacers. In addition, the molecules are tilted in the layers, and the tilt angles are estimated to be about 24° ($\mathrm{SmC_c}$ phase). On the other hand, four broad, diffuse scattering peaks are observed in the wide-angle region, suggesting liquid-like in-plane order.

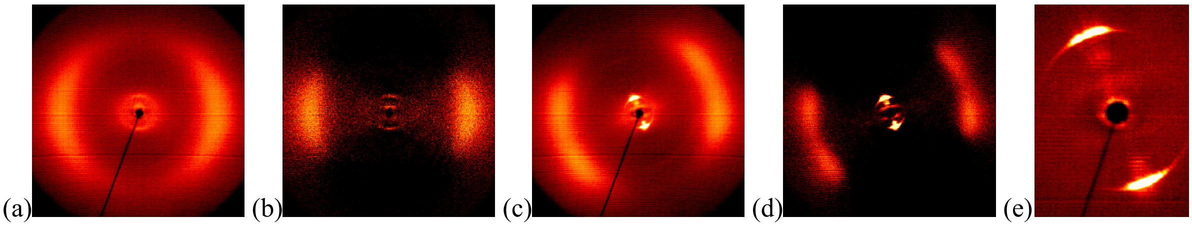

Figure 5.26: XRD patterns of an aligned sample of compound **1j** in the magnetic field on cooling; (a,b) XRD patterns of the nematic phase at 123 °C: (a) original pattern; (b) the same XRD pattern, but the intensity of the isotropic liquid is subtracted; (c-e) XRD patterns of the $\mathrm{SmC_c}$ at 119 °C: (c) original pattern; (d) the same XRD pattern, but the intensity of the isotropic liquid is subtracted; (e) small angle region.

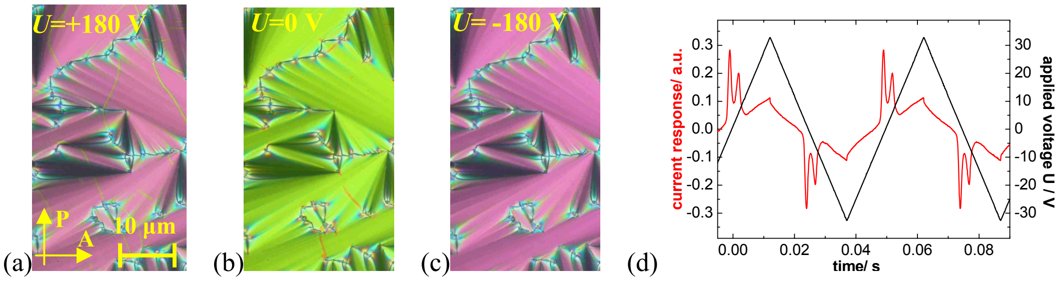

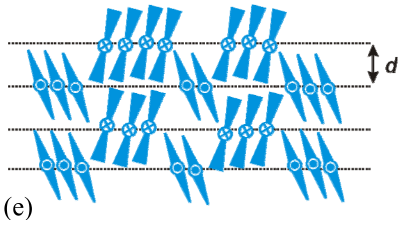

Figure 5.27: Electro-optical investigations of the $\mathrm{SmC_cP_{AF}}$ phase of compound **1j** in a 6 µm polyimide-coated ITO cell at 119 °C; textures observed between crossed polarisers in the same region of the sample under a d.c. electric field; (a,c) $U = \pm 180$ V and (b) $U = 0$ V; (d) AF switching current response obtained by applying a triangular-wave field ($U = 100\ \mathrm{V_{pp}}$, $f = 3$ Hz, $R = 5$ kΩ, $T = 119$ °C, $P_S = 300$ nC cm^{-2}); (e) model of the organisation of the molecules in the ground state.

The application of an electric field of 15 Vμm^{-1} on the SmC$_c$ phase leads to an electro-optical switching with a current response indicating an AF ground state, i.e. two polarisation current peaks per half period were recorded (P_S = 300 nC cm^{-2}), see Figure 5.27d. During the switching process the birefringence is decreasing, but the position of the defects do not change, neither on terminating nor on reversing the field. (Fig. 5.27a-c). This confirms a switching by rotation around the long axis, which changes the polar direction without changing the tilt direction of the molecules.

It follows from the X-ray investigations and the electro-optical measurements that this phase is a SmC$_c$P$_{AF}$ phase. However, it is not easy to imagine how titled molecules intercalate forming a phase in which bent-core units, calamitic moieties, terminal chains and the spacers are mixed randomly and the layer spacing is approximately one third of the molecular length and how these molecules are reorganized on switching under an applied electric field. Further experimental examinations are necessary.

5.1.2 The dimer series 2 – 6

The next point of our systematic investigation is the effect of the variation of the length of the spacer in dimers with different lengths of the terminal chains attached to the calamitic mesogenic unit and to the bent-core mesogenic moiety in dimer series **2** – **6**. To allow an appropriate comparison of the mesophase behaviour from this new perspective, the compounds **2** – **6** are listed in groups of two or three compounds which have a constant length of the *alkyloxy* chain attached to the bent-core unit (*n*) and resp. to the calamitic part (*p*), however the length of the spacer (*m*) varies (see Table 5.3.). For comparative purposes the mesophase behaviour of the dimer series **1** is included in Figure 5.28. The dimer series **1** – **6** are presented on increasing the spacer length (*m*) and the terminal chain lengths of the bent-core units (*n*) and of the calamitic moieties (*p*). This is the reason why the series **2** is presented above series **1** in Figure 5.28. The mesophase types and transition temperatures together with the associated transition enthalpies and lattice parameters for the series **2** – **6** are given in Table 5.3 and Figure 5.28. All homologues belonging to these five new series exhibit liquid crystalline behaviour. The compounds with an *even*-numbered spacer display various columnar or smectic phases, in addition to a nematic phase. Nearly all compounds with an *odd* spacer exhibit one columnar mesophase, except compound **2c**, which exhibits an enantitropic SmC$_c$P$_{FE}$ phase. The mesophases formed by the *even*-membered compounds show higher mesophase stability, as expected. Increasing the spacer length from m = 3 to m = 6 give rise to an increase of the mesophase stability. However, increasing the spacer length from m = 6 to m = 11 give rise to a reduction of the mesophase stability.

Table 5.3: Transition temperatures [°C], mesophase type, transition enthalpy values [kJ/mol], layer spacing *d* [nm], tilt angle τ of the molecules [°] with respect to the layer normal in SmC phases and with respect to the normal to *a* in Col phases, lattice parameters (*a*, *b*, *γ*) [nm, °] and P_S values [*nC*/cm^2] of dimer series **2** – **6**.[a]

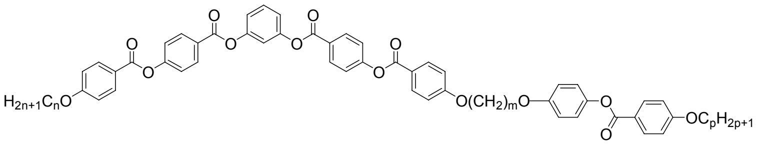

Comp	*n*	*m*	*p*	Transitions temperatures [°C] Δ*H* [kJ·mol^{-1}]	Phase type	Lattice parameters					P_S *nC/cm²*
						d [nm]	τ [°]	*a* [nm]	*b* [nm]	γ [°]	
2a	8	3	6	Cr 166 (Col_{ob} 134) I *82.2 25.2*	Col_{ob}		50	2.73	4.11	112	-
2b	8	6	6	Cr 145 (M_1 125 SmC_sP_{FE} 130) N 151 I *76.4 0.5 13.4 1.6*	N SmC_sP_{FE} M_1 [c]	 5.80 -[c]	 26 -[c]	-[c]	-[c]	-[c]	 150 -[c]
2c	8	11	6	Cr 109 SmC_cP_{FE} 147 I *46.1 23.3*	SmC_cP_{FE}	2.11	14	-	-	-	230
3a	16	3	6	Cr 136 ($Col_{ob}P_{FE}$ 129) I *60.9 22.9*	$Col_{ob}P_{FE}$		39	4.74	4.74	97.4	450
3b	16	6	6	Cr 150 (Col_x 126.5 N 142) I *65.0* -[b] *1.4*	N Col_x [c]		-[c]	-[c]	-[c]	-[c]	-[c]
3c	16	11	6	Cr 119 ($Col_{ob}P_{AF}$ 109) I *79.4 21.9*	$Col_{ob}P_{AF}$		37	4.00	5.38	94.9	530
4a	12	6	12	Cr 140 (Col_x 115.5 N 131) I *86.3* -[b] *1.6*	N Col_x [c]		-[c]	-[c]	-[c]	-[c]	-[c]
4b	12	11	12	Cr 126 (Col_rP_{AF} 121) I *57.0 7.4*	Col_rP_{AF}		29	16.1	6.76	90	450
4c	12	12	12	Cr 117 (M_3 102 M_2 110 N 114) I *69.7 0.3 13.1 1.5*	N M_2,M_3 [c]	-[c]	-[c]	-[c]	-[c]	-[c]	-[c]
5a	12	2	16	Cr 151 (M_4 121 $SmC_s'P_{AF}$ 144) SmC_sP_{AF} 160.5 N 161 I *87.5 12.0 12.4 6.3* -[b]	N SmC_sP_{AF} $SmC_s'P_{AF}$ M_4[c]	 4.88 4.83 -[c]	 41 36 -[c]	-[c]	-[c]	-[c]	 550 770 -[c]
5b	12	6	16	Cr 139 ($SmCP_{AF}$[*] 128) SmC_sP_{AF} 141 N 141.5 I *88.7 14.7 1.5 2.5*	N SmC_sP_{AF} $SmCP_{AF}$[*]	 5.56 -[c]	 32 -[c]				 580 830
5c	12	11	16	Cr 125 Col_rP_{AF} 130 I *40.8 27.2*	Col_rP_{AF}		0	13.7	7.15	90	470
6a	16	6	12	Cr 138 ($SmXP_{AF}$ 122 SmC_sP_{AF} 125 N 131) I *87.7 4.3 1.5 5.4*	N SmC_sP_{AF} $SmXP_{AF}$	 -[c] -[c]	 -[c] -[c]				 490 850
6b	16	11	12	Cr 130 (Col_rP_{AF} 125) I *74.7 34.7*	Col_rP_{AF}		0	15.3	7.11	90	770

[a] Transition temperatures (°C) and enthalpy values [kJ/mol] of dimer series **2** – **6** were taken from the second DSC heating scans (10 Kmin^{-1}); values in parentheses indicate monotropic mesophases, in this case the transition temperatures and enthalpy values were taken from the first DSC cooling scans and the transition temperatures were checked by polarising microscopy; [b] the transition is not detectable on DSC and the transition temperature value is determined by polarising microscopy; [c] could not be determined due to rapid crystallization of the sample; the M phases are unidentified phases which could not be fully investigated because of their fast crystallization immediately after formation.

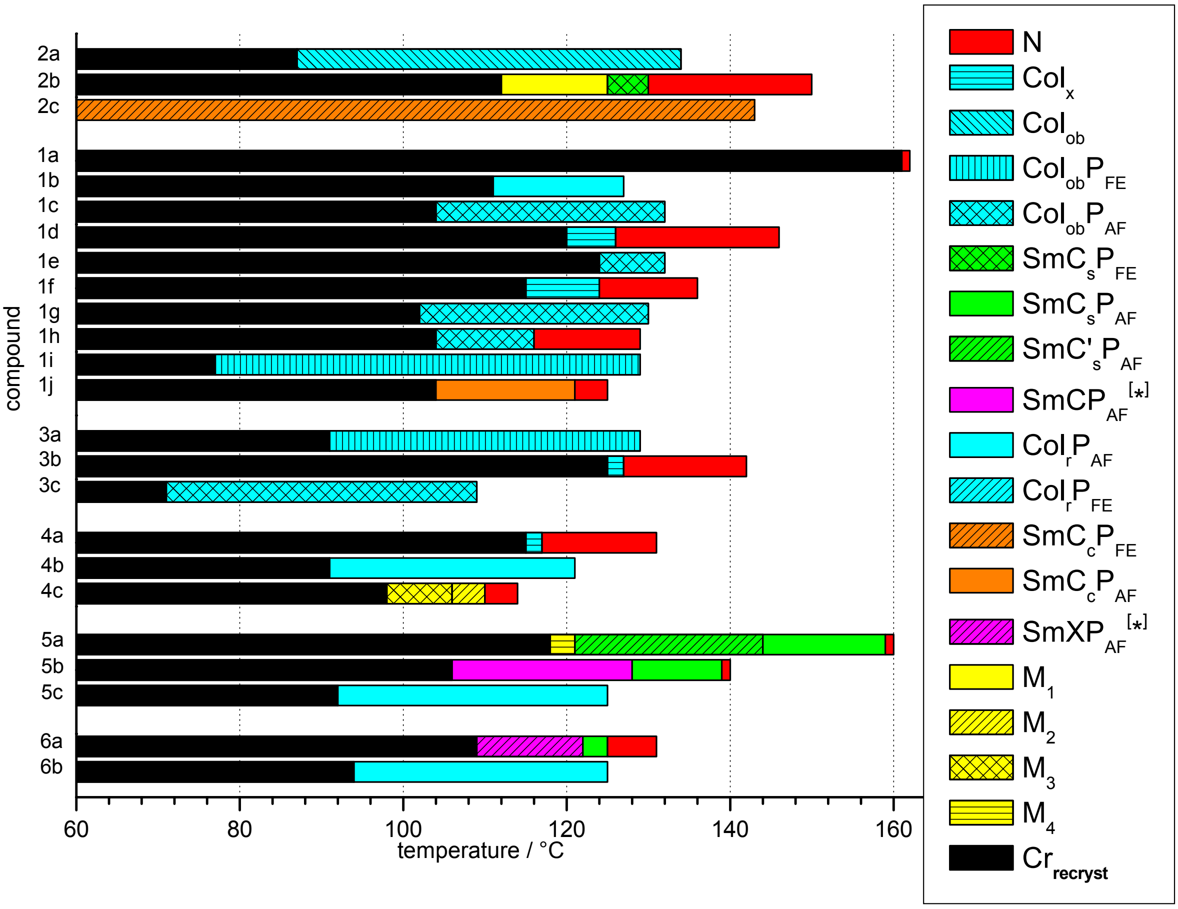

Figure 5.28: Transition temperatures (°C) of dimers **1**–**6**, taken from the first DSC cooling scans (10 Kmin^{-1}).

The study of the structure-property relationship for the dimers with $p = 6$ (**2a**, **3a**, **1i** and **3c**) revealed that on increasing the length of the terminal chain n on the bent-core moiety results in a slight increase of the values of the parameters a and b of the Col$_{\mathrm{ob}}$ phases. Meantime, the value of the oblique angle γ is slightly decreasing for these dimers. For the dimers with $p = 12$ (**4b** and **6b**), the parameter a of the Col$_\mathrm{r}$ phases are slightly decreasing, while parameter b is slightly increasing. The number of the molecules in the unit cell in the Col$_{\mathrm{ob}}$ phases with $p = 6$ is increasing, while for the dimers with $p = 12$ is slightly decreasing with increasing the length of the terminal chain on the bent-core moiety. On increasing the spacer length, m, the parameter a and the oblique angle γ of the Col$_{\mathrm{ob}}$ phases for dimers **3a** and **3c** are slightly decreasing, while parameter b is slightly increasing. The number of the molecules in the unit cell in the Col$_{\mathrm{ob}}$ phases is also slightly decreasing with increasing the spacer length. On increasing the length of the terminal chain of the calamitic unit, p, the parameter a of the Col$_\mathrm{r}$ phases for dimers **4b** and **5c** is decreasing, while parameter b is slightly increasing. The number of the molecules in the unit cell in the Col$_\mathrm{r}$ phases is also decreasing with increasing the spacer length. The correlation of a and n_{cell} speaks for the molecular being packed along a in one ribbon (b is associated to the molecular length). In the following the physical properties of the dimer series **2** – **6** will be discussed in the subchapters 5.1.2.1 to 5.1.2.4.

Table 5.4: X-ray diffraction data from aligned samples of the Col phases of compounds **1** – **6** and an estimate of the number of molecules in the cross section of the ribbons within the corresponding Col phases.

Comp.	n	m	P	T [°C]	Phase type	Parameter [nm]	$V_{\mathrm{mol,cr}}$[b] [nm^3]	$V_{\mathrm{mol,is}}$[c] [nm^3]	V_{cell}[d] [nm^3]	$n_{\mathrm{cell,cr}}$[e]	$n_{\mathrm{cell,is}}$[f]	$n_{\mathrm{cell,LC}}$[g]
2a	8	3	6	132	$\mathrm{Col_{ob}}$	$a = 2.73$ $b = 4.11$ $\gamma = 111.6$	1.376	1.751	5.42	3.94	3.10	3.52
1b	12	3	6	124	$\mathrm{Col_rP_{AF}}$	$a = 7.57$ $b = 5.51$	1.475	1.877	21.69	14.70	11.55	13.13
3a	16	3	6	123	$\mathrm{Col_{ob}P_{FE}}$	$a = 4.74$ $b = 4.74$ $\gamma = 97.4$	1.575	2.005	11.59	7.36	5.78	6.57
1i	12	11	6	125	$\mathrm{Col_{ob}P_{FE}}$	$a = 3.20$ $b = 5.00$ $\gamma = 110.0$	1.674	2.130	7.82	4.67	3.67	4.17
3c	16	11	6	104	$\mathrm{Col_{ob}P_{AF}}$	$a = 4.00$ $b = 5.38$ $\gamma = 94.9$	1.773	2.257	11.15	6.29	4.94	5.61
4b	12	11	12	120	$\mathrm{Col_rP_{AF}}$	$a = 16.06$ $b = 6.76$	1.823	2.320	56.45	30.97	24.33	27.65
5c	12	11	16	123	$\mathrm{Col_rP_{AF}}$	$a = 13.70$ $b = 7.15$	1.922	2.446	50.94	26.50	20.83	23.66
6b	16	11	12	120	$\mathrm{Col_rP_{AF}}$	$a = 15.26$ $b = 7.11$	1.922	2.446	56.42	29.35	23.07	26.21

[a] Lattice parameter with an error of the calculated parameters in the order of 0.1 nm; [b],[c],[d],[e],[f],[g] for calculation of these values see Table 5.2 in chapter 5.1.1.

5.1.2.1 The smectic $\mathrm{SmC_sP_{FE}}$ phase of dimer 2b

The mesophase behaviour of the dimer series **2** (n = 8; p = 6) is very complex (see Table 5.3). The dimer **2a** with the shortest spacer length (m = 3) exhibits a $\mathrm{Col_{ob}}$ phase, while dimer **2c** (m = 11) shows an intercalated smectic $\mathrm{SmC_cP_{FE}}$ phase. The homologue **2b** (m = 6) exhibits three different mesophases: an enantiotropic nematic and two monotropic smectic phases. The nematic phase showed typical marbled textures (Fig. 5.29a) and presents chiral domains of opposite handedness over the whole temperature range, as already described in chapter 5.1.1.2. Below this nematic phase two monotropic smectic phases appeared. The high-temperature smectic phase exhibits a fan-shaped texture (Fig. 5.29b). The transition N-SmC at 130 °C is coupled with an enthalpy change of 13.4 kJ mol^{-1}. At 125 °C a clear change of the texture occurs characterized by a change of the birefringence and the appearance of additional stripes (Fig. 5.29c). The corresponding transition enthalpy is rather low (0.5 kJ mol^{-1}).

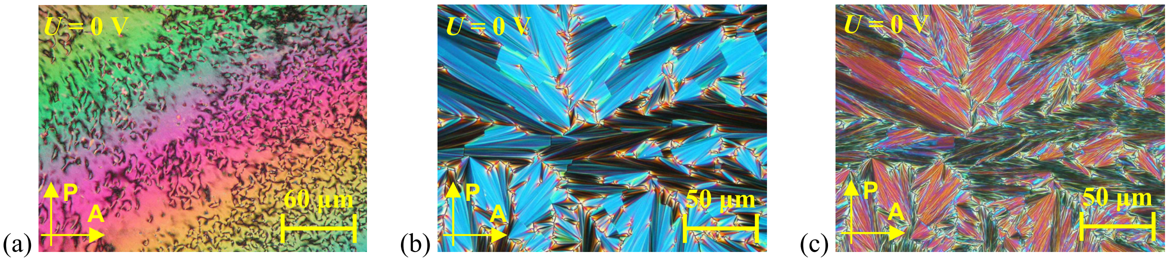

Figure 5.29: Textures of mesophases of dimer **2b** on cooling: (a) N phase at 150 °C; (b) high-temperature smectic phase at 130 °C; (c) low-temperature smectic phase at 125 °C (same region of the sample as in (b)).

X-ray measurements performed on the high-temperature mesophase of compound **2b** showed the scattering typical of a nematic phase when aligned in the magnetic field on cooling (Fig. 5.30a). The measurements at 127 °C confirmed the presence of a SmC phase and show strong small angle reflections from which a layer spacing of d = 5.76 nm could be determined (see Table 5.3 and Fig. 5.30b-d). An average tilt angle $\tau = 26°$ of the molecular long axis with respect to the layer normal can be calculated from the position of the maxima of the outer diffuse scattering in the smectic phase. The distribution of the diffuse scattering points to a synclinic tilt of the molecules. The effective molecular length L_{eff} may be calculated from these experimental results to $L_{eff} = d/\cos\tau = 6.4$ nm. Based on these experimental evidences this SmC phase was assigned as SmC$_s$ phase. On lowering the temperature to 125 °C, the second smectic phase crystallized immediately and further investigations were impossible. This phase was assigned as M$_1$ phase.

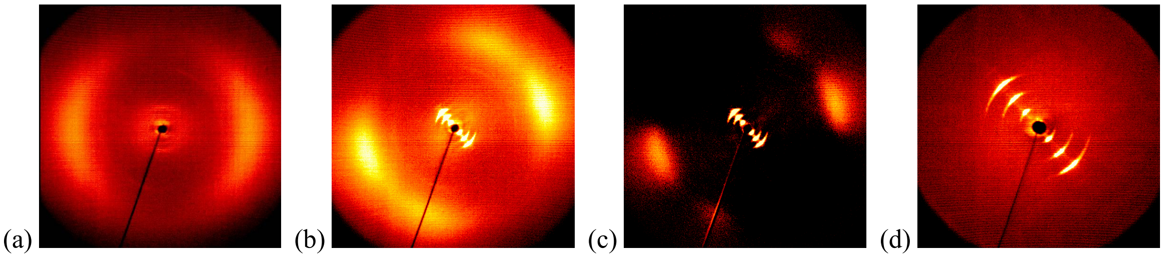

Figure 5.30: XRD patterns of an aligned sample of compound **2b** in the magnetic field on cooling: (a) nematic phase at 140 °C; (b-d) SmC$_s$ phase at 127 °C; (b) original scattering; (c) the same XRD pattern, but the intensity of the isotropic liquid is subtracted; (d) small angle region.

The nematic phase of compound **2b** shows the same unusual optical and electro-optical properties as described in section 5.1.1.2 for dimer series **1**. The SmC$_s$ phase shows an electro-optical response. Applying a sufficiently high electric field (10 Vμm^{-1}) a smoother fan-like texture is formed which is independent of the polarity of the applied field (Fig. 5.31a,c). If the field is removed the texture remains nearly unchanged, only the birefringence is slightly changed (Fig. 5.31b). This switching is accompanied by a current response with only one peak per half period of the applied field indicating a FE ground state (P_S = 150 nC cm^{-2}, Fig. 5.31d). Also only one peak per half period of the applied field could be observed under a modified triangular-wave field (when a delay is introduced at zero voltage), using non-coated ITO cells and independent of the cell thickness or glass coating (5, 6 or 10 µm).

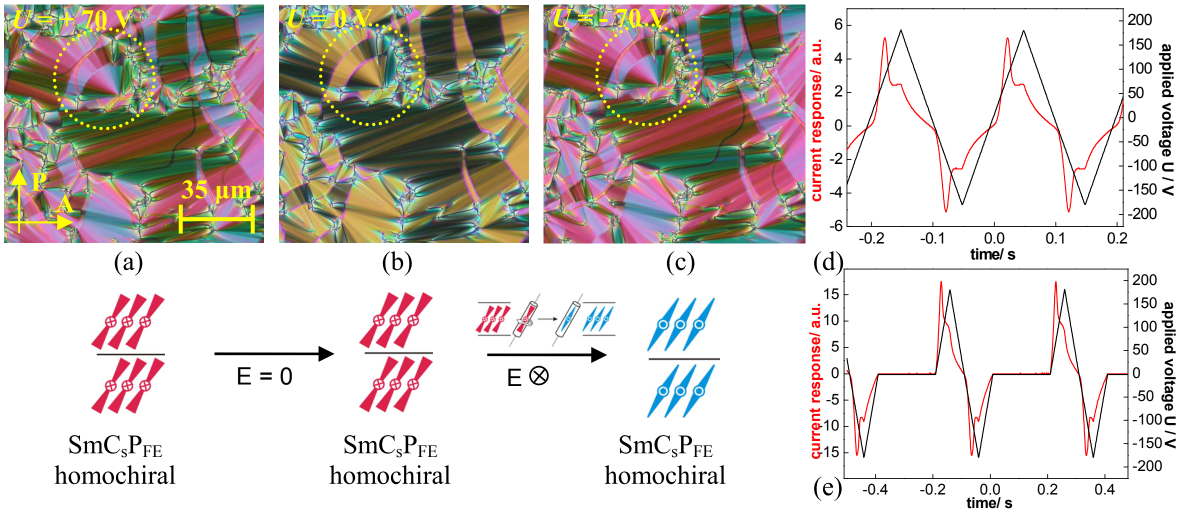

Figure 5.31: Electro-optical investigations of the SmC_sP_{FE} phase of compound **2b**: (a-c) textures observed between crossed polarisers in the same region of the sample in a 5 µm non-coated ITO cell under a d.c. electric field at 127 °C: (a,c) $U = \pm 70$ V; (b) $U = 0$ V; (a-c, down) models of the organization of the molecules in the FE states in the bistable switching process; (d,e) FE switching current response obtained by applying a simple (d) and a modified (e) triangular-wave voltage (10 µm non-coated ITO cell, $U = 360$ V_{pp}, $f = 5$ Hz, $R = 5$ kΩ, $T = 127$ °C, $P_S = 150$ nC cm^{-2}).

The extinction directions of the half circular domains make an angle of ~ 26° with the directions of the crossed polarisers indicating that the SmC_s phase has a tilted organization (Fig. 5.31a-c), as already found from XRD investigations. If the first FE ground state (Fig. 5.31a) is switched to the second FE state or *vice versa*, the extinction directions do not change. Only the birefringence is changed (Fig. 5.31c). Furthermore, this effect is independent of the polarity of the applied field. This finding suggests that the FE ground state as well as the switched FE states have a synclinic tilt and the switching corresponds to the transition from a SmC_sP_{FE} state to a SmC_sP_{FE} state. These observations suggest that the chirality of the layers switches by collective rotation of molecules around their long axes on reversing the applied field.

5.1.2.2 The mesophase behaviour of dimer series 3

All the dimers of the series **3** ($n = 16$; $p = 6$) present liquid crystalline properties (see Table 5.3). The dimers with an *odd*-spacer display polar oblique columnar phases. The dimer **3a** ($m = 3$) exhibits a $Col_{ob}P_{FE}$ phase, while the dimer **3c** ($m = 11$) forms a $Col_{ob}P_{AF}$ phase. The *even* member **3b** ($m = 6$) possesses a N-Col_x phase sequence.

5.1.2.3 The mesophase behaviour of dimer series 4

All compounds in the series **4** ($n = 12$; $p = 12$) exhibit monotropic liquid crystalline phases. Dimer **4b** with an *odd* spacer ($m = 11$) displays a Col_rP_{AF} phase while the *even* member **4a** ($m = 6$) forms a nematic and a Col_x phase (see Table 5.3). The homologue **4c** ($m = 12$) presents a N-

M_2-M_3 phase sequence. The low-temperature mesophases M_2 and M_3 are crystallizing fast and no further investigations were possible.

The dimer **4b** (m = 11) shows some beautiful and exotic textural features, independent on the glass surface preparation. On slowly cooling the isotropic liquid, spiral or double spiral nuclei arise which coalesce to a variety of optical textures such as striped focal conics, banana-leaf like textures, ribbon-like texture, spherulitic texture and circular domains, where low birefringent domains coexist with highly birefringent domains (Fig. 5.32). These textures remember of a B_7 phase,[24,32,36,61,70,101,102] or B_7' phase.[60,72,102,106]

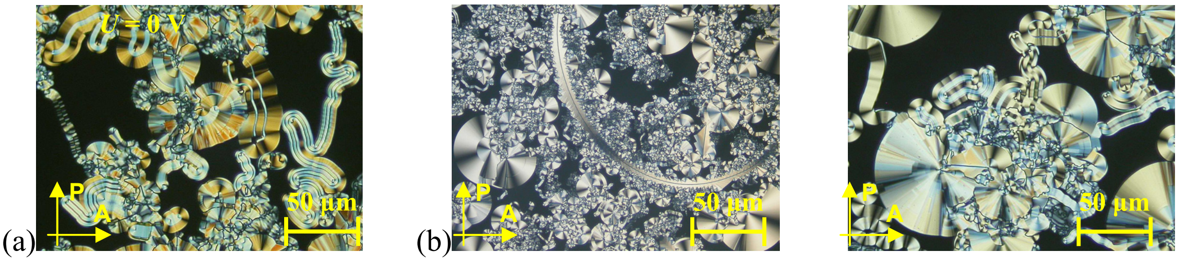

Figure 5.32: Textures of Col_r phase of compound **4b** at 121 °C at U = 0 V, on cooling from the isotropic state in a 6 µm polyimide-coated ITO cells phase (dark areas are residues of the isotropic liquid state).

The X-ray diffraction pattern is characterized by a diffuse scattering in the wide angle region and sharp BRAGG-reflections in the small angle region (Fig. 5.33a, b). The small-angle reflections can be indexed to a centred 2D rectangular lattice, with the lattice parameters a = 16.06 nm and b = 6.76 nm (see Tabel 5.3 and Fig. 5.33c). From the χ-scan of the wide angle region we could estimate a tilt angle of the molecules with respect to the normal to a-axis of the real lattice of 29°. The alignment of the long molecular axes for one preferred orientation in the fiber-like disordered sample is shown in Figure 5.33d.

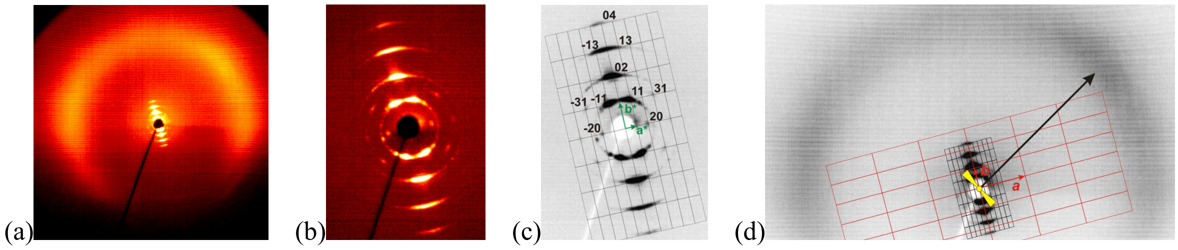

Figure 5.33: XRD patterns of a surface-aligned sample of the Col_r phase of compound **4b** at 118 °C: (a) original pattern; (b) pattern of the small-angle region; (c) reciprocal lattice with *hk* values for the observed reflections; (d) position of the maximum of the diffuse scattering (black arrow) with respect to reciprocal 2D lattice (black) and orientation of the molecules in the real lattice (red).

On applying a triangular-wave electric field above a threshold voltage of 10 V μm^{-1} the Col_r phase is switchable, i.e. two polarisation current peaks per half period were recorded indicating an AF ground state (P_S = 450 nC cm^{-2}, see Fig. 5.34e). This switching process was additionally confirmed by optical investigations. The ground state, before applying an electric field is characterized by highly birefringent stripes running parallel to the smectic layers, indicating a multidomain structure of this phase (the effect arose from a racemic nature of the domains, as a result of an alternating chirality, see Fig. 5.34a). In the ground state, the extinction crosses of the circular domains are inclined to the directions of the crossed polarisers, proving a synclinic tilted organization of the molecules (Fig. 5.34a). On applying an electric field the extinction crosses of the synclinic domains rotate into a position parallel to the crossed polarisers, as characteristic for an anticlinic organization with an equal number of layers with opposite tilt direction, corresponding to a [Col$_r$]$_a$P$_{FE}$ phase (Fig. 5.34b,d).

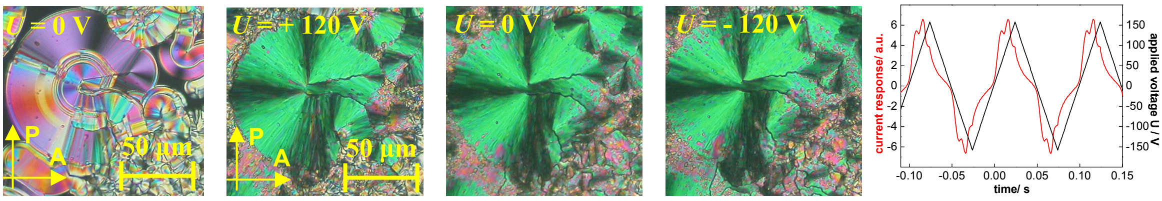

(a) [Col$_r$]$_s$P$_{AF}$ (b) [Col$_r$]$_a$P$_{FE}$ (c) ([Col$_r$]$_s$)$_a$P$_{AF}$ (d) [Col$_r$]$_a$P$_{FE}$ (e)

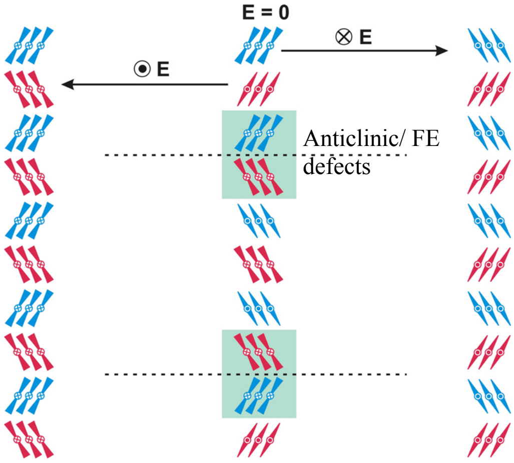

Figure 5.34: Electro-optical investigations of the Col$_r$P$_{AF}$ phase (racemic [Col$_r$]$_s$P$_{AF}$ phase) of compound **4b**: (a-d) textures observed between crossed polarisers in the same region of the sample in a 10 µm polyimide-coated ITO cell under a d.c. electric field at 118 °C; below: models showing the reorganisation of the molecules during the switching process around a cone (in analogy to references[24,36,216]), considering one column as a fragment of a smectic layer; (a) U = 0 V, AF ground state: [Col$_r$]$_s$P$_{AF}$ state; (b) U = + 120 V, field-induced FE state: [Col$_r$]$_a$P$_{FE}$ state; (c) U = 0 V, AF ground state composed of domains with opposite tilt direction and anticlinic/FE boundaries between them (areas with blue background): ([Col$_r$]$_s$)$_a$P$_{AF}$ state; (d) U = - 120 V, FE state with opposite polarity: [Col$_r$]$_a$P$_{FE}$ state; (e) AF switching current response obtained by applying a triangular-wave voltage (U = 315 V$_{pp}$, f = 10 Hz, R = 5 kΩ, T = 109 °C, P_S = 450 nC cm^{-2}).

At first sight, these observations could indicate a racemic ground state for the mesophase (racemic [Col$_r$]$_s$P$_{AF}$ phase). That means the switching process should take place between [Col$_r$]$_s$P$_{AF}$ and [Col$_r$]$_a$P$_{FE}$ states. However, the field-induced circular domains in which the extinction crosses are aligned along the directions of the crossed polarisers do not change on reversal or on removal of the field (Fig. 5.34c,d). The model described above (Fig. 5.34, model in analogy to references[24,36,216]) could be used to explain the possible modes of molecular packing in the Col$_r$P$_{AF}$ phase of compound **4b** considering one column as a fragment of a SmC$_s$P$_{AF}$ layer. The molecules are organized in ribbons with alternating polar direction along *b* in the ground-state structure. The size of the crystallographic cell of the Col$_r$P$_{AF}$ phase, seems to be sufficiently large (about 27 molecules per cross-section) to consider one column as a fragment of a SmC$_s$P$_{AF}$ layer. FOLCIA *et al.*[217] showed that the initially proposed models of the

SmC_sP_{AF} phases contradict the CURIE principle[218] , i.e. the symmetry of the SmC_aP_{FE} phase (C_{2v}) is not the intersection between the point groups of the SmC_sP_{AF} structure (C_{2h}) and the point group of the electric field ($C_{\infty v}$). Therefore these phase structures cannot be stable in bulk samples. The CURIE principle can be satisfied if an additional periodicity of equally spaced anticlinic–FE interlayer boundaries (see in the model the areas with blue background in Fig. 5.34) in the SmC_sP_{AF} phase exists along the layer normal[219,220] which changes the symmetry to C_{2v}. It means that in the ground state of the bulk materials there are mesoscopic domains with synclinic–AF interlayer interfaces separated by defects where the interlayer correlation is anticlinic–FE, i.e. the tilt direction alternates from domain to domain (Fig. 5.34b). This is in line with the domain structure and the fact that the extinction crosses still coincide with polariser and analyzer in the field-off state.[24]

5.1.2.4 The smectic polymorphism of dimers 5

The dimer series **5** (n = 12; p = 16) with an *even* methylene spacer (m = 2, 6) display various new smectic phases, in addition to the nematic phases. For the dimer with an *odd* spacer length, **5c** (m = 11), a Col_r phase is observed (see Table 5.3 and Fig. 5.35). On increasing the spacer length the mesophase stability is decreasing.

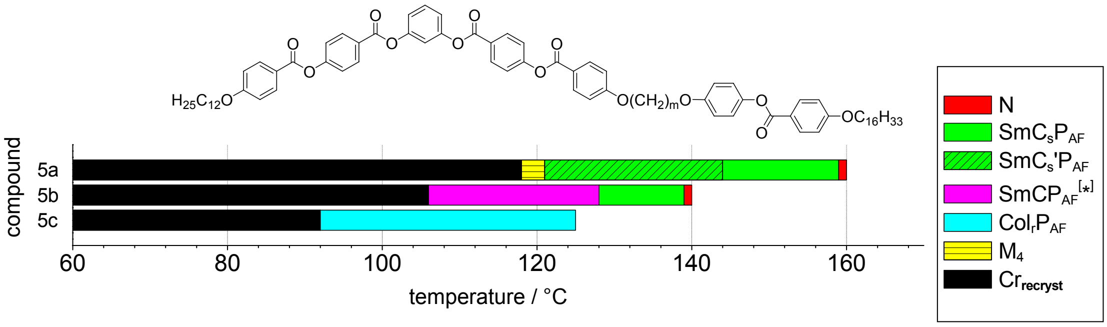

Figure 5.35 Transition temperatures (°C) of dimer series **5**, taken from the first DSC cooling scans (10 $Kmin^{-1}$).

The dimer **5a** with relatively long terminal *alkyloxy* chains (n = 12, p = 16) and a very short spacer (m = 2) exhibits two enantiotropic and two monotropic mesophases. The enantiotropic N and SmC phases were identified according to their characteristic schlieren textures. During transition from the nematic phase to the SmC phase, a typical fingerprint texture was observed. The nematic phase exists in a temperature range of 0.5 K and displays characteristic schlieren, marbled or homeotropic textures depending on the boundary conditions. If the planar oriented nematic phase is cooled down into the high-temperature smectic phase, a schlieren texture arises with singularities of $s = \pm 1$, $s = \pm 1/2$ and $s = \pm 3/2$ (Fig. 5.36a, indication of a tilted smectic mesophase) or a birefringent smooth fan-shaped texture (Fig. 5.36b). The occurrence of a schlieren texture as well as a smooth fan-shaped texture points to an anticlinic SmC phase (Fig. 5.36a,b).

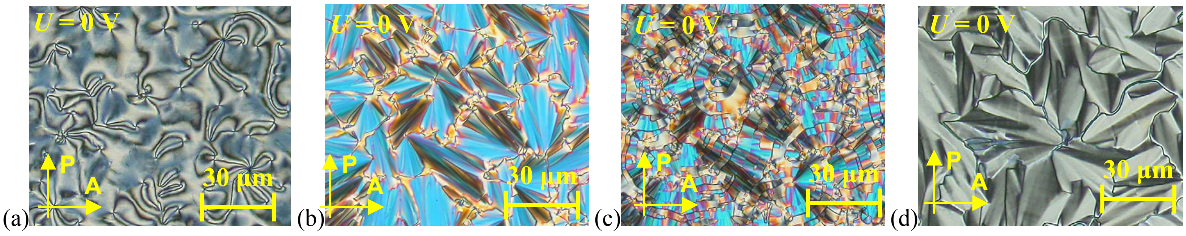

Figure 5.36: Textures of mesophases of dimer **5a** on cooling between crossed polarisers in a 5µm non-coated ITO cell: (a,b) high-temperature SmC phase at 150 °C; (c,d) low-temperature SmC phase at 140 °C.

On further cooling, a monotropic smectic phase appeared whose texture depended strongly on the texture of the preceding SmC phase. Thus, this phase appeared either with a broken fan-shaped texture (Fig. 5.36c) if cooling from a smooth fan-shaped texture or with a very low birefringent smooth fan-shaped texture (Fig. 5.36d) if cooling from schlieren SmC texture.

X-ray measurements performed on the mesophases of compound **5a** at 149 °C and at 142 °C confirmed the presence of two SmC phases with molecules tilted with respect to the layer normal and they showed very similar patterns for both phases (Fig. 5.37a-e). The layer spacing derived from the X-ray measurements on cooling are almost independent of the temperature, including the transition from the high-temperature SmC (d = 4.88 nm) to the lower-temperature SmC' phase (d' = 4.83 nm) and until the sample crystallizes. On the other hand, the appearance of second- and third-order layer reflections in the lower temperature phase (Fig. 5.37c-e) suggests a change from a sinusoidal modulation of the electron density along the layer normal found in the higher temperature phase (where only the first order is observed), to more strictly defined layers with a more pronounced segregation of the aromatic and aliphatic parts of the molecules within the intercalated structure. An average tilt angle of the molecular long axis with respect to the layer normal can be calculated from the position of the maxima for the outer diffuse scattering in the SmC phase (τ = 41°) and in the SmC'phase (τ'= 36°). The effective molecular length L_{eff} may be calculated from these experimental results for SmC to $L_{eff} = d/\cos\tau$ = 6.47 nm and for SmC' to $L_{eff}' = d'/\cos\tau'$ = 5.97 nm. On the basis of these X-ray experimental evidences these two synclinic SmC phases were assigned as SmC$_s$ and SmC$_s$' phases (in contradiction with the textural investigations which point to an anticlinic mesophase).

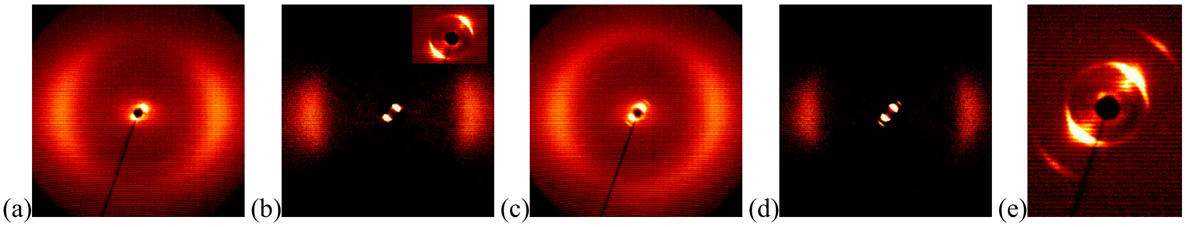

Figure 5.37: XRD patterns of an aligned sample of compound **5a** in the magnetic field on cooling; (a-b) SmC$_s$ phase at 150 °C: (a) original pattern; (b) the same XRD pattern, but the intensity of the isotropic liquid is subtracted; the inset shows the small angle region; (c-e) SmC'$_s$ phase at 130 °C: (c) original pattern; (d) the same XRD pattern, but the intensity of the isotropic liquid is subtracted; (e) small angle region.

Electro-optical measurements give evidence for an AF ground state in both SmC phases, since we found two peaks per half cycle of the applied triangular voltage (Fig. 5.38e). The switching polarisation increases with decreasing temperatures (P_S = 550 nC cm^{-2} for SmC$_s$P$_{AF}$

phase and $P_S' = 770$ nC cm^{-2} for SmC$_s$'P$_{AF}$ phase). The two SmC phases show a very different electro-optical switching. On application of a sufficiently high electric field (17 Vμm^{-1}) the SmC$_s$P$_{AF}$ phase of compound **5a** forms at 150 °C a smooth fan-like texture which is independent of the polarity of the applied field (Fig. 5.38b,d). If the field is removed the texture remains nearly unchanged, only the birefringence is slightly changed (Fig. 5.38c). This indicates that the synclinic organization of the ground-state structure is not significantly changed by the field. This confirms a switching by rotation around the long axis, which changes the polar direction without changing the tilt direction of the molecules. It should be noted that this switching process gives rise to a change of the superstructural chirality from racemic at zero voltage to homogeneously chiral under the applied field, and the change of the sign of the applied field switches between the enantiomeric chiral states (Fig. 5.38).

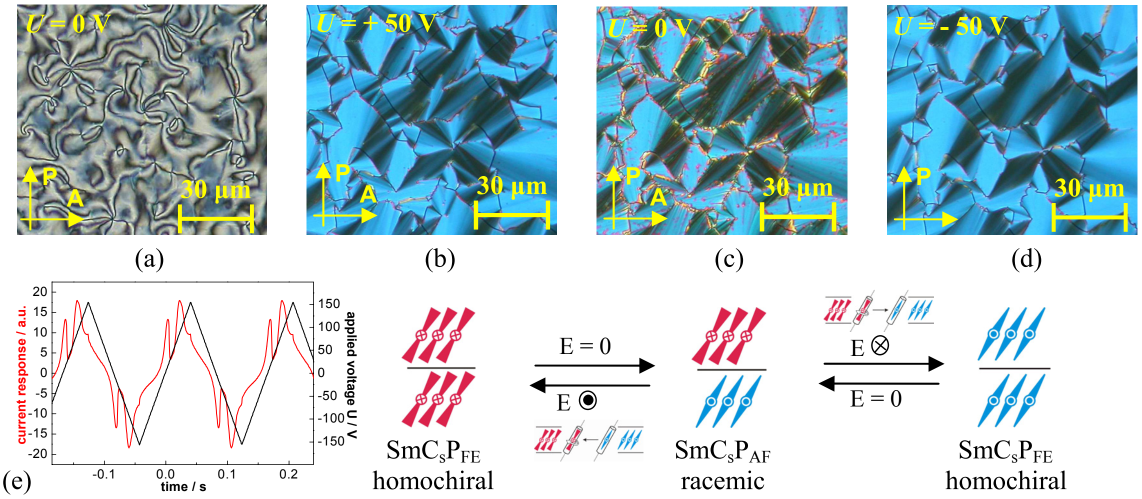
U = 0 V
U = + 50 V
U = 0 V
U = - 50 V
P
A
30 μm
(a)
(b)
(c)
(d)
(e)
current response / a.u.
applied voltage U / V
time / s
20
15
10
5
0
-5
-10
-15
-20
150
100
50
0
-50
-100
-150
-0.1
0.0
0.1
0.2
E = 0
E ⊙
E ⊗
E = 0
SmC$_s$P$_{FE}$
homochiral
SmC$_s$P$_{AF}$
racemic
SmC$_s$P$_{FE}$
homochiral

Figure 5.38: Electro-optical investigations of the SmC$_s$P$_{AF}$ phase of compound **5a**; textures observed in the same region of the sample between crossed polarisers in a 5μm non-coated ITO cell under a d.c. electric field at 150 °C: (a) U = 0 V, before starting the experiment; (b,d) U = ± 50 V; (c) U = 0 V; (e) AF switching current response obtained by applying a triangular-wave voltage ($U = 308$ V$_{pp}$, $f = 6$ Hz, $R = 5$ kΩ, $T = 150$ °C, $P_S = 550$ nC cm^{-2}); (down) models of organization of molecules in the FE states and in AF ground-state.

The low-temperature SmC$_s$'P$_{AF}$ phase of compound **5a** exhibits a complex electro-optical switching process. The first experimental findings (X-ray, electro-optic measurements, see Fig. 5.37 and 5.39) point to a SmC'$_s$P$_{AF}$ phase. However, further d.c. experiments revealed that the field-induced texture shows some special features.

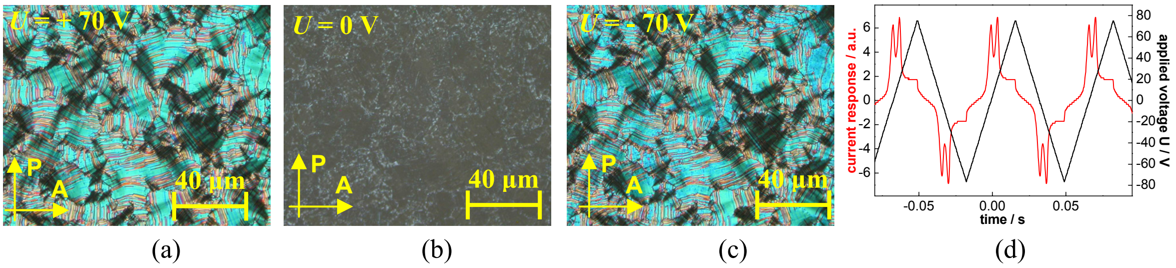
U = + 70 V
U = 0 V
U = - 70 V
P
A
40 μm
current response / a.u.
applied voltage U / V
time / s
6
4
2
0
-2
-4
-6
80
60
40
20
0
-20
-40
-60
-80
-0.05
0.00
0.05
(a)
(b)
(c)
(d)

Figure 5.39: Electro-optical investigations of the SmC'$_s$P$_{AF}$ phase of compound **5a**; textures observed in the same region of the sample between crossed polarisers under a d.c. electric field at 130 °C, in a 5μm non-coated ITO cell: (a,c) U = ± 70 V; (b) U = 0 V; (d) AF switching current response obtained by applying a triangular-wave voltage ($U = 151$ V$_{pp}$, $f = 15$ Hz, $R = 5$ kΩ, $T = 124$ °C, $P_S = 770$ nC cm^{-2}).

By applying electric fields greater than 10 Vμm^{-1}, the broken fan-shaped texture can be switched into a smoother fan-shaped texture which presents highly birefringent stripes running parallel to the smectic layers. If the field is switched off, the texture relaxes in a texture which shows nearly extinction between crossed polarisers. Rotating one polariser from the crossed position we could observe the same regions with opposite handedness as in the virgin broken fan-shaped texture. The field-free state should correspond to the anticlinic AF ground state, since this texture appears by the relaxation of the switched ferroelectric state. The nearly extinction between crossed polarisers could be the consequence of the tilt angle of the molecules. At a tilt of about 45°, in a so-called *orthoconic anticlinic director structure,*[221] the smectic layers have a *book-shelf geometry,* where the layers are perpendicular to the substrates. For bent-core molecules a deviation from a tilt angle (θ) of exactly 45° is possible if the bending angle (α) is changed according to the relation: $\alpha = 2\tan^{-1}(1/\cos\theta)$.[222] This state is non-birefringent in the direction perpendicular to the substrates, and therefore a nearly extinction between crossed polarisers is observed.[223]

On slow cooling of the sample under an external electric field circular domains could be obtained. In these circular domains the molecules are organized predominantly parallel to the surfaces. The smectic layers are more or less perpendicular to the substrates. There are rolled up in *onion-like* cylinders around the centre of the domains with the layer normal parallel to the substrates. This arrangement of the smectic layers is indicated by extinction cross. The dark brushes occur parallel and perpendicular to the molecular long axis. In this case, these brushes are inclined with the position of polariser and analyzer in the synclinic tilted phases by an angle of 36°. This value is in agreement with the results of the X-ray investigations. Interestingly, on removal of the applied electric field the relaxation of the field-induced circular domains depends on the experimental conditions. As a result, two mechanisms could be established: (a) for *fast removing of the electric field* (Fig. 5.40a-d); (b) for *slow removing of the electric field* (Fig. 5.40e).

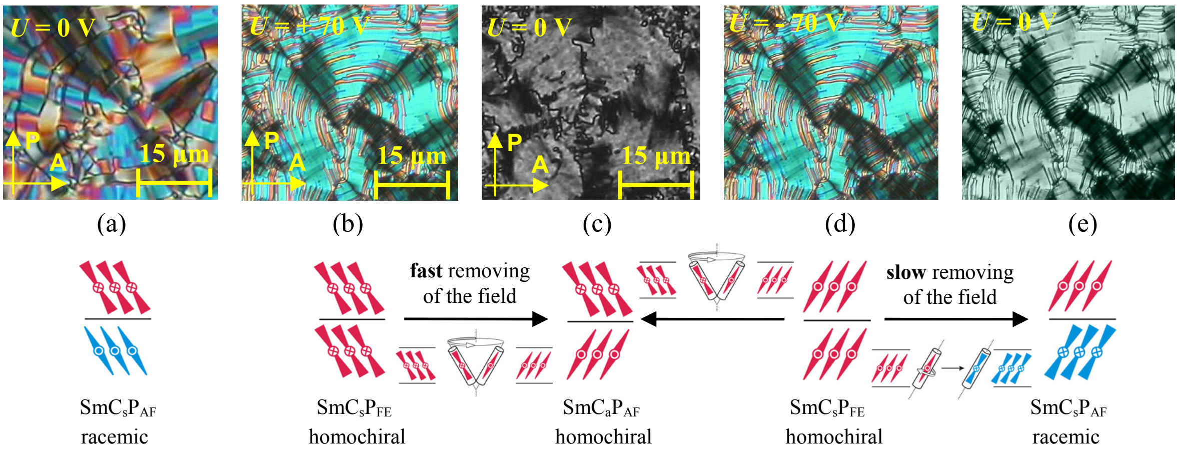

Figure 5.40: Electro-optical investigations of the SmC'$_s$P$_{AF}$ phase of compound **5a**; textures observed in the same region of the sample between crossed polarisers in a 5µm non-coated ITO cell under a d.c. electric field at 130 °C; (a) U = 0 V, before starting the experiment; (b,d) U = ± 70 V; (c) U = 0 V, on fast removing of the applied field; (e) U = 0 V, on slow removing of the field; (a-e, down) models of organization of the molecules in the FE states (b,d) and in the AF ground-states (a,c,e).

(a) On *fast removing of the electric field* the extinction crosses rotate more or less to the crossed polarisers position and the texture becomes dark, so that the crosses are now difficult to recognize (in Fig. 5.40c the intensity of the light was strongly increased for a better observation of the extinction crosses). By re-applying the electric field, the extinction crosses rotate back to the original 36° position, whereby the sense of rotation is opposite for an opposite sign of the field. The relaxation from the field-induced FE state into the AF ground state obviously corresponds to the transition from the synclinic FE state ($\mathrm{SmC_sP_{FE}}$) into the anticlinic AF state ($\mathrm{SmC_aP_{AF}}$, see Fig. 5.40c and Fig 5.41).The formation of nearly black textures, after removing the electric field, is obviously due to the tilt angle of about 45°.[65,223,224,225] Based on these observations we can conclude that such behaviour is typical for a $\mathrm{SmC_aP_{AF}}$ phase, in contradiction to the X-ray experimental findings.

(b) On *slow removing of the electric field* (0.3 Vs^{-1}) the field-induced texture with circular domains does not change, and only the birefringence slightly decreases (Fig. 5.40e). If the electric field slowly increases again, the positions of the extinction crosses do not change also on reversal or removing of the electric field. It seems that the field-induced ferroelectric state does not relax anymore into the AF ground state observed for case (a). Such transition from the field-induced $\mathrm{SmC_sP_{FE}}$ into the AF state, without rotation of the extinction crosses could be realised if, in each second layer, the molecules would rotate by 180° around their long axes. That means the chirality is changed in each second layer (transition from the chiral $\mathrm{SmC_sP_{FE}}$ into the racemic $\mathrm{SmC_sP_{AF}}$ state, see Figure 5.40e, and Figure 5.41). For such a chiral - racemic change-over in a SmCP phase (called *flipping of chirality*, already reported in the literature[94,222,226,227]) it was shown that, in the field-free state, the AF synclinic racemic state possesses a lower free energy than the corresponding anticlinic homochiral state, which is probably caused by steric reasons. A transition from a metastable into a stable state requires nucleation and needs time and this could be the reason why the effect described above is visible when the electric field is changed very slowly. Also under these conditions, the rotation around the long molecular axes needs less energy than the rotation around the tilt cone. CLARK[228] demonstrate that such a field-induced change of chirality takes place also at fast switching, but, in the main part of the sample, the chirality does not change during the switching process. These findings are very similar to those reported by SCHRÖDER *et al.*[226] for bent-core molecules. They proposed a model for this *flipping of chirality* process (Fig. 5.41).

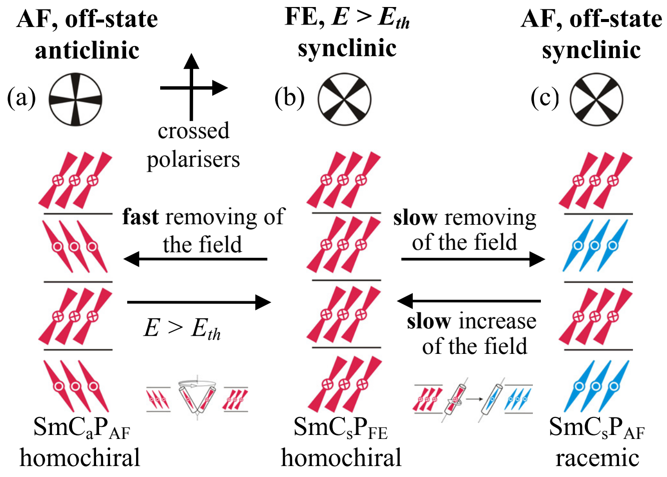

Figure 5.41: (a-c) Proposed models for the organization of the molecules over this *flipping of chirality* process; positions of the extinction crosses between crossed polarisers and related structures: (b) in the switched FE state; (a) in the AF ground state after fast removal of the applied field and (c) after very slow removal of the field. These models for the organization of the molecules are already described by SCHRÖDER *et al.*[226]

Also of interest is the additional low temperature M_4 phase. On cooling the birefringence of the texture decreases and the schlieren texture transformed into a mosaic-like texture while the broken fans became striped (Fig. 5.42a). Rapid crystallisation prevented electro-optical investigations and a clear recording of the X-ray diffraction pattern of the M phase. Textural behaviour in conjunction with the XRD pattern (see Fig. 5.42b) implies the presence of a higher ordered smectic phase.

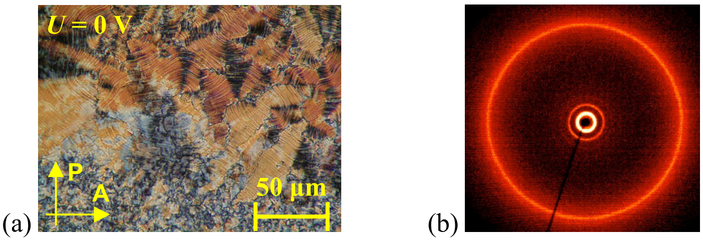

Figure 5.42: Compound **5a**: (a) texture of the potential crystal - like M_4 phase at 120 °C; (b) short take of the powder-like X-ray pattern of the M_4 phase developing on cooling from the SmC'_sP_{AF} phase at 120°C.

The dimer **5b** (m = 6) exhibits two enantiotropic phases (nematic and smectic phases), and a low-temperature monotropic smectic phase. The nematic phase and the high-temperature smectic phase were identified according to their characteristic schlieren textures (during transition from the nematic phase to the SmC phase, a typical fingerprint texture was observed, see Fig. 5.43a-c). Depending on the boundary conditions we can also observe marbled and homeotropic texture for the nematic phase and a highly birefringent smooth fan-shaped texture for the high-temperature SmC phase.

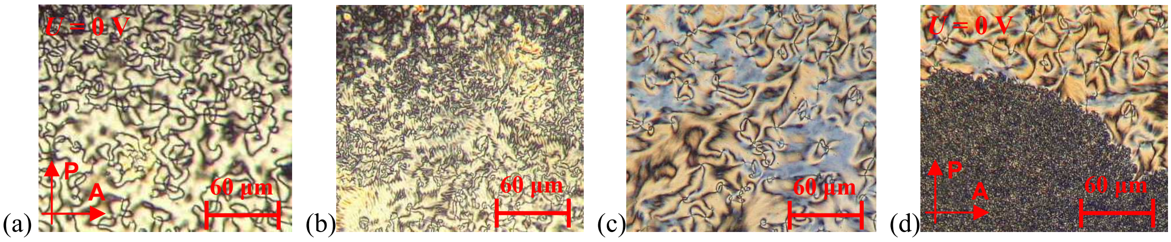

Figure 5.43: Textures of the mesophases of dimer **5b** as observed between crossed polarisers in the same region of the sample, between two untreated glass slides on cooling at U = 0 V: (a) N phase at 141.5 °C; (b) typical fingerprint texture at the transition from a N schlieren texture (top-left) to a SmC schlieren texture (bottom-right) at 141 °C; (c) SmC schlieren texture at 137 °C; (d) transition from a SmC schlieren texture (top-right) to a unspecific low birefringent texture at 128 °C.

X-ray measurements were performed on well-oriented samples of **5b** by applying a magnetic field of about 1T. The X-ray pattern at 141.2 °C shows a dumb-bell like scattering maximum in the small angle region, and a diffuse wide angle scattering located around the equator, see Figure 5.44a,b. The small-angle scattering in the nematic phase can be attributed to cybotactic groups of the SmC-type representing fluctuating arrays of molecules with a short-range order of the same type as the long-range order in the low-temperature SmC phase. The X-ray diffraction pattern of the high-temperature SmC phase of compound **5b** at 132 °C (Fig. 5.44c-e) is characterized by a diffuse scattering in the wide angle region and sharp equidistant BRAGG-reflections in the small angle region (d = 5.44 nm, SmC_s phase) and confirmed the presence of a SmC phase with molecules tilted with respect to the layer normal. An average tilt angle of the molecular long axis with respect to the layer normal can be calculated from the position of the maxima for the outer diffuse scattering in the $\mathrm{SmC_s}$ phase (τ = 32°) and the effective molecular length is $L_{eff} = d/\cos\tau = 6.56$ nm.

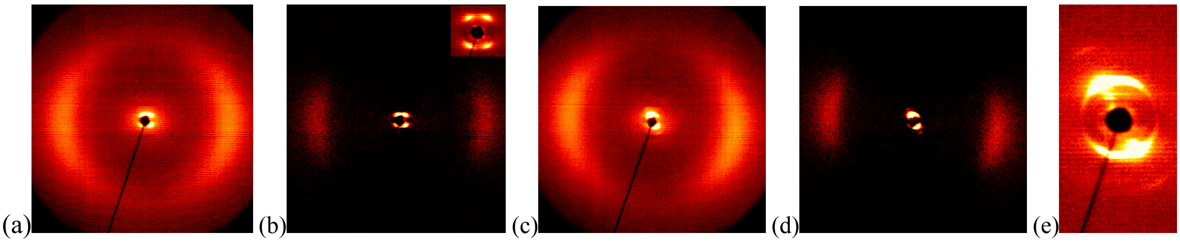

Figure 5.44: XRD patterns of an aligned sample of dimer **5b**; (a-b) N phase at 141.2 °C: (a) original pattern; (b) the same XRD pattern, but the intensity of the isotropic liquid is subtracted; the inset shows the small angle region; (c-e) $\mathrm{SmC_s}$ phase at 132 °C: (c) original pattern; (d) the same XRD pattern, but the intensity of the isotropic liquid is subtracted (suggesting a synclinic tilt of the molecules); (e) small angle region.

On electro-optical investigations the high-temperature $\mathrm{SmC_s}$ phase of compound **5b** showed the same behaviour as the high-temperature $\mathrm{SmC_sP_{AF}}$ phase of compound **5a**. The smooth fan-shaped texture induced under an electric field is independent of the reversal or removal of the field, confirming a switching by rotation around the long axis. Two peaks per half cycle of the applied triangular voltage were found ($P_S = 580$ nC cm^{-2}, $\mathrm{SmC_sP_{AF}}$ phase).

On further cooling, at 128 °C, the low-temperature smectic phase of compound **5b** appears as fractal nuclei which coalesce to a low-birefringent *grainy non-specific* texture. Rotating one polariser out of the crossed position chiral domains of opposite handedness could be observed (Fig. 5.45). The light transmission does not change when the sample is rotated. This indicates a conglomerate of macroscopically chiral domains with opposite chirality sense.[88,145,229,230,231] Moreover, these domains occur in the ratio of 1:1. In crystalline systems this type of racemic structure, in which enantiomers are organized in separate enantiomorphic crystals is called *conglomerate*.[232] Hence, this type of low-birefringent mesophases with a local chiral structure has been assigned as *dark conglomerate phases* and is indicated by the superscript '$^{[*]}$'. The mesophase has a chiral superstructure though the molecules themselves are achiral.[23,105,233] Up to now the precise structure of these phases is not clear. As already mentioned for the low-temperature $\mathrm{SmC_s'P_{AF}}$ phase of compound **5a**, the low birefringence could be an indication of an *orthoconic anticlinic director structure*[221] with a 45° tilted organization of the molecules as recently proposed for a field-induced *dark-conglomerate phase*.[234] The key difference between our results and previously published work (see for an example ref.[234]) is the fact that the low-temperature mesophase of **5b** represents a virgin structure obtained without previous application of an electric field and hence their structure could be different.

Another explanation of the low birefringent mesophase of compound **5b** can be a layer distortion which leads to a mesoscopically disordered structure, either composed of randomly ordered fragments of these layers,[235] or due to a random (*sponge-like*) deformation of the layers[230] and it is possible if the size of the domains with uniform director orientation is smaller than the wave length of light.

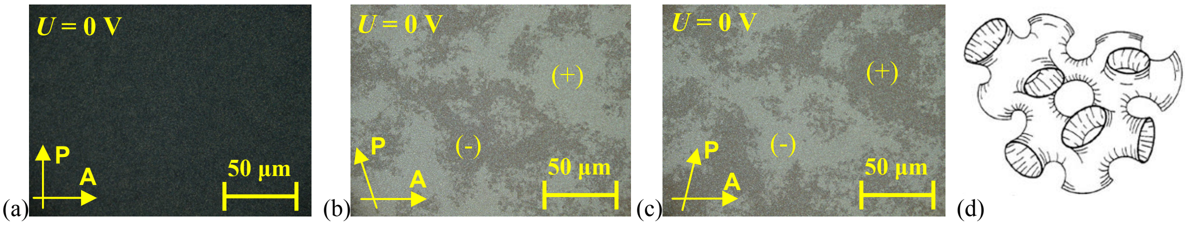

Figure 5.45: Textures of the $\mathrm{SmCP}_{\mathrm{AF}}^{[*]}$ phase of compound **5b** at 127 °C in a 5µm non-coated ITO cell at $U = 0$ V, observed in the same region of the sample: (a) between crossed polarisers and (b,c) by rotating one polariser by +15° (b) and by -15° (c) from the crossed position (chiral (+) and (–) domains); (d) model of *sponge phase* composed of deformed stacks of layers (only one layer is shown); model in analogy to the references.[211,224,236]

There are indeed strong arguments that the *dark conglomerate phases* of these molecules represent smectic phases with a strongly folded and non-regular organization of the smectic layers, similar to *sponge phases* known from lyotropic systems [211,237] (see Fig. 5.45d): (a) the microscopic observation of the growing process of the distorted structure, characterized by a fractal growing with a *grainy* and *non-specific* appearance of the mesophase (which is not typical for smectic phases with flat layers); (b) the significantly higher viscosity of this mesophase in comparison to the high-temperature *conventional* polar smectic $\mathrm{SmC_sP_{AF}}$ phase. HOUGH *et al* [238] proposed that the optical activity of the *dark conglomerate phases* arises from the layer chirality and it requires the phase structure being homogeneously chiral and the birefringence of the mesophase itself be sufficiently small.

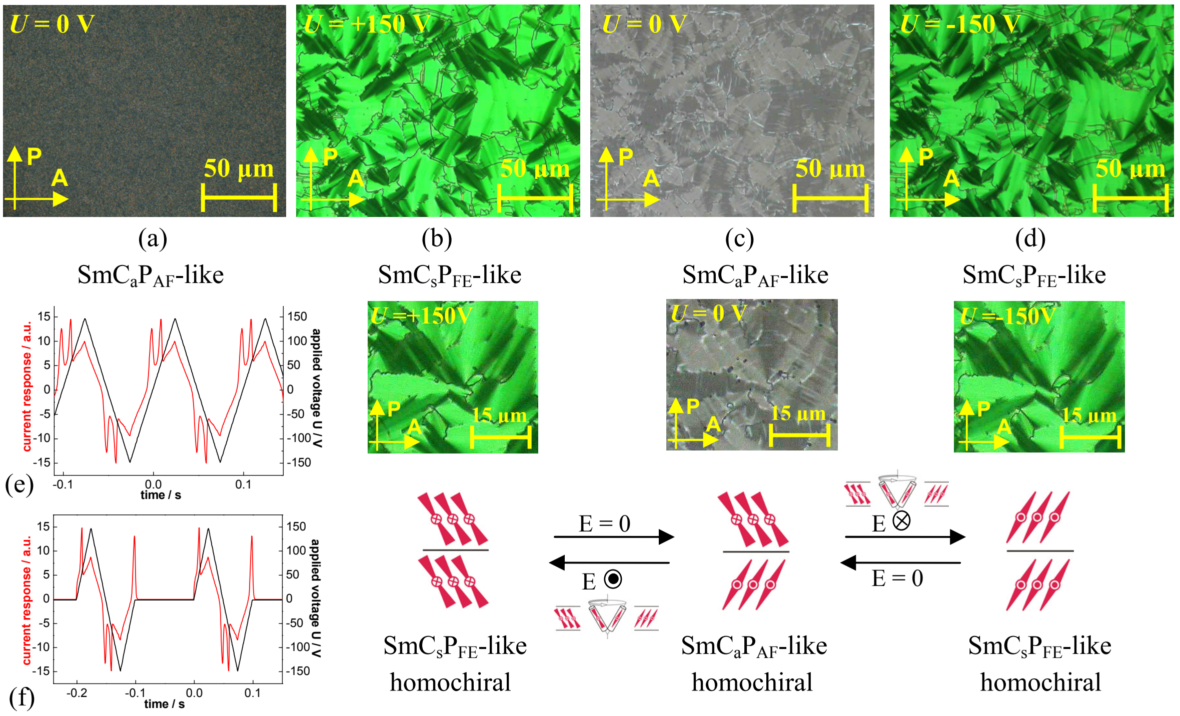

Figure 5.46: Electro-optical investigations in a 10 µm polyimide-coated ITO cell of the low-temperature phase of compound **5b** (*dark conglomerate* $\mathrm{SmCP}_{\mathrm{AF}}^{[*]}$ phase); textures observed between crossed polarisers in the same region of the sample under a d.c. electric field at 120 °C: (a,c) U = 0 V; (b,d) U = ± 150 V; (e,f) AF switching current response obtained by applying (e) a simple and (f) a modified triangular-wave voltage ($U = 298\ \mathrm{V_{pp}}$, $f = 10$ Hz, $R = 5$ kΩ, $T = 120$ °C, $P_S = 830$ nC cm^{-2}); down: models of the organization of the molecules; in the FE states (b,d) and in the AF ground-state (c).

This is a good argument for a $\mathrm{SmC_aP_{AF}}$-like ground-state structure of the low-temperature smectic phase of compound **5b**. Unfortunately, X-ray measurements were impossible in the low-temperature smectic phase of compound **5b** (this SmC phase crystallized a few minutes after its formation); however it was sufficient time to observe the textures as well as the field-induced changes of the textures in d.c. and a.c. field experiments.

The electro-optical response of this low-temperature smectic phase of dimer **5b** is different from the previously described one for the $\mathrm{SmC_sP_{AF}}$-like phase. By applying electric fields greater than about 20 $\mathrm{V\mu m^{-1}}$, this texture can be switched into a birefringent fan-shaped texture which presents circular domains with the extinction crosses inclined with the directions of polariser and analyzer evidencing a synclinic organization (Fig. 5.46). In the field-induced states the tilt angle of the extinction crosses with respect to the crossed position of the polarisers is about 45° which indicates a tilt angle of the molecules of 45°, respectively (Fig. 5.46b,g). If the field is switched off, the texture shows nearly extinction between crossed polarisers and in the circular domains the extinction crosses rotate into positions parallel to polariser and analyzer. This indicates relaxation into an anticlinic structure at 0 V (Fig. 5.46c,h; $\mathrm{SmC_aP_{AF}}$-like state). In this *non-birefringent* texture, over the whole temperature range chiral domains of opposite handedness could be observed. By applying the electric field again, the extinction crosses rotate back to the original 45° position leading to a $\mathrm{SmC_sP_{FE}}$-like structure with opposite polar direction (Fig. 5.46d,i). The current response shows two current peaks per half period of the applied triangular voltage (P_S = 830 nC $\mathrm{cm^{-2}}$, Fig. 5.46e,f). Hence, optical investigation clearly indicates a tristable switching by a collective rotation around a cone, which is an additional confirmation of the AF switching process.

Based on these experimental findings the ground state structure of the low-temperature smectic phase of compound **5b** should be AF with an anticlinic organization, a *dark conglomerate* $\mathrm{SmCP_{AF}}$[*] phase. Two different modes of switching between the $\mathrm{SmC_sP_{FE}}$–like states were described by KEITH *et al.*[212] for some bent-core molecules: a *classical* and a *non-classical* AF process (Fig. 5.47).

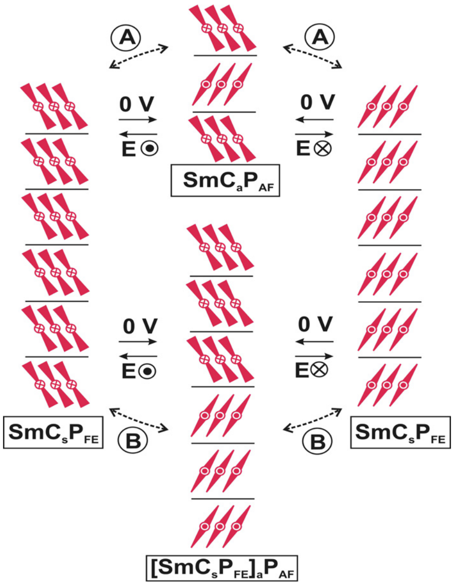

Figure 5.47: Proposed models of switching between the polar $\mathrm{SmC_sP_{FE}}$–like states: (A) in the *classical* AF switching process the relaxation of the FE states at 0 V gives rise to a $\mathrm{SmC_aP_{AF}}$–like structure where the polar direction reverses from layer to layer; (B) in the *nonclassical* AF switching the relaxation can take place by reorganization of stacks of layers, leading to an anticlinic and antipolar organization of $\mathrm{SmC_sP_{FE}}$ layer stacks and giving rise to a $\mathrm{[SmC_sP_{FE}]_aP_{AF}}$ ground-state structure. This model is described in the reference.[212]

(A) In the *classical* AF switching process the relaxation of the FE states at 0 V gives rise to a SmC$_a$P$_{AF}$–like structure where the polar direction reverses from layer to layer (discussed for the SmC$_s$'P$_{AF}$ of the compound **5a**).

(B) In the *non-classical* AF switching the relaxation takes place by reorganization of stacks of layers, as shown at the bottom of the model, leading to an anticlinic and antipolar organization of SmC$_s$P$_{FE}$ layer stacks and giving rise to a [SmC$_s$P$_{FE}$]$_a$P$_{AF}$ ground-state structure. If in this structure the size of the uniform SmC$_s$P$_{FE}$ layer stacks is smaller than the wavelength of light, only an average optical axis is seen and the extinction crosses are parallel to the polarisers. The [SmC$_s$P$_{FE}$]$_a$P$_{AF}$ structure as suggested for the *dark conglomerate phases* could also be obtained by relaxation of the polar and synclinic structure if layer deformation is inhibited (e.g. by surface stabilization).

The dimer with m = 11, **5c**, is the only compound in this series which does not show a simple layer structure but a mesophase with 2D lattice instead, i.e. a Col$_r$P$_{AF}$ phase (lattice parameters a = 13.77 nm, b = 7.15 nm, P_S = 470 nC cm^{-2}, see Table 5.3).

5.1.2.5 The smectic SmXP$_{AF}$ phase of dimer 6a

The dimer series **6** (n = 16; p = 12) contains two compounds. The dimer **6a** (m = 6) with an *even* methylene spacer displays additional to the nematic phase, various smectic phases (Table 5.3). For the dimer **6b** (m = 11) with an *odd* spacer length a Col$_r$ phase is observed. The increase of the spacer length gives rise to a reduction of the mesophase stability.

The compound **6a** exhibits three monotropic phases: a nematic and two smectic phases. On cooling from the isotropic liquid, the nematic phase showed typical schlieren texture (Fig.5.48a). The nematic phase presents over the whole temperature range chiral domains of opposite handedness, as already described in chapter 5.1.1.2. Below this nematic phase the high-temperature monotropic smectic phase appeared on cooling and the transition was accompanied by a change to a fan-like texture (Fig.5.48b). If this fan-shaped texture is cooled down into the low-temperature smectic phase (SmX) a *non-specific* texture arises (Fig.5.48c).

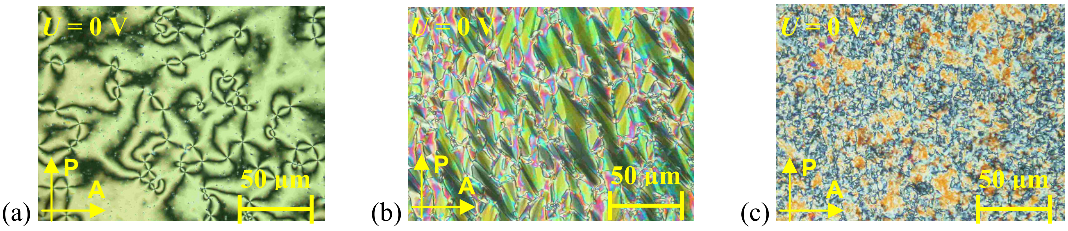

Figure 5.48: Textures of the mesophases of compound **6a** observed in a 5 µm non-coated ITO cell on cooling: (a) N phase at 130 °C; (b) high-temperature smectic at 124 °C; (c) low-temperature SmX at 121 °C.

X-ray measurements were impossible because the mesophases of compound **6a** crystallized a few minutes after formation. However it was sufficient time to observe the textures as well as the field-induced changes of the textures in a.c. and d.c. field experiments. When a relatively low field (1.0 V µm^{-1}; 27 Hz) is applied, the nematic phase of this compound shows fluctuating domains of the Williams–Kapustin type (the period of the domains corresponds to the cell thickness (5 µm), see section 5.1.1.2.).[195] Electro-optical measurements give evidence for an AF ground state in the high-temperature SmC phase of compound **6a**, since we found two peaks per half cycle of the applied triangular voltage (P_S = 490 nC cm^{-2}, Fig. 5.49d). The application of an electric field (10 Vμm^{-1}) at 124 °C leads to the formation of a smooth fan-like texture which is independent of the polarity of the applied field (Fig. 5.49a,b). If the field is removed the texture remains nearly unchanged, only the birefringence is slightly changed (Fig. 5.49c). This confirms that the switching between the AF ground state (SmC$_s$P$_{AF}$ state) and the switched FE states (SmC$_s$P$_{FE}$ states) preferably takes place through a collective rotation of the molecules around their long molecular axes (SmC$_s$P$_{AF}$ phase).

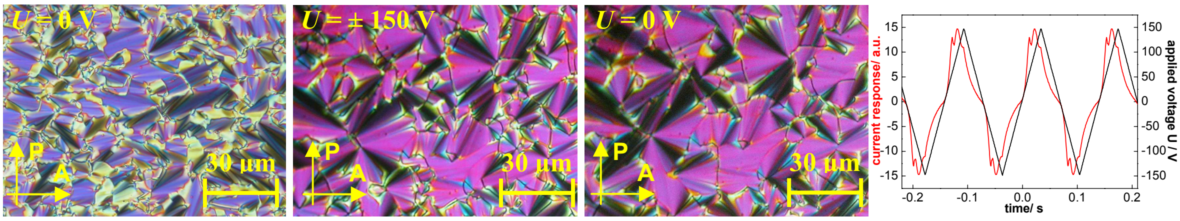

(a) SmC$_s$P$_{AF}$ (racemic) (b) SmC$_s$P$_{FE}$ (homochiral) (c) SmC$_s$P$_{AF}$ (racemic) (d)

Figure 5.49: Electro-optical investigations on the SmC$_s$P$_{AF}$ phase of compound **6a**; textures observed between crossed polarisers in the same region of the sample under a d.c. electric field in a 5 μm non-coated ITO cell at 124 °C: (a,c) $U = 0$ V; (b) $U = \pm 50$ V; (d) AF switching current response obtained by applying a triangular-wave voltage ($U = 280$ V$_{pp}$, $f = 7$ Hz, $R = 5$ kΩ, $T = 124$ °C, $P_S = 490$ nC cm^{-2}).

The low-temperature SmX phase of compound **6a** exhibits peculiar optical and electro-optical properties. The *non-specific* texture of the SmX phase exhibits no extinction condition when rotating the microscope stage between crossed polarisers which points to a twisted structure. By a small decrossing of the polarisers, domains of opposite handedness can be visualized which obviously correspond to regions of opposite director twist. Two current peaks per half-period of a triangular voltage could be recorded during the switching process indicating an AF ground state (P_S = 850 nC cm^{-2}, at 120 °C, see Fig. 5.50d). Depending on the experimental conditions two different mechanisms of the switching process of the SmX phase can be distinguished: (a) *above 117 °C*; (b) *below 115 °C.*

(a) If an electric field of 15 V μm^{-1} is applied to the planar oriented SmX phase at *121 °C* the texture becomes more *non-specific*. The texture of the switched states is independent of the polarity of the field and nearly the same as in the field-off state (Fig. 5.50a-c). This confirms that the switching between the AF ground state and the switched FE states preferably takes place through a collective rotation of the molecules around their long molecular axes. A transition into a new texture which shows complete extinction between crossed polarisers takes place on increasing the applied field to 30 V μm^{-1} (Fig. 5.51a-c). The extinction does not change when the sample is rotated. The field-induced dark texture exhibits domains of opposite handedness which can be visualized by a small decrossing of the polarisers (Fig. 5.51a,c). The border lines of these domains are identical with those of the chiral domains which are spontaneously formed in the fan-like field-free texture. On removal of the applied field, at *121 °C* the field-induced non-birefringent texture relaxes to a low-birefringent texture (Fig. 5.51b).

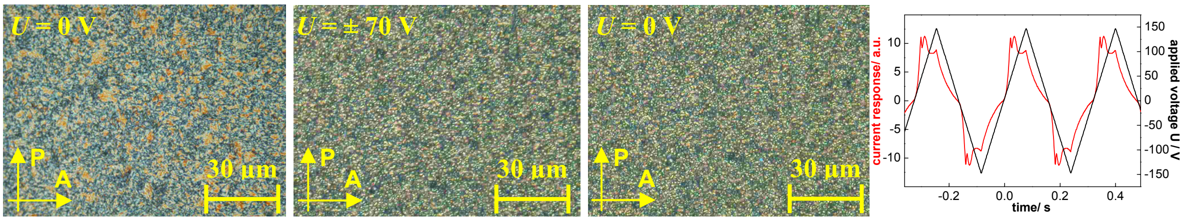

(a) SmXP$_{AF}$ (b) SmXP$_{FE}$ (c) SmXP$_{AF}$ (d)

Figure 5.50: Electro-optical investigations of the SmXP$_{AF}$ phase of compound **6a**; textures observed between crossed polarisers in the same region of the sample under a d.c. electric field at 120 °C in a 5µm non-coated ITO cell: (a, c) $U = 0$ V; (b) $U = \pm 70$ V; (d) AF switching current response obtained by applying a triangular-wave voltage ($U = 300$ V$_{pp}$, $f = 4$ Hz, $R = 5$ kΩ, $T = 120$ °C, $P_S = 850$ nC cm^{-2}).

(b) On lowering the temperature to *114 °C*, the non-birefringent field-induced texture remains unchanged when the field is removed (Fig. 5.51e). However long-time observations were not possible because of the fast crystallization of the phase. An interesting finding is that at this temperature, above critical field strength of a definite polarity (about 32 V µm^{-1}), the bright domains become dark and the dark domains become bright. This effect is reversed by a field of opposite polarity. It means that the chiral domains of opposite handedness can be reversibly switched into a state of opposite chirality by reversal of the applied electric field (Fig. 5.51d-f). The chiral domains of opposite handedness in this phase are visualized by rotation of one polariser by +5° from the crossed position. The angle between the polarisers is fixed at +5°, during these experiments (Fig. 5.51d-f). In this way, the field-induced switching of chirality can be visualized. Hence, optical investigation clearly indicates a tristable switching by a collective rotation around a cone, which is an additional confirmation of the AF switching process. However, the switching polarisation of this AF phase varies between 900 and 970 nC cm^{-2} on cooling the sample below 114 °C. Without electric field this non-birefringent texture remains unchanged on further cooling. After the removal of the field the switched states are stable up to the crystallization but it can be easily switched into the opposite FE state. This AF phase is different from that which arises spontaneously on cooling the isotropic liquid. The switching mechanism is not yet clear. On the basis of these experimental findings the low-temperature phase of compound **6a** was assigned as SmXP$_{AF}$ phase.

EREMIN[239] and PELZL[240] *et al.* reported a similar complex electro-optical behaviour for some five-ring bent-core mesogens with a 4-chlororesorcinol as central core, and WEISSFLOG *et al.*[241] for some five-ring bent-core mesogens with a 4,6-dichlororesorcinol as central core. There is proposed an alternative model which is based on the assumption that in the field-induced non-birefringent state the smectic layers are arranged parallel to the substrates and the tilted molecules form a helical superstructure. Even when the pitch is relatively large this structure should be non-birefringent in direction of the helix axis because the tilt angle is about 45°. There is assumed that the smectic layers have a triclinic (C_1) symmetry as in SmC$_G$ phases.[79,107,239,242] In the SmC$_G$ phase the director tilt has two components with respect to the layer normal: *clinic* by the angle θ and additionally in the tilt plane by the *leaning* angle α. In this case the smectic layers have a polarisation component not only parallel but also perpendicular to the smectic layers.

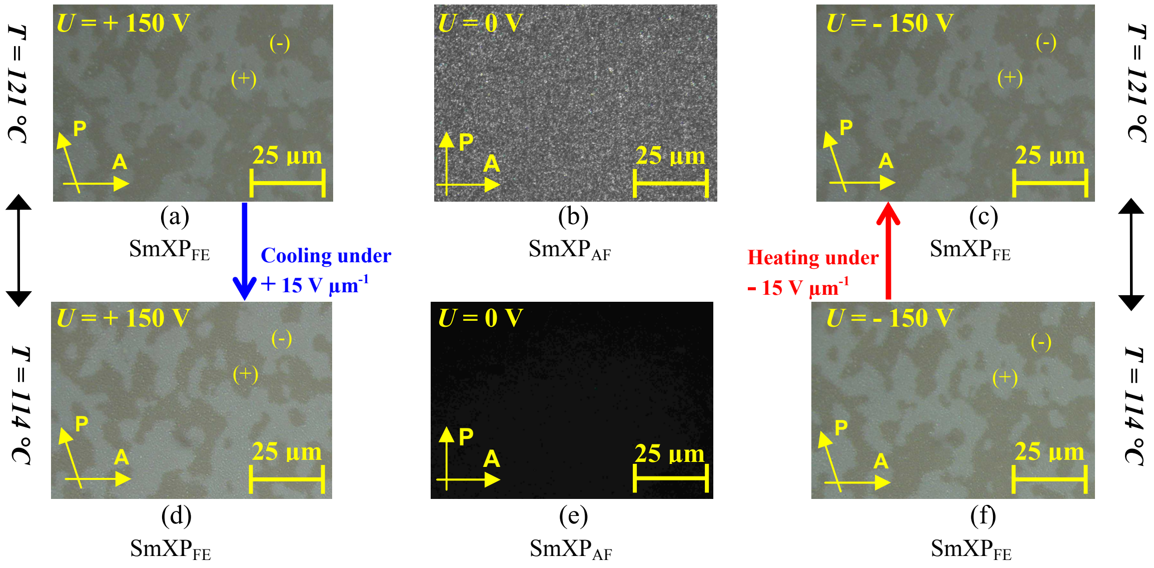

(a) SmXP$_{FE}$ (b) SmXP$_{AF}$ (c) SmXP$_{FE}$

(d) SmXP$_{FE}$ (e) SmXP$_{AF}$ (f) SmXP$_{FE}$

Figure 5.51: Electro-optical investigations of the SmXP$_{AF}$ phase of compound **6a** in a 5 µm non-coated ITO cell; the field-induced textures (a, c, d, f) between uncrossed polarisers (5°); the field-free textures (b, e) between crossed polarisers; (a-c) at 121 °C: (a) U = + 150 V, FE state; (b) U = 0 V, low-birefringent AF ground-state; (c) U = - 150 V; (d-f) at 114 °C: (d) U = + 150V, FE state; (e) U = 0 V, non-birefringent AF ground-state; (f) U = - 150V, FE state; (a,d) on cooling in the presence of a field of U = + 150 V, below 115 °C the texture is complementary to that of the starting one; (f,c) on heating in the presence of a field of U = - 150 V, over 117 °C the texture is unchanged. The intensity of the light and the contrast are increased in the optical microphotographs presented above for a better observation of the textural changes.

By coupling of the electric field with the polarisation component perpendicular to the layers the reorientation of the smectic layers from originally perpendicular to parallel to the substrates would be possible provided that the polarisation component parallel to the layer normal is larger than that perpendicular to this. In the smectic layers the molecules are tilted and form a helical superstructure which explains the extinction of this texture between crossed polarisers. In the randomly distributed chiral domains the helices possess opposite handedness. The formation of a helical structure would be advantageous from the energetically point of view because of the partial compensation of the polarisation. In the case of SmC$_G$-like layers the application of an electric field perpendicular to the layers would reverse the chirality in a simple way, by the collective rotation of the molecules around the long axes, which is accompanied by an inversion of the layer chirality (Fig. 5.52).[79]

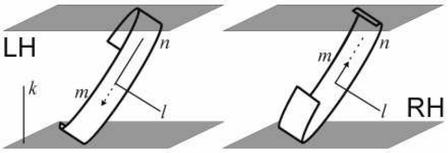

Figure 5.52: Schematic representation of the inversion of chirality in the SmC$_G$ phase through field-induced rotation of the bent molecules around their long axes (according to BRAND *et al.*[79]). k: layer normal; n: director; LH: left-handed; RH: right-handed.

REDDY *et al*[24] proposed that a field-induced optically isotropic FE phase corresponds to a *dark conglomerate phase* (SmCP$^{[*]}$ phase). It is assumed that by the action of the electric field the smectic layers of the original texture are strongly folded similar to a *lyotropic sponge phase* which can explain the optical isotropy (see also the SmCP$_{AF}^{[*]}$ phase of compound **5b**). Furthermore it is assumed that the existence of chiral domains of opposite handedness is caused by the layer chirality. As shown by HOUGH *et al*[238] the layer chirality can produce a collective chiral optical activity which is large enough to be observed in systems with very low birefringence in helix-free systems. REDDY *et al*[24] do not exclude that also the conformational chirality can play a role for the formation of chiral domains and that the reversible switching between the states of opposite chirality is based on the rotation of the molecules around their long axes. At the moment the experimental results are not sufficient to decide unambiguously between the proposed models which try to explain the reversible switching of chirality by the reversal of the field polarity. Further investigations with new experimental methods and new, similar materials should clarify what is the exact mechanism of the reversible switching of chirality by the reversal of the field polarity.

We can conclude that both smectic phases of compound **6a** are AF and the values of the spontaneous polarisation, P_S, increase on decreasing the temperature. The polar switching of the high-temperature SmC_sP_{AF} phase takes place through collective rotation of the molecules around their long axes (a similar polar switching as shown for the SmC_sP_{AF} phase of compound **5a**, i.e. which changes the polar direction without changing the tilt direction of the molecules). The low-temperature smectic phase was assigned as a probable SmC_G-like phase or as a probable *dark conglomerate phase* with a strongly folded and non-regular organization of the smectic layers and therefore it is called in this thesis $SmXP_{AF}$ phase. This low-temperature phase exhibits two different types of switching under application of an external electric field with a clear dependence of the switching mechanism on the temperature. The polar switching of the $SmXP_{AF}$ phase above 117 °C takes place through collective rotation of the molecules around their long axes, while for the same phase below 115 °C by a collective rotation around a cone. The mechanism of this polar switching is not yet clear.

5.1.2.6 The rectangular columnar Col_rP_{AF} phase of dimer 6b

The dimer **6b** whit an *odd* spacer (m = 11) exhibits a monotropic columnar phase. On slow cooling of the isotropic liquid the texture of the columnar phase shows focal conics, banana-leaf like textures, ribbon-like texture and circular domains (Fig. 5.53a). The small-angle reflections of the X-ray diffraction pattern of the columnar phase of compound **6b** can be indexed to a centred two-dimensional rectangular lattice (Col_r), with the lattice parameters a = 15.26 nm and b = 7.11 nm (see Tabel 5.3).

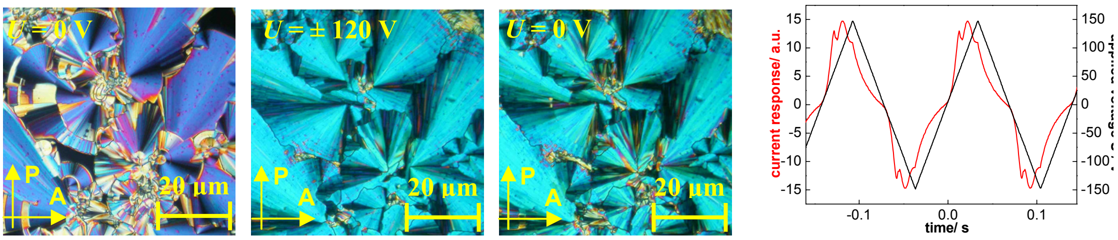

(a) $[Col_r]_sP_{AF}$ (b) $[Col_r]_aP_{FE}$ (c) $([Col_r]_s)_aP_{AF}$ (d)

Figure 5.53: Electro-optical investigations of the Col_rP_{AF} phase of compound **6b** in a 5µm non-coated ITO cell; textures observed between crossed polarisers in the same region of the sample under a d.c. electric field at 120 °C; (a, c) U = 0 V; (b) U = ± 120 V; (d) AF switching current response obtained by applying a triangular-wave voltage (U = 198 V_{pp}, f = 40 Hz, R = 5 kΩ, T = 120 °C, P_S = 410 nC cm^{-2}).

On applying a triangular-wave electric field above a threshold voltage of 25 V µm^{-1}, in a 5 µm non-coated ITO cell, the Col$_r$ phase is switchable, i.e. two polarisation current peaks per half period were recorded, which indicates an AF ground state (P_S = 410 nC cm^{-2}, Fig. 5.53).

The extinction crosses of the synclinic domains (Fig. 5.53a) rotate into a position parallel to the crossed polarisers, indicating an anticlinic organization with an equal number of layers with opposite tilt direction (Fig. 5.53b). That means the switching process takes place between [Col$_r$]$_s$P$_{AF}$ state and [Col$_r$]$_a$P$_{FE}$ states. This switching process is very similar to the one described for the Col$_r$P$_{AF}$ phase (racemic [Col$_r$]$_s$P$_{AF}$ phase) of compounds **4b** and **5c.** The field-induced circular domains in which the extinction crosses are aligned along the directions of the crossed polarisers do not change on reversal or removal of the applied field (Fig. 5.53b,c). As already described for the Col$_r$P$_{AF}$ phases of dimers **4b** and **5c**, there is assumed that in the ground state of the bulk materials there are mesoscopic domains with synclinic–AF interlayer interfaces separated by defects where the interlayer correlation is anticlinic–FE, i.e. the tilt direction alternates from domain to domain (Fig. 5.34).[24,36,216] Further investigations were impossible because of the fast crystallisation of the material and of the tendency to short at the high voltages required, but these experimental findings in the 5 µm non-coated ITO cell are indication of a racemic [Col$_r$]$_s$P$_{AF}$ phase.

Another interesting behaviour is observed on application of higher electric fields in a 6 µm polyimide-coated ITO cell. Under the influence of a triangular-wave electric field of moderate amplitude, an increase of the birefringence is observed (Fig. 5.54a,b). However, no switching current is detected, indicating that the material remains AF. Above a threshold voltage of 25 V µm^{-1}, a similar switching process to the one described previously in the 5 µm non-coated ITO cell could be detected. For sufficiently high fields (> 30 V µm^{-1}), a drastic change in the texture occurs. This is evidenced by a drastic modification of the texture, passing through an intermediate stage with a *sandy* texture (Fig. 5.54c). This change is a phase transition to a SmCP$_{AF}$ phase with a *non-specific* smectic-reminiscent texture (Fig. 5.54d), and shows the typical AF switching of this phase (Fig. 5.54f), i.e. two polarisation current peaks per half period were recorded (the value of the P_S is now much higher: P_S = 770 nC cm^{-2}). Upon removal of the field, the virgin texture of the Col$_r$ phase is not recovered, and the texture relaxed to a *non-specific* smectic-reminiscent one (Fig. 5.54e). These high electric fields make the study problematic as thin (5-6 µm) LC samples have a tendency to short at the high voltages required.

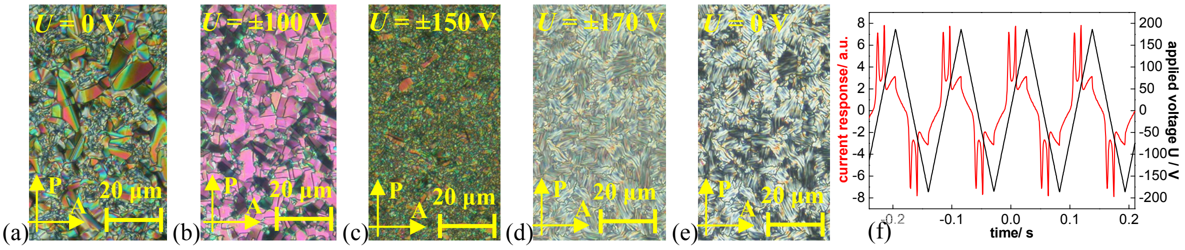

Figure 5.54: Electro-optical investigations of the Col$_r$P$_{AF}$ phase of compound **6b** in a 6 µm polyimide-coated ITO cell at 120 °C; textures observed between crossed polarisers in the same region of the sample; (a) U = 0 V; (b) field-induced mosaic-like texture at U = ± 100 V; (c) field-induced *sandy* texture at U = ± 150 V; (d) field-induced *non-specific* smectic-reminiscent texture at U = ± 170 V; (e) field-free *non-specific* smectic-reminiscent texture at U = 0 V; (f) AF switching current response obtained by applying a triangular-wave voltage (U = 372 V$_{pp}$, f = 20 Hz, R = 5 kΩ, T = 120 °C, P_S = 770 nC cm^{-2}).

Such field-induced smectic phases obtained by applying high electric fields on columnar phases were also reported by ORTEGA *et al.*[209] Consistent with their observations it takes a relatively long time for this structural transition to occur, as a major molecular rearrangement is clearly taking place. The series of images showing the possible $\mathrm{Col_r}$ to $\mathrm{SmCP_{AF}}$ transition in Figure 5.54a-e was taken over a period of 10 minutes. Unfortunately, the possible relaxation process of the field-induced texture could not be observed longer than few minutes, because of the crystallisation of the material.

The key difference between the results presented in this thesis and previously published work is the fact that the material does not relax back into the $\mathrm{Col_r}$ texture at low fields (10 V μm^{-1}) or removal of the electric field. KIRCHHOFF *et al.*[210] reported similar field-induced transitions where the material once transformed into the switching state the electric field can then be reduced significantly, down to 1 V μm^{-1}, and switching persists (the switching state has become *locked in*). Whereas ORTEGA *et al.*[209] report a return to the $\mathrm{Col_r}$ phase at zero fields, KIRCHHOFF *et al.*[210] observed a relaxation into a homeotropic texture. In the case of the $B_{1\mathrm{rev}}$ phase reported by SZYDLOWSKA *et al.*[94] the defect texture is also maintained after the onset of switching. The texture of the $\mathrm{Col_r}$ phase of dimer **6b** relaxed to a *non-specific* smectic-reminiscent texture, not very different from the field-induced texture. Although X-ray data are yet to be obtained to confirm the structure of the field-induced phase, there are strong arguments that our results reported in this thesis are another example of a $\mathrm{Col_r}$-$\mathrm{SmCP_{AF}}$ field-induced transition.

Dimer **6b** is a good example to point out that surface interactions are of great importance for the observed switching behaviour. However, if 6 µm polyimide-coated cells are used, a field-induced smectic phase with a repolarisation current curve could be observed. The reasons could be the possibility of applying an electric field above 30 V μm^{-1} (in contrast to the 5 µm cell where the material short at this high voltage required) and the better orientation of the molecules in the polyimide-coated cell. The field-induced smectic phase shows a value of the P_S much higher (P_S = 770 nC cm^{-2}). We can conclude that the AF switching is the result of the steric frustration arising from very large *alkyl* chains, either leading to the formation of unfavourable inter-ribbon interfaces ($\mathrm{Col_rP_{AF}}$ phase), or to the separation of the bent cores in the layers which reduces the polar order and hence decreases the surface coupling ($\mathrm{SmCP_{AF}}$ phase). The switching of the AF ground state into the FE state requires significant energy and the threshold voltage for this switching process becomes much higher than in the original $\mathrm{Col_r}$ phase. In summary, we have observed a $\mathrm{Col_r}$-$\mathrm{SmCP_{AF}}$ transition induced by a rather strong electric field. The transition takes place through a profound molecular reorganization, involving the alignment of the dipoles and the formation of smectic layers with tilted molecules.

5.2 Effect of the length of the terminal chain *p* attached to the calamitic mesogenic unit on the mesophase behaviour of dimer series 1 – 6

A further aspect of our systematic investigation is the influence of the length of the terminal chain *p* attached to the calamitic mesogenic unit on the mesophase behaviour of the dimer series **1** – **6**. For this reason the compounds **1** – **6** presented in sections 5.1.1 and 5.1.2 are listed in groups of two or three compounds which have a constant length of the spacer (*m*) and of the *alkyloxy* chain on the bent-core unit (*n*), however the length of the terminal chain attached to the calamitic part (*p*) varies. This allows an appropriate comparison of the mesophase behaviour from this new point of view. The mesophase behaviour and transition temperatures taken from the first DSC cooling scan (10 Kmin^{-1}) for the series **1** – **6** are given in Figure 5.55 and Table 5.3.

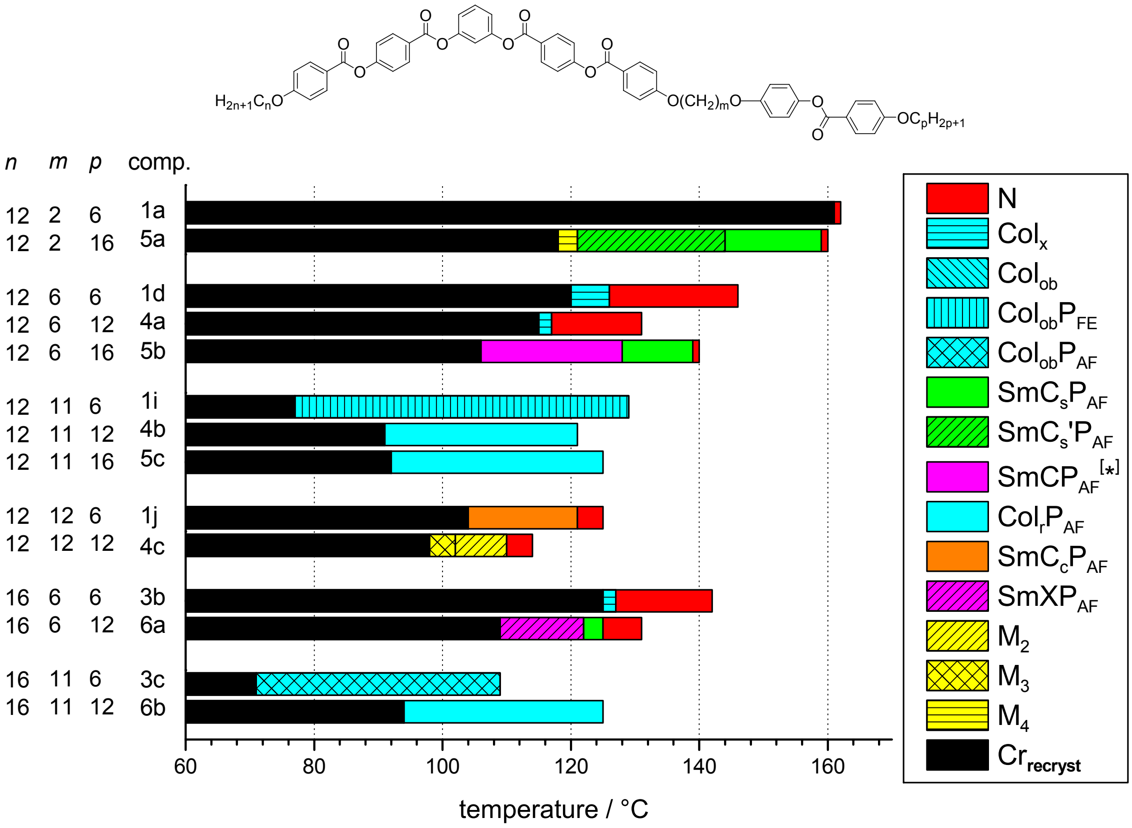

Figure 5.55: Transition temperatures (°C) of dimer series **1** – **6**, taken from the first DSC cooling scans (10 Kmin^{-1}).

For the dimers **1a** and **5a** with the shortest spacer length (m = 2) the elongation of the terminal *alkyloxy* chain attached to the calamitic mesogenic unit results in the appearance of additional polar smectic phases. The dimer **1a** displays a nematic phase, whereas the dimer **5a**, with relatively long terminal *alkyloxy* chains exhibits two enantiotropic mesophases and two monotropic mesophases (N- SmC$_s$P$_{AF}$- SmC$_s$'P$_{AF}$-M$_4$).

The dimers **1d** and **4a** (m = 6) exhibit nematic and columnar Col$_x$ phases. By further elongation of the terminal *alkyloxy p* chain, instead of columnar phases as previously found for the first two dimers, polar smectic phases could be observed, i.e. the dimer **5b** presents three mesophases: N - SmC$_s$P$_{AF}$ - SmCP$_{AF}$$^{[*]}$ (see section 5.1.2.4). For their homologue dimers **3b** and **6a** with (m = 6), with elongated terminal chains at the bent shape moiety (n = 16), similar phase sequences were observed. **3b** shows two monotropic mesophases, a nematic phase and a Col$_x$ phase. The elongation of the terminal *alkyloxy* chain attached to the calamitic mesogenic unit results in the appearance of a nematic phase and an additional polar smectic phases, i.e. the dimer **6a** (p = 12) exhibits three mesophases: N-SmC$_s$P$_{AF}$-SmXP$_{AF}$ (a probable SmC$_G$-like phase or *dark conglomerate phase*, see section 5.1.2.5).

All the dimers with m = 11 exhibit different columnar phases, independent of the chain length p. The dimer with the longest spacer length **1j** (m = 12) shows nematic and an intercalated smectic SmC_cP_{AF} phase. The elongation of the terminal *alkyloxy* chain *p* attached to the calamitic mesogenic unit results for the analogue compound **4c** in the appearance of three different monotropic phases: a high-temperature nematic phase, a M_2 (probable Col_x) phase and an optically isotropic M_3 phase (probable *dark conglomerate phase*).

A general tendency of a mesophase stabilization is found here: the transition temperatures of the dimers **1** – **6** are first decreasing with elongation of the terminal chain *p* attached to the calamitic part from $p = 6$ to 12 and then rise again by further elongation to $p = 16$.

5.3 Effect of the length of the terminal chain *n* attached to the bent-core mesogenic unit on the mesophase behaviour of dimer series 1 – 6

Next, the influence of elongating the terminal chain *n* attached to the bent-core mesogenic unit on the mesophase behaviour of the dimer series **1 - 6** shall be investigated. The accordingly rearranged list of compounds **1 - 6** presented in sections 5.1 and 5.2 are presented in groups of two or three compounds which have a constant length of the spacer (*m*) and of the *alkyloxy* chain on the calamitic part (*p*), however the length of the terminal chain attached to the bent-core unit (*n*) varies. The mesophase behaviour and transition temperatures taken from the first DSC cooling scan (10 $Kmin^{-1}$) for the series **1** – **6** are given in Figure 5.56 and Table 5.3.

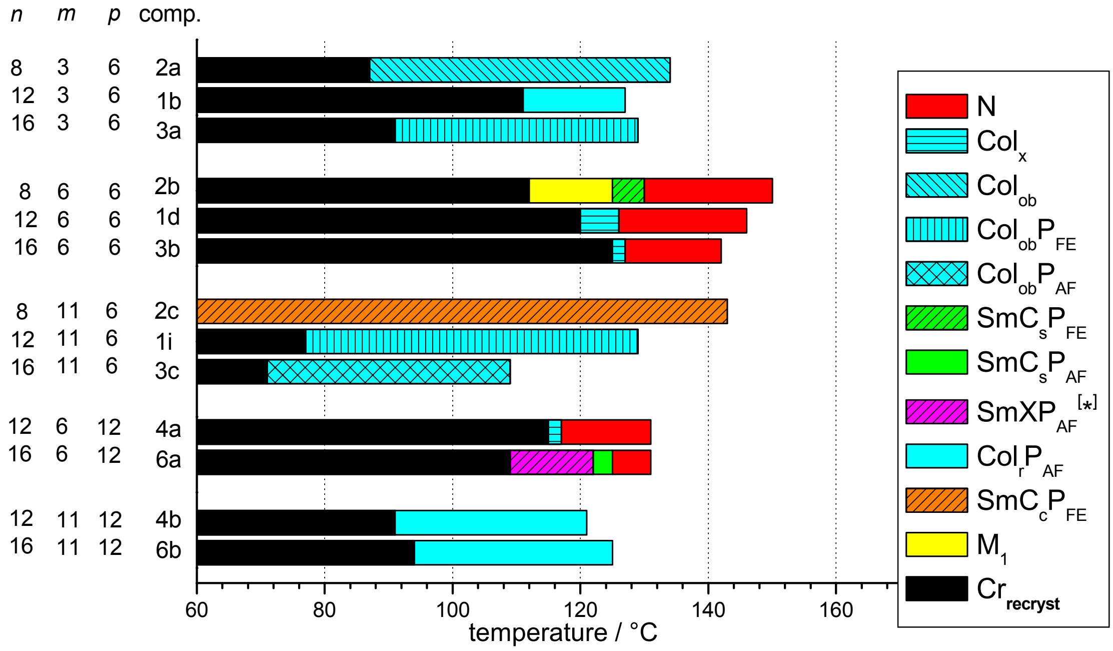

Figure 5.56: Transition temperatures (°C) of dimer series **1** – **6**, taken from the first DSC cooling scans (10 K min^{-1}).

All dimers with an *odd* number of methylene units in the flexible spacer ($m = 3$, 11) present columnar phases of different types. An exception is dimer **2c** ($n = 8$) which exhibits an enantiotropic SmC_cP_{FE} phase. The lattice parameters of the columnar phases are dependent on the length of this chain *n*. The dimer **2a** with the shortest terminal chain ($n = 8$) presents the smaller lattice parameters ($a = 2.73$ nm, $b = 4.11$ nm, see Table 5.3). On further increasing of the terminal chain length to $n = 16$, for the compound **3a** the lattice parameter *a* is 2 times higher and *b* is only slightly increased compared to the value found for the compound **2a**. The number of the molecules in the unit cell in the Col_{ob} phases is also increasing with increasing *n* length. The correlation of *a* and n_{cell} speaks for the molecular being packed along *a* in one ribbon. For the compounds **1i** and **3c** which exhibit Col_{ob} phases and resp., **4b** and **6b** which exhibit Col_rP_{AF} phases, the effect of the elongation of the terminal *alkyloxy* chain at the bent-core mesogenic unit on the lattice parameters is considerably attenuated.

All the dimers with an *even* number of methylene units in the flexible spacer (*m* = 6) exhibit a high temperature nematic phase in combination with smectic and columnar phases, independent of the chain length *n*. The dimer **2b** with the octyloxy chain (*n* = 8) exhibits an enantiotropic nematic and two monotropic phases, i.e. a N-SmC_sP_{FE} -M_1 phase sequence. On increasing the length of the terminal chain attached to the bent unit *n*, for dimer **1d** (*n* = 12) and dimer **3b** (*n* = 16) N-Col_x phase sequence could be observed.

The dimer **4a** (*n* = 12) exhibits two monotropic mesophases: a nematic and a columnar, Col_x phase. For its homologues, dimer **6a** (*n* = 16) three mesophases could be observed: N-SmC_sP_{AF}-$SmXP_{AF}$ phases (probable SmC_G-like phase or *dark conglomerate phase*, see section 5.1.2.5).

The increase of the length of the terminal chain *n* attached to the bent-core unit results in a mesophase destabilization. An exception to this tendency is found for the dimers **4b** and **6b** with an *odd* spacer (*m* = 11) and longer chain on the calamitic part (*p* = 12). An increase of the values of the spontaneous polarisation, P_S, on increasing the length of the terminal *alkyloxy* chain *n* and *p* is observed for dimers **1-6**.

5.4 Effect of the type of the groups *X*, *Y* linking the spacer to the bent-core mesogenic unit and the calamitic moiety on the mesophase behaviour of dimer series 7 – 12

This chapter is focusing on the influence of the type of the groups ***X*** and ***Y*** connecting the spacer with the two different mesogenic moieties on the mesophase behaviour in different dimer series: series **7 – 9** (connecting groups ***X*** = –**COO**- and ***Y*** = –O- and *m* = 6, 11) and series **10 – 11** (connecting groups ***X*** = –**OOC**- and ***Y*** = –O- and *m* = 5), and with different lengths of the terminal *n-alkyloxy* chains with *n* = 12, 16 and *p* = 6, 12. Furthermore, compound **12**, which has the longest spacer, *m* = 15, and different connecting groups (***X*** = –O- and ***Y*** = –**COO**-) between spacer and the two mesogenic units is presented. The mesophase behaviour of these new compounds is compared with the mesophase behaviour of the analogues dimers **1-6** with an *ether* connecting group described in chapters 5.1 -5.3. The transition temperatures and mesophase behaviour for dimer series **7 – 12** are listed in Table 5.5 and Figure 5.57.

Table 5.5: Transition temperatures [°C], mesophase types, transition enthalpy values [kJ/mol], layer spacing *d* [nm], tilt angle τ of the molecules [°] with respect to the layer normal in SmC phases and with respect to the normal to *a* in Col$_r$ phases, lattice parameters (*a*, *b*, *γ*) and P_S values of the compounds **7 – 12**.[a]

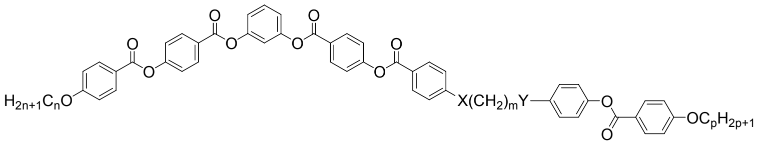

Comp.	*n*	*m*	*p*	*X*	*Y*	Transitions temperatures [°C] Δ*H* [kJ·mol^{-1}]	Phase type	Lattice parameters					P_S *nC/cm²*
								d [nm]	τ [°]	*a* [nm]	*b* [nm]	γ [°]	
7a	12	6	6	**COO**	**O**	Cr 135 (Col$_x$P$_{FE}$ 128) I *67.3 26.6*	Col$_x$P$_{FE}$		-[c]	-[c]	-[c]	-[c]	240
7b	16	6	6	**COO**	**O**	Cr 133 (Col$_r$P$_{FE}$ 126) I *66.3 27.5*	Col$_r$P$_{FE}$		0	12.45	6.28	90	370
8a	12	6	12	**COO**	**O**	Cr 129 Col$_r$P$_{FE}$ 137 I *32.3 27.6*	Col$_r$P$_{FE}$		7	11.62	6.29	90	330
8b	16	6	12	**COO**	**O**	Cr 131 Col$_r$P$_{FE}$ 139 I *33.2 25.7*	Col$_r$P$_{FE}$		27	11.38	6.63	90	390
9a	12	11	6	**COO**	**O**	Cr 109 (Col$_x$P$_{FE}$ 103 N 105) I *67.1* -[b] -[b]	N Col$_x$P$_{FE}$	-[c]	-[c]	-[c]	-[c]	-[c]	380
9b	16	11	6	**COO**	**O**	Cr 111 (N 103) I *69.6* -[b]	N						
10a	12	5	6	**OOC**	**O**	Cr 137 Cr*P$_{FE}$ 169 I *14.0 68.2*	Cr*P$_{FE}$	-	-	-	-	-	340
10b	16	5	6	**OOC**	**O**	Cr 131 Cr*P$_{FE}$ 168 I *15.2 59.7*	Cr*P$_{FE}$	-	-	-	-	-	430
11a	12	5	12	**OOC**	**O**	Cr 117 SmC’$_a$P$_{AF}$ 128 SmC$_a$P$_{AF}$ 139 N 148 I *42.8 18.8 0.4 2.3*	N SmC$_a$P$_{AF}$ SmC’$_a$P$_{AF}$	5.78 5.71	37 37				570 870
11b	16	5	12	**OOC**	**O**	Cr 115 SmC’$_s$P$_{AF}$ 123 SmC$_s$P$_{AF}$ 136 N 141 I *32.5 5.7 0.8 2.0*	N SmC$_s$P$_{AF}$ SmC’$_s$P$_{AF}$	5.87 5.80	40 44				690 890
12	12	15	16	**O**	**COO**	Cr 95 Cr* P$_{AF}$ 106.5 N 107 I *44.2 28.9* -[b]	N Cr*P$_{AF}$	-	-	-	-	-	190

[a] Transition temperatures (°C) and enthalpy values [kJ/mol] of dimers **7 – 12** were taken from the second DSC heating scans (10 Kmin^{-1}); values in parentheses indicate monotropic mesophases, in this case the transition temperatures and enthalpy values were taken from the first DSC cooling scans and the transition temperatures were checked by polarising microscopy; [b] the transition is not detectable on DSC and the transition temperature value is determined by polarising microscopy; [c] could not be determined due to rapid crystallization of the sample.

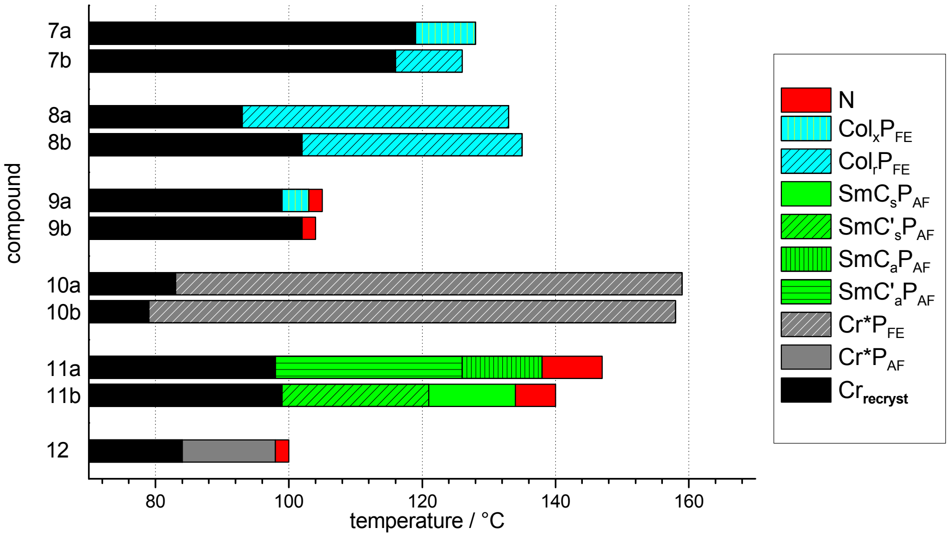

Figure 5.57: Transition temperatures (°C) of compounds **7–12**, taken from the first DSC cooling scans (10 Kmin^{-1}).

5.4.1 Substitution of the *ether* group in position *X* by the *carboxyl* group in dimer series 7 – 9

The transition temperatures of dimer series **7 – 9** (connecting groups ***X*** = –COO- and ***Y*** = –O-) and their mesophase behaviour are shown in Figure 5.57 and Table 5.5. These dimers are studied in comparison with the analogues dimers connected through an *ether* group, dimer series **1 – 6**. The dimers **9** (*m* = 11, *p* = 6) with an *even*-numbered spacer (summarizing the simple units of the flexible spacer that corresponds to an *odd* number of methylene units) display mesomorphism in accordance with their overall linear shape. Similar to the series **1 – 6**, additional to the nematic phase, also a columnar phase was found. Only columnar phases were found for the dimers series **7** (*m* = 6, *p* = 6) and **8** (*m* = 6, *p* = 12) which posses an *odd*-numbered spacer (but with an *even* number of methylene group) in accordance with the series **1 – 6**.

5.4.2 Substitution of the *ether* group in position *X* by the *oxycarbonyl* group in dimer series 10 – 11

The transition temperatures and mesophase behaviour for dimer series **10 – 11** are listed in Figure 5.57 and Table 5.5. The influence of the structure of the connecting groups ***X*** and ***Y*** on the mesophase behaviour of the dimers **10 – 11** (***X*** = –OOC- and ***Y*** = –O-) is studied in comparison with the analogues dimers **1 – 6** which are linked through *ether* groups and resp. with the dimers **7 – 9** connected through an *ester* and an *ether* group (***X*** = -COO- and ***Y*** = –O-).

There are considerable changes of the mesophase behaviour on introducing the ***X*** = –OOC- connecting group between the bent-core unit and spacer unit (actually, on reversing the *ester* linking group direction used for dimers **7 – 9**). The compounds **10** exhibit crystalline polar phases. On the other side, the compounds **11**, with an elongated terminal chain attached to the calamitic mesogenic unit, exhibit nematic and polar smectic phases. The introduction of the ***X*** = – OOC- connecting group between the bent-core unit and spacer unit resulted also in a strong effect on the mesophase stability. On increasing the length of the terminal chain of the calamitic mesogenic unit a destabilizing effect of the mesophase could be observed. On increasing the length of the terminal chain of the bent-core mesogenic unit in general, a weak destabilizing effect of the mesophase could be found.

5.4.2.1 Occurrence of a polar crystalline Cr*P_{FE} phase for dimers 10

The data listed in Table 5.5 reveal that the two dimers **10** (*m* = 5, *p* = 6, ***X*** = –OOC- and ***Y*** = –O-) with an *even* numbered spacer (summarizing the simple units of the flexible spacer that corresponds to an *odd* number of methylene units) exhibit a crystalline phase with polar switching, a Cr* phase. Such a polar switching in the crystalline modification of a bent-core compound is being reported for the first time by WEISSFLOG *et al.*[243]

The Cr* phases of the two dimers **10** present similar optical, electro-optical and structural features. As a representative example the Cr* phase of compound **10b** (*n* = 16) is described in more detail (Fig. 5.58). In the DSC scans two phases can be distinguished (Cr* and Cr) and there are no significant changes for different heating or cooling rates. X-ray investigations were performed on surface-aligned samples. They give clear evidence for the crystalline nature of the low- and high-temperature phases. The X-ray pattern of the Cr* phase of **10b** displays a lot of strong reflections in the small- and in the wide-angle region, which characterize the phase under discussion as crystalline phase (see Fig. 5.58e). It should be noted that the transition from the high-temperature crystalline phase Cr* into the low-temperature phase Cr is indicated by only very small changes of the optical texture and the X-ray scattering diagram. The crystalline nature is also supported by the high enthalpy value at the transition to the isotropic phase (68 kJ mol^{-1}) whereas the clearing temperatures of the smectic phases or columnar phases formed by other dimer series do not exceed 30-35 kJ mol^{-1}, respectively. The texture of the high-temperature Cr* phase of compound **10b** could be slightly and irreversibly deformed by applying strong mechanical stress, in contrast to the low-temperature Cr phase. Independent of the experimental conditions the Cr* phase appears on cooling as a weakly birefringent modification (Fig. 5.58a). By application of an a.c. or d.c. field this crystalline phase adopts a *non-specific* texture with small birefringent domains (Fig. 5.58b). By applying a high threshold electric field of 30 V µm^{-1} and at low frequencies (5-10 Hz), the Cr* phase of **10b** is switchable, i.e. one polarisation current peak per half period was recorded which indicates a FE ground state (P_S values are 340 nC cm^{-2} for **10a**, and 430 nC cm^{-2} for **10b**). The field-induced birefringent textures of **10b** do not change on reversal (Fig. 5.58b) or on removal of the applied field (Fig. 5.58c). This confirms a switching by rotation around the long molecular axis. The Cr* phase of **10a** (n = 12) shows the same features. On the basis of these experimental findings both Cr* phases of dimers **10** are assigned as Cr*P$_{FE}$ phases.

There are some differences between the results of this thesis and the results described in the reference[243] for *simple* bent-core mesogens. In the case of dimers **10**, no field-induced modifications of these crystalline phases could be found by the application of a sufficiently high electric field above the transition temperatures to the isotropic phase. Unfortunately, no circular domains could be obtained under a d.c. electric field for a better investigation of the switching process. The ground state of the Cr* phases of dimers **10** is FE and the corresponding P_S values calculated are much smaller than those reported in reference.[243]

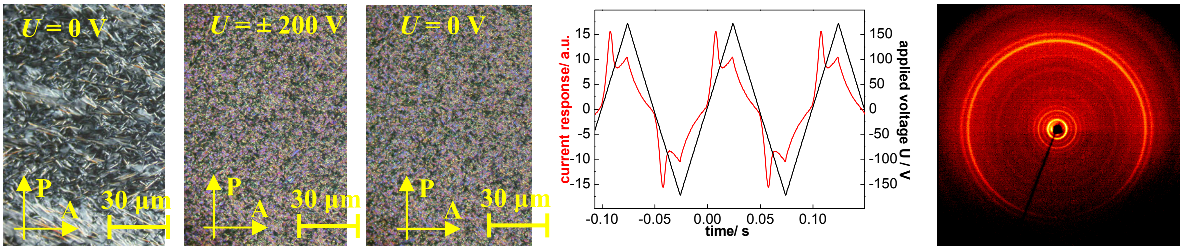

(a) (b) (c) (d) (e)

Figure 5.58: The Cr*P$_{FE}$ phase of compound **10b** at 156 °C: (a-d) electro-optical investigations of the switching process in a 5 µm non-coated ITO cell; textures observed between crossed polarisers in the same region of the sample; (a) U = 0 V, before starting the experiment; (b) U = ± 200 V; (c) U = 0 V; (d) FE switching current responses obtained by applying a triangular-wave voltage (U = 343 V$_{pp}$, f = 10 Hz, R = 5 kΩ, T = 157 °C, P_S = 430 nC cm^{-2}); (e) XRD pattern of the Cr*P$_{FE}$ phase.

5.4.2.2 Electro-optical switching behaviour of the SmC_aP_{AF} phases of dimer 11a

The two dimers **11** (*m* = 5, *p* = 12, ***X*** = –OOC- and ***Y*** = –O-) with an *even* numbered spacer and a longer terminal chain attached to the calamitic mesogenic unit exhibit enantiotropic nematic and smectic phases. The nematic phases of the two dimers are similar to the nematic phases described above in this thesis and exhibit the same unusual optical and electro-optical behaviour (see chapter 5.1.1.2). The enantiotropic nematic and the high-temperature SmC phases of compound **11a** (*n* = 12) were identified according to their characteristic schlieren textures (Fig. 5.59a). Depending on the boundary conditions a birefringent fan-shaped texture could be also observed for the high-temperature SmC phase (Fig. 5.59b). The texture of the low-temperature SmC phase depended strongly on the texture of the preceding SmC phase. This phase appeared either as a *non-specific* low-birefringent texture with small islands of birefringent broken fan-shaped texture (Fig. 5.59c) or as a very low birefringent *grainy* texture.

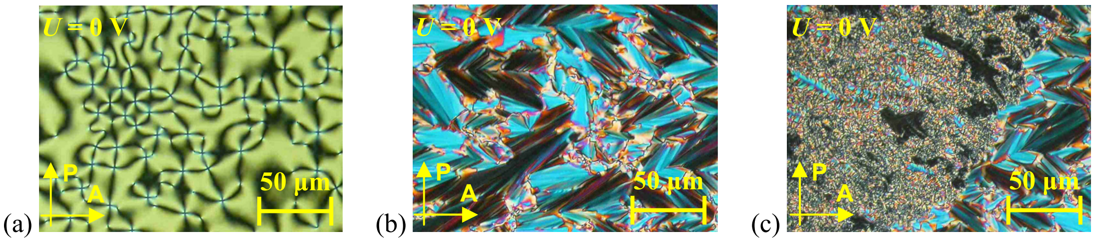

Figure 5.59: Textures of mesophases of dimer **11a** observed between crossed polarisers in the same region of the sample on cooling in a 5µm non-coated ITO cell: (a) N phase at 143 °C; (b) high-temperature SmC phase at 133 °C; (c) low-temperature SmC phase (uper-left) growing from high-temperature SmC (lower-right).

X-ray measurements performed on the high-temperature mesophase of compound **11a** at 145 °C showed the scattering typical of a nematic phase with SmC – like cybotactic groups when aligned in the magnetic field on cooling (Fig. 5.60a,b). The measurements at 130 °C and 122 °C confirmed the presence of two SmC phases with molecules tilted with respect to the layer normal and they showed very similar patterns. The X-ray measurements did not show any significant change in the layer distance on cooling, including the transition from the high-temperature SmC (Fig. 5.60c,d, *d* = 5.78 nm) to the lower-temperature SmC' phase (*d* = 5.71 nm). An average tilt angle of the molecular long axis with respect to the layer normal can be calculated from the position of the maxima of the inner scattering in both SmC phases (τ = 37°). These SmC phases were assigned as SmC_a and SmC_a' phases.

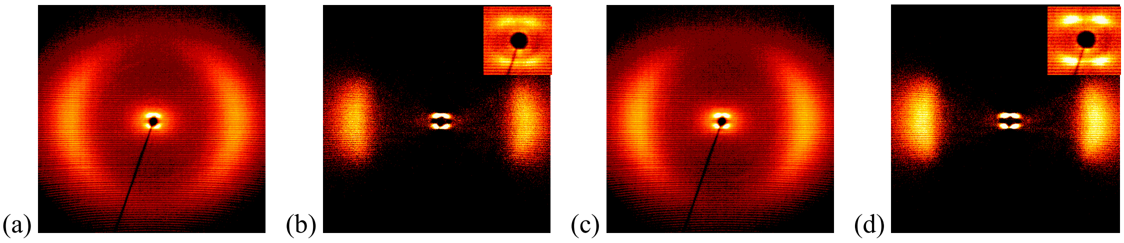

Figure 5.60: XRD patterns of an aligned sample of compound **11a**: (a-b) nematic phase at 145 °C: (a) original pattern; (b) the same XRD pattern, but the intensity of the isotropic liquid is subtracted; the inset shows the small angle scattering; (c-d) SmC_a phase at 130 °C: (c) original pattern; (d) the same XRD pattern, but the intensity of the isotropic liquid is subtracted; the inset shows the small angle scattering.

The nematic phase of compound **11a** shows the same unusual electro-optical behaviour on applying an electric field as previously described in the section 5.1.1.2. The application of an electric field (10 Vμm^{-1}) on the SmC$_a$ phase leads to the formation of a birefringent smooth fan-like texture with multiple circular domains where the extinction crosses are inclined with respect to the directions of the crossed polarisers (about 40°, which is in good agreement with the tilt angle found by X-ray investigations) evidencing a synclinic organization of the molecules between adjacent layers (Fig. 5.61a,d).

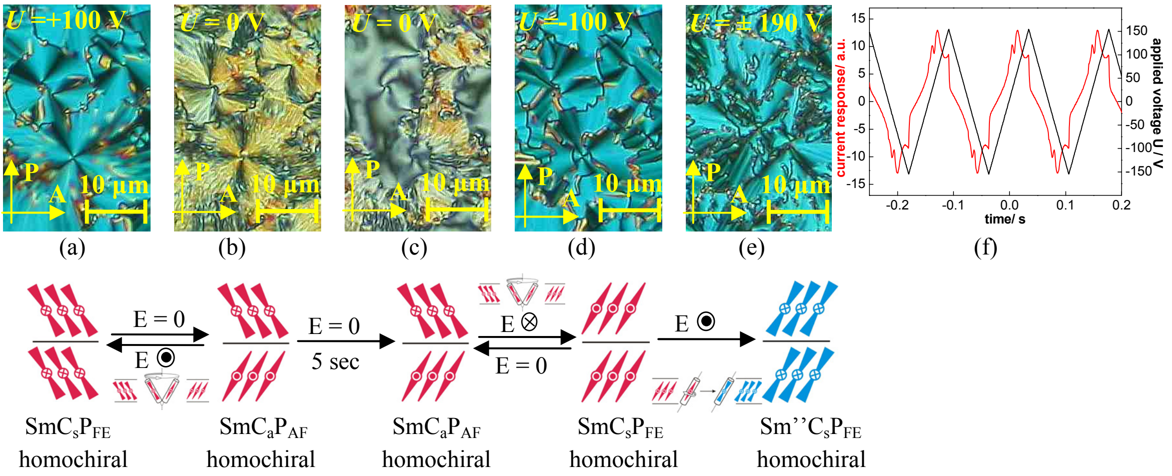

Figure 5.61: Electro-optical investigations on the SmC$_a$P$_{AF}$ phase of dimer **11a** at 130 °C; textures observed between crossed polarisers in the same region of the sample in a 5 µm non-coated ITO cell: (a,d) $U = \pm 100$ V; (b,c) $U = 0$ V; (e) the field induced SmC''$_s$P$_{FE}$ state at $U = \pm 190$ V; (f) AF switching current response obtained by applying a triangular-wave voltage (10 µm polyimide-coated ITO cell, $U = 309$ V$_{pp}$, $f = 7$ Hz, $R = 5$ kΩ, $T = 129$ °C, $P_S = 570$ nC cm^{-2}); (a-e) down: models of the organization of the molecules in the FE states (a,d,e), and in the AF ground state (b,c).

On removing the electric field the extinction crosses rotate to the position of the crossed polarisers and the birefringence significantly decreases (Fig. 5.61b). After another 5 seconds the texture relaxes to the original schlieren texture (Fig. 5.61c). By applying the electric field again, the same fan-shaped texture is induced and the extinction crosses of the circular domains rotate back to the original 40° position, whereby the sense of rotation is opposite for an opposite sign of the field. The current response presents two current peaks per half period of the applied triangular voltage (AF ground-state, $P_S = 570$ nC cm^{-2}, Fig. 5.61f). The relaxation from the field-induced FE state into the AF ground state obviously corresponds to the transition from the synclinic FE state (SmC$_s$P$_{FE}$) into the anticlinic AF state (SmC$_a$P$_{AF}$, see Fig. 5.61a-c). Hence, optical investigation clearly indicates a tristable switching by a collective rotation around a cone, which is an additional confirmation of the AF switching process. On the basis of these experimental findings the high-temperature SmC$_a$ phase of compound **11a** is AF with an anticlinic organization, i.e. a SmC$_a$P$_{AF}$ phase.

Interestingly, for a sufficiently high electric field (34 Vμm^{-1}), a change in the texture occurs which is accompanied by a slightly decrease of the birefringence and the occurrence of smaller circular domains with apparently identical inclination angle of the extinction crosses with respect to the crossed polarisers position (Fig. 5.61e). However it seems that the switching behaviour is different, that means the new field-induced fan-shaped texture is independent of the polarity of the applied field and the extinction crosses are not relaxing to the position of the crossed polarisers or to the original schlieren texture on removal of the applied field. Two current peaks per half period of the applied triangular voltage were observed also for this voltage (P_S = 590 nC cm^{-2}, is in the same range as the value found for the SmC$_a$P$_{AF}$ phase) but in contrast to the original SmC$_a$P$_{AF}$ phase, the switching process takes place by a collective rotation around the long molecular axis. This could give a hint that a Sm–Sm transition has been observed. Unfortunately, only short time observations (over a few minutes) were conducted because of the breakdown of the material at this high threshold voltage and further investigations were not possible. In the literature various reversible or irreversible field-induced transitions Sm–Sm, Col–Sm and in smectic phases, racemic to homochiral, have been reported.[107,214,225,234,244]

The low-temperature phase of compound **11a** is also an AF phase with an anticlinic organization, i.e. a SmC$'_a$P$_{AF}$ phase. The current response presents two peaks per half period of the applied triangular voltage (P_S = 870 nC cm^{-2}, Fig. 5.62f). On removing of the electric field a different relaxation mechanism could be observed depending on the experimental condition, as already discussed for the SmC'$_s$P$_{AF}$ phase of compound **5a** (see chapter 5.1.2.4).

(a) When *the field is removed fast* the extinction crosses of the birefringent field-induced texture rotate to the position of the crossed polarisers and the texture becomes dark (Fig.5.62a,b). The formation of nearly black textures, after removing the electric field, is obviously due to the tilt angle of about 45°, as already discussed in the chapter 5.1.2.4 and reported in the literature.[65,223,224,225] By applying the electric field again, the same fan-shaped texture is induced and the extinction crosses of the circular domains rotate back to the original 45° position, whereby the sense of rotation is opposite for an opposite sign of the field (Fig.5.62e). The optical investigation clearly indicates a tristable switching by a collective rotation around a cone. Such behaviour is typical for a SmC$_a$P$_{AF}$ phase.

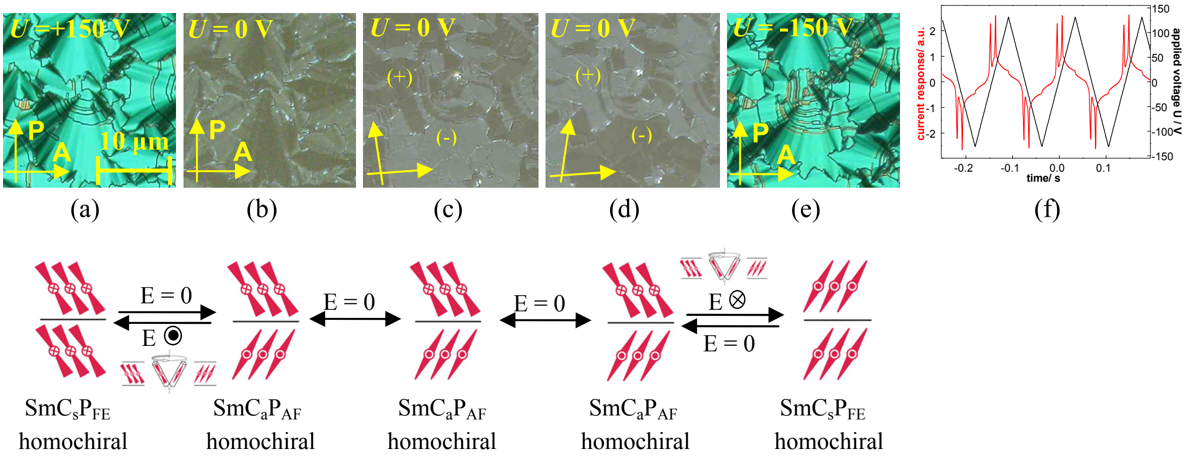

Figure 5.62: Electro-optical investigations on the SmC'$_a$P$_{AF}$ phase of dimer **11a** at 124 °C in a 5 µm non-coated ITO cell; textures observed in the same region of the sample under an applied d.c. field; (a,e) at U = ± 150 V; (b-d) at U = 0 V: (a,b,e) between crossed polarisers and (c,d) by rotating one polariser from the crossed position: (c) by +15° and (d) by -15°; (chiral (+) and (–) domains); (f) AF switching current response obtained by applying a triangular-wave voltage (U = 263 V$_{pp}$, f = 7 Hz, R = 5 kΩ, P_S = 870 nC cm^{-2}); (a-e, down): models of the organization of the molecules; in the FE states (a,e) and in the AF ground-state (b-d).

(b) On *removing* the applied field *very slowly* the extinction crosses of the birefringent field-induced texture are not moving, just the birefringence is drastically decreasing (this case is not described here because it is very similar to the switching process of the SmC'$_s$P$_{AF}$ phase of compound **5a**). If the electric field slowly increases again, the positions of the extinction crosses do not change also on reversal or again removing of the electric field. It seems that the field-induced FE state does not relax anymore into the AF ground state observed for the case (a). Such transition from the field-induced SmC$_s$P$_{FE}$ into the AF state, without rotation of the extinction cross could be realised if the chirality is changed in each second layer (*flipping of chirality*, already reported for the SmC'$_s$P$_{AF}$ phase of **5a** and in the literature[87,94,226,222]). On removal of the applied field domains of opposite handedness can be distinguished in the non-birefringent texture over the whole sample on rotating the polariser from the crossed position (Fig. 5.62c,d).

Compound **11b** (n = 16) exhibits a nematic phase and two smectic phases. The XRD measurements at 130 °C and 110 °C confirmed the presence of two SmC phases with molecules tilted with respect to the layer normal and they showed very similar patterns The X-ray measurements did not show any significant change in the layer distance on cooling, including the transition from the high-temperature SmC (d = 5.87 nm) to the lower-temperature SmC' phase (d = 5.80 nm). An average tilt angle of the molecular long axis with respect to the layer normal can be calculated from the position of the maxima of the outer diffuse scattering for the SmC phase, τ = 40°, and for the SmC' phase, τ '= 44°. On the basis of these experimental evidences the two SmC phases of compound **11b** were assigned as SmC$_s$ and SmC$_s$' phases. Electro-optical investigation showed that the nematic phase behaves similar to the nematic phases of compound **1 – 6,** but both smectic phases present different structural features and electro-optical switching processes. The switching behaviour of the two smectic phases SmC$_s$ and SmC'$_s$ phases is very similar to the already described behaviour of the SmC$_s$P$_{AF}$ and SmXP$_{AF}$ phases of compound **6a** (see Table 5.3, Fig. 5.49-5.51, section 5.1.2.5). Electro-optical measurements give evidence for an AF ground state in the high-temperature SmC$_s$P$_{AF}$ phase of compound **11b** (P_S = 690 nC cm^{-2}). The switching between the AF ground state and the switched FE states preferably takes place through the collective rotation of the molecules around their long molecular axes. The low-temperature SmC'$_s$P$_{AF}$ phase of compound **11b** exhibits quite similar optical and electro-optical properties as the one observed for the SmXP$_{AF}$ phase of compound **6a**. On the basis of these findings we can conclude that the low-temperature phase of compound **11b** is a SmC'$_s$P$_{AF}$ phase and on applying a relatively high threshold voltage a field-induced smectic SmC''$_s$P$_{AF}$ phase could be observed.

5.4.3 Substitution of the *ether* group in position *Y* by the *carboxyl* group: Occurrence of a polar crystalline Cr*P$_{AF}$ phase for dimer 12

The dimer **12** (n = 12, m = 15, p = 16, ***X*** = –O- and ***Y*** = –**COO**-) exhibits a nematic phase which exists over a very short temperature interval (0.5 K) and a crystalline phase with polar switching, a Cr* phase. The X-ray investigations, textural observations together with the DSC scans revealed that this Cr* phase is very similar to the Cr*P$_{FE}$ phase of compounds **10**. The *non-specific* weakly birefringent texture of compound **12** (Fig. 5.63b) exhibits domains of opposite handedness, visible by slightly rotating the polariser from the crossed position (Fig. 5.63c,d). In contrast to this Cr*P$_{FE}$ phase of compound **10**, the Cr* phase of compound **12** shows an AF response by applying a high threshold electric field of 30 V µm^{-1}, i.e. two polarisation current peaks per half period were recorded (P_S = 190 nC cm^{-2}). The *non-specific* texture turns into a birefringent texture with small domains (Fig. 5.63e). The application of a higher electric field (about 35 V µm^{-1}) leads to an increase of the birefringence and to a transition into a texture with bigger domains, reminiscent of a smectic-like phase (Fig. 5.63e). The field-induced textures do not change on reversal of the field (Fig. 5.63e,f) or on terminating the applied field. This confirms a switching by rotation around the long molecular axis. On the basis of these experimental findings the Cr* phases of compound **12** is assigned as Cr*P$_{AF}$ phase. There are some differences between the polar Cr* phases presented in this thesis, i.e. the ground state of the Cr* phase of the dimer **12** is AF and the corresponding P_S value is much smaller than the value reported for the Cr*P$_{FE}$.of dimers **10**.

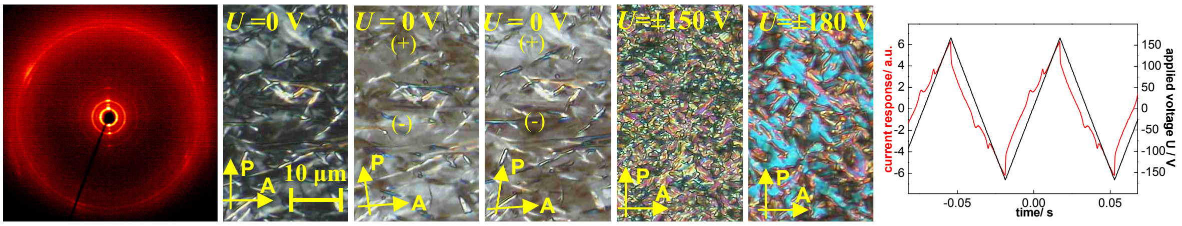

(a) (b) (c) (d) (e) (f) (g)

Figure 5.63: The Cr*P$_{AF}$ phase of compound **12** at 98 °C: (a) XRD pattern; (b-g) electro-optical investigations in a 5 µm non-coated ITO cell; textures observed in the same region of the sample on applying a d.c. electric field: (b-d) at U = 0 V as observed (b) between crossed polarisers and (c,d) by rotating one polariser by +15° (c) and by -15° (d) from the crossed position (chiral (+) and (–) domains); (e) U = ± 150 V; (f) U = ± 180 V; (g) AF switching current response obtained by applying a triangular-wave voltage (U = 334 V$_{pp}$, f = 9 Hz, R = 5 kΩ, P_S = 190 nC cm^{-2}).

Summarizing the chapter 5.4, it was found that the introduction of different connecting groups between the spacer unit and the two mesogenic units resulted in the appearance of new mesophases. A *highlight* of this thesis is the occurrence of crystalline polar phases with FE and AF ground states. It seems that the introduction of the connecting group ***X*** = -OOC- between the bent-core mesogenic unit and the spacer unit for the compounds **10** and the introduction of the connecting group ***Y*** = -COO- between spacer unit and calamitic mesogenic unit for compound **12** results in occurrence of similar crystalline polar phases. Increasing the terminal chain p attached to the calamitic mesogenic unit in dimers **11** resulted in the appearance of enantiotropic nematic and smectic phases (for **11b** in accordance with the analogue dimer connected through *ether* groups, dimer **6a)**. Also new in this chapter is the observation of a SmC'$_s$P$_{AF}$ phase for compound **11b**, very similar to the potential *dark conglomerate* or SmC$_G$ phases (SmXP$_{AF}$ phase) described for compound **6a** in chapter 5.1.2.5. It can be suggested that this SmC'$_s$P$_{AF}$ phase has similar structural features as the SmXP$_{AF}$ phase of **6a**, but there is not enough experimental evidence. The values of the spontaneous polarisation P_S of the dimers under discussion are increasing on elongating the spacer m and the terminal chains n and p attached to the mesogenic units.

5.5 Variations of the bent-core mesogenic unit of dimers 13 – 28

The next point of our systematic investigation is the study on the influence of several variations on the bent-core mesogenic unit on the mesophase behaviour of '*banana-calamit*' dimers of **type I**. It will be shown that the fine adjustment of the chemical structure in these systems leads to dimers with different mesophases and interesting variations of the physical properties.

At first, the direction of the *ester* linking groups in the bent-core unit is varied (dimers **13 - 19**). Next, the results of these investigations are combined with a study on the role of the type and the direction of the connecting groups ***X*** and ***Y*** in dimers **20 - 24**. Afterwards, the variation of the polarity of the terminal group ***R***, lateral substitution and enhancing the number of aromatic rings is discussed in detail.

5.5.1 Variation of the direction of the *ester* linking groups *E* in the bent-core mesogenic unit of dimer series 13 – 19[196]

One of the main subjects of this thesis is the influence of the direction of the *ester* linking groups on the mesophase behaviour of the discussed dimer **type I**. To obtain comparable results, the following molecular parameter have been selected: the bent-core unit contains five *phenyl* rings which are all connected by carboxylic groups ***E***; the calamitic unit is a *phenyl benzoate*; *alkyloxy* chains are attached to the two terminal positions; the *alkylene* spacer is linked to both mesogenic moieties by *ether* oxygens. Variations have been done in the length *n* and *p* of the terminal *hydrocarbon* chains and in the number *m* of methylene units in the aliphatic spacer. After that, the direction of each of the four *ester* groups ***E*** between the *phenyl* rings of the bent-core unit has been inverted.

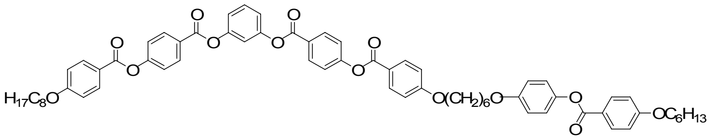

E$_0$ structure - dimer **2b** (*n*=8, *m*=6; *p*=6): Cr 145 (M$_1$ 125 SmC$_s$P$_{FE}$ 130) N 151 I

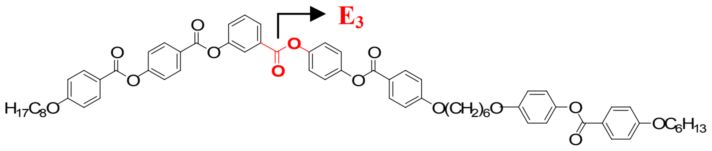

E$_3$ structure - dimer **13b** (*n*=8, *m*=6; *p*=6): Cr 147 (Col$_x$ 127 N$_x$ 129) N 167 I

Figure 5.64: Example explaining the abbreviation system for the ***E*** groups; mesophase behaviour and transition temperatures (°C) of dimers **2b** (E$_0$) and **13b** (E$_2$).

This section introduces the non-symmetrical dimers **13** – **19** (*n* = 8, 12, 16; *m* = 3, 6, 11; *p* = 6, 12). They will be compared with the analogues dimers in series **1** – **4** which have a bent-core unit possessing a central *resorcinol* fragment and both *ester* linking groups within one wing have the same direction. This is the ***reference structure*** for the bent-core unit in this thesis assigned as **E$_0$**.

Table 5.6: Transition temperatures [°C], mesophase type, transition enthalpy values [kJ/mol], layer spacing *d* [nm], tilt angle τ of the molecules [°] with respect to the layer normal in SmC phases and with respect to the normal to *a* in Col$_{ob}$ phases, lattice parameters (*a*, *b*, *γ*) and P_S values of compounds **13 – 19** and their analogues dimers **1b, 1d, 1i, 2b, 3b, 4a**.[a]

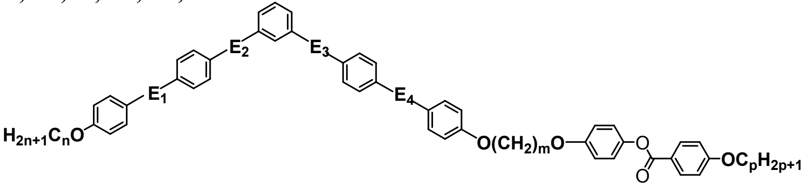

Comp.	*n*	*m*	*p*	*E*[d]	Transitions temperatures [°C] Δ*H* [kJ·mol^{-1}]	Phase type	Lattice parameters					P_S *nC/cm*^{2}
							d [nm]	τ [°]	*a* [nm]	*b* [nm]	γ [°]	
2b	8	6	6	E$_0$	Cr 145 (M$_1$ 125 SmC$_s$P$_{FE}$ 130) N 151 I *76.4 0.5 13.4 1.6*	N SmC$_s$P$_{FE}$ M$_1$ [c]	5.80 -[c]	26 -[c]	- -[c]	- -[c]	- -[c]	150 -[c]
13a	8	6	6	E$_2$	Cr 155 (SmC$_x$ 134) N 171 I *70.0* 0.7 *2.9*	N SmC$_x$ [c]	-[c]	-[c]		-	-	-[c]
13b	8	6	6	E$_3$	Cr 147 (Col$_x$ 127 N$_x$ 129) N 167 I *55.8* -[b] *1.0 4.0*	N N$_x$ Col$_x$ [c]		-[c]	-[c]	-[c]	-[c]	-[c]
1b	12	3	6	E$_0$	Cr 150 (Col$_r$P$_{AF}$ 127) I *65.7 24.0*	Col$_r$P$_{AF}$		11	7.57	5.51	90.0	350
14	12	3	6	E$_2$	Cr 147 I *54.4*		-	-	-	-	-	-
1d	12	6	6	E$_0$	Cr 148.5 (Col$_x$ 125.5 N 145.5) I *61.2 13.1 1.3*	N Col$_x$ [c]		-[c]	-[c]	-[c]	-[c]	-[c]
15a	12	6	6	E$_1$	Cr 146 SmA 149 N 150 I *48.5* -[b] *5.4*	N SmA	7.00	0				-
15b	12	6	6	E$_2$	Cr 159 (SmC$_x$ 148) N 166 I *69.8 0.04 3.1*	N SmC$_x$ [c]	-[c]	-[c]				-[c]
15c	12	6	6	E$_3$	Cr 145 (Col$_x$ 130) N 161 I *64.9* -[b] *2.6*	N Col$_x$ [c]		-[c]	-[c]	-[c]	-[c]	-[c]
15d	12	6	6	E$_4$	Cr 140 (Col$_x$ 130) N 143 I *54.1* -[b] *1.7*	N Col$_x$ [c]		-[c]	-[c]	-[c]	-[c]	-[c]
1i	12	11	6	E$_0$	Cr 121 Col$_{ob}$P$_{FE}$ 132.5 I *58.8 25.3*	Col$_{ob}$P$_{FE}$		44	3.20	5.00	110.0	380
16a	12	11	6	E$_1$	Cr 126 USmC$_a$P$_{AF}$ 130 I *39.7 24.7*	USmC$_a$P$_{AF}$		22	36.8	6.61	90.0	550
16b	12	11	6	E$_2$	Cr 131 (Col$_x$ 128 N 129) I *67.4 21.2 0.04*	N Col$_x$ [c]			-[c]	-[c]	-[c]	-[c]
3b	16	6	6	E$_0$	Cr 150 (Col$_x$ 126.5 N 142) I *65.0* -[b] *1.4*	N Col$_x$ [c]		-[c]	-[c]	-[c]	-[c]	-[c]
17a	16	6	6	E$_2$	Cr 160 (SmC$_x$ 144) SmA 163 N 164 I *63.5* -[b] *0.5 5.3*	N SmA SmC$_x$ [c]	7.19 -[c]	0 -[c]	-	-	-[c]	- -
17b	16	6	6	E$_3$	Cr 149 (Col$_x$ 133) N 158 I *58.9* -[b] *2.9*	N Col$_x$ [c]		-[c]	-[c]	-[c]	-[c]	-[c]
4a	12	6	12	E$_0$	Cr 140 (Col$_x$ 115.5 N 131) I *86.3* -[b] *1.6*	N Col$_x$ [c]		-[c]	-[c]	-[c]	-[c]	-[c]
18	12	6	12	E$_2$	Cr 140 (SmC$_s$’P$_{AF}$ 131) SmC$_s$P$_{AF}$ 163 I *88.5 8.5 11.7*	SmC$_s$P$_{AF}$ SmC$_s$’P$_{AF}$	6.19 6.10	24 32				550 780
4b	12	11	12	E$_0$	Cr 126 (Col$_r$P$_{AF}$ 121) I *57.0 7.4*	Col$_r$P$_{AF}$		29	16.06	6.76	90.0	450
19	12	11	12	E$_2$	Cr 133 (Col$_r$ 131) I *85.2 30.3*	Col$_r$		-	21.4	6.89	90.0	-

[a] Transition temperatures (°C) and enthalpy values [kJ/mol] of dimers **13** – **19** and their analogues compounds **1b, 1d, 1i, 2b, 3b, 4a** were taken from the second DSC heating scans (10 Kmin^{-1}); values in parentheses indicate monotropic mesophases, in this case the transition temperatures and enthalpy values were taken from the first DSC cooling scans and the transition temperatures were checked by polarising microscopy; [b] the transition is not detectable on DSC and the transition temperature value is determined by polarising microscopy; [c] could not be determined due to rapid crystallization of the sample; [d] the direction of the *ester* linking group **E$_1$** - **E$_4$** which is opposite to the corresponding one in the reference structure **E$_0$** (see general formula in the Figure 5.64).

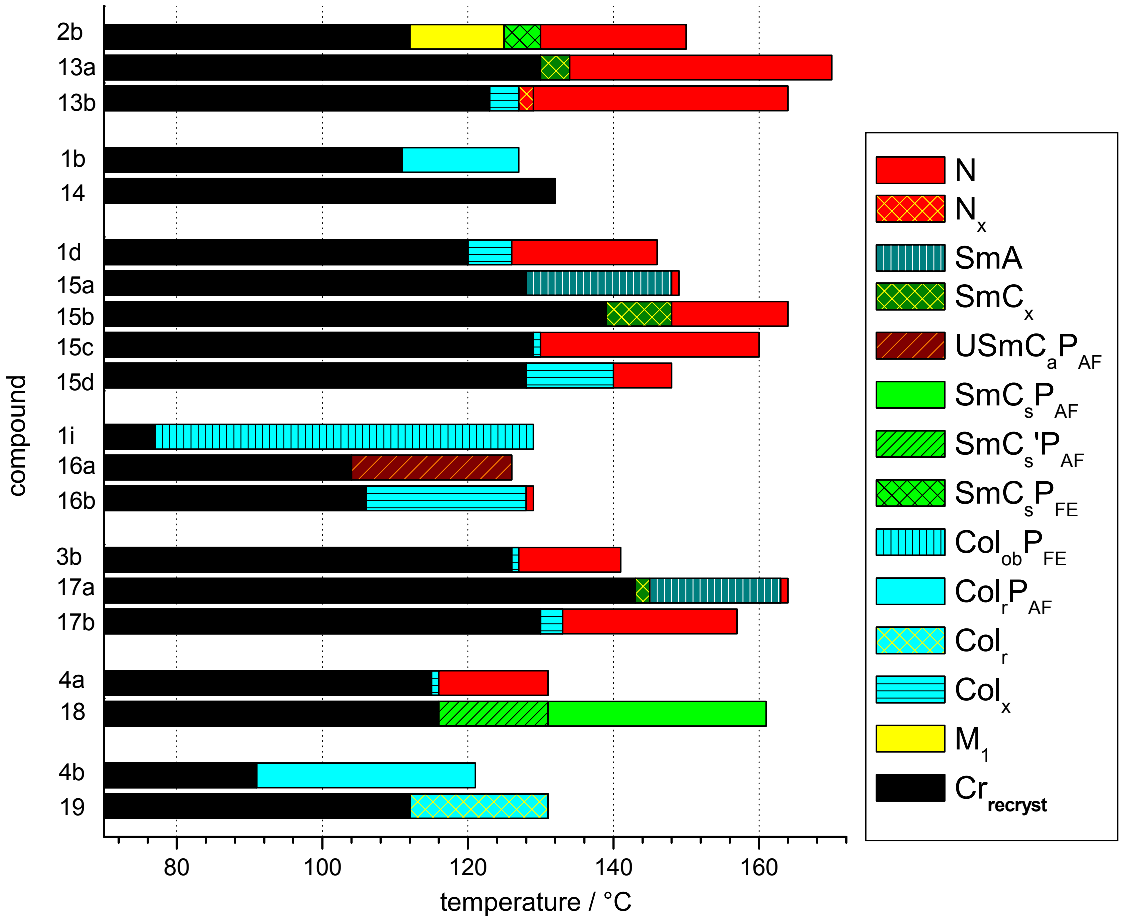

Figure 5.65: Transition temperatures (°C) of dimers **13** – **19** and their analogues compounds **1b, 1d, 1i, 2b, 3b, 4a**, taken from the first DSC cooling scans (10 Kmin^{-1}).

Since for each group of isomers the direction of only one *ester* group has been changed, the inversion of the first, second, third and fourth one is assigned as **E$_1$**, **E$_2$**, **E$_3$** and **E$_4$**, respectively (see general formula in the Figure 5.64). The synthesis and mesophase behaviour of dimers **13** – **19** were already published.[196] To explain the system of abbreviations, an example is given in Figure 5.64. The reference compound **E$_0$** (**2b**) is derived from *resorcinol*, the aliphatic chains have the lengths: $n = 8$, $m = 6$; $p = 6$. For compound **E$_3$** (**13b**) the aliphatic chains are the same, however, the direction of the carboxylic group in position **E$_3$** is inverted.

To allow an appropriate comparison, the mesophase behaviour of the new compounds **13**–**19** is presented together with that of the corresponding isomers **E$_0$** (described in the previous sections 5.1 and 5.4). The mesophase behaviour, transition temperatures together with the associated transition enthalpies, lattice parameters and P_S values of the isomers **13** – **19** and **1** – **4** are given in Table 5.6 and Figure 5.65. The compounds are listed and will be discussed with increasing length of the terminal *alkyloxy* chains *n* and *p* and increasing the length of the spacer *m*. To give more information, the mesophase behaviour on cooling is sketched in the bar charts, the transition temperatures are taken from the first DSC cooling scan (10 Kmin^{-1}), and therefore the recrystallization temperatures can be presented additionally. Nearly all compounds exhibit liquid crystalline behaviour, except compound **14** ($n = 12$, $m = 3$, $p = 6$) which is crystalline.

5.5.1.1 Occurrence of a N - N_X phase transition for dimer 13b

In the compounds **13a,b** the number *m* of methylene groups in the spacer amounts to 6, both terminal *alkyloxy* chains have similar length ($n = 8$; $m = 6$; $p = 6$). All dimers exhibit nematic phases. Additional smectic and columnar phases were found (Table 5.6 and in Figure 5.65). The analogue dimer **2b** with all *ester* linking groups in the reference orientation ($\mathbf{E_0}$) forms one enantiotropic nematic phase and two monotropic phases (a SmC_sP_{FE} and a non-classified mesophase designated as M_1 phase, see section 5.1.2.1).

The isomeric dimer **13a** ($\mathbf{E_2}$) exhibits a N-SmC_x phase sequence. The isomer **13b**, with the third *ester* linking group in inverse direction ($\mathbf{E_3}$) exhibits three mesophases which can be clearly distinguished by their textures and by differential scanning calorimetry. According to its characteristic texture the high-temperature phase can be assigned as a N phase. This N phase shows typical marbled, homeotropic and/or planar textures (Fig. 5.66a) and forms chiral domains of opposite handedness over the whole temperature range, as already described in chapter 5.1.1.2. The transition from the isotropic state to the N phase at 164 °C is coupled with an enthalpy change of 4.0 kJ mol^{-1}. On cooling the N phase a clear change in the optical texture occurs below 129 °C (Fig. 5.66b), which is accompanied by a rather low transition enthalpy (1.0 kJ mol^{-1}). The long-range director fluctuations which are characteristic of a N phase disappear and a fine structured fan-like texture develops (Fig. 5.66b). It is remarkable that this fan-like texture does not show typical focal-conic defects. On the other hand, the texture of homeotropically oriented regions remains unchanged below 129 °C, only the director fluctuations disappear and some oily strikes become visible. The occurrence of the homeotropic texture is an indication of a uniaxial phase. On cooling from this unknown phase, at 127 °C a dendritic growth of the texture can be observed, which transforms into a mosaic-like texture suggesting a columnar phase (Fig. 5.66c,d).

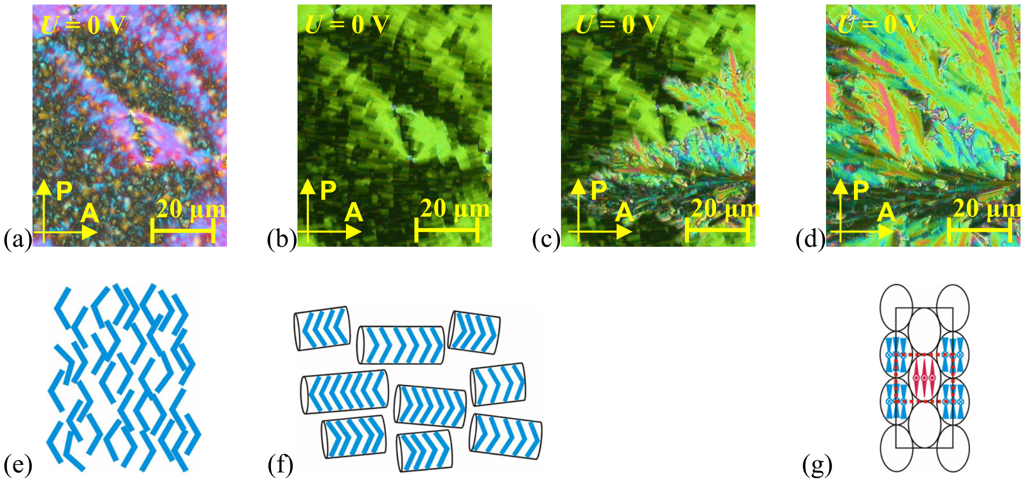

Figure 5.66: (a-d) Textures of the mesophases of compound **13b** on cooling at $U = 0$ V, observed in the same region of the sample between crossed polarisers: (a) planar texture of N phase at 163 °C; (b) fan-like texture of the N_x phase at 128 °C; (c) dendritic growing of a mosaic texture of the Col_x phase in the fan-like texture of the N_x phase at 127 °C; (d) mosaic texture of the Col_x phase at 126 °C; (e-g) proposed models for the N (e), N_x (f) and Col_r (g) phases in analogy to ref.[39]

X-ray diffraction measurements have been performed on samples of compound **13b** aligned in a magnetic field of about 1T. The results confirm that the high-temperature phase is a

N phase. The X-ray pattern shows a diffuse dumb bell-like scattering in the small angle region, and a diffuse wide angle scattering located around the equator (at 155 °C, Fig. 5.67a,b). The diffuse small-angle scattering in the N phase can be attributed to cybotactic groups representing fluctuating arrays of molecules with a short-range smectic-like order. Surprisingly, this pattern did not show significant changes at the transition to the low-temperature N_x phase (at 128 °C, Fig. 5.67c,d), although the fan-like texture indicates the existence of a smectic-like phase (see Fig. 5.67d). The distribution of the wide-angle scattering along χ and the corresponding θ-scan of the diffraction pattern in the N and N_x phases are shown in Figure 5.67e,f. The experimental results shown in Figure 5.67 prove that both nematic phases N and N_x cannot be clearly distinguished by X-ray methods. Due to the metastable nature of the low-temperature columnar phase it was not possible to characterize it by X-ray diffraction and electro-optical studies. Hence, it has been designated as an unknown columnar phase (Col_x phase).

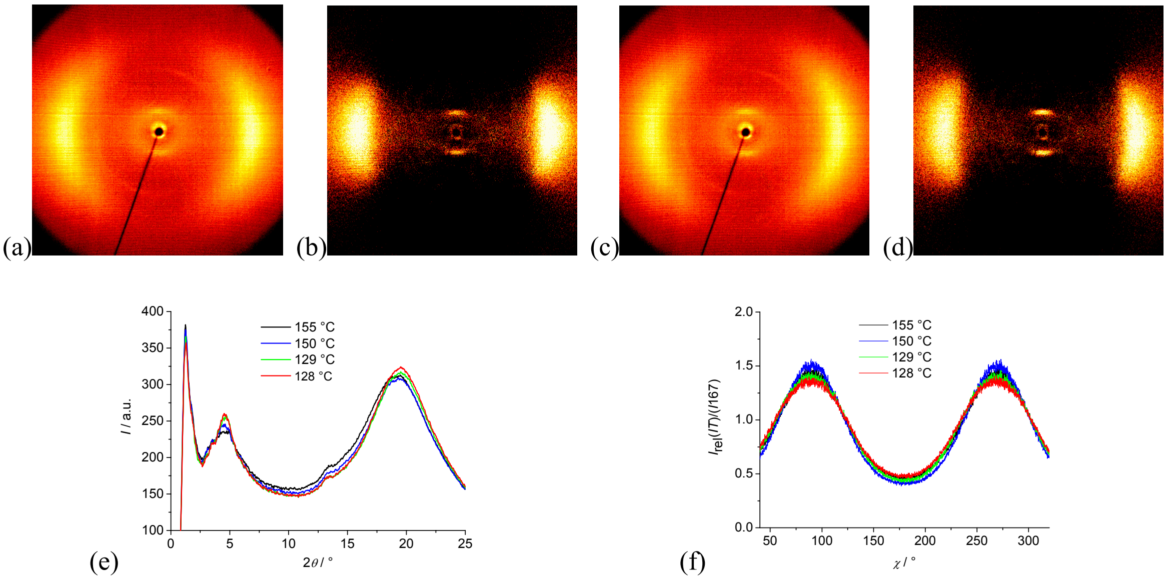

Figure 5.67: (a-d) XRD patterns of a sample of compound **13b** aligned in the magnetic field on cooling: (a,b) patterns of the nematic phase at 155 °C; (c,d) patterns of the N_x phase at 128 °C: (a,c) original scattering; (b,d) the same patterns, but the scattering of the isotropic liquid has been subtracted; (e) θ-scans of the diffraction patterns in the N and N_x phases; (g) distribution of the wide-angle scattering along χ in the nematic phase (black and blue line) and in the N_x phase (green and red line) (I_{rel} = I(T) / I(167 °C, isotropic liquid).

The results of our investigations point to a N_x phase as found for instance for liquid crystalline bent dimers of *cyanobiphenyl* connected by flexible spacers which has recently been characterized as a nematic phase with a conical twist-bend helical arrangement of the molecules and which has been called nematic twist-bend (N_{TB}) phase.[39,196,206,245,246,247,248,249]

A similar phase sequence N - N_x - Col_r was already reported by SCHROEDER *et al.* for bent-core mesogens with a central N-benzoylpiperazine fragment.[39] Based on the experimental results this unusual behaviour can be explained by the following structure model. In the N phase the molecules adopt only an orientational order with respect to the averaged molecular long axes (see Fig. 5.66e). On the other hand, in the N_x phase (see Fig. 5.66f) the molecules are stacked along the bent direction in bundles of non-defined length. Between the bundles (aggregates) only a short range positional order exists, giving rise to the diffuse scattering. In order to prevent a macroscopic polarisation, neighbouring bundles should be aligned antiparallel. On further cooling the lateral distances of the bundles are fixed and the structure passes over into a two-dimensional columnar structure (see Fig. 5.66g). That means the N_x phase can be regarded as the precursor to the following low-temperature Col_x phase. If the discussed model reflects the structure of the N_x phase correctly then it exhibits the structural feature of a N_{Col} phase as reported for discotic systems,[250] (although the texture of the N_{Col} phase of discotic systems is different to that found for the here discussed N_x phase). But in the N_{Col} phase the disc-like molecules are also stacked by intermolecular interactions one over each other forming non-ordered bundles (or columns). The existence of aggregates of bent-shaped molecules is assumed, too, to explain a field-induced transition from a layer into a columnar structure.[27]

5.5.1.2 The mesophase behaviour of dimers 15a – d

The dimer series **15** contains four compounds, thus being the series with a systematic *ester* linking group inversion, one by one from the first to the fourth group, $\mathbf{E_1}$ – $\mathbf{E_4}$. The compound **1d** with $\mathbf{E_0}$ is presented for comparison. All compounds exhibit liquid crystalline behaviour. The dimers possess an *even*-methylene spacer (*m* = 6) and similar to the series discussed in the previous chapters 5.1 - 5.4 they exhibit nematic phases. Additional smectic and columnar phases were found. The mesophase types, transition temperatures together with the associated transition enthalpies and lattice parameters for dimers **15** and **1d** are given in Table 5.6 and Figures 5.65 and 5.68.

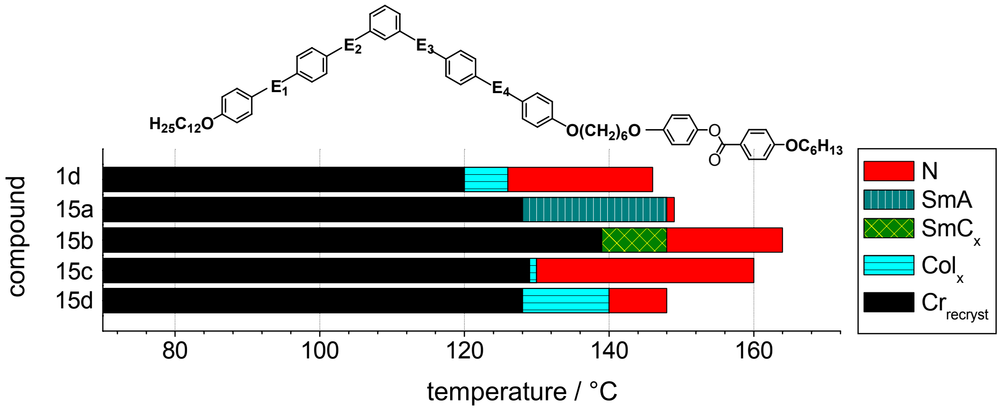

Figure 5.68: Transition temperatures (°C) of dimers **15a** – **d** and their analogue compound **1d** taken from the first DSC cooling scans (10 Kmin^{-1}).

All dimers **15** with one reversed carboxylic group exhibit beside a low-temperature phase an enantiotropic nematic phase, however, with very different ranges of existence. The reference compound **1d** ($\mathbf{E_0}$) exhibits a metastable nematic and a metastable columnar phase only. The compounds with $\mathbf{E_3}$ (**15c**) and $\mathbf{E_4}$ (**15d**) exhibit nematic and columnar (Col_x) mesophases, while the compounds with $\mathbf{E_1}$ (**15a**) and $\mathbf{E_2}$ (**15b**) form nematic and smectic mesophases. The clearing temperatures vary between 143 °C ($\mathbf{E_4}$-isomer) and 166 °C ($\mathbf{E_2}$-isomer) and increase in the following sequence: $T(E_4) < T(E_0) < T(E_1) < T(E_3) < T(E_2)$.

The dimer **15a** with the first *ester* linking group reversed ($\mathbf{E_1}$) forms two enantiotropic mesophases: a nematic and a smectic phase.

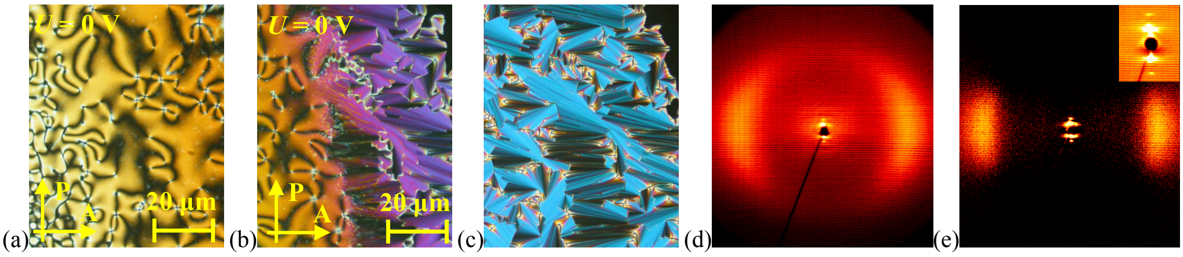

Figure 5.69: (a-c) Textures of the mesophases of compound **15a** on cooling at $U = 0$ V, observed in the same region of the sample between crossed polarisers: (a) schlieren texture of the nematic phase at 149 °C; (b) fan-shaped texture of the SmA phase growing from the schlieren texture of the nematic phase at 148.5 °C; (c) fan-shaped texture and homeotropic regions of the SmA phase at 145 °C; (d-e) XRD patterns of a surface-aligned sample in the SmA phase at 140 °C: (d) original pattern; (e) the same XRD pattern, but the intensity of the isotropic liquid is subtracted; the inset shows the small angle region.

The nematic phase of the dimer **15a** (**E_1**) exists over a very small temperature interval (1K) and shows the characteristic features of the previously discussed nematic phases in the chapter 5.1.1.2 (Fig. 5.69a). On cooling the nematic phase, a smectic phase appears characterized by a homeotropic or fan-shaped texture (Fig. 5.69b,c). The X-ray pattern of the smectic phase at 143 °C obtained from an aligned sample shows a diffuse outer scattering with the maxima located on the equator and BRAGG-reflections on the meridian, from which a layer spacing of $d = 7.0$ nm is calculated, see Table 5.6 and Figure 5.69d,e. This finding indicates a SmA phase. Additionally, no electro-optical response could be observed on applying an a.c. or a d.c. field. These experimental findings provide evidence that the low temperature smectic phase is a non-polar SmA phase.

The knowledge of the layer spacing $d = 7.0$ nm in the SmA phase could encourage a discussion on the packing of the '*banana-calamit*' molecules. A calotte model of the dimer **15a** (**E_1**) gives a similar value of $L = 6.93$ nm in its most stretched conformation, see Figure 5.70a. This is a hint at a monolayer packing, a strong intercalation of the different molecular fragments can most probably be excluded. However, a determination of the molecular shape of liquid crystalline dimers is not simple as already discussed by IMRIE and LUCKHURST.[120] This is especially true for large molecules with an unconventional shape. But for compound **16a** (**E_1**), a comparison of the lattice parameters with the corresponding calotte model would favour a more hockey-stick like or bent conformation shown in Figure 5.70b. Also in this case an intercalation can be excluded in all probability. But it should be stressed again: since the molecular conformations of the dimers are unknown and a lot of different molecular shapes can be assumed, the construction of such a structure model is rather speculative.

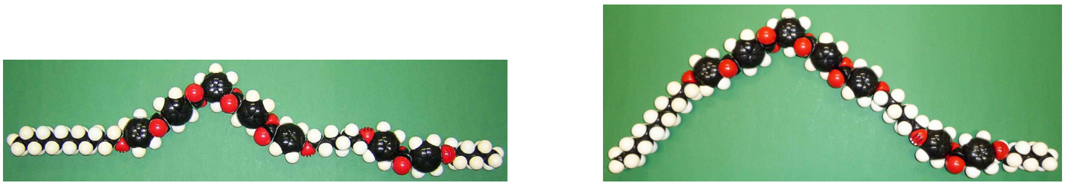
(a) $L = 6.9$ nm (b) $L = 6.2$ nm

Figure 5.70: CPK models of molecule **15a** (**E_1**) showing two possible conformations of the dimer.

The dimer **15b** (**E_2**) exhibits an enantiotropic nematic phase and a monotropic smectic SmC_x phase. The inversion of the direction of the second *ester* connecting group results in an increase of the clearing point by 20 K in comparison with the isomer **1d** (**E_0**). The nematic phase shows typical marbled and homeotropic textures and chiral domains of opposite handedness over the whole temperature range. This phase exists in a temperature range of 16 K and displays some unusual optical and electro-optical properties which will be separately discussed in the chapter 5.7. It should be mentioned that extensive physical measurements have been performed on the nematic phase of compound **15b** (**E_2**) and the results were published, see literature.[251,252,253,254,255] On cooling the homeotropic texture of the nematic phase below 148 °C, a transition into a weakly birefringent, fluctuating schlieren texture takes place indicating a biaxial smectic phase SmC_x. This transition is accompanied by a very small calorimetric peak (0.04 kJ mol^{-1}). The low-temperature smectic phase is crystallizing very fast, therefore further investigations to distinguish between a polar and a non-polar phase were impossible.

For the compounds with **E_3** (**15c**) and **E_4** (**15d**) textural and calorimetric investigations give evidences for the existence of enantiotropic nematic and monotropic columnar Col_x phases. Further electro-optical experiments and X-ray diffraction measurements were not successful because of rapid crystallization.

5.5.1.3 The undulated smectic $USmC_aP_{AF}$ phase of dimer 16a

The spacer of the following series **16** is increased from *m* = 6 to *m* = 11, that means, both mesogenic units are connected by an *odd*-numbered spacer now. A relatively short hexyloxy group is attached (*p* = 6) to the calamitic moiety, the bent-core part bears a dodecyloxy substituent (*n* = 12). Compound **16b** (**E_2**) exhibits a N-Col_x phase sequence (Table 5.6 and Figure 5.65), whereas the analogue compound **1i** (**E_0**) forms an enantiotropic $Col_{ob}P_{FE}$ phase (see section 5.1.1.3). The compound **16a** (**E_1**) shows an enantiotropic mesophase with some peculiar textural features (Fig. 5.71a-c). On cooling the isotropic liquid, this phase grows as dendritic nuclei or as spiral nuclei which coalesce to a variety of optical textures such as focal conics, banana-leaf like regions and circular domains together with ribbon-like and spherulitic textures (Fig. 5.71a-c). The growth of the phase suggests a mesophase belonging to the B_7 family (see some examples in literature[24,32,36,61,70,101,102,106]).

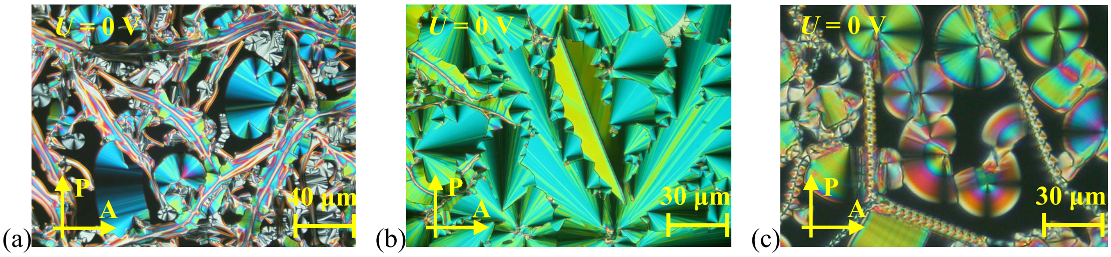

Figure 5.71: Textures of the mesophase of compound **16a** observed between crossed polarisers on cooling from the isotropic state at *U* = 0 V in: (a-b) 6 µm polyimide coated ITO cell; (c) 5 µm non-coated ITO cell.

The X-ray diffraction pattern of a surface-aligned sample of compound **16a** (**E_1**) is characterized by sharp BRAGG-reflections in the small-angle region and a diffuse scattering in the wide angle region with a maximum at 0.46 nm indicating a liquid-like lateral arrangement of the molecules within the layers (Fig. 5.72a). The layer reflections and their satellites of weak intensity are arranged in lines parallel to the equator. They can be indexed on a centred rectangular 2D lattice, with the lattice parameters $a = 36.8$ nm and $b = 6.6$ nm (see Fig. 5.72b-d). These features and the missing $h0$ reflections on the equator of the pattern (suggesting a nearly sinusoidal modulation of the electron density in direction a[192]) are typical for an undulated smectic structure. Therefore, this phase is preliminary assigned as an undulated smectic phase (USmC$_a$ phase) with a layer spacing of 6.6 nm and an undulation period of 36.8 nm. From the χ-scan of the wide angle region we could estimate a tilt angle of the molecules with respect to the layer normal of 22°.

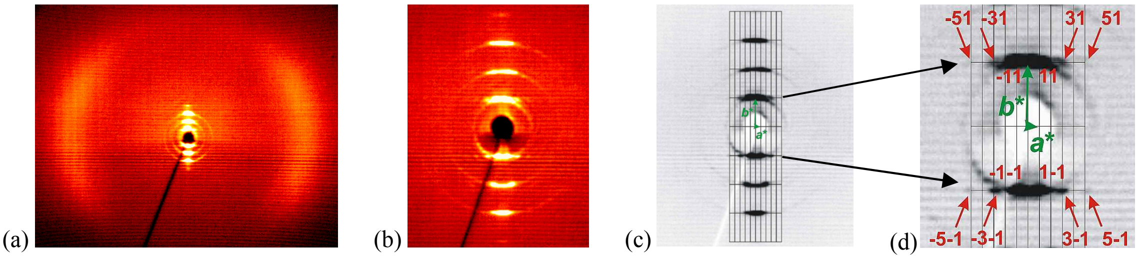

Figure 5.72: XRD patterns of a surface-aligned sample of compound **16a** in the USmC$_a$ phase at 120 °C: (a) wide-angle pattern; (b) pattern of the small-angle region; (c) reciprocal lattice for the observed reflections; (d) close-up of the reciprocal lattice with indices for the observed $h1$ and h-1 reflections.

In addition to the structural features, the electro-optical behaviour of the mesophase of dimer **16a** is also particularly interesting. Under a triangular-wave voltage antiferroelectric switching could be observed for the USmC$_a$ phase (i.e. an USmC$_a$P$_{AF}$ phase, see Fig. 5.73). The calculated value of the spontaneous polarisation is about 550 nC cm^{-2} and increases on decreasing temperature. This can be explained by a reduction of the polar order at higher temperature, possibly due to the diminished barriers for the rotation around the molecular long axis. On cooling the isotropic liquid, under a d.c. voltage of 50 V circular domains were obtained (Fig. 5.73a-c). The characteristic feature is the appearance of extinction crosses which are aligned along the direction of the crossed polarisers (Fig. 5.73a-c), indicating that the molecules adopt an anticlinic organization. The field-induced circular domains do not change on reversal of the field. However, no relaxation of the extinction crosses could be seen on terminating the applied field, apart from a small change in the birefringence (Fig. 5.73b). This means that the position and tilt of the molecules remains unchanged during the switching process, which can be explained by a polarisation reversal that takes place by rotation around the molecular long axis (see models under the Fig. 5.73a-c).

The textural features, the electro-optical behaviour, but especially the XRD pattern prove that the mesophase of compound **16a** (**E$_1$**) can be assigned as B$_7$′ phase. The reasons of the frustration of the layer organisation with formation of correlated undulated layer structures (i.e. non-interrupted, but sinusoidal deformed layers) are the mismatch of the area required by rigid bent-cores and *alkyl* chains at aromatic–aliphatic interfaces[99] as well as polar effects.[100] This gives rise to a modulation of the layers, to a tilt of the molecules and to a reduced packing density of the bent core units. COLEMAN *et al.*[102] showed that the modulated layer structures formed by bent-core molecules can be generated by splayed polarisation with domains of alternate tilt and polarisation periodically arranged in order to escape from a macroscopic polar order. The layers are slightly thicker along the splay defects than between them and this leads to an additional undulation of the layers (modulated–undulated smectic layers).

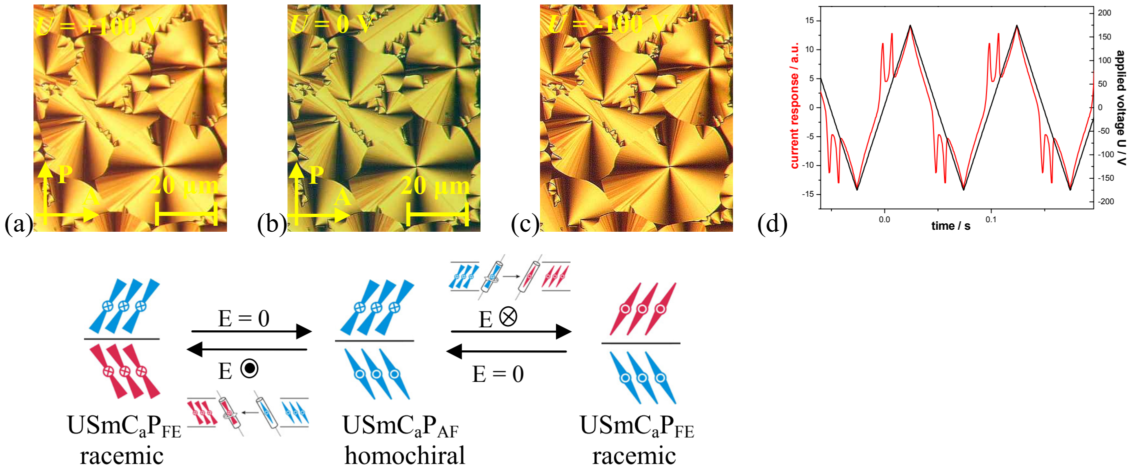

Figure 5.73: Electro-optical investigations on the USmC$_a$P$_{AF}$ phase of compound **16a** (**E$_1$**) at 120 °C in a 5µm non-coated ITO cell: (a,c) $U = \pm$ 100 V and (b) $U = 0$ V; (a-c, lower part of the figures) proposed models of the organization of the molecules in the ribbons in the FE state (a,c) and in the AF ground state (b); (d) AF switching current response obtained by applying a triangular-wave voltage ($U = 353$ V$_{pp}$, $f = 10$ Hz, $R = 5$ kΩ, $P_S = 550$ nC cm^{-2}). In the schematic model, only the bent-core parts of the dimers are sketched because the calamitic moieties are not of importance for the electro-optical behaviour under discussion.

These undulations are correlated and disregarding the polar direction it leads to a 2D-rectangular lattice with the parameter *b* corresponding to the layer distance and parameter *a* corresponding to the undulation wavelength (λ). The model suggested by COLEMAN *et al.*[102] is shown in Figure 5.74a-d. Accordingly, the molecules are organized across the splay defects in four different combinations of handedness which are indicated by different colour and orientation of the polar direction, indicated by crosses and points. This gives rise to the existence of two distinct types of defects with distinct structures with the crests and the troughs of the modulation non-equivalent (the handedness and clinicity changes (grey, crests) and the handedness remains the same and the clinicity changes (red, troughs)[24,102]). There are several possibilities for the organisation of the molecules in the undulated smectic phases. Two possible structures are shown in Figure 5.74e-f, in analogy to reference.[256] The tilt direction can change from layer to layer, which, due to the anticlinic tilt, would lead to a homogeneous chiral structure (USmC$_a$P$_{AF}$ structure, see Fig. 5.74e). In a second possible structure the correlation between the undulated layers is synclinic, but the tilt direction changes along the undulated layers (USmC$_s$P$_{AF}$ structure, see Fig. 5.74f). This structure would be racemic, but requires additional defects in the layers (positions where the tilt direction changes, see Fig. 5.74f) which are unfavourable if there is a significant tilt.

The USmC$_a$P$_{AF}$ phase of compound **16a** can be characterized by the model shown in Figure 5.74e. The AF switching is the result of the steric frustration arising from very large mesogenic groups leading to the separation of the bent cores in the layers which reduces the polar order and hence decreases the surface coupling.

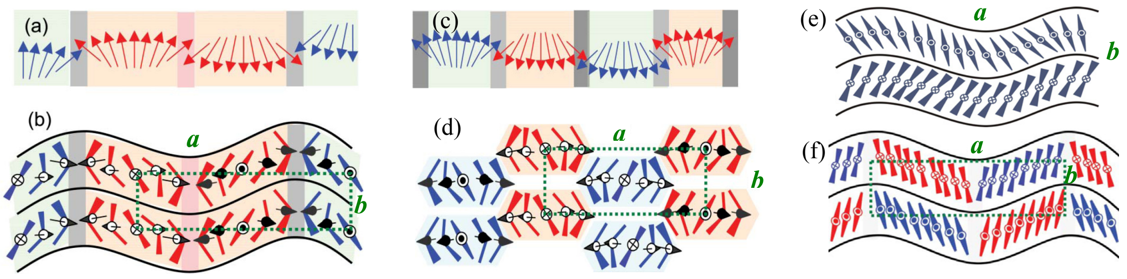

Figure 5.74: (a, b) Model of the modulated–undulated layer structure resulting from splay defects, in analogy to references[24,102]; (a) top view upon the layer, arrows indicate the direction of the polar vector; (b) front view; (c, d) model proposed for rectangular mesophases formed by the polarisation modulation leading to half-layer interdigitation of the smectic ribbons between the defects, in analogy to references; (c) top view; (d) front view along the ribbons; (e-f) models of the organisation in the undulated smectic phase, in analogy to reference;[256] (e) homogeneously chiral anticlinic AF organisation (USmC$_a$P$_{AF}$); (f) synclinic AF organisation between the layers and alternation of the tilt direction along the layers (USmC$_s$P$_{AF}$).

5.5.1.4 Field-induced enhancement of the transition temperature between the polar and non-polar smectic phases of dimer 17a

The dimer series **17** (n = 16; m = 6; p = 6) contains two compounds. The dimers **17** possess an *even*- methylene spacer (m = 6) and display nematic phases as expected. Additional smectic and columnar phases were found (Table 5.6 and Figure 5.65).

The isomer **17b** (**E$_3$**) and its analogue dimer **3b** (**E$_0$**, section 5.1.2.2) present a similar mesophase sequence (nematic and Col$_x$ phases). The dimer **17a** (**E$_2$**) exhibits two enantiotropic mesophases, a nematic and a high-temperature smectic phase, and in addition a monotropic low-temperature smectic phase. The nematic phase shows typical marbled, homeotropic or a schlieren texture (Fig. 5.75a) and forms chiral domains of opposite handedness over the whole temperature range. On cooling the nematic phase (Fig. 5.75a), a homeotropic texture as well as a smooth fan-shaped texture was observed, which is a typical feature of a SmA phase (Fig. 5.75b). On lowering the temperature (below 144 °C) the homeotropic regions transform into a weakly birefringent fluctuating schlieren texture, indicating a biaxial phase. On cooling the smooth fan-shaped texture a broken fan-shaped texture appears (Fig. 5.75c). Rapid crystallization prevents detailed investigations on this biaxial low-temperature smectic phase, which was designated as a SmC$_x$ phase.

X-ray measurements on the high-temperature phase of compound **17a** at 163 °C show the typical scattering of a N phase when aligned in the magnetic field on cooling (Fig. 5.75d). The measurements at 150 °C confirm the presence of a SmA phase and show strong small angle reflections from which a layer spacing of d = 7.19 nm could be determined (Table 5.6 and Fig. 5.75e) and two distinct wide-angle reflections with the maximum at 0.50 nm in a direction normal to the layer reflections. Based on these experimental evidences this smectic phase was assigned as a SmA phase.

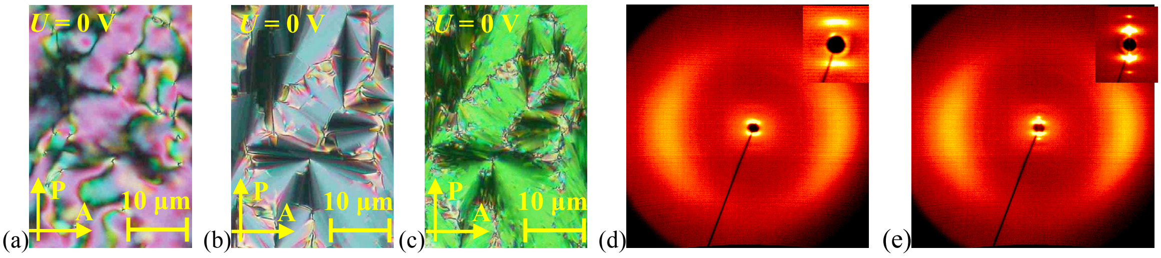

Figure 5.75: (a-c) Textures of the mesophases of compound **17a** on cooling at $U = 0$ V, observed in the same region of the sample between crossed polarisers: (a) nematic phase at 163 °C; (b) SmA phase at 148 °C; (c) SmC_x phase at 144 °C; (d-e) XRD patterns of a sample of compound **17a** aligned in the magnetic field: (d) nematic phase at 163 °C; (e) SmA phase at 150 °C; the inset shows the small angle region.

The SmA phase of compound **17a** does not show a polar electro-optical response. However, the SmA texture (Fig. 5.76a) can be transformed into an optically biaxial texture (Fig. 5.76b) under a sufficiently high electric field (~ 40 $V\mu m^{-1}$). This field-induced transition can be observed up to 4 K above the transition temperature SmC_x to SmA phase.

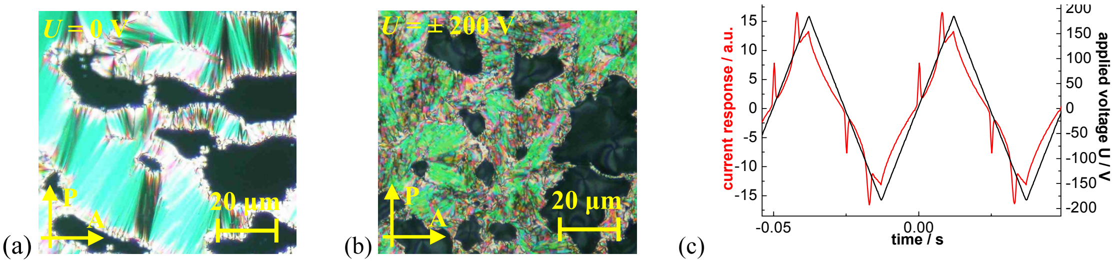

Figure 5.76: Compound **17a**: Electro-optical investigations of the field-induced SmC_xP_{AF} phase formed from the SmA phase under a d.c. electric field at 147 °C; textures observed in the same region of the sample between crossed polarisers in a 5 µm non-coated ITO cell: (a) the SmA phase at $U = 0$ V; (b) the field-induced SmC_xP_{AF} phase at $U = \pm 200$ V; (c) AF switching current response obtained by applying a triangular-wave voltage ($U = 400\ V_{pp}$, $f = 20$ Hz, $R = 5\ k\Omega$, $T = 147$ °C, $P_S = 450\ nC\ cm^{-2}$).

If the field is switched off the original fan-shaped texture of the SmA phase reappears. This field-induced transition is reversible. The field induced phase can be assigned as SmC_xP_{AF} phase because an antiferroelectric switching can be measured, as shown in Figure 5.76c. It can be assumed that the switching current response obtained in this field-induced SmC_xP_{AF} phase (Fig. 5.76c) is identical to that which could be shortly observed in the low-temperature SmC_x phase. That means the transition temperature for SmC_x to SmA can be enhanced by the application of a sufficiently high electric field. Applying a field of 40 $V\mu m^{-1}$ the enhancement of the transition temperature was found to be about 4 K. This effect may be connected with the existence of polar clusters in a short-range order region already in the non-polar SmA phase. A similar field-induced enhancement of the transition temperature between polar and non-polar phases was reported in the literature for a few 'monomeric' bent-core mesogens, especially for the phase transitions $SmCP_{AF}$ - SmA, $SmCP_{AF}$ - isotropic liquid, crystalline-polar – isotropic.[62,225] The enhancement of the transition temperature for SmC_x to SmA by the application of a sufficiently high electric field is of special interest.

5.5.1.5 The mesophase behaviour of dimer 18

In dimer **18** (**E$_2$**) both mesogenic units are connected by an even-numbered spacer (m = 6), however, both terminal chains have the same length: n, p = 12. Such symmetric substitution is of clear influence on the mesophase behaviour. The compound **18** forms two smectic phases, a high-temperature SmC$_s$ (d = 6.19 nm, τ = 24°, $L_{eff} = d/\cos\tau$ = 6.78 nm) and a low-temperature SmC$_s$' phase (d' = 6.10 nm, τ'= 32°, L_{eff}' = 7.19 nm). The intensity distribution of the outer diffuse scattering indicates a synclinic tilt of the molecules in adjacent layers in both phases, because the maxima in the upper left and the lower right quarter of the patterns are significantly stronger than those in the other two quarters.[257] It is remarkable that this result is in contradiction with the textural investigations for the high-temperature SmC$_s$ phase which point to an anticlinic mesophase. Electro-optical measurements give evidence for an antiferroelectric (AF) ground state in both SmC$_s$ phases (P_S = 550 nC cm^{-2} for SmC$_s$P$_{AF}$ phase and P_S' = 780 nC cm^{-2} for SmC$_s$'P$_{AF}$ phase). The analogue compound **4a** (**E$_0$**) exhibits a nematic – columnar dimorphism (see description in the section 5.1.2.3). Interestingly, compound **18** (**E$_2$**) is the first dimer of **type I** with an *even*-methylene spacer which does not form a nematic phase.

5.5.1.6 The mesophase behaviour of dimer 19

Defining the *odd*-numbered spacer with m = 11, in the compound **19** the two terminal chains have the same length: n, p = 12. The dimer **19** (**E$_2$**) forms a rectangular columnar phase (Col$_r$ phase, a = 21.4 nm, b = 6.89 nm) with rather large blocks. Remarkably, for this compound no electro-optical response can be observed up to a voltage of about 400 V$_{pp}$ using a 5 µm thick cell, the maximum voltage attainable from our experimental set-up. For compound **19** the inversion of the second *ester* linking group (**E$_2$**) results in an increase of the value of the lattice parameter a of the Col$_r$ phase. The analogue dimer **4b** with **E$_0$** shows a monotropic Col$_r$P$_{AF}$ phase (chapter 5.1.2.3).

To summarize the results presented in the chapter 5.5.1, different aspects are of interest. Compounds with an *even*-numbered spacer exhibit higher clearing temperatures as those with an *odd*-numbered spacer, as expected. This means that also for this dimer of **type I** the molecules with an *even* number of single units in the spacer should have a more stretched shape. Nearly all of these even-numbered dimers exhibit a nematic phase as high-temperature phase with one exception. Two polar SmC phases are formed by compound **18** (**E$_2$**), symmetrically substituted at both terminal positions by *dodecyloxy* groups. Both phases, showing a synclinic tilt of the molecules in an antiferroelectric layer arrangement, could be completely characterized. Such a SmC$_s$'P$_{AF}$ – SmC$_s$P$_{AF}$ sequence was extremely rarely found for bent-core mesogens up to now. Recently, the re-entrant behaviour SmC$_s$'P$_{AF}$ – Col$_{ob}$ - SmC$_s$P$_{AF}$ has been reported.[257] Nearly all compounds having an *odd*-numbered spacer prefer the formation of columnar phases and of an undulated SmCP phase, respectively. There is one exception: a nematic phase was found for dimer **16b** with 11 CH$_2$ groups in the spacer.

Concerning the reversion of the carboxylic groups **E$_1$** to **E$_4$**, all four *ester* groups were changed in their direction – step by step – in the isomeric series **15**. On the other hand, the *ester* linking group **E$_2$** was reversed in all the series under study which are different in the length of the aliphatic parts (n,p,m) to allow a comparison with the corresponding reference compounds

$\mathbf{E_0}$. Looking at Table 5.6, the mesophase stability of nearly all isomers $\mathbf{E_1}$-$\mathbf{E_4}$ is increased after reversing one of the carboxylic groups in the reference compounds $\mathbf{E_0}$. This allows the preparation of such '*banana-calamit'* dimers with thermodynamically stable mesophases. The strongest stabilization has been observed for the isomers $\mathbf{E_2}$ and amounts up to 32 K (compare **4a** with **18**). It is worth mentioning that the directly comparable inversion of the carboxylic group $\mathbf{E_2}$ in the corresponding 'monomeric' five-ring bent-core mesogens has a relatively low influence on the mesophase stability: the change of the clearing temperatures for the dodecyloxy substituted compound amounts to -7K, for the octyloxy homologue +3K.[192] With growing length of the terminally attached *alkyloxy* chains there is the tendency in the dimers under study that the clearing temperatures are reduced. This is in agreement with the mesophase behaviour observed for calamitic systems. For the series with the spacer m = 6 (compounds **2b**, **13a**, **13b**, **1d**, **15a-d**, **3b**, **17a**, **17b**, **4a** and **18**) we could check the influence of the *alkyloxy* wing groups in more detail. A nearly symmetric substitution (n = 8; p = 6) yielded the interesting sequence of two nematic phases N - N_x (**13b** with $\mathbf{E_3}$). For long terminal chains ($n + p > 20$) the phase behaviour of the non-symmetrically substituted compound **17a** with $\mathbf{E_2}$ (n = 16; p = 6: N, SmA, SmC_X) is very different in comparison to the symmetrically substituted dimer **18** with $\mathbf{E_2}$ (n = 12; p = 12: $SmC_s'P_{AF} - SmC_sP_{AF}$).

A multitude of new or changed phase sequences have been found by the inversion of *ester* linking groups of the reference compounds $\mathbf{E_0}$. A variety of mesophases occur (N, N_x, SmA, SmC_aP_{AF}, SmC_aP_{FE}, SmC_sP_{AF}, SmC_sP_{FE}, $USmC_aP_{AF}$, SmC_x phases) whereby the clearing temperatures vary from 121 to 171 °C. These compounds show interesting properties, such as field-induced biaxiality of uniaxial nematic phases, special electroconvection patterns and high flexoelectricity of nematic phases, field-induced inversion of chirality in $SmCP_{AF}$. Also the SmA phases exhibit unusual properties. This is proven by the experimental finding that the transition temperature SmCP – SmA can be increased on applying an electric field. For compound **17a** with $\mathbf{E_2}$**,** this enhancement amounts to 4K using $40V\mu m^{-1}$. This is clearly more than reported for a comparable 'monomeric' bent-core compound, for which an enhancement of 2K using $35V\mu m^{-1}$ was observed.[257] Up to now, it is not possible to predict which phases in which sequences will result caused by these structure variations. Such conclusion needs much more experimental work in this field. Additional work would also be justified in expectation of new materials with exciting properties. It could be shown that the direction of the *ester* linking groups has a significant influence on the dipole moment, on the conformation (in particular on the bending angle) and on the conformational flexibility (the inversion of the second *ester* linking group $\mathbf{E_2}$ have a lower conformational degree of freedom, which is responsible for higher clearing temperatures). For example, isomers in which the direction of the *ester* groups in each wing of the bent-core unit is opposite have a lower conformational degree of freedom, which is responsible for higher clearing temperatures and a distinct mesophase behaviour.[192]

5.5.2 Variations of the direction of the *ester* linking groups *E* and the type of the group *X* linking the spacer to the bent-core mesogenic unit of dimers 20 - 24

This section combines the study on the variation of the direction of the *ester* linking group ***E*** on the bent unit (see chapter 5.5.1) with the study of the variation of the connecting group ***X*** (see chapter 5.4). Therefore we compare the dimers **20** - **24** (n = 12; m = 5, 6, 11; p = 6, 12) which possess a reversed second *ester* linking group in the bent moiety, $\mathbf{E_2}$ and different directions of the connecting group ***X*** (-**COO**-/-**OOC**-) with the analogues compounds **7** – **11** (with the ***reference structure*** of the bent-core unit, $\mathbf{E_0}$, see chapter 5.5.1). The mesophase behaviour, transition temperatures together with the associated transition enthalpies, lattice parameters and P_S values for the new dimers and the comparison dimers are given in Table 5.7 and Figure 5.77.

Table 5.7: Transition temperatures [°C], mesophase types, transition enthalpy values [kJ/mol], layer spacing *d* [nm], tilt angle τ of the molecules [°] with respect to the layer normal in SmC phases and with respect to the normal to *a* in Col phases, lattice parameters (*a*, *b*, *γ*) and P_S values of the compounds **20** – **24** and their analogues compounds **7a** - **11a**.[a]

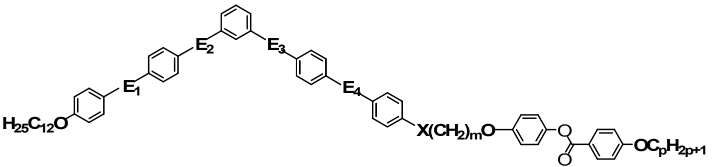

Comp	*n*	*m*	*p*	*E*[d]	*X*	Transitions temperatures [°C] Δ*H* [kJ·mol-1]	Phase type	Lattice parameters					P_S nC/cm²
								d [nm]	τ [°]	*a* [nm]	*b* [nm]	γ [°]	
7a	12	6	6	E_0	COO	Cr 135 (Col_xP_{FE} 128) I *67.3* *26.6*	Col_xP_{FE}		-[c]	-[c]	-[c]	-[c]	240
20	12	6	6	E_2	COO	Cr 138 (Col_x 117) I *37.8* -[b]	Col_x		-[c]	-[c]	-[c]	-[c]	-[c]
8a	12	6	12	E_0	COO	Cr 129 Col_rP_{FE} 137 I *32.3* *27.6*	Col_rP_{FE}		7	11.62	6.29	90	330
21	12	6	12	E_2	COO	Cr 130 Col_xP_{FE} 146 I *39.2* *32.9*	Col_xP_{FE}		-[c]	-[c]	-[c]	-[c]	250
9a	12	11	6	E_0	COO	Cr 109 (Col_xP_{FE} 103 N 105) I *67.1* -[b] -[b]	N Col_xP_{FE}		-[c]	-[c]	-[c]	-[c]	380
22	12	11	6	E_2	COO	Cr 135 (N 123) I *83.5* -[b]	N						
10a	12	5	6	E_0	OOC	Cr 137 Cr^*P_{FE} 169 I *14.0* *68.2*	Cr^*P_{FE}	-	-	-	-	-	340
23	12	5	6	E_2	OOC	Cr 176 (N 173) I *79.5* *3.4*	N						
11a	12	5	12	E_0	OOC	Cr 117 SmC'_aP_{AF} 128 SmC_aP_{AF} 139 N 148 I *42.8* *18.8* *0.4* *2.3*	N SmC_aP_{AF} SmC'_aP_{AF}	 5.78 5.71	 37 37				 570 870
24	12	5	12	E_2	OOC	Cr 142 (SmC''_sP_{AF} 118 SmC'_sP_{AF} 125) SmC_sP_{AF} 175 I *71.4* *1.8* *3.8* *12.0*	SmC_sP_{AF} SmC'_sP_{AF} SmC''_sP_{AF}	6.24 6.10 6.01	25 29 32				230 340 580

[a] Transition temperatures (°C) and enthalpy values [kJ/mol] of the compounds **20** – **24** and their analogues compounds **7a** - **11a,** were taken from the second DSC heating scans (10 $Kmin^{-1}$); values in parentheses indicate monotropic mesophases, in this case the transition temperatures and enthalpy values were taken from the first DSC cooling scans and the transition temperatures were checked by polarising microscopy; [b] the transition is not detectable on DSC and the transition temperature value is determined by polarising microscopy; [c] could not be determined due to rapid crystallization of the sample; [d] *ester* linking group, the direction of which is opposite to the corresponding one in the reference structure (see Figure 5.64 in subchapter 5.5.1).

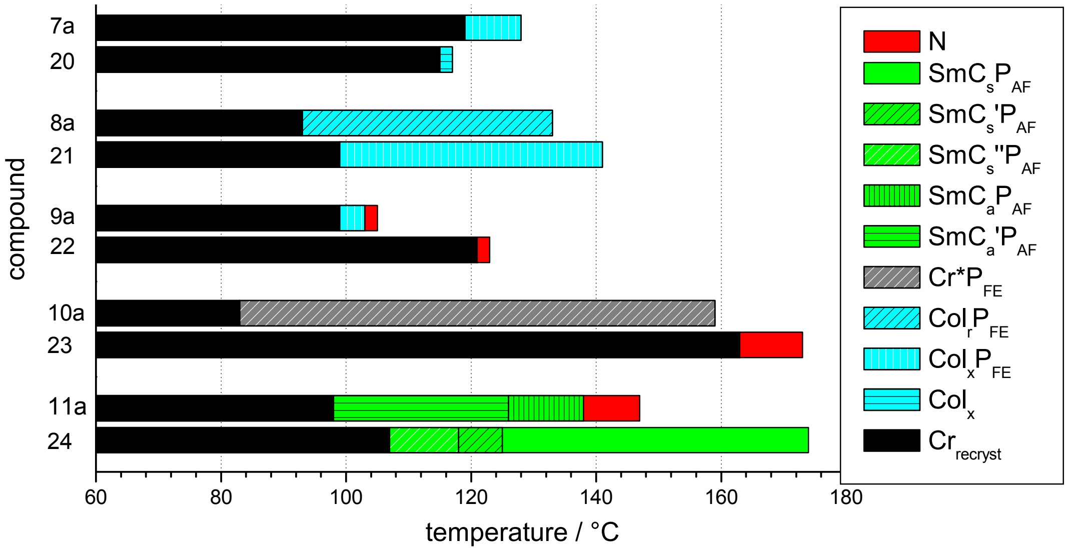

Figure 5.77: Mesophase behaviour and transition temperatures (°C) of compounds **20** – **24** and their analogues compounds **7a** - **11a,** taken from the first DSC cooling scans (10 Kmin^{-1}).

5.5.2.1 The mesophase behaviour of dimers 20 - 22

The dimers **20** - **22** (*n* = 12; *m* = 6, 11; *p* = 6, 12, **E$_2$**, ***X*** = -COO-) are studied in comparison with the corresponding dimers **7a** - **9a** with the ***reference structure*** **E$_0$** of the bent-core unit. The transition temperatures and the mesophase behaviour of dimers **20-22** and **7a-9a** are presented in Figure 5.77 and Table 5.7. Only columnar phases were found for the dimers **20** and **21** (*n* = 12; *p* = 6, 12; E$_2$) with an *odd*-numbered spacer, but with an *even* number of methylene groups (*m* = 6). This is in accordance with the results previously presented in chapters 5.1-5.3 for dimers **1** - **6**. For the Col$_x$ phase of compound **20** (**E$_2$**) no electro-optical response can be observed up to a voltage of about 400 V$_{pp}$ for a 5 µm thick cell, the maximum voltage attainable from our experimental set-up (one possibility is that there is a FE structure and the field is not strong enough to suppress the effect of modulation in this FE structure). The columnar phase of the analogue compound **7a** (**E$_0$**) was assigned as a Col$_x$P$_{FE}$ phase.

The compound **21** (**E$_2$**) presents an enantiotropic columnar phase, but fast crystallization prevent X-ray diffraction measurements for a structural characterization (Col$_x$ phase). For the Col$_x$ phase of compound **21** a FE electro-optical response could be observed (P_S = 250 nC cm^{-2}, Col$_x$P$_{FE}$ phase). The analogue compound **8a** (**E$_0$**) exhibits an enantiotropic Col$_r$P$_{FE}$ phase.

The compounds **22** (*n* = 12; *p* = 6; **E$_2$**) with an *odd* methylene spacer (*m* = 11), but an *even* number of all units in the spacer display mesomorphism in accordance with their overall linear shape, i.e. they possess nematic phases. The dimer **22** (**E$_2$**) shows only a monotropic nematic phase. The analogue isomer **9a** (**E$_0$**) exhibits two monotropic phases: a nematic and a columnar phase with a high tendency to crystallize (Col$_x$P$_{FE}$ phase).

On increasing the length of the terminal chain *p* attached to the calamitic mesogenic unit a stabilizing effect of the mesophase could be observed (dimers **20** and **21, 7a**, **8a**). On increasing the spacer *m* length for the **E$_2$**-dimers **20** and **22** the mesophase stability is increasing, which is in contrast with the tendency of mesophase destabilization found for the analogues **E$_0$**-dimers **7a** and **9a**. The value of the spontaneous polarisation P_S is increasing with decreasing the temperature and increasing the length of the spacer m and of the terminal chain p attached to the calamitic moieties, in analogy with the previously studied dimers series **1**-**19**.

5.5.2.2 The mesophase behaviour of dimers 23 and 24: Smectic polymorphism of dimer 24

The mesomorphic behaviour of dimers **23** and **24** (n = 12; m = 5; p = 6, 12, $\mathbf{E_2}$, $\boldsymbol{X}$ = -**OOC**- and $\boldsymbol{Y}$ = –**O**-) is studied in comparison with the corresponding dimers **10a** and **11a** with a ***reference structure*** $\mathbf{E_0}$ of the bent-core unit. The transition temperatures and the mesophase behaviour of dimers **23** and **24** are presented in Table 5.7. All the dimers under discussion present an overall *even* numbered spacer (m = 5, but the sum of all units in the flexible spacer is *even*).

The dimer **23** ($\mathbf{E_2}$) forms a monotropic nematic phase. The analogue isomer **10a** ($\mathbf{E_0}$) exhibits a crystalline phase with polar switching, a Cr^*P_{FE} phase.

The dimer **24** ($\mathbf{E_2}$) forms one high-temperature enantiotropic smectic phase and two monotropic smectic phases, whereas the analogues isomer **11a** ($\mathbf{E_0}$) exhibits three enantiotropic mesophases (nematic, SmC_aP_{AF} and SmC'_aP_{AF} phases). On cooling from the isotropic liquid state, at 174 °C the high-temperature smectic phase of dimer **24** ($\mathbf{E_2}$) appears as a low birefringent schlieren texture with multiple disclinations (Fig. 5.78a) and/or as a birefringent smooth fan-shaped texture that points to an anticlinic SmC phase. Over the whole temperature range chiral domains of opposite handedness could be observed. The transition to the low-temperature smectic phase at 125 °C is accompanied by the appearance of additionally fine stripes and defects on the schlieren texture (Fig. 5.78b). If the smooth fan-shaped texture is cooled down a broken texture appeared with a lower birefringence. The textural features of the above mentioned smectic phases are very similar to the features of the high-temperature SmC_s phase of compound **5a** described in section 5.1.2.4. On further cooling at 118 °C at the transition to the following low-temperature smectic phase, the schlieren texture transforms into a focal-conic texture which possesses lots of circular domains with the extinction crosses aligned with respect to the crossed polarisers (a first indication of an anticlinic organization of the molecules between adjacent layers, see Fig. 5.78c).

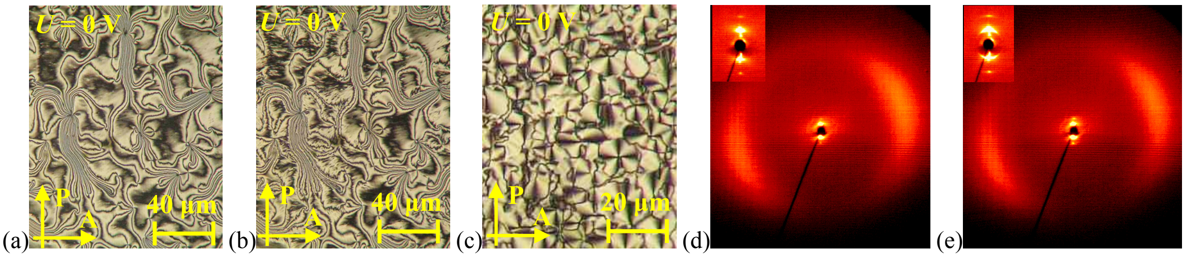

Figure 5.78: (a-c) Textures of the mesophases of compound **24** observed between two untreated glass slides on cooling: (a) high-temperature smectic phase at 150 °C; (b) second smectic phase at 123 °C; (c) low-temperature smectic phase at 116 °C (same region, but enlarged); (d-e) XRD patterns of a surface-aligned sample of compound **24**; the insets show the small angle regions; (d) high-temperature smectic phase at 145 °C; (e) low-temperature smectic phase at 116 °C.

X-ray measurements performed on the mesophases of compound **24** confirmed the presence of three SmC phases with molecules tilted with respect to the layer normal. They all showed very similar patterns indicating a synclinic tilt of the molecules in adjacent layers by the strongly different intensities of the outer diffuse scattering to the left and the right of the meridian, respectively (see X-ray diffraction patterns for the SmC$_s$ phase at 145 °C, Fig. 5.78d and for the SmC''$_s$ phase at 116 °C, Fig. 5.78e). The layer spacing derived from the X-ray measurements on cooling are almost independent of the temperature (see Table 5.9), including the transition from the high-temperature SmC$_s$ ($d = 6.24$ nm, $\tau = 25°$, $L_{eff} = d/\cos\tau = 6.89$ nm) to the lower-temperature SmC'$_s$ phase ($d' = 6.10$ nm, $\tau' = 29°$, $L_{eff}' = 6.97$ nm) to the lowest-temperature SmC''$_s$ phase ($d'' = 6.01$ nm, $\tau'' = 32°$, $L_{eff}'' = 7.08$ nm) and indeed until the sample crystallizes. On the basis of these X-ray experimental evidences these three synclinic SmC phases were assigned as SmC$_s$, SmC$_s$' and SmC$_s$'' phases (in contradiction with the textural investigations which point to anticlinic mesophases). Electro-optical measurements give evidence for an AF ground state in all SmC$_s$ phases. The switching polarisation increases with decreasing temperatures (see Table 5.9, $P_S = 230$ nC cm^{-2} for SmC$_s$P$_{AF}$ phase; $P_S' = 340$ nC cm^{-2} for SmC$_s$'P$_{AF}$ phase and $P_S'' = 580$ nC cm^{-2} for SmC$_s$''P$_{AF}$ phase). These three SmC$_s$P$_{AF}$ phases of compound **24** are very similar to the high-temperature SmC$_s$P$_{AF}$ phase of compound **5a** described in section 5.1.2.4. It was found for the selected dimers **23** and **24** and their analogues dimers **10a** and **11a** that the increase of the terminal chain length of the calamitic mesogenic unit for the **E$_2$**-dimers results in a mesophase stabilization, which is in contrast with the tendency of mesophase destabilization found for the analogue **E$_0$**-dimers. The value of the spontaneous polarisation P_S is increasing on decreasing the temperature. The inversion of the second *ester* linking group **E$_2$** results in an increasing of the clearing temperatures (4- 27 K).

It was found for the dimers **23** and **24** that in spite of the minor differences in the chemical structure a variety of mesophases occur (N, SmC$_a$P$_{AF}$, SmC'$_a$P$_{AF}$, SmC$_s$P$_{AF}$, SmC'$_s$P$_{AF}$, SmC''$_s$P$_{AF}$ phases) whereby the clearing temperatures vary from 105 °C to 175 °C. The two different types of dimers which possess different directions of the connecting group ***X*** (-**COO**-/-**OOC**-) cannot be directly compared, because of the different spacer length. But generally a tendency could be observed that the dimers with a ***X*** = -**COO**- group form columnar and/or nematic phases, while for the dimers with a ***X*** = -**OOC**- group nematic, a FE crystalline phase and several smectic phases were found. Similar studies on the influence of the direction of different connecting groups for some series of bent-core compounds were reported already in the literature.[64,192]

5.5.3 Effect of a *cyano*- group terminally attached to the bent-core mesogenic unit on the mesophase behaviour: Occurrence of a N - N$_X$ phase transition for dimer 25c[197]

In order to study the influence of the polarity of the terminal group attached to the bent unit, we synthesized dimer series **25** with five-ring bent-core moiety ($n = 12$; $m = 3, 6, 11$; $p = 6$; **E$_2$**) which possess as a terminal group ***R*** a small compact highly polar *cyano*- unit. All dimers **25** exhibit two or three mesophases. We have found that a variety of mesophases occurs (N and SmC$_x$ phases, an optically isotropic phase M$_5$, a transition N - N$_x$ and a probable smectic M$_6$ phase), whereby the clearing temperatures vary from 129 to 184 °C. All compound **25** form nematic phases which exhibit similar properties as already described in the previous chapters (marbled or schlieren texture or/with homeotropic regions, with chiral domains of opposite handedness observed by slightly rotating the polarisers from the crossed position). The mesophase behaviour, transition temperatures together with the associated transition enthalpies of these compounds are given in Table 5.8 and Figure 5.79. The synthesis and mesophase behaviour of dimers **25** were already published.[197]

Table 5.8: Transition temperatures [°C], mesophase types, transition enthalpy values [kJ/mol] of the compounds **25a - c**.[a]

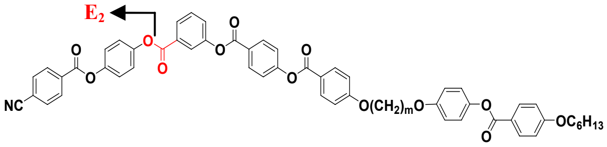

Comp	*m*	Transitions temperatures [°C] ΔH [kJ·mol^{-1}]
25a	3	Cr 166 (SmC$_x$ 127 N 132) I *71.0* *0.7*
25b	6	Cr 162 (M$_5$ 131) N 184 I *64.1* *16.4* *3.9*
25c	11	Cr 136 (M$_6$ 109 N$_x$ 115) N 145 I *71.6* *3.2* *0.8* *2.3*

[a] Transition temperatures (°C) and enthalpy values [kJ/mol] of compounds **25a** - **c** were taken from the second DSC heating scans (10 Kmin^{-1}); values in parentheses indicate monotropic mesophases, in this case the transition temperatures and enthalpy values were taken from the first DSC cooling scans and the transition temperatures were checked by polarising microscopy.

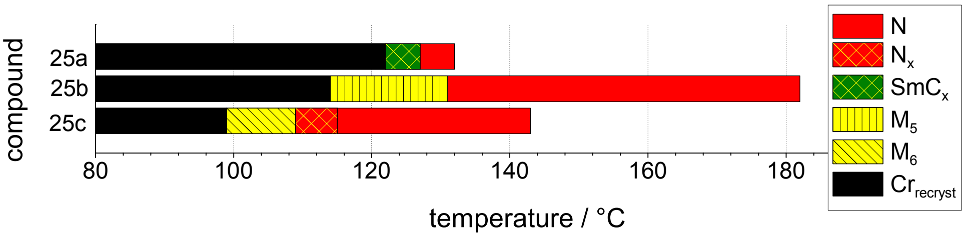

Figure 5.79: Transition temperatures (°C) of compounds **25a** - **c**, taken from the first DSC cooling scans (10 Kmin^{-1}).

The CN-substituted dimer **25a** with an *odd*-methylene spacer length (*m* = 3) exhibits two monotropic phases: a nematic and a smectic SmC$_x$ phase. a SmC$_x$ phase. The compound **25b** with an *even* methylene spacer length (*m* = 6) exhibits an enantiotropic nematic phase and an unknown monotropic phase. The low-temperature phase is characterized by the dominance of an optically isotropic texture in which regions of different chirality sense can be distinguished by rotating one polariser out of the crossed position. The light transmission changes when the sample is rotated, indicating that the M$_5$ phase of compound **25b** is not a *dark conglomerate phase*. This mesophase has a significantly higher viscosity in comparison to the high-temperature *conventional* smectic phases and does not show a polar electro-optical response. Owing to the metastable nature of this phase it was not possible to characterize it by X-ray diffraction study. Hence, it has been presently designated as an unknown phase, M$_5$ phase.

For the CN-substituted dimer **25c** (*m* = 11) three mesophases could be clearly distinguished by their textures and by differential scanning calorimetry. According to the characteristic textures, the high-temperature phases can be assigned to a nematic and a nematic

N_x phase, similar to the one described already in the section 5.5.1.1 for compound **13b**. The high-temperature nematic phase showed typical marbled, homeotropic and/or planar textures (Fig. 5.80a). The long-range director fluctuations characteristic of a nematic phase disappear upon cooling of the sample at 115 °C and a transition to another mesophase (N_x phase) occurs showing a very tiny fan-like texture, as illustrated in Figure 5.80b (the corresponding transition enthalpy is rather low, 0.8 kJ mol^{-1}). The absence of well-defined focal conics ruled out the possibility that this phase is a smectic A or C phase. On further cooling of the sample a transition to another mesophase (M_6) takes place at 109 °C, with a texture consisting of very small focal-conic fans with higher birefringence. In some regions of the slide, well-defined focal conics were seen and, therefore, the possibility that the M_6 phase is a SmA phase cannot be ruled out (Fig. 5.80c). However, when the M_6 phase was subjected to homeotropic boundary conditions (in a 5µm non-coated ITO cell, previously threaded with HTAB), it failed to produce the pseudo-isotropic texture, a characteristic feature of the SmA phase. Hence, it has been presently designated as an unknown phase, M_6 phase. The corresponding transition enthalpy is 3.2 kJ mol^{-1}. X-ray diffraction measurements have been performed on aligned samples of compound **25c** by applying a magnetic field of about 1T. The results confirm that the high-temperature phases are two nematic phases and the X-ray diffraction patterns are very similar. In the X-ray pattern of the N_x phase no evidence of a layer structure could be found, although the fan-like texture indicates the existence of a smectic-like phase. Due to the metastable nature of the M_6 phase it was not possible to characterize it by X-ray diffraction, electro-optical and/or mechanical shearing studies.

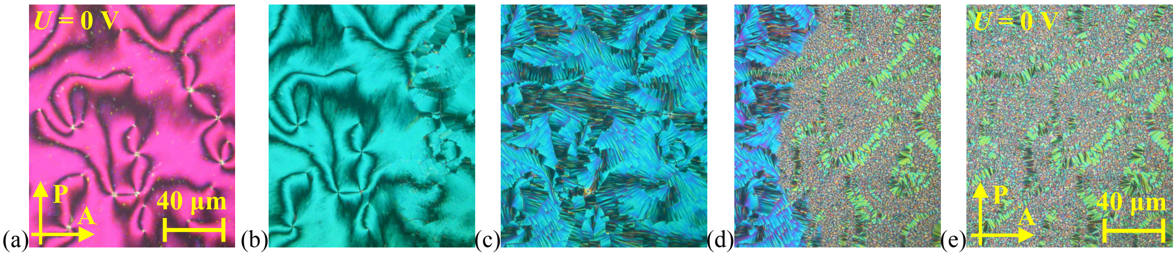

Figure 5.80: (a-e) Textures of the mesophases of compound **25c** observed between crossed polarisers in the same region of the sample, on cooling at U = 0 V in a 5µm non-coated ITO cell, which previously was threaded with HTAB: (a) schlieren texture of the nematic phase at 141 °C; (b) growing of the fan-like texture of the N_x phase from the schlieren texture of the high-temperature nematic phase at 115.5 °C; (c) fan-like texture of the N_x phase at 114 °C; (d) growing of the fan-shaped texture of the M_6 phase from the fan-like texture of the N_x phase at 109.5 °C; (e) fan-shaped texture of the M_6 phase at 108 °C.

It was found for the dimers **25** that the introduction of a polar *cyano-* unit as a terminal group at the bent segment increases the mesophase stability. All these CN-substituted dimers exhibit nematic phase over broader temperature regions than the corresponding dimers **14** – **16** with terminal *alkyloxy* substituents. The results of this work on dimers **25** were already published in a slightly modified form.[197]

5.5.4 Effect of the lateral substituents *chlorine-* and *methyl-* at the bent-core mesogenic unit on the mesophase behaviour of dimer series 26 and 27[197]

In order to study the role of the lateral substitution at the outer ring of the bent unit, we synthesized the dimer series **26** and **27** (n = 12; m = 3, 6, 11; p = 6; **E$_0$**). Two types of lateral substitution were considered: the lateral substitution by *chlorine* in 3-position at the outer ring of the bent-core (position **A**, see Table 5.9, dimer series **26**) and the lateral substitution in 2-position at the central ring of the bent-core by a *methyl-* group (position **B**, see Table 5.10, dimer series **27**). An appropriate comparison with the non-substituted corresponding homologues of series **1** followed. Parallel the role of the variation of the spacer length will be investigated. The mesophase behaviour, transition temperatures together with the associated transition enthalpies, lattice parameters and P_S values for the dimers **26** and **27** and the comparison compounds **1** are given in Table 5.9 and Table 5.10. The synthesis and mesophase behaviour of dimers **26** and **27** were already published.[197]

Table 5.9: Transition temperatures [°C], mesophase types, transition enthalpy values [kJ/mol], tilt angle τ of the molecules [°] with respect to the normal to a in Col phases, lattice parameters (a, b, γ) and P_S values of the compounds **26a - c** and their analogues compounds **1b, 1d, 1i**.[a]

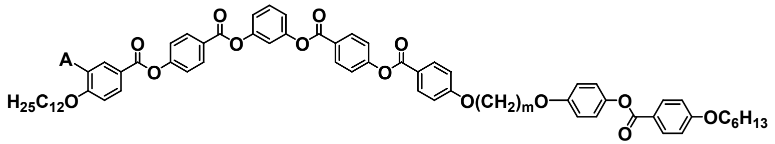

Comp.	m	A [b]	Transitions temperatures [°C] ΔH [kJ·mol^{-1}]	Phase type	Lattice parameters τ [°]	a [nm]	b [nm]	γ [°]	P_S nC/cm^2
1b	3	H	Cr 150 (Col$_r$P$_{AF}$ 127) I *65.7 24.0*	Col$_r$P$_{AF}$	11	7.57	5.51	90.0	350
26a	3	Cl	Cr 149 (Col$_r$P$_{AF}$ 139) I *72.3 27.5*	Col$_r$P$_{AF}$	-[c]	12.01	5.62	90.0	300
1d	6	H	Cr 148.5 (Col$_x$ 125.5 N 145.5) I *61.2 13.1 1.3*	N Col$_x$ [c]	-[c]	-[c]	-[c]	-[c]	-[c]
26b	6	Cl	Cr 145 (N 133) I *63.2 1.7*	N					
1i	11	H	Cr 121 Col$_{ob}$P$_{FE}$ 132.5 I *58.8 25.3*	Col$_{ob}$P$_{FE}$	44	3.20	5.00	110.0	380
26c	11	Cl	Cr 118 Col$_r$P$_{FE}$ 123 I *40.7 24.9*	Col$_r$P$_{FE}$	20	13.82	6.42	90.0	250

[a] Transition temperatures (°C) and enthalpy values [kJ/mol] of the compounds **26a - c** and their analogues compounds **1b, 1d, 1i** were taken from the second DSC heating scans (10 Kmin^{-1}); values in parentheses indicate monotropic mesophases, in this case the transition temperatures and enthalpy values were taken from the first DSC cooling scans and the transition temperatures were checked by polarising microscopy; [b] position A on the terminal ring of the bent-core unit; A = Cl, H; [c] could not be determined due to rapid crystallization of the sample.

All compounds **26** with the *chlorine* atom in 3-position at the outer ring of the bent-core exhibit liquid crystalline behaviour. The systematic study revealed that this lateral substitution with the chlorine atom does not change significantly the mesophase behaviour of the dimers. Different tendencies could be observed in the clearing temperatures of the substituted dimers **26**. That means for dimer **26a** (m = 3) a mesophase stabilization effect was observed (an increase of the clearing temperature of 12 K), while for dimer **26b** and **26c** (m = 6, 11) a decrease of the clearing temperature of 12.5 K and 9.5 K, respectively was found. The dimer **26a** (m = 3) exhibits a monotropic $\mathrm{Col_rP_{AF}}$ phase, similar to the corresponding halogen-free dimer **1b**. The dimer **26b** (m = 6) possesses a monotropic nematic phase in accordance with its overall linear shape. Its analogue compound **1d** forms a N and a $\mathrm{Col_x}$ phase.

The dimer with the longest spacer, dimer **26c** (m = 11) exhibits an enantitropic $\mathrm{Col_rP_{FE}}$ phase, while the analogue dimer **1i** forms a $\mathrm{Col_{ob}P_{FE}}$ phase. Another interesting finding on the introduction of a chlorine atom at the terminal ring of the bent unit is the enlargement of the lattice parameters for the two columnar phases of the *odd*-methylene spacers. It was found that for the member with the shortest spacer **26a** (m = 3), the lateral substitution by a *chlorine* atom in the 3-position at the outer ring of the bent-core unit results in a stabilization of nematic phase, whereas for the compounds with longer spacer it leads to a destabilization of the N or Col phase, respectively.

The effect of the lateral substitution with a *methyl-* group in 2-position at the central *phenylene* ring on the mesophase behaviour will be studied by means of compounds **27a-c** (n = 12, m = 3, 6, 11, p = 6; $\mathbf{E_0}$, see Table 5.10). The 2-methylresorcinol derivatives of five-ring bent-core mesogens are of special interest for us since DIELE *et al.*[92] gave the first report about B_5 phases for substituted five-ring bent mesogens.

Table 5.10: Transition temperatures [°C], mesophase types, transition enthalpy values [kJ/mol], tilt angle τ of the molecules [°] with respect to the normal to a in Col phases, lattice parameters (a, b, γ) and P_S values of the compounds **27a - c** and their analogues compounds **1b, 1d, 1i**.[a]

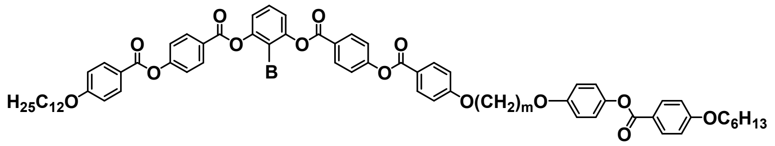

Comp.	m	B [b]	Transitions temperatures [°C] ΔH [kJ·mol^{-1}]	Phase type	Lattice parameters				P_S nC/cm^2
					τ [°]	a [nm]	b [nm]	γ [°]	
1b	3	H	Cr 150 ($\mathrm{Col_rP_{AF}}$ 127) I *65.7 24.0*	$\mathrm{Col_rP_{AF}}$	11	7.57	5.51	90.0	350
27a	3	CH_3	Cr 159 I *71.9*	-	-	-	-	-	-
1d	6	H	Cr 148.5 ($\mathrm{Col_x}$ 125.5 N 145.5) I *61.2 13.1 1.3*	N $\mathrm{Col_x}$ [c]		-[c]	-[c]	-[c]	-[c]
27b	6	CH_3	Cr 164 I *85.3*	-	-	-	-	-	-
1i	11	H	Cr 121 $\mathrm{Col_{ob}P_{FE}}$ 132.5 I *58.8 25.3*	$\mathrm{Col_{ob}P_{FE}}$	44	3.20	5.00	110.0	380
27c	11	CH_3	Cr 125 $\mathrm{Col_{ob}P_{FE}}$ 132 I *44.5 29.4*	$\mathrm{Col_{ob}P_{FE}}$	42	3.20	4.93	110	420

[a] Transition temperatures (°C) and enthalpy values [kJ/mol] of compounds **27a - c** and their analogues compounds **1b, 1d, 1i** were taken from the second DSC heating scans (10 Kmin^{-1}); values in parentheses indicate monotropic mesophases, in this case the transition temperatures and enthalpy values were taken from the first DSC cooling scans and the transition temperatures were checked by polarising microscopy; [b] position ***B*** at the central ring of the bent-core unit; ***B*** = CH_3, H); [c] could not be determined due to rapid crystallization of the sample.

This study revealed that for this type of lateral substitution at central ring of the bent unit liquid crystalline properties were found only for compound **27c**. The dimer with the longest spacer, dimer **27c** (*m* = 11) exhibits an enantiotropic $Col_{ob}P_{FE}$ phase, similar to the analogue non-substituted dimer **1i**. These findings are different than those reported for monomeric bent-shaped molecules in which the introduction of small substituents like *methyl*- groups into the obtuse angle of the molecules results in higher mesophase stabilities (e.g. ref.[258]).

5.5.5 Effect of the number of aromatic rings in the bent-core unit of dimer series 28[197]

In this section the influence of the number of aromatic rings (***q***) in the bent-core mesogenic unit will be discussed. Therefore, we synthesized the dimer series **28** with a six-ring bent-core moiety (*n* = 12; *m* = 6, 11; *p* = 6; *q* = 1; $\mathbf{E_0}$). Their mesomorphic behaviour is compared with that of the corresponding dimers **1d** and **1i**, see Table 5.11) which possess a five-ring bent-core moiety. The synthesis and mesophase behaviour of dimers **28** were already published.[197]

Monomeric bent-core compounds with six or seven aromatic rings have also been reported in the literature.[41,59,259] The general tendency is that with an increasing number of rings the transition temperatures increase.

All dimers **28** exhibit liquid crystalline behaviour. Simultaneously, a clear enhancement of the mesophase stability could be observed for these two dimers. The clearing temperatures increase by 51 K for dimer **28a** (*m* = 6) and by 10 K for dimer **28b** (*m* = 11) with respect to the corresponding value of the analogues dimers **1**.

Table 5.11: Transition temperatures [°C], mesophase types, transition enthalpy values [kJ/mol], tilt angle τ of the molecules [°] with respect to the normal to *a* in Col phases, lattice parameters (*a*, *b*, *γ*) and P_S values of the compounds **28a - c** and their analogues compounds **1d, 1i**.[a]

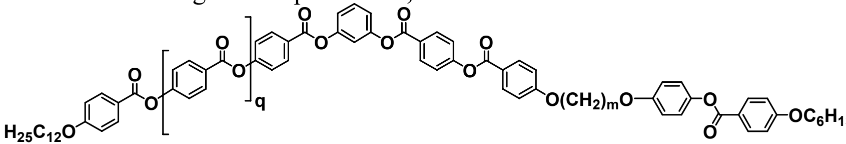

Comp.	*m*	*q*[d]	Transitions temperatures [°C] Δ*H* [kJ·mol^{-1}]	Phase type	Lattice parameters τ [°]	 *a* [nm]	 *b* [nm]	 γ [°]	P_S nC/cm^2
1d	6	0	Cr 148.5 (Col_x 125.5 N 145.5) I *61.2 13.1 1.3*	N Col_x [c]	-[c]	-[c]	-[c]	-[c]	-[c]
28a	6	1	Cr 159 Col_rP_{AF} 186 N 197 I *66.9 14.7 1.6*	N Col_rP_{AF}	0	4.33	6.75	90	400
1i	11	0	Cr 121 $Col_{ob}P_{FE}$ 132.5 I *58.8 25.3*	$Col_{ob}P_{FE}$	44	3.20	5.00	110.0	380
28b	11	1	Cr 127 Col_xP_{AF} 132 N 143 I *53.8 8.2 1.2*	N Col_xP_{AF}	-[c]	-[c]	-[c]	-[c]	570

[a] Transition temperatures (°C) and enthalpy values [kJ/mol] of the compounds **28a - c** and their analogues compounds **1d, 1i** were taken from the second DSC heating scans (10 Kmin^{-1}); values in parentheses indicate monotropic mesophases, in this case the transition temperatures and enthalpy values were taken from the first DSC cooling scans and the transition temperatures were checked by polarising microscopy; [b] the transition is not detectable on DSC and the transition temperature value is determined by polarising microscopy; [c] could not be determined due to rapid crystallization of the sample; [d] *q* is the number of the additional *benzoyloxy*-fragments in the bent–core unit.

The dimer **28a** (*m* = 6) exhibits two enantiotropic mesophases: a nematic and a columnar phase, in accordance with the analogue dimer **1d** and with its overall linear shape (*even*-methylene spacer). X-ray diffraction measurements on a surface-aligned sample give evidence for a $\mathrm{Col_r}$ phase. On applying a triangular-wave electric field above a threshold voltage of 20 V μm^{-1}, the $\mathrm{Col_r}$ phase is switchable, *i.e.*, two polarisation current peaks per half period were recorded, which indicates an AF ground state (P_S = 380 nC cm^{-2}). A field-induced phase transition to a $\mathrm{SmCP_{AF}}$ phase accompanied by a drastic change to a *non-specific* smectic-reminiscent texture occurs on applying a threshold voltage above 35 V μm^{-1} (P_S = 600 nC cm^{-2}). Upon removal of the field, the virgin texture of the $\mathrm{Col_r}$ phase is not recovered, and the texture relaxed to a *non-specific* smectic-reminiscent one. A similar field-induced phase transition was reported for the dimer **6b** in the section 5.1.2.5.

The dimer **28b** (*m* = 11) exhibits two enantiotropic mesophases: a nematic and a columnar $\mathrm{Col_xP_{AF}}$ phase (P_S = 570 nC cm^{-2}), while the analogue five-ring dimer **1i** possesses a $\mathrm{Col_{ob}P_{FE}}$ phase. The occurrence of a nematic phase for this spacer parity (*m* = 11) is in discordance with its overall zig-zag shape (*odd*-methylene spacer) and with the previously reported results for dimers **type I**. The increase of the number of rings in the bent unit leads to an increased mesophase stability and transition temperatures of the compounds **28**. A nematic phase is induced on increasing the number of rings in compound **28b** with an *odd*-methylene spacer. An increased P_S value was measured for the dimers **28**.

5.6 Variation of the molecular structure of the calamitic unit of dimer series 29 and 30

In this chapter, the mesophase properties of new dimers with calamitic mesogenic units incorporating *biphenylene* fragments (dimer series **29**) and *bis-azobenzene* segments (dimer series **30**) will be discussed. These new dimers are the only compounds presented in this work which contain three-ring calamitic mesogenic units.

The rigid *biphenyl* unit is of special interest since in literature there are reports that its introduction in the calamitic moieties leads to a stabilisation of the mesophases.[260] Numerous rod-like molecules containing *biphenyl* fragments are known to form stable smectic phases due to the parallel alignment of the rod-like moieties.[260] However, the rod-like molecules consisting of *cyanobiphenyl* units exhibit nematic phases.

Furthermore, it is well known that the introduction of photosensitive *azobenzene* groups into the polymeric matrix provides a broad range of approaches for the design of materials with applications in optical data recording and storage (see for example references [261,262]). Also, the first bent-core molecules, synthesised by VORLÄNDER *et al.*, represent *azobenzene* and *azoxybenzene* derivatives forming intercalated smectic phases (B_6 phases).[47] *Azobenzene*-containing main-chain and side-chain types of polymers[263,264] are of particular interest for holographic recording because of their large capacity for the storage of information and other advantages.

5.6.1 Introduction of a *biphenylene* unit in the calamitic moiety of dimer series 29[195]

The dimers **29** (n = 12; m = 6, 11; p = 6, 8; E$_0$; X = **-O-**/**-COO-**) posses a five-ring bent-core moiety and a weakly polar calamitic unit of different size incorporating a *biphenylene* unit (Table 5.12). The dimer **29a** contains a hexyloxybiphenyl unit, while the dimer **29b** contains an octyloxybenzoyloxybiphenyl moiety, i.e. a three-ring calamitic mesogenic unit. These new dimers will be compared with the analogues dimers **7a** and **1i** containing the calamitic hexyloxybenzoyloxyphenyl unit. All compounds exhibit liquid crystalline behaviour. The synthesis and mesophase behaviour of dimers **29** were already published.[195]

Dimer **29a** (n = 12; m = 6; p = 6; E$_0$; X = **-COO-**) which contains a calamitic hexyloxybiphenyl- unit forms a columnar mesophase, only. The columnar structure is indicated by the mosaic texture and proved by X-ray diffraction measurements. X-ray measurements performed on this mesophase at 140 °C show the typical scattering pattern of a centred, rectangular lattice (a = 17.6 nm, b = 5.84 nm, see Table 5.12). The diffuse scattering in the wide angle region points to a tilted arrangement of the mesogenic units in the cell. These are inclined with respect to the normal to a-axis of the real lattice by a tilt angle of about 28°. In contradiction to the analogue dimer **7a** which exhibits a ferroelectric columnar phase, no polar switching could be observed for the Col$_\text{r}$ phase of dimer **29a**. Dimer **29b** (n = 12; m = 11; p = 8; E$_0$; X = **-O-**) forms two enantiotropic mesophases, i.e. a N and a Col$_\text{ob}$ phase (a = 4.23 nm, b = 5.67 nm, γ = 91°). In contradiction to the analogue dimer **1i** which exhibits a ferroelectric columnar oblique phase, no polar switching could be observed for the Col$_\text{r}$ phase of dimer **29b**.

Table 5.12: Transition temperatures [°C], mesophase type, transition enthalpy values [kJ/mol], tilt angle τ of the molecules [°] with respect to the normal to a in Col$_\text{ob}$ phases, lattice parameters (a, b, γ) and P_S values of the dimers **29** and their analogues compounds **7a** and **1i**.[a]

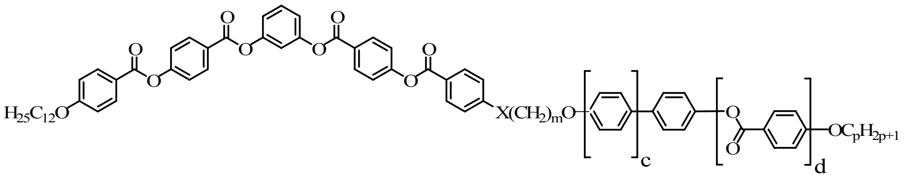

Comp	m	p	X[c]	c[d]	d[e]	Transitions temperatures [°C] ΔH [kJ·mol^{-1}]	Phase type	Lattice parameters				P_S nC/cm^2
								τ [°]	a [nm]	b [nm]	γ [°]	
7a	6	6	**COO**	0	1	Cr 135 (Col$_x$P$_{FE}$ 128) I *67.3 26.6*	Col$_x$P$_{FE}$	-[b]	-[b]	-[b]	-[b]	240
29a	6	6	**COO**	1	0	Cr 150 (Col$_r$ 144) I *62.7 29.5*	Col$_r$	28	17.6	5.84	90	-
1i	11	6	**O**	0	1	Cr 121 Col$_{ob}$P$_{FE}$ 132.5 I *58.8 25.3*	Col$_{ob}$P$_{FE}$	44	3.20	5.00	110	380
29b	11	8	**O**	1	1	Cr 144 Col$_{ob}$ 159 N 160 I *47.3 27.9 1.0*	Col$_{ob}$	40	4.23	5.67	91	-

[a] Transition temperatures (°C) and enthalpy values [kJ/mol] of dimers **29** and their analogues compounds **7a** and **1i** were taken from the second DSC heating scans (10 Kmin^{-1}); values in parentheses indicate monotropic mesophases, in this case the transition temperatures and enthalpy values were taken from the first DSC cooling scans and the transition temperatures were checked by polarising microscopy; [b] could not be determined due to rapid crystallization of the sample; [c] group X is connecting the spacer with the bent-core unit; [d] c is the number of the additional *phenyl* rings in the corresponding unit; [e] d is the number of the *benzoyloxy*- units in the calamitic unit.

The introduction of a rigid *biphenylene* segment in the calamitic moiety and the replacement of the *benzoyloxy*- unit results in a mesophase stabilization (the clearing temperature increases by about 16 K). The enlargement of the calamitic unit by the replacement of the *phenyl* unit by a *biphenyl* segment results in the case of dimers **29b** in a mesophase stabilization (the clearing temperatures is higher with 27.5 K in comparison with those of the analogue dimer **1i**) and in occurrence of an additional N phase. For both dimers **29** containing a *biphenyl* unit in the calamitic moieties a loss of the ferroelectric properties could be observed.

5.6.2 Introduction of a *bis-azobenzene* unit in the calamitic moiety of dimer series 30[198]

The non-symmetrical dimers **30** (n = 12; m = 2, 4, 6; E_0; X = **-COO-;** Y = **-O-**) posses a five-ring bent-core moiety which is connected through a flexible spacer to a three-ring calamitic mesogenic unit containing a *bis-azobenzene* unit. All dimers **30** possess an *odd*-numbered spacer (with an *even* methylene spacer (m = 2, 4, 6), but an *odd* number of all units in the spacer) and exhibit smectic phases (see Table 5.13). The dimer **30a** with the shortest spacer (m = 2) exhibits one monotropic smectic SmC_aP_{AF} phase, while dimers **30b** and **30c** (m = 4, 6) form an additional enantiotropic high-temperature smectic phase. The mesomorphic properties of these two dimers are very similar. The stability of the mesophases decreases with the elongation of the spacer unit. The synthesis and mesophase behaviour of dimers **30** were already published.[198]

Table 5.13: Transition temperatures [°C], mesophase type, transition enthalpy values [kJ/mol], layer spacing d [nm], tilt angle τ of the molecules [°] with respect to the layer normal in SmC phases and P_S values of the dimer series **30**.[a]

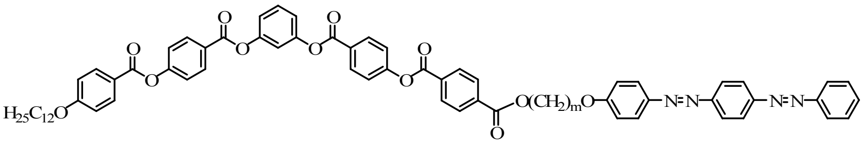

Comp.	m	Transitions temperatures [°C] ΔH [kJ·mol^{-1}]	Phase type	Lattice parameters		P_S nC/cm^2
				d [nm]	τ [°]	
30a	2	Cr 192 (SmC_aP_{AF} 184) I *86.1* -[b]	SmC_aP_{AF}	-[c]	-[c]	270
30b	4	Cr 176 (SmC_sP_{FE} 161) SmC_aP_{AF} 184 I *45.1* -[b] *27.1*	SmC_aP_{AF} SmC_sP_{FE}	6.01 6.10	22.5 20	350 470
30c	6	Cr 160 (SmC_sP_{FE} 151) SmC_aP_{AF} 175 I *66.4* *0.1* *29.0*	SmC_aP_{AF} SmC_sP_{FE}	6.30 6.30	20 20	590 770

[a] Transition temperatures (°C) and enthalpy values [kJ/mol] of dimer series **30** were taken from the second DSC heating scans (10 Kmin^{-1}); values in parentheses indicate monotropic mesophases, in this case the transition temperatures and enthalpy values were taken from the first DSC cooling scans and the transition temperatures were checked by polarising microscopy; [b] the transition is not detectable on DSC and the transition temperature value is determined by polarising microscopy; [c] could not be determined due to rapid crystallization of the sample.

For dimers **30b** and **30c** on cooling from the isotropic liquid state fascinating textures with spiral nuclei arise which coalesce to a variety of optical textures including ribbon-like and spherulitic texture, focal conics and circular domains (Figure 5.81a-c) similar to the textures of B_7 phase,[24,32,36,61,70,101,102] or B_7’ phase.[60,72,102,106]

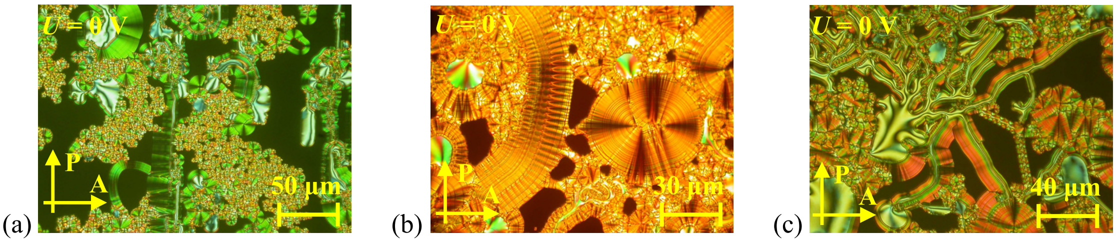

Figure 5.81: Textures between crossed polarisers of the high-temperature phase of compound **30c** at 171 °C at $U = 0$ V in (a,c) a 5 µm non-coated ITO cell and (b) a 6 µm polyimide-coated ITO cell.

The observation of a schlieren texture with multiple disclinations (Fig. 5.82a) or of a smooth fan-shaped texture is a strong indication that the high temperature phase could be an anticlinic SmC phase. Another argument for the anticlinic organization of the molecules between adjacent layers is the presence of well defined circular domains with the extinction directions parallel to the position of the crossed polarisers (Fig. 5.81a,b and 5.84). The transition into the low temperature phase is accompanied by a clear change of the optical textures. The smooth fan-shaped is transformed on cooling into a broken fan-shaped texture with irregular stripes across the fans and with circular domains where the extinction crosses are inclined with respect to the directions of the crossed polarisers. Meanwhile, the schlieren texture with multiple disclinations becomes strongly fluctuating near the transition to the low-temperature smectic phase (Fig. 5.82b) and the disclinations partially disappear (Fig. 5.82c). These are indications of a transition to a synclinic organization of the molecules between adjacent layers.

This exciting behaviour of a $\mathrm{SmC_a}$–$\mathrm{SmC_s}$ phase transition for the compounds **30b** and **30c** (m = 4, 6) is characterised by a small transition enthalpy (about 0.1 $\mathrm{kJ{\cdot}mol^{-1}}$). The phase transition can be easily observed by POM due to typical turbulences between the two smectic states (Fig. 5.82), also reported for a comparable transition between two SmC phases of hockey-stick shaped mesogens.[265] However, for the hockey-stick shaped mesogens an opposite transition, i.e. a $\mathrm{SmC_s}$–$\mathrm{SmC_a}$ phase transition was found on cooling.

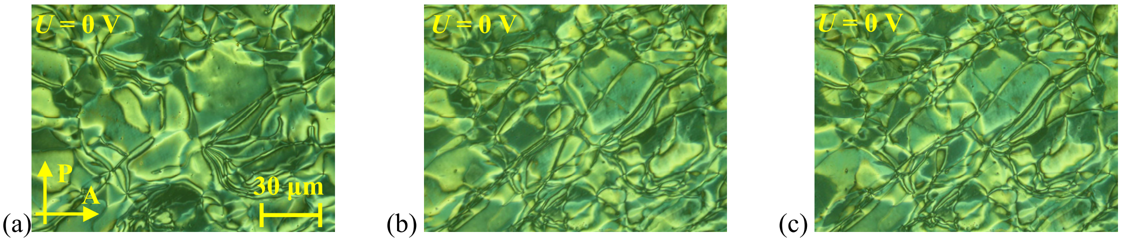

Figure 5.82: Schlieren textures of compound **30c** at $U = 0$ V in a 5 µm non-coated ITO cell, observed between crossed polarisers in the same region of the sample: (a) multiple disclinations texture of the high-temperature smectic phase at 168 °C; (b) turbulences between the two smectic states at 151 °C; (c) disturbed schlieren texture of the low-temperature smectic phase at 145 °C.

As a representative example, the X-ray investigations on the mesophases of dimer **30c** on cooling will be presented in more detail. X-ray measurements at 165 °C and at 145 °C confirmed the presence of two SmC phases. They showed very similar patterns for both phases (Fig. 5.83a-d). The layer spacing derived from the X-ray measurements on cooling is independent of the temperature, including the transition from the high-temperature SmC (6.30 nm) to the lower-temperature SmC phase (6.30 nm) and indeed until the sample crystallizes. An average tilt angle of the molecular long axis with respect to the layer normal can be calculated from the position of the maxima for the outer diffuse scattering in both SmC phases ($\tau = 20°$). An effective molecular length L_{eff} may be calculated from these experimental results for both SmC phases to $L_{eff} = d/\cos\tau = 6.70$ nm.

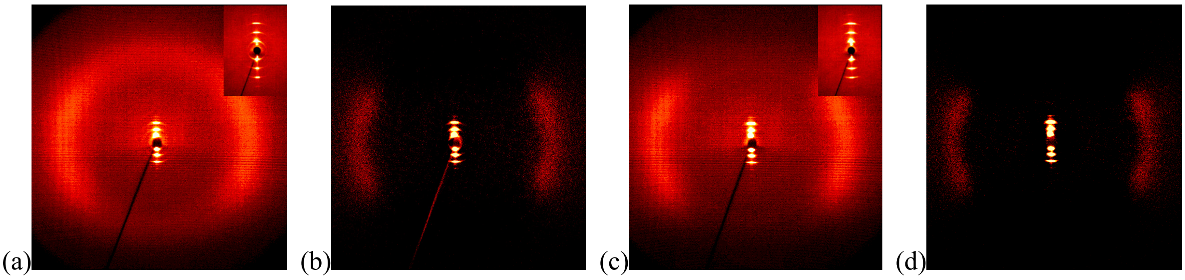

Figure 5.83: XRD patterns of an aligned sample of compound **30c**: (a-b) high-temperature SmC phase at 165 °C: (a) original pattern; (b) the same XRD pattern, but the intensity of the isotropic liquid is subtracted; (c-d) low-temperature SmC phase at 145 °C: (c) original pattern; (d) the same XRD pattern, but the intensity of the isotropic liquid is subtracted; (a,c) the insets show the small angle scattering.

The X-ray investigations on dimer **30b** evidence a similar organization of the molecules between adjacent layers. Interestingly, the layer spacing increases on cooling, from the high-temperature SmC (6.01 nm) to the lower-temperature SmC phase (6.10 nm), accompanied by a tilt angle τ decreasing from 23° in the high-temperature SmC phase to 20° in the low-temperature SmC phase as derived from the outer diffuse scattering. Because of the fibre-like disorientation of the samples, no clear evidence for a transition from an anticlinic to a synclinic organization of the molecules between adjacent layers could be found by the X-ray investigations.

Electro-optical investigations on the high-temperature SmC phases of dimers **30b** and **30c** evidenced the occurrence of two separate repolarisation peaks in each half period of the applied triangular voltage field, which is characteristic for an antiferroelectric switching (Fig. 5.84d). The calculated values of the spontaneous polarisation vary between 350 (**30b**) and 590 nC cm^{-2} (**30c**). The application of an electric field (10 $V\mu m^{-1}$) on the high-temperature SmC phase leads to formation of a smoother fan-like texture. In the circular domains the extinction crosses are aligned along the directions of the crossed polarisers and do not change on applying, on reversal (Fig. 5.84a,c) or on terminating the applied field (Fig. 5.84b). These findings suggest that the AF ground state as well as the switched FE states have an anticlinic tilt. This switching corresponds to the transition from a SmC_aP_{AF} state to a SmC_aP_{FE} state. The chirality of the layers switches by a collective rotation of the molecules around their long axes on reversing the applied field.

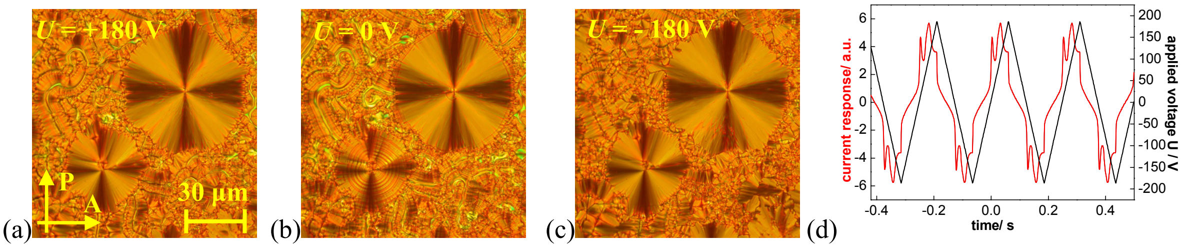

Figure 5.84: Electro-optical investigations on the SmC$_a$P$_{AF}$ phase of dimer **30c** at 165 °C, observed between crossed polarisers in the same region of the sample in a 5 µm non-coated ITO cell: (a,c) $U = \pm$ 180 V; (b) U = 0 V; (d) AF switching current response obtained by applying a triangular-wave voltage (U = 373 V$_{pp}$, f = 4 Hz, R = 5 kΩ, P_S = 590 nC cm^{-2}).

The monotropic low-temperature SmC phase presents one well defined repolarisation peak per half period of the applied triangular voltage field (SmC$_s$P$_{FE}$, see Fig. 5.85d). The calculated P_S values amounts to 470 (**30b**) and to 770 nC cm^{-2} (**30c**). The extinction directions of the circular domains make an angle of ~ 20° with the directions of the crossed polarisers indicating that this SmC phase has a tilted organization (Fig. 5.85a-c). If the first FE ground state is switched to the second FE state or *vice versa*, the extinction directions do not change and only the birefringence slightly varies (Fig. 5.85c). Furthermore, this effect is independent of the polarity of the applied field. Hence, the FE ground state as well as the switched FE states has a synclinic tilt and the switching corresponds to the transition from a SmC$_s$P$_{FE}$ state to a SmC$_s$P$_{FE}$ state. As previously found for the SmC$_a$P$_{AF}$ phase of dimers **1**-**6**, the chirality of the layers switches by a collective rotation of molecules around their long axes on reversing the applied field. On the basis of these experimental findings the high-temperature SmC$_a$ phases of compounds **30b** and **30c** are AF with an anticlinic organization, i.e. SmC$_a$P$_{AF}$ phases, while the low-temperature phases are FE with a synclinic organization, i.e. SmC$_s$P$_{FE}$ phases.

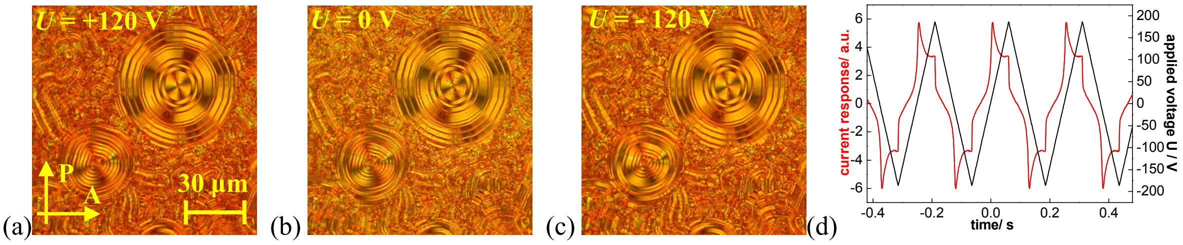

Figure 5.85: Electro-optical investigations on the SmC$_s$P$_{FE}$ phase of dimer **30c** at 145 °C, observed between crossed polarisers in the same region of the sample in a 5 µm non-coated ITO cell: (a,c) $U = \pm$ 120 V; (b) U = 0 V (e) FE switching current response obtained by applying a triangular-wave voltage (U = 372 V$_{pp}$, f = 4 Hz, R = 5 kΩ, P_S = 770 nC cm^{-2}).

Photochemical properties of dimer **30c** were studied in collaboration with Professor Dr. V. Shibaev and Dr. A. Bobrovsky (Moskow University, Russia) in the COST european project.[198] The introduction of photosensitive *azobenzene* groups into the dimers of type **I** matrix is of special interest due to the potential different applications, *e.g.*, in optical data recording and storage of information. It was found that irradiation by polarised light induces photoorientation in thin amorphous films obtained by spin-coating. Kinetics and mechanism of the photoorientation process were studied and it was shown that photoinduced order is quite stable at temperatures below the melting point.[198] The value of the photoinduced dichroism D for dimer **30c** amounts to ~0.3. Such dichroism value is more than two times lower than the maximal value obtained for *azobenzene*-containing side-chain polymers (~0.7),[266] but, nevertheless, much higher than reported before for glassy amorphous low-molar-mass compounds.[267] This relatively low dichroism value can be explained by the presence of bent-shaped fragments decreasing the uniaxial orientation and anisotropy.

To summarize the chapter 5.6.2, the dimers **30** exhibit smectic mesophases for all values of the spacer length *m*. The increase of the spacer length *m* results in a mesophase destabilization. The general tendency of increasing P_S values on increasing the spacer length and on decreasing the temperature is confirmed. Another observed tendency is the increase of the layer spacing with increasing the spacer length *m*.

5.7 Electro-optical characterization of the nematic phase of dimer 15b[251,252,253,254,255]

This section is focused on the electro-optical investigations on the enantiotropic nematic phase of compound **15b** (n = 12; m = 6; p = 6; E_2; chapter 5.5.1.2). These studies gave evidence of quantitatively and qualitatively significant differences in their electro-optical characteristics from that of conventional nematic phases of calamitic mesogens. The results presented in this chapter were already published.[251,252,253,254,255]

Nematic phases are characterized by additional degrees of freedom of the director ***n***, due to the absence of long range positional order. The nematic phases of banana-shaped mesogens behave quantitatively and qualitatively very different from ordinary nematic phases of rod-like mesogens in their electro-optical characteristics due to the prominent influences of the bent-core molecular geometry on physical properties. Some examples are the discovery of a giant bend flexoelectric coefficient e_{33} in a bent-core nematic[268] and unconventional types of electrically driven convection structures.[254,269] Consequently, their sterical shapes qualify the nematic phases of bent-core molecules as potential candidates for biaxial order. Although there has been significant theoretical work[270] and several initial experimental reports,[271,272] the biaxial nematic phases of LCs derived from calamitic mesogens have been long sought with little success.[273] Since the existence of the biaxial nematic phase has been established in complex three-component lyotropic mixtures,[161] there have been numerous efforts to find biaxiality in thermotropic nematic phases, using a variety of experimental techniques. Finally, biaxial nematics of bent-core mesogens have been identified by NMR and X-ray methods.[274,275,276] Since its theoretically prediction by FREISER in 1970,[160] the biaxial nematic (N_b) phase of LCs which possesses two orthogonal optical axes has attracted much attention. In addition to their intrinsic scientific interest, biaxial nematic phases are of potential importance to the display technology. It is to be expected that rotation of the transverse 'biaxial' optical axes might be relatively rapid and possibly faster than for the primary director ***n*** (which corresponds to the axis along which the molecular long axes tend to be parallel). This could produce a display based on in-plane switching with a fast response. The speed advantage of biaxial nematics has been proven, both experimentally[277] and from computer simulations,[278] but a number of anticipated unusual properties of the biaxial nematic phase resulting from its lower symmetry are to be successfully addressed.

5.7.1 Studies on the elastic properties[251]

The investigations of the elastic properties of the nematic phase formed by compound **15b** were realized by the analysis of one-dimensional director deformations in thin sandwich cells with defined anchoring conditions, the so-called FRÉEDERICKSZ transition (FT). The results presented in this chapter were already published.[251] The two parallel glass plates were coated with transparent indium tin-oxide (ITO) electrodes and with a rubbed polyimide layer for a planar director alignment in the x direction (Fig. 5.86a). Thus the initial director orientation $\boldsymbol{n}_0$ was along x (see Fig. 5.86). The cell gap is $d = 25$ µm. A sinusoidal electric field was applied along the z direction. Experiments were performed with monochromatic light ($\lambda = 532$ nm), between crossed polarisers (vertical and horizontal in the images), if not otherwise stated. The a.c. voltages applied to the cell were sine waves at 1 kHz, if not otherwise stated. Additional experiments were performed in a 5 µm sandwich cell with homeotropic alignment conditions in order to exclude other possible mechanisms that could lead to a change of the birefringence in the ground state (chapter 5.7.3.2). In such a cell, the director $\boldsymbol{n}$ was initially in field direction; the sample is completely black between crossed polarisers.

The analysis of the FT allowed the separate study of splay, twist or bend deformations in a pure form at the onset of the transition.[279] The initially uniform director field in the sample was deflected, e.g. by an external electric field exceeding a threshold voltage U_c which depends upon the elastic properties of the substance. The director response was retrieved from a measurement of the optical birefringence of the cell as a function of the applied external field (electric or magnetic).[280] The splay constant K_{11} determined the threshold in a planar cell when the external field was applied normal to the cell plates. With the field in the cell plane, normal to the easy axis of the planarly anchored director, the twist constant K_{22} from the threshold was obtained. In a cell with homeotropic anchoring, application of a magnetic field in the cell plane determines the threshold. A single geometry was used, i.e. a planarly oriented cell with an electric field applied normal to the cell plates. The elastic properties from the analysis of BROCHARD-LEGER (BL) walls that are formed during the splay FRÉEDERICKSZ transition in sandwich cells were investigated.

5.7.1.1 Uniform FRÉEDERICKSZ transition

The mathematical model for the uniform splay FRÉEDERICKSZ transition (FT) in the electric field has been described in great detail in literature[280] and the corresponding experiment has been extensively used for the determination of elastic coefficients of N phasess. For dimer **15b**, the optical birefringence of the material was determined in a wedge cell (commercial cell from E.H.C. with a wedge angle of 0.0135 rad) under crossed polarisers, diagonal to the rubbing direction. Two domains of opposite tilt above the transition were observed when the dynamic FT took place. Generally the domains appeared with arbitrary shapes, and they were separated by walls. Figure 5.86b shows a 25 µm cell in an electric field above the FRÉEDERICKSZ threshold (≈1.15 U_c). In each of the homogeneous regions, the director is deflected in one of the two opposite tilt directions. The domain on the concave side of the wall vanishes gradually in the electric field, on a time scale of approximately half an hour. The transmission intensity in the wall centre remains the same as in the undeformed state. Towards the two domains, several intensity minima and maxima are passed, manifesting themselves as dark and bright parallel lines. The director field in the wall was nearly planar and the director remained in good approximation in the *x, y*-plane. Figure 5.86c shows the wall under parallel polarisers, the contrast in the texture is reversed. Figure 5.86d shows the same region without polarisers (there was only a very weak shadow remaining of the wall, caused by a very small focussing effect in the inhomogeneous director field). For practical purposes, this focussing was neglected, and the light propagating through the wall locally was treated as a plane wave. All observed texture effects have to be attributed to interference of ordinary and extraordinary waves in the cell. This is also evident from Figure 5.86e, which has been recorded after the cell was rotated counter-clockwise by an angle of π / 4 (when one polariser is in the tilt plane, the texture becomes nearly black). Only a faint image of the wall remained. There was evidence for a slight director twist in the uniform domains even at very low tilt deformations above the FT, which is unusual for the splay FT. This twist is not detectable with the common diagonally crossed polariser arrangement. However, when the polariser is set parallel to the surface director, slight rotations of the analyzer out of the perpendicular direction did not produce a symmetrical response. The darkest state in a given domain was obtained when the analyzer is decrossed by about 3° either clockwise or counter-clockwise. This observed rotation was uniform inside a tilt domain. If two different domains are separated by a BL wall, the sense of rotation was opposite in the two domains. In the field-off state, the extinction was maximum at crossed polarisers, and rotation of the analyzer produces a symmetric response. In conclusion, above the FT the director has a small out-of-plane twist component. In the uniform FT, after a sufficiently long time, the walls have disappeared and the sample was a monodomain. In this monodomain state the uniform director deflection could be reversibly controlled by varying the electric field amplitude.

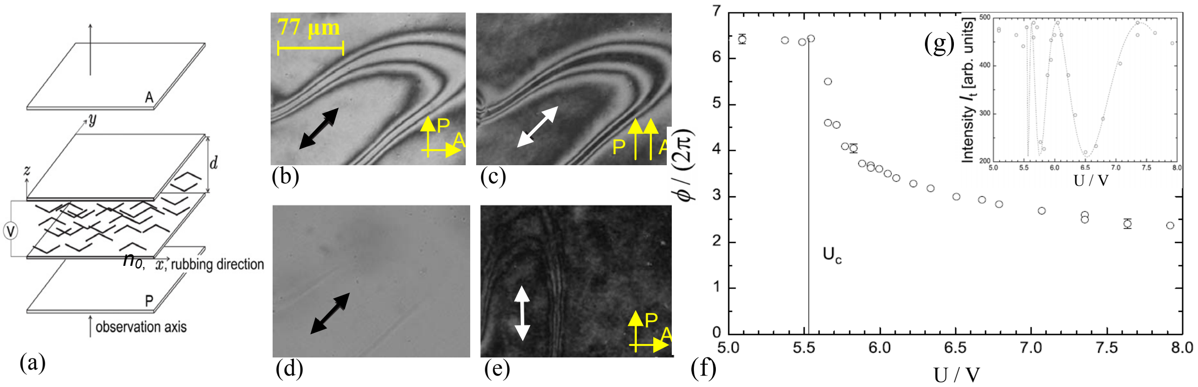

Figure 5.86: (a) Sketch of the setup with analyzer A and polariser P. The cell gap is *d*. (b-e) Textures of the nematic phase of compound **15b** in transmission, 532 nm monochromatic light; the director easy axis is marked by arrows, the electric voltage is slightly above U_c; polarisers are crossed horizontally and vertically (except images (c) and (d)). (b) two domains separated by a wall; the bottom right segment is a twist wall, the other parts contain bend; (c) same between parallel polarisers, dark and bright regions are exchanged; (d) no polarisers, the texture practically disappears; (e) sample rotated by 45° counter clockwise; the texture is nearly black since the director is in the plane of polarisation; (f) optical retardation of the 25 µm cell at $T_{NI} - 7.5$ K during the FT; the maximum $\Phi_{max} / (2\pi) = 6.4$ is related to a birefringence of $n_e - n_o = 0.136$and (g) transmission intensity I_t under crossed polarisers (the dashed line in the image only guides the eye).

Only after the cell was set to the ground state again, and the field was subsequently switched above the FRÉEDERICKSZ field, multiple domains reappeared at random positions. Inside a uniform region, the measured transmission intensity $I_t(U)$ shown in Figure 5.86g yielded the retardation $\Phi(U)$ curve in Figure 5.86f. At subcritical fields, the retardation was $\Phi_{max} = (12.8 \pm 0.1)\,\pi$ at $T = T_{NI} - 7.5$ K. The ratio $K_{11}/\Delta\varepsilon \approx (27.5\pm1.0)$ pN was calculated from the FRÉEDERICKSZ threshold of 5.54 V. This result is unaffected by possible flexoelectric terms. Compared to standard calamitic materials (e.g. 5CB), which have thresholds of the order of 1 V, the material has either a relatively large splay constant or a relatively small dielectric anisotropy ($\Delta\varepsilon < 1$). The decay of the experimental $\Phi(U)$ curve in Figure 5.86f at $U > U_c$ is much steeper than expected with the assumption $K_{33}/K_{11} \approx 1$ and $\Delta\varepsilon_{\|} << \varepsilon_{\perp}$. An assumption of a larger dielectric ratio would flatten the slope even more and an assumed larger K_{33}/K_{11} ratio as well. In order to interpret the measured characteristics, it could be assumed that K_{33} is much smaller than K_{11}, but this will be in conflict with the following description of the BROCHARD-LEGER wall profiles.

Measurements on the flexoelectric coefficients in nematic phases of bent-core mesogens[268] showed that the bend flexocoefficient e_{33} can be three orders of magnitude larger than in calamitic nematics (i.e. a huge value of the order of $e_{33} \approx 30$ nC/m has been reported). If we take into account that our material might also have a large bend flexoelectric coefficient, then the effects on the FT as well as on the wall structures could be tremendous, than we should include flexoelectric terms in the interpretation of the $\Phi(U)$ characteristics in Figure 5.86g. It is, however, not clear how the additional terms could explain the observed large drop of $\Phi(U)$ above U_c. A calculation of the effects of flexoelectric polarisations on the electric FT made by BROWN and MOTTRAM [281] reported on the contrary a flattening of the director deflection characteristics curve with an assumed increasing flexoelectric coefficient.

5.7.1.2 BROCHARD-LEGER walls

In this section the multidomain textures with walls that exhibit well separated twist and bend regions are discussed (see description in ref.[251]and Fig. 5.87a,b). This type of walls has been described first by LEGER[282] and BROCHARD[283] (in the magnetic FT). A domain surrounded by a closed wall within another uniform domain of opposite tilt is unstable. Such a region shrinks and will finally be extinguished. The final state of the LC compound in the sample is a monodomain. It has been shown that both the elliptical shape of a shrinking domain enclosed by such a BROCHARD-LEGER (BL) wall and the geometry of the wall itself carry information on the ratio of twist and bend elastic constants, $k_2 = K_{22}/K_{33}$.[282,283] In common nematic phases, e.g. 5CB, the monodomain state is reached within seconds. The domain and wall structures of the nematic phase of dimer **15b** may persist for several minutes up to about half an hour. During that time, wall segments may move, but they retain their profiles, which are determined by the equilibrium of electric and elastic forces. Sometimes walls are pinned locally by dust particles or defects in the sample, in such cases they may remain stationary. In a segment that is aligned perpendicular to the director easy axis, the BL wall contains only splay and bend deformations (Fig. 5.87f), while a straight wall segment aligned parallel to the director easy axis contains also twist deformations, and practically no bend near the FRÉEDERICKSZ threshold. Consequently, the comparison of wall profiles in different sections, served for a quantitative comparison of the related elastic constants, i.e. the ratio of wall widths in both regions provided the elastic ratio k_2.[251]

In Figure 5.87c-e some examples of digitally processed texture details are presented. The appropriately stretched and rotated images of twist sections of walls have been superimposed onto bend sections of the same walls. The director was described by the tilt angle $\theta(x, y, z)$, and it was assumed that there is no twist out of the tilt plane, $\boldsymbol{n} = (\cos\theta, 0, \sin\theta)$. The justification to exclude the out-of-plane twist in our description of the BL walls is derived from the optical appearance of the walls when the polariser is parallel to the director easy axis. Inside the walls, such out-of plane twist is not relevant, even at voltages $U > 2U_c$. The scaling procedure provided access to the ratio k_2 in a single experiment, despite the bend wall containing also splay contributions and the twist wall containing contributions of all three deformation types, and even though we had no explicit expressions for the wall profiles.

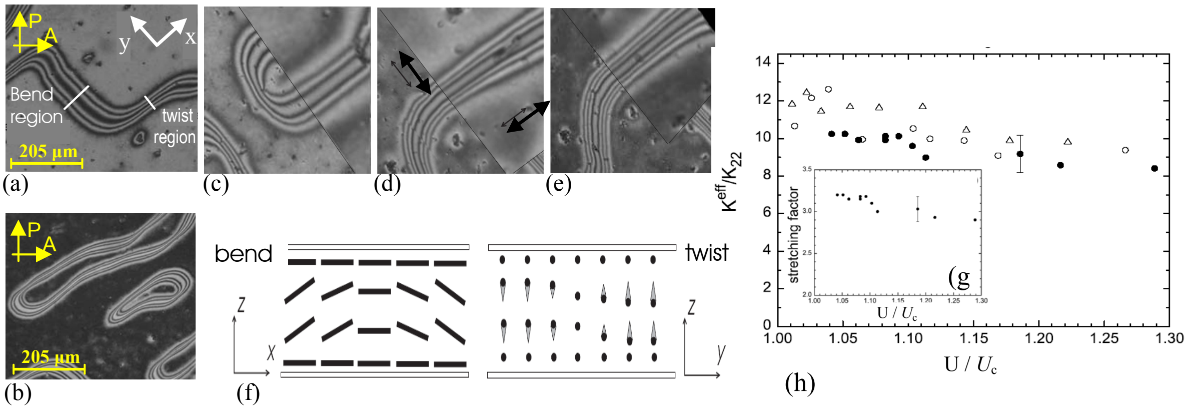

Figure 5.87: (a,b) Wall structures with clearly separated bend and twist regions; the director easy axis is along x; (a) $T = T_{NI} - 3$ K, maximum birefringence $\Phi_{max} = (12.1 \pm 0.1)\pi$ (in the dark central line of the wall); (b) $T_{NI} - 1$ K, $\Phi_{max} = (11.0 \pm 0.1)\,\pi$; (c-e) comparison of optical wall profiles in a 25 µm cell ($T = T_{NI} - 7.5$ K); (c) $U = 1.07\ U_c$; (d) $U = 1.14\ U_c$; (e) $U = 1.20\ U_c$; the images each show a bend section of the wall in original size and a twist section of the same wall rotated and uniformly stretched so that the inner features of both bend and twist walls coincide; the stretching factors are 3.15 (c), 3.03 (d) and 2.90 (e), respectively; the rubbing direction in the bend and twist parts is indicated by arrows in the image in the middle; (f) sketch of the director field in the cross sections of the bend and twist walls; (g) stretching factor obtained from the comparison of the widths of the core regions of the walls at $T = T_{NI} - 7.5$ K; (h) ratio of elastic constants at $T_{NI} - 3$ K (open symbols) and $T_{NI} - 7.5$ K (solid symbols), determined from the squares of the stretching factors (while the data for a given temperature should approach the actual K_{33}/K_{22} ratio near the FRÉEDERICKSZ threshold U_c, the increasing influence of lateral splay at larger voltages changes this ratio to lower values; different symbols mark sets of data obtained in different runs of the experiment).

A simple procedure to extract this ratio from the textures was derived: if the optical image of a twist wall segment was stretched with a factor of $\sqrt{1/k_2}$) that it matched a bend region of the same wall. The elastic ratio was directly obtained from the stretching factor. In the classical experiment with the calamitic material MBBA,[282,283] the ratio $\sqrt{k_2}$ has been only 1.7. Close to the FRÉEDERICKSZ transition, the wall shapes were quite similar to the analytical functions.[284] The uniformly stretched twist wall matched the profile of the bend segment quite well. With increasing electric fields, corrections due to lateral splay took effect. Estimation for the bend to twist ratio could be obtained on comparing the inner parts of the walls. In the outer parts, bend was gradually replaced by splay, and the scaled profiles did not match. The outer part of the bend walls was narrower than the digitally scaled twist wall profile when the central parts fitted satisfactorily for our material. The regions where bend was partially substituted by splay were narrower than expected from the two-constant model, i.e. K_{11} should be noticeably smaller than K_{33}. This was consistent with the observation that the apparent K^{eff}_{33} /K_{22} ratio determined from the scaling (Fig. 5.87g) decreases with increasing voltage (larger director deflection). Figure 5.87h shows an electric field strength dependence of the apparent ratio K^{eff}_{33} /K_{22}, which has been obtained from the square of the wall width ratio. To compare walls which cannot be brought to a complete match by linear scaling, the distances between the first interference minima next to the centre as the criterion of comparison were arbitrarily chosen. There, the tilt angle $\theta(d/2)$ in the cell midplane was roughly 25°. The correct k_2 is found from the extrapolation to U_c. A numerical solution of the EULER-LAGRANGE equation in two dimensions could in principle help to calculate exact wall profiles for arbitrary sets of K_{11}, K_{22}, K_{33} and to fit all three constants. These results presented for the elastic ratio k_2 depended upon the model assumptions that neglect flexoelectric contributions. Flexoelectric polarisation would affect the interpretation of the BL wall shapes, i.e. the bend walls may be broadened by flexoelectric polarisation terms, which tend to suppress bend. Any relevant interaction of the induced polarisation in a bend wall with the external a.c. field could be excluded since the field alternated with 1 kHz, while the wall profiles were quasi-static. The argument that the free ions in the LC cell will at least partially screen the lateral internal fields created by the stationary flexoelectric polarisation of a bend wall was considered against the necessity to consider flexoelectric field terms. Additionally, the results for the bend flexocoefficient e_{33} reported by HARDEN,[268] cannot be directly transfered to the dimer **15b.** The reasons are the much smaller lateral dipole moment, due to the missing chlorine from the chemical structure of our compound **15b** and the positive value of $\Delta\varepsilon$ for all frequencies. Nevertheless, this question needs further clarification.

The measurements on the elastic properties of the nematic phase of dimer **15b** revealed an extremely large anisotropy of BROCHARD-LEGER walls in the splay FT,as compared to similar structures in the N phases of calamitic mesogens. A reasonable explanation is an extremely small twist elastic constant K_{22} of the material as compared to the bend elastic constant K_{33}, i.e. being more than one order of magnitude smaller than K_{33}.

5.7.2 Longitudinal and normal electroconvection rolls above the splay FRÉEDERICKSZ transition[251,254,255]

In the following section, an experimental characterization of different pattern types developed above the splay FRÉEDERICKSZ transition in planar alignment in the nematic phase of dimer **15b** is presented. The results presented in this chapter were already published.[251,254,255]
The basic features of this type of instability have been described by STANNARIUS.[254] It is known that the electrohydrodynamic convection (EHC) of nematic LCs is a well suited system to study pattern formation in anisotropic fluids. It is driven electrically and yields a large variety of spatially extended patterns with different dynamics. EHC in calamitic nematic LCs has been studied experimentally for a long time.[285]

5.7.2.1 Model for an instability leading to a novel type of electroconvection patterns

The nematic phase of **15b** develops unconventional electroconvection patterns above the splay FRÉEDERICKSZ transition in planar alignment, e.g. longitudinal rolls that are oriented parallel or nearly parallel to the initial director $\boldsymbol{n}_0$ (for a description of the FRÉEDERICKSZ transition, see, e.g. [286]). This is in contrast to the classical normal rolls with an orientation perpendicular to $\boldsymbol{n}_0$ in the negative dielectric and positive conductivity anisotropy case (in accordance with the standard model, see[287]). A mechanism leading to the formation of longitudinal rolls at electric fields above the FRÉEDERICKSZ transition has been introduced and explained within a basic model.[254] Therein, a periodic twist modulation is constitutive for the longitudinal patterns that are described as standard EHC. The parallel non-standard patterns investigated here do not produce shadowgraph patterns near the convection threshold. Note that in the type of material investigated in this study with positive dielectric and negative conductivity anisotropy there are EHC in homeotropic cells without preceding FRÉEDERICKSZ transition.[253] The basic features of this type of instability have been described in ref.[254] by STANNARIUS *et al.* A small initial fluctuation is considered a periodic modulation of the director, with a wave vector perpendicular to $\boldsymbol{n}_0$ (see Fig. 5.88). This twist mode does not grow from the undistorted ground state $\boldsymbol{n} \equiv \boldsymbol{n}_0$ but from a uniformly distorted state, i.e. a homogeneous tilt out of the x-y plane that is realized in experiments by the splay FRÉEDERICKSZ transition.

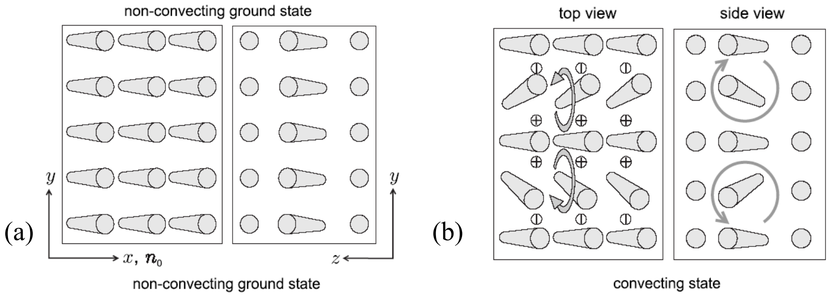

Figure 5.88: Top view left (xy) and side view right (yz) of the director configuration assumed in ref.:[254] (a) homogeneously tilted ground state; (b) periodic modulation. The cylinders symbolize the locally preferred director configuration. The director alignment at the plates is $\boldsymbol{n}_0$. x-y is the cell plane, z is normal to the cell.

The periodic deflections of the director out of the tilt plane cause a spatially modulated charge transport and a charge segregation in the y direction, in the same way as periodic tilt deflections in the classical CARR-HELFRICH structures lead to a charge segregation along x. This modulated charge couples via COULOMB forces to the external electric field and leads to a shear flow of the nematic sample in convection rolls that are oriented along the initial director. A simpler ansatz has been used to demonstrate the principal instability mechanism.[254] The stability of the tilted, in-plane homogeneous ground state has been tested within a one-dimensional model, i.e. the particular director profile in the z direction is not considered. This model yields some specific conditions for the conductivity and viscous parameters of the material which are necessary for the instability to occur. The combination of negative conductivity anisotropy with a positive viscosity coefficient α_3 seems to be fulfilled in particular in materials which are close to a nematic-smectic transition. A pattern with a wave vector perpendicular to the x direction and to $\boldsymbol{n}_0$ was produced.

5.7.2.2 Measurements of the anisotropies

In order to determine the character of the electrohydrodynamic instability was necessary to know the combination of the signs of dielectric anisotropy, $\Delta\varepsilon$, and conductivity anisotropy, $\Delta\sigma$. The nematic phase of dimer **15b** develops in planar alignment unconventional electroconvection patterns above the splay FRÉEDERICKSZ transition. The existence of this splay type transition evidences that the dielectric constant is necessarily positive[286] (indices $\perp$ and $\|$ refer to the director $\boldsymbol{n}$). The sign of the conductivity anisotropy $\Delta\sigma = \sigma_{\|} - \sigma_{\perp}$ was determined by using electric field dependent current measurements and recording the voltages U_{cell} and U_{R0} of the nematic sandwich cell and of a serial reference resistance $R_0 = 100\ \text{k}\Omega$, respectively, at an excitation frequency $f_0 = 1$ kHz. The E.H.C. cell represents a parallel circuit of Ohmic and capacitive elements, but the capacitive contributions can be neglected due to the rather high Ohmic conductivity in our material.

The measured effective conductivity $\sigma_{\text{eff}} = [d/(R_0 A)](U_{R_0}/U_{\text{cell}})$ as a function of the voltage U_{cell}, with the electrode area $A = 1\ \text{cm}^{-1}$ cm and the cell gap d =25 µm at $T - T_{\text{iso}} = -0.5$ K is shown in Figure 5.89. The director remains in the untilted ground state below the FRÉEDERICKSZ transition (FT, dash-dotted line). This means that the relevant component of the conductivity tensor is $\sigma_{\perp}$ and the effective conductivity is practically constant (Fig. 5.89). On the other hand, above the FRÉEDERICKSZ transition σ_{eff} decreases, while the director changes gradually from a perpendicular to a more parallel alignment with respect to the applied electric field (see inset in Fig. 5.89). The kink of σ_{eff} (Fig. 5.89) represents the optical visibility of the FRÉEDERICKSZ transition in the polarising microscope.[251] From the measured values a negative value of the conductivity anisotropy could be concluded ($\Delta\sigma = \sigma_{\|} - \sigma_{\perp} < 0$).

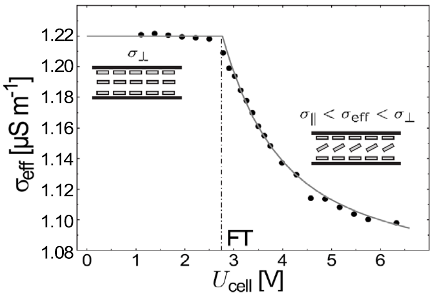

Figure 5.89: Dependence of the effective conductivity σ_{eff} on the voltage U_{cell}. Below the FRÉEDERICKSZ transition (FT, dash-dotted line) the measured conductivity corresponds to the conductivity perpendicular to the director $\boldsymbol{n}$ (inset sketch on the left). Above the FT, the effective conductivity contains contributions of both, $\sigma_{\|}$ and $\sigma_{\perp}$ (inset sketch on the right).

The anisotropy of the electric conductivity is determined to be $\Delta\sigma = -0.17\ \mu\text{S m}^{-1}$ and $\Delta\sigma/\sigma_{\perp} = -0.14$. The director deflection $\Phi(z)$ can be calculated as the inversion of the elliptic integral for U_{cell}, with the voltage U_F at the FRÉEDERICKSZ transition.[286] Following approximations for the model of this fit were made: (a) the constant electric field $E = U_{\text{cell}}/d$ was used as an approximation for the actual z-dependent electric field; (b) the elastic approximation: $K_{11} = K_{33} = K$ was applied for the elastic splay and bend constants K_{11}, K_{33}, and assumption $\varepsilon_{\|} \approx \varepsilon_{\perp}$ was used. The model curve in Figure 5.89 is correct only for the limits $U < U_F$ and $U >> U_F$, but the qualitative characteristics could be reproduced also for intermediate fields. Another interesting finding is that the absolute value of $\Delta\sigma$ is highest near the transition to the SmC phase at lower temperatures and decreases for higher temperatures. At the transition temperature T_{iso} to the isotropic phase, $|\Delta\sigma|$ is minimal. Note that there is no sign inversion of $\Delta\sigma$ in the interesting temperature range.

5.7.2.3 Longitudinal electroconvection rolls above the splay FRÉEDERICKSZ transition

The parallel non-standard patterns investigated here do not produce shadowgraph patterns near the convection threshold voltage U_c (Fig. 5.90a), i.e. at pattern onset the rolls are only visible with two polarisers. Thus the longitudinal rolls at onset are interference patterns. In contrast to the shadowgraph patterns that appear at a few percent above the threshold voltage (Fig. 5.90c), the image is generated only by the modulation of the optical phase profile of ordinary and extraordinary waves. The model derived in ref.[254] by STANNARIUS *et al.* (see Fig. 5.90) yields patterns that will not produce shadowgraph patterns at onset, because the z component of $\boldsymbol{n}$ is not modulated in the cell plane. Hence the features predicted by the model agree with our experimental observations: the longitudinal orientation as well as the optical appearance as interference patterns. The model also explains the pattern onset above the FRÉEDERICKSZ threshold.

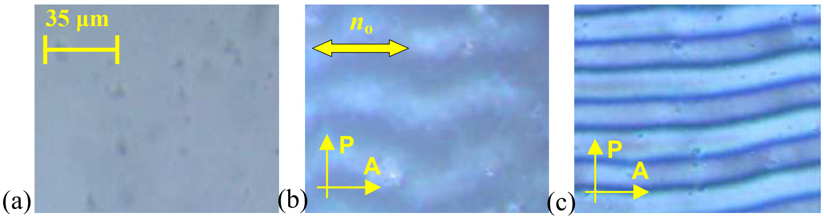

Figure 5.90: Polarising microscopy images of longitudinal rolls (a) without polarisers at $U \approx U_c$; (b,c) crossed polarisers, at (b) $U \approx U_c$; (c) $U = 1.04\ U_c$. The initial director orientation $\boldsymbol{n}_0$ is marked, $f_0 = 1$ kHz, $U_c = 6.5$ V.

Additionally, the pattern dynamics and dynamic regimes under a.c. electric fields i.e. conduction rolls, dielectric rolls and subharmonic structures.[288] were studied in the nematic phase of dimer **15b**.[254,255] Qualitative structural changes as a consequence of the variation of excitation parameters (frequency and voltage) and sample temperature could be observed on the electro-optical experiments in the nematic phase of dimer **15b** (i.e. a transition between longitudinal and normal rolls).[254,255]

Another interesting finding is the presence of convection structures that develop from the metastable ground state (N_b, see for further details chapter 5.7.3 and ref.[251,253]) of the planar cell and their voltage dependent reorientation in the metastable domains. In this new ground state N_b, one can reversibly generate a splay FRÉEDERICKSZ transition, and one observes EHC patterns above that transition. The optical characteristics of these EHC patterns are equivalent to those of the patterns in the original domains described in chapter 5.7.2 and ref.[253]. The obvious qualitative difference is that twist normal (TN) rolls in the N_b domains travel at onset, whereas rolls in the original domains are stationary.

Novel types of electroconvection patterns could be found in the dimer **15b**. These patterns show previously unobserved optical and structural properties. However, the nature of the observed structural changes is not clear so far. It is to be expected that similar patterns play a role and have to be considered in the electro-optical application of similar types of materials, in particular in N phases of bent-core mesogens (strong tendency to form layered structures). These experiments show that this type of molecules appears to be promising candidates for display and sensor materials, due to their unique material properties. They combine easy alignment and switchability of nematic phases of calamitic mesogens with biaxial optical properties, potential polar effects and the existence of spontaneous electric polarisations, and consequently new types of electro-optic switching mechanisms.

5.7.3 Field-induced texture transitions by means of an electric field[252,253]

This section is focused on the study of the formation of a second, metastable ground state in the nematic phase of compound **15b** which occurs when the cell has been exposed to electric fields of the order of 1 MV/m. The results presented in this chapter were already published.[252,253] This ground state in absence of electric fields was optically different from the planar original ground state, and the effective birefringence was reduced by about 15%. In this way evidence was found that in a sufficiently strong external electric field, one can transform the uniaxial nematic phase (denoted N_u) of compound **15b** into a metastable biaxial state (denoted N_b), either in the complete cell or in domains coexisting with domains in the original uniaxial state. The field-induced metastable state is identified by its optical and electric properties. After the field is switched off, the original and induced states can coexist in domains for about one hour in planar sandwich cells. During this time, the induced domains gradually shrinked but they could be stabilized in moderate electric fields. The occurrence of similar domains in homeotropic cells suggested that the transition into a metastable biaxial state was observed and the biaxial state was not imposed by boundary conditions of the cell but represented a thermodynamically metastable biaxial phase. In the field-free planar ground state, the formation of inversion walls was observed inside the metastable domains.

5.7.3.1 Electro-optical experiments in planar cells

Commercial sandwich cell (E.H.C.) with a cell gap of $d = 25$ µm and rubbed polyimide coating of the glass plates for planar surface alignment were used for this experiment. The splay FRÉEDERICKSZ transition (FT) evidenced that the dielectric anisotropy $\Delta\varepsilon = \varepsilon_{\|} - \varepsilon_{\perp}$ is positive.[251] A study of the splay FT in an electric field applied normal to the glass substrate[289] revealed that when the applied field is sufficiently strong (a few hundred kV/m to 1 MV/m), a transition into a certain new state of order takes place, which leads to an altered ground state after the removal of the field. This second ground state differed optically from the planar ground state of the original uniaxial nematic phase. The so far unidentified new state was designated here as N_b. The direction of the largest refractive index of N_b in the cell plane was unchanged with respect to the optical axis of N_u in the planar cell (rubbing direction). With polarisers crossed parallel and perpendicular to the rubbing direction of the cell, both N_u and N_b states appear almost black. Between crossed polarisers diagonal to the director easy axis, the two states were easily distinguished by the change of birefringence. The effective birefringence in the off state was reduced by about 15%. With a compensator we measure a drop of $\Delta n = n_e - n_o = 0.136$ in N_u to $\Delta n' = \Delta n - \delta n = n_1 - n_2 = 0.115$ in N_b. Here, n_e and n_o are extraordinary and ordinary refractive indices of N_u, while n_1; n_2 are the corresponding effective refractive indices in N_b, for normally incident light polarised parallel and perpendicular to the alignment axis, respectively.

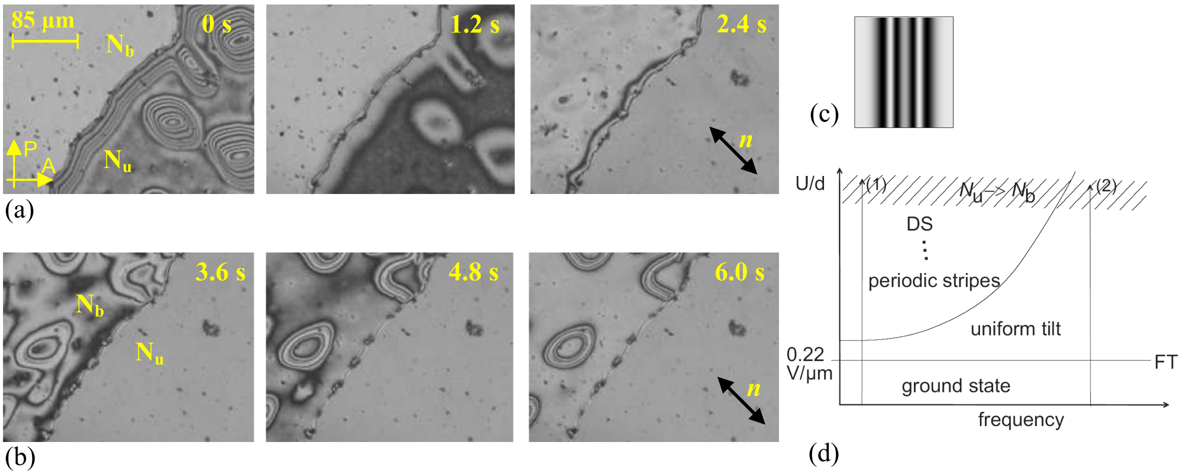

Figure 5.91: (a,b) Two coexisting domains in the N_b (top left) and N_u (bottom right) planar ground states after a voltage of 7.35 V has been switched off. The N_b domain contains a closed inversion wall loop. The director easy axis $\boldsymbol{n}$ is in the direction of the arrow; (c) texture simulation of a wall of the second director $\boldsymbol{n}_2$ in the N_b state. The images are taken in 1.2 s intervals. In the N_u domain, the BL walls disappear and the sample relaxes to the all-planar state while in the N_b domain a new type of walls appears in the off state; (d) sketch of the N_u orientational states in a 25 µm cell in the voltage-frequency space. The transition to N_b is indicated.

On applying an electric field it was possible to transform the complete region under the cell electrodes into the new state, but also textures where N_u and N_b domains coexisted (Fig. 5.91a,b). These domains were separated by sharp borders which had not the appearance of walls but of either defect lines or phase boundaries. After the field was switched off, the original and induced states could coexist in domains for about one hour. The N_b domains shrink slowly when the electric field was off. After approximately one hour, the uniform N_u ground state was re-established in the whole cell. During this time, it was possible to stabilize the induced domains N_b by applying a moderate electric field. At a few hundred MV/m, there was a clear progression of existing N_b domains. It could be observed that N_b domains often contained walls in the off state, in contrast to N_u domains which always relaxed to a uniform planar texture even if BL walls[282] had formed during the FT (Fig. 5.91). The walls in the N_b field-off state had widths that were nearly independent of their orientations. This distinguishes them from the BL walls[251] in N_u above the FRÉEDERICKSZ threshold. Moreover, they appeared when the cell was switched off, irrespective of whether the tilted state above the FT was uniform or not, and they disappeared again above the FRÉEDERICKSZ threshold. The walls often form closed loops that shrink in minutes. Optical textures on both sides of the wall are indistinguishable between crossed diagonal polarisers.

The state diagram of N_u in the 25 µm cell in the field strength and frequency parameter space is sketched schematically in the Figure 5.91d. It can be observed that the FT has the lowest threshold, nearly frequency independent. Above, there is a transition into a periodically distorted state, formed by electrically driven convection[254] and, after further instabilities, into a dynamic scattering (DS) regime. The electro-optic characteristics of N_u are previously described in the sections 5.7.2 and 5.7.3 and in the ref.[251,254] A similar behaviour is found in N_b domains, but the thresholds in both states differ from each other. If one chooses path (1), the transition $N_u \rightarrow N_b$ appears in the turbulent DS pattern and the transformation itself is difficult to identify. Varying the field along path (2), one can observe the nucleation of N_b domains, preferentially inside BL walls.

5.7.3.2 Electro-optical experiments in homeotropic cells

Additional experiments were performed in a 5 μm sandwich cell with homeotropic alignment in order to exclude other possible mechanisms that could lead to a change of the birefringence in the ground state. The two states N_u and N_b were observed there as well. In a homeotropic cell, the director $\boldsymbol{n}$ is initially in field direction and the sample is completely black between crossed polarisers in the N_u phase. In this geometry the electric field applied normal to the glass plates cannot align the second director and a mechanism that tilts the director out of the normal orientation first was necessary. At high electric fields, electrically driven convection patterns were formed in the homeotropic cells (Fig. 5.92a the onset of an electroconvection pattern; Fig. 5.92b the fully developed convection pattern in the cell). This situation is typical for a material with negative conductivity anisotropy and positive dielectric anisotropy.[287,290]

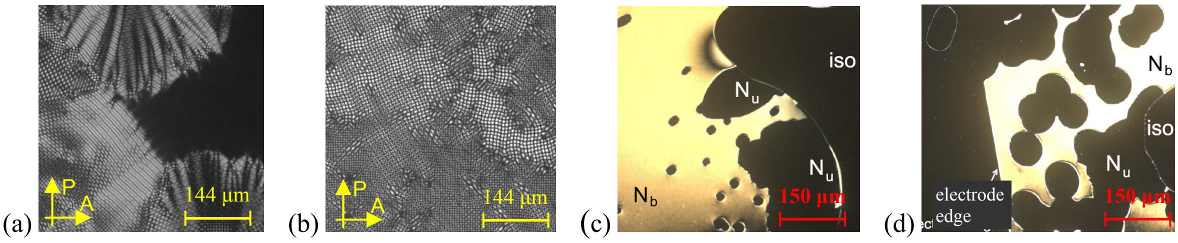

Figure 5.92: Textures in a 5 μm thick homeotropic cell: (a) onset of electroconvection; (b) fully developed electroconvection pattern at 1 kHz a.c. excitation; (c) texture at zero electric field, after application of a strong ac field (10 MV/m, 1 kHz), white light illumination. The region in the right-hand part has undergone a N-isotropic transition. The region N_b is characterized by a bright schlieren texture. Dark spots inside this area represent small domains of the N_u phase. (d) biaxial nematic phase N_b with enclosed circular domains of the N_u phase. Outside the electrode area (left in the image), the sample is still N_u. The temperature is between T_NI and $T_\mathrm{NI}-7.5$ K.

The pattern undergoes a transition to a dynamic scattering state at higher voltages, as well as in the planar cells. When electric fields above 10 MV/m are applied, a similar transition to N_b as in the planar case is observed. A disadvantage of this experiment is that it cannot be performed under isothermal conditions. The electroconvection pattern is highly dissipative and the cell heats up during the high-field application. When the field was suddenly switched off after a few seconds, the sample temperature was already close to the clearing point and the electroconvection pattern breaked down immediately after the field was off (see Fig. 5.92c; the isotropic phase (right), the homeotropic biaxial nematic state (left), and domains of the homeotropic uniaxial nematic state, near the NI phase boundary and in the small circular spots). The N_u domains are black in the field off state, while the N_b domains are characterized by a bright schlieren texture of the second director (Fig. 5.92c,d). Apparently, the second director in N_b was hardly aligned by the lateral phase boundaries, but it varies slightly across the cell plane. Inversion walls of the second director appeared as schlieren in the top central part and at the bottom of Figure 5.92c. On removal of the electric field, the cell cooled rapidly to the original temperature 7.5 K below the clearing point, and the isotropic phase retreated. At the same time, the N_u domains growed inside the N_b domain (Fig. 5.92d). After approximately 1 minute, they covered the whole cell. In the Figure 5.92d can be observed that the biaxial domain was only formed in the region of the electrodes. Outside the electrode area, no transition has taken place.

The observation of metastable, optically biaxial domains in the homeotropic cell and of domains with reduced birefringence in planar cells can be explained by a field-induced transition from a uniaxial into a biaxial nematic state for the dimer **15b**. This field-induced domains are stabilized in moderate (<1 MV/m) fields. The combined results in planar and homeotropic cells revealed that N_b is not merely a biaxial state in a thin planar cell but represents a biaxial nematic phase, induced by an electric field. The interpretation of anchoring transitions leading to N_u-N_b phase transition[291] failed. Our a.c. electric field experiments could not test whether the second director axis is polar or not. The molecular shape would suggest a polar ordering. This problem could be solved on d.c. field experiments, but so far the onset of strong convective flow at d.c. excitation prevented a reliable evaluation of the experimental data.

Another possible explanation is the assumption that there exist cybotactic clusters of mesogens with short range biaxial order. Owing to a random orientation of the second axis of these clusters, biaxiality averages out in the uniaxial phase and only after application of the electric field these collective clusters of mesogens are aligned to form a state with macroscopical biaxial order. This property to form clusters with biaxial order in the uniaxial nematic phase is a prerequisite for the observed effect. This is a unique property of bent-core mesogens like the dimer **15b**. The biaxially ordered phase persisted after the field was removed, but it was metastable; the uniaxial phase was energetically preferred in the field-free state. A transition back into the uniaxial state occured via nucleation of small uniaxial domains and growth of the uniaxial domains by the propagation of phase boundaries. It was pointed out that for the appearance of the N_b state the mesogens have to be sufficiently flat, but smectic order has to be absent. The bent-core unit of the dimer **15b** is sufficiently anisotropic to match the first condition, and the twin structure with a rod-like subunit reduces the tendency to form smectic layers. The positive dielectric anisotropy $\Delta\varepsilon$ caused by the absence of large lateral dipole moments is a special feature of the nematic phase of dimer **15b**, and is a prerequisite for the splay FT in a planar cell, and it is essential for the electro-optic effects described here. Negative $\Delta\varepsilon$ (lateral molecular dipoles) may provide even better conditions to induce N_b since such nematics favor $\boldsymbol{n}$ perpendicular to E.[274] In our samples, this effect was hidden by the reorientation of $\boldsymbol{n}_1$ in the electric field. Independent switching of the first and second directors in a biaxial nematic phase has been recently reported by LEE *et al.*[277] VAN LE *et al.* [292] argued that for materials having positive dielectric anisotropy, the biaxiality can be clearly verified or excluded by measuring the transmitted light intensity as a function of the electric field, but the proposed method failed to prove biaxiality of the studied bent-core mesogens.

6 Mesophase behaviour of dimers of type II

The next point is the study on the influence of the position to connect the calamitic moiety to the bent-core mesogenic unit *via* a flexible *hydrocarbon* spacer on the mesophase behaviour of '*banana – calamit*' dimers.

The linking of the bent-core unit to the calamitic moiety *via* a flexible spacer can be realized in different ways (see Fig. 6.1). In this chapter we focused on the structure-properties relationship of ***laterally - terminally*** linked dimers of **type II** (see Fig. 6.1b,d) and the comparison with the previously presented ***terminally - terminally*** connected dimers of **type I** (dimers **1** – **30**, Fig 6.1a). It is to expect that the polymorphism and the mesophase stability depend strongly on the position of the attachment as this should alter the segregation of the different dimer parts.

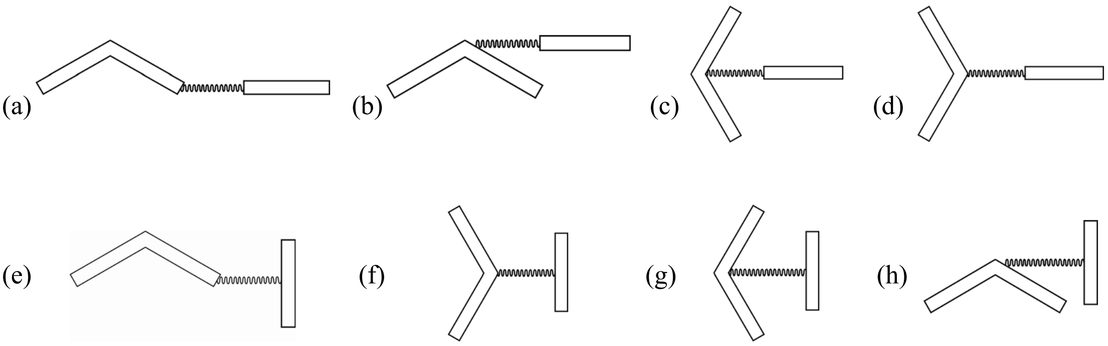

Figure 6.1: General sketch of different possibilities to design '*banana – calamit*' dimers.

For this reason two new series of '*banana - calamit*' dimers, each containing two homologues members were synthesized (see Table 6.1). In dimers **31** the calamitic moieties are connected ***laterally - terminally*** in the *5* – position (here assigned as **L – *5* - T**) of the central *resorcinol* fragment of the bent-core moiety, whereas in the dimers **32** the connection is at the *4* – position (**L – *4* - T)**. The spacer is a *hydrocarbon* chain (*m* = 6, 11) which is connected through *ester* and *ether* groups to the mesogenic units. These new compounds **31** and **32** have a constant length of the *alkyloxy* chain attached to the bent-core unit (*n* = 12) and to the calamitic part (*p* = 6).

6.1 The mesophase behaviour of dimers 31 and 32

In the following a description on the influence of the linking position of the *spacer-calamit* unit on the bent-core moiety on the mesophase behaviour of dimers **31** and **32** (*n* = 12; *m* = 6, 11; *p* = 6; $\mathbf{E_0}$; ***laterally – terminally*** connected) is given (see Table 6.1). To allow an appropriate comparison, the mesophase behaviour of the analogues dimers of **type I**, the compounds **7a** and **9a** (see section 5.4) is listed**.**

Table 6.1: Transition temperatures [°C], mesophase type, transition enthalpy values [kJ/mol], layer spacing *d* [nm], tilt angle τ of the molecules [°] with respect to the layer normal in SmC phases and with respect to the normal to *a* in Col phases, lattice parameters (*a*, *b*, *γ*) and P_S values of dimers **31**, **32** and their analogues dimers **7a** and **9a**.[a]

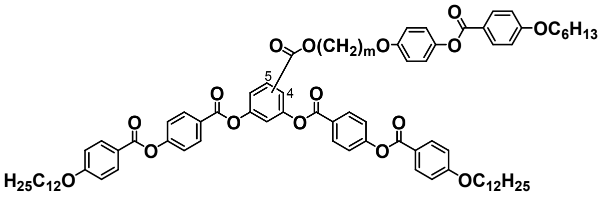

Comp	*m*	Linking position	Transitions temperatures [°C] Δ*H* [kJ·mol^{-1}]	Phase type	Lattice parameters					P_S *nC/cm*^{2}
					d [nm]	τ [°]	*a* [nm]	*b* [nm]	γ [°]	
31a	6	L-*5*-T	Cr 95 ($\mathrm{Col_rP_{FE}}$ 84) I *50.7 22.3*	$\mathrm{Col_rP_{FE}}$		-	3.90	5.15	90	230
31b	11	L-*5*-T	Cr 76 $\mathrm{Col_rP_{FE}}$ 89 I *47.5 26.1*	$\mathrm{Col_rP_{FE}}$		-	4.00	4.51	90	300
32a	6	L-*4*-T	Cr 107 $\mathrm{SmC_xP_{AF}}$ 119 $\mathrm{SmAP_{AF}}$ 121 N 123 I *46.9 0.8 1.5 9.7*	N $\mathrm{SmAP_{AF}}$ $\mathrm{SmC_xP_{AF}}$	 -[c] -[c]	 -[c] -[c]				 240 330
32b	11	L-*4*-T	Cr 105 $\mathrm{SmAP_{AF}}$ 144 N 151 I *67.7 2.3 8.5*	N $\mathrm{SmAP_{AF}}$	 3.24	 0				 370
7a	6	T-T	Cr 135 ($\mathrm{Col_xP_{FE}}$ 128) I *67.3 26.6*	$\mathrm{Col_xP_{FE}}$		-[c]	-[c]	-[c]	-[c]	240
9a	11	T-T	Cr 109 ($\mathrm{Col_xP_{FE}}$ 103 N 105) I *67.1* -[b] -[b]	N $\mathrm{Col_xP_{FE}}$		 -[c]	 -[c]	 -[c]	 -[c]	 380

[a] Transition temperatures (°C) and enthalpy values [kJ/mol] of dimers **31**, **32** and their analogues dimers **7a** and **9a** were taken from the second DSC heating scans (10 Kmin^{-1}); values in parentheses indicate monotropic mesophases, in this case the transition temperatures and enthalpy values were taken from the first DSC cooling scans and the transition temperatures were checked by polarising microscopy; [b] the transition is not detectable on DSC and the transition temperature value is determined by polarising microscopy; [c] could not be determined due to rapid crystallization of the sample.

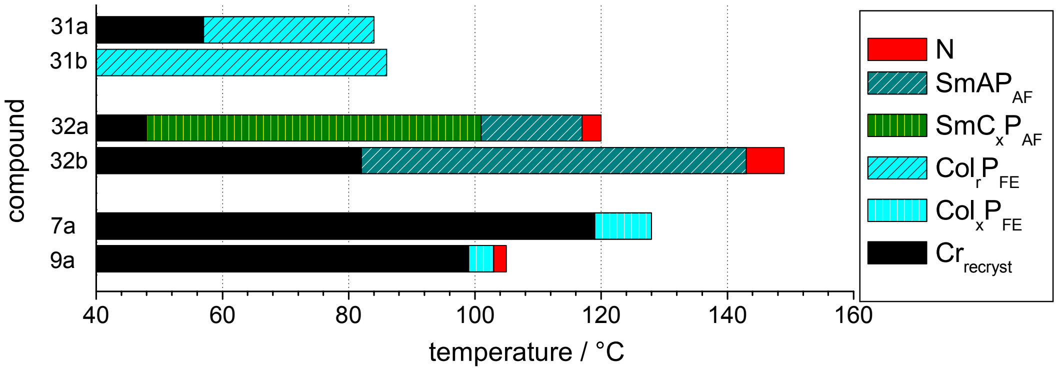

Figure 6.2: Transition temperatures (°C) of dimers **31**, **32** and their analogues dimers **7a** and **9a**, taken from the first DSC cooling scans (10 Kmin^{-1}).

6.1.1 Dimers 31 bearing the *spacer-calamit* unit in the *5*-position on the central *resorcinol* fragment of the bent-core moiety

The compounds **31** (*n* = 12; *m* = 6, 11; *p* = 6; $\mathbf{E_0}$) connected ***laterally - terminally*** in the *5*-position on the central *resorcinol* fragment of the bent-core moiety (here assigned as **L – 5 - T**) form columnar phases. The dimer **31a** with an *odd*-numbered spacer (summarizing the single units of the flexible spacer that corresponds to an *even* number of methylene units, *m* = 6) possesses a monotropic columnar phase. Meanwhile, dimer **31b** with an *even*-numbered spacer (but with an *odd* methylene spacer, *m* = 11) exhibits an enantiotropic columnar phase. The transition temperatures and the mesophase behaviour are given in Table 6.1 and in Figure 6.2.

On cooling from the isotropic liquid state a dendritic growth of the texture could be observed (Fig. 6.3a). The small-angle reflections found in the X-ray diffraction pattern of the mesophase of dimer **31a** can be indexed to a centred two-dimensional rectangular lattice, with the lattice parameters *a* = 3.90 nm and *b* = 5.15 nm (see Table 6.1 and Fig. 6.3b,c).

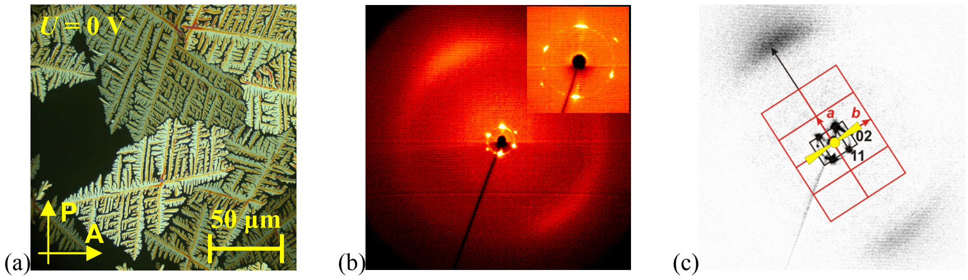

Figure 6.3: Columnar phase of dimer **31a**: (a) dendritic growing on cooling from the isotropic liquid at 84 °C; (b, c) XRD patterns of a surface-aligned sample in the Col phase at 83 °C: (b) original pattern; the inset shows the small angle region; (c) position of the maximum of the diffuse scattering (black arrow) with respect to the reciprocal 2D lattice and orientation of the molecules in the corresponding real lattice (red, arbitrary size).

The $\mathrm{Col_r}$ phase of dimer **31a** shows an electro-optical switching on application of a relatively high threshold electric field of about 30 $\mathrm{V\mu m^{-1}}$. The switching is accompanied by a current response with only one sharp current peak in the half period of a triangular wave voltage, also at low frequencies (down to 0.1 Hz) indicating a FE ground state (P_S = 230 $\mathrm{nCcm^{-2}}$). Additionally, using a modified triangular wave field, where a delay is introduced at zero voltage, independent of the temperature and the thickness of the non-coated ITO cells (5, 10 µm) only one peak is observed. This indicates that a bistable switching takes place, and that switching always occurs after zero-voltage crossing of the applied field. The $\mathrm{Col_r}$ phase of dimer **31b** (*m* = 11, Ps = 300 nC $\mathrm{cm^{-2}}$) behaves very similar in a.c. and d.c. experiments. All these compounds form Col phases which show a similar bistable polar switching by rotation around the long molecular axis.

6.1.2 Dimers 32 bearing the *spacer-calamit* unit in the *4*-position on the central *resorcinol* fragment of the bent-core moiety

The compounds **32** (*n* = 12; *m* = 6, 11; *p* = 6; $\mathbf{E_0}$) are dimers connected ***laterally - terminally*** in the *4*-position on the central *resorcinol* fragment of the bent-core moiety (here assigned as **L –**

4 **- T**, see Table 6.1). On changing the connecting position of the *spacer-calamit* unit to the position *4* on the bent-core moiety, an increase of the mesophase stability was observed for the dimers **32**. The transition temperatures and the mesophase behaviour of compounds **32** are given in Table 6.1 and in Figure 6.2. The dimer **32a** (m = 6) presents three enantiotropic mesophases: a nematic and two smectic phases. The compound **32b** (m = 11) forms two enantiotropic mesophases: a nematic and a smectic phase. A significant increase of the mesophase stability could be observed for this dimer.

The mesomorphic properties of the compound **32b** (with an *even*-numbered spacer, but an *odd* number of methylene units, m = 11) will be discussed in more detail. The high-temperature phase of compound **32b** can be assigned as a nematic phase. This phase shows typical schlieren (Fig. 6.4a), marbled, homeotropic and/or planar textures. Over the whole existence range of the nematic phase, chiral domains of opposite handedness can be observed. Furthermore, the N phase shows a similar unusual electro-optical response, similar to the one described for the nematic phase of dimer **1h** (**type I**) in subchapter 5.1.1.2. On application of a relatively low a.c. field (1.0 V μm^{-1}, 20 Hz) to the planar oriented N phase of compound **32b** in a 6 µm polyimide-coated cell, fluctuating domains of the WILLIAMS–KAPUSTIN type appeared (their period, d_{dom}, corresponds to the cell thickness). Applying higher fields and higher frequencies (3.0 V μm^{-1}, 150 Hz) to the planar oriented N phase, domains with equidistant stripes parallel to the original orientation of the director n_o appear (longitudinal patterns, with a period of these domains clearly greater than the sample thickness). Further increase of the voltage results in a decrease of the domain period, i.e. 6 µm at 5 Vμm^{-1}, 4 µm at 10 Vμm^{-1}. Unusual effects are observed like a transition between longitudinal, zigzag and normal rolls (5 V μm^{-1}, 3 kHz; Fig. 6.4b), controlled by the excitation frequency. Details on such rare electro-optical behaviour have been reported already in chapter 5.7 [254,255] for the N phase of the '*banana-calamit*' dimer of **type I**, compound **15b**. With increasing voltage (above 12 Vμm^{-1}) a *myelin* - like texture with fine equidistant stripes appears (Fig. 6.4c). At higher a.c. field (above 30 V μm^{-1}) the stripes disappear and an optical texture results which is reminiscent of a smectic fan-shaped texture (Fig. 6.4d). This field-induced fan-shaped texture is observed in the whole existence region of the N phase. However, during the electro-optical experiments no polar switching was detected. If the electric field is removed, the smectic-like texture disappears and the texture of the planar oriented N phase reappears. This means that the nematic phases of the two different type of dimers ***laterally – terminally*** connected (dimers **32**, of **type II**) and ***terminally - terminally*** connected (dimer **9a**, of **type I**) exhibit very similar optical and electro-optical properties.

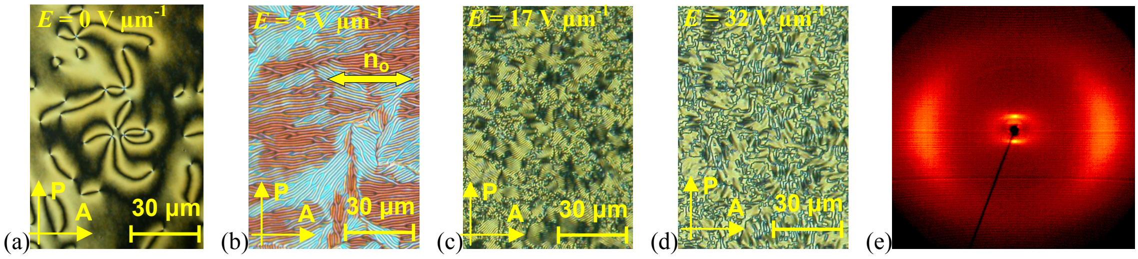

Figure 6.4: (a-d) Textures of the nematic phase of compound **32b** at 147 °C observed between crossed polarisers in the same region of the sample in a 6 µm polyimide-coated ITO cell: (a) at U = 0 V; (b-d) field-induced texture changes of the nematic phase by application of an a.c. field; the electric field strength E is increasing: (b) 5 Vμm^{-1}, 3 kHz; (c) 17 Vμm^{-1}; (d) 32 Vμm^{-1}; the orientation of the initial director $\mathbf{n_o}$ is marked; (e) XRD pattern of an aligned sample of the nematic phase of compound **32b** at 147 °C.

X-ray measurements performed on a sample of the compound **32b** at 147 °C by applying a magnetic field of about 1T confirm the presence of a nematic phase, i.e. a diffuse scattering in the small angle region located on the meridian, and a diffuse wide angle scattering located around the equator (Fig. 6.4e). The diffuse, small-angle scattering in the nematic phase can be attributed to cybotactic groups representing fluctuating arrays of molecules with a short-range order of the same type as the long-range order in the low-temperature smectic phase.

On cooling the nematic phase of compound **32b**, a smectic phase separates in the form of *batônnets* which then coalesce and form a fan-shaped texture (Fig. 6.5a). The X-ray pattern of the smectic phase at 140 °C obtained from an aligned sample shows a diffuse outer scattering with the maxima located on the equator and BRAGG-reflections on the meridian, from which a layer spacing of d = 3.24 nm is calculated (Table 6.1 and Fig. 6.5d). This finding indicates a SmA phase.

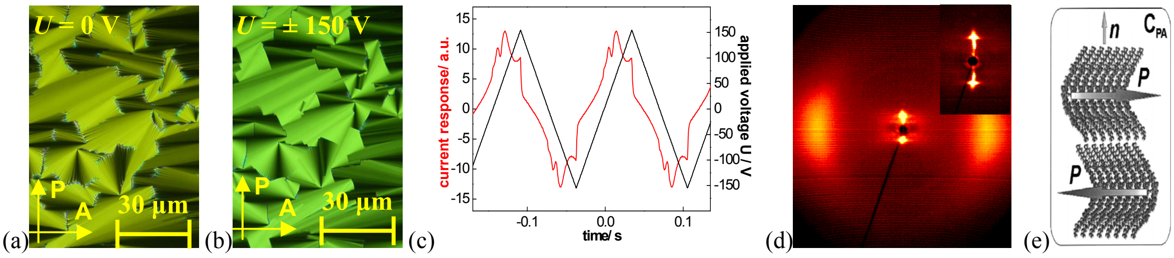

Figure 6.5: (a-c) Electro-optical investigations of the SmAP$_{AF}$ phase of **32b** at 140 °C in a 6 µm polyimide-coated ITO cell; textures observed between polarisers in the same region of the sample: (a,b) under a d.c. electric field at (a) U = 0 V and (b) U = ± 150 V; (c) AF switching current response obtained by applying a triangular-wave voltage (U = 315 V$_{pp}$, f = 10 Hz, R = 5 kΩ, P_S = 370 nC cm^{-2}); (d) XRD patterns of a surface-aligned sample in the SmAP$_{AF}$ phase of **32b** at 140 °C; the inset shows the small angle region; (e) packing of the molecules in the C_{PA} phase described by EREMIN *et al.* in ref.[82]

Interestingly, an electro-optical response could be observed on applying an a.c. or a d.c. field on the low-temperature phase of compound **32b**, i.e. an orthogonal polar smectic phase was observed. On applying an electric field to the fan-shaped texture of the SmA phase the birefringence is slightly changing and the stripes within the fans disappear (Fig. 6.5b). Furthermore, it was found that the texture of the switched state is independent of the polarity of the applied field (Fig. 6.5b). The switching in this polar SmA mesophase takes place by rotation around the long molecular axis. Furthermore, this switching process is rather slow due to steric hindrance of the rotation by the lateral attached *spacer-calamit* unit. As a consequence the current response peaks could only hardly be recorded. However, during detailed a.c. experiments, two current peaks per half period of a triangular voltage could be recorded (Fig. 6.5c) indicating the switching from an AF ground state into FE states. The field-induced SmAP$_{FE}$ phase is metastable and relaxes back to the SmAP$_{AF}$ ground state after removal of the field (Fig. 6.5a). We can conclude from these experimental findings that the low-temperature phase of compound **32b** is an antiferroelectric variant of a polar biaxial SmA phase which was theoretically predicted by BRAND *et al.*,[79,159] i.e. a SmAP$_{AF}$ phase (there designated as C$_{PA}$). In this phase the smectic layers have C_{2v} symmetry whereas in the SmCP$_{AF}$ phase a C_2 symmetry exists. A C$_{PA}$ phase was experimentally proved in a pure banana-shaped 4-cyanoresorcinol derivative for the first time by EREMIN *et al.*[82] There, the banana-shaped molecules are packed in the bent direction, which is identical with the polar axis. The smectic layers have C_{2v}

symmetry, i.e. a twofold symmetry axis (which coincides with the polar axis) and a vertical mirror plane including the two-fold axis and the layer normal. In addition, the polar direction alternates from layer to layer giving rise to the antiferroelectric structure of the SmAP$_{AF}$ phase. EREMIN *et al.*[82] proposed a packing of the so-called C$_{PA}$ phase (Fig.6.5e) which can still serve us only as a rough approximation of the structural model.

The homologous compound **32a** (*m* = 6) forms three enantiotropic mesophases: a nematic and two smectic phases. Detailed POM, DSC and electro-optical experiments proved that the two high-temperature phases of dimer **32a** are a nematic and a SmAP$_{AF}$ phase (P_S = 240 nC cm^{-2}). This SmAP$_{AF}$ phase presents a similar electro-optical behaviour as the one observed for compound **32b** (*m* = 6). However, on further cooling of the SmAP$_{AF}$ phase some additional irregular stripes parallel to the smectic layers arises. Applying an electric field to the fan-shaped texture of the low-temperature phase, optically equivalent textures of the switched and ground states can be seen under a polarising microscope, as a consequence of the switching which takes place by rotation around the long molecular axis. They differ from each other only by a small change in the birefringence. It was found that the low-temperature smectic phase of dimer **32a** is also AF, i.e. a SmC$_x$P$_{AF}$ phase (U = 340 V$_{pp}$, f = 10 Hz, R = 5 kΩ, T = 95 °C, P_S = 330 nC cm^{-2}). No X-ray investigations were possible due to a fast crystallization of the sample.

Summarizing chapter 6.1, it was found that on increasing the spacer length for the dimers **type II** the mesophases are stabilized, contrarily to the tendency found for the analogues dimers of **type I** (see Table 6.1 and Figure 6.2). Another interesting point is the structure-property relationship on varying the length of the spacer *m* resulting in columnar phases for dimers **L – *5* - T** (compounds **31**). The lattice parameters of the Col$_r$ phases of compounds **31** depend on the length of the flexible spacer *m* (see Table 6.1). On increasing the spacer length the parameter *a* of the Col$_r$ phases is slightly increasing, while parameter *b* is slightly decreasing. The number of the molecules in the unit cell in the Col$_r$ phases of compounds **31** is decreasing with increasing spacer length. This means that the size of the ribbons of the Col$_r$ phases is decreasing on increasing the spacer length. The number of molecules in a unit cell of the Col$_r$ phase of dimers **31**, $n_{cell,LC}$ (calculated using ref. [03,204] see also chapter 5.1.2 for a detailed description) was found to be 5 for dimer **31a** and 4 for dimer **31b**. The values of the spontaneous polarisation, P_S, found for the polar phases of dimers **31** and **32** are increasing on elongating the spacer *m* and on decreasing the temperature, as observed for the analogues dimers **7a** and **9a** (**T – T**).

The connection of the mesogenic units in a ***laterally - terminally*** way in the *4*-position (**L – *4* - T**) on the central *resorcinol* fragment of the bent-core moiety, results for the dimers **32**, in appearance of new mesophases with new mesomorphic properties, i.e. SmAP$_{AF}$ phases (see Table 6.1 and Fig. 6.5). A phase sequence N -> SmAP$_{AF}$ -> SmC$_x$P$_{AF}$ has been observed for compound **32a**. The transition SmAP$_{AF}$ -> SmC$_x$P$_{AF}$ was found to be first order (with a transition enthalpy value of 0.8 kJ mol^{-1}). This means that on changing the connecting position resulted in the appearance of AF smectic phases.

6.2 The effect of the linking position of the mesogenic units on the mesophase behaviour of the analogues dimers of types I and II

The investigation of the effect of the connecting position of the *spacer - calamit* unit on the bent-core moiety on the mesophase behaviour showed that for the analogues dimers with spacer length $m = 6$, the linking of the mesogenic units in a ***laterally - terminally*** way results in compounds with lower mesophase stabilities than that found for the corresponding dimers of **type I** linked ***terminally - terminally*** (see Table 6.1 and Fig. 6.6). Thus, the compound **7a** (**T - T**) has the highest mesophase stability and is followed by the dimer **32a** (**L – *4* - T**). The dimer **31a** (**L – 5 - T**) exhibits the lowest mesophase stability.

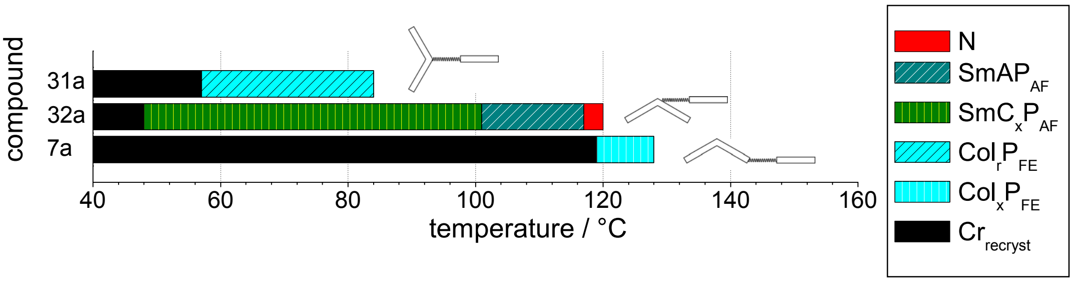

Figure 6.6: Transition temperatures (°C) of dimers **31a**, **32a** and their analogue dimer **7a** taken from the first DSC cooling scans (10 Kmin^{-1}).

A different situation could be observed for the dimers with eleven methylene units in the spacer. Surprisingly, it was observed that for the dimers **type II**, the highest mesophase stability is obtained for the ***laterally - terminally*** connected dimer **32b** (**L – *4* - T** dimer, see Table 6.1 and Fig. 6.7). Similar to the dimers with 6 methylene units in the spacer, the dimer **31b** with the *spacer-calamit* unit attached at the top of the bent-core unit (**L – 5 - T** dimer) exhibits the lowest mesophase stability.

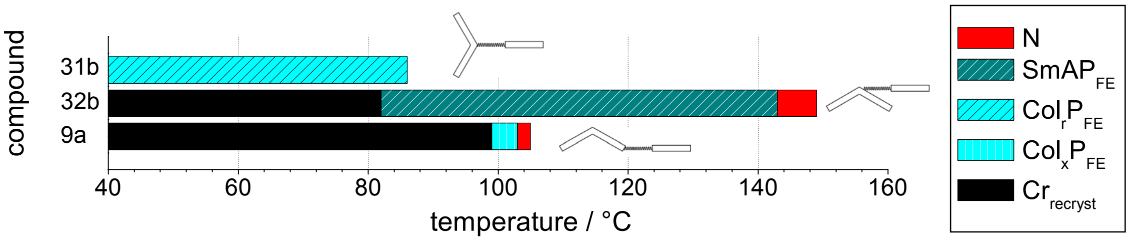

Figure 6.7: Transition temperatures (°C) of dimers **31b**, **32b** and their analogue dimer **9a** taken from the first DSC cooling scans (10 Kmin^{-1}).

On connecting the *spacer-calamit* unit in a ***laterally - terminally*** modality in the *5*-position (**L – 5 - T**) on the central *resorcinol* fragment of the bent-core moiety, only Col$_r$P$_{FE}$ mesophases were found for dimers **31**. Interestingly, the analogue connection in the *4*-position (**L – *4* - T**) on the central *resorcinol* fragment of the bent-core moiety results for dimers **32** in appearance of new mesophases with interesting mesomorphic properties, i.e. SmAP$_{AF}$ phases.

7 Mesophase behaviour of *'calamit–banana-calamit'* trimers

This chapter is focused on *'calamit – banana - calamit'* trimers of **type I** containing two identical calamitic mesogenic moieties connected *via* two equal flexible spacers to a bent-core unit in a linear fashion (***terminally – terminally*** connection). The trimers **type II**, *'banana - calamit – banana'* trimers, containing two identical bent-core mesogenic units connected to a calamitic mesogenic moiety in a linear fashion will be presented in the next chapter 8. The combination in the trimers under discussion should clarify if also such componds can exhibit '*banana phases*' (SmCP, Col) as well as mesophases typical for calamitic compounds (N, SmA, SmC) which were found for dimeric mesogens (see ref.[138,139,195,251] and chapters 5 and 6) and in the binary mixtures of bent-core and calamitic compounds.[183]

Several molecular architectures are possible for the design of such liquid crystal trimers, e.g. ***terminally – terminally*** connection (see a general example in Fig. 7.1a), ***laterally – terminally*** linking (Fig. 7.1b,c).

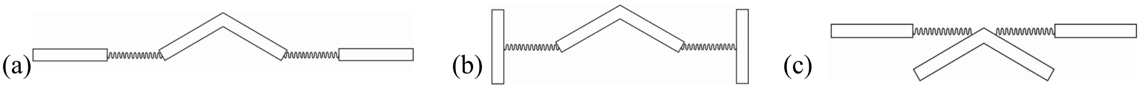

Figure 7.1: General sketch of *'calamit – banana - calamit'* trimers ***terminally – terminally*** connected (a) and ***laterally*** – ***terminally*** linked (b,c).

We used five- or seven-ring bent-core moieties (q = 0, 1, see Table 7.1) with different direction of the *ester* groups ***Z***, ***W***, i.e. a *resorcinol* fragment for trimers **33**, **35a** and **36** or an *isophthalic acid* unit for trimers **34** and **35b**. The bent-core moieties are tied to two identical calamitic alkyloxybenzoyloxyphenyl units (p = 6, 16) *via* flexible spacers in a linear fashion (***terminally – terminally*** connection). The three mesogenic units are linked using aliphatic spacers of equal size. The linkages between the two spacers and the mesogenic moieties are *ether* groups. The compounds **33**, **34** and **35** possess a five-ring bent-core moiety (q = 0), while the trimer **36** contains a seven-ring bent-core moiety (q = 1).

All compounds exhibit liquid crystalline behaviour. The mesophase types, transition temperatures together with the associated transition enthalpies, lattice parameters and P_S values of the trimers **33** - **36** are given in Table 7.1. To give more information, the mesophase behaviour on cooling is sketched in the bar charts (Fig. 7.2). Nearly all compounds exhibit smectic mesophases (several in combination with a nematic phase). Trimer **34a** exhibits only a monotropic nematic phase. The influence of this new constellation on the mesophase behaviour is discussed based on electro-optical and X-ray measurements.

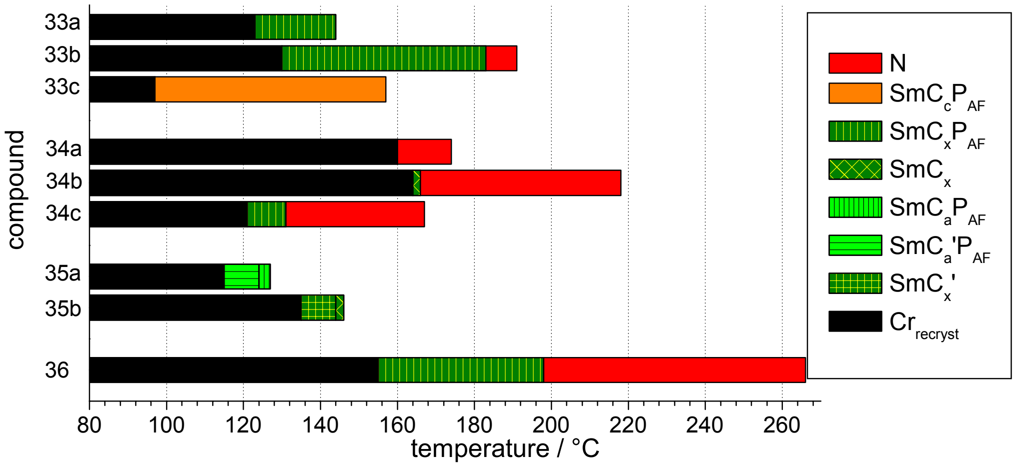

Figure 7.2: Transition temperatures (°C) of trimers **33** - **36**, taken from the first DSC cooling scans (10 Kmin^{-1}).

Table 7.1: Transition temperatures [°C], mesophase type, transition enthalpy values [kJ/mol], layer spacing d [nm], tilt angle τ of the molecules [°] with respect to the layer normal in SmC phases and P_S values of trimers **33 - 36**.[a]

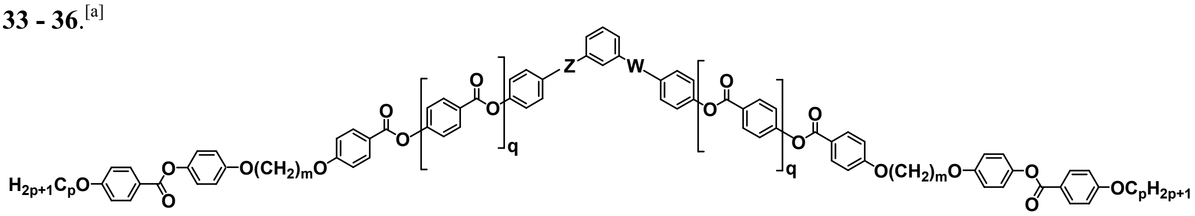

Comp	*m*	*p*	*Z*	*W*	*q*	Transitions temperatures [°C] Δ*H* [kJ·mol^{-1}]	Phase type	Lattice parameters *d* [nm]	τ [°]	P_S *nC/cm²*
33a	3	6	COO	OOC	0	Cr 156 (SmC$_x$P$_{AF}$ 144) I *67.6 21.4*	SmC$_x$P$_{AF}$	-[c]	-[c]	270
33b	6	6	COO	OOC	0	Cr 176 SmC$_x$P$_{AF}$ 185 N 193 I *58.9 21.1 7.7*	N SmC$_x$P$_{AF}$	-[c]	-[c]	300
33c	11	6	COO	OOC	0	Cr 130 SmC$_c$P$_{AF}$ 161 I *77.6 33.7*	SmC$_c$P$_{AF}$	2.12	24	340
34a	3	6	OOC	COO	0	Cr 186 (N 174) I *88.4 2.4*	N			
34b	6	6	OOC	COO	0	Cr 186 (SmC$_x$ 166) N 220 I *71.2* -[b] *11.9*	N SmC$_x$	-[c]	-[c]	-[c]
34c	11	6	OOC	COO	0	Cr 143 (SmC$_x$P$_{AF}$ 131) N 171 I *114.3 6.1 7.5*	N SmC$_x$P$_{AF}$	-[c]	-[c]	270
35a	11	16	COO	OOC	0	Cr 126 (SmC'$_a$P$_{AF}$ 125) SmC$_a$P$_{AF}$ 130 I *44.5 22.2 34.7*	SmC$_a$P$_{AF}$ SmC'$_a$P$_{AF}$	6.90 -[c]	- -[c]	330 370
35b	11	16	OOC	COO	0	Cr 142 SmC'$_x$ 146 SmC$_x$ 149 I *121.9 0.3 21.2*	SmC$_x$ SmC'$_x$	-[d] 7.54	-[d] -	-[d] -
36	6	6	COO	OOC	1	Cr 165 SmC$_x$P$_{AF}$ 200 N 267 I *43.2 15.0 7.1*	N SmC$_x$P$_{AF}$	-[c]	-[c]	430

[a] Transition temperatures (°C) and enthalpy values [kJ/mol] of trimers **33 - 36** were taken from the second DSC heating scans (10 Kmin^{-1}); values in parentheses indicate monotropic mesophases, in this case the transition temperatures and enthalpy values were taken from the first DSC cooling scans and the transition temperatures were checked by polarising microscopy; [b] the transition is not detectable on DSC and the transition temperature value is determined by polarising microscopy; [c] not determined due to rapid crystallization of the sample; [d] not determined due to fast transition to the low-temperature smectic phase.

7.1 Trimers 33 containing a *resorcinol* fragment in central position of the bent-core moiety

The symmetric trimers **33** have a five-ring bent-core unit possessing a central *resorcinol* fragment (***Z*** = -**COO**-, ***W*** = -**OOC**-, E_0) and two calamitic hexyloxybenzoyloxyphenyl units (p = 6). The three mesogenic units are connected by two equal methylene spacer (m = 3, 6, 11). It is important to note that the varied spacer contains *odd* as well as *even* number of atoms linking the three mesogenic units. The mesophase behaviour, transition temperatures together with the associated transition enthalpies, lattice parameters and P_S values of the trimers **33** are collected in the Table 7.1.

The homologue with *even*-numbered spacer length **33b** (m = 6) give rise to both nematic and smectic phases. The *odd*-numbered trimers exhibit exclusively smectic phases, however of different types. For trimer **33a** with m = 3 a monotropic smectic phase, here assigned as SmC_xP_{AF} phase could be found, while trimer **33c** (m = 11) forms an intercalated smectic SmC_cP_{AF} phase.

The nematic phase of the trimer **33b** shows typical schlieren (Fig. 7.3a), marbled, homeotropic and / or planar textures and chiral domains of opposite handedness. Moreover, the nematic phase shows a similar unusual electro-optical response, as the one described for the nematic phases of dimers of **type I** and **II** by application of an a.c. field (see for an example the compound **1h**, subchapter 5.1.1.2). Unusual effects are observed like a transition between longitudinal, zigzag and normal rolls (5 V μm^{-1}, 3 kHz; Fig. 7.3b), controlled by the excitation frequency. Above 12 Vμm^{-1}, on increasing the voltage, a *myelin*-like texture with fine equidistant stripes appears (Fig. 7.3c). At higher a.c. field (above 30 V μm^{-1}) the stripes disappear and an optical texture results which is reminiscent of a smectic fan-shaped texture (Fig. 7.3d). This field-induced fan-shaped texture is observed in the whole existence region of the nematic phase. It is important to note that during these electro-optical experiments no polar switching was detected. If the electric field is removed, the smectic-like texture disappears and the texture of the original planar oriented nematic phase reappears. This means that the nematic phases of the two different type of dimers '*banana - calamit*' **type I** and **II** (***terminally - terminally*** and ***laterally – terminally*** connected) exhibit very similar optical and electro-optical properties to those of the nematic phases of trimers of *'calamit – banana - calamit'* trimers. The low-temperature phases of trimers **33a** and **33b** were assigned as SmC_xP_{AF} phases.

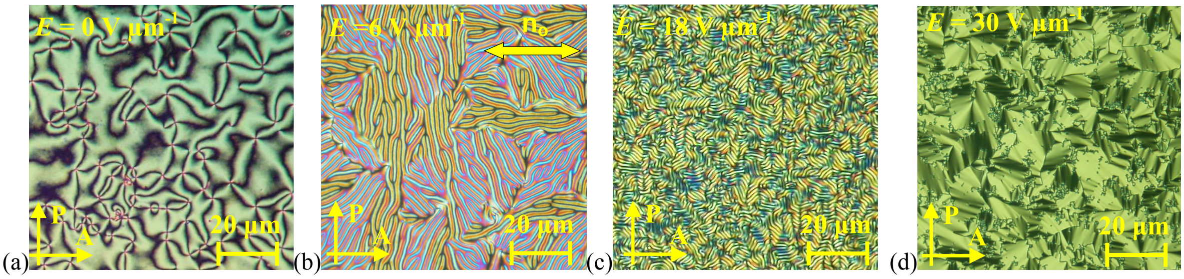

Figure 7.3: (a-d) Textures of the N phase of trimer **33b** at 187 °C observed between crossed polarisers in a 6 µm polyimide-coated ITO cell in the same region of the sample: (a) at U = 0 V, schlieren texture; (b-d) field-induced texture changes of the nematic phase by application of an a.c. field; the electric field strength E is increasing: (b) 6 Vμm^{-1}, f_0=4 kHz, longitudinal, zigzag and normal rolls; (c) 18 Vμm^{-1}, *myelin*-like texture; (d) 30 Vμm^{-1}, smectic fan-shaped reminiscent texture; the orientation of the initial director $\mathbf{n_o}$ is marked.

The trimer **33c** (*m* = 11) exhibits an enantiotropic smectic phase. It follows from the X-ray investigations and the electro-optical measurements that this phase is a SmC_cP_{AF} phase with only one layer reflection corresponding to a periodicity smaller than half the molecular length in the small-angle region (d = 2.12 nm). An electro-optical switching with a current response indicating an AF ground state could be obtained, i.e. two polarisation current peaks per half period were recorded (P_S = 340 nC cm^{-2}), with a switching mechanism by rotation around the long axis, which changes the polar direction without changing the tilt direction of the molecules.

7.2 Trimers 34 containing an *isophthalic acid* unit in central position of bent-core moiety

The trimer series **34** (*m* = 3, 6, 11; *p* = 6) differs from the series **33** only by the direction of the connecting *ester* linking groups of the central aromatic ring (***Z*** = -OOC-, ***W*** =-COO-), i.e. they posses a five-ring bent part with a central *isophthalic acid* unit. The mesophase behaviour, transition temperatures together with the associated transition enthalpies, lattice parameters and P_S values of the trimers **34** are collected in the Table 7.1.

All trimers of the series **34** form nematic phases, contrarily to the previously presented homologous series **33** (only the *even*-membered trimer **33b** forms a nematic phase). The trimer **34b** (*m* = 6) exhibits a nematic and a monotropic non-polar SmC phase (assigned here as SmC_x phase). The trimer **34c** (*m* = 11) forms a nematic and a polar SmC_x phase. The SmC_x phase possesses a polar switching very similar to that of the SmC_xP_{AF} phase of compound **33b**, i.e. a switching mechanism by rotation around the long axis, which changes the polar direction without changing the tilt direction of the molecules (SmC_xP_{AF} phase, P_S = 270 nC cm^{-2}).

The inversion of the two *ester* linking groups of the central aromatic ring ***Z*** and ***W*** results in a mesophase stabilization in comparison with the analogues trimers **33**. On increasing the spacer length for the trimers with *m* = 3 (**34a**) to the trimer with *m* = 6 (**34b**), the mesophases are stabilized. However, on further increasing the spacer length to *m* = 11 (**34c**), a mesophase destabilization could be detected, associated with the appearance of a polar smectic phase.

7.3 Trimers 35 bearing long terminal chains *p*

The trimer series **35** (*m* = 11; *p* = 16; see Table 7.1) incorporate bent-core units derived from *resorcinol* (trimer **35a**, ***Z*** = -COO-, ***W*** = -OOC-; $\mathbf{E_0}$ orientation) and from *isophthalic acid* (trimer **35b**, ***Z*** = -OOC-, ***W*** =-COO-). The elongation of the spacer and of the terminal chain leads to drastic consequences. The mesophase behaviour, transition temperatures together with the associated transition enthalpies, lattice parameters and P_S values of the trimers **35** are collected in the Table 7.1.

The trimer **35a** exhibits two smectic phases. On cooling from isotropic state a schlieren texture arises with singularities of $s = \pm1$, $s = \pm1/2$ and $s = \pm3/2$ (Fig. 7.4a, indication of a tilted smectic mesophase) and / or a birefringent smooth fan-shaped texture which points to an anticlinic SmC phase (Fig. 7.4a,b). Over the whole temperature range complementary domains of opposite handedness could be observed on rotating the polariser from the crossed position.

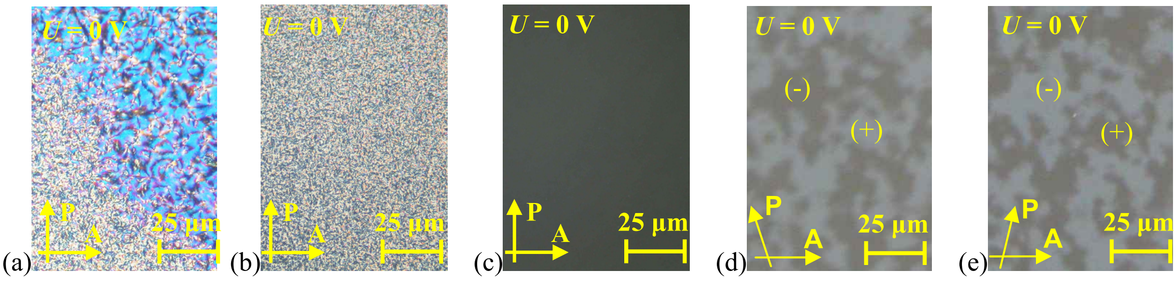

Figure 7.4: Textures of the mesophases of trimer **35a** as observed between two untreated glass slides on cooling at $U = 0$ V (same region is presented in all cases): (a) at the transition from the high-temperature SmC phase (schlieren texture, top-right) to the low-temperature smectic phase (*non-specific grainy* texture, bottom-left) at 125 °C; (b) the *non-specific grainy* texture of the low-temperature smectic phase at 124 °C; (c) optically isotropic texture of the low-temperature smectic phase at 122 °C (after 5 minutes); (a-c) textures observed between crossed polarisers, and (d,e) by rotating one polariser by +15° (d) and by -15° (e) from the crossed position (chiral (+) and (–) domains).

The X-ray diffraction pattern of the high-temperature phase of compound **35a** confirmed the presence of a SmC phase. Electro-optical investigations evidenced the occurrence of two separate repolarisation peaks in each half period of the applied triangular voltage field, which is characteristic for an AF switching (SmC_aP_{AF} phase). In the circular domains the extinction crosses are aligned along the directions of the crossed polarisers and do not change on applying, on reversal or on terminating the applied field. These findings suggest that the AF ground state as well as the switched FE states have an anticlinic tilt. This switching corresponds to the transition from a SmC_aP_{AF} state to a SmC_aP_{FE} state. The chirality of the layers switches by a collective rotation of the molecules around their long axes on reversing the applied field.

The texture of the low-temperature smectic phase of compound **35a** depended strongly on the texture of the preceding smectic phase and on the boundary conditions. This phase appeared either as a *non-specific* low-birefringent texture with small islands of birefringent broken fan-shaped texture or as a low birefringent *non-specific grainy* texture (Fig. 7.4b), which transforms into an optically isotropic texture (it appears dark between crossed polarisers on cooling and / or after several minutes, Fig. 7.4c). Rotating one polariser out of the crossed position chiral domains of opposite handedness could be observed (Fig. 7.4d,e). The features of this phase are similar to those found for the $SmCP_{AF}{}^{[*]}$ phase of compound **5b**. These findings would point out to a strongly distorted and hence optically isotropic layer structure similar to that proposed for the *dark conglomerate* phases (the mesophase has a chiral superstructure though the molecules themselves are achiral). The *dark conglomerate* phase exhibits little birefringence but is optically active and exhibits large homochiral domains in cells.[88,195,212]

However, there are strong arguments against the theory of a *dark conglomerate phase*, i.e. no fractal growing of the *grainy non-specific* texture of the mesophase, and no significantly higher viscosity of this mesophase in comparison to the high-temperature *conventional* polar smectic SmC_aP_{AF} phase (on shearing experiments) could be observed. Also the appearance of a *non-specific* low-birefringent texture with small islands of birefringent broken fan-shaped texture on cooling to the low-temperature phase of compound **35a** in a 5 µm non-coated ITO cell speaks for a non-typical *dark conglomerate phase*. It is assumed that in this mesophase microscopically sized domains with distinct tilt direction and polar directions are organized in layers. The X-ray measurements are indicating that this is not a conventional *dark* *conglomerate phase* as our sample was partially aligned and second- and third-order layer reflections in the lower temperature phase appeared. X-Ray investigations on the typical *dark conglomerate phase* indicate a simple layer structure; the layer reflections are not resolution limited and indicate a relatively short correlation length of the smectic layers.

There is a second different type of mesophases showing this type of *dark conglomerate* textures. In contrast to the typical *dark conglomerate phase*, which are simple layer structures without in-plane order, this second type has additional order and is assumed to be a soft crystalline phase, assigned as $B_4^{[*]}$ phases.[23] This means that several properties of the low-temperature phase of compound **35a** present similarities to those observed for related phases described above, however there are some significant differences. Therefore a *sponge-like* distorted structure or a soft crystalline $B_4^{[*]}$ phase structure cannot be assumed and hence their structure could be different.

The electro-optical response of the low-temperature phase of compound **35a** is different from the one observed for the high-temperature SmC_aP_{AF} phase. By applying electric fields greater than about 18 $V\mu m^{-1}$, this texture can be switched into a birefringent fan-shaped texture which presents circular domains with the extinction crosses inclined with respect to the directions of polariser and analyzer evidencing a synclinic organization of the molecules between adjacent layers in the field-induced state (Fig. 7.5a). The tilt angle of the extinction crosses with respect to the crossed position of the polarisers in the field-induced states is about 45° which indicates a tilt angle of the molecules of 45°, respectively (Fig. 7.5a,b,d). If the field is switched off, the texture shows nearly extinction between crossed polarisers and in the circular domains the extinction crosses rotate into positions parallel to polariser and analyzer. This indicates relaxation into an anticlinic structure at 0 V (Fig. 7.5c; SmC_aP_{AF}-like state). In this *non-birefringent* texture, over the whole temperature range chiral domains of opposite handedness could be observed. By applying the electric field again, the extinction crosses rotate back to the position where the tilt angle of the extinction crosses with respect to the crossed position of the polarisers in the field-induced states is about 45° (Fig. 7.5d). This indicates the existence of a SmC_sP_{FE}-like structure with opposite polar direction. The current response shows two current peaks per half period of the applied triangular voltage ($P_S = 370$ nC cm^{-2}, Fig. 7.5e). Hence, optical investigation clearly indicates a tristable switching by a collective rotation around a cone, which is an additional confirmation of the AF switching process.

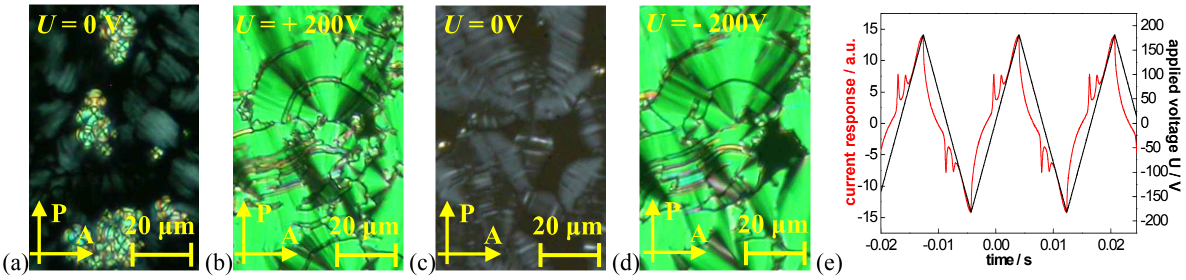

Figure 7.5: Electro-optical investigations of the SmC'_aP_{AF} phase of trimer **35a** at 120 °C in a 5 µm non-coated ITO cell (same region is presented in all cases): (a,c) U = 0 V; (b,d) U = ± 200 V; (e) AF switching current response obtained by applying a triangular-wave voltage ($U = 380$ V_{pp}, $f = 30$ Hz, $R = 5$ kΩ, $P_S = 370$ nC cm^{-2}); in images (a) and (c) the intensity of the light was strongly increased for a better observation of the extinction crosses).

Based on these experimental findings the ground state structure of the low-temperature smectic phase of trimer **35a** should be AF with an anticlinic organization, a SmC'_aP_{AF} phase.

The low birefringence could be explained with a SmC$_a$P$_{AF}$ phase structure with a 45° tilted organization of the molecules and a bending angle of the aromatic cores of about 109° (*orthoconic anticlinic director structure*[221]), as already mentioned for the low-temperature smectic phase of compound **5b**, a *dark conglomerate* SmCP$_{AF}$[*] phase (see chapter 5.1.2.4). Also for the low-temperature smectic phase of trimer **35a** the optically measured tilt angles in the field-induced textures of the SmC$_s$P$_{FE}$-like structure are in the range of 40–45°. Another explanation of the low birefringent mesophase can be a layer distortion which leads to a mesoscopically disordered structure, either composed of randomly ordered fragments of these layers,[235] or due to a random (*sponge-like*) deformation of the layers[250] and it is possible if the size of the domains with uniform director orientation is smaller than the wave length of light.

The structure of the trimer **35b** (m = 11; p = 16; ***Z*** = -**OOC**-, ***W*** =-**COO**-) differs from the trimer **35a** only by the direction of the connecting *ester* linking groups of the central aromatic ring. The inversion of these two *ester* linking groups of the central aromatic ring results in a mesophase stabilization (about 19 K), conform to the previously described tendency discovered for the trimers series **33** and **34**. The trimer **35b** exhibits two enantiotropic smectic mesophases. Based on the textural observations and of the X-ray diffraction pattern the mesophases of compound **35b** were assigned as SmC$_x$ and SmC’$_x$ phases. The comparison with the analogues trimers **33** and **34** revealed that the elongation of the spacer and of the terminal chain resulted in a mesophase destabilization for compounds **35**.

7.4 Trimer 36 containing a seven-ring bent-core unit

The trimer **36** possesses a seven-ring bent-core unit (q = 1) derived from *resorcinol* (***Z*** = -**COO**-, ***W*** = -**OOC**-; **E$_0$** orientation) and two calamitic hexyloxy-benzoyloxyphenyl units (p = 6). The three mesogenic units are connected to the methylene spacer (m = 6) through the *ether* groups. The influence of varying the number of aromatic rings of the bent-core unit on the mesomorphic properties will be investigated in comparison with the analogue trimer **33b** (m = 6; p = 6; ***Z*** = -**COO**-, ***W*** = -**OOC**-), which contains a five-ring bent-core unit (q = 0). The mesophase behaviour, transition temperatures together with the associated transition enthalpies, lattice parameters and P_S values of the trimer **36** are presented in the Table 7.1.

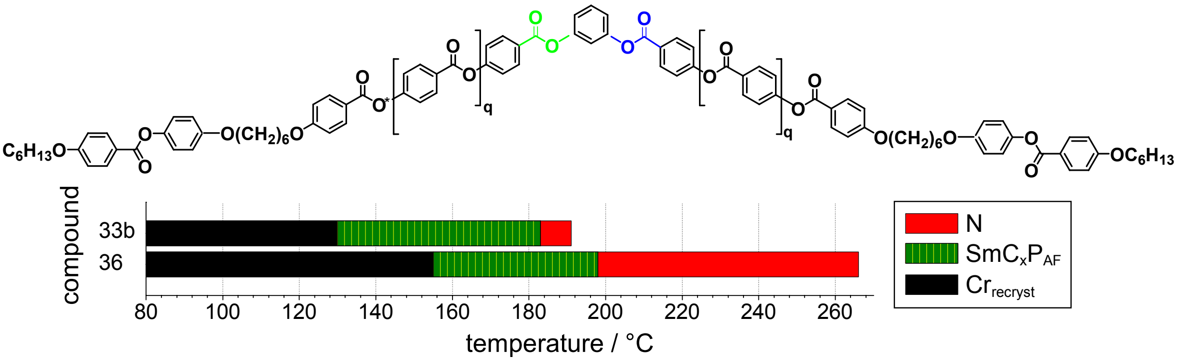

Figure 7.6: Transition temperatures (°C) of trimers **33b** and **36**, taken from the first DSC cooling scans (10 Kmin^{-1}).

The trimer **36** exhibits two enantiotropic phases: a nematic and a smectic phase, in accordance with the analogue trimer **33b** (N-SmC$_x$ phase sequence) and with its overall linear shape (*even*-methylene spacer). The application of an electric field of 20 Vμm^{-1} on the smectic phase leads to an electro-optical switching with a current response indicating an AF ground state, i.e. two polarisation current peaks per half period were recorded (P_S = 430 nC cm^{-2}). Over the whole temperature range complementary domains of opposite handedness could be observed (in the 0 V state and in the field-induced states). Based on these experimental findings, the low-temperature phase of trimer **36** was assigned as a SmC$_x$P$_{AF}$ phase. We can conclude that the enhancement of the number of rings in the bent unit (actually of the number of the benzoyloxy- units) results in an increased mesophase stability (Fig. 7.6), along with an increased P_S value.

Summarizing chapter 7, it was found that similar to the dimers '*banana - calamit*' of **type I**, for the trimers **type I** (*'calamit – banana - calamit'* trimers) the combination of two identical calamitic mesogenic units connected *via* two equal flexible spacers to a bent-core unit in a linear fashion ***terminally*** – ***terminally*** leads to compounds exhibiting polymorphism variants with phases typical for bent-core molecules (SmCP$_{AF}$) as well as mesophases characteristic for calamitic compounds (N). These nematic phases exhibit special properties similar to the nematic phases of dimers **type I** and **II** presented in previous chapters 5 and 6, e.g. special electro-convection pattern, as well as possible field induced transitions into smectic phases. New polar smectic phases, i.e. SmC$_c$P$_{AF}$ phases, as well as new phase sequences with non-polar and polar phases of special interest (nematic – smectic, nematic – polar smectic phases) appeared, similar to the combination '*banana - calamit*' of dimers of **type I**. It was found that the inversion of the two *ester* linking groups of the central aromatic ring ***Z*** and ***W*** results in a mesophase stabilization. The *even* - numbered spacer compounds (m = 6) presents the higher mesophase stability (see Table 7.1), similar to the dimers **type I**. The enhancement of the number of rings in the bent unit results in an increase of the mesophase stability, similar to the dimers **type I**.

All the polar SmC phases are AF and the values of the spontaneous polarisation, P_S, increase on increasing the length of the spacer m and of the terminal *alkyloxy* chain p attached to the calamitic mesogens and on decreasing the temperature, similar to the dimers **type I**.

8 Mesophase behaviour of ‘*banana–calamit-banana’* trimers

In this chapter, the mesophase behaviour of the symmetric trimers ‘*banana-calamit-banana’* of **type II** containing two identical bent-core mesogenic segments connected through two equal flexible spacer units in a linear *end-to–end* manner to a calamitic moiety incorporating different segments will be discussed. This combination in the trimers of **type II** should permit us a clearer understanding of the correlation between the overall molecular structure and thermal properties of these trimeric molecules. Furthermore, the trimers facilitate our understanding of the origin of the thermal behavior from dimers to the polymers.

The linking of the two bent-core units to the calamitic moiety *via* two flexible spacers can be realized in different ways: ***terminally* - *terminally*** (the trimers **type IIa** which will be in the following described, Fig. 8.1a), ***laterally* - *terminally*** **(**trimers **type IIb**, see Fig. 8.1b,c) and ***laterally* - *laterally*** (trimers **type IId**, see Fig. 8.1d).

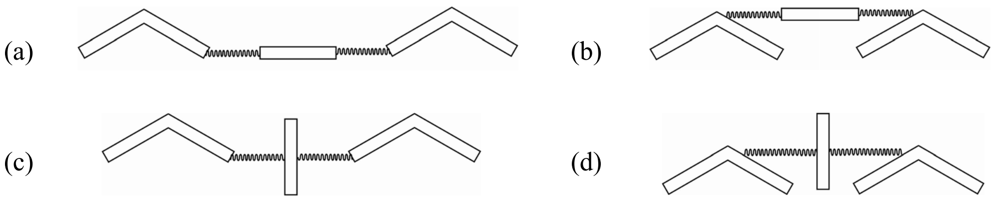

Figure 8.1: Different possibilities to design ‘*banana – calamit - banana*’ trimers.

Phenylene and *biphenylene* fragments (dimer series **37**) and *azobenzene* segments (dimer series **38**) were used as the calamitic moieties. We used the five-ring bent-core moiety possessing a central *resorcinol* ring with its *reference structure* **E$_0$**.

8.1 Trimers 37 containing *phenylene* and *biphenylene* units

The symmetric trimers **37** possess two five-ring bent-core mesogenic units (n = 12; **E$_0$**) and a calamitic structural unit containing a 1,4-disubstituted *benzene* ring or a *4,4’*-disubstituted *biphenylene* unit. The three mesogenic units are connected to the methylene spacer (m = 4, 11) through *ester* and *ether* groups. The mesophase behaviour, transition temperatures together with the associated transition enthalpies, lattice parameters and P_S values of the trimers **37** are collected in the Table 8.1 and Figure 8.2. All compounds **37** exhibit liquid crystalline behaviour.

Table 8.1: Transition temperatures [°C], mesophase type, transition enthalpy values [kJ/mol], layer spacing *d* [nm], tilt angle τ of the molecules [°] with respect to the layer normal in SmC phases and P_S values of trimers **37**.[a]

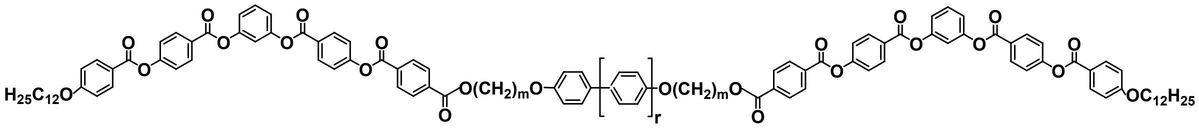

Comp	*m*	*r*[d]	Transitions temperatures [°C] Δ*H* [kJ·mol^{-1}]	Phase type	Lattice parameters					P_S *nC/cm*^{2}
					d [nm]	τ [°]	*a* [nm]	*b* [nm]	γ [°]	
37a	4	0	Cr 162 SmC_aP_{AF} 189 I *54.3* *14.7*	SmC_aP_{AF}	5.66	44				270
37b	4	1	Cr 153 SmC_aP_{AF} 191 I *59.1* *15.9*	SmC_aP_{AF}	6.09	-[e]				140
37c	11	1	Cr 158 (M_7 153) I *107.7* -[b]	M_7	-[c]	-[c]	-[c]	-[c]	-[c]	-[c]

[a] Transition temperatures (°C) and enthalpy values [kJ/mol] of trimers **37** were taken from the second DSC heating scans (10 Kmin^{-1}); values in parentheses indicate monotropic mesophases, in this case the transition temperatures and enthalpy values were taken from the first DSC cooling scans and the transition temperatures were checked by polarising microscopy; [b] the transition is not detectable on DSC and the transition temperature value is determined by polarising microscopy; [c] not determined due to rapid crystallization of the sample; [d] *r* is the number of additional *phenyl* rings in the corresponding calamitic unit; [e] the tilt angle could not be determined because only a powder-like pattern was obtained during the X-ray investigations.

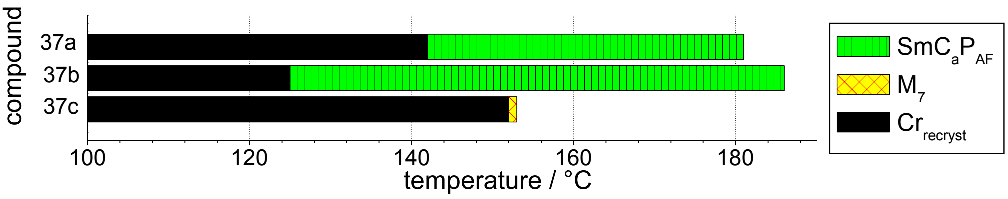

Figure 8.2: Transition temperatures (°C) of compounds **37**, taken from the first DSC cooling scans (10 Kmin^{-1}).

Only smectic phases were found for the trimers **37a** and **37b** with an *odd*-numbered of single units per spacer. The two compounds differ only by the calamitic rigid unit, i.e. the trimer **37a** possesses a *1,4*-disubstituted benzene ring ($r = 0$), while the trimer **37b** contains a *4,4'*-disubstituted *biphenylene* moiety ($r = 1$) as calamitic unit. Surprisingly, the stability of the mesophase of compound **37b** is only slightly higher.

The mesophases of the trimers **37a** and **37b** have similar physical properties. On slow cooling, the mesophase of trimer **37a** shows banana leaf-like and ribbon-like textures and numerous circular domains. The direction of the extinction crosses in the circular domains is parallel to the position of the crossed polarisers, indicating an anticlinic organization of the molecules between adjacent layers (Fig. 8.3a). The X-ray diffraction pattern of a surface-aligned sample of the mesophase of trimer **37a** is characterized by a diffuse scattering in the wide angle region and layer reflections of the first and second order with *d* = 5.66 nm (Table 8.1 and Fig. 8.3b). The well-defined layer structure confirms a smectic phase. Based on the cumulated experimental findings of the POM and X-ray investigations this phase is designed as a SmC_a phase.

Electro-optical investigations on the enantiotropic SmC$_a$ phases of trimers **37a** and **37b** evidenced the occurrence of two separate repolarisation peaks in each half period of the applied triangular voltage field, which is characteristic for an antiferroelectric switching (U = 300 V$_{pp}$, f = 10 Hz, R = 5 kΩ, T = 170 °C, SmC$_a$P$_{AF}$ phase, see Fig. 8.3d; P_S = 270 nC cm^{-2} for **37a** and P_S = 140 nC cm^{-2} for **37b**). Upon applying a sufficiently strong electric field (25 Vµm^{-1}) the texture becomes *non-specific* and the birefringence increases. The field-induced texture is independent of the polarity of the applied field (Fig. 8.3c) and does not relax on removal of the electric field. This confirms that the switching process takes place by a collective rotation around the long molecular axis, which changes the polar direction without changing the tilt direction of the molecules.

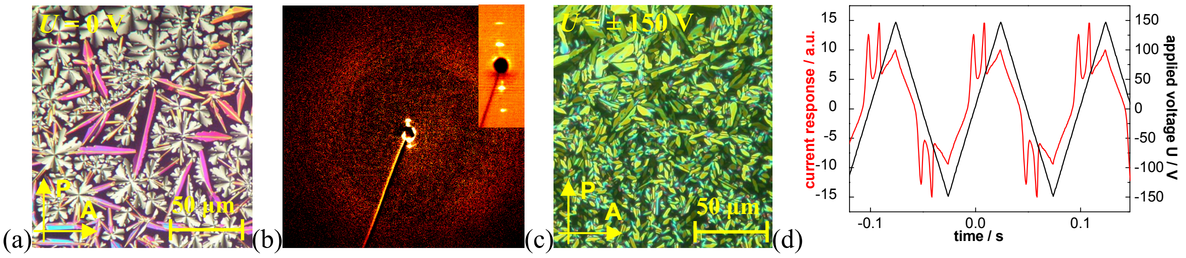

Figure 8.3: The SmC$_a$P$_{AF}$ phase of trimer **37a**: (a) Texture on cooling from the isotropic liquid at 180 °C at U = 0 V (dark areas are residues of isotropic liquid); (b) XRD patterns of a surface-aligned sample at 174.5 °C (the intensity of the isotropic liquid is subtracted); inset shows the small angle region; (c) d.c. field experiments at 170 °C in a 5µm non-coated ITO cell (U = ± 150 V); (d) AF switching current response by applying a triangular-wave voltage (U = 300 V$_{pp}$, f = 10 Hz, R = 5 kΩ, T = 170 °C; P_S = 270 nC cm^{-2}).

Compound **37c** having an *odd* number of methylene units per spacer (m = 11) and with a calamitic unit consisting of a *4,4'*-disubstituted *biphenylene* unit (r = 1) forms a mesophase which appears completely dark between crossed polarisers. This texture exhibits domains of opposite handedness which can be visualized by a small decrossing of the polarisers (Fig. 8.4a,b). This mesophase shows a high viscosity, similar to *dark conglomerate* phases or cubic phases. The significantly higher viscosity of this mesophase in comparison to the *conventional* polar smectic phase obtained for the homologous trimer **37b** (m = 4) was tested by shearing experiments (Fig. 8.4c). Further characterization by X-ray diffraction and electro-optical studies was not possible due to the metastable nature of this phase. The unidentified mesophase of compound **37c** was assigned as a M$_7$ phase.

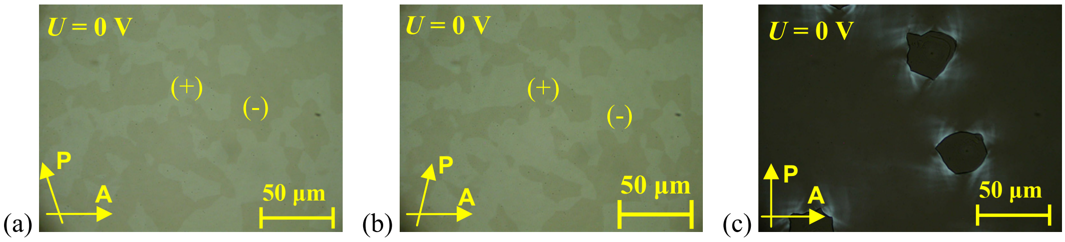

Figure 8.4: Textures of the M$_7$ phase of compound **37c** at 152.5 °C in a 5 µm non-coated ITO cell at U = 0 V observed by rotating one polariser by +10° (a) and by -10° (b) from the crossed position (chiral (+) and (–) domains); (c) same section observed between crossed polarisers, after shearing the sample.

Despite the smaller size of the *1,4*-disubstituted benzene unit (trimer **37a**; *r* = 0) in comparison to the *4,4'-biphenylene* unit (trimer **37b**; *r* = 1) these compounds have a relatively similar mesophase stability. This is surprising since the calamitic *biphenylene* unit is much more rigid and has a larger size, which should disturb the packing of the bent-core mesogenic units. On the other hand, a significant stabilization of the mesophase would be expected because of the stronger π-stacking interactions in the aromatic sublayers containing the *biphenyl* fragment (in comparison to the benzene ring sublayers). Obviously, the two effects compensate each other for these compounds. Other interesting findings are the higher melting point and the smaller mesophase range observed for the *benzene* derived trimer **37a** due to the smaller disturbing effect of the smaller size of the *phenylene* unit (see Table 8.1). The mesophase range for trimer **37a** is 27 K, while for trimer **37b** a mesophase interval of 38 K was found. It is also interesting to note that the trimers **37a** and **37b** require very high voltages for electro-optical switching ($U = 300$ - $400\ V_{pp}$). Hence, this might also be caused by the relatively strong π-stacking interactions which provide a more dense packing of the molecules. On increasing the spacer length (trimer **37c**, *m* = 11), the polar phases are replaced by the unidentified M_7 phase. Additionally, a strong mesophase destabilization could be observed for the *even*-numbered spacer, i.e. the clearing temperature of trimer **37c** (*m* = 11) is 38 K lower than the one corresponding to the homologous trimer **37b** (*m* = 4).

8.2 Trimers 38 containing an *azobenzene* unit[198]

In this chapter, the mesophase behaviour of the symmetric trimers **38** which possess two five-ring bent-core mesogenic moieties (*n* = 12; $\mathbf{E_0}$) and a calamitic structural unit containing an *azobenzene* fragment will be discussed. The three mesogenic units are connected to the methylene spacer (*m* = 2, 4, 5, 6) through *ester* and *ether* groups. The mesophase behaviour, transition temperatures together with the associated transition enthalpies, lattice parameters and P_S values of the trimers **38** are collected in the Table 8.2 and Figure 8.5. All compounds **38** exhibit monotropic mesophases. The synthesis and mesophase behaviour of trimers **38** were already published by us.[198]

The trimers **38a** and **38b** with *odd*-numbered spacers (with an *even* number of methylene groups (*m* = 2, 4)) exhibit monotropic optical isotropic mesophases. No chiral domains of opposite handedness could be detected by slightly uncrossing the polarisers. Further characterization by X-ray diffraction and electro-optical studies was not possible due to the metastable nature of these phases. The unidentified mesophases of compounds **38a** and **38b** were assigned as M_8 and M_9 phases.

The trimer **38c** (*m* = 5) forms two phases which could be identified as tilted smectic phases by their characteristic textures, i.e. schlieren textures, high- and low-birefringence fan-shaped textures and regions with circular domains, where the extinction crosses are aligned or inclined with respect to the position of the crossed polarisers. It was impossible to obtain homeotropic textures either by shearing or by surface treatment, which implies phases with tilted molecules. The corresponding phase transition is characterised by a small transition enthalpy (about 0.3 $kJ \cdot mol^{-1}$). Fast crystallization prevented X-ray diffraction measurements and electro-optical studies. The unidentified mesophases of compound **38c** were assigned as SmC_x and SmC'_x phases.

Table 8.2: Transition temperatures [°C], mesophase type, transition enthalpy values [kJ/mol], layer spacing d [nm], tilt angle τ of the molecules [°] with respect to the layer normal in SmC phases and P_S values of trimer series **38**.[a]

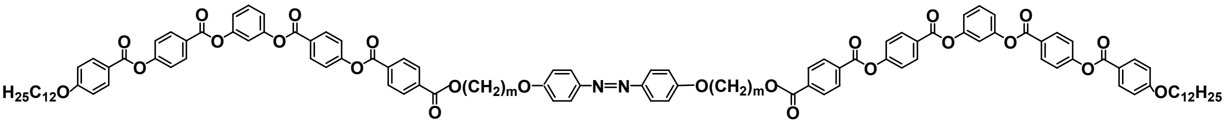

Comp.	m	Transitions temperatures [°C] ΔH [kJ·mol^{-1}]	Phase type	Lattice parameters		P_S nC/cm^2
				d [nm]	τ [°]	
38a	2	Cr 216 (M_8 203) I *111.7* -[b]	M_8	-[c]	-[c]	-[c]
38b	4	Cr 185 (M_9 181) I *135.9 44.1*	M_9	-[c]	-[c]	-[c]
38c	5	Cr 187 (SmC'$_x$ 162 SmC$_x$ 176) I *132.4 0.3 33.4*	SmC$_x$ SmC'$_x$	-[c] -[c]	-[c] -[c]	-[c] -[c]
38d	6	Cr 162 (SmC$_a$P$_{AF}$ 157) I *113.1 43.1*	SmC$_a$P$_{AF}$	6.21	-[d]	270

[a] Transition temperatures (°C) and enthalpy values [kJ/mol] of trimers **38** were taken from the second DSC heating scans (10 Kmin^{-1}); values in parentheses indicate monotropic mesophases, in this case the transition temperatures and enthalpy values were taken from the first DSC cooling scans and the transition temperatures were checked by polarising microscopy; [b] the transition is not detectable on DSC and the transition temperature value is determined by polarising microscopy; [c] not determined due to rapid crystallization of the sample; [d] the tilt angle could not be determined because only a powder-like pattern was obtained during the X-ray investigations.

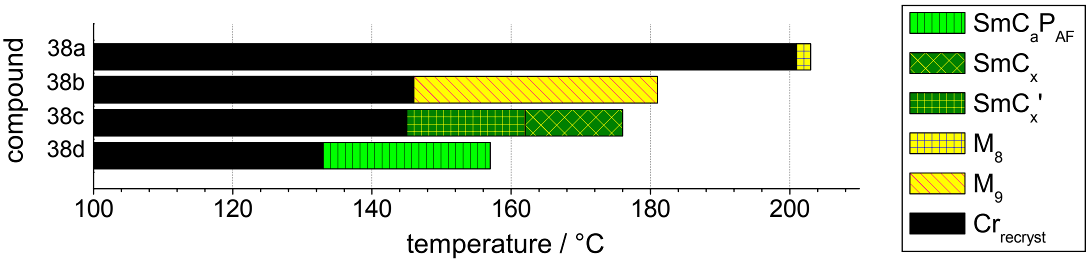

Figure 8.5: Transition temperatures (°C) of trimer series **38**, taken from the first DSC cooling scans (10 Kmin^{-1}).

The trimer **38d** with the longest spacers (m = 6) exhibits one monotropic smectic phase. The growth of this phase suggests a columnar or an undulated smectic phase, i.e. a dendritic growing, banana leaf-like texture and numerous circular domains with the direction of the extinction crosses parallel to the crossed polarisers position (suggestion of an anticlinic organization of the molecules between adjacent layers, see Fig. 8.6a,b) could be observed. However, in the XRD pattern only layer reflections can be found with d = 6.21 nm, confirming a smectic phase (see Table 8.2 and Fig. 8.6c). In electro-optical investigations an AF polar switching could be observed, and therefore, the mesophase is assigned as a SmC$_a$P$_{AF}$ phase. Two current peaks per half-period of a triangular voltage could be recorded during the switching process indicating an AF ground state (P_S = 270 nC cm^{-2}). If an electric field of 25 V µm^{-1} is applied to the phase of trimer **38d** the texture becomes *non-specific* and the birefringence slightly increases. The texture of the switched states is independent of the polarity of the field and nearly the same as in the field-off state (Fig. 8.6d). This confirms that the switching between the AF ground state and the switched FE states preferably takes place by the collective rotation of the molecules around their long axes.

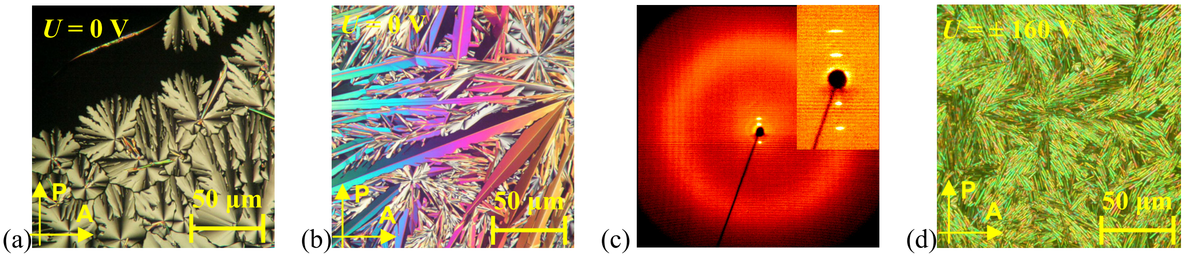

Figure 8.6: The SmC$_a$P$_{AF}$ phase of trimer **38d**: (a,b) Textures on cooling from the isotropic liquid at $U = 0$ V (a) at 157 °C and (b) at 150 °C; (c) XRD patterns of a surface-aligned sample at 148 °C; the inset shows the small angle region; (d) d.c. field experiments at 150 °C in a 5µm non-coated ITO cell ($U = \pm 160$ V).

Similar to the dimer **30a** containing a *bis-azobenzene* calamitic mesogen (chapter 5.6.2), photochemical properties of trimer **38d** were studied by Professor Dr. V. SHIBAEV and Dr. A. BOBROVSKY (MOSKOW University, Russia) in collaboration within the COST european project.[198] The introduction of photosensitive *azobenzene* groups into the trimers of **type II** matrix is of special interest due to the potential different applications, e.g. in optical data recording and storage of information. On analyzing the photochemical properties of trimer **38d** it was found that the irradiation by polarised light induces photoorientation in thin amorphous films obtained by spin-coating. On studying the kinetics and the mechanism of the photoorientation process it was shown that the photoinduced order is quite stable at temperatures below the melting point.

The increase of the length of the spacer *m* resulted in a destabilization of the mesophases and a reduction of the transition temperatures for the compounds with two *odd*-numbered spacer (with an *even* number of methylene groups, $m = 2, 4, 6$).

9 Summary

Liquid crystals are complex and challenging systems for theoretical and experimental research, and especially for their technological applications. Bent-core liquid crystals represent one of the major topics of the actual condensed matter research due to their ability to form new mesophases with unusual properties. Despite their achiral molecular structure, bent-core molecules show polar order and chiral superstructures in their LC mesophases. The relationships between the chemical structure of bent-core molecules and the type and physical properties of the exhibited mesophases are the subject of many studies and yet relatively unknown in detail. Attempted calculation and modelling of such systems can be made with numerous limitations and simplifications. In order to obtain reliable predictions concerning the impact of variation of the structure of the molecules and the properties of the resulting mesophases our factual knowledge need to be broadened.

In this work a comprehensive investigation of the impact of molecular design on the mesomorphic behaviour of new oligomeric liquid crystal systems, i.e. dimers and trimers containing bent-shaped and calamitic mesogens connected covalently *via* flexible spacers was conducted. It is well known that members of the different mesogenic groups form different types of mesophases. If mesogens belonging to different groups are covalently connected to each other, the existence and the type of mesophases of the new materials cannot be foreseen. The general formula of the novel non-symmetrical '*banana – calamit'* dimers (**type I** and **type II**), symmetrical '*calamit – banana – calamit'* trimers (**type I**) and '*banana – calamit – banana'* trimers (**type II**) are given in Figure 9.1. Numerous variations on the structure of the bent-core moiety and calamitic mesogenic units, the length and parity of the flexible spacer connecting the different mesogenic units, the nature of linking groups between the mesogenic units, as well as the fashion of linking the units were conducted.

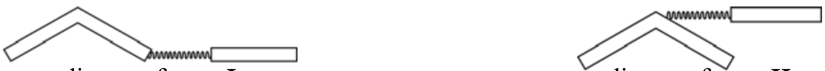
dimers of **type I**
(compounds **1** - **30**; chapter 5)

dimers of **type II**
(compounds **31**, **32**; chapter 6)

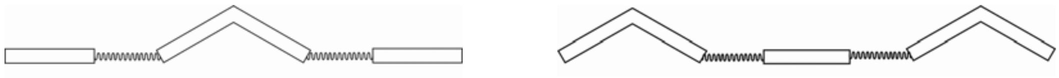
trimers of **type I**
(compounds **33** - **36**; chapter 7)

trimers of **type II**
(compounds **37**, **38**; chapter 8)

Figure 9.1: General formula of the synthesized compounds.

These variations were introduced for two reasons: to investigate the direct influence of these structural variations on the mesomorphic properties and hence, to make possible a detailed analyse of the potential '*competition*' of the contribution of the calamitic and bent-core moieties on the mesomorphic behaviour of the oligomeric systems. The question was whether this combination would result into polymorphism variants with '*banana phases*' (columnar and polar smectic phases) and/or mesophases typical for calamitic compounds (N, SmA, SmC phases). A further point of interest was the question as to whether the nematic, SmA or SmC phases formed by these oligomeric systems could exhibit the properties of calamitic mesogens, or perhaps the features of the phases formed by corresponding monomeric bent-core mesogens. The main target when designing these LCs systems was to identify novel chemically stable compounds with switchable enantiotropic mesophases that exhibit a wide range of temperature (as near to room temperature as possible) with potential use in display devices.

In the oligomeric molecules under discussion it was found that there is a '*competition*' between these two moieties. Almost all these compounds have interesting liquid crystalline properties. A large variety of new mesophases could be induced by covalently linking bent-core and calamitic moieties of different size and nature, by means of varied structure of the connecting groups, length and parity of the different chains, introduction of polar groups and lateral substituents, etc. Several novelties concerning the phase behaviour of these substances were found:

- the combinations lead to compounds exhibiting polymorphism variants with phases typical for bent-core molecules ($SmCP_A$, Col) as well as mesophases characteristic for calamitic compounds (N, SmA),
- appearance of new phase sequences with non-polar and polar phases of special interest: nematic-columnar and nematic-smectic,
- an unusual *odd-even* effect: the appearance of the nematic phase only for the *even*-membered dimers,
- the nematic phases exhibit special properties, e.g. special electro-convection pattern, biaxiality, high flexoelectricity, and possible field induced transitions into smectic-like phases,
- the occurrence of N – N_X phase transition characterised by a low transition enthalpy; the N_X phase probably possesses a conical twist-bend helical arrangement of the molecules (called nematic twist-bend N_{TB} phase in literature[39,196,206,245-249]).
- the existence of a SmC_s – SmC_a phase transition with a small transition enthalpy,
- rich polymorphism of polar switchable phases typical for bent-core mesogens,
- the appearance of new intercalated smectic phases for some longer spacer length.

Chiral domains could be observed in the nematic phases of all dimers and trimers under study, although the molecules themselves are not chiral. Remarkably, in contrast to conventional calamitic nematics, it was found that these nematic phases exhibit a positive dielectric and negative conductivity anisotropy (e.g. **15b**). The SmA phases of these dimers exhibit also unusual properties (dimers **13** – **19**).

On the basis of these studies, it was found that the transition temperatures and phase behaviour of dimers and trimers under study depend on a series of factors as follows: the length and parity of the flexible spacer, molecular structure of the constituent mesogenic groups, the nature of connecting groups between the corresponding units, the nature of terminal groups.

A good insight on the role of the length of the flexible spacer *m* on the mesophase behaviour of these new dimeric systems is given on the analysis of the dimers series **1** (see Fig. 9.2). All compounds **1** exhibit liquid crystalline behaviour. A dependence of transition temperatures on the number of methylene units, *m*, in the flexible spacer was found, i.e. a clear alternation of the clearing temperatures, where the *even* members exhibit the higher values. Nearly all compounds **1** exhibit columnar mesophases (several in combination with a nematic phase). Interestingly, we could observe the N phase only for the *even*-membered dimers **1**. This means that also for '*banana-calamit*' dimers the molecules with an *even* number of single units in the spacer should have a more stretched shape. The *odd*-numbered dimers **1** exhibit exclusively columnar phases, however of different types. The homologue with the shortest spacer length (m = 2) exhibit nematic behaviour, while the compound with m = 3 presents only columnar behaviour. The next homologues with *even*-numbered spacer lengths (m = 6, 8, 10) give rise to both nematic and columnar phases, while for the longer member with m = 12, nematic and smectic (SmC_cP_{AF}) phases are observed. Thus, increasing spacer length (m = 12) appears to promote smectic over columnar behaviour. At the N-I transition temperatures, one can observe a monotone decrease on increasing the spacer length from 163 °C (m = 2) to 125 °C (m = 12). The alternation of the phase type in dependence of spacer length is highly unusual, especially in the combination type N-Col phases.

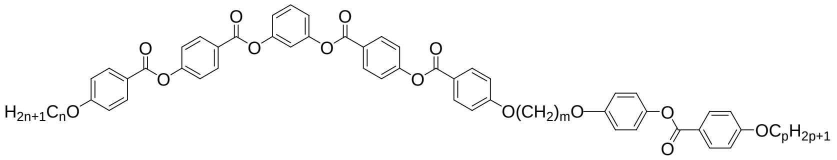

1: n = 12; m = 2, 3, 5-12; p = 6
2: n = 8; m = 3, 6, 11; p = 6
3: n = 16; m = 3, 6, 11; p = 6
4: n = 12; m = 6, 11,12; p = 12
5: n = 12; m = 2, 6, 11; p = 16
6: n = 16; m = 6, 11; p = 12

Figure 9.2: Compounds **1 - 6** with variations of the length of the spacer and of the terminal chains attached to the bent-core and calamitic mesogenic units.

Different columnar phases occurred on varying the length of the spacer of dimers **1** (Col_rP_{AF} phase (m = 3), $Col_{ob}P_{AF}$ phases (m = 5, 7, 9, 10) and non-identified Col_x phases (m = 6, 8). A dependence of the lattice parameters of the columnar phases on the length of the flexible spacer was observed, i.e. on increasing the spacer length the parameter a of the Col_{ob} phases is slightly decreasing, while parameter b and the oblique angle (γ) are slightly increasing. The number of the molecules in the unit cell in the Col_{ob} phases is also slightly decreasing with increasing spacer length. The correlation of a and n_{cell} speaks for the molecules being packed along a in ribbons (b is associated to the molecular length). Remarkably, a dependence of the values of the spontaneous polarisation P_S with the length of the *hydrocarbon* spacer was observed for the first time, i.e. for the homologues of series **1** with $Col_{ob}P_{AF}$ phases an increase of the value of P_S could be detected on elongating spacer length m.

Further investigations on the impact of the length of the spacer m and of the terminal *alkyloxy-* chains n and p attached to the two mesogenic units on the mesomorphic behaviour of dimer series **2** – **30** (see Fig. 9.2-9.8) revealed that the tendencies found for the mesophase behaviour and transitional temperatures of the series **1** can be generalized for the '*banana-calamit'* dimers of **type I** (dimer series **1-30**). For the dimers **1** – **6** all these variations bring some alterations, but also some similarities to the general tendencies as follows:

- A general tendency of decreasing of the mesophase stability on increasing n, m and p; an exception is dimer **6b** bearing the longest *hydrocarbon* chains (n = 16, m = 11, p = 12).

- In spite of the minor differences in the lengths of the flexible chains, a variety of new mesophases occur: N, non-polar and polar Col$_{\mathrm{ob}}$, Col$_{\mathrm{r}}$, Col$_{\mathrm{x}}$, SmC$_{\mathrm{s}}$, SmC$_{\mathrm{a}}$, SmC$_{\mathrm{c}}$, SmCP$_{\mathrm{AF}}$[*], non fully identified SmX and resp. M$_{\mathrm{x}}$ phases.
- Elongation of the length of terminal chain *p* attached to the calamitic mesogenic unit resulted for *even* dimers **5** (*n* = 12, *m* = 2, 6; *p* = 16) in appearance of additional polar smectic phases (**5b**: N-SmC$_{\mathrm{s}}$P$_{\mathrm{AF}}$-SmCP$_{\mathrm{AF}}$[*]).
- Increasing of terminal chain *n* attached to the bent-core mesogenic unit (from *n* = 8 to 12 to 16) resulted in the appearance of polar columnar phases for some dimers with an *odd* –numbered spacer (comparing dimers **2** with *n* = 8, which exhibit smectic phases, and resp. analogues dimers **1** and **3,** with *n* = 12, 16, which form columnar phases).
- A nearly symmetric substitution (*n* = 8; *m* = 6, *p* = 6) resulted in a phase sequence N–SmC$_{\mathrm{s}}$P$_{\mathrm{FE}}$–M$_{\mathrm{I}}$ (**2b**) on cooling. The analogues dimers **1d, 3b**, **4a** (*n* = 6, 12, 16; *p* = 6, 12) with *m* = 6 and longer terminal chains (n + p < 24) exhibit a sequence N-Col$_{\mathrm{x}}$ phase. For longest terminal chains (n + p > 24) the dimers **5b** and **6a** (*n* = 12, 16; *p* = 12, 16) showed three mesophases: N-SmC$_{\mathrm{s}}$P$_{\mathrm{AF}}$-SmCP$_{\mathrm{AF}}$[*] (**5b**) and resp. N-SmC$_{\mathrm{s}}$P$_{\mathrm{AF}}$-SmXP$_{\mathrm{AF}}$ phase sequence (**6a**).

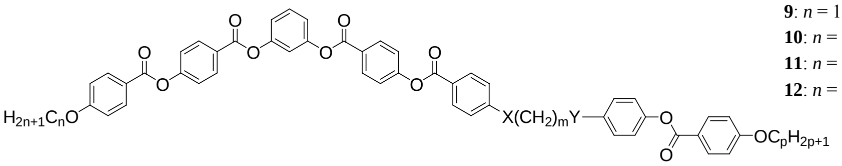

7: *n* = 12, 16; *m* = 6; *p* = 6; *X* = COO; *Y* = O
8: *n* = 12, 16; *m* = 6; *p* = 12; *X* = COO; *Y* = O
9: *n* = 12, 16; *m* = 11; *p* = 6; *X* = COO; *Y* = O
10: *n* = 12, 16; *m* = 5; *p* = 6; *X* = OOC; *Y* = O
11: *n* = 12, 16; *m* = 5; *p* = 12; *X* = OOC; *Y* = O
12: *n* = 12; *m* = 15; *p* = 16; *X* = O; *Y* = COO

Figure 9.3: Dimers **7**-**12** (*X* = -COO-, -OOC-, -O-; *Y* = -COO-, -O-) with variation of connecting groups ***X*** and ***Y***, the length of the spacer and the terminal chains attached to bent-core and calamitic mesogenic units.

Introduction of different groups ***X*** and ***Y*** connecting the spacer with the two different mesogenic moieties resulted in the appearance of new mesophases for dimers **7 - 9** (*X* = –COO-, *Y* = –O-), **10 - 11** (*X* = –OOC-, *Y* = –O-) and dimer **12** (***X*** = –O-, ***Y*** = –COO-, Fig. 9.3). These variations results in changes in the general behaviour found for dimers **1 -6** as follow:

- A *highlight* of this thesis is the occurrence of crystalline polar phases with FE and AF ground states. Dimers **10 (*X*** = -OOC-, ***Y*** = –O-) exhibit crystalline FE polar phases, whereas its analogues, dimers **1d** and **3b** (***X*, *Y*** = -O-) show a N-Col$_{\mathrm{x}}$ phase sequence. Compound **12** (*m* = 15, ***X*** = –O-, ***Y*** = –COO-) presents a novel polymorphism, i.e. a nematic and a crystalline polar AF phase.
- Similar to the results found for the dimers **1**–**6**, a nematic phase as a high-temperature phase was found for most of dimers **9**–**12** with an *even* number of the single units in the connecting bridge between the two mesogenic fragments.
- Introduction of group ***X*** = -COO- resulted in a decreasing of the mesophase stability for dimers **7**–**9** (comparing **7a** and **1e**, and resp. **9a** and **1j**). Moreover, in the case of dimer **9a** different phase sequence was found, i.e. a N-Col sequence on cooling, whereas the analogue dimer **1j** with *ether* group connection exhibits a N–Sm sequence.
- Contrarily, for the dimers **11** the introduction of the invers ***X*** = -OOC- group resulted into a mesophase stabilization, as well in a variation of the mesophase behaviour

(comparing dimers **11a** and **4a**, and resp. **11b** and **6a**). The dimer **11a** (m = 5) form N and two polar smectic phases, whereas its analogue **4a** exhibits a N – Col sequence.

- Only columnar phases were found for dimers **7** and **8** (m = 6) with an *odd* number of the single units in the connecting bridge between mesogenic units, similar to behaviour found for dimers **1**.
- The melting points of dimers **7-11** do not change remarkably on increasing the length of the terminal *alkyloxy-* chains attached to the two mesogenic units.

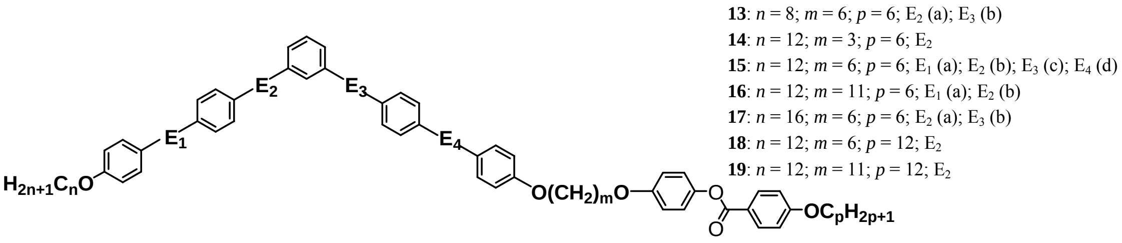

13: n = 8; m = 6; p = 6; E_2 (a); E_3 (b)
14: n = 12; m = 3; p = 6; E_2
15: n = 12; m = 6; p = 6; E_1 (a); E_2 (b); E_3 (c); E_4 (d)
16: n = 12; m = 11; p = 6; E_1 (a); E_2 (b)
17: n = 16; m = 6; p = 6; E_2 (a); E_3 (b)
18: n = 12; m = 6; p = 12; E_2
19: n = 12; m = 11; p = 12; E_2

Figure 9.4: Dimers **13 - 19** with variation of direction of *ester* linking groups $\mathbf{E_x}$ (-COO- or –OOC-) in the bent-core unit.

The variation of direction of *ester* linking groups $\mathbf{E_x}$ (-COO- or –OOC-) in the bent-core unit radically effects the phase behaviour and the clearing points of the non-symmetrical dimer series **13** – **19** (Fig. 9.4). These variations bring about changes as follows:

- A variety of mesophases and new phase sequences occur on reversal of the *ester* linking groups of the reference compounds E_0 (used before in dimers **1**–**12**), i.e. interesting sequences of two nematic phases N – N_x (**13b**), a N – SmA (**15a**) or N – SmA – SmC_x (**17a**), and a SmC_sP_{AF} – $SmC_{s'}P_{AF}$ phase sequence (**18**) on cooling, and an $USmC_aP_{AF}$ phase (**16a**).
- Compounds with an *even* – numbered spacer exhibit a N phase with the exception of the compound **18** (n, p = 12, m = 6) which forms a SmC_sP_{AF} – $SmC_{s'}P_{AF}$ sequence on cooling.
- Nearly all compounds having an *odd* - numbered spacer prefer the formation of Col and undulated $USmC_aP_{AF}$ phases (excepting **16b** which forms a N phase).
- The mesophase stability of all the isomers E_1-E_3 with an *even*-numbered spacer is increased after reversing one of the *carboxylic* groups in the reference compounds E_0. Hence, this concept of designing new molecules allows the preparation of compounds with thermodynamically stable mesophases. The strongest stabilisation has been observed for the isomers E_2 and amounts up to 32 K (compare **4a** with **18**). It is worth mentioning that the directly comparable inversion of the *carboxylic* group E_2 in the corresponding monomeric five-ring bent-core mesogens has a relatively low influence on the mesophase stability.
- Contrarily, for *odd*-spacered isomers E_1-E_2 **14**, **16** and **19** the mesophase stability is slightly decreasing after reversing one of the *carboxylic* groups in the reference compounds E_0 (excepting **19**).
- Similar to the E_0 isomers, with growing length of the terminally attached *alkyloxy-* chains n and p there is the tendency for the clearing temperatures to be reduced.

- Remarkably, a nearly symmetric substitution at terminal chains ($n = 8$; $p = 6$) yielded for the series with the spacer $m = 6$ to an interesting phase sequence of two nematic phases, i.e. a N – N_x transition (**13b**). The results of our investigations point to a N_x phase as found for instance for liquid crystalline bent dimers of *cyanobiphenyl* fragments connected by flexible spacers which has recently been characterized as a nematic phase with a conical twist-bend helical arrangement of the molecules and which has been called nematic twist-bend N_{TB} phase.[39,196,206,245-249]
- Exceptionally, in contrast to conventional calamitic nematics, it was found that the N phases of these new '*banana-calamit*' dimers exhibit a positive dielectric and negative conductivity anisotropy (e.g. dimer **15b**). Different types of electrically driven patterns formation in nematics have been found. These patterns are distinguished by their respective orientation of the convection roles which can be influenced by frequency, voltage amplitude, and temperature.[251,254,255] A field-induced transition from a uniaxial to an optically biaxial N state was found. The biaxially ordered phase persists after the field is removed, but is metastable. The original and the field-induced state can coexist in domains for about 1 h.[253] The measurements on the elastic properties of N phase of **15b** revealed an extremely large anisotropy of BROCHARD-LEGER walls in the splay FRÉEDERICKSZ transition (as compared to similar structures in calamitic N phases). A reasonable explanation is an extremely small twist elastic constant K_{22} of the material as compared to bend elastic constant K_{33}, i.e. being more than one order of magnitude smaller than K_{33}.
- Compound **17a** with long terminal chains ($n + p > 20$; $n = 16$; $p = 6$: N, SmA, SmC_x) behave very different to the symmetrically substituted dimer **18** ($n = 12$; $p = 12$: $SmC_{s'}P_{AF}$–SmC_sP_{AF}).
- The SmA phases of these dimers exhibit also unusual properties. Interestingly, the transition temperature SmC_x - SmA phase of compound **17a** can be increased on applying an electric field, i.e., up to 4 K using 40 V μm^{-1}. For a comparable 'monomeric' bent-core compound an enhancement of 2 K using 35 V μm^{-1} was observed.[257]

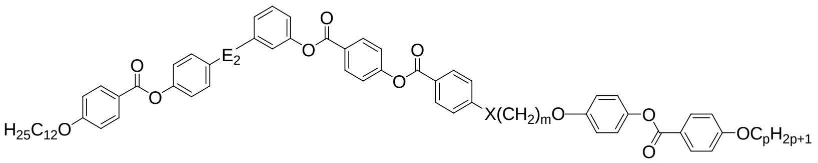

20: $m = 6$; $p = 6$; E_2; X = COO
21: $m = 6$; $p = 12$; E_2; X = COO
22: $m = 11$; $p = 6$; E_2; X = COO
23: $m = 5$; $p = 6$; E_2; X = OOC
24: $m = 5$; $p = 12$; E_2; X = OOC

Figure 9.5: Dimers **20 - 24** with variation of direction of *ester* linking groups $\mathbf{E_2}$ in the bent-core unit in combination with the variation of connecting group **X** (-COO- or -OOC-).

Inversion of direction of second *ester* linking groups $\mathbf{E_2}$ in the bent-core unit, combined with the introduction of different connecting groups ***X*** (-**COO**-/-**OOC**-) resulted in the appearance of new mesophases for dimers **23** and **24** (***X*** = -**OOC**-) and increase of melting points for all the dimers **20** – **24** (Fig. 9.5). These variations bring about changes as follow:

- In spite of the minor differences in the chemical structure a variety of mesophases occur (N, SmC_sP_{AF}, SmC'_sP_{AF}, SmC''_sP_{AF} and polar and non-polar Col_x phases).

- Inversion of $\boldsymbol{E_2}$ group yielded an increase of clearing points (amounts 9 K comparing **8a** and **21** (***X*** = **-COO-**)**,** and up to 30 K comparing **11a** with **24** (***X*** = **-OOC**-).
- Inversion of E_2 yielded the occurrence of a N phase for dimer **23** (***X*** = **-OOC**-), whereas its E_0 analogue **10a** possess a Cr^*P_{FE} phase. Elongation of terminal chain attached to the calamitic moiety resulted in a unique phase sequence SmC_sP_{AF}-SmC'_sP_{AF}-SmC''_sP_{AF} on cooling (**24,** ***X*** = -OOC-).

Introduction of a terminal *cyano* group attached to the bent unit in position *R* (dimers **25**, Fig. 9.6) results in formation of N and SmC_x phases, an optically isotropic phase M_5, a transition N - N_x - M_6 and also in an increase of mesophase stability. The clearing temperatures vary from 145 to 184 °C. Remarkably, independent of the parity of spacer all dimers **25** form N phases with broader temperature regions than the N phases found for analogues dimers **14**–**16** with terminal *alkyloxy*- substituents.

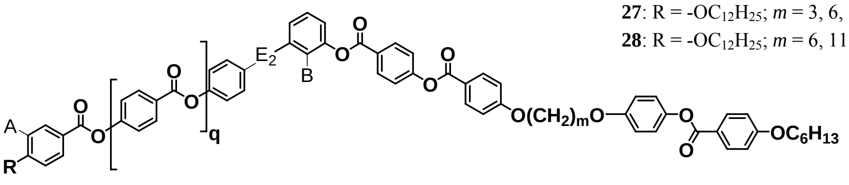

25: R = -CN; *m* = 3, 6, 11; E_2; *A* = H; *B* = H; *q* = 0
26: R = $-OC_{12}H_{25}$; *m* = 3, 6, 11; E_0; *A* = Cl; *B* = H; *q* = 0
27: R = $-OC_{12}H_{25}$; *m* = 3, 6, 11; E_0; *A* = H; *B* = CH_3; *q* = 0
28: R = $-OC_{12}H_{25}$; *m* = 6, 11; E_0; *A* = H; *B* = H; *q* = 1

Figure 9.6: Further variations on the bent-core unit of dimers **25** (**E_2**, R = CN), **26** (A = Cl), **27** (B = CH_3), **28** (q = 1).

Lateral substitution by *chlorine*- in 3-position at the outer ring of the bent-core unit (position **A** in Fig. 9.6) reduces the stability of the mesophases for dimers **26**. The chlorinated derivatives with an *odd*-numbered spacer (*m* = 3, 11) (**26a** and **26c**) exhibit columnar mesophase as well as the non-chlorinated ones (**1b** and **1i**). The *even*- spacered dimer **26b** (*m* = 6) exhibits a N phase, whereas his non-chlorinated analogue compound **1d** forms a N and a columnar phase. At the introduction of a *methyl*- group in the 2-position at the central ring (position **B** in Fig. 9.6) in dimers **27** liquid crystalline behaviour could be found only for dimer **27c** (*m* = 11) which exhibits a $Col_{ob}P_{FE}$ phase, similar to the non-substituted analogue **1i**.

Enlargement of the number of aromatic rings ***q*** in the bent-core mesogenic unit (dimers **28**, Fig. 9.6) dramatically increases the mesophase stability (50 K for dimer **28a** with a six-ring bent-core moiety, comparing to analogue dimer **1d** with five-ring bent-core segment).

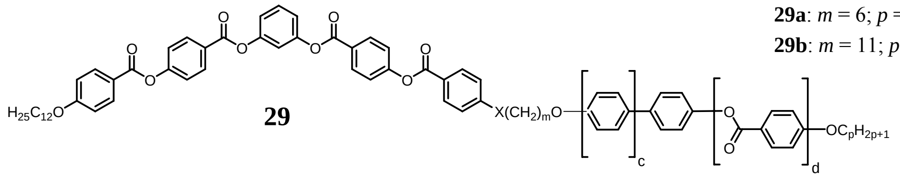

29a: *m* = 6; *p* = 6; *X* = COO; *c* = 1; *d* = 0
29b: *m* = 11; *p* = 8; *X* = O; *c* = 1; *d* = 1

Figure 9.7: Variations on the calamitic mesogenic unit, compounds **29**.

Linking of a bent-core mesogen to calamitic mesogenic units incorporating *biphenylene* units (dimers **29**, Fig. 9.7) results in dimers that exhibit phase sequences N-Col and a stabilization of the mesophase (16 K and resp. 27.5 K comparing to analogues *phenyl benzoates* compounds **7a** and **1i**). Contrarily to the findings for dimers **1**–**6**, the *odd*-numbered spacer dimer **29b** (*m* = 11, *X, Y* = **- O -**) exhibits a N-Col$_{ob}$ phase sequence. Its analogue, dimer **1i** forms a Col$_{ob}$P$_{FE}$ phase.

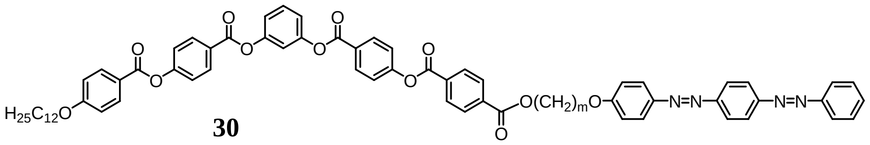

30

30: *m* = 2, 4, 6

Figure 9.8: Variations on the calamitic mesogenic unit, compounds **30**.

Linking of a bent-core mesogen with *bis-azobenzene* segments results in dimers **30** (Fig. 9.8) which exhibit polar smectic phases for all values of spacer *m*. Dimer **30a** (*m* = 2) possesses a SmC$_a$P$_{AF}$ phase, whereas compounds **30b** and **30c** (*m* = 4 and 6) present a SmC$_a$P$_{AF}$-SmC$_s$P$_{FE}$ phase sequence on cooling. The increase of the spacer length *m* results in a mesophase destabilization and in an increase of the layer spacing of the smectic phases. The synclinic – anticlinic phase sequence SmC$_s$–SmC$_a$ found for homologues **30b** and **30c** have been reported so far in an inverse sequence SmC$_a$–SmC$_s$ only for *hockey stick* mesogens and for terminally branched mesogens. The photochemical properties of these dimers proved that irradiation by polarised light induce photo-orientation in thin amorphous films obtained by spin coating.[198]

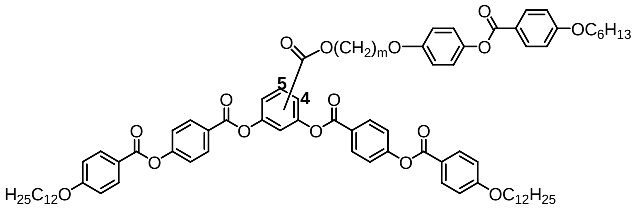

31: *m* = 6, 11; L-5-T
32: *m* = 6, 11; L-4-T

Figure 9.9: Dimers **31** and **32** of **type II** connected *laterally - terminally* (L – T) in the *5* and *4*– position.

The ***lateral - terminal*** covalent linking of *spacer-calamit* unit to the central *resorcinol* fragment of bent-core moiety in *5* – position (**L – *5* - T**) and resp., in *4* - position (**L – *4* - T**) resulted in occurrence of different mesophases and interesting variations of physical properties (dimers of **type II**, **31** and **32**, Fig. 9.9). These variations results in the following findings:

- Connection in *4*-position resulted in formation of SmAP$_{AF}$ phases (dimers **32**). A phase sequence N-SmAP$_{AF}$-SmC$_x$P$_{AF}$ has been observed for compound **32a**. The transition SmAP$_{AF}$-SmC$_x$P$_{AF}$ was found to be first order. The linking in the *5*-position yielded Col$_r$P$_{FE}$ mesophases (**31**), similar to the ***terminally - terminally*** linked analogues dimers **7a** and **9a**. Hence, in this type of connection of the mesogenic units the ferroelectricity is retained. Changing the connecting position from **L–*5*–T** to **L–*4*–T** resulted in a loss of ferroelectricity and appearance of AF polar smectic phases.
- On increasing the length of the spacer *m* of dimers **L–*4*–T** the mesophases are stabilized, contrarily to the tendency found for analogues dimers of **type I** and **L–*5*–T**.
- By the lateral connection a destabilization of mesophases was found. Dimers **31** (**L–*5*-T**) exhibit the lowest mesophase stability. Destabilization of mesophase of dimers with

an *odd*-parity of the spacer amounts 40 K (**31a**, **L–5-T**) and resp., 12 K (**32a**, **L–*4*-T**), in comparison with the transition temperature found for the analogue dimer **7a** (**T-T**).

- Interestingly, for *odd* – parity of the connecting-bridge in **32a** (**L–*4*-T,** m = 6) a nematic phase could be observed, contrarily to the tendency found for analogues dimers **type I**.
- Elongation of the spacer (m = 6 to 11) results in a small increase of parameter a of the Col$_r$ phases of **L–5-T** dimers **31**, while parameter b is slightly decreasing. Simultaneously, a decrease of the number of molecules in the unit cell in the Col$_r$ phases of **31** is determined, i.e. the size of the ribbons of the Col$_r$ phases decrease on increasing the length of the spacer m.

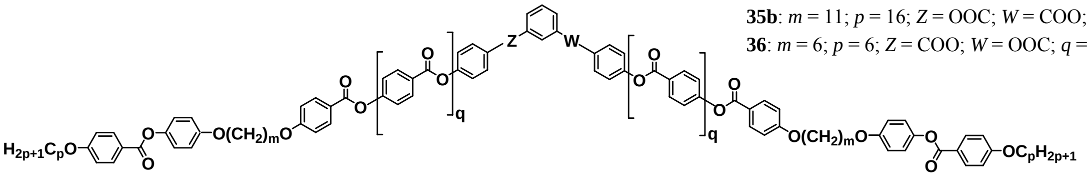

33: m = 3, 6, 11; p = 6; Z = COO; W = OOC; q = 0
34: m = 3, 6, 11; p = 6; Z = OOC; W = COO; q = 0
35a: m = 11; p = 16; Z = COO; W = OOC; q = 0
35b: m = 11; p = 16; Z = OOC; W = COO; q = 0
36: m = 6; p = 6; Z = COO; W = OOC; q = 1

Figure 9.10: General formula of trimers **33-36**, *'calamit – banana - calamit'* of **type I**.

Trimers of **type I** *'calamit – banana - calamit'* with a *resorcinol* unit (**33**, **35a** and **36,** q = 0, 1, Fig. 9.1 and 9.10) and resp., an *isophthalic acid* fragment (**34** and **35b**) exhibit polymorphism variants with phases typical for bent-core molecules ($SmCP_{AF}$), as well as mesophases characteristic for calamitic compounds (N). New polar smectic phases (SmC_cP_{AF}), as well as phase sequences with non-polar and polar phases of special interest, i.e. nematic – smectic, nematic – polar smectic phases appeared, similar to '*banana - calamit*' dimers of **type I**. Similar to the nematic phases of dimers **I** and **II**, these nematic phases exhibit special properties, e.g. special electro-convection pattern, possible field induced transitions into smectic-like phases.

Trimer **33b** with an *even* - numbered spacer (m = 6) and a central *resorcinol* fragment on the bent-core unit presents higher mesophase stability, in analogy to the general tendency found for dimers '*banana - calamit*' of **type I**. Trimer **33b** forms N and smectic phases. Its analogue, dimer **1d**, possesses a N–Col$_x$ phase sequence. The *odd*-numbered trimers **33a** and **33c** exhibit exclusively smectic phases, whereas their analogues dimers **1b** and **1i** (m = 3, 11) exhibit N – polar Col phase sequences.

Inversion of the two *ester* linking groups ***Z*** and ***W*** of the central aromatic ring (Fig. 9.10) results for the *isophthalic acid* derivative trimers **34** in occurrence of N phases for all members and a mesophase stabilization (about 27 K on comparison of **34b** (m = 6) with the analogue trimer **33b**). On increasing the spacer length for trimers with m = 3 (**34a**) to m = 6 (**34b**), the mesophases are stabilized and a SmC phase occurs. However, on further increasing the spacer length to m = 11 (**34c**), a mesophase destabilization could be detected, associated with the appearance of a polar smectic phase.

Further elongation of spacer m and of terminal chain p attached to the calamitic mesogenic units (m = 11; p = 16) yielded smectic phases, several in combination with a N phase. Also a destabilization of the mesophases was determined for trimers **35** (in comparison with analogues

33 and **34**). The inversion of these two *ester* linking groups ***Z*** and ***W*** of the central aromatic ring results in a mesophase stabilization (about 19 K, comparing trimers **35a** and **35b**).

Enhancement of the number of units in the bent-core segment (q = 1) from five to seven rings results in an increased mesophase stability. Trimer **36** exhibits two enantiotropic phases: a N and a smectic phase, in accordance with the analogue trimer **33b** (N-SmC$_x$) and with its overall linear shape (*even*-methylene spacer). Generally, all the polar SmC phases of trimers **33** - **36** are AF and the values of the spontaneous polarisation, P_S, increase on elongating the spacer m and the terminal *alkyloxy*- chain p attached to the calamitic mesogens, similar to the dimers of **type I**. The value of P_S is also increasing on decreasing the temperature.

37a: m = 4; r = 0
37b: m = 4; r = 1
37c: m = 11; r = 1

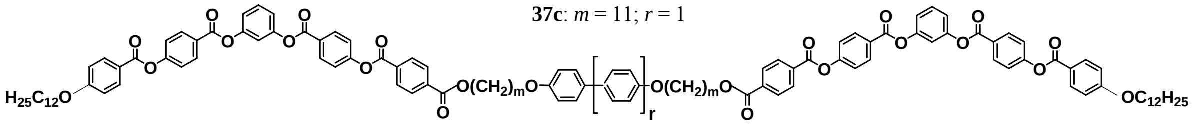

Figure 9.11: Trimers **37** of **type II**, *'banana-calamit–banana'* trimers containing *phenylene* and *biphenylene* units.

The introduction of the *phenylene* and *biphenylene* units in the calamitic moiety of trimers *'banana - calamit – banana'* of **type II** (trimers **37**, Fig. 9.1 and Fig. 9.11) resulted in occurrence of only smectic phases for an *odd* number of single units per spacer segment. Interestingly, for trimers **37a** and **37b** it was found that despite the smaller size of the *1,4*-disubstituted *benzene* ring (trimer **37a**; r = 0) in comparison to the *4,4'-biphenylene* unit (trimer **37b**; r = 1) these compounds have a relatively similar mesophase stability.

38: m = 2, 4, 5, 6

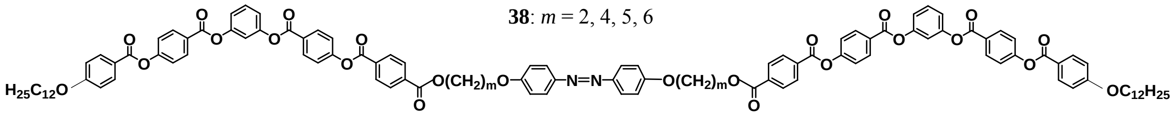

Figure 9.12: Trimers **38** of **type II**, *'banana-calamit–banana'* trimers containing *azobenzene* segments.

For the *'banana - calamit – banana'* trimeric systems **38** (Fig. 9.12) containing *azobenzene* segments, smectic phases could be found only for the homologues with a spacer length of m = 5 (**38c**: SmC$_x$ - SmC'$_x$), and m = 6 (**38d**: SmC$_a$P$_{AF}$).[198] Trimers **38a** and **38b** with a spacer length m = 2 and 4 exhibit monotropic optically isotropic mesophases. Increasing of the spacer length results in a destabilization of the mesophases. Irradiation with polarised light induces photo-orientation in thin amorphous films obtained by spin-coating of trimer **38d** and the photoinduced order is relatively stable at temperatures below the melting point.

Comparison between the mesophase behaviour of the analogues monomers, dimers and trimers revealed that the trimers show the highest isotropization temperatures followed by the dimers and monomers, as reported for calamitic oligomeric systems.[109] For example, comparing the dimers of **type I, 1b**, **1d** and **1i** with analogues trimers of **type I**, **33a**, **33b** and **33c** a stabilization of the mesophase for the trimeric systems up to 47 K could be determined. Moreover, similar to the calamitic oligomeric systems, the isotropization transition temperatures of the dimers under study show a pronounced alternation, which attenuates on increasing the length of spacer *m* (the *even* – numbered members exhibit the higher values, see dimer series **1**).

Up to now, it was not possible to predict which phases in which sequences will result from the structural variations of banana-shaped mesogens and much more experimental work in this field is needed. Further work would also be justified in the expectation of new materials with exciting properties. The chemical structure of the molecules under study should be further changed, i.e. shorten the terminal *alkyloxy*- chains, decouple the mesogens by longer spacer or chemically different spacer, or change the ratio between bent core and calamitic moieties. For the photochemical properties, the increase of the photo-orientational effect would be of interest. A further elongation of the oligomeric molecules could achieve this. The '*banana – calamit'* dimers as well as the '*banana-calamit-banana*' and resp. '*calamit-banana-calamit*' trimers are suitable materials for studying the boundary between bent-core and calamitic compounds. This is shown by the existence of phase sequences combining nematic and/or SmA phases (characteristic for classical calamitic mesogens) with polar columnar and/or polar smectic phases (typical for bent-core mesogens).

The covalently linking of bent-core mesogens with calamitic moieties via flexible spacers resulting in '*banana – calamit*' dimers, '*banana – calamit –banana*' trimers and '*calamit – banana – calamit*' trimers has been a remarkably successful project. Furthermore, the mesomorphic properties of such oligomeric systems are still of great interest.

10 Experimental Section

10.1 General aspects

The purification and drying of the used solvents was performed according to the methods described in the literature,[293] distilled under inert atmosphere and stored over appropriate size molecular sieves. Thin-layer chromatography (TLC) was performed using aluminium sheets coated with silica gel 60 F_{254} (*Merck*, Germany) and visualised using iodine vapour or under UV-light (λ = 254 nm, resp. 354 nm) or spraying with a solution of *Molybdenum blue* (solution of 12.5 g phosphomolybdic acid, 5g of Cerium (IV) sulphate, 30 ml conc. H_2SO_4 in 470 ml water) followed by heating of the TLC plates. Silica Gel 60 was used for column chromatography purification (average particle size 40-63 µm, for flash chromatography and resp. 63-200 µm, for column chromatography, *Merck*, Germany). Purification steps always lower the yield and the reported chemical yields in this work usually refer to the yield of the final purified product and are not optimized.

The structure of the intermediates and final compounds was confirmed by ^{1}H-NMR and ^{13}C-NMR and by elemental analysis. The elemental analysis was performed by a *Leco* CHNS-932 instrument (*Leco Co.* elemental analyzer, *Leco Co.*, USA). NMR spectra were recorded on a *Varian* Gemini 200 and *Varian* Unity 400 and 500 spectrometers. If not otherwise stated, in this work the spectra of the compounds were made at 27 °C in $CDCl_3$, with TMS $\delta_H = 0$ as the internal standard or residual protic solvent ($CDCl_3$, $\delta_H = 7.26$). Chemical shifts are given in units of parts per million ppm (δ) and expressed relative to the signals of deuterated solvents. Coupling constants (*J*) are reported in Hertz (Hz). In general, the ^{1}H NMR were recorded at 400 MHz; ^{13}C recorded at 100.5 MHz with the central peak of $CDCl_3$ (δ_C =77.0 ppm), as the internal reference. The signal types in ^{1}H-NMR are given using the following nomenclature: s (singlet), d (dublet), t (triplet), q (quartet), m (multiplet) and b (broad peak).

Transition temperatures were determined using a *Linkam* TP 92 (*Linkam*, UK) heating stage or a *Mettler* FP 82 HT (*Mettler-Toledo*, Switzerland) heating stage and control unit in conjunction with a *Nikon* Labophot-2A (*Nikon*, Japan) polarizing microscope and were confirmed using differential scanning calorimetry. The calorimetric measurements were made using a *Perkin Elmer* Pyris 1 (*Perkin Elmer*, *Inc.*, USA) differential scanning calorimeter with a heating-cooling rate of 10 °C·min^{-1} (if no other specified). If no other specified the phase transition of the LC are taken from the first heating scan and are given in °C, while the enthalpy values are given in [kJ/mol]. Photos of the micrographs were taken with the help of a *Nikon Coolpix 5400* digital camera (*Nikon*, Japan).

The assignment of the mesophases is based on combined results of optical textures and X-ray diffraction (XRD). X-ray investigations on powder-like samples were carried out with a Guinier equipment (film camera and goniometer, both by *Huber* Diffraktionstechnik GmbH, Germany) with samples in a temperature controlled heating stage using quartz-monochromatized CuKα radiation (Cu-$K_{\alpha 1}$-radiation; λ = 0.154 nm). The calibration of the film patterns was made with the powder pattern of $Pb(NO_3)_2$. The substances had to be heated, for orientation, into the isotropic liquid during the sample preparation for the X-ray investigations.

The samples for the Guinier measurements were sealed in glass capillaries (with a outside diameter of 0.8 mm to 1 mm and wall thickness of 0.01 mm, manufactured by the *Hilgenberg GmbH*, Germany). Two-dimensional patterns for aligned samples on a temperature controlled heating stage were recorded with a 2D wire detector (*HI-Star, Siemens AG*, Germany). The samples for the 2D measurements were either sealed in same type of glass capillaries (0.8 mm to 1 mm) or were prepared as drops on a glass plate aligned at the sample – glass or at the sample – air interface. Alignment was achieved either in thin capillaries under a magnetic field (B = 1 T) or by slow cooling a small drop of the sample on a glass substrate; the incident X-ray beam was in this case nearly parallel to the glass plate.

In this chapter, in section 10.4, the synthetic procedure and the analytical data for one final compound, dimer **1a**, are given as an example. The synthetic procedures and the analytical data for all the final products and one or two instances of intermediates compounds are given in Appendix. The rest of analytical data is available in the working group of Professor WEISSFLOG. The compounds which are not described here were either commercially available (see list below) or they were available in the inventary of the working group of Professor WEISSFLOG and are described elsewhere (see list below). The methods of purification by means of column chromatography, and/or by destillation or by recrystallization are described for each compound separately.

10.2 Starting materials

The following substances were commercial available and used without further purification:

n-Alkyl bromides (Acros)
α,ω-Dibromoalkanes (Acros)
n-Alkanols (Acros)
α,ω-Bromoalkanols (Acros)
α,ω-Diols (Acros)
Benzyl bromide (Acros)
Benzyl chloride (Acros)
Benzyl 4-hydroxybenzoate (Acros)
4-Benzyloxybenzoic acid
4-(Benzyloxy)phenol (Acros)
16-Bromohexadecanoic acid (Aldrich)
6-Bromohexanoyl chloride (Aldrich)
Caessium carbonate (*Aldrich*)
Chloroform-d (Chemotrade)
3-Chloro-4-hydroxybenzoic acid (Aldrich)
Dimethyl sulfoxide-d6 (Chemotrade)
N,N'-Dicyclohexylcarbodiimide (Fluka)
Diethyl azodicarboxylate (Lancaster)
3, 5-Dihydroxybenzoic acid methyl ester (Acros)

3-Hydroxybenzaldehyde (Acros)
4-Hydroxybenzaldehyde (Acros)
Isophthalic acid (Acros)
Methyl 4-hydroxybenzoate (Acros)
2-Methylresorcinol (Aldrich)
Oxalyl chloride
Palladium on activated carbon (Aldrich) (5%, 10%)
Potassium hydroxide (Acros)
Potassium iodide (Acros)
Potassium carbonate (Acros)
Resorcinol (Aldrich)
Resorcinol monobenzoate
Silica gel 40-63 µm (J. T. Baker)
Silica gel 63-200 µm (J. T. Baker)
Sodium chlorite (Aldrich)
Sodium dihydrogenphosphate monohydrate (Acros)
Sodium hydride (60% dispersion in mineral oil (Acros)
Sodium hydroxide (Merck)
Sodium sulfate anhydrous (Merck)

2, 4-Dihydroxybenzoic acid methyl ester (Acros)
4-Dimethylaminopyridine (Merck)
Ethyl 3-hydroxybenzoate (Merck)
4-Formylbenzoic acid (Aldrich)
Tetrabutylammonium iodide (Fluka)
Triethylamine (Merck)
Thionylchloride
Triphenylphosphine (Acros)

The following compounds were available in our laboratory:
4-(ω-hydroxyalkyloxy)bisazobenzenes[199]
4,4'-*bis*(ω-hydroxyalkyloxy)azobenzenes[200]
4,4'-*bis*(ω-hydroxyalkyloxy)biphenyls[200]
4,4'-*bis*(ω-hydroxyalkyloxy)phenyls[200]

10.3 General procedures

10.3.1 WILLIAMSON etherification

Methode A:[185]
The corresponding phenolic derivative (1 eq.) was dissolved under nitrogen atmosphere in dry dimethylformamide (DMF), dry butan-2-one, dry acetonitrile (CH_3CN) or dry acetone (20-30 ml pro 1 mmol phenol). 1.05 eq. of *n*-alkyl halide (1.05 eq pro phenolic group), pulverized dry potassium carbonate or caesium carbonate (2 – 5 eq.) and catalytic amount potassium iodide or tetrabutylammonium iodide were given to it. The reaction mixture was heated under reflux for 12 - 84 hours (TLC monitoring). For the reactions using DMF as solvent the reaction mixture was heated at 75 -80 °C for 6 - 12 h (TLC monitoring). The cold reaction mixture was poured into ice-water mixture and diluted to the double volume. The organic and aqueous phases were separated. The aqueous phase was extracted 3x with diethylether (and additionally 3x with ethyl acetate for compounds with a low solubility). The unified organic phases were extracted 3x with supersaturated LiCl solution (only for the reaction using DMF as solvent), 3x with water and supersaturated NaCl solution and dried over sodium sulphate (Na_2SO_4) overnight. The method of purification is described for each compound separately.

Methode B:
The sodium hydride NaH (60% dispersion in mineral oil, 1.7 eq.) was suspended in dry DMF (2 ml per 1 mmol phenol) under cooling and nitrogen atmosphere. To the cooled suspension, solution of the corresponding phenol derivative (1 eq.) in dry DMF (1 ml per 1 mmol phenol) was drop-wise added and the resulting mixture stirred until evolution of hydrogen stopped (~30 min.). To the obtained solution, solution of benzyl bromide (1.1 eq.) in dry DMF (1 ml per 1 mmol phenol) was added and the reaction mixture stirred 1h at 0 °C and 1 h at room temperature. The reaction mixture was then poured into water; the resulting precipitate was filtered off and washed with water.

Methode C:
The corresponding phenolic derivative (1 eq.) was dissolved under nitrogen atmosphere in dry ethanol (20-30 ml per 1 mmol phenol). 1.1 eq. of *n*-alkyl halide, pulverized potassium hydroxyde (2 eq.) and catalytic amount potassium iodide were given to it. The reaction mixture was heated at 75 -80 °C for 6 - 12 h. After cooling, the reaction mixture was poured into ice-water mixture. The organic and aqueous phases were separated. The aqueous phase was extracted with diethylether (and additionally with ethyl acetate for compounds with a low solubility). The unified organic phases were extracted twice with water and supersaturated LiCl solution and with supersaturated NaCl solution and dried over Na_2SO_4 overnight.

10.3.2 MITSUNOBU etherification[186,187]

The corresponding phenolic derivative (1 eq.) and triphenylphosphine PPh_3 (1.1 eq.) were dissolved under nitrogen atmosphere in dry THF (20-30 ml per 1 mmol phenol). The reaction mixture was cooled down to 0°C (ice-water bath). A solution of *n*-alkanol (1.1 eq.) in dry THF was added to the cooled reaction mixture. Diethyl azodicarboxylate (DEAD) diluted with THF was dripped to it over ~ 30 – 60 minutes. After giving all DEAD to the reaction, the mixture was stirred at room temperature for about twenty four hours (TLC monitoring). The solvent was evaporated, and diethylether was given to the crude product. White precipitation (triphenylphosphine oxide, $O{=}PPh_3$) forms after two days of stirring at room temperature. The precipitate was filtered off and after evaporation of the solvent the crude product was purified by column chromatography (silica gel, eluent: dichloromethane: chloroform = 1:1 or just dichloromethane) and recrystallization from ethanol and/or *n*-hexane.

10.3.3 STEGLICH esterification[184]

The corresponding acid (1 eq.), the phenolic derivative (1 eq.) and *N,N'*-dicyclohexyl-carbodiimide (DCC, 1.1 eq.) were dissolved under nitrogen atmosphere in dry dichloromethane (20 ml pro 1 mmol acid). Catalytic amount of 4-dimethylaminopyridine (DMAP, a top of spatula) was given to it. It was stirred at room temperature for 6 – 24h (TLC monitoring). The precipitated white crystals (*N,N'*-dicyclohexylurea, DCU) were filtered out and the solvent was evaporated. The crude product was recrystallized from ethyl acetate (or from a mixture of ethyl acetate with ethanol, or dimethylformamide with ethanol) or purified by means of column chromatography.

10.3.4 Esterification via acid chlorides

Methode A:[146]
The corresponding acid (1 eq.) was suspended in dry dichloromethane (20 ml pro 1 mmol acid) and a solution of oxalylchloride in dichloromethane (4 eq., 2M solution in CH_2Cl_2) was added to the suspension, followed by a drop of pyridine. The obtained mixture was heated to reflux and stirred until the suspension cleared out (1 – 2 h). The mixture was cooled to room

temperature. The solvent and the excess of oxalylchloride were removed under reduced pressure. To the crude product dry CH_2Cl_2 was added 2x and removed with traces of reagent in vacuum (or using dry toluene). The obtained crude acylchloride was dissolved in dichloromethane (20 ml pro 1 mmol) and corresponding phenol- derivative (1.1 eq.) was added, followed by catalytic amount of DMAP. Afterwards, 1.3 eq. of triethylamine was added drop-wise to the reaction mixture. The reaction was stirred at room temperature for 12 h, followed by heating under reflux for another 6 – 12 h and observed *via* TLC. The reaction was stopped when all of one of the starting materials disappeared or the TLC showed no further progress. To the reaction mixture was added a 5% aqueous solution of HCl. The resulting layers were separated. The aqueous layers were washed 2x with dichloromethane and the combined organic fractions were washed successively with 5% aqueous solution of HCl, 5% aqueous solution of NaOH (2x, only in cases where low molecular acid or phenol was used in excess in the reaction) and brine. The resulting solution was dried with anhydrous Na_2SO_4, solvent was removed in vacuum.

Methode B:[58]
The corresponding acid (1 eq.) was suspended in dry dichloromethane (20 ml pro 1 mmol acid) and thionylchloride (3 eq.) was added to the suspension and the obtained mixture was heated to reflux and stirred for 2 h. The mixture was cooled to room temperature. The solvent and the excess of thionylchloride were removed under reduced pressure. To the crude product dry toluene was added 2x and removed with traces of reagent in vacuum. After the obtained crude acylchloride was dissolved in dry dichloromethane or toluene (20 ml pro 1 mmol) and corresponding phenol - derivative (1.1 eq.) was added, followed by catalytic amount of DMAP. After addition of triethylamine (1.3 eq.), the reaction mixture was stirred and heated under reflux for another 6 – 12 h and observed via TLC. The reaction was stopped when all of one of the starting materials disappeared or the TLC showed no further progress. To the cold reaction mixture water was added and the resulting layers were separated. The aqueous layers were washed 3x with dichloromethane and the combined organic fractions were washed successively with 5% aqueous solution of HCl, supersaturated solution of $NaHCO_3$ and water. The resulting solution was dried with anhydrous Na_2SO_4. After removal of the solvent in vacuum, the crude product was purified by column chromatography, by destillation or recrystallization.

10.3.5 Oxidation with sodium chlorite[188,189]

The corresponding aldehyde-derivative (1 eq.) and resorcinol (1.3 eq.) were dissolved in THF or in t-Butanol (10 ml pro 1 mmol aldehyde). To this solution, a solution of sodium chlorite ($NaClO_2$, 80%, 5.8 eq.) and sodium dihydrogenphosphate dihydrate ($NaH_2PO_4 \cdot 2\ H_2O$, 3 eq) in 20 ml water (1 ml per 1 mmol $NaClO_2$) was added dropwise over 10 - 30 minutes. The resulting pale yellow reaction mixture was then stirred at room temperature under TLC control. The reaction was stopped when the starting materials disappeared or the TLC showed no further progress. Volatile components were removed in vacuo and the residue was dissolved in water. The aqueous solution was acidified to pH = 2 by adding 1M solution of HCl. The precipitate was filtered, washed with water and *n*-hexane, and dried in vacuum. The crystals were then recrystallized from acetic acid glacial.

10.3.6 Deprotection of benzylether and benzylesters by means of hydrogenolysis

Methode A:[190]

Under a nitrogen atmosphere the corresponding benzyl-protected compound (1 eq.) was suspended or dissolved in THF or ethyl acetate and a catalytic amount of 10% Pd/C (10 mg pro 1 mmol of starting material) was given to it. After purging the solution with nitrogen, hydrogen was led into it. The reaction mixture was stirred for 12 -48 h (TLC monitoring) under hydrogen, at room temperature. The Pd/C catalyst was filtered off of the hot reaction mixture through a pad of Celite. The filter pad was washed with THF or ethyl acetate, and the combined filtrate was concentrated. The remaining solids were purified by means of recrystallization.

Methode B:[191]

The corresponding benzyl-protected compound (1 eq.) was suspended or dissolved in acetone (30 ml pro 1 mmol of starting material) under nitrogen atmosphere and ammonium formate (5 eq. pro 1 mol of protected compound) was added, followed by 10% Pd/C (10 mg pro 1 mmol of starting material). The reaction mixture was stirred and heated to reflux under nitrogen atmosphere and observed by means of TLC. The reaction was stopped when all starting material disappeared, usually after 30 – 60 minutes. The hot mixture was 2x filtered to remove the catalyst through a pad of Celite. In the case of products with low solubility in acetone, hot THF or ethyl acetate were used to wash the filter pad. The combined filtrate was concentrated. In case of deprotection of alcohols, the solvent was removed in vacuum. In case of deprotection of acids the amount of solvent was reduced to 1/2 and the solution poured into mixture of 5% aqueous solution of HCl and ice-water, filtered and the resulting solids were washed 2x with water. The remaining solids were purified by means of recrystallization.

10.3.7 Alkaline hydrolysis of benzyl substituted benzoates

The corresponding benzylated compound was added into a mixture 1:1 of ethanol (or methanol) and water (20 ml pro 1 mmol of starting material), KOH or NaOH (3 eq.), heated to reflux and observed by means of TLC. The reaction was stopped when all starting material disappeared. The cold reaction mixture was poured into ice-water mixture and diluted to the 5 fold volume with water. The resulting solution was then acidified to pH = 2 by adding 5% aqueous solution of HCl. The precipitate was filtered, washed with water and dried in vacuum. The crude product was purified by destillation or recrystallization.

10.4 Synthesis of compound 1a

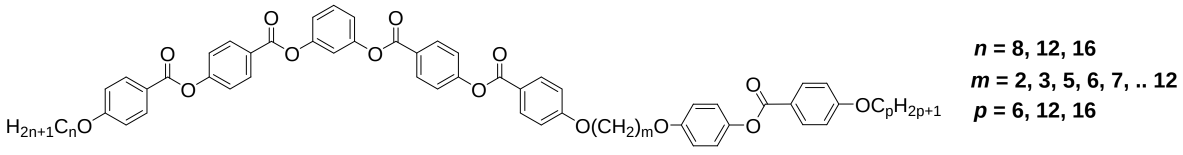

4-(3-{[4-({4-[2-(4-{[4-(Hexyloxy)phenyl]carbonyloxy}phenoxy)ethoxy]phenyl}-carbonyloxy)phenyl]carbonyloxy}phenoxycarbonyl)phenyl 4-(dodecyloxy)benzoate **1a** (*n* = 12, *m* = 2, *p* = 6)

Formula:	$C_{67}H_{70}O_{14}$, M = 1099.30 g/mol
Synthesis:	according to the general procedure 10.3.3
Reagents:	580 mg (0.91 mmol) 4-{3-[(4-hydroxyphenyl)carbonyloxy]phenoxycarbonyl}phenyl 4-(dodecyloxy)benzoate **i9(12)** 440 mg (0.91 mmol) 4-[2-(4-{[4-(hexyloxy)phenyl]carbonyloxy}-phenoxy)ethoxy]benzoic acid **i14(2,6)** 210 mg (1.00 mmol) DCC 5 mg DMAP 40 ml dichloromethane
Purification:	column chromatography, eluent: $CHCl_3$/EtOAc (10/0.2) and further recrystallisation from EtOAc/EtOH (10/0.2)
Yield:	770 mg (77 %), colorless solid
Transition temp.:	Cr 178 (N 163) I
^{1}H-NMR:	($CDCl_3$, *J*/Hz, 400 MHz) δ 8.26 (dd, *J* = 8.8, 2.0 Hz, 4H, Ar-H), 8.21 – 8.08 (m, 6H, Ar-H), 7.48 (t, *J* = 8.0 Hz, 1H, Ar-H), 7.40 – 7.34 (m, 4H, Ar-H), 7.22 – 7.15 (m, 3H, Ar-H), 7.12 (d, *J* = 9.0 Hz, 2H, Ar-H), 7.05 (d, *J* = 8.9 Hz, 2H, Ar-H), 7.02 – 6.91 (m, 6H, Ar-H), 4.45 – 4.34 (m, 4H, OCH_2), 4.03 (q, 6.5 Hz, 4H, OCH_2), 1.88 – 1.75 (m, 4H, $OCH_2C\mathbf{H}_2$), 1.52 – 1.41 (m, 4H, CH_2), 1.41 – 1.20 (m, 20H, CH_2), 0.90 (t, *J* = 6.9 Hz, 3H, CH_3), 0.87 (t, *J* = 6.8 Hz, 3H, CH_3).
^{13}C-NMR:	($CDCl_3$, 100 MHz) δ 165.12, 164.17, 164.06, 163.97, 163.96, 163.75, 163.43, 163.13, 156.03, 155.44, 155.38, 151.39, 145.06, 132.43, 132.37, 132.18, 131.81, 131.80, 129.82, 126.69, 122.68, 122.10, 119.24, 115.78, 115.43, 114.63, 114.44, 114.30, 68.50, 68.43, 66.95, 66.91, 32.06, 31.66, 29.79, 29.77, 29.73, 29.69, 29.50, 29.48, 29.25, 29.23, 26.14, 25.81, 22.84, 22.73, 14.26, 14.16.
EA:	calculated: C: 73.21 %, H: 6.42 %; found: C: 73.20 %, H: 6.41 %

The synthetic procedures and the analytical data for all other final compounds and one or two instances of intermediates are given in the Appendix.

References

1 F. Reinitzer, *Monatsh Chem.,* **1888**, *9*, 421.

2 D. Demus, J. Goodby, G. W. Gray, H.- W. Spiess, V. Vill, *Handbook of Liquid Crystals*, Wiley-VCH, Weinheim, **1998**.

3 M. Baron, *Pure Appl. Chem*., **2001**, *73*, 845.

4 A. J. Leadbetter, in *Thermotropic Liquid Crystals*, *Critical Reports on Applied Chemistry,* ed.: G. W. Gray, Wiley, Chichester, UK, **1987,** *22*, 1.

5 G. W. Gray, J. W. Goodby, *Smectic Liquid Crystals, Textures and Structures*, Leonard Hill, Philadelphia, **1984.**

6 K. Praefcke, D. Blunk, J. Hempel, *Mol. Cryst. Liq. Cryst.*, **1994**, *243*, 323.

7 S. Hoffmann, in *Handbook of Liquid Crystals*, ed. D. Demus, J. Goodby, G. W. Gray, H.-W. Spiess and V. Vill, Wiley-VCH, Weinheim, **1998**, *3*, 393.

8 J. M. Seddon and R. H. Templerin, in *Handbook of Biological Physics,* ed. R. Lipowsky and E. Sackmann, Elsevier, Amsterdam, **1995**, *1*, 97.

9 P. Zugenmaier, in *Handbook of Liquid Crystals*, ed. D. Demus, J. Goodby, G. W. Gray, H.-W. Spiess and V. Vill, Wiley-VCH, Weinheim, **1998**, *3*, 453.

10 C. Tschierske, *Annu. Rep. Prog. Chem., Sect. C: Phys. Chem*., **2001**, *97*, 191.

11 J. W. Goodby, in *Handbook of Liquid Crystals*, ed. D. Demus, J. Goodby, G. W. Gray, H.-W. Spiess and V. Vill, Wiley-VCH, Weinheim, **1998**, *2A*, 3.

12 H.-S. Kitzerow and C. Bahr, *Chirality in Liquid Crystals*, ed. H.-S. Kitzerow and C. Bahr, Springer-Verlag, New York, **2001**.

13 D. Demus, *Liq. Cryst.,* **1989**, *5*, 75.

14 H. R.Brand, P. E. Cladis and H. Pleiner, *Int. J. Eng. Sci.,* **2000**, *38*, 1099.

15 L. A. Madsen, T. J. Dingemans, M. Nakata and E. T. Samulski *Phys. Rev. Lett.,* **2004**, *92*, 145505.

16 B. R. Acharya, A. Primak, S. Kumar, *Phys. Rev. Lett*., **2004**, *92*, 145506.

17 W. Mormann, J. G. Zimmermann, *Liq. Cryst*., **1995**, *19*, 481.

18 S. Chandrasekhar, B. K. Sadashiva, K. A. Suresh, *Pranama*, **1977**, *9*, 471.

19 G. Ungar and X. Zeng, *Soft Matter*, **2005**, *1*, 95.

20 S. Diele and P. Goering, in *Handbook of Liquid Crystals*, ed. D. Demus, J. Goodby, G. W. Gray, H.-W. Spiess and V. Vill, Wiley-VCH, Weinheim, **1998**, *2B*, 887.

21 D. Vorländer, *Ber. Dtsch. Chem. Ges*., **1929**, *62*, 2831.

22 T. Niori, F. Sekine, J. Watanabe, T. Furukawa and H. Takezoe, *J. Mater. Chem.,* **1996**, *6*, 1231.

23 T. Sekine, T. Niori, J. Watanabe, T. Furukawa, S. W. Choi and H. Takezoe, *J. Mater. Chem*., **1997**, *8*, 1307.

24 R. Amaranatha Reddy and C. Tschierske, *J. Mater. Chem.,* **2006**, *16*, 907.

25 J. P. Bedel, J. C Rouillon, J. P. Marcerou, M. Laguerre, M. F. Achard and H. T. Nguyen, *Liq. Cryst*., **2000**, *27*, 103.

26 D. Shen, S. Diele, I. Wirth and C. Tschierske, *Chem. Commun*., **1998**, *23*, 2573.

27 Y. Takanishi, T. Izumi, J. Watanabe, K. Ishikawa, H. Takezoe and A. Iida, *J. Mater. Chem.*, **1999**, *9*, 2771.

28 J. Thisayukta, Y. Nakayama and J. Watanabe, *Liq. Cryst.*, **2000**, *27*, 1129.

29 K. Pelz, W. Weissflog, U. Baumeister and S. Diele, *Liq. Cryst.*, **2003**, *30*, 1151.

30 T. J. Dingemans, N. S. Murthy and E. T. Samulski, *J. Phys. Chem. B*, **2001**, *105*, 8845.

31 G. S. Attard, and A. G. Douglass, *Liq. Cryst.*, **1997**, *22*, 349.

32 G. Pelzl, S. Diele and W. Weissflog, *Adv. Mater.*, **1999**, *11*, 707.

33 C. V. Yelamaggad, I. Shashikala, D. S. S. Rao and S. K. Prasad, *Liq. Cryst.*, **2004**, *31*, 1027.

34 R. Achten, A. Koudijs, Z. Karzcmarzyk, A. T. M. Marcelis and E. J. R. Sudhölter, *Liq. Cryst.*, **2004**, *31*, 215.

35 R. Amaranatha Reddy and B. K. Sadashiva, *J. Mater. Chem.*, **2004**, *14*, 310.

36 H. Takezoe and Y. Takanishi, *Jpn. J. Appl. Phys.*, **2006**, *2A*, 597.

37 A. Eremin, A. Jakli, *Soft Matter*, **2012**, *9*, 615.

38 I. Wirth, S. Diele, A. Eremin, G. Pelzl, S. Grande, L. Kovalenko, N. Pancenko and W. Weissflog, *J. Mater. Chem.*, **2001**, *11*, 1642.

39 M. W. Schröder, S. Diele, G. Pelzl, U. Dunemann, H. Kresse, W. Weissflog, *J. Mater. Chem.*, **2003**, *13*, 1877.

40 G. Gesekus, I. Dierking, S. Gerber, M. Wulf and V. Vill, *Liq. Cryst.*, **2004**, *31*, 145.

41 D. Shen, S. Diele, G. Pelzl, I. Wirth and C. Tschierske, *J. Mater. Chem.*, **1999**, *9*, 661.

42 S. I. Torgova, T. A. Geivandova, O. Francescangeli and A. Strigazzi, *Pramana*, **2003**, *61*, 239.

43 T. J. Dingemans and E. T. Samulski, *Liq. Cryst.*, **2000**, *27*, 131.

44 D. M. Walba, E. Korblova, R. Shao and N. A. Clark, *J. Mater. Chem.*, **2001**, *11*, 2743.

45 C. V. Yelamaggad, U. S. Hiremath, S. A. Nagamani, D. S. S. Rao and S.K. Prasad, *J. Mater. Chem.*, **2001**, *11*, 1818.

46 V. Prasad and A. Jakli, *Liq. Cryst.*, **2004**, *31*, 473.

47 G. Pelzl, I. Wirth and W. Weissflog, *Liq. Cryst.*, **2001**, *28*, 969.

48 R. Amaranatha Reddy, M. W. Schröder, M. Bodyagin, H. Kresse, S. Diele, G. Pelzl and W. Weissflog, Angew. *Chem., Int. Ed.*, **2005**, *44*, 774.

49 H. N. Shreenivasa Murthy and B. K. Sadashiva, *J. Mater. Chem.*, **2005**, *15*, 2056.

50 D. M. Walba, E. Körblova, R. Shao, J. E. Maclennan, D. R. Link, M. A. Glaser and N. A. Clark, *J. Phys. Org. Chem.*, **2000**, *12*, 830.

51 K. Kishikawa, S. Nakahara, Y. Nishikawa, S. Kohmoto and M. Yamamoto, *J. Am. Chem. Soc.*, **2005**, *127*, 2565.

52 J. Malthete, A. M. Levelut and L. Liebert, *Adv. Mater.*, **1992**, *4*, 37.

53 L. Kovalenko, W. Weissflog, S. Grande, S. Diele, G. Pelzl, I. Wirth, *Liq. Cryst.*, **2000**, *27*, 683.

54 W. Weissflog, U. Baumeister, M.-G. Tamba, G. Pelzl, H. Kresse, R. Friedemann, G. Hempel, R. Kurz, M. Roos, K. Merzweiler, A. Jákli, C. Zhang, N. Diorio, R. Stannarius, A. Eremin, U. Kornek, *Soft Matter,* **2012,** *8,* 2671.

55 S. Kang, Y. Saito, N. Watanabe, M. Tokita, Y. Takanishi, H. Takezoe and J. Watanabe, *J. Phys. Chem. B*, **2006**, *110*, 5205.

56 W. Weissflog, U. Dunemann, S. Findeisen-Tandel, M.-G. Tamba, H. Kresse, G. Pelzl, S. Diele, U. Baumeister, A. Eremin, S. Stern and R. Stannarius, *Soft Matter*, **2009**, *5*, 1840.

57 R. Deb, R. K. Nath, M. K. Paul, N. V. S. Rao, F. Tuluri, Y. Shen, R. Shao, D. Chen, C. Zhu, I. I. Smalyukh and N. A. Clark, *J. Mater. Chem*., **2010**, *20*, 7332.

58 R. Achten, R. Cuypers, M. Giesbers, A. Koudijs, A. T. M. Marcelis and E. J. R. Sudhölter, *Liq. Cryst.*, **2004**, *31*, 1167.

59 B. K. Sadashiva, H. N. S. Murthy and S. Dhara, *Liq. Cryst.*, **2001**, *28*, 483.

60 S. Umadevi and B. K. Sadashiva, *Liq. Cryst.,* **2005**, *32*, 287.

61 W. Weissflog, H. Nadasi, U. Dunemann, G. Pelzl, S. Diele, A. Eremin and H. Kresse, *J. Mater. Chem.,* **2001**, *11*, 2748.

62 W. Weissflog, G. Pelzl, *Thermotropic Liquid Crystals: Recent Advances*, ed.Ayyalusamy Ramamoorthy, Springer, **2007**.

63 R. Amaranatha Reddy and B. K. Sadashiva, *J. Mater. Chem*., **2002**, *12*, 2627.

64 G. Pelzl, A. Eremin, S. Diele, H. Kresse and W. Weissflog, *J. Mater. Chem.,* **2002**, *12,* 2591.

65 K. Fodor-Csorba, A. Vajda, G. Galli, A. Jakli, D. Demus, S. Holly, and E. Gacs-Baitz, *Macromol. Chem. Phys*., **2002**, *203,* 1556.

66 M. Kaspar, V. Hamplova, V. Novotna, M. Glogarova, and P. Vanek, *J. Mater. Chem*., **2002**, *12*, 2221.

67 W. Weissflog, L. Kovalenko, I. Wirth, S. Diele, G. Pelzl, H. Schmalfuss, and H. Kresse, *Liq. Cryst*., **2000**, *27*, 667.

68 H. Dehne, M. Potter, S. Sokolowski, W. Weissflog, S. Diele, G. Pelzl, I. Wirth, H. Kresse, H. Schmalfuss, and S. Grande, *Liq. Cryst*., **2001**, *28*, 1269.

69 S. Shubashree, B. K. Sadashiva, S. Dhara, *Liq. Cryst*., **2002**, *29*, 789.

70 R. Amaranatha Reddy and B. K. Sadashiva, *Liq. Cryst.,* **2003**, *30*, 1031.

71 S. Rauch, C. Selbmann, P. Bault, H. Sawade, G. Heppke, O. Morales-Saavedra, M. Y. M. Huang and A. Jakli, *Phys. Rev. E*, **2004**, *69*, 021707.

72 D. M. Walba, E. Korblova, R. Shao, J. E. Maclennan, D. R. Link, M. A. Glaser and N. A. Clark, *Science,* **2000**, *288*, 2181.

73 E. Gorecka, D. Pociecha, J. Mieczkowski, J. Matraszek, D. Guillon and B. Donnio, *J. Am. Chem. Soc.,* **2004**, *126*, 15946.

74 N. Gimeno, M. B. Ros, J. L. Serrano and M. R. de la Fuente, *Angew. Chem. Int. Ed.,* **2004**, *43*, 5235.

75 D. Kardas, M. Prehm, U. Baumeister, D. Pociecha, R. Amaranatha Reddy, G. H. Mehl and C. Tschierske, *J. Mater. Chem.,* **2005**, *15*, 1722.

76 A. Fukuda, Y. Takanishi, T. Ishikawa, K. Ishikawa and H. Takezoe, *J. Mater. Chem*., **1994**, *4*, 997.

77 J. Thisayukta and E. T. Samulski, *J. Mater. Chem*., **2004**, *14,* 1554.

78 D. R. Link, G. Natale, R. Shao, J. E. Maclennan, N. A. Clark, E. Körblova and D. M. Walba, *Science*, **1997**, *278*, 1924.

79 H. R. Brand, P. E. Cladis and H. Pleiner, *Eur. Phys. J. B.*, **1998**, *6*, 347; Erratum: *Eur. Phys. J. B,* **2003**, *31*, 147.

80 L. M. Blinov, *Liq. Cryst.*, **1998**, *24*, 143.

81 T. C. Lubensky, *Mol. Cryst. Liq. Cryst.*, **2001**, *13*, 1.

82 A. Eremin, S. Diele, G. Pelzl, H. Nádasi, W. Weissflog, J. Salfetnikova, H. Kresse, *Phys. Rev. E,* **2001**, *64,* 051707.

83 D. R. Link, N. A. Clark, B. I. Ostrovskii, E. A. Soto Bustamante, *Phys. Rev. E,* **2000**, *61*, R37.

84 D. J. Earl, M. A. Osipov, H. Takezoe, Y. Takanishi and M. R. Wilson, *Phys. Rev. E,* **2005**, *71,* 021706.

85 T. C. Lubensky, A. B. Harris, R. D. Kamien, G. Yan, *Ferroelectrics,* **1998**, *212,* 1.

86 A. B. Harris, R. D. Kamien, T. C. Lubensky, *Rev. Mod. Phys.*, **1999**, *71*, 1745.

87 G. Heppke, A. Jakli and H. Sawade, *Phys. Rev. E,* **1999**, *60*, 5575.

88 G. Dantlgraber, S. Diele and C. Tschierske, *Chem. Commun.*, **2002**, 2768.

89 R. B. Meyer, L. Liebert, L. Strzelecki and P. Keller, *J. Phys. Fr. Lett.*, (Paris), **1975**, *36,* L69.

90 A. D. L. Chandani, Y. Ouchi, H. Takezoe, A. Fukuda, K. Terashima, K. Furukawa and A. Kishi, *Jpn. J. Appl. Phys.*, **1989**, *28*, L1261.

91 R. B. Meyer, *Mol. Cryst. Liq. Cryst.*, **1977**, *40*, 33.

92 S. Diele, H. Grande, H. Kruth, Ch. Lischka, G. Pelzl, W. Weissflog and I. Wirth, *Ferroelectrics,* **1998**, *212,* 169.

93 J. Watanabe, T. Niori, T. Sekine, T. Furukawa and H. Takezoe, *Jpn. J. Appl. Phys.*, **1998**, *37,* L139.

94 J. Szydlowska, J. Mieczkowski, J. Matraszek, D. W. Bruce, E. Gorecka, D. Pociecha and D. Guillon, *Phys. Rev. E,* **2003**, *67*, 031702.

95 J. Mieczkowski, K. Gomola, J. Koseska, D. Pociecha, J. Szydlowska and E. Gorecka, *J. Mater. Chem.*, **2003**, *13,* 2132.

96 C. Tschierske, G. Pelzl, S. Diele and M. Müller, *Angew. Chem.*, **2004**, *116*, 6340.

97 S. Diele, G. Pelzl and W. Weissflog, *Liq. Cryst. Today,* **1999**, *9*, 8.

98 W. Weissflog, I. Wirth, S. Diele, G. Pelzl, H. Schmalfuss, T. Schoss, A. Würflinger, *Liq. Cryst.*, **2001**, *28,* 1603.

99 H.-T. Nguyen, C. Destrade and J. Malthete, in *Handbook of Liquid Crystals*, ed. D. Demus, J. Goodby, G. W. Gray, H.-W. Spiess and V. Vill, Wiley-VCH, Weinheim, **1998**, *2A*, 3865.

100 F. Hardouin, A. M. Levelut, M. F. Achard and G. Sigaud, *J. Chim. Phys.*, **1983**, *80,* 53.

101 G. Pelzl, S. Diele, A. Jakli, C. Lischka, I. Wirth, and W. Weissflog, *Liq. Cryst.*, **1999**, *26,* 135.

102 D. A. Coleman, J. Fernsler, N. Chattham, M. Nakata, Y. Takanishi, E. Korblova, D. R. Link, R.-F. Shao, W. G. Jang, J. E. Maclennan, O. Mondainn-Monval, C. Boyer, W. Weissflog, G. Pelzl, L.-C. Chien, J. Zasadzinski, J. Watanabe, D. M. Walba, H. Takezoe and N. A. Clark, *Science,* **2003**, *301*, 1204.

103 S. W. Choi, Y. Kinoshita, B. Park, H. Takezoe, T. Niori and J. Watanabe, *Jpn. J. Appl.*

Phys., **1998**, *37*, 3408.

104 L. E. Hough , H. -T. Jung , D. Krüerke , M. S. Heberling , M. Nakata , C. D. Jones , D. Chen , D. R. Link , J. Zasadzinski , G. Heppke , J. P. Rabe , W. Stocker , E. Körblova , D. M. Walba , M. A. Glaser , N. A. Clark, *Science*, **2009**, *325*, 456.

105 H. Niwano, M. Nakata, J. Thisayukta, D. R. Link, H. Takezoe and J. Watanabe, *J. Phys. Chem. B,* **2004**, *108,* 14889.

106 V. Prasad, *Liq. Cryst.,* **2001**, *28*, 1115.

107 J. P. Bedel, J. C. Rouillon, J. P. Marcerou, H. T. Nguyen and M. F. Achard, *Phys. Rev. E*, **2004**, *69*, 061702.

108 P. G. de Gennes, *The Physics of Liquid Crystals,* Clarendon Press, Oxford, **1974**, 277.

109 C. T. Imrie, P. A. Henderson and G.-Y. Yeap, *Liq. Cryst.*, **2009**, *36*, 755.

110 C. T. Imrie, P. A. Henderson, *Chem. Soc. Rev*., **2007**, *36*, 2096.

111 C. T. Imrie and P. A. Henderson, *Curr. Opin. Colloid Interface Sci.*, **2002**, *7*, 298.

112 P. A. Henderson, A. G. Cook, C. T. Imrie, *Liq. Cryst*., **2004**, *31*, 1427.

113 A. T. M. Marcelis, A. Koudijs, Z. Karczmarzyk, E. J. R. Sudhölter. *Liq. Cryst*., **2003**, *30*, 1357.

114 Y. S. Park, K.-H. Lee, J.-W. Lee, J.-I. Jin, *Liq. Cryst*., **2003**, *30*, 173.

115 S. Diez, D. A. Dunmur, M. R. de la Fuente, P. K. Karahaliou, G. Mehl, T. Meyer, M. A. P. Jubindo, D. J. Photinos, *Liq. Cryst*., **2003**, *30*, 1021.

116 J. Watanabe, H. Komura and T. Niori, *Liq. Cryst.*, **1993**, *13*, 455.

117 A. C. Griffin and T. R. Britt, *J. Am. Chem. Soc.*, **1981**, *103*, 4957.

118 J. Watanabe, T. Izumi, T. Niori, M. Zennyoji, Y. Takanishi and H. Takezoe, *Mol. Cryst. Liq. Cryst.*, **2000**, *346*, 77.

119 T. Niori, S. Adachi and J. Watanabe, *Liq. Cryst.*, **1995**, *19*, 139.

120 C. T. Imrie and G. R. Luckhurst, in *Handbook of Liquid Crystals*, ed. D. Demus, J. W. Goodby, G. W. Gray, H. W. Spiess and V. Vill, Wiley-VCH, Weinheim, **1998**, 801.

121 J. Watanabe, T. Niori, S.-W. Choi, Y. Takanishi and H. Takezoe, *Jpn. J. Appl. Phys*., **1998**, *37*, L401.

122 S. W. Choi, M. Zennyoji, Y. Takanishi, H. Takezoe, T. Niori and J. Watanabe, *Mol. Cryst. Liq. Cryst.*, **1999**, *328*, 185.

123 G. W. Gray, *The molecular Physics of Liquid Crysyals,* **1979**, *chapter 12*.

124 R. W. Date, C. T. Imrie, G. R. Luckhurst and J. M. Seddon, *Liq. Cryst.*, **1992**, *12*, 203.

125 G. S. Attard, R. W. Date, C. T. Imrie, G. R. Luckhurst, S. J. Roskilly, J. M. Seddon and L. Taylor, *Liq. Cryst.*, **1994**, *16*, 529.

126 A. E. Blatch and G. R. Luckhurst, *Liq. Cryst.*, **2000**, *27*, 775.

127 P. E. Cladis, *Mol. Cryst. Liq. Cryst.*, **1981**, *67*, 177.

128 G. R. Luckhurst, *Liq. Cryst*., **2005**, *32*, 1335.

129 A. E. Blatch, I. D. Fletcher and G. R. Luckhurst, *Liq. Cryst.*, **1995**, *18*, 801.

130 A. del Campo, A. Meyer, E. Pérez, A. Bello, *Liq. Cryst*., **2004**, *31*, 109.

131 S.-L. Wu, S. Senthil, *Liq. Cryst*., **2004**, *31*, 1573.

132 I. Nishiyama, J. Yamamoto, J. W. Goodby, H. Yokoyama, *Liq. Cryst*., **2004**, *31*, 1495.

133 R. Centore, *Liq. Cryst.*, **2007**, *34*, 729.

134 A. Yoshizawa, H. Iwamochi, S. Segawa, M. Sato, *Liq. Cryst.*, **2007**, *34*, 1039.

135 R. Achten, A. Koudijs, M. Giesbers, A. T. M. Marcelis, E. J. R. Sudhölter, M. W. Schröder, W. Weissflog, *Liq. Cryst.*, **2007**, *34*, 59.

136 C. V. Yelamaggad, I. S. Shashikala, U. S. Hiremath, D. S. S. Rao, S. K. Prasad, *Liq. Cryst.*, **2007**, *34*, 153.

137 R. W. Date, D. W. Bruce, *J. Am. Chem. Soc.*, **2003**, *125*, 9012.

138 C. V. Yelamaggad, S. K. Prasad, G. G. Nair, I. S. Shashikala, D. S. S. Rao, C. V. Lobo and S. Chandrasekhar, *Angew. Chem., Int. Ed.*, **2004**, *43*, 3429.

139 C. V. Yelamaggad, I. S. Shashikala, G. X. Liao, D. S. S. Rao, S. K. Prasad, Q. Li and A. Jakli, *Chem. Mater.*, **2006**, *18*, 6100.

140 A. Jakli, G. Liao, I. Shashikala, U. S. Hiremath and C. V. Yelamaggad, *Phys. Rev. E: Stat., Nonlinear, Soft Matter Phys.*, **2006**, *74*, 041706.

141 H. Wang, R. Shao, C. Zhu, B. Bai, C. Gong, P. Zhang, F. Li, M. Li, N. A. Clark, *Liq. Cryst.*, **2008**, *35*, 967.

142 E. Bialecka - Florjanczyk, I. Sledzinska, E. Gorecka, J. Przedmojski, *Liq. Cryst.*, **2008**, *35*, 401.

143 S. M. Morris, M. J. Clarke, A. E. Blatch, H. J. Coles, *Phys. Rev. E.*, **2007**, *75*, 041701.

144 R. M. Srivastava, R. A. W. N. Filho, R. Schneider, A. A. Vieira, H. Gallardo, *Liq. Cryst.*, **2008**, *35*, 737.

145 C. Keith, R. A. Reddy, U. Baumeister, H. Hahn, H. Lang and C. Tschierske, *J. Mater. Chem.*, **2006**, *16*, 3444.

146 B. Kosata, M.-G. Tamba, U. Baumeister, K. Pelz, S. Diele, G. Pelzl, G. Galli, S. Samaritani, E. V. Agina, N. I. Boiko, V. P. Shibaev and W. Weissflog, *Chem. Mater.*, **2006**, *18*, 691.

147 S. Umadevi, B. K. Sadashiva, H. N. Shreenivasa Murthy, V. A. Raghunathan, *Soft Matter*, **2006**, *2*, 210.

148 S. Radhika, B. K. Sadashiva and V. A. Raghunathan, *Liq. Cryst.*, **2013**, *40*, 1209.

149 S. K. Prasad, G. G. Nair, D. S. S. Rao, C. V. Lobo, I. S. Shashikala, C. V. Yelamaggad, *Mol. Cryst. Liq. Cryst.*, **2005**, *437*, 211.

150 H. P. Hinov, Y. G. Marinov, A. G. Petrov, U. S. Hiremath, C. V. Yelamaggad, *J. Optoelectronics Adv. Mater.*, **2009**, *11*, 1194.

151 C. Keith, A. Lehmann, U. Baumeister, M. Prehm, C. Tschierske, *Soft Matter*, **2010**, *6*, 1704.

152 Y. Wang, H. G. Yoon, H. K. Bisoyi, S. Kumar, Q. Li, *J. Mater. Chem.*, **2012**, *22*, 20363.

153 M. Nagaraj, Y. P. Panarin, J. K. Vij, C. Keith and C. Tschierske, *Appl. Phys. Lett.*, **2010**, *97*, 213505.

154 Y. Shombo, Y. Takanishi, K. Ishikawa, E. Gorecka, D. Pociecha, J. Mieczkowski, K. Gomola and H. Takezoe, *Jpn. J. Appl. Phys.*, **2006**, *45*, L282.

155 R. A. Reddy, C. Zhu, R. Shao, E. Korblova, T. Gong, Y. Shen, E. Garcia, M. A. Glaser, J. E. Maclennan, D. M. Walba and N. A. Clark, *Science*, **2011**, *332*, 72.

156 G. Lee, H.-C. Jeong, F. Araoka, K. Ishikawa, J. G. Lee, K.-T. Kang, M. Cepic, H. Takezoe, *Liq. Cryst.*, **2010**, *37*, 883.

157 G. Shanker, M. Prehm, C. Tschierske, *Beilstein J. Org. Chem.*, **2012**, *8*, 472.

158 G. Shanker, M. Prehm, C. Tschierske, *J. Mater. Chem.*, **2012**, *22*, 168.

159 H. R. Brand, P. E. Cladis and H. Pleiner, *Macromolecules*, **1992**, *25*, 7223.

160 M. J. Freiser, *Phys. Rev. Lett.*, **1970**, *24*, 1041.

161 L. J. Yu and A. Saupe, *Phys. Rev. Lett.*, **1980**, *45*, 1000.

162 J. Malthete, H. T. Nguyen and A. M. Levelut, *J. Chem. Soc., Chem. Commun.*, **1986**, 1548.

163 G. R. Luckhurst, *Thin Solid Films*, **2001**, *393*, 40.

164 P. I. C. Teixeira, A. J. Masters and B. M. Mulder, *Mol. Cryst. Liq. Cryst.*, **1998**, *323*, 167.

165 C. V. Yelamaggad, S. Anitha Nagamani, U. S. Hiremath, D. S. Shankar Rao and S. Krishna Prasad, *Liq. Cryst.*, **2002**, *29*, 1401.

166 C. T. Imrie, G. R. Luckhurst, *J. Mater. Chem.*, **1998**, *8*, 1339.

167 W. Kreuder, H. Ringsdorf, O. Herrmann-Schonherr, J. H. Wendorff, *Angew. Chem. Int. Ed. Engl.*, **1987**, *26*, 1249.

168 J. F. Li, V. Percec, C. Rosenblatt, O. D. Lavrentovich, *Europhys. Lett.*, **1994**, *25*, 199.

169 K. Zab, D. Joachimi, E. Novotna, S. Diele, C. Tschierske, *Liq. Cryst.*, **1995**, *18*, 631.

170 G. R. Luckhurst, *Macromol. Symp.*, **1995**, *96*, 1.

171 C. V. Yelamaggad, S. Anitha Nagamani, U. S. Hiremath, D. S. Shankar Rao, S. Krishna Prasad, *Liq. Cryst.*, **2001**, *28*, 1581.

172 A. Yoshizawa, *J. Mater. Chem.*, **2008**, *18*, 2877.

173 C. V. Yelamaggad, I. S. Shashikala and Q. Li, *Chem. Mater.*, **2007,** *19*, 6561.

174 E. Gorecka, M. Nakata, J. Mieczkowski, Y. Takanishi, K. Ishikawa, J. Watanabe, H. Takezoe, S. H. Eichhorn and T. M. Swager, *Phys. Rev. Lett.*, **2000**, *85*, 2526.

175 P. K. Maiti, Y. Lansac, M. A. Glaser and N. A. Clark, *Phys. Rev. Lett.*, **2002**, *88*, 065504.

176 R. Pratibha, N. V. Madhusudana and B. K. Sadashiva, *Science*, **2000**, *288*, 2184.

177 R. Pratibha, N. V. Madhusudana and B. K. Sadashiva, *Phys. Rev. E*, **2005**, *71*, 011701.

178 Y. Takanishi, G. J. Shin, J. C. Jung, S. W. Choi, K. Ishikawa, J. Watanabe, H. Takezoe and P. Toledano, *J. Mater. Chem.*, **2005**, *15*, 4020.

179 A. Jakli, W. Cao, Y. Huang, C. K. Lee and L.-C. Chien, *Liq. Cryst.*, **2001**, *28*, 1279.

180 M. Y. M. Huang, A. M. Pedreira, O. G. Martins, A. M. Figueiredo Neto and A. Jakli, *Phys. Rev. E*, **2002**, *66*, 031708.

181 M. W. Schröder, S. Diele, N. Pancenko, W. Weissflog and G. Pelzl, *J. Mater. Chem.*, **2002**, *12*, 1331.

182 M. W. Schröder, S. Diele, G. Pelzl, N. Pancenko and W. Weissflog, *Liq. Cryst.*, **2002**, *29*, 1039.

183 S. Haddawi, M.-G. Tamba, G. Pelzl, W. Weissflog and U. Baumeister, *Soft Matter*, **2010**, *6*, 1170.

184 B. Neises, W. Steglich, *Angew. Chem.*, **1978**, *90*, 556.

185 S. Coco, P. Espinet, J. M. Martín-Alvarez, A.-M. Levelut, *J. Mater. Chem.*, **1997**, *7*, 19.

186 O. Mitsunobu, Y. Yamada, *Bull. Chem. Soc. Japan,* **1967**, *40*, 2380.

187 D. L. Hughes, *Organic Reactions*, **1992**, *42*, 335.

188 B. O. Lindgren, T. Nilsson, S. Husebye, Y. Mikalsen, K. Leander, C.-G. Swahn, *Acta Chemica Scandinavica*, **1973**, *27*, 888.

189 R. Achten, A. Koudijs, M. Giesbers, A. T. Marcelis, E. J. R. Sudhölter, *Liq. Cryst.*, 2005, **32**, *3*, 277.

190 C. H. Heathcock, R. Ratcliffe, *J. Am. Chem. Soc.*, **1971**, *93*, 1746.

191 T. Bieg, W. Szeja, *Synthesis*, **1985**, 76.

192 W. Weissflog, G. Naumann, B. Kosata, M. W. Schröder, A. Eremin, S. Diele, H. Kresse, R. Friedemann, A. Rama Krishnan, *J. Mater. Chem.*, **2005**, *15*, 4328.

193 H. N. S. Murthy, B. K. Sadashiva, *Liq. Cryst.*, **2004**, *31*, 1347.

194 H. N. S.Murthy and B.K. Sadashiva, *J. Mater. Chem.*, **2004**, *14*, 2813.

195 M. G. Tamba, B. Kosata, K. Pelz, S. Diele, G. Pelzl, Z. Vakhovskaya, H. Kresse, W. Weissflog, *Soft Matter*, **2006**, *2*, 60.

196 M.-G. Tamba, U. Baumeister, G. Pelzl, W. Weissflog, *Liq. Cryst.*, **2010**, *37*, 853.

197 M.-G. Tamba, G. Pelzl, U. Baumeister and W. Weissflog, Ferroelectrics, **2014**, accepted.

198 M.-G. Tamba, A. Bobrovsky, V. Shibaev, G. Pelzl, U. Baumeister, W. Weissflog, *Liq. Cryst.*, **2011**, *38*, 1531.

199 U. Rötz, J. Lindau, G. Reinhold, F. Kuschel, *Z. Chem.*, **1987**, *27*, 293.

200 U. Rötz, J. Lindau, W. Weissflog, G. Reinhold, W. Unseld, F. Kuschel, *Mol. Cryst. Liq. Cryst.*, **1989**, *170*, 185.

201 P. Martinot-Lagarde, *J. Phys., Lett.*, **1977**, *38*, 1.

202 K. Miyasato, S. Abe, H. Takezoe, A. Fukuda, E. Kuze, *Jpn. J. Appl. Phys.*, **1983**, *22*, L661.

203 A. Immirzi, B. Perini, *Acta Cryst. Sect. A*, **1977**, *33*, 216.

204 A. I. Kitaigorodski, *Molekülkristalle*, Akademieverlag Berlin, **1979**.

205 W. Weissflog, S. Sokolowski, H. Dehne, B. Das, S. Grande, M. W. Schroeder, A. Eremin, S. Diele, G. Pelzl and H. Kresse, *Liq. Cryst.*, **2004**, *31*, 923.

206 I. Dozov, *Europhys. Lett.*, **2002**, *56*, 247.

207 R. Memmer, *Liq. Cryst.*, **2002**, *29*, 483.

208 L. Kovalenko, M. W. Schroeder, R. Amaranatha Reddy, S. Diele, G. Pelzl and W. Weissflog, *Liq. Cryst.*, **2005**, *32*, 857.

209 J. Ortega, M. R. de la Fuente, J. Etxebarria, C. L. Folcia, S. Dıez, J. A. Gallastegui, N. Gimeno, M. B. Ros, and M. A. Perez-Jubindo, *Phys. Rev. E*, **2004**, *69*, 011703.

210 J. Kirchhoff, L. S. Hirst; K. M. Fergusson and M. Hird, *Appl. Phys. Lett.*, **2007**, *90*, 161905.

211 C. Keith, R. Amaranatha Reddy, M. Prehm, U. Baumeister, H. Kresse, J. Lorenzo Chao, H. Hahn, H. Lang, and C. Tschierske, *Chem. Eur. J.*, **2007**, *13*, 2556.

212 C. Keith, G. Dantlgraber, R. Amaranatha Reddy, U. Baumeister, and C. Tschierske, *Chem. Mater.*, **2007,** *19*, 694.

213 M. Nakata, D. R. Link, Y. Takanishi, Y. Takahasi, J. Thisayukta, H. Niwano, D. A. Coleman, J. Watanabe, A. Iida, N. A. Clark, H. Takezoe, *Phys. Rev. E*, **2005**, *71*, 011705.

214 J. Etxebarria, C. L. Folcia, J. Ortega, M. B. Ros, *Phys. Rev. E*, **2003**, *67*, 042702.

215 C. T. Imrie, *Struct. Bonding*, **1999**, *95*, 149.

216 M. Zennyoji, Y. Takanishi, K. Ishikawa, J. Thisayukta, J. Watanabe and H. Takezoe, *J. Mater. Chem.*, **1999**, *9*, 2775.

217 C. L. Folcia, J. Ortega and J. Etxebaria, *Liq. Cryst.*, **2003**, *30*, 1189.

218 M. Avalos, R. Babiano, P. Cintas, J. L. Jimenez and J. C. Palacios, *Tetrahedron: Asymmetry*, **2004**, *15*, 3171.

219 D. M. Walba, in *Topics in Stereochemistr*y, ed. M. M. Green, R. J. M. Nolte, E. W. Meijer, Wiley, **2003**, *42*, 475.

220 P. Pyc, J. Mieczkowski, D. Pociecha, E. Gorecka, B. Donnio and D. Guillon, *J. Mater. Chem.*, **2004**, *14*, 2374.

221 K. D'Have, A. Dahlgren, P. Rudquist, J. P. F. Lagerwall, G. Andersson, M. Matuszczyk, S. T. Lagerwall, R. Dabrowski, W. Drzewinski, *Ferroelectrics*, **2000**, *244*, 415.

222 A. Jakli, C. Lischka, W. Weissflog, G. Pelzl, S. Rauch, G. Heppke, *Ferroelectrics*, **2002**, *243*, 239.

223 S. Lagerwall, A. Dahlgren, P. Jaegemalm, P. Rudquist, K. D.'Have, H. Pauwels, R. Dabrowski, W. Drzewinski, *Adv. Funct. Mater.*, **2001**, *11*, 87.

224 G. Dantlgraber, A. Eremin, S. Diele, A. Hauser, H. Kresse, G. Pelzl, C. Tschierske, *Angew. Chem.*, **2002**, 114, 2514 ; *Angew. Chem. Int. Ed.*, **2002**, *41*, 2408.

225 W. Weissflog, M. W. Schröder, S. Diele, G. Pelzl, *Adv. Mater.*, **2003**, *15*, 630.

226 M. W. Schröder, S. Diele, G. Pelzl, and W. Weissflog, *Chem. Phys. Chem.*, **2004**, *5*, 99.

227 G. Heppke, A. Jakli, S. Rauch, H. Sawade, *Phys. Rev. E*, **1999**, *60*, 5575.

228 N. A. Clark, personal communication.

229 G. Dantlgraber, U. Baumeister, S. Diele, H. Kresse, B. Lühmann, H. Lang, C. Tschierske, *J. Am. Chem. Soc.*, **2002**, *124*, 14852.

230 C. Keith, R. Amaranatha Reddy, A. Hauser, U. Baumeister, C. Tschierske, *J. Am. Chem. Soc.*, **2006**, 128, *9*, 3051.

231 R. Amaranatha Reddy, G. Dantlgraber, U. Baumeister, C. Tschierske, *Angew. Chem.*, **2006**, 118, 1962; *Angew. Chem. Int. Ed.*, **2006**, *45*, 1928.

232 E. L. Eliel, S. H. Wilen, L. N. Mander, *Stereochemistry of Organic Compounds*, Wiley, New York, **1994**, 159.

233 F. Araoka, N. Y. Ha, Y. Kinoshita, B. Park, J. W. Wu, H. Takezoe, *Phys. Rev. Lett.*, **2005**, *94*, 137801.

234 A. Jakli, Y. M. Huang, K. Fodor-Csorba, A. Vajda, G. Galli, S. Diele, G. Pelzl, *Adv. Mater.*, **2003**, *15*, 1606.

235 G. Liao, S. Stojadinovic, G. Pelzl, W. Weissflog, S. Sprunt, A. Jakli, *Phys. Rev. E*, **2005**, *72*, 021710.

236 C. Keith, R. A. Reddy, A. Hauser, U. Baumeister, C. Tschierske, *J. Am. Chem. Soc.*, **2006**, *126*, 3051.

237 M. Spannuth, L. Hough, D. Coleman, C. Jones, M. Nakata, Y. Takanishi, H. Takezoe, J. Watanabe, C. Tschierske, E. Körblova, D. Walba, N. A. Clark, Poster presented at the 9th *International Liquid Crystal Conference*, Ljubljana, July 4 –9, **2004**, Book of Abstracts, SYN-P026.

238 L. E. Hough, N. A. Clark, *Phys. Rev. Lett.*, **2005**, *95*, 107802.

239 A. Eremin, S. Diele, G. Pelzl, H. Nadasi, W. Weissflog, *Phys. Rev. E,* **2003**, *67*, 020702.

240 G. Pelzl, M. W. Schröder, A. Eremin, S. Diele, B. Das, S. Grande, H. Kresse, and W. Weissflog, *Eur. Phys. J. E*, **2006**, *21*, 293.

241 W. Weissflog, U. Dunemann, M. W. Schröder, S. Diele, G. Pelzl, H. Kresse and S. Grande, *J. Mater. Chem*., **2005**, *15*, 939.

242 A. Jakli, D. Krüerke, H. Sawade, G. Heppke, *Phys. Rev. Lett*., **2001**, *86*, 5715.

243 G. Pelzl, H. N. Shreenivasa Murthy, M. W. Schröder, S. Diele, Z. Vakhovskaya, H. Kresse and W. Weissflog, *J. Mater. Chem*., **2006**, *16*, 1702.

244 G. Heppke, D. D. Parghi and H. Sawade, *Liq. Cryst*., **2000**, *27*, 313

245 D. Chen, M. Nakata, R. Shao, M. R. Tuchband, M. Shuai, U. Baumeister, W. Weissflog, D. M. Walba, M. A. Glaser, J. E. MacLennan, N. A. Clark., *Phys. Rev. E*, **2014**, *89*, 022506.

246 P. A. Henderson, C. T. Imrie, *Liq. Cryst*., **2011**, *38*, 1407.

247 M. Cestari, S. Diez-Berart, D. A. Dunmur, A. Ferrarini, M. R. de la Fuente, D. J. B. Jackson, D. O. Lopez, G. R. Luckhurst, M. A. Perez-Jubindo, R. M. Richardson, J. Salud, B. A. Timimi, H. Zimmermann, *Phys. Rev. E,* **2011**, *84*, 031704.

248 M. Sepelj, U. Baumeister, T. Ivsic, A. Lesac, *J Phys Chem B*, **2013**, *117*, 8918.

249 V. P. Panov, M. Nagaraj, J. K. Vij, YuP Panarin, A. Kohlmeier, M. G. Tamba, R. A. Lewis, G. H. Mehl, *Phys. Rev. Lett.*, **2010**, *105*, 167801.

250 K. Praefcke, D. Singer, B. Kohne, M. Ebert, A. Liebmann and H. J. Wendorff, *Liq. Cryst*., **1991**, *10*, 147.

251 M.-G. Tamba, W. Weissflog, A. Eremin, J. Heuer, and R. Stannarius, *Eur. Phys. J. E,* **2007**, *22*, 85.

252 R. Stannarius, A. Eremin, M.-G. Tamba, G. Pelzl, W. Weissflog, *e-Liq. Cryst. Comm*., **2006**.

253 R. Stannarius, A. Eremin, M.-G. Tamba, G. Pelzl, and W. Weissflog, *Phys. Rev. E*, **2007**, *76*, 061704.

254 R. Stannarius and J. Heuer, *Eur. Phys. J. E* , **2007**, *24*, 27.

255 J. Heuer, R. Stannarius, M.-G. Tamba, and W. Weissflog, *Phys. Rev. E*, **2008**, *77***,** 056206.

256 C. Keith, R. Amaranatha Reddy, U. Baumeister and C. Tschierske, *J. Am. Chem. Soc*., **2004**, *126*, 14312.

257 H. N. Shreenivasa Murthy, M. Bodyagin, S. Diele, U. Baumeister, G. Pelzl, W Weissflog, *J. Mater. Chem*., **2006**, *16*, 1634.

258 W. Weissflog, C. Lischka, I. Benne, T. Scharf, G. Pelzl, S. Diele and H. Kruth, *Proc. SPIE: Int. Soc. Opt. Eng*., **1998**, *3319*, 14.

259 D. Shen, A. Pegenau, S. Diele, I. Wirth and C. Tschierske, *J. Am. Chem. Soc*., **2000**, *122*, 1593.

260 F. Hentrich, C. Tschierske, S. Diele, C. Sauer, *J. Mater. Chem*., **1994**, *4*, 1547.

261 O. Nuyken, C. Scherer, A. Baindl, A. R. Brenner, U. Dahn, R. Gaertner, S. Kaiser-Roehrich, R. Kollefrath, P. Matusche, B. Voit, *Prog. Polym. Sci*., **1997**, *22*, 93.

262 A. Bobrovsky, N. Boiko, V. Shibaev, J. Wendorff, *Liq. Cryst*., **2004**, *31*, 351.

263 V. Shibaev, A. Bobrovsky, N. Boiko, *Prog. Polym. Sci.*, **2003**, *28*, 729.

264 F.H. Kreuzer. In *Polymers as Electrooptical and Photooptical Active Media*, edited by V.P. Shibaev, Springer-Verlag, Berlin, **1996**.

265 B. Das, S. Grande, W. Weissflog, A. Eremin, M.W. Schröder, G. Pelzl, S. Diele, H. Kresse, *Liq. Cryst.*, **2003**, *30*, 529.

266 I. Zebger, M. Rutloh, U. Hoffmann, J. Stumpe, H. W. Siesler, S. Hvilsted, *J. Phys. Chem.* A, **2002**, *106*, 3454.

267 S.Yu. Grebenkin, B.V. Bol'shakov, *J Photochem. Photobiol. A, Chemistry*, **2006**, *184*, 155.

268 J. Harden, B. Mbanga, N. Eber, K. Fodor-Csorba, S. Sprunt, J.T. Gleeson, A. Jakli, *Phys. Rev. Lett.*, **2006**, *97*, 157802.

269 D. Wiant, J. T. Gleeson, N. Eber, K. Fodor-Csorba, A. Jakli and T. Toth-Katona, *Phys. Rev. E,* **2005**, *72*, 041712.

270 R. Alben, *J. Chem. Phys*., **1973,** *59*, 4299; *Phys. Rev. Lett*., **1973**, *30*, 778.

271 S. Chandrasekhar, V. N. Raja, and B. K. Sadashiva, *Mol. Cryst. Liq. Cryst. Lett.*, **1990**, *7*, 65.

272 J. Malthete, A.-M. Levelut and Y. C. R. Galerne, *Acad. Sc. Paris*, **1986**, *303*, 1073.

273 J. Hughes, G. Kothe, G. R. Luckhurst, J. Malthete, M. E. Neubert, I. G. Shenouda, B. A. Timimi, and M. Titlebach, *J. Chem. Phys*., **1997**, *107*, 9252.

274 B. R. Acharya, A. Primak, and S. Kumar, *Phys. Rev. Lett.*, **2004**, *92*, 145506.

275 L. A. Madsen, T. J. Dingemans, M. Nakata, and E. T. Samulski, *Phys. Rev. Lett.*, **2004**, *92*, 145505.

276 G. R. Luckhurst, *Nature* (London), **2004**, *430*, 413.

277 J.-H. Lee, T. K. Lim, W. T. Kim, J. I. Jin, *J. Appl. Phys.*, **2007,** *101*, 034105.

278 R. Berardi, L. Muccioli, C. Zannoni, *J. Chem. Phys*., **2008,** *128*, 024905.

279 V. Fréedericksz, V. Zolina, *Z. Kristallogr.*, **1931**, *79*, 225.

280 R. Stannarius, in *Handbook of Liquid Crystals*, edited by D. Demus, J.W. Goodby, G.W. Gray, H.W. Spiess, V. Vill, Wiley-VCH, Weinheim, **1998**, Chap. 2.1., Vol. 2A.

281 C.V. Brown, N.J. Mottram, *Phys. Rev. E*, **2003**, *68*, 031702.

282 L. Leger, *Mol. Cryst. Liq. Cryst*., **1973**, *24*, 33; L. Leger, *Solid State Commun.*, **1972**, *11*, 1499.

283 F. Brochard, *J. Phys. France*, **1972**, *33*, 607; P. Schiller, F. Zeitler, *J. Phys. II France*, **1996**, *6*, 1175.

284 A. Scharkowski, H. Schmiedel, R. Stannarius, E. Weisshuhn, *Z. Naturforschung A*., **1990**, *45*, 37.

285 Á. Buka, N. Éber, W. Pesch, and L. Kramer, in *Self-Assembly, Pattern Formation and Growth Phenomena in Nano-Systems*, edited by A. A. Golovin and A. A. Nepomnyashchy (Springer, Secaucus, NJ), **2006**, 55.

286 I. W. Stewart, *The Static and Dynamic Continuum Theory of Liquid Crystals,* Taylor and Francis, London, **2004**.

287 Á. Buka, B. Dressel, W. Otowski, K. Camara, T. Toth-Katona, L. Kramer, J. Lindau, G. Pelzl, and W. Pesch, *Phys. Rev. E*, **2002**, *66*, 051713.

288 T. John, J. Heuer, and R. Stannarius, *Phys. Rev. E*, **2005**, *71*, 056307.

289 H. Gruler, G. Meier, *Mol. Cryst. Liq. Cryst.*, **1972**, *16*, 299.

290 P. Toth, A. Buka, J. Peinke, and L. Kramer, *Phys. Rev. E*, **1998**, *58*, 1983.

291 J. S. Patel and H. Yokoyama, *Nature* (London), **1993**, *362*, 525.

292 K. Van Le, M. Mathews, M. Chambers, J. Harden, Q. Li, H. Takezoe, and A. Jákli, *Phys. Rev. E*, **2009**, *79*, 030701.

293 Autorenkollektiv, *Organikum*, Deutscher Verlag der Wissenschaften, Leipzig, 20. Auflage **1996**.

Appendix

In the first part of the appendix (A1 – A53) the synthetic procedures and the analytical data for all of the final compounds are given. Similar, one or two instances of each intermediates compounds are given in the second part of the appendix (A54 – A87). The rest of analytical data is available in the working group of Professor WEISSFLOG. The methods of purification by means of column chromatography, and/or by destillation or recrystallization are described for each compound separately.

Final compounds

Compounds 1-6

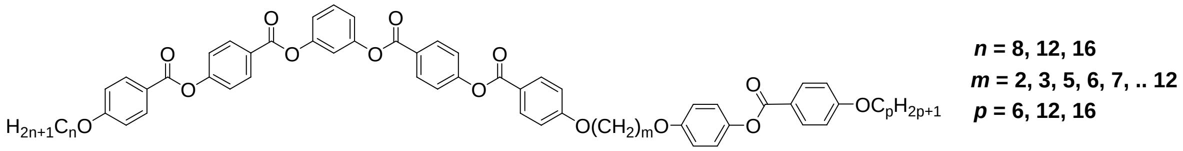

4-(3-{[4-({4-[2-(4-{[4-(Hexyloxy)phenyl]carbonyloxy}phenoxy)ethoxy]phenyl}carbonyloxy)-phenyl]carbonyloxy}phenoxycarbonyl)phenyl 4-(dodecyloxy)benzoate **1a**
(*n* = 12, *m* = 2, *p* = 6)

Formula:	$C_{67}H_{70}O_{14}$, M = 1099.30 g/mol
Synthesis:	according to the general procedure 10.3.3
Reagents:	580 mg (0.91 mmol) 4-{3-[(4-hydroxyphenyl)carbonyloxy]phenoxycarbonyl}phenyl 4-(dodecyloxy)benzoate **i9(12)** 440 mg (0.91 mmol) 4-[2-(4-{[4-(hexyloxy)phenyl]carbonyloxy}phenoxy)ethoxy]benzoic acid **i14(2,6)** 210 mg (1.00 mmol) DCC 5 mg DMAP 40 ml dichloromethane
Purification:	column chromatography, eluent: $CHCl_3$/EtOAc (10/0.2) and further recrystallisation from EtOAc/EtOH (10/0.2)
Yield:	770 mg (77 %), colorless solid
Transition temp.:	Cr 178 (N 163) I
^{1}H-NMR:	($CDCl_3$, *J*/Hz, 400 MHz) δ 8.26 (dd, *J* = 8.8, 2.0 Hz, 4H, Ar-H), 8.21 – 8.08 (m, 6H, Ar-H), 7.48 (t, *J* = 8.0 Hz, 1H, Ar-H), 7.40 – 7.34 (m, 4H, Ar-H), 7.22 – 7.15 (m, 3H, Ar-H), 7.12 (d, *J* = 9.0 Hz, 2H, Ar-H), 7.05 (d, *J* = 8.9 Hz, 2H, Ar-H), 7.02 – 6.91 (m, 6H, Ar-H), 4.45 – 4.34 (m, 4H, OCH_2), 4.03 (q, 6.5 Hz, 4H, OCH_2), 1.88 – 1.75 (m, 4H, $OCH_2\mathbf{CH_2}$), 1.52 – 1.41 (m, 4H, CH_2), 1.41 – 1.20 (m, 20H, CH_2), 0.90 (t, *J* = 6.9 Hz, 3H, CH_3), 0.87 (t, *J* = 6.8 Hz, 3H, CH_3).
^{13}C-NMR:	($CDCl_3$, 100 MHz) δ 165.12, 164.17, 164.06, 163.97, 163.96, 163.75, 163.43, 163.13, 156.03, 155.44, 155.38, 151.39, 145.06, 132.43, 132.37, 132.18, 131.81, 131.80, 129.82, 126.69, 122.68, 122.10, 119.24, 115.78, 115.43, 114.63, 114.44, 114.30, 68.50, 68.43, 66.95, 66.91, 32.06, 31.66, 29.79, 29.77, 29.73, 29.69, 29.50, 29.48, 29.25, 29.23, 26.14, 25.81, 22.84, 22.73, 14.26, 14.16.
EA:	calculated: C: 73.21 %, H: 6.42 %; found: C: 73.20 %, H: 6.41 %

4-(3-{[4-({4-[3-(4-{[4-(Hexyloxy)phenyl]carbonyloxy}phenoxy)propoxy]phenyl}carbonyloxy)phenyl]carbonyloxy}phenoxycarbonyl)phenyl 4-(dodecyloxy)benzoate **1b**

(*n* = 12, *m* = 3, *p* = 6)

Formula: $C_{68}H_{72}O_{14}$, M = 1113.32 g/mol
Synthesis: according to the general procedure 10.3.3
Reagents: 400 mg (0.63 mmol) 4-{3-[(4-hydroxyphenyl)carbonyloxy]phenoxycarbonyl}phenyl 4-(dodecyloxy)benzoate **i9(12)**
310 mg (0.63 mmol) 4-[3-(4-{[4-(hexyloxy)phenyl]carbonyloxy}phenoxy)propoxy]benzoic acid **i14(3,6)**
140 mg (0.69 mmol) DCC
5 mg DMAP
40 ml dichloromethane
Purification: column chromatography, eluent: $CHCl_3$/EtOAc (10/0.2) and further recrystallisation from EtOAc/EtOH (10/0.2)
Yield: 350 mg (56 %), colorless solid
Transition temp.: Cr 150 (Col$_r$P$_{AF}$ 127) I
^{1}H-NMR: ($CDCl_3$, *J*/Hz, 400 MHz) δ 8.26 (d, *J* = 8.7 Hz, 4H, Ar-H), 8.17 – 8.08 (m, 6H, Ar-H), 7.47 (t, *J* = 8.2 Hz, 1H, Ar-H), 7.37 (dd, *J* = 8.6, 1.3 Hz, 4H, Ar-H), 7.22 (t, *J* = 2.1 Hz, 1H, Ar-H), 7.18 (dd, *J* = 8.2, 2.2 Hz, 2H, Ar-H), 7.11 (d, *J* = 9.0 Hz, 2H, Ar-H), 7.03 – 6.90 (m, 8H, Ar-H), 4.27 (t, *J* = 6.2 Hz, 2H, OCH_2), 4.18 (t, *J* = 6.0 Hz, 2H, OCH_2), 4.04 (q, *J* = 6.5 Hz, 4H, OCH_2), 2.31 (p, *J* = 6.1 Hz, 2H, $OCH_2C\mathbf{H}_2$), 1.86 – 1.77 (m, 4H, $OCH_2C\mathbf{H}_2$), 1.52 – 1.43 (m, 4H, CH_2), 1.42 – 1.24 (m, 20H, CH_2), 0.95 – 0.85 (m, 6H, CH_3).
^{13}C-NMR: ($CDCl_3$, 100 MHz) δ 165.11, 164.16, 164.09, 163.96, 163.89, 163.55, 156.42, 155.60, 155.58, 151.59, 145.00, 132.43, 132.38, 132.16, 131.78, 129.75, 126.80, 126.78, 122.58, 122.05, 121.89, 121.60, 121.22, 119.16, 115.73, 115.30, 114.59, 114.55, 114.39, 68.54, 68.46, 65.03, 64.91, 31.95, 31.58, 29.68, 29.66, 29.61, 29.58, 29.38, 29.35, 29.19, 29.17, 26.05, 25.71, 22.69, 22.58, 14.04, 13.94.
EA: calculated: C: 73.36 %, H: 6.52 %; found: C: 73.39 %, H: 6.48 %

4-[3-({4-[(4-{[5-(4-{[4-(Hexyloxy)phenyl]carbonyloxy}phenoxy)pentyl]oxy}phenyl)carbonyloxy]phenyl}carbonyloxy)phenoxycarbonyl]phenyl 4-(dodecyloxy)benzoate **1c**

(*n* = 12, *m* = 5, *p* = 6)

Formula: $C_{70}H_{76}O_{14}$, M = 1141.38 g/mol
Synthesis: according to the general procedure 10.3.3
Reagents: 560 mg (0.88 mmol) 4-{3-[(4-hydroxyphenyl)carbonyloxy]phenoxycarbonyl}phenyl 4-(dodecyloxy)benzoate **i9(12)**
460 mg (0.88 mmol) 4-{[5-(4-{[4-(hexyloxy)phenyl]carbonyloxy}phenoxy)pentyl]oxy}-benzoic acid **i14(5,6)**
100 mg (0.96 mmol) DCC
5 mg DMAP
40 ml dichloromethane
Purification: column chromatography, eluent: $CHCl_3$/EtOAc (10/0.2) and further recrystallisation from EtOAc/EtOH (10/0.2)
Yield: 680 mg 68 %), colorless solid
Transition temp.: Cr 137 (Col$_{ob}$P$_{AF}$ 132) I
^{1}H-NMR: ($CDCl_3$, *J*/Hz, 400 MHz) δ 8.26 (d, *J* = 8.5 Hz, 4H, Ar-H), 8.17 – 8.08 (m, 6H, Ar-H), 7.48 (t, *J* = 8.1 Hz, 1H, Ar-H), 7.36 (d, *J* = 8.6 Hz, 4H, Ar-H), 7.20 – 7.15 (m, 3H, Ar-H), 7.12 – 7.06 (m, 2H, Ar-H), 7.00 – 6.88 (m, 8H, Ar-H), 4.08 (t, *J* = 6.4 Hz, 2H, OCH_2), 4.06 – 3.97 (m, 6H, OCH_2), 1.95 – 1.76 (m, 8H, $OCH_2C\mathbf{H}_2$), 1.73 – 1.63 (m, 2H, CH_2), 1.52 – 1.41 (m, 4H, CH_2), 1.40 – 1.21 (m, 20H, CH_2), 0.94 – 0.84 (m, 6H, CH_3).
^{13}C-NMR: ($CDCl_3$, 100 MHz) δ 165.17, 164.16, 164.12, 163.96, 163.75, 163.63, 163.38, 156.55, 155.43, 151.39, 144.52, 132.40, 132.37, 132.15, 131.79, 129.81, 126.63, 122.50, 122.09, 121.70,

121.11, 121.00, 119.24, 115.78, 115.11, 114.45, 114.28, 68.50, 68.42, 68.23, 32.05, 31.68, 29.79, 29.77, 29.72, 29.69, 29.49, 29.48, 29.24, 29.23, 29.16, 29.01, 26.13, 25.81, 22.89, 22.83, 22.73, 14.26, 14.16.

EA: calculated: C: 73.66 %, H: 6.71 %; found: C: 73.63 %, H: 6.72 %

4-[3-({4-[(4-{[6-(4-{[4-(Hexyloxy)phenyl]carbonyloxy}phenoxy)hexyl]oxy}phenyl)carbonyloxy]phenyl}carbonyloxy)phenoxycarbonyl]phenyl 4-(dodecyloxy)benzoate **1d** ($n = 12$, $m = 6$, $p = 6$)

Formula: $C_{71}H_{78}O_{14}$, M = 1155.40 g/mol

Synthesis: according to the general procedure 10.3.3

Reagents: 330 mg (0.52 mmol) 4-{3-[(4-hydroxyphenyl)carbonyloxy]phenoxycarbonyl}phenyl 4-(dodecyloxy)benzoate **i9(12)**
280 mg (0.52 mmol) 4-{[6-(4-{[4-(hexyloxy)phenyl]carbonyloxy}phenoxy)hexyl]oxy}-benzoic acid **i14(6,6)**
130 mg (0.62 mmol) DCC
5 mg DMAP
40 ml dichloromethane

Purification: column chromatography, eluent: $CHCl_3$/EtOAc (10/0.2) and further recrystallisation from EtOAc/EtOH (10/0.2)

Yield: 380 mg (63 %), colorless solid

Transition temp.: Cr 148.5 (Col_x 125.5 N 145.5) I

^{1}H-NMR: ($CDCl_3$, *J*/Hz, 400 MHz) δ 8.26 (d, *J* = 8.4 Hz, 4H, Ar-H), 8.16 – 8.08 (m, 6H, Ar-H), 7.48 (t, *J* = 8.1 Hz, 1H, Ar-H), 7.36 (d, *J* = 8.8 Hz, 4H, Ar-H), 7.21 – 7.15 (m, 3H, Ar-H), 7.08 (d, *J* = 9.0 Hz, 2H, Ar-H), 7.00 – 6.87 (m, 8H, Ar-H), 4.09 – 3.95 (m, 8H, OCH_2), 1.90 – 1.76 (m, 8H, $OCH_2C\mathbf{H_2}$), 1.60 – 1.54 (m, 4H, CH_2), 1.51 – 1.41 (m, 4H, CH_2), 1.39 – 1.20 (m, 20H, CH_2), 0.93 – 0.84 (m, 6H, CH_3).

^{13}C-NMR: ($CDCl_3$, 100 MHz) δ 165.23, 164.19, 164.00, 163.74, 163.67, 163.37, 156.59, 155.45, 151.36, 144.41, 132.38, 132.16, 131.82, 126.61, 122.50, 122.10, 121.66, 121.03, 120.93, 115.08, 114.43, 114.29, 68.50, 68.41, 68.28, 32.07, 31.70, 29.81, 29.75, 29.51, 29.37, 29.22, 26.16, 25.97, 25.82, 22.87, 22.76, 14.30, 14.21.

EA: calculated: C: 73.81 %, H: 6.80 %; found: C: 73.91 %, H: 6.90 %

4-[3-({4-[(4-{[7-(4-{[4-(Hexyloxy)phenyl]carbonyloxy}phenoxy)heptyl]oxy}phenyl)carbonyloxy]phenyl}carbonyloxy)phenoxycarbonyl]phenyl 4-(dodecyloxy)benzoate **1e** ($n = 12$, $m = 7$, $p = 6$)

Formula: $C_{72}H_{80}O_{14}$, M = 1169.43 g/mol

Synthesis: according to the general procedure 10.3.3

Reagents: 550 mg (0.86 mmol) 4-{3-[(4-hydroxyphenyl)carbonyloxy]phenoxycarbonyl}phenyl 4-(dodecyloxy)benzoate **i9(12)**
470 mg (0.86 mmol) 4-{[7-(4-{[4-(hexyloxy)phenyl]carbonyloxy}phenoxy)heptyl]oxy}-benzoic acid **i14(7,6)**
190 mg (0.94 mmol) DCC
5 mg DMAP
40 ml dichloromethane

Purification: column chromatography, eluent: $CHCl_3$/EtOAc (10/0.2) and further recrystallisation from EtOAc/EtOH (10/0.2)

Yield: 720 mg (72 %), colorless solid

Transition temp.: Cr 147 ($Col_{ob}P_{AF}$ 132) I

^{1}H-NMR: ($CDCl_3$, *J*/Hz, 400 MHz) δ 8.26 (d, *J* = 8.9 Hz, 4H, Ar-H), 8.16 – 8.08 (m, 6H, Ar-H), 7.47 (t, *J* = 7.9 Hz, 1H, Ar-H), 7.35 (d, *J* = 8.8 Hz, 4H, Ar-H), 7.21 – 7.15 (m, 3H, Ar-H), 7.08 (d, *J* = 9.1 Hz, 2H, Ar-H), 7.00 – 6.88 (m, 8H, Ar-H), 4.08 – 3.99 (m, 6H, OCH_2), 3.96 (t, *J* = 6.5 Hz, 2H, OCH_2), 1.87 – 1.75 (m, 8H, $OCH_2C\mathbf{H}_2$), 1.51 – 1.41 (m, 6H, CH_2), 1.38 – 1.22 (m, 24H, CH_2), 0.93 – 0.83 (m, 6H, CH_3).

^{13}C-NMR: ($CDCl_3$, 100 MHz) δ 165.19, 164.16, 163.96, 163.74, 163.70, 163.36, 156.63, 155.42, 151.37, 144.42, 132.38, 132.14, 131.79, 129.81, 126.61, 122.46, 122.10, 121.69, 121.01, 119.24, 115.78, 115.08, 114.43, 114.26, 68.49, 68.40, 68.38, 32.05, 31.68, 29.79, 29.72, 29.70, 29.49, 29.34, 29.24, 26.14, 26.09, 25.81, 22.84, 22.73, 14.27, 14.17.

EA: calculated: C: 73.95 %, H: 6.90 %; found: C: 73.93 %, H: 6.87 %

4-[3-({4-[(4-{[8-(4-{[4-(Hexyloxy)phenyl]carbonyloxy}phenoxy)octyl]oxy}phenyl)carbonyl-oxy]phenyl}carbonyloxy)phenoxycarbonyl]phenyl 4-(dodecyloxy)benzoate **1f**

(n = 12, m = 8, p = 6)

Formula: $C_{73}H_{82}O_{14}$, M = 1183.46 g/mol

Synthesis: according to the general procedure 10.3.3

Reagents: 540 mg (0.86 mmol) 4-{3-[(4-hydroxyphenyl)carbonyloxy]phenoxycarbonyl}phenyl 4-(dodecyloxy)benzoate **i9(12)**
480 mg (0.86 mmol) 4-{[8-(4-{[4-(hexyloxy)phenyl]carbonyloxy}phenoxy)octyl]oxy}benzoic acid **i14(8,6)**
190 mg (0.93 mmol) DCC
5 mg DMAP
40 ml dichloromethane

Purification: column chromatography, eluent: $CHCl_3$/EtOAc (10/0.2) and further recrystallisation from EtOAc/EtOH (10/0.2)

Yield: 660 mg (65 %), colorless solid

Transition temp.: Cr 141 (Col$_x$ 124 N 136) I

^{1}H-NMR: ($CDCl_3$, J/Hz, 400 MHz) δ 8.26 (d, J = 8.7 Hz, 4H, Ar-H), 8.13 (d, J = 8.9 Hz, 4H, Ar-H), 8.10 (d, J = 8.9 Hz, 2H, Ar-H), 7.47 (t, J = 8.1 Hz, 1H, Ar-H), 7.36 (d, J = 8.7 Hz, 4H, Ar-H), 7.20 – 7.14 (m, 3H, Ar-H), 7.08 (d, J = 9.0 Hz, 2H, Ar-H), 7.00 – 6.87 (m, 8H, Ar-H), 4.07 – 3.99 (m, 6H, OCH_2), 3.95 (t, J = 6.5 Hz, 2H, OCH_2), 1.87 – 1.74 (m, 8H, $OCH_2C\mathbf{H}_2$), 1.53 – 1.22 (m, 32H, CH_2), 0.93 – 0.84 (m, 6H, CH_3).

^{13}C-NMR: ($CDCl_3$, 100 MHz) δ 165.26, 164.23, 164.03, 163.81, 163.79, 163.43, 156.71, 155.48, 151.43, 144.45, 132.40, 132.17, 131.82, 129.84, 126.63, 122.47, 122.12, 121.71, 120.98, 119.26, 115.80, 115.09, 114.44, 114.27, 68.44, 68.38, 68.36, 31.97, 31.60, 29.71, 29.69, 29.64, 29.61, 29.41, 29.32, 29.15, 29.14, 26.04, 25.99, 25.72, 22.75, 22.64, 14.17, 14.07.

EA: calculated: C: 74.09 %, H: 6.98 %; found: C: 74.09 %, H: 6.93 %

4-[3-({4-[(4-{[9-(4-{[4-(Hexyloxy)phenyl]carbonyloxy}phenoxy)nonyl]oxy}phenyl)carbonyl-oxy]phenyl}carbonyloxy)phenoxycarbonyl]phenyl 4-(dodecyloxy)benzoate **1g**

(n = 12, m = 9, p = 6)

Formula: $C_{74}H_{84}O_{14}$, M = 1197.49 g/mol

Synthesis: according to the general procedure 10.3.3

Reagents: 540 mg (0.84 mmol) 4-{3-[(4-hydroxyphenyl)carbonyloxy]phenoxycarbonyl}phenyl 4-(dodecyloxy)benzoate **i9(12)**
480 mg (0.84 mmol) 4-{[9-(4-{[4-(hexyloxy)phenyl]carbonyloxy}phenoxy)nonyl]oxy}-benzoic acid **i14(9,6)**
190 mg (0.92 mmol) DCC
5 mg DMAP
40 ml dichloromethane

Purification: column chromatography, eluent: $CHCl_3$/EtOAc (10/0.2) and further recrystallisation from EtOAc/EtOH (10/0.2)

Yield: 740 mg (74 %), colorless solid

Transition temp.: Cr 136 (Col$_{ob}$P$_{AF}$ 130) I

^{1}H-NMR: ($CDCl_3$, *J*/Hz, 400 MHz) δ 8.26 (dd, *J* = 8.9, 1.0 Hz, 4H, Ar-H), 8.13 (d, *J* = 9.0 Hz, 4H, Ar-H), 8.10 (d, *J* = 9.0 Hz, 2H, Ar-H), 7.48 (t, *J* = 8.2 Hz, 1H, Ar-H), 7.36 (d, *J* = 8.4 Hz, 4H, Ar-H), 7.20 – 7.17 (m, 2H, Ar-H), 7.16 (d, *J* = 2.2 Hz, 1H, Ar-H), 7.08 (d, *J* = 9.1 Hz, 2H, Ar-H), 6.99 – 6.88 (m, 8H, Ar-H), 4.06 – 4.00 (m, 6H, OCH_2), 3.95 (t, *J* = 6.5 Hz, 2H, OCH_2), 1.86 – 1.74 (m, 8H, $OCH_2\mathbf{CH_2}$), 1.52 – 1.42 (m, 8H, CH_2), 1.42 – 1.23 (m, 26H, CH_2), 0.93 – 0.85 (m, 6H, CH_3).

^{13}C-NMR: ($CDCl_3$, 100 MHz) δ 165.19, 164.16, 163.96, 163.75, 163.37, 156.68, 155.44, 151.39, 144.42, 132.37, 132.14, 131.79, 129.81, 126.62, 122.44, 122.10, 121.71, 120.99, 119.24, 115.78, 115.10, 114.44, 114.27, 68.49, 68.46, 68.41, 32.06, 31.69, 29.80, 29.77, 29.73, 29.70, 29.59, 29.50, 29.49, 29.41, 29.24, 26.17, 26.14, 26.12, 25.81, 22.84, 22.73, 14.26, 14.16.

EA: calculated: C: 74.22 %, H: 7.07 %; found: C: 74.22 %, H: 7.10 %

4-[3-({4-[(4-{[10-(4-{[4-(Hexyloxy)phenyl]carbonyloxy}phenoxy)decyl]oxy}phenyl)carbonyloxy]phenyl}carbonyloxy)phenoxycarbonyl]phenyl 4-(dodecyloxy)benzoate **1h**

(*n* = 12, *m* = 10, *p* = 6)

Formula: $C_{75}H_{86}O_{14}$, M = 1211.51 g/mol

Synthesis: according to the general procedure 10.3.3

Reagents:
530 mg (0.83 mmol) 4-{3-[(4-hydroxyphenyl)carbonyloxy]phenoxycarbonyl}phenyl 4-(dodecyloxy)benzoate **i9(12)**
490 mg (0.83 mmol) 4-{[10-(4-{[4-(hexyloxy)phenyl]carbonyloxy}phenoxy)decyl]oxy}-benzoic acid **i14(10,6)**
190 mg (0.91 mmol) DCC
5 mg DMAP
40 ml dichloromethane

Purification: column chromatography, eluent: $CHCl_3$/EtOAc (10/0.2) and further recrystallisation from EtOAc/EtOH (10/0.2)

Yield: 710 mg (71 %), colorless solid

Transition temp.: Cr 130 ($Col_{ob}P_{AF}$ 116 N 129) I

^{1}H-NMR: ($CDCl_3$, *J*/Hz, 400 MHz) δ 8.26 (d, *J* = 8.8 Hz, 4H, Ar-H), 8.13 (d, *J* = 8.9 Hz, 4H, Ar-H), 8.10 (d, *J* = 8.9 Hz, 2H, Ar-H), 7.47 (t, *J* = 8.1 Hz, 1H, Ar-H), 7.35 (d, *J* = 8.8 Hz, 4H, Ar-H), 7.20 – 7.17 (m, 2H, Ar-H), 7.16 (d, *J* = 2.1 Hz, 1H, Ar-H), 7.07 (d, *J* = 9.0 Hz, 2H, Ar-H), 6.99 – 6.86 (m, 8H, Ar-H), 4.07 – 3.99 (m, 6H, OCH_2), 3.94 (t, *J* = 6.5 Hz, 2H, OCH_2), 1.86 – 1.73 (m, 8H, $OCH_2\mathbf{CH_2}$), 1.52 – 1.41 (m, 8H, CH_2), 1.41 – 1.22 (m, 28H, CH_2), 0.93 – 0.84 (m, 6H, CH_3).

^{13}C-NMR: ($CDCl_3$, 100 MHz) δ 165.26, 164.23, 164.03, 163.81, 163.42, 156.73, 155.48, 151.43, 144.43, 132.40, 132.17, 131.82, 129.84, 126.63, 122.45, 122.11, 121.72, 120.99, 119.26, 115.79, 115.09, 114.44, 114.26, 68.45, 68.36, 31.97, 31.60, 29.71, 29.69, 29.64, 29.61, 29.52, 29.40, 29.34, 29.15, 29.14, 26.09, 26.04, 25.72, 22.74, 22.63, 14.16, 14.07.

EA: calculated: C: 74.36 %, H: 7.16 %; found: C: 74.42 %, H: 7.18 %

4-[3-({4-[(4-{[11-(4-{[4-(Hexyloxy)phenyl]carbonyloxy}phenoxy)undecyl]oxy}phenyl)-carbonyloxy]phenyl}carbonyloxy)phenoxycarbonyl]phenyl 4-(dodecyloxy)benzoate **1i**

(*n* = 12, *m* = 11, *p* = 6)

Formula: $C_{76}H_{88}O_{14}$, M = 1225.54 g/mol

Synthesis: according to the general procedure 10.3.3

Reagents:
470 mg (0.73 mmol) 4-{3-[(4-hydroxyphenyl)carbonyloxy]phenoxycarbonyl}phenyl 4-(dodecyloxy)benzoate **i9(12)**
440 mg (0.73 mmol) 4-{[11-(4-{[4-(hexyloxy)phenyl]carbonyloxy}phenoxy)undecyl]oxy}-benzoic acid **i14(11,6)**
170 mg (0.81 mmol) DCC
5 mg DMAP

40 ml dichloromethane

Purification: column chromatography, eluent: $CHCl_3$/EtOAc (10/0.2) and further recrystallisation from EtOAc/EtOH (10/0.2)

Yield: 590 mg (66 %), colorless solid

Transition temp.: Cr 121 $\mathrm{Col_{ob}P_{FE}}$ 132.5 I

^{1}H-NMR: ($CDCl_3$, *J*/Hz, 400 MHz) δ 8.26 (d, *J* = 8.3 Hz, 4H, Ar-H), 8.13 (d, *J* = 8.9 Hz, 4H, Ar-H), 8.10 (d, *J* = 9.0 Hz, 2H, Ar-H), 7.47 (t, *J* = 8.2 Hz, 1H, Ar-H), 7.35 (d, *J* = 8.5 Hz, 4H, Ar-H), 7.20 – 7.16 (m, 2H, Ar-H), 7.15 (d, *J* = 2.1 Hz, 1H, Ar-H), 7.07 (d, *J* = 9.0 Hz, 2H, Ar-H), 6.99 – 6.87 (m, 8H, Ar-H), 4.07 – 3.99 (m, 6H, OCH_2), 3.94 (t, *J* = 6.5 Hz, 2H, OCH_2), 1.86 – 1.74 (m, 8H, $OCH_2C\mathbf{H_2}$), 1.50 – 1.40 (m, 8H, CH_2), 1.39 – 1.23 (m, 30H, CH_2), 0.93 – 0.84 (m, 6H, CH_3).

^{13}C-NMR: ($CDCl_3$, 100 MHz) δ 164.19, 163.98, 163.75, 163.36, 156.68, 155.42, 151.37, 144.37, 132.37, 132.14, 131.80, 129.83, 126.60, 122.43, 122.10, 121.69, 120.96, 119.24, 115.79, 115.09, 114.43, 114.25, 68.49, 68.40, 32.06, 31.69, 29.83, 29.80, 29.78, 29.73, 29.70, 29.67, 29.66, 29.62, 29.50, 29.49, 29.43, 29.24, 26.19, 26.13, 25.81, 22.84, 22.73, 14.27, 14.17.

EA: calculated: C: 74.49 %, H: 7.24 %; found: C: 74.48 %, H: 7.24 %

4-[3-({4-[(4-{[12-(4-{[4-(Hexyloxy)phenyl]carbonyloxy}phenoxy)dodecyl]oxy}phenyl)-carbonyloxy]phenyl}carbonyloxy)phenoxycarbonyl]phenyl 4-(dodecyloxy)benzoate **1j** (n = 12, m = 12, p = 6)

Formula: $C_{77}H_{90}O_{14}$, M = 1239.57 g/mol

Synthesis: according to the general procedure 10.3.3

Reagents: 520 mg (0.81 mmol) 4-{3-[(4-hydroxyphenyl)carbonyloxy]phenoxycarbonyl}phenyl 4-(dodecyloxy)benzoate **i9(12)**

500 mg (0.81 mmol) 4-{[12-(4-{[4-(hexyloxy)phenyl]carbonyloxy}phenoxy)dodecyl]oxy}-benzoic acid **i14(12,6)**

180 mg (0.89 mmol) DCC

5 mg DMAP

40 ml dichloromethane

Purification: column chromatography, eluent: $CHCl_3$/EtOAc (10/0.2) and further recrystallisation from EtOAc/EtOH (10/0.2)

Yield: 820 mg (82 %), colorless solid

Transition temp.: Cr 135 ($\mathrm{SmC_cP_{AF}}$ 121 N 125) I

^{1}H-NMR: ($CDCl_3$, *J*/Hz, 200 MHz) δ 8.26 (d, *J* = 8.7 Hz, 4H, Ar-H), 8.20 – 8.03 (m, 6H, Ar-H), 7.59 – 7.30 (m, 5H, Ar-H), 7.17 – 6.82 (m, 13H, Ar-H), 4.18 – 3.87 (m, 8H, OCH_2), 1.96 – 1.68 (m, 8H, $OCH_2C\mathbf{H_2}$), 1.61 – 1.20 (m, 40H, CH_2), 0.97 – 0.80 (m, 6H, CH_3).

^{13}C-NMR: ($CDCl_3$, 125 MHz) δ 165.29, 164.25, 164.05, 163.80, 163.41, 156.73, 155.46, 151.39, 144.37, 132.38, 132.15, 131.81, 129.84, 126.58, 122.42, 122.10, 121.66, 120.91, 119.25, 115.78, 115.04, 114.39, 114.21, 68.39, 68.37, 68.28, 31.88, 31.51, 29.62, 29.60, 29.52, 29.34, 29.32, 29.25, 29.05, 29.04, 26.01, 25.95, 25.62, 22.64, 22.55, 14.08, 13.98.

EA: calculated: C: 74.61 %, H: 7.32 %; found: C: 74.64 %, H: 7.31 %

4-(3-{[4-({4-[3-(4-{[4-(Hexyloxy)phenyl]carbonyloxy}phenoxy)propoxy]phenyl}carbonyl-oxy)phenyl]carbonyloxy}phenoxycarbonyl)phenyl 4-(octyloxy)benzoate **2a** (n = 8, m = 3, p = 6)

Formula: $C_{64}H_{64}O_{14}$, M = 1057.22 g/mol

Synthesis: according to the general procedure 10.3.3

Reagents: 350 mg (0.60 mmol) 4-{3-[(4-hydroxyphenyl)carbonyloxy]phenoxycarbonyl}phenyl 4-(octyloxy)benzoate **i9(8)**

300 mg (0.60 mmol) 4-[3-(4-{[4-(hexyloxy)phenyl]carbonyloxy}phenoxy)propoxy]benzoic acid **i14(3,6)**

140 mg (0.66 mmol) DCC
5 mg DMAP
40 ml dichloromethane

Purification: column chromatography, eluent: $CHCl_3$/EtOAc (10/0.2) and further recrystallisation from EtOAc/EtOH (10/0.2)

Yield: 460 mg (72 %), colorless solid

Transition temp.: Cr 166 (Col_{ob} 134) I

^{1}H-NMR: ($CDCl_3$, *J*/Hz, 400 MHz) δ 8.26 (d, *J* = 8.7 Hz, 4H, Ar-H), 8.17 – 8.13 (m, 4H, Ar-H), 8.11 (d, *J* = 8.9 Hz, 2H, Ar-H), 7.48 (t, *J* = 8.2 Hz, 1H, Ar-H), 7.36 (dd, *J* = 8.7, 1.9 Hz, 4H, Ar-H), 7.20 (t, *J* = 2.0 Hz, 1H, Ar-H), 7.18 (d, *J* = 2.2 Hz, 1H, Ar-H), 7.17 (d, *J* = 2.2 Hz, 1H, Ar-H), 7.10 (d, *J* = 9.0 Hz, 2H, Ar-H), 7.01 (d, *J* = 8.9 Hz, 2H, Ar-H), 6.97 (d, *J* = 8.9 Hz, 2H, Ar-H), 6.96 – 6.92 (m, 4H, Ar-H), 4.26 (t, *J* = 6.1 Hz, 2H, OCH_2), 4.18 (t, *J* = 6.0 Hz, 2H, OCH_2), 4.06 – 4.00 (m, 4H, OCH_2), 2.34 – 2.28 (m, 2H, $OCH_2C\mathbf{H}_2$), 1.85 – 1.77 (m, 4H, $OCH_2C\mathbf{H}_2$), 1.50 – 1.43 (m, 4H, CH_2), 1.39 – 1.26 (m, 12H, CH_2), 0.93 – 0.86 (m, 6H, CH_3).

^{13}C-NMR: ($CDCl_3$, 100 MHz) ($CDCl_3$, 100 MHz) δ 165.31, 164.32, 164.26, 164.11, 163.87, 163.53, 163.52, 156.39, 155.53, 155.50, 151.46, 144.76, 132.50, 132.45, 132.24, 131.88, 129.91, 126.67, 126.65, 122.65, 122.17, 121.64, 121.33, 120.98, 119.31, 115.84, 115.14, 114.49, 114.46, 114.30, 68.43, 68.35, 64.83, 64.61, 31.82, 31.57, 29.34, 29.24, 29.20, 29.11, 29.09, 26.01, 25.68, 22.68, 22.60, 14.12, 14.04.

EA: calculated: C: 72.71 %, H: 6.10 %; found: C: 72.71 %, H: 6.15 %

4-[3-({4-[(4-{[6-(4-{[4-(Hexyloxy)phenyl]carbonyloxy}phenoxy)hexyl]oxy}phenyl)-carbonyloxy]phenyl}carbonyloxy)phenoxycarbonyl]phenyl 4-(octyloxy)benzoate **2b** ($n = 8$, $m = 6$, $p = 6$)

Formula: $C_{67}H_{70}O_{14}$, M = 1099.30 g/mol

Synthesis: according to the general procedure 10.3.3

Reagents: 350 mg (0.60 mmol) 4-{3-[(4-hydroxyphenyl)carbonyloxy]phenoxycarbonyl}phenyl 4-(octyloxy)benzoate **i9(8)**
320 mg (0.60 mmol) 4-{[6-(4-{[4-(hexyloxy)phenyl]carbonyloxy}phenoxy)hexyl]oxy}-benzoic acid **i14(6,6)**
140 mg (0.66 mmol) DCC
5 mg DMAP
40 ml dichloromethane

Purification: column chromatography, eluent: $CHCl_3$/EtOAc (10/0.2) and further recrystallisation from EtOAc/EtOH (10/0.2)

Yield: 460 mg (70 %), colorless solid

Transition temp.: Cr 145 (M_1 125 SmC_sP_{FE} 130) N 151 I

^{1}H-NMR: ($CDCl_3$, *J*/Hz, 400 MHz) δ 8.26 (d, *J* = 8.5 Hz, 4H, Ar-H), 8.14 (dd, *J* = 8.9, 2.0 Hz, 4H, Ar-H), 8.11 (d, *J* = 8.9 Hz, 2H, Ar-H), 7.48 (t, *J* = 8.1 Hz, 1H, Ar-H), 7.36 (d, *J* = 8.8 Hz, 4H, Ar-H), 7.21 – 7.17 (m, 2H, Ar-H), 7.16 (d, *J* = 2.2 Hz, 1H, Ar-H), 7.09 (d, *J* = 9.0 Hz, 2H, Ar-H), 7.01 – 6.94 (m, 5H, Ar-H), 6.94 – 6.88 (m, 3H, Ar-H), 4.09 – 4.00 (m, 6H, OCH_2), 3.98 (t, *J* = 6.4 Hz, 2H, OCH_2), 1.91 – 1.76 (m, 8H, $OCH_2C\mathbf{H}_2$), 1.60 – 1.55 (m, 4H, CH_2), 1.52 – 1.42 (m, 4H, CH_2), 1.40 – 1.24 (m, 12H, CH_2), 0.93 – 0.86 (m, 6H, CH_3).

^{13}C-NMR: ($CDCl_3$, 100 MHz) δ 165.20, 164.17, 163.99, 163.80, 163.73, 163.43, 156.66, 155.48, 151.44, 144.54, 132.39, 132.37, 132.14, 131.78, 129.79, 126.64, 122.46, 122.07, 121.74, 121.09, 121.03, 119.20, 115.75, 115.11, 114.45, 114.27, 68.44, 68.36, 68.24, 31.82, 31.57, 29.34, 29.25, 29.23, 29.09, 26.02, 25.89, 25.83, 25.69, 22.67, 22.60, 14.09, 14.01.

EA: calculated: C: 73.21 %, H: 6.42 %
found: C: 73.38 %, H: 6.46 %

4-[3-({4-[(4-{[11-(4-{[4-(Hexyloxy)phenyl]carbonyloxy}phenoxy)undecyl]oxy}phenyl)-carbonyloxy]phenyl}carbonyloxy)phenoxycarbonyl]phenyl 4-(octyloxy)benzoate **2c** (*n* = 8, *m* = 11, *p* = 6)

Formula:	$C_{72}H_{80}O_{14}$, M = 1169.43 g/mol
Synthesis:	according to the general procedure 10.3.3
Reagents:	350 mg (0.60 mmol) 4-{3-[(4-hydroxyphenyl)carbonyloxy]phenoxycarbonyl}phenyl 4-(octyloxy)benzoate **i9(8)** 360 mg (0.60 mmol) 4-{[11-(4-{[4-(hexyloxy)phenyl]carbonyloxy}phenoxy)undecyl]oxy}-benzoic acid **i14(11,6)** 140 mg (0.66 mmol) DCC 5 mg DMAP 40 ml dichloromethane
Purification:	column chromatography, eluent: $CHCl_3$/EtOAc (10/0.2) and further recrystallisation from EtOAc/EtOH (10/0.2)
Yield:	520 mg (74 %), colorless solid
Transition temp.:	Cr 109 SmC_cP_{FE} 147 I
^{1}H-NMR:	($CDCl_3$, *J*/Hz, 400 MHz) δ 8.26 (d, *J* = 8.9 Hz, 4H, Ar-H), 8.13 (d, *J* = 9.0 Hz, 4H, Ar-H), 8.10 (d, *J* = 9.0 Hz, 2H, Ar-H), 7.47 (t, *J* = 8.0 Hz, 1H, Ar-H), 7.35 (d, *J* = 8.9 Hz, 4H, Ar-H), 7.21 – 7.15 (m, 3H, Ar-H), 7.07 (d, *J* = 9.0 Hz, 2H, Ar-H), 7.00 – 6.94 (m, 5H, Ar-H), 6.94 – 6.87 (m, 3H, Ar-H), 4.06 – 3.99 (m, 6H, OCH_2), 3.94 (t, *J* = 6.5 Hz, 2H, OCH_2), 1.86 – 1.74 (m, 8H, $OCH_2C\mathbf{H_2}$), 1.59 – 1.55 (m, 4H, CH_2), 1.52 – 1.41 (m, 4H, CH_2), 1.40 – 1.23 (m, 22H, CH_2), 0.93 – 0.85 (m, 6H, CH_3).
^{13}C-NMR:	($CDCl_3$, 100 MHz) δ 165.14, 164.13, 163.93, 163.76, 163.37, 156.71, 155.46, 151.43, 144.46, 132.35, 132.12, 131.76, 129.77, 126.64, 122.40, 122.06, 121.79, 121.03, 119.20, 115.75, 115.13, 114.46, 114.28, 68.56, 68.51, 68.36, 31.91, 31.66, 29.62, 29.59, 29.47, 29.43, 29.32, 29.24, 26.18, 26.12, 25.79, 22.77, 22.69, 14.19, 14.11.
EA:	calculated: C: 73.95 %, H: 6.90 %; found: C: 74.03 %, H: 7.02 %

4-(3-{[4-({4-[3-(4-{[4-(Hexyloxy)phenyl]carbonyloxy}phenoxy)propoxy]phenyl}carbonyl-oxy)phenyl]carbonyloxy}phenoxycarbonyl)phenyl 4-(hexadecyloxy)benzoate **3a** (*n* = 16, *m* = 3, *p* = 6)

Formula:	$C_{72}H_{80}O_{14}$, M = 1169.43 g/mol
Synthesis:	according to the general procedure 10.3.3
Reagents:	400 mg (0.58 mmol) 4-{3-[(4-hydroxyphenyl)carbonyloxy]phenoxycarbonyl}phenyl 4-(hexadecyloxy)benzoate **i9(16)** 280 mg (0.58 mmol) 4-[3-(4-{[4-(hexyloxy)phenyl]carbonyloxy}phenoxy)propoxy]benzoic acid **i14(3,6)** 130 mg (0.63 mmol) DCC 5 mg DMAP 40 ml dichloromethane
Purification:	column chromatography, eluent: $CHCl_3$/EtOAc (10/0.2) and further recrystallisation from EtOAc/EtOH (10/0.2)
Yield:	460 mg (68 %), colorless solid
Transition temp.:	Cr 136 ($Col_{ob}P_{FE}$ 129) I
^{1}H-NMR:	($CDCl_3$, *J*/Hz, 400 MHz) δ 8.19 (d, *J* = 8.7 Hz, 4H, Ar-H), 8.10 – 8.02 (m, 6H, Ar-H), 7.41 (t, *J* = 8.2 Hz, 1H, Ar-H), 7.30 (dd, *J* = 8.7, 1.8 Hz, 4H, Ar-H), 7.15 (t, *J* = 2.2 Hz, 1H, Ar-H), 7.11 (dd, *J* = 8.2, 2.2 Hz, 2H, Ar-H), 7.04 (d, *J* = 9.0 Hz, 2H, Ar-H), 6.94 (d, *J* = 8.9 Hz, 2H, Ar-H), 6.91 (d, *J* = 8.9 Hz, 2H, Ar-H), 6.89 – 6.85 (m, 4H, Ar-H), 4.21 (t, *J* = 6.1 Hz, 2H, OCH_2), 4.12 (t, *J* = 6.0 Hz, 2H, OCH_2), 3.97 (q, 6.7 Hz, 4H, OCH_2), 2.27 – 2.21 (m, 2H, $OCH_2C\mathbf{H_2}$), 1.79 – 1.71 (m, 4H, $OCH_2C\mathbf{H_2}$), 1.44 – 1.37 (m, 4H, CH_2), 1.34 – 1.18 (m, 28H, CH_2), 0.86 – 0.79 (m, 6H, CH_3).
^{13}C-NMR:	($CDCl_3$, 125 MHz) δ 165.38, 164.41, 164.35, 164.22, 164.09, 163.74, 156.61, 155.77, 155.75,

151.74, 145.11, 132.64, 132.59, 132.37, 132.00, 129.98, 126.94, 126.92, 122.78, 122.27, 121.98, 121.69, 121.32, 119.39, 115.94, 115.43, 114.73, 114.69, 114.53, 68.65, 68.58, 65.11, 64.96, 32.09, 31.71, 29.85, 29.83, 29.81, 29.74, 29.71, 29.52, 29.51, 29.46, 29.30, 29.28, 26.17, 25.83, 22.83, 22.72, 14.21, 14.10.

EA: calculated: C: 73.95 %, H: 6.90 %; found: C: 73.84 %, H: 6.89 %

4-[3-({4-[(4-{[6-(4-{[4-(Hexyloxy)phenyl]carbonyloxy}phenoxy)hexyl]oxy}phenyl)carbonyloxy]phenyl}carbonyloxy)phenoxycarbonyl]phenyl 4-(hexadecyloxy)benzoate **3b**

($n = 16$, $m = 6$, $p = 6$)

Formula: $C_{75}H_{86}O_{14}$, M = 1211.51 g/mol

Synthesis: according to the general procedure 10.3.3

Reagents: 390 mg (0.56 mmol) 4-{3-[(4-hydroxyphenyl)carbonyloxy]phenoxycarbonyl}phenyl 4-(hexadecyloxy)benzoate **i9(16)**
300 mg (0.56 mmol) 4-{[6-(4-{[4-(hexyloxy)phenyl]carbonyloxy}phenoxy)hexyl]oxy}-benzoic acid **i14(6,6)**
130 mg (0.62 mmol) DCC
5 mg DMAP
40 ml dichloromethane

Purification: column chromatography, eluent: $CHCl_3$/EtOAc (10/0.2) and further recrystallisation from EtOAc/EtOH (10/0.2)

Yield: 520 mg (77 %), colorless solid

Transition temp.: Cr 150 (Col_x 126.5 N 142) I

^{1}H-NMR: ($CDCl_3$, *J*/Hz, 400 MHz) δ 8.26 (d, *J* = 8.4 Hz, 4H, Ar-H), 8.16 – 8.08 (m, 6H, Ar-H), 7.48 (t, *J* = 8.2 Hz, 1H, Ar-H), 7.36 (d, *J* = 8.7 Hz, 4H, Ar-H), 7.20 – 7.17 (m, 2H, Ar-H), 7.16 (d, *J* = 2.2 Hz, 1H, Ar-H), 7.08 (d, *J* = 9.1 Hz, 2H, Ar-H), 7.00 – 6.88 (m, 8H, Ar-H), 4.09 – 4.00 (m, 6H, OCH_2), 3.97 (t, *J* = 6.4 Hz, 2H, OCH_2), 1.90 – 1.76 (m, 8H, $OCH_2C\mathbf{H}_2$), 1.60 – 1.54 (m, 4H, CH_2), 1.51 – 1.41 (m, 8H, CH_2), 1.39 – 1.23 (m, 28H, CH_2), 0.93 – 0.84 (m, 6H, CH_3).

^{13}C-NMR: ($CDCl_3$, 100 MHz) δ 165.06, 164.17, 163.97, 163.75, 163.38, 156.58, 155.43, 151.38, 144.44, 132.39, 132.37, 132.15, 131.79, 129.82, 126.61, 122.47, 122.10, 121.69, 120.99, 119.24, 115.78, 115.10, 114.44, 114.27, 68.41, 68.30, 32.06, 31.68, 29.83, 29.79, 29.72, 29.49, 29.35, 29.24, 29.22, 29.20, 26.13, 26.01, 25.80, 22.84, 22.72, 21.31, 14.26, 14.16.

EA: calculated: C: 74.36, H: 7.16 %; found: C: 74.28, H: 7.15 %

4-[3-({4-[(4-{[11-(4-{[4-(Hexyloxy)phenyl]carbonyloxy}phenoxy)undecyl]oxy}phenyl)-carbonyloxy]phenyl}carbonyloxy)phenoxycarbonyl]phenyl 4-(hexadecyloxy)benzoate **3c**

($n = 16$, $m = 11$, $p = 6$)

Formula: $C_{80}H_{96}O_{14}$, M = 1281.65 g/mol

Synthesis: according to the general procedure 10.3.3

Reagents: 350 mg (0.60 mmol) 4-{3-[(4-hydroxyphenyl)carbonyloxy]phenoxycarbonyl}phenyl 4-(hexadecyloxy)benzoate **i9(16)**
320 mg (0.60 mmol) 4-{[11-(4-{[4-(hexyloxy)phenyl]carbonyloxy}phenoxy)undecyl]oxy}-benzoic acid **i14(11,6)**
140 mg (0.66 mmol) DCC
5 mg DMAP
40 ml dichloromethane

Purification: column chromatography, eluent: $CHCl_3$/EtOAc (10/0.2) and further recrystallisation from EtOAc/EtOH (10/0.2)

Yield: 480 mg (62 %), colorless solid

Transition temp.: Cr 119 ($Col_{ob}P_{AF}$ 109) I

^{1}H-NMR: ($CDCl_3$, *J*/Hz, 400 MHz) δ 8.26 (d, *J* = 8.9 Hz, 4H, Ar-H), 8.16 – 8.08 (m, 6H, Ar-H), 7.48 (t, *J* = 8.2 Hz, 1H), 7.36 (d, *J* = 8.8 Hz, 4H, Ar-H), 7.21 – 7.14 (m, 3H, Ar-H), 7.08 (d, *J* = 9.1

Hz, 2H, Ar-H), 7.00 – 6.87 (m, 8H, Ar-H), 4.08 – 3.99 (m, 6H, OCH_2), 3.94 (t, *J* = 6.5 Hz, 2H, OCH_2), 1.87 – 1.73 (m, 8H, $OCH_2C\mathbf{H}_2$), 1.51 – 1.41 (m, 8H, CH_2), 1.41 – 1.22 (m, 38H, CH_2), 0.93 – 0.84 (m, 6H, CH_3).

^{13}C-NMR: ($CDCl_3$, 100 MHz) δ 165.20, 164.15, 163.96, 163.75, 163.36, 156.69, 155.44, 151.40, 144.41, 132.36, 132.13, 131.79, 129.80, 126.63, 122.42, 122.09, 121.74, 120.99, 119.23, 115.77, 115.10, 114.44, 114.27, 68.53, 68.50, 68.41, 32.06, 31.68, 29.83, 29.79, 29.72, 29.49, 29.25, 26.19, 26.13, 25.81, 22.83, 22.72, 14.25, 14.15.

EA: calculated: C: 74.97, H: 7.55 %; found: C: 74.87, H: 7.80 %

4-[3-({4-[(4-{[6-(4-{[4-(Dodecyloxy)phenyl]carbonyloxy}phenoxy)hexyl]oxy}phenyl)-carbonyloxy]phenyl}carbonyloxy)phenoxycarbonyl]phenyl 4-(dodecyloxy)benzoate **4a** (*n* = 12, *m* = 6, *p* = 12)

Formula: $C_{77}H_{90}O_{14}$, M = 1239.57 g/mol

Synthesis: according to the general procedure 10.3.3

Reagents:
310 mg (0.48 mmol) 4-{3-[(4-hydroxyphenyl)carbonyloxy]phenoxycarbonyl}phenyl 4-(dodecyloxy)benzoate **i9(12)**
300 mg (0.48 mmol) 4-{[6-(4-{[4-(dodecyloxy)phenyl]carbonyloxy}phenoxy)hexyl]oxy}-benzoic acid **i14(6,12)**
110 mg (0.53 mmol) DCC
5 mg DMAP
40 ml dichloromethane

Purification: column chromatography, eluent: $CHCl_3$/EtOAc (10/0.2) and further recrystallisation from EtOAc/EtOH (10/0.2)

Yield: 450 mg (75 %), colorless solid

Transition temp.: Cr 140 (Col_x 115.5 N 131) I

^{1}H-NMR: ($CDCl_3$, *J*/Hz, 400 MHz) δ 8.26 (d, *J* = 8.9 Hz, 4H, Ar-H), 8.14 (dd, *J* = 9.0, 2.1 Hz, 4H, Ar-H), 8.11 (d, *J* = 9.0 Hz, 2H, Ar-H), 7.48 (t, *J* = 8.2 Hz, 1H, Ar-H), 7.36 (d, *J* = 8.8 Hz, 4H, Ar-H), 7.20 – 7.17 (m, 2H, Ar-H), 7.16 (d, *J* = 2.1 Hz, 1H, Ar-H), 7.08 (d, *J* = 9.1 Hz, 2H, Ar-H), 7.00 – 6.94 (m, 4H, Ar-H), 6.94 – 6.88 (m, 4H, Ar-H), 4.09 – 4.00 (m, 6H, OCH_2), 3.97 (t, *J* = 6.4 Hz, 2H, OCH_2), 1.90 – 1.76 (m, 8H, $OCH_2C\mathbf{H}_2$), 1.60 – 1.54 (m, 4H, CH_2), 1.51 – 1.40 (m, *J* = 3.6 Hz, 4H, CH_2), 1.39 – 1.23 (m, 32H, CH_2), 0.90 – 0.84 (m, 6H, CH_3).

^{13}C-NMR: ($CDCl_3$, 100 MHz) δ 164.16, 163.97, 163.75, 162.80, 155.43, 151.38, 132.39, 132.37, 132.14, 131.79, 126.62, 122.47, 122.10, 119.24, 115.10, 114.44, 114.27, 68.50, 68.42, 68.30, 32.05, 31.33, 29.79, 29.77, 29.72, 29.69, 29.49, 29.48, 29.24, 26.13, 26.01, 22.83, 14.26.

EA: calculated: C: 74.61 %, H: 7.32 %; found: C: 74.52 %, H: 7.30 %

4-[3-({4-[(4-{[11-(4-{[4-(Dodecyloxy)phenyl]carbonyloxy}phenoxy)undecyl]oxy}phenyl)-carbonyloxy]phenyl}carbonyloxy)phenoxycarbonyl]phenyl 4-(dodecyloxy)benzoate **4b** (*n* = 12, *m* = 11, *p* = 12)

Formula: $C_{82}H_{100}O_{14}$, M = 1309.70 g/mol

Synthesis: according to the general procedure 10.3.3

Reagents:
290 mg (0.46 mmol) 4-{3-[(4-hydroxyphenyl)carbonyloxy]phenoxycarbonyl}phenyl 4-(dodecyloxy)benzoate **i9(12)**
320 mg (0.46 mmol) 4-{[11-(4-{[4-(dodecyloxy)phenyl]carbonyloxy}phenoxy)undecyl]oxy}-benzoic acid **i14(11,12)**
100 mg (0.50 mmol) DCC
5 mg DMAP
40 ml dichloromethane

Purification: column chromatography, eluent: $CHCl_3$/EtOAc (10/0.2) and further recrystallisation from EtOAc/EtOH (10/0.2)

Yield: 440 mg (73 %), colorless solid

Transition temp.: Cr 126 (Col_rP_{AF} 121) I

^{1}H-NMR: ($CDCl_3$, *J*/Hz, 400 MHz) δ 8.28 – 8.23 (m, 4H, Ar-H), 8.13 (d, *J* = 8.8 Hz, 4H, Ar-H), 8.10 (d, *J* = 9.0 Hz, 2H, Ar-H), 7.47 (t, *J* = 8.4 Hz, 1H, Ar-H), 7.35 (d, *J* = 8.5 Hz, 4H, Ar-H), 7.20 – 7.14 (m, 3H, Ar-H), 7.07 (d, *J* = 9.1 Hz, 2H, Ar-H), 6.99 – 6.87 (m, 8H, Ar-H), 4.06 – 3.99 (m, 6H, OCH_2), 3.94 (t, *J* = 6.5 Hz, 2H, OCH_2), 1.85 – 1.73 (m, 8H, $OCH_2\mathbf{CH_2}$), 1.50 – 1.40 (m, 8H, CH_2), 1.40 – 1.22 (m, 42H, CH_2), 0.90 – 0.84 (m, 6H, CH_3).

^{13}C-NMR: ($CDCl_3$, 100 MHz) δ 164.17, 163.97, 163.75, 155.43, 151.38, 132.37, 132.14, 131.79, 129.81, 126.61, 122.43, 122.09, 120.98, 119.23, 115.78, 115.09, 114.44, 114.26, 68.52, 68.49, 68.41, 32.05, 29.79, 29.77, 29.72, 29.69, 29.65, 29.50, 29.48, 29.25, 26.19, 26.13, 22.83, 14.33, 14.26.

EA: calculated: C: 75.20 %, H: 7.70 %; found: C: 75.08 %, H: 7.60 %

4-[3-({4-[(4-{[12-(4-{[4-(Dodecyloxy)phenyl]carbonyloxy}phenoxy)dodecyl]oxy}phenyl)-carbonyloxy]phenyl}carbonyloxy)phenoxycarbonyl]phenyl 4-(dodecyloxy)benzoate **4c**

(*n* = 12, *m* = 12, *p* = 12)

Formula: $C_{83}H_{102}O_{14}$, M = 1323.73 g/mol

Synthesis: according to the general procedure 10.3.3

Reagents:
480 mg (0.76 mmol) 4-{3-[(4-hydroxyphenyl)carbonyloxy]phenoxycarbonyl}phenyl 4-(dodecyloxy)benzoate **i9(12)**
530 mg (0.76 mmol) 4-{[12-(4-{[4-(dodecyloxy)phenyl]carbonyloxy}phenoxy)dodecyl]oxy}-benzoic acid **i14(12,12)**
180 mg (0.83 mmol) DCC
5 mg DMAP
40 ml dichloromethane

Purification: column chromatography, eluent: $CHCl_3$/EtOAc (10/0.2) and further recrystallisation from EtOAc/EtOH (10/0.2)

Yield: 670 mg (67 %), colorless solid

Transition temp.: Cr 117 (M_3 102 M_2 110 N 114) I

^{1}H-NMR: ($CDCl_3$, *J*/Hz, 200 MHz) δ 8.26 (d, *J* = 8.7 Hz, 4H, Ar-H), 8.18 – 8.06 (m, 6H, Ar-H), 7.48 (t, *J* = 8.0 Hz, 1H, Ar-H), 7.36 (d, *J* = 8.8 Hz, 4H, Ar-H), 7.21 – 7.03 (m, 5H, Ar-H), 7.02 – 6.85 (m, 8H, Ar-H), 4.09 – 3.89 (m, 8H, OCH_2), 1.90 – 1.69 (m, 8H, $OCH_2\mathbf{CH_2}$), 1.52 – 1.19 (m, 52H, CH_2), 0.87 (t, *J* = 6.3 Hz, 6H, CH_3).

^{13}C-NMR: ($CDCl_3$, 100 MHz) δ 165.19, 164.17, 163.97, 163.75, 163.36, 156.69, 155.43, 151.38, 144.38, 132.37, 132.14, 131.80, 129.82, 126.61, 122.43, 122.10, 121.71, 120.97, 119.25, 115.79, 115.09, 114.44, 114.26, 68.53, 68.49, 68.41, 32.06, 29.80, 29.78, 29.73, 29.70, 29.50, 29.44, 29.26, 26.20, 26.14, 22.84, 14.27.

EA: calculated: C: 75.31 %, H: 7.77 %; found: C: 75.41 %, H: 7.79 %

4-(3-{[4-({4-[2-(4-{[4-(Hexadecyloxy)phenyl]carbonyloxy}phenoxy)ethoxy]phenyl}carbonyl-oxy)phenyl]carbonyloxy}phenoxycarbonyl)phenyl 4-(dodecyloxy)benzoate **5a**

(*n* = 12, *m* = 2, *p* = 16)

Formula: $C_{77}H_{90}O_{14}$, M = 1239.57 g/mol

Synthesis: according to the general procedure 10.3.3

Reagents:
360 mg (0.56 mmol) 4-{3-[(4-hydroxyphenyl)carbonyloxy]phenoxycarbonyl}phenyl 4-(dodecyloxy)benzoate **i9(12)**
350 mg (0.56 mmol) 4-[2-(4-{[4-(hexadecyloxy)phenyl]carbonyloxy}phenoxy)ethoxy]-benzoic acid **i14(2,16)**
130 mg (0.62 mmol) DCC
5 mg DMAP
40 ml dichloromethane

Purification: column chromatography, eluent: $CHCl_3$/EtOAc (10/0.2) and further recrystallisation from

EtOAc/EtOH (10/0.2)

Yield: 510 mg (73 %), colorless solid

Transition temp.: Cr 151 (M$_4$ 121 SmC$_s$'P$_{AF}$ 144) SmC$_s$P$_{AF}$ 160.5 N 161 I

^{1}H-NMR: (CDCl$_3$, *J*/Hz, 400 MHz) δ 8.27 (dd, *J* = 8.8, 2.3 Hz, 4H, Ar-H), 8.20 – 8.10 (m, 6H, Ar-H), 7.48 (t, *J* = 8.3 Hz, 1H, Ar-H), 7.38 (d, *J* = 8.6 Hz, 4H, Ar-H), 7.24 – 7.12 (m, 3H, Ar-H), 7.06 (d, *J* = 8.8 Hz, 2H, Ar-H), 7.02 – 6.94 (m, 8H, Ar-H), 4.46 – 4.36 (m, 4H, OCH$_2$), 4.05 (q, *J* = 6.7 Hz, 4H, OCH$_2$), 1.87 – 1.78 (m, 4H, OCH$_2$C**H**$_2$), 1.48 – 1.44 (m, 4H, CH$_2$), 1.41 – 1.23 (m, 40H, CH$_2$), 0.92 – 0.86 (m, 6H, CH$_3$).

^{13}C-NMR: (CDCl$_3$, 100 MHz) δ = δ 165.09, 164.17, 164.05, 163.97, 163.90, 163.58, 163.29, 156.17, 155.61, 155.55, 151.60, 145.35, 132.45, 132.39, 132.19, 131.79, 129.76, 126.85, 126.78, 122.67, 122.05, 121.96, 121.84, 121.23, 119.17, 115.74, 115.61, 114.76, 114.55, 114.41, 68.54, 68.48, 67.13, 67.01, 31.96, 29.72, 29.70, 29.68, 29.66, 29.61, 29.58, 29.39, 29.37, 29.36, 29.21, 29.20, 26.06, 22.70, 14.05.

EA: calculated: C: 74.61 %, H: 7.32 %; found: C: 74.56 %, H: 7.31 %

4-[3-({4-[(4-{[6-(4-{[4-(Hexadecyloxy)phenyl]carbonyloxy}phenoxy)hexyl]oxy}phenyl)-carbonyloxy]phenyl}carbonyloxy)phenoxycarbonyl]phenyl 4-(dodecyloxy)benzoate **5b**

(*n* = 12, *m* = 6, *p* = 16)

Formula: C$_{81}$H$_{98}$O$_{14}$, M = 1295.68 g/mol

Synthesis: according to the general procedure 10.3.3

Reagents: 260 mg (0.42 mmol) 4-{3-[(4-hydroxyphenyl)carbonyloxy]phenoxycarbonyl}phenyl 4-(dodecyloxy)benzoate **i9(12)**
280 mg (0.42 mmol) 4-{[6-(4-{[4-(hexadecyloxy)phenyl]carbonyloxy}phenoxy)hexyl]oxy}-benzoic acid **i14(6,16)**
90 mg (0.46 mmol) DCC
5 mg DMAP
40 ml dichloromethane

Purification: column chromatography, eluent: CHCl$_3$/EtOAc (10/0.2) and further recrystallisation from EtOAc/EtOH (10/0.2)

Yield: 390 mg (72 %), colorless solid

Transition temp.: Cr 139 (SmCP$_{AF}$[*] 128) SmC$_s$P$_{AF}$ 141 N 141.5 I

^{1}H-NMR: (CDCl$_3$, *J*/Hz, 400 MHz) δ 8.26 (d, *J* = 8.5 Hz, 4H, Ar-H), 8.14 (dd, *J* = 9.0, 2.3 Hz, 4H, Ar-H), 8.11 (d, *J* = 8.6 Hz, 2H, Ar-H), 7.48 (t, *J* = 8.5 Hz, 1H, Ar-H), 7.37 (d, *J* = 8.6 Hz, 4H, Ar-H), 7.25 – 7.21 (m, 1H, Ar-H), 7.18 (d, *J* = 8.5 Hz, 2H, Ar-H), 7.10 (d, *J* = 8.8 Hz, 2H, Ar-H), 6.99 – 6.97 (m, 4H, Ar-H), 6.96 – 6.90 (m, 4H, Ar-H), 4.08 – 3.99 (m, 8H, OCH$_2$), 1.84 – 1.81 (m, 8H, OCH$_2$C**H**$_2$), 1.60 – 1.54 (m, 4H, CH$_2$), 1.51 – 1.46 (m, 4H, CH$_2$), 1.39 – 1.26 (m, 24H, CH$_2$), 0.88 – 0.86 (m, 6H, CH$_3$).

^{13}C-NMR: (CDCl$_3$, 100 MHz) δ 164.16, 163.98, 163.84, 163.53, 155.62, 151.61, 132.41, 132.39, 132.16, 131.79, 129.75, 126.80, 122.47, 122.06, 119.17, 115.74, 115.27, 114.57, 114.40, 68.55, 68.48, 68.44, 68.36, 31.97, 29.72, 29.68, 29.66, 29.62, 29.59, 29.40, 29.37, 29.36, 29.22, 29.20, 29.15, 26.06, 25.93, 25.87, 22.70, 14.04.

EA: calculated: C: 75.09 %, H: 7.62 %; found: C: 75.08 %, H: 7.65 %

4-[3-({4-[(4-{[11-(4-{[4-(Hexadecyloxy)phenyl]carbonyloxy}phenoxy)undecyl]oxy}phenyl)-carbonyloxy]phenyl}carbonyloxy)phenoxycarbonyl]phenyl 4-(dodecyloxy)benzoate **5c**

(*n* = 12, *m* = 11, *p* = 16)

Formula: C$_{86}$H$_{108}$O$_{14}$, M = 1365.81 g/mol

Synthesis: according to the general procedure 10.3.3

Reagents: 330 mg (0.52 mmol) 4-{3-[(4-hydroxyphenyl)carbonyloxy]phenoxycarbonyl}phenyl 4-(dodecyloxy)benzoate **i9(12)**
380 mg (0.52 mmol) 4-{[11-(4-{[4-(hexadecyloxy)phenyl]carbonyloxy}phenoxy)undecyl]-

oxy}benzoic acid **i14(11,16)**
120 mg (0.56 mmol) DCC
5 mg DMAP
40 ml dichloromethane

Purification: column chromatography, eluent: $CHCl_3$/EtOAc (10/0.2) and further recrystallisation from EtOAc/EtOH (10/0.2)

Yield: 460 mg (65 %), colorless solid

Transition temp.: Cr 125 (Col$_r$P$_{AF}$ 130) I

^{1}H-NMR: ($CDCl_3$, *J*/Hz, 400 MHz) δ 8.26 (d, *J* = 8.9 Hz, 4H, Ar-H), 8.13 (d, *J* = 8.7 Hz, 4H, Ar-H), 8.10 (d, *J* = 9.0 Hz, 2H, Ar-H), 7.47 (t, *J* = 8.2 Hz, 1H, Ar-H), 7.36 (d, *J* = 8.4 Hz, 4H, Ar-H), 7.21 (t, *J* = 2.1 Hz, 1H, Ar-H), 7.17 (dd, *J* = 8.2, 2.2 Hz, 2H, Ar-H), 7.08 (d, *J* = 9.1 Hz, 2H, Ar-H), 6.97 (d, *J* = 8.9 Hz, 4H, Ar-H), 6.95 – 6.87 (m, 4H, Ar-H), 4.08 – 4.00 (m, 6H, OCH_2), 3.95 (t, *J* = 6.5 Hz, 2H, OCH_2), 1.86 – 1.74 (m, 8H, $OCH_2C\mathbf{H}_2$), 1.53 – 1.42 (m, 8H, CH_2), 1.42 – 1.24 (m, 50H, CH_2), 0.91 – 0.85 (m, *J* = 16.2 Hz, 6H, CH_3).

^{13}C-NMR: ($CDCl_3$, 100 MHz) δ 164.17, 163.98, 163.91, 156.85, 155.62, 151.61, 132.39, 132.16, 131.79, 126.80, 122.42, 122.06, 121.25, 119.17, 115.74, 115.27, 114.57, 114.39, 68.67, 68.55, 68.47, 31.96, 29.72, 29.69, 29.62, 29.59, 29.55, 29.52, 29.40, 29.37, 29.22, 29.20, 26.12, 26.06, 22.70, 14.05.

EA: calculated: C: 75.63 %, H: 7.97 %; found: C: 75.56 %, H: 8.08 %

4-[3-({4-[(4-{[6-(4-{[4-(Dodecyloxy)phenyl]carbonyloxy}phenoxy)hexyl]oxy}phenyl)-carbonyloxy]phenyl}carbonyloxy)phenoxycarbonyl]phenyl 4-(hexadecyloxy)benzoate **6a** (*n* = 16, *m* = 6, *p* = 12)

Formula: $C_{81}H_{98}O_{14}$, M = 1295.68 g/mol

Synthesis: according to the general procedure 10.3.3

Reagents: 320 mg (0.46 mmol) 4-{3-[(4-hydroxyphenyl)carbonyloxy]phenoxycarbonyl}phenyl 4-(hexadecyloxy)benzoate **i9(16)**
280 mg (0.46 mmol) 4-{[6-(4-{[4-(dodecyloxy)phenyl]carbonyloxy}phenoxy)hexyl]oxy}-benzoic acid **i14(6,12)**
110 mg (0.51 mmol) DCC
5 mg DMAP
40 ml dichloromethane

Purification: column chromatography, eluent: $CHCl_3$/EtOAc (10/0.2) and further recrystallisation from EtOAc/EtOH (10/0.2)

Yield: 400 mg (67 %), colorless solid

Transition temp.: Cr 138 (SmXP$_{AF}$ 122 SmC$_s$P$_{AF}$ 125 N 131) I

^{1}H-NMR: ($CDCl_3$, *J*/Hz, 400 MHz) δ 8.26 (d, *J* = 8.4 Hz, 4H, Ar-H), 8.13 (dd, *J* = 9.0, 2.2 Hz, 4H, Ar-H), 8.10 (d, *J* = 9.0 Hz, 2H, Ar-H), 7.47 (t, *J* = 8.3 Hz, 1H, Ar-H), 7.35 (d, *J* = 8.8 Hz, 4H, Ar-H), 7.20 – 7.14 (m, 3H, Ar-H), 7.08 (d, *J* = 9.1 Hz, 2H, Ar-H), 7.00 – 6.93 (m, 5H, Ar-H), 6.93 – 6.87 (m, 3H, Ar-H), 4.09 – 3.99 (m, 6H, OCH_2), 3.97 (t, *J* = 6.3 Hz, 2H, OCH_2), 1.90 – 1.75 (m, 8H, $OCH_2C\mathbf{H}_2$), 1.60 – 1.54 (m, 4H, CH_2), 1.49 – 1.41 (m, 4H, CH_2), 1.38 – 1.21 (m, 40H, CH_2), 0.86 (t, *J* = 6.8 Hz, 6H, CH_3).

^{13}C-NMR: ($CDCl_3$, 100 MHz) δ 165.47, 164.43, 164.23, 163.98, 163.91, 163.61, 156.83, 155.64, 151.58, 144.63, 132.59, 132.57, 132.34, 131.99, 130.02, 126.77, 122.66, 122.28, 121.81, 121.18, 121.10, 119.43, 115.96, 115.22, 114.58, 114.40, 68.55, 68.47, 68.33, 32.07, 32.07, 29.84, 29.83, 29.80, 29.78, 29.74, 29.70, 29.51, 29.49, 29.35, 29.24, 29.19, 26.13, 26.01, 25.95, 22.84, 14.26.

EA: calculated: C: 75.09 %, H: 7.62 %; found: C: 74.86 %, H: 7.72 %

4-[3-({4-[(4-{[11-(4-{[4-(Dodecyloxy)phenyl]carbonyloxy}phenoxy)undecyl]oxy}phenyl)-carbonyloxy]phenyl}carbonyloxy)phenoxycarbonyl]phenyl 4-(hexadecyloxy)benzoate **6b** (*n* = 16, *m* = 11, *p* = 12)

Formula:	$C_{86}H_{108}O_{14}$, M = 1365.81 g/mol
Synthesis:	according to the general procedure 10.3.3
Reagents:	310 mg (0.44 mmol) 4-{3-[(4-hydroxyphenyl)carbonyloxy]phenoxycarbonyl}phenyl 4-(hexadecyloxy)benzoate **i9(16)** 300 mg (0.44 mmol) 4-{[11-(4-{[4-(dodecyloxy)phenyl]carbonyloxy}phenoxy)undecyl]oxy}-benzoic acid **i14(11,12)** 100 mg (0.48 mmol) DCC 5 mg DMAP 40 ml dichloromethane
Purification:	column chromatography, eluent: $CHCl_3$/EtOAc (10/0.2) and further recrystallisation from EtOAc/EtOH (10/0.2)
Yield:	490 mg (82 %), colorless solid
Transition temp.:	Cr 130 (Col$_r$P$_{AF}$ 125) I
^{1}H-NMR:	($CDCl_3$, *J*/Hz, 400 MHz) δ 8.26 (d, *J* = 8.3 Hz, 4H, Ar-H), 8.13 (d, *J* = 8.9 Hz, 4H, Ar-H), 8.10 (d, *J* = 9.0 Hz, 2H, Ar-H), 7.48 (t, *J* = 8.3 Hz, 1H, Ar-H), 7.36 (d, *J* = 8.5 Hz, 4H, Ar-H), 7.20 – 7.17 (m, 2H, Ar-H), 7.16 (d, *J* = 2.2 Hz, 1H, Ar-H), 7.08 (d, *J* = 9.1 Hz, 2H, Ar-H), 6.99 – 6.87 (m, 8H, Ar-H), 4.06 – 3.99 (m, 6H, OCH_2), 3.94 (t, *J* = 6.5 Hz, 2H, OCH_2), 1.86 – 1.73 (m, 8H, $OCH_2C\mathbf{H_2}$), 1.50 – 1.40 (m, 8H, CH_2), 1.38 – 1.20 (m, 50H, CH_2), 0.89 – 0.80 (m, 6H, CH_3).
^{13}C-NMR:	($CDCl_3$, 100 MHz) δ 164.27, 164.07, 163.81, 155.47, 151.41, 132.40, 131.83, 129.86, 126.60, 122.44, 122.11, 120.93, 119.26, 115.79, 115.05, 114.41, 114.23, 68.38, 31.91, 29.67, 29.65, 29.64, 29.57, 29.53, 29.34, 29.07, 25.96, 22.67, 14.09.
EA:	calculated: C: 75.63 %, H: 7.97 %; found: C: 75.35 %, H: 8.04 %

Compounds 7-9

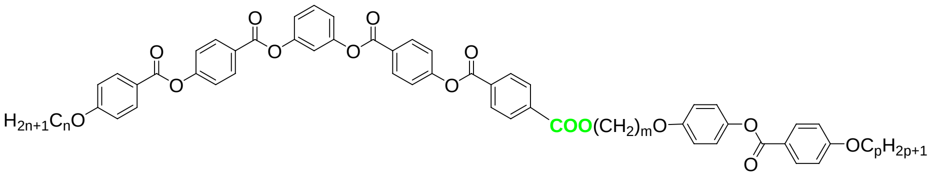

dimer series 7-9
7a: *n* = 12; *m* = 6; *p* = 6
7b: *n* = 16; *m* = 6; *p* = 6
8a: *n* = 12; *m* = 6; *p* = 12
8b: *n* = 16; *m* = 6; *p* = 12
9a: *n* = 12; *m* = 11; *p* = 6
9b: *n* = 16; *m* =11; *p* = 6

1-(4-{3-[(4-{[4-(Dodecyloxy)phenyl]carbonyloxy}phenyl)carbonyloxy]phenoxycarbonyl}-phenyl) 4-[6-(4-{[4-(hexyloxy)phenyl]carbonyloxy}phenoxy)hexyl]benzene-1,4-dicarboxylate **7a** (*n* = 12, *m* = 6, *p* = 6)

Formula:	$C_{72}H_{78}O_{15}$, M = 1183.42 g/mol
Synthesis:	according to the general procedure 10.3.3
Reagents:	110 mg (0.18 mmol) 4-{3-[(4-hydroxyphenyl)carbonyloxy]phenoxycarbonyl}phenyl 4-(dodecyloxy)benzoate **i9(12)** 100 mg (0.18 mmol) 4-({[6-(4-{[4-(hexyloxy)phenyl]carbonyloxy}phenoxy)hexyl]oxy}-carbonyl)benzoic acid **i17(6,6)** 40 mg (0.20 mmol) DCC 5 mg DMAP 30 ml dichloromethane
Purification:	column chromatography, eluent: $CHCl_3$/EtOAc (10/0.2) and further recrystallisation from EtOAc/EtOH (10/0.2)
Yield:	160 mg (75 %), colorless solid
Transition temp.:	Cr 135 (Col$_x$P$_{FE}$ 128) I

^{1}H-NMR: ($CDCl_3$, *J*/Hz, 400 MHz) δ 8.30 – 8.23 (m, 6H, Ar-H), 8.19 – 8.07 (m, 6H, Ar-H), 7.48 (t, *J* = 8.1 Hz, 1H, Ar-H), 7.41 – 7.33 (m, 4H, Ar-H), 7.21 – 7.15 (m, 3H, Ar-H), 7.08 (d, *J* = 8.9 Hz, 2H, Ar-H), 6.99 – 6.86 (m, 6H, Ar-H), 4.38 (t, *J* = 6.6 Hz, 2H, $COOCH_2$), 4.07 – 3.99 (m, 4H, OCH_2), 3.97 (t, *J* = 6.3 Hz, 2H, OCH_2), 1.88 – 1.75 (m, 8H, $OCH_2C\mathbf{H}_2$, $COOCH_2C\mathbf{H}_2$), 1.60 – 1.53 (m, 4H, CH_2), 1.50 – 1.41 (m, 4H, CH_2), 1.39 – 1.23 (m, 20H, CH_2), 0.93 – 0.84 (m, 6H, CH_3).

^{13}C-NMR: ($CDCl_3$, 100 MHz) δ 167.37, 163.37, 155.45, 154.95, 151.40, 144.47, 132.67, 132.37, 132.14, 131.90, 131.79, 130.18, 129.83, 129.73, 122.47, 122.10, 121.93, 115.76, 115.09, 114.44, 114.26, 68.50, 68.41, 68.28, 65.66, 32.05, 31.68, 29.79, 29.72, 29.69, 29.49, 29.32, 29.24, 28.79, 26.13, 26.00, 25.80, 22.83, 22.73, 14.26, 14.16.

EA: calculated: C: 73.08 %, H: 6.64 %; found: C: 73.09 %, H: 6.69 %

1-(4-{3-[(4-{[4-(Hexadecyloxy)phenyl]carbonyloxy}phenyl)carbonyloxy]phenoxycarbonyl}-phenyl) 4-[6-(4-{[4-(hexyloxy)phenyl]carbonyloxy}phenoxy)hexyl]benzene-1,4-dicarboxylate **7b** (*n* = 16, *m* = 6, *p* = 6)

Formula: $C_{76}H_{86}O_{15}$, M = 1239.52 g/mol

Synthesis: according to the general procedure 10.3.3

Reagents: 130 mg (0.18 mmol) 4-{3-[(4-hydroxyphenyl)carbonyloxy]phenoxycarbonyl}phenyl 4-(hexadecyloxy)benzoate **i9(16)**
100 mg (0.18 mmol) 4-({[6-(4-{[4-(hexyloxy)phenyl]carbonyloxy}phenoxy)hexyl]oxy}-carbonyl)benzoic acid **i17(6,6)**
40 mg (0.20 mmol) DCC
5 mg DMAP
30 ml dichloromethane

Purification: column chromatography, eluent: $CHCl_3$/EtOAc (10/0.2) and further recrystallisation from EtOAc/EtOH (10/0.2)

Yield: 150 mg (67 %), colorless solid

Transition temp.: Cr 133 (Col_xP_{FE} 126) I

^{1}H-NMR: ($CDCl_3$, *J*/Hz, 400 MHz) δ 8.30 – 8.23 (m, 6H, Ar-H), 8.19 – 8.07 (m, 6H, Ar-H), 7.48 (t, *J* = 8.1 Hz, 1H, Ar-H), 7.41 – 7.34 (m, 4H, Ar-H), 7.21 – 7.15 (m, 3H, Ar-H), 7.08 (d, *J* = 9.0 Hz, 2H, Ar-H), 6.99 – 6.87 (m, 6H, Ar-H), 4.39 (t, *J* = 6.6 Hz, 2H, $COOCH_2$), 4.07 – 3.99 (m, 4H, OCH_2), 3.97 (t, *J* = 6.3 Hz, 2H, OCH_2), 1.89 – 1.75 (m, 8H, $OCH_2C\mathbf{H}_2$, $COOCH_2C\mathbf{H}_2$), 1.61 – 1.54 (m, 4H, CH_2), 1.50 – 1.42 (m, 4H, CH_2), 1.40 – 1.22 (m, 28, CH_2), 0.93 – 0.84 (m, 6H, CH_3).

^{13}C-NMR: ($CDCl_3$, 100 MHz) δ 173.54, 165.52, 165.17, 165.12, 164.17, 163.96, 163.82, 163.76, 163.68, 163.37, 156.59, 155.45, 154.95, 151.40, 151.32, 144.47, 135.14, 132.67, 132.37, 132.14, 131.91, 131.79, 130.18, 129.73, 127.11, 126.60, 122.47, 122.11, 121.88, 120.97, 119.28, 119.21, 115.76, 115.09, 114.44, 114.26, 68.50, 68.41, 68.27, 65.66, 32.06, 31.68, 29.83, 29.79, 29.72, 29.50, 29.33, 29.24, 29.22, 28.79, 26.13, 26.00, 25.97, 25.80, 22.84, 22.73, 14.26, 14.16.

EA: calculated: C: 73.65 %, H: 6.99 %; found: C: 73.57 %, H: 6.99 %

1-[6-(4-{[4-(Dodecyloxy)phenyl]carbonyloxy}phenoxy)hexyl] 4-(4-{3-[(4-{[4-(dodecyloxy)-phenyl]carbonyloxy}phenyl)carbonyloxy]phenoxycarbonyl}phenyl)benzene-1,4-dicarboxylate **8a** (*n* = 12, *m* = 6, *p* = 12)

Formula: $C_{78}H_{90}O_{15}$, M = 1267.58 g/mol

Synthesis: according to the general procedure 10.3.3

Reagents: 200 mg (0.31 mmol) 4-{3-[(4-hydroxyphenyl)carbonyloxy]phenoxycarbonyl}phenyl 4-(dodecyloxy)benzoate **i9(12)**
200 mg (0.31 mmol) 4-({[6-(4-{[4-(dodecyloxy)phenyl]carbonyloxy}phenoxy)hexyl]oxy}-carbonyl)benzoic acid **i17(6,12)**

70 mg (0.34 mmol) DCC
5 mg DMAP
30 ml dichloromethane

Purification: column chromatography, eluent: $CHCl_3$/EtOAc (10/0.2) and further recrystallisation from EtOAc/EtOH (10/0.2)

Yield: 260 mg (66 %), colorless solid

Transition temp.: Cr 129 Col_rP_{FE} 137 I

^{1}H-NMR: ($CDCl_3$, *J*/Hz, 400 MHz) δ 8.30 – 8.24 (m, 6H, Ar-H), 8.17 (d, *J* = 8.6 Hz, 2H, Ar-H), 8.13 (d, *J* = 8.9 Hz, 2H, Ar-H), 8.10 (d, *J* = 8.9 Hz, 2H, Ar-H), 7.48 (t, *J* = 8.0 Hz, 1H, Ar-H), 7.41 – 7.34 (m, 4H, Ar-H), 7.21 – 7.15 (m, 3H, Ar-H), 7.08 (d, *J* = 9.0 Hz, 2H, Ar-H), 6.99 – 6.87 (m, 6H, Ar-H), 4.39 (t, *J* = 6.6 Hz, 2H, $COOCH_2$), 4.07 – 3.99 (m, 4H, OCH_2), 3.97 (t, *J* = 6.4 Hz, 2H, OCH_2), 1.88 – 1.75 (m, 8H, $OCH_2\mathbf{CH_2}$, $COOCH_2\mathbf{CH_2}$), 1.60 – 1.53 (m, 4H, CH_2), 1.50 – 1.41 (m, 4H, CH_2), 1.39 – 1.22 (m, 32H, CH_2), 0.90 – 0.84 (m, 6H, CH_3).

^{13}C-NMR: ($CDCl_3$, 100 MHz) δ 165.61, 165.29, 164.27, 164.06, 163.92, 163.82, 163.78, 163.44, 156.64, 155.49, 154.99, 151.42, 151.35, 144.47, 135.14, 132.66, 132.40, 132.17, 131.94, 131.83, 130.21, 129.88, 129.76, 127.09, 126.58, 122.48, 122.13, 121.95, 121.63, 120.92, 119.22, 115.77, 115.04, 114.41, 114.23, 68.38, 68.30, 68.14, 65.57, 31.90, 29.63, 29.61, 29.56, 29.53, 29.34, 29.32, 29.15, 29.08, 28.61, 25.96, 25.83, 25.80, 22.67, 14.09.

EA: calculated: C: 73.91 %, H: 7.16 %; found: C: 73.82 %, H: 7.15 %

1-[6-(4-{[4-(Dodecyloxy)phenyl]carbonyloxy}phenoxy)hexyl] 4-(4-{3-[(4-{[4-(hexadecyloxy)phenyl]carbonyloxy}phenyl)carbonyloxy]phenoxycarbonyl}phenyl)benzene-1,4-dicarboxylate **8b** (*n* = 16, *m* = 6, *p* = 12)

Formula: $C_{82}H_{98}O_{15}$, M = 1323.69 g/mol

Synthesis: according to the general procedure 10.3.3

Reagents: 210 mg (0.30 mmol) 4-{3-[(4-hydroxyphenyl)carbonyloxy]phenoxycarbonyl}phenyl 4-(hexadecyloxy)benzoate **i9(16)**
200 mg (0.30 mmol) 4-({[6-(4-{[4-(dodecyloxy)phenyl]carbonyloxy}phenoxy)hexyl]oxy}-carbonyl)benzoic acid **i17(6,12)**
70 mg (0.33 mmol) DCC
5 mg DMAP
40 ml dichloromethane

Purification: column chromatography, eluent: $CHCl_3$/EtOAc (10/0.2) and further recrystallisation from EtOAc/EtOH (10/0.2)

Yield: 270 mg (68 %), colorless solid

Transition temp.: Cr 131 Col_rP_{FE} 139 I

^{1}H-NMR: ($CDCl_3$, *J*/Hz, 400 MHz) δ 8.30 – 8.23 (m, 6H, Ar-H), 8.17 (d, *J* = 8.3 Hz, 2H, Ar-H), 8.13 (d, *J* = 8.7 Hz, 2H, Ar-H), 8.09 (d, *J* = 8.7 Hz, 2H, Ar-H), 7.48 (t, *J* = 8.1 Hz, 1H, Ar-H), 7.41 – 7.33 (m, 4H, Ar-H), 7.21 – 7.15 (m, 3H, Ar-H), 7.08 (d, *J* = 8.9 Hz, 2H, Ar-H), 6.99 – 6.87 (m, 6H, Ar-H), 4.38 (t, *J* = 6.6 Hz, 2H, $COOCH_2$), 4.06 – 3.99 (m, 4H, OCH_2), 3.97 (t, *J* = 6.3 Hz, 2H, OCH_2), 1.88 – 1.75 (m, 8H, $OCH_2\mathbf{CH_2}$, $COOCH_2\mathbf{CH_2}$), 1.59 – 1.53 (m, 4H, CH_2), 1.50 – 1.40 (m, 4H, CH_2), 1.39 – 1.21 (m, 40H, CH_2), 0.86 (t, *J* = 6.8 Hz, 6H, CH_3).

^{13}C-NMR: ($CDCl_3$, 100 MHz) δ 165.51, 165.17, 164.16, 163.96, 163.82, 163.76, 163.37, 156.59, 155.45, 154.95, 151.40, 151.33, 144.47, 135.14, 132.67, 132.37, 132.14, 131.91, 131.79, 130.18, 129.84, 129.73, 127.11, 126.60, 122.47, 122.10, 121.93, 121.68, 120.97, 119.31, 119.17, 115.76, 115.09, 114.44, 114.26, 68.50, 68.41, 68.28, 65.66, 32.06, 32.05, 29.83, 29.79, 29.77, 29.72, 29.69, 29.50, 29.48, 29.32, 29.25, 28.79, 26.13, 26.00, 25.97, 22.83, 14.26.

EA: calculated: C: 74.41 %, H: 7.46 %; found: C: 74.37 %, H: 7.51 %

1-(4-{3-[(4-{[4-(Dodecyloxy)phenyl]carbonyloxy}phenyl)carbonyloxy]phenoxycarbonyl}-phenyl) 4-[11-(4-{[4-(hexyloxy)phenyl]carbonyloxy}phenoxy)undecyl]benzene-1,4-dicarboxylate **9a** (*n* = 12, *m* = 11, *p* = 6)

Formula:	$C_{77}H_{88}O_{15}$, M = 1253.55 g/mol
Synthesis:	according to the general procedure 10.3.3
Reagents:	300 mg (0.47 mmol) 4-{3-[(4-hydroxyphenyl)carbonyloxy]phenoxycarbonyl}phenyl 4-(dodecyloxy)benzoate **i9(12)** 300 mg (0.47 mmol) 4-({[10-(4-{[4-(hexyloxy)phenyl]carbonyloxy}phenoxy)decyl]oxy}-carbonyl)benzoic acid **i17(11,6)** 110 mg (0.52 mmol) DCC 5 mg DMAP 40 ml dichloromethane
Purification:	column chromatography, eluent: $CHCl_3$/EtOAc (10/0.2) and further recrystallisation from EtOAc/EtOH (10/0.2)
Yield:	420 mg (71 %), colorless solid
Transition temp.:	Cr 109 (Col_xP_{FE} 103 N 105) I
^{1}H-NMR:	($CDCl_3$, *J*/Hz, 400 MHz) δ 8.31 – 8.24 (m, 6H, Ar-H), 8.17 (d, *J* = 8.4 Hz, 2H, Ar-H), 8.13 (d, *J* = 8.8 Hz, 2H, Ar-H), 8.10 (d, *J* = 8.8 Hz, 2H, Ar-H), 7.48 (t, *J* = 8.1 Hz, 1H, Ar-H), 7.41 – 7.34 (m, 4H, Ar-H), 7.21 – 7.15 (m, 3H, Ar-H), 7.07 (d, *J* = 9.0 Hz, 2H, Ar-H), 6.99 – 6.86 (m, 6H, Ar-H), 4.36 (t, *J* = 6.7 Hz, 2H, $COOCH_2$), 4.06 – 3.99 (m, 4H, OCH_2), 3.94 (t, *J* = 6.5 Hz, 2H, OCH_2), 1.85 – 1.73 (m, 8H, $OCH_2C\mathbf{H}_2$, $COOCH_2C\mathbf{H}_2$), 1.51 – 1.40 (m, 8H, CH_2), 1.40 – 1.23 (m, 30H, CH_2), 0.93 – 0.84 (m, 6H, CH_3).
^{13}C-NMR:	($CDCl_3$, 100 MHz) δ 165.52, 165.18, 164.16, 163.96, 163.82, 163.76, 163.69, 163.36, 156.69, 155.45, 154.95, 151.40, 151.33, 144.39, 135.23, 132.64, 132.37, 132.14, 131.91, 131.79, 130.16, 129.84, 129.73, 127.13, 126.60, 122.42, 122.10, 121.93, 121.73, 120.97, 119.30, 119.20, 115.76, 115.09, 114.45, 114.26, 68.53, 68.50, 68.41, 65.85, 32.05, 31.68, 29.79, 29.77, 29.72, 29.69, 29.67, 29.63, 29.51, 29.49, 29.48, 29.44, 29.40, 29.24, 29.23, 28.83, 26.20, 26.17, 26.13, 25.81, 22.83, 22.73, 14.26, 14.16.
EA:	calculated: C: 73.78 %, H: 7.08 %; found: C: 73.75 %, H: 7.16 %

1-(4-{3-[(4-{[4-(Hexadecyloxy)phenyl]carbonyloxy}phenyl)carbonyloxy]phenoxycarbonyl}-phenyl) 4-[11-(4-{[4-(hexyloxy)phenyl]carbonyloxy}phenoxy)undecyl]benzene-1,4-dicarboxylate **9b** (*n* = 16, *m* = 11, *p* = 6)

Formula:	$C_{81}H_{96}O_{15}$, M = 1309.66 g/mol
Synthesis:	according to the general procedure 10.3.3
Reagents:	330 mg (0.47 mmol) 4-{3-[(4-hydroxyphenyl)carbonyloxy]phenoxycarbonyl}phenyl 4-(hexadecyloxy)benzoate **i9(16)** 300 mg (0.47 mmol) 4-({[10-(4-{[4-(hexyloxy)phenyl]carbonyloxy}phenoxy)decyl]oxy}-carbonyl)benzoic acid **i17(11,6)** 110 mg (0.52 mmol) DCC 5 mg DMAP 40 ml dichloromethane
Purification:	column chromatography, eluent: $CHCl_3$/EtOAc (10/0.2) and further recrystallisation from EtOAc/EtOH (10/0.2)
Yield:	400 mg (65 %), colorless solid
Transition temp.:	Cr 111 (N 103) I
^{1}H-NMR:	($CDCl_3$, *J*/Hz, 400 MHz) δ 8.31 – 8.24 (m, 6H, Ar-H), 8.17 (d, *J* = 8.5 Hz, 2H, Ar-H), 8.14 (d, *J* = 8.9 Hz, 2H, Ar-H), 8.10 (d, *J* = 8.9 Hz, 2H, Ar-H), 7.48 (t, *J* = 8.1 Hz, 1H, Ar-H), 7.41 – 7.34 (m, 4H, Ar-H), 7.21 – 7.15 (m, 3H, Ar-H), 7.07 (d, *J* = 9.0 Hz, 2H, Ar-H), 6.97 (d, *J* = 8.9 Hz, 2H, Ar-H), 6.94 (d, *J* = 8.9 Hz, 2H, Ar-H), 6.89 (d, *J* = 9.0 Hz, 2H, Ar-H), 4.36 (t, *J* = 6.7 Hz, 2H, $COOCH_2$), 4.07 – 3.99 (m, 4H, OCH_2), 3.94 (t, *J* = 6.5 Hz, 2H, OCH_2), 1.85 – 1.73 (m, 8H, $OCH_2C\mathbf{H}_2$, $COOCH_2C\mathbf{H}_2$), 1.51 – 1.40 (m, 8H, CH_2), 1.39 – 1.22 (m, 38H, CH_2), 0.93

	– 0.84 (m, 6H, CH_3).
^{13}C-NMR:	($CDCl_3$, 100 MHz) δ 165.68, 165.35, 164.32, 164.12, 163.98, 163.87, 163.84, 163.47, 156.79, 155.54, 155.04, 151.48, 151.41, 144.44, 135.28, 132.68, 132.45, 132.22, 132.00, 131.88, 130.24, 129.94, 129.80, 127.16, 126.63, 122.49, 122.18, 122.00, 121.72, 120.97, 119.37, 119.28, 115.83, 115.10, 114.46, 114.28, 68.44, 68.34, 65.82, 31.96, 31.58, 29.72, 29.71, 29.69, 29.62, 29.59, 29.56, 29.53, 29.39, 29.31, 29.30, 29.12, 29.10, 28.70, 26.07, 26.05, 26.01, 25.69, 22.72, 22.61, 14.15, 14.05.
EA:	calculated: C: 74.29 %, H: 7.39 %; found: C: 74.18 %, H: 7.39 %

Compounds 10-11

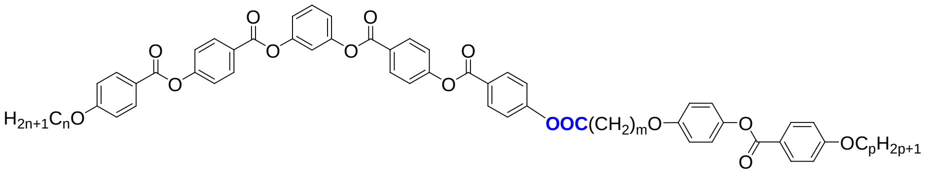

dimer series 10-11

10a: *n* = 12; *m* = 5; *p* = 6
10b: *n* = 16; *m* = 5; *p* = 6
11a: *n* = 12; *m* = 5; *p* = 12
11b: *n* = 16; *m* = 5; *p* = 12

4-[3-({4-[(4-{[6-(4-{[4-(Hexyloxy)phenyl]carbonyloxy}phenoxy)hexanoyl]oxy}phenyl)-carbonyloxy]phenyl}carbonyloxy)phenoxycarbonyl]phenyl 4-(dodecyloxy)benzoate **10a** (*n* = 12, *m* = 5, *p* = 6)

Formula:	$C_{71}H_{76}O_{15}$, M = 1169.39 g/mol
Synthesis:	according to the general procedure 10.3.3
Reagents:	330 mg (0.51 mmol) 4-{3-[(4-hydroxyphenyl)carbonyloxy]phenoxycarbonyl}phenyl 4-(dodecyloxy)benzoate **i9(12)** 280 mg (0.51 mmol) 4-{[6-(4-{[4-(hexyloxy)phenyl]carbonyloxy}phenoxy)hexanoyl]oxy}-benzoic acid **i20(5,6)** 120 mg (0.56 mmol) DCC 5 mg DMAP 40 ml dichloromethane
Purification:	column chromatography, eluent: $CHCl_3$/EtOAc (10/0.2) and further recrystallisation from EtOAc/EtOH (10/0.2)
Yield:	490 mg (82 %), colorless solid
Transition temp.:	Cr 137 Cr*P_{FE} 169 I
^{1}H-NMR:	($CDCl_3$, *J*/Hz, 400 MHz) δ 8.26 (d, *J* = 8.3 Hz, 4H, Ar-H), 8.17 – 8.08 (m, 6H, Ar-H), 7.47 (t, *J* = 8.3 Hz, 1H, Ar-H), 7.36 (d, *J* = 8.5 Hz, 4H, Ar-H), 7.22 – 7.15 (m, 5H, Ar-H), 7.11 (d, *J* = 9.1 Hz, 2H, Ar-H), 7.00 – 6.92 (m, 6H, Ar-H), 4.08 (t, *J* = 6.3 Hz, 2H, OCH_2), 4.06 – 4.00 (m, 4H, OCH_2), 2.61 (t, *J* = 7.4 Hz, 2H, CH_2COO), 1.94 – 1.76 (m, 8H, $OCH_2C\mathbf{H}_2$, $C\mathbf{H}_2CH_2COO$), 1.68 – 1.58 (m, 2H, CH_2), 1.50 – 1.41 (m, 4H, CH_2), 1.39 – 1.23 (m, 20H, CH_2), 0.93 – 0.84 (m, 6H, CH_3).
^{13}C-NMR:	($CDCl_3$, 100 MHz) δ 171.70, 167.21, 164.66, 164.17, 163.96, 163.77, 163.75, 163.58, 163.54, 155.42, 151.38, 149.34, 148.41, 147.95, 132.41, 132.37, 132.23, 131.79, 129.81, 126.62, 122.60, 122.31, 122.09, 119.24, 114.43, 114.34, 68.49, 68.44, 68.05, 34.35, 32.05, 31.68, 29.79, 29.77, 29.72, 29.69, 29.49, 29.48, 29.24, 29.21, 28.95, 26.13, 25.80, 25.75, 24.77, 22.83, 22.72, 14.26, 14.16.
EA:	calculated: C: 72.93 %, H: 6.55 %; found: C: 72.91 %, H: 6.63 %

4-[3-({4-[(4-{[6-(4-{[4-(Hexyloxy)phenyl]carbonyloxy}phenoxy)hexanoyl]oxy}phenyl)-carbonyloxy]phenyl}carbonyloxy)phenoxycarbonyl]phenyl 4-(hexadecyloxy)benzoate **10b** (*n* = 16, *m* = 5, *p* = 6)

Formula: $C_{75}H_{84}O_{15}$, M = 1225.50 g/mol

Synthesis: according to the general procedure 10.3.3

Reagents: 340 mg (0.49 mmol) 4-{3-[(4-hydroxyphenyl)carbonyloxy]phenoxycarbonyl}phenyl 4-(hexadecyloxy)benzoate **i9(16)**
270 mg (0.49 mmol) 4-{[6-(4-{[4-(hexyloxy)phenyl]carbonyloxy}phenoxy)hexanoyl]oxy}-benzoic acid **i20(5,6)**
120 mg (0.54 mmol) DCC
5 mg DMAP
40 ml dichloromethane

Purification: column chromatography, eluent: $CHCl_3$/EtOAc (10/0.2) and further recrystallisation from EtOAc/EtOH (10/0.2)

Yield: 450 mg (75 %), colorless solid

Transition temp.: Cr 131 Cr*P_{FE} 168 I

^{1}H-NMR: ($CDCl_3$, *J*/Hz, 400 MHz) δ 8.26 (d, *J* = 8.3 Hz, 4H, Ar-H), 8.16 – 8.08 (m, 6H, Ar-H), 7.47 (t, *J* = 8.3 Hz, 1H, Ar-H), 7.36 (d, *J* = 8.5 Hz, 4H, Ar-H), 7.21 – 7.15 (m, 5H, Ar-H), 7.11 (d, *J* = 9.1 Hz, 2H, Ar-H), 7.00 – 6.92 (m, 6H, Ar-H), 4.08 (t, *J* = 6.3 Hz, 2H, OCH_2), 4.06 – 4.00 (m, 4H, OCH_2), 2.61 (t, *J* = 7.4 Hz, 2H, CH_2COO), 1.94 – 1.76 (m, 8H, $OCH_2C\mathbf{H}_2$, $C\mathbf{H}_2CH_2COO$), 1.67 – 1.59 (m, 2H, CH_2), 1.50 – 1.42 (m, 4H, CH_2), 1.39 – 1.22 (m, 28H, CH_2), 0.93 – 0.84 (m, 6H, CH_3).

^{13}C-NMR: ($CDCl_3$, 100 MHz) δ 164.17, 164.14, 163.97, 163.75, 163.57, 163.53, 163.51, 155.41, 151.38, 148.39, 147.95, 132.41, 132.37, 132.23, 131.80, 129.82, 126.62, 122.61, 122.31, 122.10, 121.34, 120.97, 119.25, 115.79, 114.43, 114.33, 68.50, 68.44, 68.05, 34.35, 32.06, 31.68, 29.84, 29.80, 29.73, 29.50, 29.21, 28.95, 26.14, 25.81, 25.75, 24.77, 22.84, 22.73, 14.27, 14.17.

EA: calculated: C: 73.51 %, H: 6.91 %; found: C: 73.63 %, H: 6.95 %

4-[3-({4-[(4-{[6-(4-{[4-(Dodecyloxy)phenyl]carbonyloxy}phenoxy)hexanoyl]oxy}phenyl)-carbonyloxy]phenyl}carbonyloxy)phenoxycarbonyl]phenyl 4-(dodecyloxy)benzoate **11a** (*n* = 12, *m* = 5, *p* = 12)

Formula: $C_{77}H_{88}O_{15}$, M = 1253.55 g/mol

Synthesis: according to the general procedure 10.3.3

Reagents: 300 mg (0.47 mmol) 4-{3-[(4-hydroxyphenyl)carbonyloxy]phenoxycarbonyl}phenyl 4-(dodecyloxy)benzoate **i9(12)**
300 mg (0.47 mmol) 4-{[6-(4-{[4-(dodecyloxy)phenyl]carbonyloxy}phenoxy)hexanoyl]oxy}-benzoic acid **i20(5,12)**
110 mg (0.52 mmol) DCC
5 mg DMAP
40 ml dichloromethane

Purification: column chromatography, eluent: $CHCl_3$/EtOAc (10/0.2) and further recrystallisation from EtOAc/EtOH (10/0.2)

Yield: 460 mg (78 %), colorless solid

Transition temp.: Cr 117 SmC'_aP_{AF} 128 SmC_aP_{AF} 139 N 148 I

^{1}H-NMR: ($CDCl_3$, *J*/Hz, 400 MHz) δ 8.26 (d, *J* = 8.9 Hz, 4H, Ar-H), 8.16 – 8.07 (m, 6H, Ar-H), 7.47 (t, *J* = 8.2 Hz, 1H, Ar-H), 7.36 (d, *J* = 8.9 Hz, 4H, Ar-H), 7.21 – 7.14 (m, 5H, Ar-H), 7.14 – 7.08 (m, 2H, Ar-H), 7.00 – 6.91 (m, 6H, Ar-H), 4.11 – 3.99 (m, 6H, OCH_2), 2.61 (t, *J* = 7.3 Hz, 2H, CH_2COO), 1.94 – 1.75 (m, 8H, $OCH_2C\mathbf{H}_2$, $C\mathbf{H}_2CH_2COO$), 1.68 – 1.58 (m, 2H, CH_2), 1.51 – 1.40 (m, 4H, CH_2), 1.39 – 1.21 (m, 32H, CH_2), 0.90 – 0.83 (m, 6H, CH_3).

^{13}C-NMR: ($CDCl_3$, 100 MHz) δ 171.63, 164.63, 164.13, 164.09, 163.93, 163.77, 163.59, 163.55, 155.45, 151.43, 148.44, 147.99, 132.39, 132.35, 132.21, 131.76, 129.77, 126.66, 122.56, 122.27, 122.06, 121.42, 121.23, 121.04, 119.20, 115.75, 114.46, 114.36, 68.51, 68.46, 68.07, 34.34, 32.03, 29.76, 29.74, 29.69, 29.66, 29.47, 29.45, 29.24, 28.94, 26.12, 25.74, 24.76, 22.80, 14.21.

EA: calculated: C: 73.78 %, H: 7.08 %; found: C: 73.96 %, H: 7.07 %

4-[3-({4-[(4-{[6-(4-{[4-(Dodecyloxy)phenyl]carbonyloxy}phenoxy)hexanoyl]oxy}phenyl)-carbonyloxy]phenyl}carbonyloxy)phenoxycarbonyl]phenyl 4-(hexadecyloxy)benzoate **11b** (*n* = 16, *m* = 5, *p* = 12)

Formula: $C_{81}H_{96}O_{15}$, M = 1309.66 g/mol

Synthesis: according to the general procedure 10.3.3

Reagents: 300 mg (0.43 mmol) 4-{3-[(4-hydroxyphenyl)carbonyloxy]phenoxycarbonyl}phenyl 4-(hexadecyloxy)benzoate **i9(16)**
270 mg (0.43 mmol) 4-{[6-(4-{[4-(dodecyloxy)phenyl]carbonyloxy}phenoxy)hexanoyl]oxy}-benzoic acid **i20(5,12)**
100 mg (0.47 mmol) DCC
5 mg DMAP
40 ml dichloromethane

Purification: column chromatography, eluent: $CHCl_3$/EtOAc (10/0.2) and further recrystallisation from EtOAc/EtOH (10/0.2)

Yield: 380 mg (67 %), colorless solid

Transition temp.: Cr 115 SmC'$_s$P$_{AF}$ 123 SmC$_s$P$_{AF}$ 136 N 141 I

^{1}H-NMR: ($CDCl_3$, *J*/Hz, 400 MHz) δ 8.26 (d, *J* = 8.7 Hz, 4H, Ar-H), 8.18 – 8.07 (m, 6H, Ar-H), 7.47 (t, *J* = 8.1 Hz, 1H, Ar-H), 7.36 (d, *J* = 8.6 Hz, 4H, Ar-H), 7.23 – 7.09 (m, 5H, Ar-H), 7.03 – 6.92 (m, 6H, Ar-H), 4.12 – 3.99 (m, 6H, OCH_2), 2.61 (t, *J* = 7.3 Hz, 2H, CH_2COO), 1.96 – 1.75 (m, 8H, $OCH_2\mathbf{CH_2}$, $\mathbf{CH_2}CH_2COO$), 1.70 – 1.58 (m, 2H, CH_2), 1.52 – 1.41 (m, 4H, CH_2), 1.39 – 1.20 (m, 40H, CH_2), 0.87 (t, *J* = 6.7 Hz, 6H, CH_3).

^{13}C-NMR: ($CDCl_3$, 100 MHz) δ 171.64, 164.64, 164.13, 164.10, 163.94, 163.77, 163.59, 163.55, 155.45, 151.42, 148.43, 147.98, 132.39, 132.35, 132.22, 131.77, 129.78, 126.65, 122.58, 122.28, 122.07, 119.21, 115.76, 114.46, 114.36, 68.50, 68.46, 68.07, 34.34, 32.05, 29.82, 29.78, 29.71, 29.68, 29.48, 29.25, 28.94, 26.13, 25.74, 24.76, 22.82, 14.23.

EA: calculated: C: 74.29 %, H: 7.39 %; found: C: 74.31 %, H: 7.39 %

Compounds 12

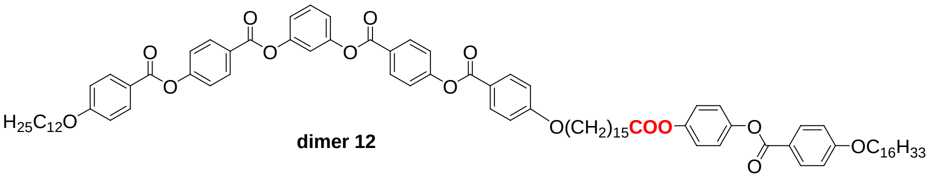

dimer 12

4-[3-({4-[(4-{[16-(4-{[4-(Hexadecyloxy)phenyl]carbonyloxy}phenoxy) 16-oxohexadecyl]-oxy}phenyl)carbonyloxy]phenyl}carbonyloxy)phenoxycarbonyl]phenyl 4-(dodecyloxy)-benzoate **12** (*n* = 12, *m* = 15, *p* = 16)

Formula: $C_{91}H_{116}O_{15}$, M = 1449.93 g/mol

Synthesis: according to the general procedure 10.3.3

Reagents: 310 mg (0.48 mmol) 4-{3-[(4-hydroxyphenyl)carbonyloxy]phenoxycarbonyl}phenyl 4-(dodecyloxy)benzoate **i9(12)**
400 mg (0.48 mmol) 4-{[16-(4-{[4-(hexadecyloxy)phenyl]carbonyloxy}phenoxy)-16-oxohexadecyl]oxy}benzoic acid **i23(15,16)**
110 mg (0.53 mmol) DCC
5 mg DMAP

40 ml dichloromethane

Purification: column chromatography, eluent: $CHCl_3$/EtOAc (10/0.2) and further recrystallisation from EtOAc/EtOH (10/0.2)

Yield: 450 mg (65 %), colorless solid

Transition temp.: Cr 95 Cr* P_{AF} 106.5 N 107 I

^{1}H-NMR: ($CDCl_3$, J/Hz, 400 MHz) δ 8.26 (d, J = 8.7 Hz, 4H, Ar-H), 8.13 (d, J = 8.7 Hz, 4H, Ar-H), 8.10 (d, J = 8.8 Hz, 2H, Ar-H), 7.47 (t, J = 8.1 Hz, 1H, Ar-H), 7.36 (d, J = 8.6 Hz, 4H, Ar-H), 7.22 – 7.15 (m, J = 9.5 Hz, 5H, Ar-H), 7.11 (d, J = 8.9 Hz, 2H, Ar-H), 7.00 – 6.92 (m, 6H, Ar-H), 4.08 – 4.00 (m, 6H, OCH_2), 2.54 (t, J = 7.3 Hz, 2H, CH_2COO), 1.86 – 1.71 (m, 8H, $OCH_2\mathbf{CH_2}$, $\mathbf{CH_2}CH_2COO$), 1.52 – 1.42 (m, 8H, CH_2), 1.41 – 1.22 (m, 58H, CH_2), 0.91 – 0.84 (m, 6H, CH_3).

^{13}C-NMR: ($CDCl_3$, 100 MHz) δ 171.95, 164.15, 163.93, 163.82, 163.58, 155.51, 155.44, 151.43, 132.95, 132.79, 132.29, 131.71, 131.68, 131.08, 126.65, 122.68, 122.43, 122.02, 121.32, 121.05, 119.38, 115.25, 114.35, 114.19, 113.60, 69.91, 69.09, 68.37, 67.82, 31.86, 30.21, 30.10, 29.55, 29.49, 29.24, 29.05, 28.96, 28.92, 25.91, 22.58, 13.80.

EA: calculated: C: 75.38 %, H: 8.06 %; found: C: 75.27 %, H: 8.05 %

Compounds 15a and 16a with E_1-group

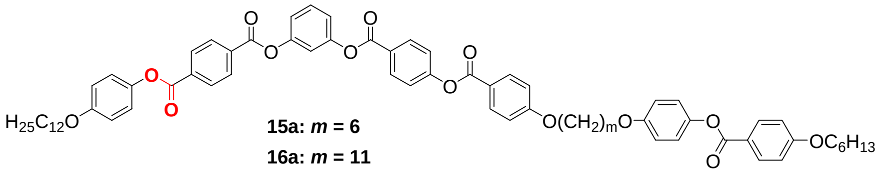

15a: m **= 6**

16a: m **= 11**

1-[4-(Dodecyloxy)phenyl] 4-[3-({4-[(4-{[6-(4-{[4-(hexyloxy)phenyl]carbonyloxy}phenoxy)-hexyl]oxy}phenyl)carbonyloxy]phenyl}carbonyloxy)phenyl]benzene-1,4-dicarboxylate **15a** (n = 12, m = 6, p = 6)

Formula: $C_{71}H_{78}O_{14}$, M = 1155.40 g/mol

Synthesis: according to the general procedure 10.3.3

Reagents: 300 mg (0.47 mmol) 1-[4-(dodecyloxy)phenyl] 4-{3-[(4-hydroxyphenyl)carbonyloxy]phenyl} benzene-1,4-dicarboxylate **i31(12)**
250 mg (0.47 mmol) 4-{[6-(4-{[4-(hexyloxy)phenyl]carbonyloxy}phenoxy)hexyl]oxy}-benzoic acid **i14(6,6)**
110 mg (0.52 mmol) DCC
5 mg DMAP
40 ml dichloromethane

Purification: column chromatography, eluent: $CHCl_3$/EtOAc (10/0.2) and further recrystallisation from EtOAc/EtOH (10/0.2)

Yield: 440 mg (81 %), colorless solid

Transition temp.: Cr 146 SmA 149 N 150

^{1}H-NMR: ($CDCl_3$, J/Hz, 400 MHz) δ 8.31 (s, 4H, Ar-H), 8.26 (d, J = 8.8 Hz, 2H, Ar-H), 8.14 (d, J = 8.9 Hz, 2H, Ar-H), 8.11 (d, J = 8.9 Hz, 2H, Ar-H), 7.49 (t, J = 8.2 Hz, 1H, Ar-H), 7.36 (d, J = 8.8 Hz, 2H, Ar-H), 7.23 – 7.17 (m, 3H, Ar-H), 7.13 (d, J = 9.0 Hz, 2H, Ar-H), 7.08 (d, J = 9.0 Hz, 2H, Ar-H), 6.98 (d, J = 8.9 Hz, 2H, Ar-H), 6.96 – 6.87 (m, 6H, Ar-H), 4.06 (t, J = 6.4 Hz, 2H, OCH_2), 4.02 (t, J = 6.6 Hz, 2H, OCH_2), 3.99 – 3.93 (m, 4H, OCH_2), 1.90 – 1.73 (m, 8H, $OCH_2\mathbf{CH_2}$), 1.61 – 1.52 (m, 4H, CH_2), 1.51 – 1.40 (m, 4H, CH_2), 1.39 – 1.22 (m, 20H, CH_2), 0.94 – 0.84 (m, 6H, CH_3).

^{13}C-NMR: ($CDCl_3$, 100 MHz) δ 165.15, 164.43, 164.12, 163.93, 163.77, 163.71, 163.39, 157.07, 156.63, 155.50, 151.48, 151.22, 144.53, 144.06, 134.24, 133.55, 132.38, 132.13, 131.77, 130.22, 130.21, 129.88, 126.57, 122.46, 122.17, 122.10, 121.75, 121.08, 119.44, 119.06, 115.68, 115.24, 115.13, 114.48, 114.29, 68.62, 68.42, 68.32, 32.05, 31.67, 29.79, 29.76, 29.73, 29.71, 29.53, 29.47, 29.43, 29.35, 29.22, 29.19, 26.20, 26.00, 25.94, 25.80, 22.82, 22.71, 14.23,

	14.13.
EA:	calculated: C: 73.81 %, H: 6.80 %; found: C: 73.77 %, H: 6.81 %

1-[4-(Dodecyloxy)phenyl] 4-[3-({4-[(4-{[11-(4-{[4-(hexyloxy)phenyl]carbonyloxy}phenoxy)-undecyl]oxy}phenyl)carbonyloxy]phenyl}carbonyloxy)phenyl]benzene-1,4-dicarboxylate **16a**

(n = 12, m = 11, p = 6)

Formula:	$C_{76}H_{88}O_{14}$, M = 1225.54 g/mol
Synthesis:	according to the general procedure 10.3.3
Reagents:	300 mg (0.47 mmol) 1-[4-(dodecyloxy)phenyl] 4-{3-[(4-hydroxyphenyl)carbonyloxy]phenyl} benzene-1,4-dicarboxylate **i31(12)** 280 mg (0.47 mmol) 4-{[6-(4-{[4-(hexyloxy)phenyl]carbonyloxy}phenoxy)hexyl]oxy}-benzoic acid **i14(6,6)** 110 mg (0.52 mmol) DCC 5 mg DMAP 40 ml dichloromethane
Purification:	column chromatography, eluent: $CHCl_3$/EtOAc (10/0.2) and further recrystallisation from EtOAc/EtOH (10/0.2)
Yield:	460 mg (80 %), colorless solid
Transition temp.:	Cr 126 USmC$_a$P$_{AF}$ 130 I
^{1}H-NMR:	($CDCl_3$, J/Hz, 400 MHz) δ 8.31 (s, J = 7.6 Hz, 4H, Ar-H), 8.26 (d, J = 8.7 Hz, 2H, Ar-H), 8.13 (d, J = 8.8 Hz, 2H, Ar-H), 8.10 (d, J = 8.9 Hz, 2H, Ar-H), 7.50 (t, J = 8.1 Hz, 1H, Ar-H), 7.36 (d, J = 8.7 Hz, 2H, Ar-H), 7.23 – 7.17 (m, 3H, Ar-H), 7.13 (d, J = 9.0 Hz, 2H, Ar-H), 7.08 (d, J = 8.9 Hz, 2H, Ar-H), 6.97 (d, J = 8.9 Hz, 2H, Ar-H), 6.95 – 6.87 (m, 6H, Ar-H), 4.07 – 3.99 (m, 4H, OCH_2), 3.98 – 3.91 (m, 4H, OCH_2), 1.86 – 1.73 (m, 8H, $OCH_2C\mathbf{H}_2$), 1.52 – 1.40 (m, 8H, CH_2), 1.40 – 1.23 (m, 30H, CH_2), 0.93 – 0.84 (m, 6H, CH_3).
^{13}C-NMR:	($CDCl_3$, 100 MHz) δ 165.18, 164.45, 164.15, 163.94, 163.79, 163.78, 163.37, 157.06, 156.69, 155.49, 151.46, 151.18, 146.43, 144.43, 134.22, 133.55, 132.36, 132.13, 131.78, 130.23, 130.22, 129.90, 126.55, 122.42, 122.18, 122.11, 121.75, 119.45, 119.08, 115.69, 115.22, 115.11, 114.46, 114.27, 68.61, 68.54, 68.50, 68.41, 32.05, 31.67, 29.79, 29.76, 29.73, 29.71, 29.65, 29.64, 29.61, 29.53, 29.48, 29.47, 29.43, 29.24, 29.22, 26.19, 26.12, 25.80, 22.82, 22.71, 14.24, 14.14.
EA:	calculated: C: 74.49 %, H: 7.24 %; found: C: 74.62 %, H: 7.21 %

Compounds 13a, 14, 15b, 16b, 17a, 18 and 19 with E$_2$-group

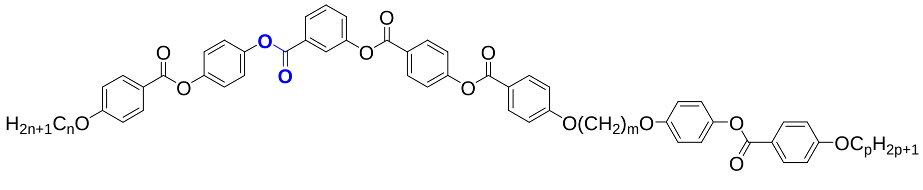

13a: n = 8; m = 6; p = 6
14: n = 12; m = 3; p = 6
15b: n = 12; m = 6; p = 6
16b: n = 12; m = 11; p = 6
17a: n = 16; m = 6; p = 6
18: n = 12; m = 6; p = 12
19: n = 12; m = 11; p = 12

4-{[3-({4-[(4-{[6-(4-{[4-(Hexyloxy)phenyl]carbonyloxy}phenoxy)hexyl]oxy}phenyl)carbonyl-oxy]phenyl}carbonyloxy)phenyl]carbonyloxy}phenyl 4-(octyloxy)benzoate **13a**

(n = 8, m = 6, p = 6)

Formula:	$C_{67}H_{70}O_{14}$, M = 1099.30 g/mol
Synthesis:	according to the general procedure 10.3.3
Reagents:	330 mg (0.56 mmol) 4-({3-[(4-hydroxyphenyl)carbonyloxy]phenyl}carbonyloxy)phenyl 4-(octyloxy)benzoate **i37(8)** 300 mg (0.56 mmol) 4-{[6-(4-{[4-(hexyloxy)phenyl]carbonyloxy}phenoxy)hexyl]oxy}-

benzoic acid **i14(6,6)**
130 mg (0.62 mmol) DCC
5 mg DMAP
40 ml dichloromethane

Purification: column chromatography, eluent: $CHCl_3$/EtOAc (10/0.2) and further recrystallisation from EtOAc/EtOH (10/0.2)

Yield: 450 mg (73 %), colorless solid

Transition temp.: Cr 155 (SmC_x 134) N 171 I

^{1}H-NMR: ($CDCl_3$, J/Hz, 400 MHz) δ 8.26 (d, J = 8.7 Hz, 2H, Ar-H), 8.12 (d, J = 8.8 Hz, 4H, Ar-H), 8.09 (d, J = 9.1 Hz, 4H, Ar-H), 8.05 – 8.02 (m, 1H, Ar-H), 7.56 (t, J = 7.9 Hz, 1H, Ar-H), 7.51 – 7.47 (m, 1H, Ar-H), 7.35 (d, J = 8.7 Hz, 2H, Ar-H), 7.21 (d, J = 8.8 Hz, 2H, Ar-H), 7.06 (d, J = 9.0 Hz, 2H d, Ar-H), 6.97 – 6.90 (m, 7H, Ar-H), 6.88 (d, J = 9.0 Hz, 2H d, J = 8.7 Hz, Ar-H), 4.04 (t, J = 6.4 Hz, 2H, OCH_2), 4.02 – 3.97 (m, 4H, OCH_2), 3.95 (t, J = 6.4 Hz, 2H, OCH_2), 1.87 – 1.74 (m, 8H, $OCH_2C\mathbf{H}_2$), 1.57 – 1.51 (m, 4H, CH_2), 1.48 – 1.40 (m, 4H, CH_2), 1.36 – 1.22 (m, 12H, CH_2), 0.90 – 0.84 (m, 6H, CH_3).

^{13}C-NMR: ($CDCl_3$, 125 MHz) δ 165.33, 164.79, 164.29, 164.27, 164.16, 163.80, 163.63, 163.48, 156.69, 155.63, 151.04, 148.68, 148.12, 144.50, 132.46, 132.32, 132.21, 131.90, 131.09, 129.79, 127.77, 127.24, 126.42, 123.56, 122.78, 122.53, 122.51, 122.22, 121.68, 121.37, 121.00, 115.09, 114.46, 114.35, 114.27, 68.37, 68.33, 68.22, 68.19, 31.82, 31.56, 29.34, 29.23, 29.22, 29.12, 29.08, 29.06, 26.00, 25.87, 25.81, 25.67, 22.67, 22.60, 14.11, 14.04.

EA: calculated: C: 73.21 %, H: 6.42 %; found: C: 73.10 %, H: 6.52 %

4-[(3-{[4-({4-[3-(4-{[4-(Hexyloxy)phenyl]carbonyloxy}phenoxy)propoxy]phenyl}carbonyloxy)phenyl]carbonyloxy}phenyl)carbonyloxy]phenyl 4-(dodecyloxy)benzoate **14** (n = 12, m = 3, p = 6)

Formula: $C_{68}H_{72}O_{14}$, M = 1113.32 g/mol

Synthesis: according to the general procedure 10.3.3

Reagents: 400 mg (0.63 mmol) 4-({3-[(4-hydroxyphenyl)carbonyloxy]phenyl}carbonyloxy)phenyl 4-(dodecyloxy)benzoate **i37(12)**
310 mg (0.63 mmol) 4-[3-(4-{[4-(hexyloxy)phenyl]carbonyloxy}phenoxy)propoxy]benzoic acid **i14(3,6)**
150 mg (0.69 mmol) DCC
5 mg DMAP
40 ml dichloromethane

Purification: column chromatography, eluent: $CHCl_3$/EtOAc (10/0.2) and further recrystallisation from EtOAc/EtOH (10/0.2)

Yield: 470 mg (67 %), colorless solid

Transition temp.: Cr 147 I

^{1}H-NMR: ($CDCl_3$, J/Hz, 400 MHz) δ 8.29 (d, J = 8.9 Hz, 2H, Ar-H), 8.17 – 8.08 (m, 7H, Ar-H), 7.59 (t, J = 7.9 Hz, 1H, Ar-H), 7.53 – 7.49 (m, 1H, Ar-H), 7.38 (d, J = 8.8 Hz, 2H, Ar-H), 7.26 (s, 5H, Ar-H), 7.10 (d, J = 9.1 Hz, 2H, Ar-H), 7.01 (d, J = 9.0 Hz, 2H, Ar-H), 6.98 – 6.91 (m, 6H, Ar-H), 4.27 (t, J = 6.1 Hz, 2H, OCH_2), 4.18 (t, J = 6.0 Hz, 2H, OCH_2), 4.06 – 4.00 (m, 4H, OCH_2), 2.35 – 2.27 (m, 2H, $OCH_2C\mathbf{H}_2$), 1.85 – 1.76 (m, 4H, $OCH_2C\mathbf{H}_2$), 1.51 – 1.42 (m, 4H, CH_2), 1.39 – 1.23 (m, 20H, CH_2), 0.93 – 0.84 (m, 6H, CH_3).

^{13}C-NMR: ($CDCl_3$, 100 MHz) δ 164.65, 164.16, 164.06, 163.69, 163.56, 156.43, 155.72, 151.21, 148.81, 148.24, 145.02, 132.45, 132.27, 132.17, 131.84, 131.29, 130.03, 129.67, 127.66, 123.51, 122.67, 122.59, 122.40, 122.13, 121.90, 121.66, 121.57, 115.32, 114.61, 114.47, 114.40, 68.50, 68.48, 65.05, 64.92, 31.96, 31.59, 29.68, 29.66, 29.61, 29.59, 29.39, 29.36, 29.21, 29.18, 26.06, 25.72, 22.70, 22.59, 14.05, 13.94.

EA: calculated: C: 73.36 %, H: 6.52 %; found: C: 73.23 %, H: 6.61 %

4-{[3-({4-[(4-{[6-(4-{[4-(Hexyloxy)phenyl]carbonyloxy}phenoxy)hexyl]oxy}phenyl)carbonyloxy]phenyl}carbonyloxy)phenyl]carbonyloxy}phenyl 4-(dodecyloxy)benzoate **15b** (*n* = 12, *m* = 6, *p* = 6)

Formula:	$C_{71}H_{78}O_{14}$, M = 1155.40 g/mol
Synthesis:	according to the general procedure 10.3.3
Reagents:	360 mg (0.56 mmol) 4-({3-[(4-hydroxyphenyl)carbonyloxy]phenyl}carbonyloxy)phenyl 4-(dodecyloxy)benzoate **i37(12)** 300 mg (0.56 mmol) 4-{[6-(4-{[4-(hexyloxy)phenyl]carbonyloxy}phenoxy)hexyl]oxy}-benzoic acid **i14(6,6)** 130 mg (0.62 mmol) DCC 5 mg DMAP 40 ml dichloromethane
Purification:	column chromatography, eluent: $CHCl_3$/EtOAc (10/0.2) and further recrystallisation from EtOAc/EtOH (10/0.2)
Yield:	400 mg (62 %), colorless solid
Transition temp.:	Cr 159 (SmC_x 148) N 166 I
^{1}H-NMR:	($CDCl_3$, *J*/Hz, 400 MHz) δ 8.28 (d, *J* = 8.9 Hz, 2H, Ar-H), 8.17 – 8.08 (m, 7H, Ar-H), 8.07 – 8.04 (m, 1H, Ar-H), 7.59 (t, *J* = 8.0 Hz, 1H, Ar-H), 7.53 – 7.49 (m, 1H, Ar-H), 7.38 (d, *J* = 8.8 Hz, 2H, Ar-H), 7.26 (s, 4H, Ar-H), 7.08 (d, *J* = 9.1 Hz, 2H, Ar-H), 6.98 (d, *J* = 9.0 Hz, 3H, Ar-H), 6.96 – 6.88 (m, 5H, Ar-H), 4.09 – 4.00 (m, 6H, OCH_2), 3.98 (t, *J* = 6.4 Hz, 2H, OCH_2), 1.91 – 1.76 (m, 8H, $OCH_2C\mathbf{H}_2$), 1.60 – 1.54 (m, 4H, CH_2), 1.51 – 1.41 (m, 6H, CH_2), 1.39 – 1.23 (m, 18H, CH_2), 0.93 – 0.84 (m, 6H, CH_3).
^{13}C-NMR:	($CDCl_3$, 100 MHz) δ 164.59, 164.11, 163.99, 163.55, 163.40, 156.63, 155.60, 151.05, 148.67, 148.10, 144.78, 132.37, 132.23, 132.12, 131.80, 129.66, 127.64, 123.48, 122.67, 122.44, 122.40, 122.12, 115.15, 114.49, 114.38, 114.30, 68.47, 68.44, 68.36, 68.33, 32.03, 31.66, 29.76, 29.74, 29.69, 29.66, 29.47, 29.44, 29.35, 29.25, 29.22, 29.19, 26.12, 25.99, 25.93, 25.78, 22.79, 22.68, 14.18, 14.09.
EA:	calculated: C: 73.81 %, H: 6.80 %; found: C: 73.80 %, H: 6.87 %

4-{[3-({4-[(4-{[11-(4-{[4-(Hexyloxy)phenyl]carbonyloxy}phenoxy)undecyl]oxy}phenyl)-carbonyloxy]phenyl}carbonyloxy)phenyl]carbonyloxy}phenyl 4-(dodecyloxy)benzoate **16b** (*n* = 12, *m* = 11, *p* = 6)

Formula:	$C_{76}H_{88}O_{14}$, M = 1225.54 g/mol
Synthesis:	according to the general procedure 10.3.3
Reagents:	500 mg (0.78 mmol) 4-({3-[(4-hydroxyphenyl)carbonyloxy]phenyl}carbonyloxy)phenyl 4-(dodecyloxy)benzoate **i37(12)** 470 mg (0.78 mmol) 4-{[11-(4-{[4-(hexyloxy)phenyl]carbonyloxy}phenoxy)undecyl]oxy}-benzoic acid **i14(11,6)** 180 mg (0.86 mmol) DCC 5 mg DMAP 60 ml dichloromethane
Purification:	column chromatography, eluent: $CHCl_3$/EtOAc (10/0.2) and further recrystallisation from EtOAc/EtOH (10/0.2)
Yield:	720 mg (75 %), colorless solid
Transition temp.:	Cr 131 (Col_x 128 N 129) I
^{1}H-NMR:	($CDCl_3$, *J*/Hz, 400 MHz) δ 8.28 (d, *J* = 8.7 Hz, 2H, Ar-H), 8.17 – 8.08 (m, 7H, Ar-H), 8.07 – 8.04 (m, 1H, Ar-H), 7.59 (t, *J* = 7.9 Hz, 1H, Ar-H), 7.54 – 7.49 (m, 1H, Ar-H), 7.38 (d, *J* = 8.7 Hz, 2H, Ar-H), 7.26 (s, 4H, Ar-H), 7.08 (d, *J* = 9.0 Hz, 2H, Ar-H), 7.00 – 6.86 (m, 8H, Ar-H), 4.08 – 3.99 (m, 6H, OCH_2), 3.94 (t, *J* = 6.5 Hz, 2H, OCH_2), 1.86 – 1.73 (m, 8H, $OCH_2C\mathbf{H}_2$), 1.52 – 1.41 (m, 8H, CH_2), 1.40 – 1.22 (m, 30H, CH_2), 0.94 – 0.84 (m, 6H, CH_3).
^{13}C-NMR:	($CDCl_3$, 100 MHz) δ 165.18, 164.65, 164.15, 164.03, 163.78, 163.54, 163.36, 156.69, 155.56, 150.99, 148.63, 148.06, 144.40, 132.38, 132.25, 132.14, 131.83, 131.08, 129.70, 127.69,

127.43, 127.16, 126.40, 123.51, 122.72, 122.45, 122.43, 122.16, 121.73, 121.40, 120.95, 115.10, 114.46, 114.35, 114.26, 68.53, 68.50, 68.45, 68.41, 32.05, 31.68, 29.79, 29.77, 29.72, 29.69, 29.66, 29.65, 29.62, 29.50, 29.48, 29.44, 29.25, 29.23, 26.19, 26.13, 25.81, 22.83, 22.73, 14.26, 14.16.

EA: calculated: C: 74.49 %, H: 7.24 %; found: C: 74.34 %, H: 7.32 %

4-{[3-({4-[(4-{[6-(4-{[4-(Hexyloxy)phenyl]carbonyloxy}phenoxy)hexyl]oxy}phenyl)carbonyloxy]phenyl}carbonyloxy)phenyl]carbonyloxy}phenyl 4-(hexadecyloxy)benzoate **17a**

(n = 16, m = 6, p = 6)

Formula: $C_{75}H_{86}O_{14}$, M = 1211.51 g/mol

Synthesis: according to the general procedure 10.3.3

Reagents: 390 mg (0.56 mmol) 4-({3-[(4-hydroxyphenyl)carbonyloxy]phenyl}carbonyloxy)phenyl 4-(hexadecyloxy)benzoate **i37(16)**
300 mg (0.56 mmol) 4-{[6-(4-{[4-(hexyloxy)phenyl]carbonyloxy}phenoxy)hexyl]oxy}-benzoic acid **i14(6,6)**
130 mg (0.62 mmol) DCC
5 mg DMAP
40 ml dichloromethane

Purification: column chromatography, eluent: $CHCl_3$/EtOAc (10/0.2) and further recrystallisation from EtOAc/EtOH (10/0.2)

Yield: 450 mg (66 %), colorless solid

Transition temp.: Cr 160 (SmC_x 144) SmA 163 N 164 I

^{1}H-NMR: ($CDCl_3$, *J*/Hz, 500 MHz) δ 8.26 (d, *J* = 8.7 Hz, 2H, Ar-H), 8.12 (d, *J* = 9.1 Hz, 3H, Ar-H), 8.09 (d, *J* = 9.0 Hz, 4H, Ar-H), 8.04 – 8.02 (m, 1H, Ar-H), 7.56 (t, *J* = 7.9 Hz, 1H, Ar-H), 7.51 – 7.47 (m, 1H, Ar-H), 7.36 (d, *J* = 8.7 Hz, 2H, Ar-H), 7.23 (d, *J* = 8.8 Hz, 4H, Ar-H), 7.06 (d, *J* = 9.0 Hz, 2H, Ar-H), 6.98 – 6.90 (m, 6H, Ar-H), 6.88 (d, *J* = 9.0 Hz, 2H, Ar-H), 4.04 (t, *J* = 6.4 Hz, 2H, OCH_2), 4.03 – 3.98 (m, 4H, OCH_2), 3.95 (t, *J* = 6.4 Hz, 2H, OCH_2), 1.87 – 1.74 (m, 8H, $OCH_2C\mathbf{H}_2$), 1.57 – 1.52 (m, 4H, CH_2), 1.47 – 1.40 (m, 4H, CH_2), 1.36 – 1.29 (m, 8H, CH_2), 1.28 – 1.20 (m, 20H, CH_2), 0.88 (t, *J* = 7.1 Hz, 3H, CH_3), 0.84 (t, *J* = 6.9 Hz, 3H, CH_3).

^{13}C-NMR: ($CDCl_3$, 125 MHz) δ 165.34, 164.79, 164.29, 164.17, 163.80, 163.63, 163.47, 156.69, 155.62, 151.03, 148.68, 148.11, 144.49, 132.46, 132.31, 132.21, 131.90, 131.09, 129.78, 127.77, 127.23, 126.42, 123.56, 122.78, 122.52, 122.50, 122.22, 121.67, 121.37, 121.00, 115.09, 114.46, 114.34, 114.27, 68.37, 68.33, 68.22, 68.19, 31.94, 31.55, 29.70, 29.69, 29.67, 29.60, 29.57, 29.37, 29.21, 29.11, 29.08, 29.05, 25.99, 25.87, 25.81, 25.67, 22.70, 22.59, 14.12, 14.02.

EA: calculated: C: 74.36 %, H: 7.16 %; found: C: 74.30 %, H: 7.27 %

4-{[3-({4-[(4-{[6-(4-{[4-(Dodecyloxy)phenyl]carbonyloxy}phenoxy)hexyl]oxy}phenyl)-carbonyloxy]phenyl}carbonyloxy)phenyl]carbonyloxy}phenyl 4-(dodecyloxy)benzoate **18**

(n = 12, m = 6, p = 12)

Formula: $C_{77}H_{90}O_{14}$, M = 1239.57 g/mol

Synthesis: according to the general procedure 10.3.3

Reagents: 310 mg (0.48 mmol) 4-({3-[(4-hydroxyphenyl)carbonyloxy]phenyl}carbonyloxy)phenyl 4-(dodecyloxy)benzoate **i37(12)**
300 mg (0.48 mmol) 4-{[6-(4-{[4-(dodecyloxy)phenyl]carbonyloxy}phenoxy)hexyl]oxy}-benzoic acid **i14(6,12)**
110 mg (0.53 mmol) DCC
5 mg DMAP
40 ml dichloromethane

Purification: column chromatography, eluent: $CHCl_3$/EtOAc (10/0.2) and further recrystallisation from EtOAc/EtOH (10/0.2)

Yield: 420 mg (71 %), colorless solid

Transition temp.: Cr 140 ($SmC_s'P_{AF}$ 131) SmC_sP_{AF} 163 I

^{1}H-NMR: ($CDCl_3$, *J*/Hz, 400 MHz) δ 8.28 (d, *J* = 8.8 Hz, 2H, Ar-H), 8.16 – 8.08 (m, 7H, Ar-H), 8.06 – 8.04 (m, 1H, Ar-H), 7.59 (t, *J* = 7.9 Hz, 1H, Ar-H), 7.53 – 7.49 (m, 1H, Ar-H), 7.38 (d, *J* = 8.8 Hz, 2H, Ar-H), 7.26 (s, 4H, Ar-H), 7.08 (d, *J* = 9.1 Hz, 2H, Ar-H), 6.98 (d, *J* = 9.0 Hz, 3H, Ar-H), 6.96 – 6.92 (m, 3H, Ar-H), 6.90 (d, *J* = 9.1 Hz, 2H, Ar-H), 4.09 – 4.00 (m, 6H, OCH_2), 3.98 (t, *J* = 6.4 Hz, 2H, OCH_2), 1.81 (m, 8H, $OCH_2C\mathbf{H}_2$), 1.59 – 1.54 (m, 4H, CH_2), 1.49 – 1.41 (m, 4H, CH_2), 1.39 – 1.23 (m, 32H, CH_2), 0.90 – 0.84 (m, 6H, CH_3).

^{13}C-NMR: ($CDCl_3$, 100 MHz) δ 165.35, 164.81, 164.30, 164.19, 163.82, 163.65, 163.49, 156.71, 155.65, 151.06, 148.70, 148.13, 144.51, 132.48, 132.33, 132.22, 131.92, 131.11, 129.80, 127.79, 127.25, 126.44, 123.58, 122.80, 122.54, 122.53, 122.24, 121.69, 121.39, 121.02, 115.11, 114.48, 114.37, 114.29, 68.38, 68.35, 68.24, 68.21, 31.95, 29.68, 29.66, 29.62, 29.58, 29.39, 29.38, 29.24, 29.13, 29.07, 26.01, 25.89, 25.83, 22.72, 14.15.

EA: calculated: C: 74.61 %, H: 7.32 %; found: C: 74.52 %, H: 7.39 %

4-{[3-({4-[(4-{[11-(4-{[4-(Dodecyloxy)phenyl]carbonyloxy}phenoxy)undecyl]oxy}phenyl)-carbonyloxy]phenyl}carbonyloxy)phenyl]carbonyloxy}phenyl 4-(dodecyloxy)benzoate **19** (*n* = 12, *m* = 11, *p* = 12)

Formula: $C_{82}H_{100}O_{14}$, M = 1309.70 g/mol

Synthesis: according to the general procedure 10.3.3

Reagents: 290 mg (0.46 mmol) 4-({3-[(4-hydroxyphenyl)carbonyloxy]phenyl}carbonyloxy)phenyl 4-(dodecyloxy)benzoate **i37(12)**
320 mg (0.46 mmol) 4-{[11-(4-{[4-(dodecyloxy)phenyl]carbonyloxy}phenoxy)undecyl]oxy}-benzoic acid **i14(11,12)**
110 mg (0.51 mmol) DCC
5 mg DMAP
40 ml dichloromethane

Purification: column chromatography, eluent: $CHCl_3$/EtOAc (10/0.2) and further recrystallisation from EtOAc/EtOH (10/0.2)

Yield: 430 mg (71 %), colorless solid

Transition temp.: Cr 133 (Col_r 131) I

^{1}H-NMR: ($CDCl_3$, *J*/Hz, 400 MHz) δ 8.28 (d, *J* = 8.9 Hz, 2H, Ar-H), 8.16 – 8.08 (m, 7H, Ar-H), 8.07 – 8.04 (m, 1H, Ar-H), 7.59 (t, *J* = 8.0 Hz, 1H, Ar-H), 7.53 – 7.49 (m, 1H, Ar-H), 7.38 (d, *J* = 8.9 Hz, 2H, Ar-H), 7.26 (s, 4H, Ar-H), 7.08 (d, *J* = 9.1 Hz, 2H, Ar-H), 7.00 – 6.92 (m, 6H, Ar-H), 6.90 (d, *J* = 9.1 Hz, 2H, Ar-H), 4.03 (m, 6H, OCH_2), 3.94 (t, *J* = 6.5 Hz, 2H, OCH_2), 1.86 – 1.73 (m, 8H, $OCH_2C\mathbf{H}_2$), 1.51 – 1.40 (m, 8H, CH_2), 1.40 – 1.23 (m, 42H, CH_2), 0.90 – 0.84 (m, 6H, CH_3).

^{13}C-NMR: ($CDCl_3$, 100 MHz) δ 165.35, 164.81, 164.31, 164.19, 163.89, 163.65, 163.48, 156.79, 155.65, 151.06, 148.70, 148.13, 144.44, 132.46, 132.33, 132.22, 131.92, 131.11, 129.80, 127.79, 127.26, 126.43, 123.58, 122.80, 122.52, 122.49, 122.24, 121.71, 121.39, 120.95, 115.10, 114.47, 114.37, 114.28, 68.44, 68.38, 68.35, 31.95, 29.68, 29.66, 29.62, 29.58, 29.56, 29.55, 29.51, 29.39, 29.38, 29.31, 29.13, 26.07, 26.01, 22.72, 14.14.

EA: calculated: C: 75.20 %, H: 7.70 %; found: C: 75.07 %, H: 7.68 %

Compounds 13b, 15c and 17b with E$_3$-group

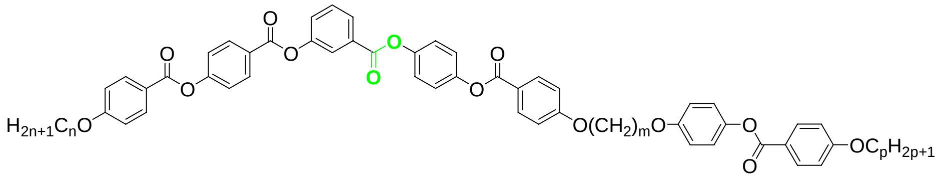

13b: *n* = 8; *m* = 6; *p* = 6
15c: *n* = 12; *m* = 6; *p* = 6
17b: *n* = 16; *m* = 6; *p* = 6

4-(3-{4-[(4-{[6-(4-{[4-(Hexyloxy)phenyl]carbonyloxy}phenoxy)hexyl]oxy}phenyl)carbonyloxy]phenoxycarbonyl}phenoxycarbonyl)phenyl 4-(octyloxy)benzoate **13b** (*n* = 8, *m* = 6, *p* = 6)

Formula:	$C_{67}H_{70}O_{14}$, M = 1099.30 g/mol
Synthesis:	according to the general procedure 10.3.3
Reagents:	330 mg (0.56 mmol) 4-[3-(4-hydroxyphenoxycarbonyl)phenoxycarbonyl]phenyl 4-(octyloxy)-benzoate **i41(8)** 300 mg (0.56 mmol) 4-{[6-(4-{[4-(hexyloxy)phenyl]carbonyloxy}phenoxy)hexyl]oxy}-benzoic acid **i14(6,6)** 130 mg (0.62 mmol) DCC 5 mg DMAP 40 ml dichloromethane
Purification:	column chromatography, eluent: $CHCl_3$/EtOAc (10/0.2) and further recrystallisation from EtOAc/EtOH (10/0.2)
Yield:	420 mg (68 %), colorless solid
Transition temp.:	Cr 147 (Col$_x$ 127 N$_x$ 129) N 167 I
^{1}H-NMR:	($CDCl_3$, *J*/Hz, 500 MHz) δ 8.29 (d, *J* = 8.8 Hz, 2H, Ar-H), 8.16 – 8.09 (m, 7H, Ar-H), 8.07 – 8.05 (m, 1H, Ar-H), 7.59 (t, *J* = 7.9 Hz, 1H, Ar-H), 7.53 – 7.50 (m, 1H, Ar-H), 7.38 (d, *J* = 8.8 Hz, 2H, Ar-H), 7.26 (s, 4H, Ar-H), 7.09 (d, *J* = 9.0 Hz, 2H, Ar-H), 7.00 – 6.92 (m, 6H, Ar-H), 6.90 (d, *J* = 9.0 Hz, 2H, Ar-H), 4.08 – 4.00 (m, 6H, OCH_2), 3.97 (t, *J* = 6.4 Hz, 2H, OCH_2), 1.89 – 1.77 (m, 8H, OCH_2**C**$\mathbf{H_2}$), 1.59 – 1.53 (m, 4H, CH_2), 1.50 – 1.43 (m, 4H, CH_2), 1.39 – 1.25 (m, 12H, CH_2), 0.92 – 0.86 (m, 6H, CH_3).
^{13}C-NMR:	($CDCl_3$, 125 MHz) δ 165.33, 164.78, 164.29, 164.16, 163.87, 163.56, 163.47, 156.70, 155.63, 151.04, 148.68, 148.12, 144.49, 132.44, 132.34, 132.21, 131.90, 131.09, 129.78, 127.77, 127.23, 126.42, 123.56, 122.78, 122.52, 122.51, 122.22, 121.69, 121.44, 120.93, 115.09, 114.45, 114.35, 114.27, 68.42, 68.33, 68.20, 68.17, 31.81, 31.56, 29.33, 29.23, 29.10, 29.08, 26.00, 25.88, 25.82, 25.67, 22.67, 22.59, 14.11, 14.03.
EA:	calculated: C: 73.21 %, H: 6.42 %; found: C: 73.07 %, H: 6.57 %

4-(3-{4-[(4-{[6-(4-{[4-(Hexyloxy)phenyl]carbonyloxy}phenoxy)hexyl]oxy}phenyl)carbonyloxy]phenoxycarbonyl}phenoxycarbonyl)phenyl 4-(dodecyloxy)benzoate **15c** (*n* = 12, *m* = 6, *p* = 6)

Formula:	$C_{71}H_{78}O_{14}$, M = 1155.40 g/mol
Synthesis:	according to the general procedure 10.3.3
Reagents:	360 mg (0.57 mmol) 4-[3-(4-hydroxyphenoxycarbonyl)phenoxycarbonyl]phenyl 4-(dodecyloxy)benzoate **i41(12)** 300 mg (0.57 mmol) 4-{[6-(4-{[4-(hexyloxy)phenyl]carbonyloxy}phenoxy)hexyl]oxy}-benzoic acid **i14(6,6)** 130 mg (0.63 mmol) DCC 5 mg DMAP 40 ml dichloromethane
Purification:	column chromatography, eluent: $CHCl_3$/EtOAc (10/0.2) and further recrystallisation from EtOAc/EtOH (10/0.2)
Yield:	400 mg (61 %), colorless solid
Transition temp.:	Cr 145 (Col$_x$ 130) N 161 I

^{1}H-NMR: (CDCl$_3$, *J*/Hz, 400 MHz) δ 8.29 (d, *J* = 8.7 Hz, 2H, Ar-H), 8.16 – 8.09 (m, 7H, Ar-H), 8.07 – 8.05 (m, 1H, Ar-H), 7.59 (t, *J* = 7.9 Hz, 1H, Ar-H), 7.54 – 7.49 (m, 1H, Ar-H), 7.40 – 7.35 (m, 2H, Ar-H), 7.26 (s, 4H, Ar-H), 7.09 (d, *J* = 9.0 Hz, 2H, Ar-H), 7.00 – 6.93 (m, 6H, Ar-H), 6.90 (d, *J* = 9.0 Hz, 2H, Ar-H), 4.08 – 4.00 (m, 6H, OCH$_2$), 3.97 (t, *J* = 6.4 Hz, 2H, OCH$_2$), 1.89 – 1.77 (m, 8H, OCH$_2$C$\mathbf{H}_2$), 1.60 – 1.54 (m, 4H, CH$_2$), 1.46 (m, 4H, CH$_2$), 1.38 – 1.22 (m, 20H, CH$_2$), 0.93 – 0.84 (m, 6H, CH$_3$).

^{13}C-NMR: (CDCl$_3$, 125 MHz) δ 165.33, 164.78, 164.29, 164.16, 163.87, 163.56, 163.46, 156.70, 155.63, 151.03, 148.68, 148.12, 144.49, 132.44, 132.34, 132.21, 131.91, 131.09, 129.78, 127.77, 127.23, 126.42, 123.56, 122.78, 122.51, 122.21, 121.69, 121.44, 120.92, 115.09, 114.45, 114.35, 114.27, 68.42, 68.32, 68.20, 68.17, 31.93, 31.56, 29.67, 29.64, 29.60, 29.57, 29.36, 29.22, 29.10, 29.08, 25.99, 25.88, 25.82, 25.67, 22.70, 22.59, 14.13, 14.03.

EA: calculated: C: 73.81 %, H: 6.80 %; found: C: 73.74 %, H: 6.82 %

4-(3-{4-[(4-{[6-(4-{[4-(Hexyloxy)phenyl]carbonyloxy}phenoxy)hexyl]oxy}phenyl)carbonyloxy]phenoxycarbonyl}phenoxycarbonyl)phenyl 4-(hexadecyloxy)benzoate **17b** (n = 16, m = 6, p = 6)

Formula: C$_{75}$H$_{86}$O$_{14}$, M = 1211.51 g/mol

Synthesis: according to the general procedure 10.3.3

Reagents: 390 mg (0.56 mmol) 4-[3-(4-hydroxyphenoxycarbonyl)phenoxycarbonyl]phenyl 4-(hexadecyloxy)benzoate **i41(16)**
300 mg (0.56 mmol) 4-{[6-(4-{[4-(hexyloxy)phenyl]carbonyloxy}phenoxy)hexyl]oxy}-benzoic acid **i14(6,6)**
130 mg (0.62 mmol) DCC
5 mg DMAP
40 ml dichloromethane

Purification: column chromatography, eluent: CHCl$_3$/EtOAc (10/0.2) and further recrystallisation from EtOAc/EtOH (10/0.2)

Yield: 450 mg (66 %), colorless solid

Transition temp.: Cr 149 (Col$_x$ 133) N 158 I

^{1}H-NMR: (CDCl$_3$, *J*/Hz, 400 MHz) δ 8.26 (d, *J* = 8.5 Hz, 2H, Ar-H), 8.15 – 8.06 (m, 7H, Ar-H), 8.05 – 8.02 (m, 1H, Ar-H), 7.56 (t, *J* = 7.9 Hz, 1H, Ar-H), 7.52 – 7.47 (m, 1H, Ar-H), 7.36 (d, *J* = 8.6 Hz, 2H, Ar-H), 7.22 (s, 4H, Ar-H), 7.06 (d, *J* = 8.8 Hz, 2H, Ar-H), 6.98 – 6.92 (m, 5H, Ar-H), 6.92 – 6.85 (m, 3H, Ar-H), 4.07 – 3.98 (m, 6H, OCH$_2$), 3.95 (t, *J* = 6.4 Hz, 2H, OCH$_2$), 1.88 – 1.73 (m, 8H, OCH$_2$C$\mathbf{H}_2$), 1.58 – 1.52 (m, 4H, CH$_2$), 1.49 – 1.39 (m, 4H, CH$_2$), 1.38 – 1.20 (m, 28H, CH$_2$), 0.91 – 0.81 (m, 6H, CH$_3$).

^{13}C-NMR: (CDCl$_3$, 100 MHz) δ 165.18, 164.64, 164.15, 164.03, 163.77, 163.46, 163.37, 156.62, 155.56, 148.62, 148.06, 132.38, 132.27, 132.15, 131.84, 131.08, 129.71, 127.70, 127.16, 126.41, 125.65, 123.51, 122.72, 122.47, 122.45, 122.16, 121.47, 120.95, 115.10, 114.45, 114.35, 114.27, 68.51, 68.41, 68.31, 68.25, 32.06, 31.68, 29.83, 29.79, 29.73, 29.69, 29.50, 29.36, 29.24, 29.23, 26.14, 26.02, 25.96, 25.81, 22.84, 22.73, 14.26, 14.16.

EA: calculated: C: 74.36 %, H: 7.16 %; found: C: 74.31 %, H: 7.23 %

Compound 15d with E_4-group

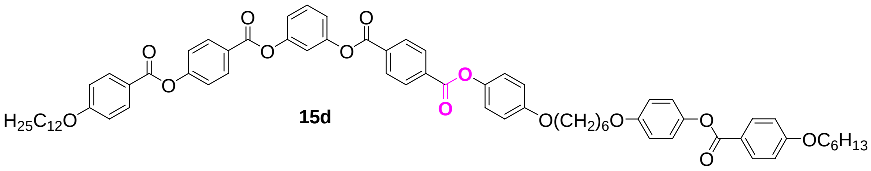

15d

1-{3-[(4-{[4-(Dodecyloxy)phenyl]carbonyloxy}phenyl)carbonyloxy]phenyl} 4-(4-{[6-(4-{[4-(hexyloxy)phenyl]carbonyloxy}phenoxy)hexyl]oxy}phenyl)benzene-1,4-dicarboxylate **15d** (*n* = 12, *m* = 6, *p* = 6)

Formula:	$C_{71}H_{78}O_{14}$, M = 1155.40 g/mol
Synthesis:	according to the general procedure 10.3.3
Reagents:	490 mg (0.73 mmol) 4-{3-[(4-{[4-(dodecyloxy)phenyl]carbonyloxy}phenyl)carbonyloxy]-phenoxycarbonyl}benzoic acid **i43(12)** 370 mg (0.73 mmol) 4-{[6-(4-hydroxyphenoxy)hexyl]oxy}phenyl 4-(hexyloxy)benzoate **i45(6,6)** 170 mg (0.80 mmol) DCC 5 mg DMAP 40 ml dichloromethane
Purification:	column chromatography, eluent: $CHCl_3$/EtOAc (10/0.2) and further recrystallisation from EtOAc/EtOH (10/0.2)
Yield:	560 mg (66 %), colorless solid
Transition temp.:	Cr 145 (Col_x 130) N 161 I
^{1}H-NMR:	($CDCl_3$, *J*/Hz, 400 MHz) δ 8.31 (s, 4H, Ar-H), 8.26 (d, *J* = 8.7 Hz, 2H, Ar-H), 8.13 (d, *J* = 8.9 Hz, 2H, Ar-H), 8.10 (d, *J* = 8.8 Hz, 2H, Ar-H), 7.49 (t, *J* = 8.1 Hz, 1H, Ar-H), 7.36 (d, *J* = 8.7 Hz, 2H, Ar-H), 7.23 – 7.17 (m, 3H, Ar-H), 7.13 (d, *J* = 9.0 Hz, 2H, Ar-H), 7.08 (d, *J* = 9.0 Hz, 2H, Ar-H), 6.99 – 6.87 (m, 8H, Ar-H), 4.06 – 3.94 (m, 8H, OCH_2), 1.87 – 1.75 (m, 8H, $OCH_2\mathbf{CH_2}$), 1.59 – 1.51 (m, 4H, CH_2), 1.51 – 1.42 (m, 4H, CH_2), 1.39 – 1.22 (m, 20H, CH_2), 0.93 – 0.84 (m, 6H, CH_3).
^{13}C-NMR:	($CDCl_3$, 100 MHz) δ 165.14, 164.42, 164.13, 163.93, 163.78, 163.37, 157.00, 156.65, 155.50, 151.47, 151.21, 144.48, 144.10, 134.23, 133.53, 132.36, 132.13, 131.77, 130.22, 129.88, 126.57, 122.44, 122.21, 122.10, 121.78, 121.00, 119.44, 119.06, 115.68, 115.24, 115.13, 114.46, 114.28, 68.51, 68.42, 68.38, 32.04, 31.67, 29.78, 29.76, 29.71, 29.68, 29.48, 29.46, 29.39, 29.37, 29.24, 29.23, 26.13, 26.01, 25.80, 22.82, 22.71, 14.23, 14.13.
EA:	calculated: C: 73.81 %, H: 6.80 %; found: C: 73.76 %, H: 6.72 %

Compounds 20-22

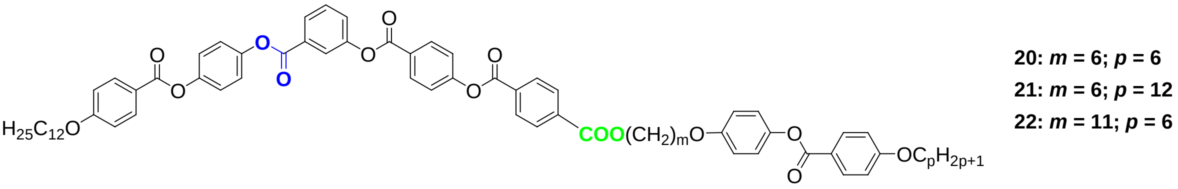

20: *m* = 6; *p* = 6
21: *m* = 6; *p* = 12
22: *m* = 11; *p* = 6

1-{4-[3-(4-{[4-(Dodecyloxy)phenyl]carbonyloxy}phenoxycarbonyl)phenoxycarbonyl]phenyl} 4-[6-(4-{[4-(hexyloxy)phenyl]carbonyloxy}phenoxy)hexyl]benzene-1,4-dicarboxylate **20** (*n* = 12, *m* = 6, *p* = 6)

Formula:	$C_{72}H_{78}O_{15}$, M = 1183.42 g/mol
Synthesis:	according to the general procedure 10.3.3
Reagents:	110 mg (0.18 mmol) 4-({3-[(4-hydroxyphenyl)carbonyloxy]phenyl}carbonyloxy)phenyl 4-

(dodecyloxy)benzoate **i37(12)**
100 mg (0.18 mmol) 4-({[6-(4-{[4-(hexyloxy)phenyl]carbonyloxy}phenoxy)hexyl]oxy}carbonyl)benzoic acid **i17(6,6)**
40 mg (0.20 mmol) DCC
5 mg DMAP
30 ml dichloromethane
Purification: column chromatography, eluent: $CHCl_3$/EtOAc (10/0.2) and further recrystallisation from EtOAc/EtOH (10/0.2)
Yield: 140 mg (66 %), colorless solid
Transition temp.: Cr 138 (Col_x 117) I
^{1}H-NMR: ($CDCl_3$, J/Hz, 400 MHz) δ 8.30 (d, J = 8.6 Hz, 2H, Ar-H), 8.28 – 8.22 (m, J = 8.4 Hz, 2H, Ar-H), 8.18 (d, J = 8.3 Hz, 2H, Ar-H), 8.15 – 8.02 (m, 6H, Ar-H), 7.59 (t, J = 7.8 Hz, 1H, Ar-H), 7.54 – 7.49 (m, 1H, Ar-H), 7.41 (d, J = 8.6 Hz, 2H, Ar-H), 7.26 (s, 4H, Ar-H), 7.08 (d, J = 9.0 Hz, 2H, Ar-H), 6.98 – 6.87 (m, 6H, Ar-H), 4.39 (t, J = 6.6 Hz, 2H, $COOCH_2$), 4.02 (q, J = 6.5 Hz, 4H, OCH_2), 3.97 (t, J = 6.3 Hz, 2H, OCH_2), 1.88 – 1.75 (m, 8H, $OCH_2C\mathbf{H}_2$, $COOCH_2C\mathbf{H}_2$), 1.61 – 1.54 (m, 4H, CH_2), 1.49 – 1.41 (m, 4H, CH_2), 1.39 – 1.23 (m, 20H, CH_2), 0.93 – 0.84 (m, 6H, CH_3).
^{13}C-NMR: ($CDCl_3$, 100 MHz) δ 165.67, 165.35, 164.83, 164.18, 163.83, 163.66, 163.50, 156.70, 155.17, 151.02, 148.72, 148.13, 144.52, 135.23, 132.69, 132.34, 132.23, 132.05, 131.93, 131.15, 130.28, 129.83, 127.22, 126.94, 123.57, 122.82, 122.54, 122.53, 122.08, 121.69, 121.38, 115.11, 114.38, 114.29, 68.40, 68.20, 65.64, 31.96, 31.58, 29.69, 29.67, 29.62, 29.59, 29.38, 29.21, 29.14, 29.10, 28.67, 26.02, 25.86, 25.69, 22.73, 22.62, 14.15, 14.05.
EA: calculated: C: 73.08 %, H: 6.64 %; found: C: 72.89 %, H: 6.79 %

1-[6-(4-{[4-(Dodecyloxy)phenyl]carbonyloxy}phenoxy)hexyl] 4-{4-[3-(4-{[4-(dodecyloxy)phenyl]carbonyloxy}phenoxycarbonyl)phenoxycarbonyl]phenyl}benzene-1,4-dicarboxylate **21** (*n* = 12, *m* = 6, *p* = 12)

Formula: $C_{78}H_{90}O_{15}$, M = 1267.58 g/mol
Synthesis: according to the general procedure 10.3.3
Reagents: 200 mg (0.31 mmol) 4-({3-[(4-hydroxyphenyl)carbonyloxy]phenyl}carbonyloxy)phenyl 4-(dodecyloxy)benzoate **i37(12)**
200 mg (0.31 mmol) 4-({[6-(4-{[4-(dodecyloxy)phenyl]carbonyloxy}phenoxy)hexyl]oxy}carbonyl)benzoic acid **i17(6,12)**
70 mg (0.34 mmol) DCC
5 mg DMAP
40 ml dichloromethane
Purification: column chromatography, eluent: $CHCl_3$/EtOAc (10/0.2) and further recrystallisation from EtOAc/EtOH (10/0.2)
Yield: 280 mg (71 %), colorless solid
Transition temp.: Cr 130 Col_xP_{FE} 146 I
^{1}H-NMR: ($CDCl_3$, J/Hz, 400 MHz) δ 8.30 (d, J = 8.8 Hz, 2H, Ar-H), 8.27 (d, J = 8.7 Hz, 2H, Ar-H, Ar-H), 8.18 (d, J = 8.7 Hz, 2H, Ar-H, Ar-H), 8.15 – 8.05 (m, 6H, Ar-H), 7.59 (t, J = 7.9 Hz, 1H, Ar-H), 7.54 – 7.50 (m, 1H, Ar-H), 7.41 (d, J = 8.8 Hz, 2H, Ar-H), 7.26 (s, 4H, Ar-H), 7.08 (d, J = 9.1 Hz, 2H, Ar-H), 6.98 – 6.91 (m, 4H, Ar-H), 6.90 (d, J = 9.1 Hz, 2H, Ar-H), 4.39 (t, J = 6.6 Hz, 2H, $COOCH_2$), 4.02 (q, J = 14.1, 6.6 Hz, 4H, OCH_2), 3.97 (t, J = 6.3 Hz, 2H, OCH_2), 1.88 – 1.75 (m, 8H, $OCH_2C\mathbf{H}_2$, $COOCH_2C\mathbf{H}_2$), 1.60 – 1.54 (m, 4H, CH_2), 1.50 – 1.40 (m, 4H, CH_2), 1.39 – 1.22 (m, 32H, CH_2), 0.90 – 0.84 (m, 6H, CH_3).
^{13}C-NMR: ($CDCl_3$, 100 MHz) δ 165.66, 165.21, 164.69, 164.05, 163.70, 163.57, 163.40, 156.61, 155.08, 150.94, 148.64, 148.06, 144.52, 135.16, 132.63, 132.25, 132.14, 131.95, 131.09, 130.18, 129.74, 127.75, 127.11, 126.88, 123.48, 122.72, 122.46, 122.43, 121.98, 121.65, 121.35, 115.06, 114.32, 114.23, 68.37, 68.33, 68.19, 65.59, 31.94, 29.67, 29.65, 29.60, 29.57, 29.38, 29.36, 29.20, 29.13, 28.67, 26.01, 25.88, 25.85, 22.71, 14.13.
EA: calculated: C: 73.91 %, H: 7.16 %; found: C: 73.87 %, H: 7.15 %

1-{4-[3-(4-{[4-(Dodecyloxy)phenyl]carbonyloxy}phenoxycarbonyl)phenoxycarbonyl]phenyl} 4-[11-(4-{[4-(hexyloxy)phenyl]carbonyloxy}phenoxy)undecyl]benzene-1,4-dicarboxylate **22** (*n* = 12, *m* = 11, *p* = 6)

Formula:	$C_{77}H_{88}O_{15}$, M = 1253.55 g/mol
Synthesis:	according to the general procedure 10.3.3
Reagents:	200 mg (0.32 mmol) 4-({3-[(4-hydroxyphenyl)carbonyloxy]phenyl}carbonyloxy)phenyl 4-(dodecyloxy)benzoate **i37(12)** 200 mg (0.32 mmol) 4-({[6-(4-{[4-(dodecyloxy)phenyl]carbonyloxy}phenoxy)hexyl]oxy}-carbonyl)benzoic acid **i17(6,12)** 70 mg (0.35 mmol) DCC 5 mg DMAP 40 ml dichloromethane
Purification:	column chromatography, eluent: $CHCl_3$/EtOAc (10/0.2) and further recrystallisation from EtOAc/EtOH (10/0.2)
Yield:	280 mg (70 %), colorless solid
Transition temp.:	Cr 135 (N 123) I
^{1}H-NMR:	($CDCl_3$, *J*/Hz, 400 MHz) δ 8.29 (d, *J* = 8.6 Hz, 2H, Ar-H), 8.25 (d, *J* = 8.3 Hz, 2H, Ar-H), 8.15 (d, *J* = 8.3 Hz, 2H, Ar-H), 8.13 – 8.05 (m, 5H, Ar-H), 8.05 – 8.02 (m, 1H, Ar-H), 7.57 (t, *J* = 7.9 Hz, 1H, Ar-H), 7.52 – 7.47 (m, 1H, Ar-H), 7.38 (d, *J* = 8.7 Hz, 2H, Ar-H), 7.22 (s, 4H, Ar-H), 7.05 (d, *J* = 8.9 Hz, 2H, Ar-H), 6.96 – 6.84 (m, 6H, Ar-H), 4.34 (t, *J* = 6.7 Hz, 2H, COOCH$_2$), 4.00 (q, *J* = 12.1, 6.5 Hz, 4H, OCH$_2$), 3.92 (t, *J* = 6.5 Hz, 2H, OCH$_2$), 1.83 – 1.70 (m, 8H, OCH$_2$**CH**$_2$, COOCH$_2$C**H**$_2$), 1.48 – 1.39 (m, 8H, CH$_2$), 1.38 – 1.21 (m, 30H, CH$_2$), 0.91 – 0.82 (m, 6H, CH$_3$).
^{13}C-NMR:	($CDCl_3$, 100 MHz) δ 165.51, 165.17, 164.65, 164.01, 163.67, 163.54, 163.36, 156.69, 155.07, 150.94, 148.64, 148.05, 144.40, 135.26, 132.61, 132.25, 132.13, 131.96, 131.11, 130.16, 129.74, 127.74, 127.11, 126.92, 123.48, 122.72, 122.43, 122.42, 121.99, 121.74, 121.39, 115.10, 114.35, 114.26, 68.53, 68.45, 68.41, 65.86, 32.05, 31.68, 29.79, 29.76, 29.72, 29.69, 29.66, 29.63, 29.49, 29.47, 29.44, 29.40, 29.25, 29.22, 28.83, 26.19, 26.17, 26.13, 25.80, 22.83, 22.72, 14.25, 14.15.
EA:	calculated: C: 73.78 %, H: 7.08 %; found: C: 73.72 %, H: 7.12 %

Compounds 23 and 24

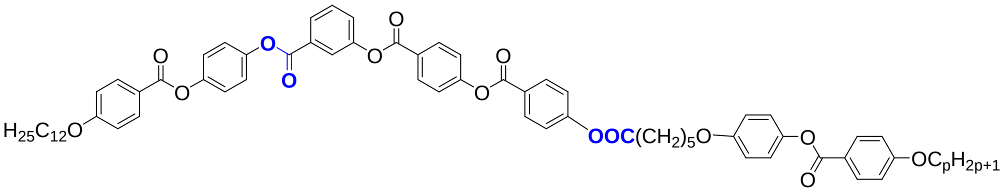

23: ***p*** **= 6**
24: ***p*** **= 12**

4-{[3-({4-[(4-{[6-(4-{[4-(Hexyloxy)phenyl]carbonyloxy}phenoxy)hexanoyl]oxy}phenyl)-carbonyloxy]phenyl}carbonyloxy)phenyl]carbonyloxy}phenyl 4-(dodecyloxy)benzoate **23** (*n* = 12, *m* = 5, *p* = 6)

Formula:	$C_{71}H_{76}O_{15}$, M = 1169.39 g/mol
Synthesis:	according to the general procedure 10.3.3
Reagents:	330 mg (0.51 mmol) 4-({3-[(4-hydroxyphenyl)carbonyloxy]phenyl}carbonyloxy)phenyl 4-(dodecyloxy)benzoate **i37(12)** 280 mg (0.51 mmol) 4-{[6-(4-{[4-(hexyloxy)phenyl]carbonyloxy}phenoxy)hexanoyl]oxy}-benzoic acid **i20(5,6)** 120 mg (0.56 mmol) DCC 5 mg DMAP

40 ml dichloromethane
Purification: column chromatography, eluent: $CHCl_3$/EtOAc (10/0.2) and further recrystallisation from EtOAc/EtOH (10/0.2)
Yield: 390 mg (65 %), colorless solid
Transition temp.: Cr 176 (N 173) I
^{1}H-NMR: ($CDCl_3$, *J*/Hz, 400 MHz) δ 8.28 (d, *J* = 8.9 Hz, 2H, Ar-H), 8.14 (d, *J* = 8.9 Hz, 4H, Ar-H), 8.12 – 8.08 (m, 3H, Ar-H), 8.06 – 8.04 (m, 1H, Ar-H), 7.58 (t, *J* = 7.9 Hz, 1H, Ar-H), 7.53 – 7.49 (m, 1H, Ar-H), 7.38 (d, *J* = 8.9 Hz, 2H, Ar-H), 7.26 (s, 4H, Ar-H), 7.20 (d, *J* = 9.2 Hz, 2H, Ar-H), 7.11 (d, *J* = 9.1 Hz, 2H, Ar-H), 7.00 – 6.92 (m, 6H, Ar-H), 4.08 (t, *J* = 6.3 Hz, 2H, OCH_2), 4.05 – 4.00 (m, 4H, OCH_2), 2.61 (t, *J* = 7.4 Hz, 2H, CH_2COO), 1.94 – 1.76 (m, 8H, $OCH_2C\mathbf{H}_2$, $C\mathbf{H}_2CH_2COO$), 1.68 – 1.59 (m, 2H, CH_2), 1.50 – 1.42 (m, 4H, CH_2), 1.39 – 1.23 (m, 20H, CH_2), 0.93 – 0.84 (m, 6H, CH_3).
^{13}C-NMR: ($CDCl_3$, 100 MHz) δ 171.88, 164.81, 164.79, 164.29, 164.25, 164.17, 163.70, 163.63, 155.62, 151.04, 148.69, 148.47, 148.12, 148.02, 132.48, 132.32, 132.30, 131.91, 131.09, 129.79, 127.77, 127.24, 126.43, 123.56, 122.78, 122.67, 122.51, 122.37, 122.22, 121.37, 121.33, 121.10, 114.45, 114.35, 68.37, 67.98, 34.21, 31.93, 31.56, 29.67, 29.65, 29.60, 29.57, 29.38, 29.36, 29.12, 29.07, 28.81, 26.00, 25.67, 25.60, 24.62, 22.71, 22.60, 14.14, 14.04.
EA: calculated: C: 72.93 %, H: 6.55 %; found: C: 72.83 %, H: 6.55 %

4-{[3-({4-[(4-{[6-(4-{[4-(Dodecyloxy)phenyl]carbonyloxy}phenoxy)hexanoyl]oxy}phenyl)-carbonyloxy]phenyl}carbonyloxy)phenyl]carbonyloxy}phenyl 4-(dodecyloxy)benzoate **24** (*n* = 12, *m* = 5, *p* = 12)

Formula: $C_{77}H_{88}O_{15}$, M = 1253.55 g/mol
Synthesis: according to the general procedure 10.3.3
Reagents: 300 mg (0.47 mmol) 4-({3-[(4-hydroxyphenyl)carbonyloxy]phenyl}carbonyloxy)phenyl 4-(dodecyloxy)benzoate **i37(12)**
300 mg (0.47 mmol) 4-{[6-(4-{[4-(dodecyloxy)phenyl]carbonyloxy}phenoxy)hexanoyl]oxy}-benzoic acid **i20(5,12)**
110 mg (0.52 mmol) DCC
5 mg DMAP
40 ml dichloromethane
Purification: column chromatography, eluent: $CHCl_3$/EtOAc (10/0.2) and further recrystallisation from EtOAc/EtOH (10/0.2)
Yield: 380 mg (64 %), colorless solid
Transition temp.: Cr 142 ($\mathrm{SmC''_sP_{AF}}$ 118 $\mathrm{SmC'_sP_{AF}}$ 125) $\mathrm{SmC_sP_{AF}}$ 175 I
^{1}H-NMR: ($CDCl_3$, *J*/Hz, 400 MHz) δ 8.28 (d, *J* = 8.9 Hz, 2H, Ar-H), 8.14 (d, *J* = 8.9 Hz, 4H, Ar-H), 8.12 – 8.08 (m, 3H, Ar-H), 8.06 – 8.04 (m, 1H, Ar-H), 7.58 (t, *J* = 8.1 Hz, 1H, Ar-H), 7.53 – 7.49 (m, 1H, Ar-H), 7.37 (d, *J* = 8.9 Hz, 2H, Ar-H), 7.26 (s, 4H, Ar-H), 7.19 (d, *J* = 9.1 Hz, 2H, Ar-H), 7.11 (d, *J* = 9.1 Hz, 2H, Ar-H), 7.00 – 6.92 (m, 6H, Ar-H), 4.08 (t, *J* = 6.3 Hz, 2H, OCH_2), 4.05 – 4.00 (m, 4H, OCH_2), 2.61 (t, *J* = 7.4 Hz, 2H, CH_2COO), 1.94 – 1.75 (m, 8H, $OCH_2C\mathbf{H}_2$, $C\mathbf{H}_2CH_2COO$), 1.68 – 1.58 (m, 2H, CH_2), 1.50 – 1.40 (m, 4H, CH_2), 1.40 – 1.19 (m, 32H, CH_2), 0.87 (t, *J* = 6.5 Hz, 6H, CH_3).
^{13}C-NMR: ($CDCl_3$, 100 MHz) δ 171.64, 167.01, 164.63, 164.10, 163.63, 163.56, 163.52, 151.03, 149.42, 147.98, 145.02, 132.41, 132.24, 132.22, 131.82, 129.68, 127.67, 127.12, 126.44, 123.50, 122.69, 122.58, 122.42, 122.28, 122.14, 121.43, 114.47, 114.37, 68.46, 68.07, 35.17, 34.34, 32.03, 29.76, 29.74, 29.69, 29.67, 29.47, 29.45, 29.24, 28.93, 26.11, 25.74, 24.75, 22.80, 14.60, 14.20.
EA: calculated: C: 73.78 %, H: 7.08 %; found: C: 73.85 %, H: 7.14 %

Compounds 25

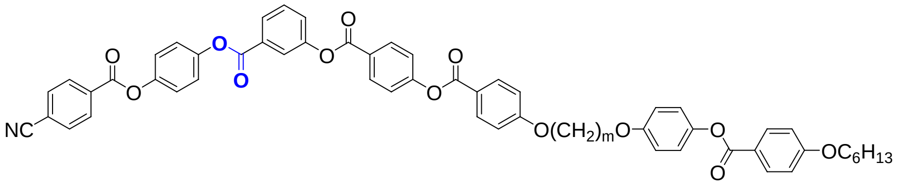

25a: ***m* = 3**
25b: ***m* = 6**
25c: ***m* = 11**

4-[(3-{[4-({4-[3-(4-{[4-(Hexyloxy)phenyl]carbonyloxy}phenoxy)propoxy]phenyl}carbonyloxy)phenyl]carbonyloxy}phenyl)carbonyloxy]phenyl 4-cyanobenzoate **25a** (*m* = 3, *p* = 6)

Formula:	$C_{57}H_{47}O_{13}N$, M = 954.01 g/mol
Synthesis:	according to the general procedure 10.3.3
Reagents:	350 mg (0.73 mmol) 4-({3-[(4-hydroxyphenyl)carbonyloxy]phenyl}carbonyloxy)phenyl 4-cyanobenzoate **i49** 360 mg (0.73 mmol) 4-[3-(4-{[4-(hexyloxy)phenyl]carbonyloxy}phenoxy)propoxy]benzoic acid **i14(3,6)** 170 mg (0.80 mmol) DCC 5 mg DMAP 40 ml dichloromethane
Purification:	column chromatography, eluent: $CHCl_3$/EtOAc (10/0.2) and further recrystallisation from EtOAc/EtOH (10/0.2)
Yield:	520 mg (75 %), colorless solid
Transition temp.:	Cr 166 (SmC_x 127 N 132) I
^{1}H-NMR:	($CDCl_3$, *J*/Hz, 500 MHz) δ 8.23 (d, *J* = 8.5 Hz, 2H, Ar-H), 8.10 (d, *J* = 8.7 Hz, 2H, Ar-H), 8.08 – 8.01 (m, 6H, Ar-H), 7.55 (t, *J* = 7.9 Hz, 1H, Ar-H), 7.50 – 7.48 (m, 1H, Ar-H), 7.35 (d, *J* = 8.5 Hz, 2H, Ar-H), 7.32, (s, 4H, Ar-H), 7.26 (d, *J* = 8.3 Hz, 2H, Ar-H), 7.06 (d, *J* = 8.9 Hz, 2H, Ar-H), 6.98 (d, *J* = 8.8 Hz, 2H, Ar-H), 6.91 (d, *J* = 8.8 Hz, 2H, Ar-H), 6.90 (d, *J* = 8.8 Hz, 2H, Ar-H), 5.00 (t, *J* = 6.1 Hz, 2H, OCH_2), 4.15 (t, *J* = 6.0 Hz, 2H, OCH_2), 4.00 (t, *J* = 6.5 Hz, 2H, OCH_2), 2.29 – 2.24 (m, 2H, $OCH_2\mathbf{CH_2}$), 1.79 – 1.73 (m, 2H, $OCH_2\mathbf{CH_2}$), 1.79 – 1.73 (m, 2H, CH_2), 1.45 – 1.40 (m, 2H, CH_2), 1.33 – 1.30 (m, 4H, CH_2), 0.87 (t, *J* = 7.1 Hz, 3H, CH_3).
^{13}C-NMR:	($CDCl_3$, 125 MHz) δ 164.85, 164.49, 163.91, 163.85, 163.81, 163.35, 163.30, 156.17, 155.44, 150.90, 148.43, 148.00, 144.64, 144.26, 132.16, 131.86, 131.53, 130.85, 129.92, 129.50, 129.06, 127.36, 126.90, 126.46, 126.22, 123.20, 122.39, 122.30, 122.20, 121.90, 121.47, 121.12, 114.99, 114.34, 114.13, 114.13, 68.13, 64.70, 64.55, 31.20, 28.96, 28.77, 25.32, 22.20, 21.38, 13.62.
EA:	calculated: C: 71.76 %, H: 4.97 %, N 1.47 %; found: C: 71.72 %, H: 5.07 %, N 1.40 %

4-{[3-({4-[(4-{[6-(4-{[4-(Hexyloxy)phenyl]carbonyloxy}phenoxy)hexyl]oxy}phenyl)-carbonyloxy]phenyl}carbonyloxy)phenyl]carbonyloxy}phenyl 4-cyanobenzoate **25b** (*m* = 6, *p* = 6)

Formula:	$C_{60}H_{53}O_{13}N$, M = 996.09 g/mol
Synthesis:	according to the general procedure 10.3.3
Reagents:	360 mg (0.70 mmol) 4-({3-[(4-hydroxyphenyl)carbonyloxy]phenyl}carbonyloxy)phenyl 4-cyanobenzoate **i49** 370 mg (0.70 mmol) 4-{[6-(4-{[4-(hexyloxy)phenyl]carbonyloxy}phenoxy)hexyl]oxy}-benzoic acid **i14(6,6)** 160 mg (0.77 mmol) DCC 5 mg DMAP 40 ml dichloromethane
Purification:	column chromatography, eluent: $CHCl_3$/EtOAc (10/0.2) and further recrystallisation from EtOAc/EtOH (10/0.2)
Yield:	490 mg (70 %), colorless solid

Transition temp.: Cr 162 (M_5 131) N 184 I

^{1}H-NMR: ($CDCl_3$, *J*/Hz, 500 MHz) δ 8.22 (d, *J* = 8.7 Hz, 2H, Ar-H), 8.08 (d, *J* = 8.8 Hz, 2H, Ar-H), 8.04 (d, *J* = 8.8 Hz, 2H, Ar-H), 8.03 – 8.00 (m, 4H, Ar-H), 7.53 (t, *J* = 7.9 Hz, 1H, Ar-H), 7.48 – 7.47 (m, 1H, Ar-H), 7.33 (d, *J* = 8.7 Hz, 2H, Ar-H), 7.26 – 7.22 (m, 6H, Ar-H), 7.03 (d, *J* = 9.0 Hz, 2H, Ar-H), 6.93 (d, *J* = 8.8 Hz, 2H, Ar-H), 6.89 (d, *J* = 8.8 Hz, 2H, Ar-H), 6.85 (d, *J* = 8.9 Hz, 2H, Ar-H), 4.02 (t, *J* = 6.4 Hz, 2H, OCH_2), 3.98 (t, *J* = 6.6 Hz, 2H, OCH_2), 3.93 (t, *J* = 6.3 Hz, 2H, OCH_2), 1.81 – 1.73 (m, 6H, $OCH_2C\mathbf{H}_2$), 1.53 – 1.50 (m, 4H, CH_2), 1.42 – 1.40 (m, 2H, CH_2), 1.31 – 1.28 (m, 4H, CH_2), 0.85 (t, *J* = 7.1 Hz, 3H, CH_3).

^{13}C-NMR: ($CDCl_3$, 125 MHz) δ 165.10, 164.88, 164.10, 164.09, 163.98, 163.76, 163.42, 156.63, 155.61, 151.04, 148.58, 148.15, 144.53, 144.39, 132.30, 132.04, 131.72, 131.03, 130.10, 129.63, 129.20, 127.55, 127.05, 126.63, 126.36, 123.39, 122.55, 122.36, 122.06, 121.69, 121.00, 115.07, 114.43, 114.24, 68.27, 68.20, 68.16, 31.38, 29.08, 28.95, 28.91, 25.71, 25.65, 25.50, 22.39, 21.55, 13.79.

EA: calculated: C: 72.35 %, H: 5.36 %, N 1.41 %; found: C: 72.22 %, H: 5.42 %, N 1.37 %

4-{[3-({4-[(4-{[11-(4-{[4-(Hexyloxy)phenyl]carbonyloxy}phenoxy)undecyl]oxy}phenyl)-carbonyloxy]phenyl}carbonyloxy)phenyl]carbonyloxy}phenyl 4-cyanobenzoate **25c** (*m* = 11, *p* = 6)

Formula: $C_{65}H_{63}O_{13}N$, M = 1066.23 g/mol

Synthesis: according to the general procedure 10.3.3

Reagents: 320 mg (0.66 mmol) 4-({3-[(4-hydroxyphenyl)carbonyloxy]phenyl}carbonyloxy)phenyl 4-cyanobenzoate **i49**
400 mg (0.66 mmol) 4-{[11-(4-{[4-(hexyloxy)phenyl]carbonyloxy}phenoxy)undecyl]oxy}-benzoic acid **i14(11,6)**
150 mg (0.73 mmol) DCC
5 mg DMAP
40 ml dichloromethane

Purification: column chromatography, eluent: $CHCl_3$/EtOAc (10/0.2) and further recrystallisation from EtOAc/EtOH (10/0.2)

Yield: 510 mg (72 %), colorless solid

Transition temp.: Cr 136 (M_6 109 N_x 115) N 145 I

^{1}H-NMR: ($CDCl_3$, *J*/Hz, 500 MHz) δ 8.24 (d, *J* = 8.8 Hz, 2H, Ar-H), 8.09 (d, *J* = 8.8 Hz, 2H, Ar-H), 8.07 – 8.02 (m, 6H, Ar-H), 7.57 (t, *J* = 8.0 Hz, 1H, Ar-H), 7.51 – 7.49 (m, 1H, Ar-H), 7.37 (s, 4H, Ar-H), 7.35 (d, *J* = 8.7 Hz, 2H, Ar-H), 7.27 (d, *J* = 9.0 Hz, 2H, Ar-H), 7.03 (d, *J* = 8.8 Hz, 2H, Ar-H), 6.95 (d, *J* = 8.8 Hz, 2H, Ar-H), 6.91 (d, *J* = 8.9 Hz, 2H, Ar-H), 6.86 (d, *J* = 8.8 Hz, 2H, Ar-H), 4.03 – 3.98 (m, 4H, OCH_2), 3.92 (t, *J* = 6.4 Hz, 2H, OCH_2), 1.80 – 1.71 (m, 6H, $OCH_2C\mathbf{H}_2$), 1.44 – 1.39 (m, 6H, CH_2), 1.31 – 1.29 (m, 14H, CH_2), 0.87 (t, *J* = 7.0 Hz, 3H, CH_3).

^{13}C-NMR: ($CDCl_3$, 125 MHz) δ 164.74, 164.55, 163.76, 163.66, 163.52, 163.11, 156.39, 155.30, 150.72, 148.26, 147.82, 144.15, 144.10, 131.96, 131.69, 131.38, 130.63, 129.76, 129.40, 128.94, 127.22, 126.80, 126.23, 126.00, 123.05, 122.27, 122.08, 121.79, 121.31, 120.53, 114.73, 114.15, 113.96, 68.10, 68.04, 67.95, 31.05, 29.02, 29.00, 28.97, 28.86, 28.83, 28.63, 28.61, 25.56, 25.50, 25.17, 22.06, 21.26, 13.51.

EA: calculated: C: 73.22 %, H: 5.96 %, N 1.31 %; found: C: 73.25 %, H: 6.08 %, N 1.37 %

Compounds 26

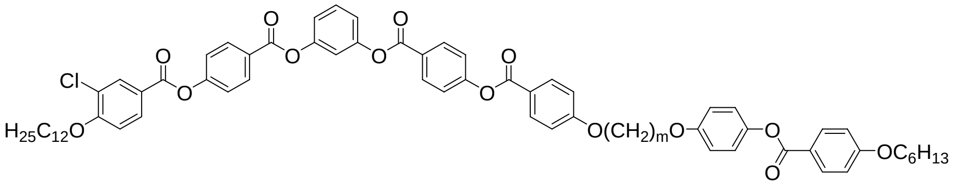

dimer series 26
26a: $m = 3$
26b: $m = 6$
26c: $m = 11$

4-(3-{[4-({4-[3-(4-{[4-(Hexyloxy)phenyl]carbonyloxy}phenoxy)propoxy]phenyl}carbonyloxy)phenyl]carbonyloxy}phenoxycarbonyl)phenyl 3-chloro-4-(dodecyloxy)benzoate **26a** ($n = 12$, $m = 3$, $p = 6$)

Formula:	$C_{68}H_{71}ClO_{14}$, M = 1147.77 g/mol
Synthesis:	according to the general procedure 10.3.3
Reagents:	500 mg (0.75 mmol) 4-{3-[(4-hydroxyphenyl)carbonyloxy]phenoxycarbonyl}phenyl 3-chloro-4-(dodecyloxy)benzoate **i56** 370 mg (0.75 mmol) 4-[3-(4-{[4-(hexyloxy)phenyl]carbonyloxy}phenoxy)propoxy]benzoic acid **i14(3,6)** 170 mg (0.83 mmol) DCC 5 mg DMAP 40 ml dichloromethane
Purification:	column chromatography, eluent: $CHCl_3$/EtOAc (10/0.2) and further recrystallisation from EtOAc/EtOH (10/0.2)
Yield:	520 mg (60 %), colorless solid
Transition temp.:	Cr 149 ($\mathrm{Col_rP_{AF}}$ 139) I
^{1}H-NMR:	($CDCl_3$, *J*/Hz, 400 MHz) δ 8.29 – 8.24 (m, 4H, Ar-H), 8.21 (d, *J* = 2.1 Hz, 1H, Ar-H), 8.15 (d, *J* = 8.9 Hz, 2H, Ar-H), 8.11 (d, *J* = 8.9 Hz, 2H, Ar-H), 8.06 (dd, *J* = 8.6, 2.2 Hz, 1H, Ar-H), 7.48 (t, *J* = 8.1 Hz, 1H, Ar-H), 7.36 (dd, *J* = 8.8, 2.5 Hz, 4H, Ar-H), 7.21 – 7.14 (m, 3H, Ar-H), 7.10 (d, *J* = 9.0 Hz, 2H, Ar-H), 7.03 – 6.91 (m, 7H, Ar-H), 4.26 (t, *J* = 6.1 Hz, 2H, OCH_2), 4.17 (t, *J* = 6.0 Hz, 2H, OCH_2), 4.11 (t, *J* = 6.5 Hz, 2H, OCH_2), 4.02 (t, *J* = 6.5 Hz, 2H, OCH_2), 2.34 – 2.27 (m, 2 H, $OCH_2C\mathbf{H}_2$), 1.92 – 1.76 (m, 4H, $OCH_2C\mathbf{H}_2$), 1.55 – 1.42 (m, 4H, CH_2), 1.41 – 1.21 (m, 20H, CH_2), 0.93 – 0.84 (m, 6H, CH_3).
^{13}C-NMR:	($CDCl_3$, 100 MHz) δ 165.10, 164.07, 163.93, 163.86, 163.42, 163.21, 159.11, 156.30, 155.44, 155.17, 151.40, 144.79, 132.41, 132.35, 132.23, 132.14, 131.82, 131.77, 130.55, 129.79, 126.88, 126.66, 123.29, 122.57, 122.07, 121.97, 121.83, 121.70, 121.39, 119.20, 115.75, 115.17, 114.50, 114.30, 112.33, 69.62, 68.43, 64.96, 64.78, 32.04, 31.67, 29.77, 29.76, 29.69, 29.65, 29.46, 29.41, 29.38, 29.22, 29.06, 26.04, 25.80, 22.81, 22.70, 14.23, 14.12.
EA:	calculated: C: 71.16 %, H: 6.24 %; found: C: 71.30 %, H: 6.21 %

4-[3-({4-[(4-{[6-(4-{[4-(Hexyloxy)phenyl]carbonyloxy}phenoxy)hexyl]oxy}phenyl)carbonyloxy]phenyl}carbonyloxy)phenoxycarbonyl]phenyl 3-chloro-4-(dodecyloxy)benzoate **26b** ($n = 12$, $m = 6$, $p = 6$)

Formula:	$C_{71}H_{77}ClO_{14}$, M = 1189.85 g/mol
Synthesis:	according to the general procedure 10.3.3
Reagents:	500 mg (0.75 mmol) 4-{3-[(4-hydroxyphenyl)carbonyloxy]phenoxycarbonyl}phenyl 3-chloro-4-(dodecyloxy)benzoate **i56** 400 mg (0.75 mmol) 4-{[6-(4-{[4-(hexyloxy)phenyl]carbonyloxy}phenoxy)hexyl]oxy}-benzoic acid **i14(6,6)** 170 mg (0.83 mmol) DCC 5 mg DMAP 40 ml dichloromethane
Purification:	column chromatography, eluent: $CHCl_3$/EtOAc (10/0.2) and further recrystallisation from

EtOAc/EtOH (10/0.2)

Yield: 550 mg (62 %), colorless solid

Transition temp.: Cr 145 (N 133) I

^{1}H-NMR: (CDCl$_3$, *J*/Hz, 400 MHz) δ 8.29 – 8.23 (m, 4H, Ar-H), 8.21 (d, *J* = 2.2 Hz, 1H, Ar-H), 8.14 (d, *J* = 8.9 Hz, 2H, Ar-H), 8.11 (d, *J* = 8.9 Hz, 2H, Ar-H), 8.06 (dd, *J* = 8.7, 2.2 Hz, 1H, Ar-H), 7.48 (t, *J* = 8.2 Hz, 1H, Ar-H), 7.39 – 7.33 (m, 4H, Ar-H), 7.21 – 7.15 (m, 3H, Ar-H), 7.08 (d, *J* = 9.0 Hz, 2H, Ar-H), 7.01 – 6.88 (m, 7H, Ar-H), 4.11 (t, *J* = 6.5 Hz, 2H, OCH$_2$), 4.06 (t, *J* = 6.4 Hz, 2H, OCH$_2$), 4.02 (t, *J* = 6.6 Hz, 2H, OCH$_2$), 3.97 (t, *J* = 6.4 Hz, 2H, OCH$_2$), 1.92 – 1.76 (m, 8H, OCH$_2$C$\mathbf{H}_2$), 1.59 – 1.53 (m, 4H, CH$_2$), 1.53 – 1.42 (m, 4H, CH$_2$), 1.41 – 1.22 (m, 20H, CH$_2$), 0.93 – 0.84 (m, 6H, CH$_3$).

^{13}C-NMR: (CDCl$_3$, 100 MHz) δ 165.14, 164.12, 163.93, 163.86, 163.70, 163.39, 163.20, 159.11, 156.62, 155.46, 155.17, 151.43, 144.53, 132.37, 132.22, 132.13, 131.82, 131.76, 130.55, 129.79, 126.88, 126.63, 123.28, 122.46, 122.08, 121.97, 121.71, 121.10, 119.23, 119.19, 115.75, 115.13, 114.47, 114.29, 112.33, 69.62, 68.42, 68.31, 32.04, 31.67, 29.77, 29.68, 29.64, 29.46, 29.41, 29.35, 29.22, 29.19, 29.05, 26.04, 26.00, 25.94, 25.79, 22.81, 22.70, 14.23, 14.12.

EA: calculated: C: 71.67 %, H: 6.52 %; found: C: 71.75 %, H: 6.50 %

4-[3-({4-[(4-{[11-(4-{[4-(Hexyloxy)phenyl]carbonyloxy}phenoxy)undecyl]oxy}phenyl)-carbonyloxy]phenyl}carbonyloxy)phenoxycarbonyl]phenyl 3-chloro-4-(dodecyloxy)benzoate **26c** (*n* = 12, *m* = 11, *p* = 6)

Formula: C$_{76}$H$_{87}$ClO$_{14}$, M = 1259.99 g/mol

Synthesis: according to the general procedure 10.3.3

Reagents:
440 mg (0.66 mmol) 4-{3-[(4-hydroxyphenyl)carbonyloxy]phenoxycarbonyl}phenyl 3-chloro-4-(dodecyloxy)benzoate **i56**
400 mg (0.66 mmol) 4-{[11-(4-{[4-(hexyloxy)phenyl]carbonyloxy}phenoxy)undecyl]oxy}-benzoic acid **i14(11,6)**
150 mg (0.73 mmol) DCC
5 mg DMAP
40 ml dichloromethane

Purification: column chromatography, eluent: CHCl$_3$/EtOAc (10/0.2) and further recrystallisation from EtOAc/EtOH (10/0.2)

Yield: 540 mg (65 %), colorless solid

Transition temp.: Cr 118 Col$_r$P$_{FE}$ 123 I

^{1}H-NMR: (CDCl$_3$, *J*/Hz, 400 MHz) δ 8.29 – 8.23 (m, 4H, Ar-H), 8.21 (d, *J* = 2.2 Hz, 1H, Ar-H), 8.13 (d, *J* = 8.7 Hz, 2H, Ar-H), 8.10 (d, *J* = 9.0 Hz, 2H, Ar-H), 8.06 (dd, *J* = 8.6, 2.2 Hz, 1H, Ar-H), 7.48 (t, *J* = 8.1 Hz, 1H, Ar-H), 7.36 (d, *J* = 8.7 Hz, 4H, Ar-H), 7.20 – 7.15 (m, 3H, Ar-H), 7.08 (d, *J* = 8.8 Hz, 2H, Ar-H), 7.00 – 6.93 (m, 4H, Ar-H), 6.93 – 6.87 (m, 3H, Ar-H), 4.11 (t, *J* = 6.5 Hz, 2H, OCH$_2$), 4.06 – 3.99 (m, 4H, OCH$_2$), 3.94 (t, *J* = 6.5 Hz, 2H, OCH$_2$), 1.91 – 1.73 (m, 8H, OCH$_2$C$\mathbf{H}_2$), 1.53 – 1.41 (m, 8H, CH$_2$), 1.40 – 1.22 (m, 30H, CH$_2$), 0.93 – 0.84 (m, 6H, CH$_3$).

^{13}C-NMR: (CDCl$_3$, 100 MHz) δ 165.12, 164.11, 163.92, 163.84, 163.77, 163.38, 163.19, 159.12, 156.71, 155.47, 155.17, 151.45, 151.40, 144.47, 132.35, 132.23, 132.11, 131.81, 131.75, 130.53, 129.77, 126.90, 126.64, 123.31, 122.40, 122.06, 121.95, 119.17, 115.73, 115.14, 114.47, 114.29, 112.34, 69.63, 68.58, 68.51, 68.42, 32.03, 31.66, 29.76, 29.75, 29.67, 29.64, 29.45, 29.40, 29.24, 29.22, 29.06, 26.18, 26.12, 26.03, 25.79, 22.80, 22.69, 14.20, 14.10.

EA: calculated: C: 72.45 %, H: 6.96 %; found: C: 72.44 %, H: 6.97 %

Compounds 27

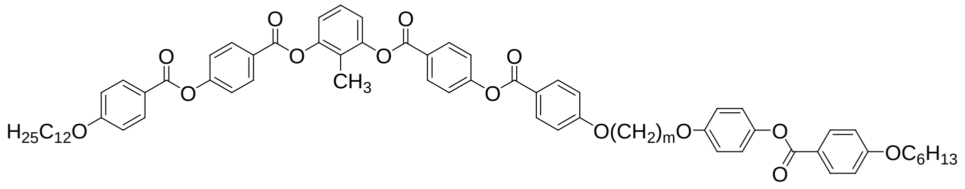

dimer series 27
27a: ***m*** **= 3**
27b: ***m*** **= 6**
27c: ***m*** **= 11**

4-(3-{[4-({4-[3-(4-{[4-(Hexyloxy)phenyl]carbonyloxy}phenoxy)propoxy]phenyl}carbonyloxy)phenyl]carbonyloxy}-2-methylphenoxycarbonyl)phenyl 4-(dodecyloxy)benzoate **27a** (*n* = 12, *m* = 3, *p* = 6)

Formula:	$C_{69}H_{74}O_{14}$, M = 1127.35 g/mol
Synthesis:	according to the general procedure 10.3.3
Reagents:	400 mg (0.62 mmol) 4-{3-[(4-hydroxyphenyl)carbonyloxy]-2-methylphenoxycarbonyl}phenyl 4-(dodecyloxy)benzoate **i60** 300 mg (0.62 mmol) 4-[3-(4-{[4-(hexyloxy)phenyl]carbonyloxy}phenoxy)propoxy]benzoic acid **i14(3,6)** 140 mg (0.68 mmol) DCC 5 mg DMAP 40 ml dichloromethane
Purification:	column chromatography, eluent: $CHCl_3$ and $CHCl_3$/EtOAc (10/0.2) and further recrystallisation from EtOAc/EtOH (10/0.2)
Yield:	420 mg (60 %), colorless solid
Transition temp.:	Cr 159 I
^{1}H-NMR:	($CDCl_3$, *J*/Hz, 400 MHz) δ 8.29 (d, *J* = 8.7 Hz, 4H, Ar-H), 8.18 – 8.08 (m, 6H, Ar-H), 7.37 (dd, *J* = 8.6, 1.5 Hz, 4H, Ar-H), 7.32 (t, *J* = 8.1 Hz, 1H, Ar-H), 7.15 – 7.07 (m, 4H, Ar-H), 7.03 – 6.91 (m, 8H, Ar-H), 4.26 (t, *J* = 6.1 Hz, 2H, OCH_2), 4.18 (t, *J* = 5.9 Hz, 2H, OCH_2), 4.03 (q, *J* = 6.6 Hz, 4H, OCH_2), 2.35 – 2.27 (m, 2H, $OCH_2\mathbf{CH_2}$), 2.11 (s, 3H, Ar-CH_3), 1.85 – 1.76 (m, 4H, $OCH_2\mathbf{CH_2}$), 1.51 – 1.40 (m, 4H, CH_2), 1.39 – 1.22 (m, 20H, CH_2), 0.94 – 0.84 (m, 6H, CH_3).
^{13}C-NMR:	($CDCl_3$, 100 MHz) δ 165.31, 164.36, 164.30, 163.95, 163.88, 163.53, 163.52, 156.39, 155.54, 150.31, 144.76, 132.51, 132.46, 132.24, 131.90, 126.68, 126.59, 124.02, 122.65, 122.23, 121.64, 121.32, 120.96, 120.00, 115.15, 114.50, 114.46, 114.30, 68.44, 68.35, 64.84, 64.61, 31.95, 31.57, 29.68, 29.66, 29.61, 29.58, 29.38, 29.21, 29.12, 29.10, 26.01, 25.69, 22.72, 22.61, 14.15, 14.05, 12.13.
EA:	calculated: C: 73.51 %, H: 6.62 %; found: C: 73.63 %, H: 6.64 %

4-[3-({4-[(4-{[6-(4-{[4-(Hexyloxy)phenyl]carbonyloxy}phenoxy)hexyl]oxy}phenyl)carbonyloxy]phenyl}carbonyloxy)-2-methylphenoxycarbonyl]phenyl 4-(dodecyloxy)benzoate **27b** (*n* = 12, *m* = 6, *p* = 6)

Formula:	$C_{72}H_{80}O_{14}$, M = 1169.43 g/mol
Synthesis:	according to the general procedure 10.3.3
Reagents:	390 mg (0.60 mmol) 4-{3-[(4-hydroxyphenyl)carbonyloxy]-2-methylphenoxycarbonyl}phenyl 4-(dodecyloxy)benzoate **i60** 320 mg (0.60 mmol) 4-{[6-(4-{[4-(hexyloxy)phenyl]carbonyloxy}phenoxy)hexyl]oxy}-benzoic acid **i14(6,6)** 140 mg (0.66 mmol) DCC 5 mg DMAP 40 ml dichloromethane
Purification:	column chromatography, eluent: $CHCl_3$ and $CHCl_3$/EtOAc (10/0.2) and further recrystallisation from EtOAc/EtOH (10/0.2)

Yield: 510 mg (73 %), colorless solid

Transition temp.: Cr 164 I

^{1}H-NMR: ($CDCl_3$, *J*/Hz, 400 MHz) δ 8.29 (d, *J* = 8.6 Hz, 4H, Ar-H), 8.17 – 8.08 (m, 6H, Ar-H), 7.37 (d, *J* = 8.7 Hz, 4H, Ar-H), 7.32 (t, *J* = 8.2 Hz, 1H, Ar-H), 7.12 (d, *J* = 8.2 Hz, 2H, Ar-H), 7.09 (d, *J* = 9.0 Hz, 2H, Ar-H), 7.00 – 6.88 (m, 8H, Ar-H), 4.09 – 4.00 (m, 6H, OCH_2), 3.97 (t, *J* = 6.3 Hz, 2H, OCH_2), 2.11 (s, 3H, Ar-CH_3), 1.90 – 1.76 (m, 8H, $OCH_2C\mathbf{H}_2$), 1.60 – 1.53 (m, 4H, CH_2), 1.51 – 1.42 (m, 4H, CH_2), 1.39 – 1.23 (m, 20H, CH_2), 0.93 – 0.84 (m, 6H, CH_3).

^{13}C-NMR: ($CDCl_3$, 100 MHz) δ 165.36, 164.36, 163.96, 163.81, 163.49, 156.71, 155.54, 150.31, 144.51, 132.48, 132.46, 132.23, 131.90, 126.59, 124.02, 122.54, 122.24, 121.70, 121.04, 120.00, 115.11, 114.47, 114.29, 68.44, 68.35, 68.22, 31.95, 31.58, 29.69, 29.66, 29.62, 29.59, 29.38, 29.24, 29.10, 26.01, 25.89, 25.83, 25.69, 22.72, 22.61, 14.15, 14.05, 12.13.

EA: calculated: C: 73.95 %, H: 6.90 %; found: C: 74.05 %, H: 6.90 %

4-[3-({4-[(4-{[11-(4-{[4-(Hexyloxy)phenyl]carbonyloxy}phenoxy)undecyl]oxy}phenyl)-carbonyloxy]phenyl}carbonyloxy)-2-methylphenoxycarbonyl]phenyl 4-(dodecyloxy)benzoate **27c** (*n* = 12, *m* = 11, *p* = 6)

Formula: $C_{77}H_{90}O_{14}$, M = 1239.57 g/mol

Synthesis: according to the general procedure 10.3.3

Reagents: 370 mg (0.56 mmol) 4-{3-[(4-hydroxyphenyl)carbonyloxy]-2-methylphenoxycarbonyl}phenyl 4-(dodecyloxy)benzoate **i60**
340 mg (0.56 mmol) 4-{[11-(4-{[4-(hexyloxy)phenyl]carbonyloxy}phenoxy)undecyl]oxy}-benzoic acid **i14(11,6)**
130 mg (0.62 mmol) DCC
5 mg DMAP
40 ml dichloromethane

Purification: column chromatography, eluent: $CHCl_3$ and $CHCl_3$/EtOAc (10/0.2) and further recrystallisation from EtOAc/EtOH (10/0.2)

Yield: 490 mg (71 %), colorless solid

Transition temp.: Cr 125 $Col_{ob}P_{FE}$ 132 I

^{1}H-NMR: ($CDCl_3$, *J*/Hz, 400 MHz) δ 8.29 (d, *J* = 8.6 Hz, 4H, Ar-H), 8.17 – 8.08 (m, 6H, Ar-H), 7.37 (d, *J* = 8.6 Hz, 4H, Ar-H), 7.32 (t, *J* = 8.2 Hz, 1H, Ar-H), 7.12 (d, *J* = 8.1 Hz, 2H, Ar-H), 7.08 (d, *J* = 9.0 Hz, 2H, Ar-H), 7.01 – 6.87 (m, 8H, Ar-H), 4.08 – 3.99 (m, 6H, OCH_2), 3.94 (t, *J* = 6.5 Hz, 2H, OCH_2), 2.11 (s, 3H, Ar-CH_3), 1.86 – 1.73 (m, 8H, $OCH_2C\mathbf{H}_2$), 1.46 (d, *J* = 4.6 Hz, 8H, CH_2), 1.40 – 1.21 (m, 30H, CH_2), 0.94 – 0.84 (m, 6H, CH_3).

^{13}C-NMR: ($CDCl_3$, 100 MHz) δ 165.35, 164.36, 163.95, 163.87, 163.47, 156.79, 155.53, 150.31, 144.43, 132.46, 132.22, 131.90, 126.67, 126.58, 124.02, 122.49, 122.23, 121.72, 120.96, 120.00, 115.10, 114.46, 114.28, 68.43, 68.34, 31.95, 31.57, 29.68, 29.66, 29.61, 29.58, 29.56, 29.51, 29.38, 29.38, 29.31, 29.12, 29.10, 26.06, 26.01, 25.69, 22.72, 22.61, 14.14, 14.04, 12.12.

EA: calculated: C: 74.61 %, H: 7.32 %; found: C: 74.80 %, H: 7.35 %

Compounds 28

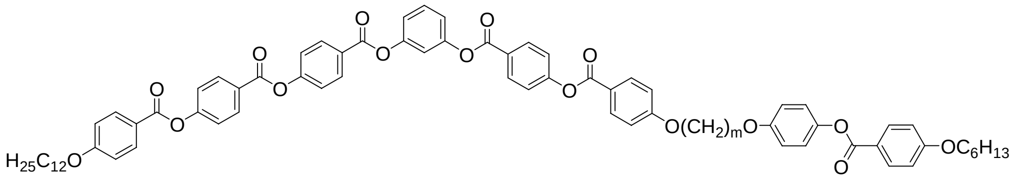

dimer series 28
28a: ***m*** **= 6**
28b: ***m*** **= 11**

4-[3-({4-[(4-{[6-(4-{[4-(Hexyloxy)phenyl]carbonyloxy}phenoxy)hexyl]oxy}phenyl)carbonyloxy]phenyl}carbonyloxy)phenoxycarbonyl]phenyl 4-{[4-(dodecyloxy)phenyl]carbonyloxy}-benzoate **28a** (*n* = 12, *m* = 6, *p* = 6)

Formula: $C_{78}H_{82}O_{16}$, M = 1275.51 g/mol

Synthesis: according to the general procedure 10.3.3

Reagents: 400 mg (0.53 mmol) 4-{3-[(4-hydroxyphenyl)carbonyloxy]phenoxycarbonyl}phenyl 4-{[4-dodecyloxy)phenyl]carbonyloxy}benzoate **i66**
280 mg (0.53 mmol) 4-{[6-(4-{[4-(hexyloxy)phenyl]carbonyloxy}phenoxy)hexyl]oxy}-benzoic acid **i14(6,6)**
120 mg (0.58 mmol) DCC
5 mg DMAP
40 ml dichloromethane

Purification: column chromatography, eluent: $CHCl_3$ and $CHCl_3$/EtOAc (10/0.2 – 10/0.5) and further recrystallisation from EtOAc/EtOH (10/0.2)

Yield: 470 mg (70 %), colorless solid

Transition temp.: Cr 159 $\mathrm{Col_rP_{AF}}$ 186 N 197 I

^{1}H-NMR: ($CDCl_3$, *J*/Hz, 400 MHz) δ 8.31 – 8.24 (m, 6H, Ar-H), 8.14 (d, *J* = 8.7 Hz, 4H, Ar-H), 8.11 (d, *J* = 8.9 Hz, 2H, Ar-H), 7.48 (t, *J* = 8.1 Hz, 1H, Ar-H), 7.41 – 7.34 (m, 6H, Ar-H), 7.22 – 7.15 (m, 3H, Ar-H), 7.09 (d, *J* = 9.0 Hz, 2H, Ar-H), 7.01 – 6.88 (m, 8H, Ar-H), 4.10 – 4.00 (m, 6H, OCH_2), 3.97 (t, *J* = 6.3 Hz, 2H, OCH_2), 1.91 – 1.76 (m, 8H, $OCH_2\mathbf{CH_2}$), 1.60 – 1.52 (m, 4H, CH_2), 1.51 – 1.42 (m, 4H, CH_2), 1.40 – 1.22 (m, 20H, CH_2), 0.93 – 0.84 (m, 6H, CH_3).

^{13}C-NMR: ($CDCl_3$, 100 MHz) δ 165.35, 164.31, 164.12, 164.05, 163.91, 163.80, 163.49, 156.71, 155.70, 155.53, 155.24, 151.47, 144.51, 132.46, 132.23, 131.95, 131.88, 129.92, 126.96, 126.64, 126.36, 122.54, 122.27, 122.17, 122.10, 121.69, 121.06, 120.91, 119.30, 115.84, 115.11, 114.47, 114.29, 68.45, 68.35, 68.21, 42.90, 31.95, 31.57, 29.69, 29.66, 29.62, 29.58, 29.38, 29.23, 29.10, 29.07, 26.01, 25.89, 25.83, 25.69, 22.72, 22.61, 14.15, 14.05.

EA: calculated: C: 73.45 %, H: 6.48 %; found: C: 73.30 %, H: 6.60 %

4-[3-({4-[(4-{[11-(4-{[4-(Hexyloxy)phenyl]carbonyloxy}phenoxy)undecyl]oxy}phenyl)-carbonyloxy]phenyl}carbonyloxy)phenoxycarbonyl]phenyl 4-{[4-(dodecyloxy)phenyl]-carbonyloxy}benzoate **28b** (*n* = 12, *m* = 11, *p* = 6)

Formula: $C_{83}H_{92}O_{16}$, M = 1345.65 g/mol

Synthesis: according to the general procedure 10.3.3

Reagents: 350 mg (0.46 mmol) 4-{3-[(4-hydroxyphenyl)carbonyloxy]phenoxycarbonyl}phenyl 4-{[4-dodecyloxy)phenyl]carbonyloxy}benzoate **i66**
280 mg (0.46 mmol) 4-{[11-(4-{[4-(hexyloxy)phenyl]carbonyloxy}phenoxy)undecyl]oxy}-benzoic acid **i14(11,6)**
100 mg (0.51 mmol) DCC
5 mg DMAP
40 ml dichloromethane

Purification: column chromatography, eluent: $CHCl_3$ and $CHCl_3$/EtOAc (10/0.2 – 10/0.5) and further recrystallisation from EtOAc/EtOH (10/0.2)

Yield: 410 mg (66 %), colorless solid

Transition temp.: Cr 127 $\mathrm{Col_xP_{AF}}$ 132 N 143 I

^{1}H-NMR: (CDCl$_3$, *J*/Hz, 400 MHz) δ 8.32 – 8.24 (m, 6H, Ar-H), 8.14 (dd, *J* = 8.9, 1.7 Hz, 4H, Ar-H), 8.11 (d, *J* = 8.9 Hz, 2H, Ar-H), 7.53 – 7.46 (m, 1H, Ar-H), 7.43 – 7.34 (m, 6H, Ar-H), 7.21 – 7.15 (m, 3H, Ar-H), 7.08 (d, *J* = 9.0 Hz, 2H, Ar-H), 7.00 – 6.94 (m, 4H, Ar-H), 6.94 – 6.84 (m, 4H, Ar-H), 4.07 – 4.00 (m, 6H, OCH$_2$), 3.99 – 3.92 (m, 2H, OCH$_2$), 1.86 – 1.73 (m, 8H, OCH$_2$C**H**$_2$), 1.53 – 1.41 (m, 8H, CH$_2$), 1.40 – 1.23 (m, 30H, CH$_2$), 0.94 – 0.84 (m, 6H, CH$_3$).

^{13}C-NMR: (CDCl$_3$, 100 MHz) δ 165.18, 164.14, 163.96, 163.89, 163.79, 163.75, 163.73, 163.36, 156.69, 155.62, 155.45, 155.16, 151.40, 151.37, 144.40, 132.38, 132.14, 131.95, 131.87, 131.79, 129.82, 129.01, 126.93, 126.61, 126.33, 122.43, 122.19, 122.10, 122.03, 121.73, 120.99, 120.92, 119.27, 119.23, 115.78, 115.10, 114.46, 114.45, 114.32, 114.27, 77.38, 77.07, 76.75, 68.53, 68.51, 68.41, 32.57, 32.06, 31.68, 31.02, 29.79, 29.77, 29.73, 29.69, 29.67, 29.62, 29.50, 29.44, 29.25, 28.98, 26.47, 26.19, 26.14, 25.81, 24.67, 22.84, 22.73, 14.26, 14.16.

EA: calculated: C: 74.09 %, H: 6.89 %; found: C: 73.96 %, H: 7.03 %

Compounds 30

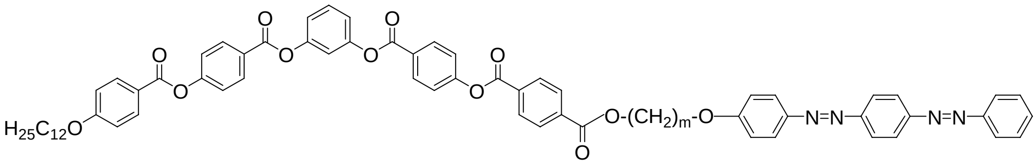

dimer series 30
30a: *m* = 2
30b: *m* = 4
30c: *m* = 6

1-(4-{3-[(4-{[4-(Dodecyloxy)phenyl]carbonyloxy}phenyl)carbonyloxy]phenoxycarbonyl}-phenyl) 4-[2-(4-{2-[4-(2-phenyldiazen-1-yl)phenyl]diazen-1-yl}phenoxy)ethyl]benzene-1,4-dicarboxylate **30a** (*n* = 12, *m* = 2)

Formula: $C_{67}H_{62}N_4O_{12}$, M = 1115.26 g/mol

Synthesis: according to the general procedure 10.3.3

Reagents: 480 mg (0.61 mmol) 4-(4-{3-[(4-{[4-(dodecyloxy)phenyl]carbonyloxy}phenyl)carbonyloxy]-phenoxycarbonyl}phenoxycarbonyl)benzoic acid **i70**
210 mg (0.61 mmol) 2-(4-{2-[4-(2-phenyldiazen-1-yl)phenyl]diazen-1-yl}phenoxy)ethan-1-ol **(*m* = 2)**
140 mg (0.67 mmol) DCC
5 mg DMAP
40 ml dichloromethane

Purification: column chromatography, eluent: CHCl$_3$/EtOAc (10/0.5) and further recrystallisation from CHCl$_3$/CH$_3$CN (10/0.2)

Yield: 460 mg (68 %), colorless solid

Transition temp.: Cr 192 (SmC$_a$P$_{AF}$ 184) I

^{1}H-NMR: (CDCl$_3$, *J*/Hz, 400 MHz) δ 8.30 – 8.23 (m, 6H, Ar-H), 8.19 (d, *J* = 8.8 Hz, 2H, Ar-H), 8.13 (d, *J* = 9.0 Hz, 2H, Ar-H), 8.00-7.97 (m, 4H, Ar-H), 7.98 – 7.91 (m, 4H, Ar-H), 7.54 – 7.44 (m, 4H, Ar-H), 7.40 – 7.33 (m, 4H, Ar-H), 7.20 – 7.14 (m, 3H, Ar-H), 7.08 (d, *J* = 9.1 Hz, 2H, Ar-H), 6.97 (d, *J* = 9.0 Hz, 2H, Ar-H), 4.78 – 4.74 (m, 2H, COOCH$_2$), 4.46 – 4.42 (m, 2H, OCH$_2$), 4.03 (t, *J* = 6.6 Hz, 2H, OCH$_2$), 1.85 – 1.77 (m, 2H, OCH$_2$C**H**$_2$), 1.51 – 1.41 (m, 2H, CH$_2$), 1.39 – 1.22 (m, 16H, CH$_2$), 0.89 – 0.85 (m, 3H, CH$_3$).

^{13}C-NMR: (CDCl$_3$, 100 MHz) δ 165.37, 164.17, 163.97, 163.81, 163.76, 163.71, 163.59, 161.16, 155.45, 154.89, 153.79, 153.37, 152.70, 151.39, 151.31, 147.51, 134.42, 132.99, 132.37, 131.92, 131.79, 131.26, 130.22, 129.95, 129.84, 129.10, 127.15, 126.59, 125.07, 123.73, 123.47, 123.00, 122.11, 121.91, 120.96, 119.30, 119.21, 115.76, 115.02, 114.44, 68.50, 66.31, 63.82, 32.05, 31.08, 29.79, 29.77, 29.72, 29.69, 29.50, 29.48, 29.24, 26.13, 22.84, 14.27.

EA: calculated: C: 72.16 %, H: 5.60 %, N: 5.02 %; found: C: 72.16 %, H: 5.67 %, N: 5.05 %

1-(4-{3-[(4-{[4-(Dodecyloxy)phenyl]carbonyloxy}phenyl)carbonyloxy]phenoxycarbonyl}-phenyl) 4-[4-(4-{2-[4-(2-phenyldiazen-1-yl)phenyl]diazen-1-yl}phenoxy)butyl]benzene-1,4-dicarboxylate **30b** (*n* = 12, *m* = 4)

Formula:	$C_{69}H_{66}N_4O_{12}$, M = 1143.31 g/mol
Synthesis:	according to the general procedure 10.3.3
Reagents:	480 mg (0.61 mmol) 4-(4-{3-[(4-{[4-(dodecyloxy)phenyl]carbonyloxy}phenyl)carbonyloxy]-phenoxycarbonyl}phenoxycarbonyl)benzoic acid **i70** 230 mg (0.61 mmol) 4-(4-{2-[4-(2-phenyldiazen-1-yl)phenyl]diazen-1-yl}phenoxy)butan-1-ol **i73(4)** 140 mg (0.67 mmol) DCC 5 mg DMAP 40 ml dichloromethane
Purification:	column chromatography, eluent: $CHCl_3$/EtOAc (10/0.5) and further recrystallisation from $CHCl_3$/CH_3CN (10/0.2)
Yield:	470 mg (67 %), colorless solid
Transition temp.:	Cr 176 (SmC_sP_{FE} 161) SmC_aP_{AF} 184 I
^{1}H-NMR:	($CDCl_3$, *J*/Hz, 400 MHz) δ 8.28 – 8.22 (m, 6H, Ar-H), 8.17 – 8.11 (m, 4H, Ar-H), 8.05-7.98 (m, 4H, Ar-H), 7.95 – 7.91 (m, 4H, Ar-H), 7.53 – 7.43 (m, 4H, Ar-H), 7.38 – 7.33 (m, 4H, Ar-H), 7.19 – 7.13 (m, 3H, Ar-H), 7.01 (d, *J* = 9.1 Hz, 2H, Ar-H), 6.97 (d, *J* = 9.0 Hz, 2H, Ar-H), 4.47 (t, *J* = 6.0 Hz, 2H, $COOCH_2$), 4.15 (t, *J* = 5.7 Hz, 2H, OCH_2), 4.03 (t, *J* = 6.6 Hz, 2H, OCH_2), 2.06 – 1.99 (m, 4H, $COOCH_2C\mathbf{H}_2$), 1.85 – 1.77 (m, 2H, $OCH_2C\mathbf{H}_2$), 1.51 – 1.41 (m, 2H, CH_2), 1.39 – 1.23 (m, 16H, CH_2), 0.87 (t, *J* = 6.9 Hz, 3H, CH_3).
^{13}C-NMR:	($CDCl_3$, 100 MHz) δ 165.45, 164.17, 163.96, 163.80, 163.76, 163.62, 161.63, 155.45, 154.90, 153.85, 153.28, 152.70, 151.38, 151.31, 147.16, 134.91, 132.75, 132.37, 131.90, 131.79, 131.22, 130.18, 129.83, 129.73, 129.09, 127.12, 126.60, 125.05, 123.72, 123.41, 122.99, 122.11, 121.90, 120.96, 119.20, 115.75, 114.81, 114.44, 68.49, 67.69, 65.29, 32.06, 31.02, 29.79, 29.77, 29.73, 29.69, 29.50, 29.24, 26.13, 25.65, 25.19, 22.84, 14.84, 14.27.
EA:	calculated: C: 72.49 %, H: 5.82 %, N: 4.90 %; found: C: 72.45 %, H: 5.82 %, N: 4.89 %

1-(4-{3-[(4-{[4-(Dodecyloxy)phenyl]carbonyloxy}phenyl)carbonyloxy]phenoxycarbonyl}-phenyl) 4-[6-(4-{2-[4-(2-phenyldiazen-1-yl)phenyl]diazen-1-yl}phenoxy)hexyl]benzene-1,4-dicarboxylate **30c** (*n* = 12, *m* = 6)

Formula:	$C_{71}H_{70}N_4O_{12}$, M = 1171.37 g/mol
Synthesis:	according to the general procedure 10.3.3
Reagents:	1.00 g (1.27 mmol) 4-(4-{3-[(4-{[4-(dodecyloxy)phenyl]carbonyloxy}phenyl)carbonyloxy]-phenoxycarbonyl}phenoxycarbonyl)benzoic acid **i70** 0.51 g (1.27 mmol) 6-(4-{2-[4-(2-phenyldiazen-1-yl)phenyl]diazen-1-yl}phenoxy)hexan-1-ol **i73(6)** 0.29 g (1.40 mmol) DCC 10 mg DMAP 100 ml dichloromethane
Purification:	column chromatography, eluent: $CHCl_3$/EtOAc (10/0.5) and further recrystallisation from $CHCl_3$/CH_3CN (10/0.2)
Yield:	0.90 g (60 %), colorless solid
Transition temp.:	Cr 160 (SmC_sP_{FE} 151) SmC_aP_{AF} 175 I
^{1}H-NMR:	($CDCl_3$, *J*/Hz, 400 MHz) δ 8.30 – 8.23 (m, 6H, Ar-H), 8.17 (d, *J* = 8.5 Hz, 2H, Ar-H), 8.13 (d, *J* = 8.9 Hz, 2H, Ar-H), 8.06 – 7.97 (m, 4H, Ar-H), 7.93 (d, *J* = 8.9 Hz, 4H, Ar-H), 7.54 – 7.44 (m, 4H, Ar-H), 7.40 – 7.34 (m, 4H, Ar-H), 7.20 – 7.14 (m, 3H, Ar-H), 7.00 (d, *J* = 9.0 Hz, 2H, Ar-H), 6.97 (d, *J* = 8.9 Hz, 2H, Ar-H), 4.40 (t, *J* = 6.6 Hz, 2H, $COOCH_2$), 4.10 – 4.01 (m, 4H, OCH_2), 1.91 – 1.77 (m, 6H, $COOCH_2C\mathbf{H}_2$, $OCH_2C\mathbf{H}_2$), 1.64 – 1.54 (m, 4H, CH_2), 1.51 – 1.42 (m, 2H, CH_2), 1.39 – 1.23 (m, 16H, CH_2), 0.87 (t, *J* = 6.8 Hz, 3H, CH_3).
^{13}C-NMR:	($CDCl_3$, 100 MHz) δ 165.51, 164.17, 163.96, 163.76, 163.65, 161.89, 155.45, 154.92, 153.89,

	153.26, 152.72, 151.39, 151.32, 147.07, 135.10, 132.71, 132.37, 131.91, 131.79, 131.20, 130.18, 129.83, 129.73, 129.08, 127.13, 126.60, 125.03, 123.72, 123.39, 122.99, 122.11, 121.91, 120.97, 119.28, 119.20, 115.76, 114.79, 114.45, 68.50, 68.24, 65.60, 52.23, 32.05, 29.79, 29.77, 29.72, 29.69, 29.48, 29.24, 28.77, 26.13, 25.96, 25.93, 22.83, 14.26.
EA:	calculated: C: 72.80 %, H: 6.02 %, N: 4.78 %; found: C: 72.77 %, H: 6.23 %, N: 4.69 %

Compounds 31

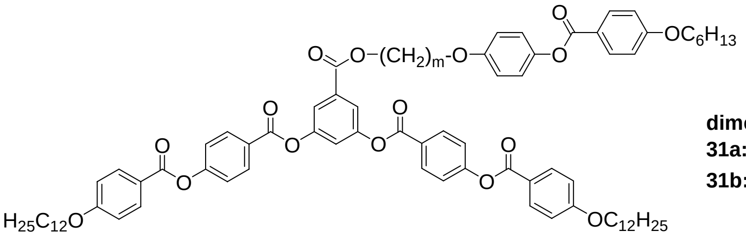

dimer series 31
31a: *m* = 6
31b: *m* = 11

6-(4-{[4-(Hexyloxy)phenyl]carbonyloxy}phenoxy)hexyl 3,5-bis[(4-{[4-(dodecyloxy)phenyl]-carbonyloxy}phenyl)carbonyloxy]benzoate **31a** (*m* = 6)

Formula:	$C_{84}H_{102}O_{16}$, M = 1367.74 g/mol
Synthesis:	according to the general procedure 10.3.3
Reagents:	770 mg (1.82 mmol) 4-{[4-(dodecyloxy)phenyl]carbonyloxy}benzoic acid **i3(12)** 500 mg (0.91 mmol) 6-(4-{[4-(hexyloxy)phenyl]carbonyloxy}phenoxy)hexyl 3,5-dihydroxybenzoate **i75(6), L-5-T** 410 mg (2.00 mmol) DCC 10 mg DMAP 40 ml dichloromethane
Purification:	column chromatography, eluent: $CHCl_3$/EtOAc (10/0.2) and further recrystallisation from EtOAc/EtOH (10/0.2)
Yield:	850 mg (68 %), colorless solid
Transition temp.:	Cr 95 ($\mathrm{Col_rP_{FE}}$ 84) I
^{1}H-NMR:	($CDCl_3$, *J*/Hz, 400 MHz) δ 8.26 (d, *J* = 8.7 Hz, 4H, Ar-H), 8.13 (d, *J* = 8.8 Hz, 4H, Ar-H), 8.10 (d, *J* = 8.8 Hz, 2H, Ar-H), 7.84 (d, *J* = 2.2 Hz, 2H, Ar-H), 7.42 (t, *J* = 2.2 Hz, 1H, Ar-H), 7.37 (d, *J* = 8.7 Hz, 4H, Ar-H), 7.07 (d, *J* = 8.9 Hz, 2H, Ar-H), 6.97 (d, *J* = 8.9 Hz, 4H, Ar-H), 6.95 – 6.86 (m, 4H, Ar-H), 4.36 (t, *J* = 6.6 Hz, 2H, $COOCH_2$), 4.07 – 3.99 (m, 6H, OCH_2), 3.95 (t, *J* = 6.4 Hz, 2H, OCH_2), 1.86 – 1.75 (m, 10H, $COOCH_2C\mathbf{H}_2$, $OCH_2C\mathbf{H}_2$), 1.51 – 1.41 (m, 8H, CH_2), 1.40 – 1.21 (m, 38H, CH_2), 0.93 – 0.84 (m, 9H, CH_3).
^{13}C-NMR:	($CDCl_3$, 100 MHz) δ 165.18, 164.86, 164.16, 163.83, 163.79, 163.36, 156.64, 155.62, 151.24, 144.43, 132.79, 132.37, 132.13, 131.86, 126.22, 122.41, 122.16, 120.93, 120.47, 115.06, 114.42, 114.22, 68.42, 68.32, 68.25, 65.60, 31.94, 31.57, 29.67, 29.65, 29.60, 29.57, 29.38, 29.36, 29.23, 29.12, 28.67, 26.01, 25.88, 25.83, 25.69, 22.71, 22.60, 14.13, 14.03.
EA:	calculated: C: 73.77 %, H: 7.52 %; found: C: 73.73 %, H: 7.52 %

11-(4-{[4-(Hexyloxy)phenyl]carbonyloxy}phenoxy)undecyl 3,5-bis[(4-{[4-(dodecyloxy)-phenyl]carbonyloxy}phenyl)carbonyloxy]benzoate **31b** (*m* = 11)

Formula:	$C_{89}H_{112}O_{16}$, M = 1437.88 g/mol
Synthesis:	according to the general procedure 10.3.3
Reagents:	620 mg (1.45 mmol) 4-{[4-(dodecyloxy)phenyl]carbonyloxy}benzoic acid **i3(12)** 450 mg (0.73 mmol) 11-(4-{[4-(hexyloxy)phenyl]carbonyloxy}phenoxy)undecyl 3,5-dihydroxybenzoate **i75(11), L-5-T** 330 mg (1.61 mmol) DCC 10 mg DMAP

40 ml dichloromethane

Purification: column chromatography, eluent: $CHCl_3$/EtOAc (10/0.2) and further recrystallisation from EtOAc/EtOH (10/0.2)

Yield: 720 mg (69 %), colorless solid

Transition temp.: Cr 76 Col_rP_{FE} 89 I

^{1}H-NMR: ($CDCl_3$, *J*/Hz, 400 MHz) δ 8.26 (d, *J* = 8.6 Hz, 4H, Ar-H), 8.13 (d, *J* = 8.8 Hz, 4H, Ar-H), 8.10 (d, *J* = 8.8 Hz, 2H, Ar-H), 7.83 (d, *J* = 2.2 Hz, 2H, Ar-H), 7.41 (t, *J* = 2.1 Hz, 1H, Ar-H), 7.37 (d, *J* = 8.7 Hz, 4H, Ar-H), 7.06 (d, *J* = 8.9 Hz, 2H, Ar-H), 6.97 (d, *J* = 8.9 Hz, 4H, Ar-H), 6.95 – 6.86 (m, 4H, Ar-H), 4.33 (t, *J* = 6.7 Hz, 2H, $COOCH_2$), 4.07 – 3.99 (m, 6H, OCH_2), 3.92 (t, *J* = 6.5 Hz, 2H, OCH_2), 1.86 – 1.71 (m, 10H, $COOCH_2C\mathbf{H}_2$, $OCH_2C\mathbf{H}_2$), 1.51 – 1.40 (m, 10H, CH_2), 1.39 – 1.22 (m, 46H, CH_2), 0.93 – 0.84 (m, 9H, CH_3).

^{13}C-NMR: ($CDCl_3$, 100 MHz) δ 165.14, 164.83, 164.11, 163.78, 163.34, 156.71, 155.61, 151.22, 144.38, 132.89, 132.37, 132.13, 131.85, 126.26, 122.38, 122.16, 120.96, 120.45, 115.11, 114.46, 114.25, 68.56, 68.50, 68.40, 65.85, 32.05, 31.68, 29.78, 29.76, 29.71, 29.68, 29.63, 29.60, 29.49, 29.47, 29.44, 29.39, 29.24, 28.82, 26.18, 26.13, 25.80, 22.82, 22.72, 14.24, 14.14.

EA: calculated: C: 74.35 %, H: 7.85 %; found: C: 74.27 %, H: 7.74 %

Compounds 32

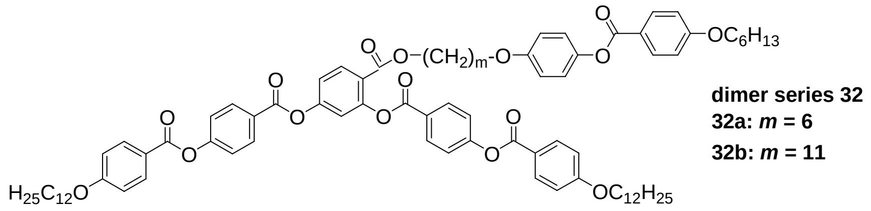

6-(4-{[4-(Hexyloxy)phenyl]carbonyloxy}phenoxy)hexyl 2,4-bis[(4-{[4-(dodecyloxy)phenyl]-carbonyloxy}phenyl)carbonyloxy]benzoate **32a** (*m* = 6)

Formula: $C_{84}H_{102}O_{16}$, M = 1367.74 g/mol

Synthesis: according to the general procedure 10.3.3

Reagents: 210 mg (0.51 mmol) 4-{[4-(dodecyloxy)phenyl]carbonyloxy}benzoic acid **i3(12)**
500 mg (0.51 mmol) 6-(4-{[4-(hexyloxy)phenyl]carbonyloxy}phenoxy)hexyl 2,4-dihydroxybenzoate **i75(6), L-4-T**
120 mg (0.56 mmol) DCC
5 mg DMAP
40 ml dichloromethane

Purification: column chromatography, eluent: $CHCl_3$/EtOAc (10/0.2) and further recrystallisation from EtOAc/EtOH (10/0.2)

Yield: 510 mg (73 %), colorless solid

Transition temp.: Cr 107 SmC_xP_{AF} 119 $SmAP_{AF}$ 121 N 123 I

^{1}H-NMR: ($CDCl_3$, *J*/Hz, 400 MHz) δ 8.23 (d, *J* = 8.7 Hz, 2H, Ar-H), 8.13 (d, *J* = 8.9 Hz, 2H, Ar-H), 8.09 (d, *J* = 8.9 Hz, 4H, Ar-H), 7.89 (d, *J* = 8.7 Hz, 1H, Ar-H), 7.35 (d, *J* = 8.7 Hz, 2H, Ar-H), 7.08 (d, *J* = 9.0 Hz, 4H, Ar-H), 6.97 (d, *J* = 8.9 Hz, 4H, Ar-H), 6.93 (d, *J* = 8.9 Hz, 2H, Ar-H), 6.90 (d, *J* = 9.0 Hz, 4H, Ar-H), 6.86 (d, *J* = 2.2 Hz, 1H, Ar-H), 6.76 (dd, *J* = 8.7, 2.2 Hz, 1H, Ar-H), 4.37 (t, *J* = 6.5 Hz, 2H, $COOCH_2$), 4.07 – 3.99 (m, 4H, OCH_2), 3.97 (t, *J* = 6.3 Hz, 2H, OCH_2), 1.87 – 1.75 (m, 10H, $COOCH_2C\mathbf{H}_2$, $OCH_2C\mathbf{H}_2$), 1.51 – 1.41 (m, 8H, CH_2), 1.39 – 1.22 (m, 38H, CH_2), 0.93 – 0.84 (m, 9H, CH_3).

^{13}C-NMR: ($CDCl_3$, 100 MHz) δ 169.58, 165.13, 164.11, 163.78, 163.51, 163.36, 162.93, 156.60, 156.39, 155.54, 144.51, 132.36, 132.13, 131.82, 131.04, 126.43, 122.46, 122.10, 121.77, 120.98, 115.11, 114.46, 114.27, 113.16, 112.39, 112.26, 68.51, 68.41, 68.28, 65.52, 32.04, 31.68, 29.78, 29.76, 29.71, 29.68, 29.48, 29.47, 29.30, 29.24, 29.23, 28.70, 26.13, 25.93, 25.92, 25.80, 22.82, 22.71, 14.23, 14.13.

EA: calculated: C: 73.77 %, H: 7.52 %; found: C: 73.66 %, H: 7.46 %

11-(4-{[4-(Hexyloxy)phenyl]carbonyloxy}phenoxy)undecyl 2,4-bis[(4-{[4-(dodecyloxy)-phenyl]carbonyloxy}phenyl)carbonyloxy]benzoate **32b** (*m* = 11)

Formula:	$C_{89}H_{112}O_{16}$, M = 1437.88 g/mol
Synthesis:	according to the general procedure 10.3.3
Reagents:	240 mg (0.49 mmol) 4-{[4-(dodecyloxy)phenyl]carbonyloxy}benzoic acid **i3(12)** 480 mg (0.49 mmol) 11-(4-{[4-(hexyloxy)phenyl]carbonyloxy}phenoxy)undecyl 2,4-dihydroxybenzoate **i75(11), L-4-T** 110 mg (0.54 mmol) DCC 5 mg DMAP 40 ml dichloromethane
Purification:	column chromatography, eluent: $CHCl_3$/EtOAc (10/0.2) and further recrystallisation from EtOAc/EtOH (10/0.2)
Yield:	490 mg (68 %), colorless solid
Transition temp.:	Cr 105 $SmAP_{AF}$ 144 N 151 I
^{1}H-NMR:	($CDCl_3$, *J*/Hz, 400 MHz) δ 8.24 (d, *J* = 8.8 Hz, 2H, Ar-H), 8.17 – 8.05 (m, 6H, Ar-H), 7.90 (d, *J* = 8.7 Hz, 1H, Ar-H), 7.35 (d, *J* = 8.8 Hz, 2H, Ar-H), 7.07 (d, *J* = 9.0 Hz, 5H, Ar-H), 7.01 – 6.83 (m, 10H, Ar-H), 6.77 (dd, *J* = 8.7, 2.3 Hz, 1H, Ar-H), 4.35 (t, *J* = 6.7 Hz, 2H, $COOCH_2$), 4.09 – 3.87 (m, 8H, OCH_2), 1.89 – 1.68 (m, 10H, $COOCH_2\mathbf{CH_2}$, $OCH_2\mathbf{CH_2}$), 1.51 – 1.19 (m, 56H, CH_2), 0.95 – 0.80 (m, 9H, CH_3).
^{13}C-NMR:	($CDCl_3$, 125 MHz) δ 169.69, 165.28, 164.23, 163.81, 163.63, 163.39, 162.95, 156.73, 156.35, 155.55, 144.35, 132.38, 132.15, 131.86, 131.08, 126.37, 122.41, 122.14, 121.74, 121.67, 120.87, 115.04, 114.39, 114.20, 113.11, 112.35, 112.28, 68.37, 68.27, 65.62, 31.88, 31.51, 29.61, 29.59, 29.55, 29.51, 29.49, 29.44, 29.31, 29.24, 29.18, 29.03, 28.53, 26.00, 25.94, 25.91, 25.62, 22.65, 22.54, 14.07, 13.98.
EA:	calculated: C: 74.35 %, H: 7.85 %; found: C: 74.48 %, H: 7.92 %

Compounds 33 and 35a

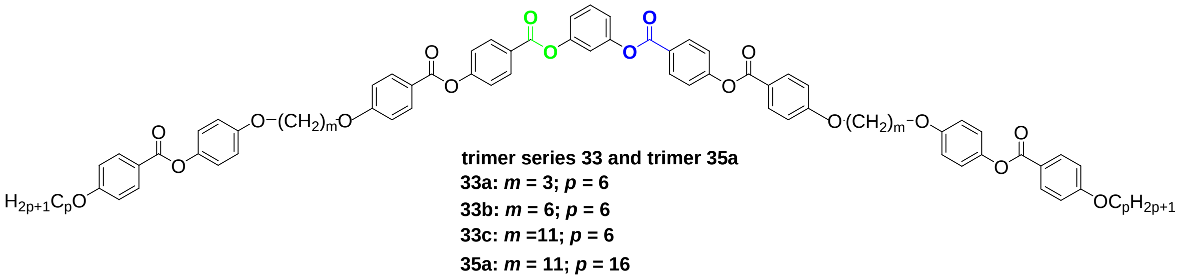

4-(3-{[4-({4-[3-(4-{[4-(Hexyloxy)phenyl]carbonyloxy}phenoxy)propoxy]phenyl}carbonyl-oxy)phenyl]carbonyloxy}phenoxycarbonyl)phenyl 4-[3-(4-{[4-(hexyloxy)phenyl]carbonyl-oxy}phenoxy)propoxy]benzoate **33a** (*m* = 3, p = 6)

Formula:	$C_{78}H_{74}O_{18}$, M = 1299.45 g/mol
Synthesis:	according to the general procedure 10.3.3
Reagents:	190 mg (0.54 mmol) 3-[(4-hydroxyphenyl)carbonyloxy]phenyl 4-hydroxybenzoate **i77** 530 mg (1.08 mmol) 4-[3-(4-{[4-(hexyloxy)phenyl]carbonyloxy}phenoxy)propoxy]benzoic acid **i14(3,6)** 240 mg (1.19 mmol) DCC 10 mg DMAP 40 ml dichloromethane
Purification:	column chromatography, eluent: $CHCl_3$/EtOAc (10/0.2) and further recrystallisation from $CHCl_3$/PE (10/0.2)
Yield:	470 mg (67 %), colorless solid
Transition temp.:	Cr 156 (SmC_xP_{AF} 144) I

^{1}H-NMR: ($CDCl_3$, *J*/Hz, 400 MHz) δ 8.26 (d, *J* = 8.8 Hz, 4H, Ar-H), 8.15 (d, *J* = 8.9 Hz, 4H, Ar-H), 8.11 (d, *J* = 8.9 Hz, 4H, Ar-H), 7.48 (t, *J* = 8.1 Hz, 1H, Ar-H), 7.36 (d, *J* = 8.8 Hz, 4H, Ar-H), 7.21 – 7.15 (m, 3H, Ar-H), 7.10 (d, *J* = 9.0 Hz, 4H, Ar-H), 7.00 (d, *J* = 8.9 Hz, 4H, Ar-H), 6.97 – 6.91 (m, 8H, Ar-H), 4.26 (t, *J* = 6.1 Hz, 4H, OCH_2), 4.18 (t, *J* = 5.9 Hz, 4H, OCH_2), 4.02 (t, *J* = 6.6 Hz, 4H, OCH_2), 2.35 – 2.27 (m, 4H, $OCH_2C\mathbf{H}_2$), 1.85 – 1.76 (m, 4H, $OCH_2C\mathbf{H}_2$), 1.51 – 1.42 (m, 4H, CH_2), 1.39 – 1.31 (m, 8H, CH_2), 0.90 (t, *J* = 7.0 Hz, 6H, CH_3).

^{13}C-NMR: ($CDCl_3$, 100 MHz) δ 165.12, 164.09, 163.94, 163.41, 156.30, 155.42, 151.41, 144.76, 132.41, 132.15, 131.78, 129.79, 126.66, 122.57, 122.08, 121.68, 121.38, 119.22, 115.77, 115.16, 114.49, 114.29, 68.43, 64.94, 64.76, 31.67, 29.37, 29.22, 25.80, 22.71, 14.14.

EA: calculated: C: 72.10 %, H: 5.74 %; found: C: 72.21 %, H: 5.80 %

4-[3-({4-[(4-{[6-(4-{[4-(Hexyloxy)phenyl]carbonyloxy}phenoxy)hexyl]oxy}phenyl)carbonyloxy]phenyl}carbonyloxy)phenoxycarbonyl]phenyl 4-{[6-(4-{[4-(hexyloxy)phenyl]carbonyloxy}phenoxy)hexyl]oxy}benzoate **33b** (*m* = 6, p = 6)

Formula: $C_{84}H_{86}O_{18}$, M = 1383.61 g/mol

Synthesis: according to the general procedure 10.3.3

Reagents: 180 mg (0.50 mmol) 3-[(4-hydroxyphenyl)carbonyloxy]phenyl 4-hydroxybenzoate **i77**
530 mg (1.00 mmol) 4-{[6-(4-{[4-(hexyloxy)phenyl]carbonyloxy}phenoxy)hexyl]oxy}-benzoic acid **i14(6,6)**
230 mg (1.10 mmol) DCC
10 mg DMAP
40 ml dichloromethane

Purification: column chromatography, eluent: $CHCl_3$/EtOAc (10/0.2) and further recrystallisation from $CHCl_3$/PE (10/0.2)

Yield: 450 mg (65 %), colorless solid

Transition temp.: Cr 176 SmC_xP_{AF} 185 N 193 I

^{1}H-NMR: ($CDCl_3$, *J*/Hz, 400 MHz) δ 8.26 (d, *J* = 8.7 Hz, 4H, Ar-H), 8.14 (d, *J* = 8.9 Hz, 4H, Ar-H), 8.11 (d, *J* = 8.9 Hz, 4H, Ar-H), 7.48 (t, *J* = 8.1 Hz, 1H, Ar-H), 7.36 (d, *J* = 8.7 Hz, 4H, Ar-H), 7.21 – 7.17 (m, 2H, Ar-H), 7.16 (d, *J* = 2.2 Hz, 1H, Ar-H), 7.09 (d, *J* = 9.0 Hz, 4H, Ar-H), 6.98 (d, *J* = 8.9 Hz, 4H, Ar-H), 6.94 (d, *J* = 8.9 Hz, 4H, Ar-H), 6.90 (d, *J* = 9.0 Hz, 4H, Ar-H), 4.07 (t, *J* = 6.4 Hz, 4H, OCH_2), 4.02 (t, *J* = 6.6 Hz, 4H, OCH_2), 3.97 (t, *J* = 6.4 Hz, 4H, OCH_2), 1.91 – 1.76 (m, 12H, $OCH_2C\mathbf{H}_2$), 1.61 – 1.52 (m, 8H, CH_2), 1.51 – 1.42 (m, 4H, CH_2), 1.38 – 1.31 (m, 8H, CH_2), 0.90 (t, *J* = 7.0 Hz, 6H, CH_3).

^{13}C-NMR: ($CDCl_3$, 100 MHz) δ 165.19, 164.17, 163.98, 163.73, 163.42, 156.65, 155.48, 151.44, 144.53, 132.38, 132.14, 131.77, 129.78, 126.64, 122.45, 122.07, 121.74, 121.09, 119.20, 115.74, 115.11, 114.44, 114.27, 68.35, 68.24, 31.56, 29.24, 29.11, 29.08, 25.89, 25.83, 25.68, 22.59, 14.00.

EA: calculated: C: 72.92 %, H: 6.27 %; found: C: 72.94 %, H: 6.34 %

4-[3-({4-[(4-{[11-(4-{[4-(Hexyloxy)phenyl]carbonyloxy}phenoxy)undecyl]oxy}phenyl)-carbonyloxy]phenyl}carbonyloxy)phenoxycarbonyl]phenyl 4-{[11-(4-{[4-(hexyloxy)phenyl]-carbonyloxy}phenoxy)undecyl]oxy}benzoate **33c** (*m* = 11, p = 6)

Formula: $C_{94}H_{106}O_{18}$, M = 1523.88 g/mol

Synthesis: according to the general procedure 10.3.3

Reagents: 160 mg (0.46 mmol) 3-[(4-hydroxyphenyl)carbonyloxy]phenyl 4-hydroxybenzoate **i77**
560 mg (0.92 mmol) 4-{[11-(4-{[4-(hexyloxy)phenyl]carbonyloxy}phenoxy)undecyl]oxy}-benzoic acid **i14(11,6)**
210 mg (1.01 mmol) DCC
10 mg DMAP
40 ml dichloromethane

Purification: column chromatography, eluent: $CHCl_3$/EtOAc (10/0.2) and further recrystallisation from

$\mathrm{CHCl_3}$/PE (10/0.2)

Yield: 460 mg (66 %), colorless solid

Transition temp.: Cr 130 $\mathrm{SmC_cP_{AF}}$ 161 I

^{1}H-NMR: ($\mathrm{CDCl_3}$, *J*/Hz, 400 MHz) δ 8.26 (d, *J* = 8.7 Hz, 4H, Ar-H), 8.13 (d, *J* = 8.9 Hz, 4H, Ar-H), 8.10 (d, *J* = 8.9 Hz, 4H, Ar-H), 7.48 (t, *J* = 8.2 Hz, 1H, Ar-H), 7.36 (d, *J* = 8.7 Hz, 4H, Ar-H), 7.20 – 7.17 (m, 2H, Ar-H), 7.16 (d, *J* = 2.2 Hz, 1H, Ar-H), 7.08 (d, *J* = 9.0 Hz, 4H, Ar-H), 6.97 (d, *J* = 9.0 Hz, 4H, Ar-H), 6.94 (d, *J* = 8.9 Hz, 4H, Ar-H), 6.90 (d, *J* = 9.0 Hz, 4H, Ar-H), 4.07 – 3.99 (m, 8H, $\mathrm{OCH_2}$), 3.94 (t, *J* = 6.5 Hz, 4H, $\mathrm{OCH_2}$), 1.86 – 1.73 (m, 12H, $\mathrm{OCH_2C\mathbf{H}_2}$), 1.51 – 1.41 (m, 12H, $\mathrm{CH_2}$), 1.40 – 1.29 (m, 28H, $\mathrm{CH_2}$), 0.90 (t, *J* = 7.1 Hz, 6H, $\mathrm{CH_3}$).

^{13}C-NMR: ($\mathrm{CDCl_3}$, 100 MHz) δ 165.17, 164.16, 163.96, 163.75, 163.36, 156.70, 155.44, 151.39, 144.41, 132.36, 132.13, 131.78, 129.78, 126.62, 122.42, 122.09, 121.01, 119.22, 115.78, 115.10, 114.45, 114.27, 68.53, 68.49, 68.41, 31.67, 29.64, 29.61, 29.47, 29.43, 29.22, 26.18, 26.12, 25.80, 22.71, 14.14.

EA: calculated: C: 74.09 %, H: 7.01 %; found: C: 74.20 %, H: 7.08 %

4-[3-({4-[(4-{[11-(4-{[4-(Hexadecyloxy)phenyl]carbonyloxy}phenoxy)undecyl]oxy}phenyl)-carbonyloxy]phenyl}carbonyloxy)phenoxycarbonyl]phenyl 4-{[11-(4-{[4-(hexadecyloxy)-phenyl]carbonyloxy}phenoxy)undecyl]oxy}benzoate **35a** (*m* = 11, p = 16)

Formula: $\mathrm{C_{114}H_{146}O_{18}}$, M = 1804.42 g/mol

Synthesis: according to the general procedure 10.3.3

Reagents: 160 mg (0.46 mmol) 3-[(4-hydroxyphenyl)carbonyloxy]phenyl 4-hydroxybenzoate **i77**
680 mg (0.92 mmol) 4-{[11-(4-{[4-(hexadecyloxy)phenyl]carbonyloxy}phenoxy)undecyl]-oxy}benzoic acid **i14(11,16)**
210 mg (1.01 mmol) DCC
10 mg DMAP
40 ml dichloromethane

Purification: column chromatography, eluent: $\mathrm{CHCl_3}$/EtOAc (10/0.2) and further recrystallisation from $\mathrm{CHCl_3/CH_3CN}$ (10/0.2)

Yield: 530 mg (64 %), colorless solid

Transition temp.: Cr 126 ($\mathrm{SmC'_aP_{AF}}$ 125) $\mathrm{SmC_aP_{AF}}$ 130 I

^{1}H-NMR: ($\mathrm{CDCl_3}$, *J*/Hz, 400 MHz) δ 8.26 (d, *J* = 8.7 Hz, 4H, Ar-H), 8.13 (d, *J* = 8.9 Hz, 4H, Ar-H), 8.10 (d, *J* = 8.9 Hz, 4H, Ar-H), 7.48 (t, *J* = 8.1 Hz, 1H, Ar-H), 7.36 (d, *J* = 8.7 Hz, 4H, Ar-H), 7.21 – 7.17 (m, 2H, Ar-H), 7.16 (d, *J* = 2.3 Hz, 1H, Ar-H), 7.08 (d, *J* = 8.9 Hz, 4H, Ar-H), 6.97 (d, *J* = 8.9 Hz, 4H, Ar-H), 6.94 (d, *J* = 8.9 Hz, 4H, Ar-H), 6.90 (d, *J* = 9.0 Hz, 4H, Ar-H), 4.07 – 3.99 (m, 8H, $\mathrm{OCH_2}$), 3.94 (t, *J* = 6.5 Hz, 4H, $\mathrm{OCH_2}$), 1.86 – 1.73 (m, 12H, $\mathrm{OCH_2C\mathbf{H}_2}$), 1.51 – 1.41 (m, 12H, $\mathrm{CH_2}$), 1.40 – 1.20 (m, 68H, $\mathrm{CH_2}$), 0.86 (t, *J* = 6.7 Hz, 6H, $\mathrm{CH_3}$).

^{13}C-NMR: ($\mathrm{CDCl_3}$, 100 MHz) δ 171.17, 165.15, 163.37, 161.36, 156.71, 154.71, 144.44, 132.12, 129.00, 122.40, 115.12, 114.34, 114.28, 68.56, 68.42, 68.35, 57.79, 49.68, 32.56, 32.04, 31.01, 29.87, 29.80, 29.77, 29.70, 29.67, 29.65, 29.61, 29.47, 29.43, 29.26, 26.46, 26.18, 26.12, 25.57, 25.47, 24.64, 22.81, 14.21.

EA: calculated: C: 75.88 %, H: 8.16 %; found: C: 75.73 %, H: 8.13 %

Compounds 34 and 35b

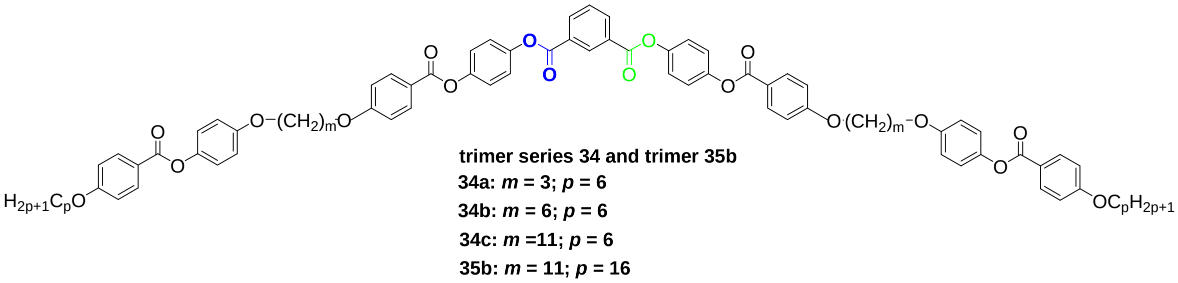

1,3-Bis[4-({4-[3-(4-{[4-(hexyloxy)phenyl]carbonyloxy}phenoxy)propoxy]phenyl}carbonyloxy)phenyl]benzene-1,3-dicarboxylate **34a** (*m* = 3, p = 6)

Formula: $C_{78}H_{74}O_{18}$, M = 1299.45 g/mol

Synthesis: according to the general procedure 10.3.3

Reagents:
- 140 mg (0.41 mmol) 1,3-bis(4-hydroxyphenyl)benzene-1,3-dicarboxylate **i79**
- 200 mg (0.82 mmol) 4-[3-(4-{[4-(hexyloxy)phenyl]carbonyloxy}phenoxy)propoxy]benzoic acid **i14(3,6)**
- 180 mg (0.90 mmol) DCC
- 10 mg DMAP
- 40 ml dichloromethane

Purification: column chromatography, eluent: $CHCl_3$/EtOAc (10/0.2) and further recrystallisation from $CHCl_3/CH_3CN$ (10/0.2)

Yield: 390 mg (73 %), colorless solid

Transition temp.: Cr 186 (N 174) I

^{1}H-NMR: ($CDCl_3$, *J*/Hz, 400 MHz) δ 9.01 (s, 1H, Ar-H), 8.46 (dd, *J* = 7.8, 1.7 Hz, 2H, Ar-H), 8.15 (d, *J* = 8.9 Hz, 5H, Ar-H), 8.11 (d, *J* = 8.9 Hz, 5H, Ar-H), 7.69 (t, *J* = 7.8 Hz, 1H, Ar-H), 7.25 (d, *J* = 12.5 Hz, 2H, Ar-H), 7.10 (d, *J* = 9.0 Hz, 5H, Ar-H), 7.00 (d, *J* = 8.9 Hz, 5H, Ar-H), 6.97 – 6.91 (m, 10H, Ar-H), 4.26 (t, *J* = 6.1 Hz, 4H, OCH_2), 4.18 (t, *J* = 5.9 Hz, 4H, OCH_2), 4.02 (t, *J* = 6.6 Hz, 4H, OCH_2), 2.31 (p, *J* = 5.9 Hz, 4H, $OCH_2C\mathbf{H}_2$), 1.85 – 1.76 (m, 4H, $OCH_2C\mathbf{H}_2$), 1.51 – 1.42 (m, 4H, CH_2), 1.39 – 1.29 (m, 8H, CH_2), 0.90 (t, *J* = 7.0 Hz, 6H, CH_3).

^{13}C-NMR: ($CDCl_3$, 100 MHz) δ 165.13, 164.57, 163.97, 163.40, 163.22, 156.31, 148.71, 148.01, 144.74, 134.93, 132.31, 132.15, 131.75, 130.26, 129.09, 122.77, 122.57, 122.42, 121.74, 121.68, 115.16, 114.41, 114.29, 68.42, 64.91, 64.79, 31.68, 29.38, 29.23, 25.81, 22.72, 14.15.

EA: calculated: C: 72.10 %, H: 5.74 %; found: C: 72.09 %, H: 5.76 %

1,3-Bis({4-[(4-{[6-(4-{[4-(hexyloxy)phenyl]carbonyloxy}phenoxy)hexyl]oxy}phenyl)carbonyloxy]phenyl})benzene-1,3-dicarboxylate **34b** (*m* = 6, p = 6)

Formula: $C_{84}H_{86}O_{18}$, M = 1383.61 g/mol

Synthesis: according to the general procedure 10.3.3

Reagents:
- 0.35 g (1.00 mmol) 1,3-bis(4-hydroxyphenyl)benzene-1,3-dicarboxylate **i79**
- 1.07 g (2.00 mmol) 4-{[6-(4-{[4-(hexyloxy)phenyl]carbonyloxy}phenoxy)hexyl]oxy}benzoic acid **i14(6,6)**
- mg (2.20 mmol) DCC
- 0.45 g DMAP
- 60 ml dichloromethane

Purification: column chromatography, eluent: $CHCl_3$/EtOAc (10/0.2) and further recrystallisation from $CHCl_3/CH_3CN$ (10/0.2)

Yield: 870 mg (63 %), colorless solid

Transition temp.: Cr 186 (SmC_x 166) N 220 I

^{1}H-NMR: Due to the low solubility of the compound the ^{1}H-NMR could not be measured.

^{13}C-NMR: Due to the low solubility of the compound ^{13}C-NMR could not be measured.

EA: calculated: C: 72.92 %, H: 6.27 %; found: C: 72.96 %, H: 6.37 %

1,3-Bis({4-[(4-{[11-(4-{[4-(hexyloxy)phenyl]carbonyloxy}phenoxy)undecyl]oxy}phenyl)-carbonyloxy]phenyl})benzene-1,3-dicarboxylate **34c** (*m* = 11, p = 6)

Formula: $C_{94}H_{106}O_{18}$, M = 1523.88 g/mol
Synthesis: according to the general procedure 10.3.3
Reagents: 160 mg (0.46 mmol) 1,3-bis(4-hydroxyphenyl)benzene-1,3-dicarboxylate **i79**
560 mg (0.92 mmol) 4-{[11-(4-{[4-(hexyloxy)phenyl]carbonyloxy}phenoxy)undecyl]oxy}-benzoic acid **i14(11,6)**
210 mg (1.01 mmol) DCC
10 mg DMAP
40 ml dichloromethane
Purification: column chromatography, eluent: $CHCl_3$/EtOAc (10/0.2) and further recrystallisation from $CHCl_3$/CH_3CN (10/0.2)
Yield: 480 mg (68 %), colorless solid
Transition temp.: Cr 143 (SmC_xP_{AF} 131) N 171 I
^{1}H-NMR: ($CDCl_3$, *J*/Hz, 400 MHz) δ 9.01 (s, 1H, Ar-H), 8.45 (dd, *J* = 7.8, 1.7 Hz, 2H, Ar-H), 8.16 – 8.07 (m, 10H, Ar-H), 7.68 (t, *J* = 7.8 Hz, 1H, Ar-H), 7.32 – 7.25 (m, 2H, Ar-H), 7.07 (d, *J* = 9.0 Hz, 5H, Ar-H), 7.00 – 6.87 (m, 15H, Ar-H), 4.06 – 3.99 (m, 8H, OCH_2), 3.94 (t, *J* = 6.5 Hz, 4H, OCH_2), 1.86 – 1.72 (m, 12H, $OCH_2C\mathbf{H}_2$), 1.52 – 1.41 (m, 12H, CH_2), 1.40 – 1.28 (m, 28H, CH_2), 0.90 (t, *J* = 7.0 Hz, 6H, CH_3).
^{13}C-NMR: ($CDCl_3$, 100 MHz) δ 165.14, 164.61, 163.95, 163.57, 163.37, 156.71, 148.74, 148.00, 144.45, 134.90, 132.24, 132.12, 131.73, 130.29, 129.05, 122.75, 122.40, 122.39, 121.80, 121.41, 115.13, 114.38, 114.28, 68.57, 68.46, 68.42, 31.67, 29.65, 29.61, 29.48, 29.44, 29.26, 29.22, 26.19, 26.13, 25.79, 22.70, 14.12.
EA: calculated: C: 74.09 %, H: 7.01 %; found: C: 74.10 %, H: 6.93 %

1,3-Bis({4-[(4-{[11-(4-{[4-(hexadecyloxy)phenyl]carbonyloxy}phenoxy)undecyl]oxy}phenyl)-carbonyloxy]phenyl})benzene-1,3-dicarboxylate **35b** (*m* = 11, p = 16)

Formula: $C_{114}H_{146}O_{18}$, M = 1804.42 g/mol
Synthesis: according to the general procedure 10.3.3
Reagents: 160 mg (0.46 mmol) 1,3-bis(4-hydroxyphenyl)benzene-1,3-dicarboxylate **i79**
690 mg (0.92 mmol) 4-{[11-(4-{[4-(hexadecyloxy)phenyl]carbonyloxy}phenoxy)undecyl]-oxy}benzoic acid **i14(11,16)**
210 mg (1.01 mmol) DCC
10 mg DMAP
60 ml dichloromethane
Purification: column chromatography, eluent: $CHCl_3$/EtOAc (10/0.2) and further recrystallisation from $CHCl_3$/CH_3CN (10/0.2)
Yield: 590 mg (71 %), colorless solid
Transition temp.: Cr 142 SmC'_x 146 SmC_x 149 I
^{1}H-NMR: ($CDCl_3$, *J*/Hz, 400 MHz) δ 9.01 (s, 1H, Ar-H), 8.46 (dd, *J* = 7.8, 1.7 Hz, 2H, Ar-H), 8.15 – 8.08 (m, 10H, Ar-H), 7.68 (t, *J* = 7.8 Hz, 1H, Ar-H), 7.28 (d, *J* = 2.0 Hz, 2H, Ar-H), 7.07 (d, *J* = 9.0 Hz, 5H, Ar-H), 6.99 – 6.91 (m, 10H, Ar-H), 6.89 (d, *J* = 9.0 Hz, 5H, Ar-H), 4.06 – 3.99 (m, 8H, OCH_2), 3.94 (t, *J* = 6.6 Hz, 4H, OCH_2), 1.85 – 1.73 (m, 12H, $OCH_2C\mathbf{H}_2$), 1.50 – 1.40 (m, 12H, CH_2), 1.39 – 1.22 (m, 68H, CH_2), 0.86 (t, *J* = 6.8 Hz, 6H, CH_3).
^{13}C-NMR: ($CDCl_3$, 100 MHz) δ 171.31, 165.16, 163.51, 161.52, 156.85, 154.81, 144.64, 132.15, 129.06, 122.41, 115.26, 114.46, 114.38, 68.66, 68.47, 68.42, 57.88, 49.67, 32.52, 31.97, 31.00, 29.72, 29.68, 29.62, 29.56, 29.52, 29.40, 29.21, 26.44, 26.12, 26.06, 25.55, 25.44, 24.56, 22.70, 14.05.
EA: calculated: C: 75.88 %, H: 8.16 %; found: C: 75.77 %, H: 8.07 %

Compound 36

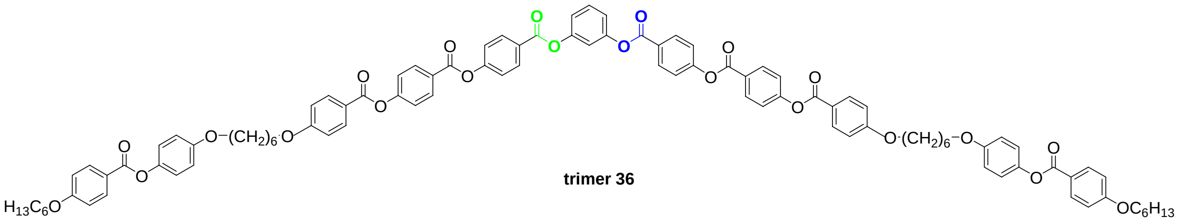

trimer 36

4-(3-{[4-({4-[(4-{[6-(4-{[4-(Hexyloxy)phenyl]carbonyloxy}phenoxy)hexyl]oxy}phenyl)-carbonyloxy]phenyl}carbonyloxy)phenyl]carbonyloxy}phenoxycarbonyl)phenyl 4-[(4-{[6-(4-{[4-(hexyloxy)phenyl]carbonyloxy}phenoxy)hexyl]oxy}phenyl)carbonyloxy]benzoate **36** (*m* = 6, p = 6)

Formula:	$C_{98}H_{94}O_{22}$, M = 1623.83 g/mol
Synthesis:	according to the general procedure 10.3.3
Reagents:	300 mg (0.46 mmol) 4-[(4-{[6-(4-{[4-(hexyloxy)phenyl]carbonyloxy}phenoxy)hexyl]oxy}-phenyl)carbonyloxy]benzoic acid **i81** 80 mg (0.23 mmol) 3-[(4-hydroxyphenyl)carbonyloxy]phenyl 4-hydroxybenzoate **i77** 100 mg (0.51 mmol) DCC 10 mg DMAP 40 ml dichloromethane
Purification:	column chromatography, eluent: $CHCl_3$/EtOAc (10/0.2) and further recrystallisation from $CHCl_3/CH_3CN$ (10/0.2)
Yield:	260 mg (70 %), colorless solid
Transition temp.:	Cr 165 SmC_xP_{AF} 200 N 267 I
^{1}H-NMR:	($CDCl_3$, *J*/Hz, 400 MHz) δ 8.31 – 8.25 (m, 8H, Ar-H), 8.14 (d, *J* = 8.8 Hz, 4H, Ar-H), 8.11 (d, *J* = 8.8 Hz, 4H, Ar-H), 7.49 (t, *J* = 8.2 Hz, 1H, Ar-H), 7.38 (dd, *J* = 8.7, 2.4 Hz, 8H, Ar-H), 7.22 – 7.16 (m, 3H, Ar-H), 7.09 (d, *J* = 9.0 Hz, 4H, Ar-H), 6.98 (d, *J* = 8.9 Hz, 4H, Ar-H), 6.94 (d, *J* = 8.8 Hz, 4H, Ar-H), 6.90 (d, *J* = 9.0 Hz, 4H, Ar-H), 4.07 (t, *J* = 6.4 Hz, 4H, OCH_2), 4.02 (t, *J* = 6.6 Hz, 4H, OCH_2), 3.97 (t, *J* = 6.4 Hz, 4H, OCH_2), 1.91 – 1.76 (m, 12H, $OCH_2\mathbf{CH_2}$), 1.61 – 1.55 (m, 8H, CH_2), 1.51 – 1.42 (m, 4H, CH_2), 1.39 – 1.30 (m, 8H, CH_2), 0.90 (t, *J* = 7.0 Hz, 6H, CH_3).
^{13}C-NMR:	($CDCl_3$, 100 MHz) δ 165.17, 164.12, 163.88, 163.72, 163.39, 156.62, 155.63, 155.18, 151.39, 144.51, 132.40, 132.14, 131.85, 126.94, 126.34, 122.47, 122.18, 122.02, 121.73, 121.03, 119.25, 115.76, 115.12, 114.48, 114.28, 68.42, 68.32, 31.67, 29.36, 29.23, 29.19, 26.00, 25.94, 25.80, 22.71, 14.14.
EA:	calculated: C: 72.49 %, H: 5.83 %; found: C: 72.61 %, H: 5.84 %

Compound 37

1-{4-[4-(4-{[4-(4-{3-[(4-{[4-(Dodecyloxy)phenyl]carbonyloxy}phenyl)carbonyloxy]phenoxy-carbonyl}phenoxycarbonyl)phenyl]carbonyloxy}butoxy)phenoxy]butyl} 4-(4-{3-[(4-{[4-(dodecyloxy)phenyl]carbonyloxy}phenyl)carbonyloxy]phenoxycarbonyl}phenyl)benzene-1,4-dicarboxylate **37a** (*m* = 4, p = 12)

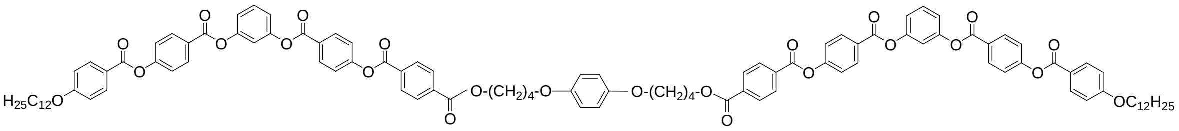

trimer 37a

Formula:	$C_{108}H_{110}O_{24}$, M = 1792.07 g/mol

Synthesis: according to the general procedure 10.3.3
Reagents: 130 mg (0.49 mmol) 4-[4-(4-hydroxybutoxy)phenoxy]butan-1-ol
770 mg (0.98 mmol) 4-(4-{3-[(4-{[4-(dodecyloxy)phenyl]carbonyloxy}phenyl)carbonyloxy]-phenoxycarbonyl}phenoxycarbonyl)benzoic acid **i70**
220 mg (1.08 mmol) DCC
10 mg DMAP
60 ml dichloromethane
Purification: column chromatography, eluent: $CHCl_3$/EtOAc (10/0.2) and further recrystallisation from $CHCl_3/CH_3CN$ (10/0.2)
Yield: 0.58 mg (66 %), colorless solid
Transition temp.: Cr 162 SmC_aP_{AF} 189 I
^{1}H-NMR: ($CDCl_3$, J/Hz, 400 MHz) δ 8.31 (s, 3H, Ar-H), 8.30 – 8.23 (m, 10H, Ar-H), 8.18 – 8.15 (m, 2H, Ar-H), 8.13 (d, J = 8.9 Hz, 4H, Ar-H), 7.51 – 7.45 (m, 2H, Ar-H), 7.42 – 7.33 (m, 8H, Ar-H), 7.21 – 7.12 (m, 8H, Ar-H), 6.99 – 6.92 (m, 6H, Ar-H), 6.82 (s, 1H, Ar-H), 4.49 – 4.41 (m, 4H, OCH_2), 4.09 – 4.01 (m, 8H, OCH_2), 2.06 – 1.90 (m, 8H, $OCH_2C\mathbf{H}_2$), 1.85 – 1.77 (m, 4H, $OCH_2C\mathbf{H}_2$), 1.51 – 1.42 (m, 4H, CH_2), 1.40 – 1.22 (m, 32H), 0.87 (t, J = 6.8 Hz, 6H, CH_3).
^{13}C-NMR: ($CDCl_3$, 100 MHz) δ 164.20, 164.00, 163.84, 163.78, 160.31, 155.47, 154.95, 151.42, 151.34, 132.41, 132.37, 131.91, 131.80, 130.28, 130.20, 129.85, 129.75, 126.59, 122.30, 122.10, 121.92, 119.20, 115.76, 115.21, 114.43, 96.53, 68.45, 65.31, 31.98, 29.71, 29.69, 29.64, 29.61, 29.42, 29.16, 26.05, 22.75, 14.17.
EA: calculated: C: 72.39 %, H: 6.19 %; found: C: 72.32 %, H: 6.23 %

1-(4-{4-[4-(4-{[4-(4-{3-[(4-{[4-(Dodecyloxy)phenyl]carbonyloxy}phenyl)carbonyloxy]-phenoxycarbonyl}phenoxycarbonyl)phenyl]carbonyloxy}butoxy)phenyl]phenoxy}butyl) 4-(4-{3-[(4-{[4-(dodecyloxy)phenyl]carbonyloxy}phenyl)carbonyloxy]phenoxycarbonyl}phenyl)-benzene-1,4-dicarboxylate **37b** (*m* = 4, p = 12)

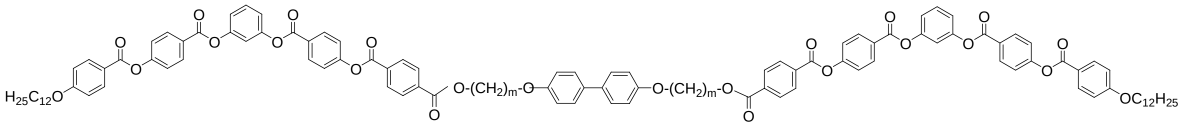

trimers 37b and 37c
37b: *m* = 4
37c: *m* = 6

Formula: $C_{114}H_{114}O_{24}$, M = 1868.17 g/mol
Synthesis: according to the general procedure 10.3.3
Reagents: 120 mg (0.49 mmol) 4-{4-[4-(4-hydroxybutoxy)phenyl]phenoxy}butan-1-ol **(*m* = 4)**
770 mg (0.98 mmol) 4-(4-{3-[(4-{[4-(dodecyloxy)phenyl]carbonyloxy}phenyl)carbonyloxy]-phenoxycarbonyl}phenoxycarbonyl)benzoic acid **i70**
220 mg (1.08 mmol) DCC
10 mg DMAP
60 ml dichloromethane
Purification: column chromatography, eluent: $CHCl_3$/EtOAc (10/0.2) and further recrystallisation from $CHCl_3/CH_3CN$ (10/0.2)
Yield: 670 mg (73 %), colorless solid
Transition temp.: Cr 153 SmC_aP_{AF} 191 I
^{1}H-NMR: ($CDCl_3$, J/Hz, 400 MHz)) δ 8.28 (d, J = 8.8 Hz, 8H, Ar-H), 8.23 (d, J = 8.6 Hz, 8H, Ar-H), 8.18 – 8.10 (m, 6H, Ar-H), 7.53 – 7.41 (m, 4H, Ar-H), 7.36 (dd, J = 8.6, 4.0 Hz, 8H, Ar-H), 7.23 – 7.14 (m, 6H, Ar-H), 7.01 – 6.89 (m, 8H, Ar-H), 4.45 (t, J = 5.9 Hz, 4H, OCH_2), 4.10 – 4.00 (m, 8H, OCH_2), 2.08 – 1.94 (m, 8H, $OCH_2C\mathbf{H}_2$), 1.87 – 1.77 (m, 4H, $OCH_2C\mathbf{H}_2$), 1.52 – 1.41 (m, 4H, CH_2), 1.41 – 1.23 (m, 32H, CH_2), 0.87 (t, J = 6.7 Hz, 6H, CH_3).
^{13}C-NMR: ($CDCl_3$, 100 MHz) δ 165.49, 163.86, 163.79, 154.95, 151.42, 151.34, 146.42, 132.38, 131.91, 131.80, 130.16, 129.86, 129.74, 127.67, 122.11, 121.93, 119.31, 115.76, 114.77, 114.43, 68.45, 67.35, 65.36, 31.98, 29.71, 29.65, 29.61, 29.42, 29.16, 26.15, 26.05, 25.60, 22.75, 14.17.

EA: calculated: C: 73.29 %, H: 6.15 %; found: C: 73.16 %, H: 6.32 %

1-[6-(4-{4-[(6-{[4-(4-{3-[(4-{[4-(Dodecyloxy)phenyl]carbonyloxy}phenyl)carbonyloxy]-phenoxycarbonyl}phenoxycarbonyl)phenyl]carbonyloxy}hexyl)oxy]phenyl}phenoxy)hexyl] 4-(4-{3-[(4-{[4-(dodecyloxy)phenyl]carbonyloxy}phenyl)carbonyloxy]phenoxycarbonyl}phenyl) benzene-1,4-dicarboxylate **37c** (*m* = 6, p = 12)

Formula:	$C_{128}H_{142}O_{24}$, M = 2064.54 g/mol
Synthesis:	according to the general procedure 10.3.3
Reagents:	250 mg (0.47 mmol) 6-(4-{4-[(6-hydroxyhexyl)oxy]phenyl}phenoxy)hexan-1-ol **(*m* = 6)** 740 mg (0.94 mmol) 4-(4-{3-[(4-{[4-(dodecyloxy)phenyl]carbonyloxy}phenyl)carbonyloxy]-phenoxycarbonyl}phenoxycarbonyl)benzoic acid **i70** 210 mg (1.03 mmol) DCC 10 mg DMAP 60 ml dichloromethane
Purification:	column chromatography, eluent: $CHCl_3$/EtOAc (10/0.2) and further recrystallisation from $CHCl_3$/CH_3CN (10/0.2)
Yield:	710 mg (73 %), colorless solid
Transition temp.:	Cr 158 (M_7 153) I
^{1}H-NMR:	($CDCl_3$, *J*/Hz, 400 MHz) δ 8.27 (t, *J* = 8.5 Hz, 12H, Ar-H), 8.17 (d, *J* = 8.4 Hz, 4H, Ar-H), 8.13 (d, *J* = 8.8 Hz, 4H, Ar-H), 7.48 (t, *J* = 8.1 Hz, 2H, Ar-H), 7.43 (d, *J* = 8.7 Hz, 4H, Ar-H), 7.41 – 7.34 (m, 8H, Ar-H), 7.21 – 7.15 (m, 6H, Ar-H), 6.97 (d, *J* = 8.9 Hz, 4H, Ar-H), 6.91 (d, *J* = 8.7 Hz, 4H, Ar-H), 4.35 (t, *J* = 6.7 Hz, 4H, OCH_2), 4.04 (t, *J* = 6.5 Hz, 4H, OCH_2), 3.96 (t, *J* = 6.5 Hz, 4H, OCH_2), 1.86 – 1.74 (m, 12H, $OCH_2C\mathbf{H}_2$), 1.51 – 1.41 (m, 12H, CH_2), 1.40 – 1.22 (m, 54H, CH_2), 0.87 (t, *J* = 6.8 Hz, 6H, CH_3).
^{13}C-NMR:	($CDCl_3$, 100 MHz) 165.57, 164.22, 164.01, 163.87, 155.51, 154.99, 151.38, 151.36, 147.16, 135.25, 133.35, 132.66, 132.38, 131.92, 131.80, 130.45, 130.17, 129.84, 129.74, 127.61, 127.15, 126.61, 122.10, 121.92, 119.19, 115.76, 114.77, 114.45, 68.44, 68.13, 65.77, 31.94, 29.66, 29.61, 29.57, 29.52, 29.37, 29.28, 29.13, 28.71, 26.11, 26.01, 22.71, 14.12.
EA:	calculated: C: 74.47 %, H: 6.93 %; found: C: 74.40 %, H: 6.83 %

Compounds 38

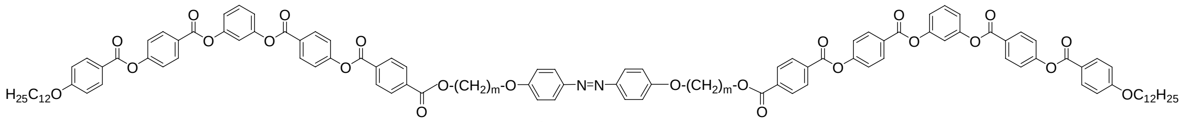

trimer series 38

38a: *m* = 2; 38b: *m* = 4

38c: *m* = 5; 38d: *m* = 6

1-[2-(4-{2-[4-(2-{[4-(4-{3-[(4-{[4-(Dodecyloxy)phenyl]carbonyloxy}phenyl)carbonyloxy]-phenoxycarbonyl}phenoxycarbonyl)phenyl]carbonyloxy}ethoxy)phenyl]diazen-1-yl}-phenoxy)ethyl] 4-(4-{3-[(4-{[4-(dodecyloxy)phenyl]carbonyloxy}phenyl)carbonyloxy]-phenoxycarbonyl}phenyl)benzene-1,4-dicarboxylate **38a** (*m* = 2, p = 12)

Formula:	$C_{110}H_{106}N_2O_{24}$, M = 1840.07 g/mol
Synthesis:	according to the general procedure 10.3.3
Reagents:	100 mg (0.35 mmol) 2-(4-{2-[4-(2-hydroxyethoxy)phenyl]diazen-1-yl}phenoxy)ethan-1-ol **(*m* = 2)** 550 mg (0.70 mmol) 4-(4-{3-[(4-{[4-(dodecyloxy)phenyl]carbonyloxy}phenyl)carbonyloxy]-phenoxycarbonyl}phenoxycarbonyl)benzoic acid **i70** 160 mg (0.77 mmol) DCC 10 mg DMAP

60 ml dichloromethane

Purification: column chromatography, eluent: $CHCl_3$/EtOAc (10/0.5) and further recrystallisation from $CHCl_3$/CH_3CN (10/0.2)

Yield: 480 mg (75 %), colorless solid

Transition temp.: Cr 216 (M_8 203) I

^{1}H-NMR: ($CDCl_3$, *J*/Hz, 400 MHz) δ 8.32 – 8.22 (m, 12H, Ar-H), 8.19 (d, *J* = 8.3 Hz, 4H, Ar-H), 8.13 (d, *J* = 8.8 Hz, 4H, Ar-H), 7.88 (d, *J* = 8.8 Hz, 4H, Ar-H), 7.48 (t, *J* = 8.1 Hz, 1H, Ar-H), 7.36 (t, *J* = 8.3 Hz, 8H, Ar-H), 7.21 – 7.14 (m, 7H, Ar-H), 7.04 (d, *J* = 8.9 Hz, 4H, Ar-H), 6.96 (d, *J* = 8.8 Hz, 4H, Ar-H), 4.79 – 4.71 (m, 4H, OCH_2), 4.45 – 4.38 (m, 4H, OCH_2), 4.03 (t, *J* = 6.5 Hz, 4H, OCH_2), 1.86 – 1.76 (m, 4H, $OCH_2C\mathbf{H}_2$), 1.51 – 1.41 (m, 6H, CH_2), 1.40 – 1.20 (m, 30H, CH_2), 0.87 (t, *J* = 6.7 Hz, 6H, CH_3).

^{13}C-NMR: ($CDCl_3$, 100 MHz) δ 165.38, 164.37, 164.17, 164.02, 163.75, 163.59, 160.42, 155.44, 154.90, 151.40, 151.31, 134.45, 132.37, 131.91, 131.79, 130.21, 129.94, 129.85, 127.14, 126.59, 124.44, 122.72, 122.11, 121.91, 120.96, 119.31, 115.76, 114.93, 114.44, 68.49, 66.26, 63.87, 32.05, 31.02, 29.79, 29.77, 29.72, 29.69, 29.49, 29.48, 29.24, 26.13, 22.83, 14.26.

EA: calculated: C: 71.80 %, H: 5.81 %, N: 1.52 %; found: C: 71.77 %, H: 5.84 %, N: 1.41 %

1-[4-(4-{2-[4-(4-{[4-(4-{3-[(4-{[4-(Dodecyloxy)phenyl]carbonyloxy}phenyl)carbonyloxy]-phenoxycarbonyl}phenoxycarbonyl)phenyl]carbonyloxy}butoxy)phenyl]diazen-1-yl}-phenoxy)butyl] 4-(4-{3-[(4-{[4-(dodecyloxy)phenyl]carbonyloxy}phenyl)carbonyloxy]-phenoxycarbonyl}phenyl)benzene-1,4-dicarboxylate **38b** (*m* = 4, p = 12)

Formula: $C_{114}H_{114}N_2O_{24}$, M = 1896.18 g/mol

Synthesis: according to the general procedure 10.3.3

Reagents: 100 mg (0.35 mmol) 4-(4-{2-[4-(4-hydroxybutoxy)phenyl]diazen-1-yl}phenoxy)butan-1-ol **(*m* = 4)**

550 mg (0.70 mmol) 4-(4-{3-[(4-{[4-(dodecyloxy)phenyl]carbonyloxy}phenyl)carbonyloxy]-phenoxycarbonyl}phenoxycarbonyl)benzoic acid **i70**

160 mg (0.77 mmol) DCC

10 mg DMAP

60 ml dichloromethane

Purification: column chromatography, eluent: $CHCl_3$/EtOAc (10/0.5) and further recrystallisation from $CHCl_3$/CH_3CN (10/0.2)

Yield: 460 mg (69 %), colorless solid

Transition temp.: Cr 185 (M_9 181) I

^{1}H-NMR: ($CDCl_3$, *J*/Hz, 400 MHz) δ 8.28 – 8.21 (m, 12H, Ar-H), 8.16 – 8.11 (m, 8H, Ar-H), 7.83 (d, *J* = 9.0 Hz, 4H, Ar-H), 7.48 (t, *J* = 8.2 Hz, 1H, Ar-H), 7.35 (d, *J* = 8.5 Hz, 8H, Ar-H), 7.21 – 7.15 (m, 7H, Ar-H), 6.96 (d, *J* = 9.1 Hz, 8H, Ar-H), 4.46 (t, *J* = 6.2 Hz, 4H, OCH_2), 4.12 (t, *J* = 5.5 Hz, 4H, OCH_2), 4.03 (t, *J* = 6.6 Hz, 4H, OCH_2), 2.05 – 1.94 (m, 8H, $OCH_2C\mathbf{H}_2$), 1.85 – 1.76 (m, 4H, $OCH_2C\mathbf{H}_2$), 1.49 – 1.41 (m, 4H, CH_2), 1.39 – 1.22 (m, 32H), 0.87 (t, *J* = 6.9 Hz, 6H, CH_3).

^{13}C-NMR: ($CDCl_3$, 100 MHz) δ 165.45, 164.17, 163.97, 163.83, 163.76, 163.63, 160.78, 155.45, 154.91, 151.40, 151.33, 134.93, 132.72, 132.37, 131.89, 131.80, 130.17, 129.85, 129.73, 127.08, 126.59, 124.33, 122.72, 122.11, 121.92, 120.95, 119.31, 115.77, 114.67, 114.44, 68.50, 67.60, 65.35, 32.05, 31.02, 29.79, 29.77, 29.72, 29.69, 29.48, 29.24, 26.13, 25.62, 22.84, 14.27.

EA: calculated: C: 72.21 %, H: 6.06 %, N: 1.48 %; found: C: 72.17 %, H: 6.17 %, N: 1.30 %

1-{6-[4-(2-{4-[(6-{[4-(4-{3-[(4-{[4-(Dodecyloxy)phenyl]carbonyloxy}phenyl)carbonyloxy]-phenoxycarbonyl}phenoxycarbonyl)phenyl]carbonyloxy}hexyl)oxy]phenyl}diazen-1-yl)-phenoxy]hexyl} 4-(4-{3-[(4-{[4-(dodecyloxy)phenyl]carbonyloxy}phenyl)carbonyloxy]-phenoxycarbonyl}phenyl)benzene-1,4-dicarboxylate **38c** (*m* = 6, p = 12)

Formula: $C_{116}H_{118}N_2O_{24}$, M = 1924.23 g/mol

Synthesis: according to the general procedure 10.3.3

Reagents: 140 mg (0.35 mmol) 6-[4-(2-{4-[(6-hydroxyhexyl)oxy]phenyl}diazen-1-yl)phenoxy]hexan-1-ol **(*m* = 6)**
550 mg (0.70 mmol) 4-(4-{3-[(4-{[4-(dodecyloxy)phenyl]carbonyloxy}phenyl)carbonyloxy]-phenoxycarbonyl}phenoxycarbonyl)benzoic acid **i70**
160 mg (0.77 mmol) DCC
10 mg DMAP
60 ml dichloromethane

Purification: column chromatography, eluent: CHCl$_3$/EtOAc (10/0.5) and further recrystallisation from CHCl$_3$/CH$_3$CN (10/0.2)

Yield: 490 mg (73 %), colorless solid

Transition temp.: Cr 187 (SmC’$_x$ 162 SmC$_x$ 176) I

^{1}H-NMR: (CDCl$_3$, *J*/Hz, 400 MHz) δ 8.30 – 8.23 (m, 12H, Ar-H), 8.16 (d, *J* = 8.5 Hz, 4H, Ar-H), 8.13 (d, *J* = 8.9 Hz, 4H, Ar-H), 7.83 (d, *J* = 8.9 Hz, 4H, Ar-H), 7.48 (t, *J* = 8.1 Hz, 1H, Ar-H), 7.40 – 7.33 (m, 8H, Ar-H), 7.21 – 7.15 (m, 7H, Ar-H), 6.96 (d, *J* = 8.9 Hz, 8H, Ar-H), 4.41 (t, *J* = 6.6 Hz, 4H, OCH$_2$), 4.09 – 4.01 (m, 8H, OCH$_2$), 1.95 – 1.85 (m, *J* = 14.8 Hz, 8H, OCH$_2$C**H**$_2$), 1.85 – 1.77 (m, 4H, OCH$_2$C**H**$_2$), 1.50 – 1.41 (m, 4H, CH$_2$), 1.38 – 1.21 (m, 36H, CH$_2$), 0.87 (t, *J* = 6.9 Hz, 6H, CH$_3$).

^{13}C-NMR: (CDCl$_3$, 100 MHz) δ 165.49, 164.17, 163.97, 163.82, 163.76, 163.66, 160.91, 155.45, 154.93, 151.39, 151.32, 147.00, 135.05, 132.70, 132.37, 131.91, 131.79, 130.18, 129.85, 129.74, 127.11, 126.59, 124.30, 122.70, 122.11, 121.92, 120.95, 119.20, 115.77, 114.65, 114.44, 68.49, 67.97, 66.02, 65.51, 32.05, 31.02, 29.79, 29.77, 29.72, 29.69, 29.48, 29.24, 29.01, 28.60, 26.13, 22.84, 14.27.

EA: calculated: C: 72.41 %, H: 6.18 %, N: 1.46 %; found: C: 72.21 %, H: 6.15 %, N: 1.38 %

1-{8-[4-(2-{4-[(8-{[4-(4-{3-[(4-{[4-(Dodecyloxy)phenyl]carbonyloxy}phenyl)carbonyloxy]-phenoxycarbonyl}phenoxycarbonyl)phenyl]carbonyloxy}octyl)oxy]phenyl}diazen-1-yl)-phenoxy]octyl} 4-(4-{3-[(4-{[4-(dodecyloxy)phenyl]carbonyloxy}phenyl)carbonyloxy]-phenoxycarbonyl}phenyl)benzene-1,4-dicarboxylate **38d** (*m* = 8, p = 12)

Formula: C$_{118}$H$_{122}$N$_2$O$_{24}$, M = 1952.29 g/mol

Synthesis: according to the general procedure 10.3.3

Reagents: 210 mg (0.51 mmol) 8-[4-(2-{4-[(8-hydroxyoctyl)oxy]phenyl}diazen-1-yl)phenoxy]octan-1-ol **(*m* = 8)**
800 mg (1.02 mmol) 4-(4-{3-[(4-{[4-(dodecyloxy)phenyl]carbonyloxy}phenyl)carbonyloxy]-phenoxycarbonyl}phenoxycarbonyl)benzoic acid **i70**
230 mg (1.12 mmol) DCC
10 mg DMAP
60 ml dichloromethane

Purification: column chromatography, eluent: CHCl$_3$/EtOAc (10/0.5) and further recrystallisation from CHCl$_3$/CH$_3$CN (10/0.2)

Yield: 620 mg (62 %), colorless solid

Transition temp.: Cr 162 (SmC$_a$P$_{AF}$ 157) I

^{1}H-NMR: (CDCl$_3$, *J*/Hz, 400 MHz) δ 8.28 (d, *J* = 9.0 Hz, 6H, Ar-H), 8.23 (d, *J* = 8.6 Hz, 6H, Ar-H), 8.17 – 8.11 (m, 8H, Ar-H), 7.48 (t, *J* = 8.1 Hz, 1H, Ar-H), 7.44 (d, *J* = 8.7 Hz, 4H, Ar-H), 7.39 – 7.33 (m, 8H, Ar-H), 7.21 – 7.15 (m, 7H, Ar-H), 6.97 (d, *J* = 8.9 Hz, 4H, Ar-H), 6.92 (d, *J* = 8.8 Hz, 4H, Ar-H), 4.45 (t, *J* = 5.9 Hz, 4H, OCH$_2$), 4.09 – 4.01 (m, 8H, OCH$_2$), 2.07 – 1.94 (m, 8H, OCH$_2$C**H**$_2$), 1.85 – 1.77 (m, 4H, OCH$_2$C**H**$_2$), 1.51 – 1.42 (m, 4H, CH$_2$), 1.39 – 1.22 (m, 40H, CH$_2$), 0.87 (t, *J* = 6.8 Hz, 6H, CH$_3$).

^{13}C-NMR: (CDCl$_3$, 100 MHz) δ 165.50, 164.16, 163.96, 163.76, 163.65, 160.98, 155.45, 154.93, 151.41, 151.33, 146.97, 135.12, 132.36, 131.89, 131.79, 130.17, 129.83, 129.72, 127.11, 126.60, 124.28, 122.10, 121.91, 119.20, 115.76, 114.65, 114.45, 68.50, 68.15, 65.62, 32.05, 29.79, 29.77, 29.72, 29.69, 29.48, 29.24, 28.76, 26.13, 25.97, 25.93, 22.83, 14.25.

EA: calculated: C: 72.60 %, H: 6.30 %, N: 1.43 %; found: C: 72.41 %, H: 6.47 %, N: 1.27 %

Intermediate compounds

4-(Dodecyloxy)benzoic acid **i1(12)**

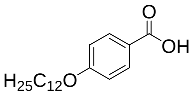

Formula: $C_{19}H_{30}O_3$, M = 306.44 g/mol
Synthesis: according to the general procedure 11.3.1 methode C
Reagents: 12.90 g (93.40 mmol) 4-hydroxybenzoic acid
34.95 g (140.25 mmol) 1-bromododecane
12.18 g (186.80 mmol) KOH
40 ml ethanol
20 ml water
Purification: recrystallisation from EtOH/CH_3COOH (5/1)
Yield: 22.04 g (77 %), colorless solid
Transition temp.: Cr 94 [61.2] SmC 132 [4.0] N 138 [4.6] I
^{1}H-NMR: ($CDCl_3$, *J*/Hz, 400 MHz) δ 8.02 (d, *J* = 9.0 Hz, 2H, Ar-H), 6.91 (d, *J* = 9.0 Hz, 2H, Ar-H), 4.00 (t, *J* = 6.6 Hz, 2H, OCH_2), 1.83 – 1.74 (m, 2H, $OCH_2C\mathbf{H}_2$), 1.49 – 1.39 (m, 2H, CH_2), 1.38 – 1.22 (m, 16H, CH_2), 0.86 (t, *J* = 6.9 Hz, 3H, CH_3).

4-[(Benzyloxy)carbonyl]phenyl 4-(dodecyloxy)benzoate **i2(12)**

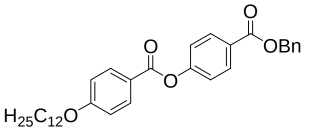

Formula: $C_{33}H_{40}O_5$, M = 516.67 g/mol
Synthesis: according to the general procedure 11.3.3
Reagents: 7.00 g (22.84 mmol) 4-(dodecyloxy)benzoic acid **i1(12)**
5.21 g (22.84 mmol) benzyl 4-hydroxybenzoate
5.19 g (25.16 mmol) DCC
0.05 g DMAP
50 ml dichloromethane
Purification: recrystallisation from EtOAc/EtOH (10/0.1)
Yield: 10.05 g (85 %), colorless solid
Transition temp.: Cr 64 [31.6] Iso
^{1}H-NMR: ($CDCl_3$, *J*/Hz, 400 MHz) δ 8.16 – 8.09 (m, 4H, Ar-H), 7.46 – 7.41 (m, 2H, Ar-H), 7.41 – 7.31 (m, 3H, Ar-H), 7.30 – 7.23 (m, 2H, Ar-H), 6.95 (d, *J* = 8.8 Hz, 2H, Ar-H), 5.36 (s, 2H, CH_2Ph), 4.03 (t, *J* = 6.6 Hz, 2H, OCH_2), 1.86 – 1.76 (m, 2H, $OCH_2C\mathbf{H}_2$), 1.50 – 1.42 (m, 2H, CH_2), 1.26 (s, 16H, CH_2), 0.87 (t, *J* = 6.8 Hz, 3H, CH_3).

4-{[4-(Dodecyloxy)phenyl]carbonyloxy}benzoic acid **i3(12)**

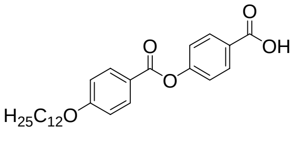

Formula: $C_{26}H_{34}O_5$, M = 426.55 g/mol
Synthesis: according to the general procedure 11.3.6 methode A
Reagents: 10.00 g (19.35 mmol) 4-[(benzyloxy)carbonyl]phenyl 4-(dodecyloxy)benzoate **i2(12)**
1 g Pd/C
100 ml ethyl acetate

Purification: recrystallisation from CH_3COOH
Yield: 7.30 g (88 %), colorless solid
Transition temp.: Cr 120 [27.1] SmC 211 [4.5] N 223 [4.6] I
^{1}H-NMR: ($CDCl_3$, *J*/Hz, 400 MHz) δ 8.17 (d, *J* = 8.6 Hz, 2H, Ar-H), 8.12 (d, *J* = 8.8 Hz, 2H, Ar-H), 7.32 (d, *J* = 8.6 Hz, 2H, Ar-H), 6.96 (d, *J* = 8.9 Hz, 2H, Ar-H), 4.04 (t, *J* = 6.5 Hz, 2H, OCH_2), 1.86 – 1.76 (m, 2H, $OCH_2\mathbf{CH_2}$), 1.51 – 1.42 (m, 2H, CH_2), 1.26 (s, 16H, CH_2), 0.87 (t, *J* = 6.8 Hz, 3H, CH_3).

3-(Benzyloxy)phenyl benzoate **i4**

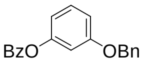

Formula: $C_{21}H_{18}O_3$, M = 318.37 g/mol
Synthesis: according to the general procedure 11.3.1, methode B
Reagents: 20.00 g (102.80 mmol) 3-(hydroxy)phenyl benzoate
13 ml (107.80 mmol) benzyl bromide
4.32 g (180.40 mmol) sodium hydrate (60% dispersion in mineral oil)
150 ml dimethylformamide
Purification: The crude compound **i4** was then used into the next reaction without further purification.
Yield: -
Transition temp.: brown oil
^{1}H-NMR: -

3-(Benzyloxy)phenol **i5**

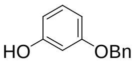

Formula: $C_{13}H_{12}O_2$, M = 200.23 g/mol
Synthesis: according to the general procedure 11.3.7
Reagents: ~19.00 g (102.80 mmol) crude 3-(benzyloxy)phenyl benzoate **i4**
16.00 g (400.00 mmol) sodium hydroxide
100 ml methanol
150 ml water
Purification: column chromatography, eluent: *n*-heptane/EtOAc (1/1)
Yield: 15.40 g (74.83 %), pinkish low-melting crystals
Transition temp.: Cr 54 [4.0] I
^{1}H-NMR: ($CDCl_3$, *J*/Hz, 400 MHz) δ 7.43 – 7.28 (m, 5H, Ar-H), 7.11 (t, *J* = 8.2 Hz, 1H, Ar-H),), 6.57 – 6.53 (m, 1H, Ar-H), 6.46 (t, *J* = 2.3 Hz, 1H, Ar-H),), 6.44 – 6.38 (m, 1H, Ar-H),), 5.02 (s, 2H, CH_2Ph).

4-[3-(Benzyloxy)phenoxycarbonyl]phenyl 4-(dodecyloxy)benzoate **i6(12)**

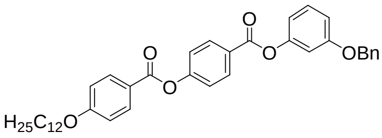

Formula: $C_{39}H_{44}O_6$, M = 608.76 g/mol
Synthesis: according to the general procedure 11.3.3
Reagents: 2.00 g (4.66 mmol) 3-(benzyloxy)phenol **i5**
0.94 g (4.68 mmol) 4-{[4-(dodecyloxy)phenyl]carbonyloxy}benzoic acid **i3(12)**

	1.01 g (4.92 mmol) DCC
	0.05 g DMAP
	40 ml methylene chlorid
Purification:	recrystallisation from EtOAc/EtOH (10/0.1)
Yield:	2.38 g (84 %), colorless solid
Transition temp.:	Cr 100 [58.7] I
^{1}H-NMR:	($CDCl_3$, *J*/Hz, 400 MHz) δ 8.25 (d, *J* = 8.8 Hz, 2H, Ar-H), 8.14 (d, *J* = 8.9 Hz, 2H, Ar-H), 7.45 – 7.29 (m, 8H, Ar-H), 6.97 (d, *J* = 8.9 Hz, 2H, Ar-H), 6.91 – 6.85 (m, 2H, Ar-H), 6.85 – 6.81 (m, 1H, Ar-H), 5.06 (s, 2H, CH_2Ph), 4.04 (t, *J* = 6.6 Hz, 2H, OCH_2), 1.86 – 1.77 (m, 2H, $OCH_2C\mathbf{H}_2$), 1.51 – 1.42 (m, 2H, CH_2), 1.40 – 1.22 (m, 16H, CH_2), 0.87 (t, *J* = 6.9 Hz, 3H, CH_3).

4-(3-Hydroxyphenoxycarbonyl)phenyl 4-(dodecyloxy)benzoate **i7(12)**

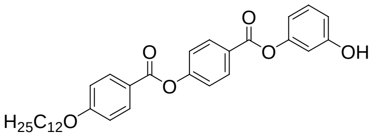

Formula:	$C_{32}H_{38}O_6$, M = 518.66 g/mol
Synthesis:	according to the general procedure 11.3.6 methode A
Reagents:	2.10 g (3.44 mmol) 4-[3-(benzyloxy)phenoxycarbonyl]phenyl 4-(dodecyloxy)benzoate **i6(12)**
	0.21 g Pd/C
	45 ml ethyl acetate
Purification:	recrystallisation from DMF/EtOH
Yield:	1.48 g (83 %), colorless solid
Transition temp.:	Cr 127 [40.7] (N 117 [1.0]) I
^{1}H-NMR:	($CDCl_3$, *J*/Hz, 400 MHz) δ 8.24 (d, *J* = 8.8 Hz, 2H, Ar-H), 8.13 (d, *J* = 8.9 Hz, 2H, Ar-H), 7.34 (d, *J* = 8.8 Hz, 2H, Ar-H), 7.27 – 7.20 (m, 1H, Ar-H), 6.97 (d, *J* = 8.9 Hz, 2H, Ar-H), 6.78 – 6.73 (m, 1H, Ar-H), 6.71 – 6.66 (m, 2H, Ar-H), 4.03 (t, *J* = 6.6 Hz, 2H, OCH_2), 1.85 – 1.76 (m, 2H, $OCH_2C\mathbf{H}_2$), 1.51 – 1.41 (m, 2H, CH_2), 1.40 – 1.20 (m, 16H, CH_2), 0.87 (t, *J* = 6.9 Hz, 3H, CH_3).

4-(3-{[4-(Benzyloxy)phenyl]carbonyloxy}phenoxycarbonyl)phenyl 4-(dodecyloxy)benzoate **i8(12)**

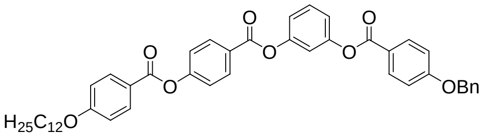

Formula:	$C_{46}H_{48}O_8$, M = 728.87 g/mol
Synthesis:	according to the general procedure 11.3.3
Reagents:	1.40 g (2.70 mmol) 4-(3-hydroxyphenoxycarbonyl)phenyl 4-(dodecyloxy)benzoate **i7(12)**
	0.62 g (2.70 mmol) 4-(benzyloxy)benzoic acid
	0.67 g (3.24 mmol) DCC
	0.03 g DMAP
	40 ml dichloromethane
Purification:	recrystallisation from EtOAc/EtOH (10/0.1)
Yield:	1.56 g (79 %), colorless solid
Transition temp.:	Cr 123 [46.4] I
^{1}H-NMR:	($CDCl_3$, *J*/Hz, 400 MHz) δ 8.25 (d, *J* = 8.8 Hz, 2H, Ar-H), 8.13 (d, *J* = 8.9 Hz, 4H, Ar-H), 7.50 – 7.31 (m, 9H, Ar-H), 7.18 – 7.11 (m, 2H, Ar-H), 7.05 (d, *J* = 9.0 Hz, 2H, Ar-H), 6.97 (d, *J* = 8.9 Hz, 2H, Ar-H), 5.15 (s, 2H, CH_2Ph), 4.04 (t, *J* = 6.5 Hz, 2H, OCH_2), 1.87 – 1.76 (m, 2H,

$OCH_2C\mathbf{H}_2$), 1.51 – 1.41 (m, 2H, CH_2), 1.40 – 1.19 (m, 16H, CH_2), 0.87 (t, *J* = 6.8 Hz, 3H, CH_3).

4-{3-[(4-Hydroxyphenyl)carbonyloxy]phenoxycarbonyl}phenyl 4-(dodecyloxy)benzoate **i9(12)**

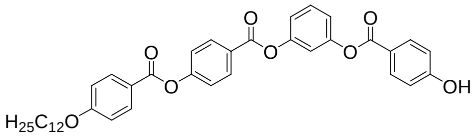

Formula: $C_{39}H_{42}O_8$, M = 638.75 g/mol

Synthesis: according to the general procedure 11.3.6 methode A

Reagents: 1.56 g (2.14 mmol) 4-(3-{[4-(benzyloxy)phenyl]carbonyloxy}phenoxycarbonyl)phenyl 4-(dodecyloxy)benzoate **i8(12)**
0.16 g Pd/C
30 ml ethyl acetate

Purification: recrystallisation from EtOAc/EtOH (10/0.1)

Yield: 0.98 g (72 %), colorless solid

Transition temp.: Cr 187 [67.3] I

^{1}H-NMR: ($CDCl_3$, *J*/Hz, 400 MHz) δ 8.25 (d, *J* = 8.4 Hz, 2H, Ar-H), 8.14 (d, *J* = 8.6 Hz, 2H, Ar-H), 8.10 (d, *J* = 8.4 Hz, 2H, Ar-H), 7.45 (t, *J* = 8.2 Hz, 1H, Ar-H), 7.36 (d, *J* = 8.4 Hz, 2H, Ar-H), 7.19 – 7.13 (m, 3H, Ar-H), 6.97 (d, *J* = 8.6 Hz, 2H, Ar-H), 6.90 (d, *J* = 8.5 Hz, 2H, Ar-H), 4.05 (t, *J* = 6.7 Hz, 2H, OCH_2), 1.86 – 1.78 (m, 2H, $OCH_2C\mathbf{H}_2$), 1.51 – 1.43 (m, 2H, CH_2), 1.40 – 1.24 (m, 16H, CH_2), 0.88 (t, *J* = 6.8 Hz, 3H, CH_3).

4-(Benzyloxy)phenyl 4-(hexyloxy)benzoate **i10 (6)**

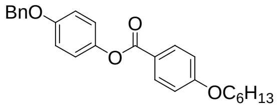

Formula: $C_{26}H_{28}O_4$, M = 404.50 g/mol

Synthesis: according to the general procedure 11.3.3

Reagents: 12.94 g (58.21 mmol) 4-(hexyloxy)benzoic acid
11.66 g (58.21 mmol) 4-(benzyloxy)phenol
12.60 g (61.07 mmol) DCC
0.05 g DMAP
50 ml dichloromethane

Purification: recrystallisation from EtOAc

Yield: 20.01 g (85 %), colorless solid

Transition temp.: Cr 124 [49.4] (N 99 [1.5]) I

^{1}H-NMR: ($CDCl_3$, *J*/Hz, 400 MHz) δ 8.15 – 8.09 (m, 2H, Ar-H), 7.46 – 7.35 (m, 4H, Ar-H), 7.35 – 7.29 (m, 1H, Ar-H), 7.10 (d, *J* = 9.0 Hz, 2H, Ar-H), 6.99 (d, *J* = 9.0 Hz, 2H, Ar-H), 6.95 (d, *J* = 8.9 Hz, 2H, Ar-H), 5.06 (s, 2H, CH_2Ph), 4.03 (t, *J* = 6.6 Hz, 2H, OCH_2), 1.86 – 1.76 (m, 2H, $OCH_2C\mathbf{H}_2$), 1.52 – 1.43 (m, 2H, CH_2), 1.39 – 1.30 (m, 4H, CH_2), 0.91 (t, *J* = 6.9 Hz, 3H, CH_3).

4-Hydroxyphenyl 4-(hexyloxy)benzoate **i11(6)**

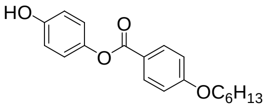

Formula: $C_{19}H_{22}O_4$, M = 314.38 g/mol
Synthesis: according to the general procedure 11.3.6 methode A
Reagents: 16.00 g (39.55 mmol) 4-(benzyloxy)phenyl 4-(hexyloxy)benzoate **i10(6)**
1.60 g Pd/C
300 ml THF
Purification: recrystallisation from EtOH
Yield: 11.15 g (90 %), colorless solid
Transition temp.: Cr 115 [26.9] I
^{1}H-NMR: ($CDCl_3$, *J*/Hz, 400 MHz) δ 8.11 (d, *J* = 8.9 Hz, 2H, Ar-H), 7.00 (d, *J* = 8.9 Hz, 2H, Ar-H), 6.95 (d, *J* = 8.9 Hz, 2H, Ar-H), 6.78 (d, *J* = 8.9 Hz, 2H, Ar-H), 4.03 (t, *J* = 6.6 Hz, 2H, OCH_2), 1.85 – 1.76 (m, 2H, $OCH_2C\mathbf{H}_2$), 1.51 – 1.42 (m, 2H, CH_2), 1.39 – 1.29 (m, 4H, CH_2), 0.90 (t, *J* = 7.0 Hz, 3H, CH_3).

4-[(6-Bromohexyl)oxy]phenyl 4-(hexyloxy)benzoate **i12(6,6)**

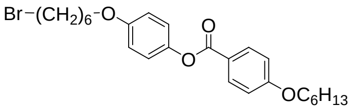

Formula: $C_{25}H_{33}BrO_4$, M = 477.43 g/mol
Synthesis: according to the general procedure 11.3.2
Reagents: 3.86 g (12.28 mmol) 4-hydroxyphenyl 4-(hexyloxy)benzoate **i11(6)**1eq
2.45 g (13.51 mmol) 6-bromohexan-1-ol 1eq
3.54 g (13.51 mmol) PPh_3
2.30 g (13.51 mmol) DEAD
150 ml tetrahydrofurane
Purification: column chromatography, eluent: $CHCl_3/CH_2Cl_2$ (1/1) and further recrystallisation from *n*-hexane
Yield: 3.73 g (64 %), colorless solid
Transition temp.: Cr 58 [38.8] N 82 [1.0] I
^{1}H-NMR: ($CDCl_3$, *J*/Hz, 400 MHz) δ 8.11 (d, *J* = 8.8 Hz, 2H, Ar-H), 7.08 (d, *J* = 8.9 Hz, 2H, Ar-H), 6.94 (d, *J* = 8.8 Hz, 2H, Ar-H), 6.89 (d, *J* = 8.9 Hz, 2H, Ar-H), 4.02 (t, *J* = 6.5 Hz, 2H, OCH_2), 3.95 (t, *J* = 6.4 Hz, 2H, OCH_2), 3.41 (t, *J* = 6.8 Hz, 2H, $BrCH_2$), 1.94 – 1.74 (m, 6H, $OCH_2C\mathbf{H}_2$, $BrCH_2C\mathbf{H}_2$), 1.56 – 1.38 (m, 6H, CH_2), 1.38 – 1.29 (m, 4H), 0.90 (t, *J* = 6.9 Hz, 3H, CH_3).

4-[(6-{4-[(Benzyloxy)carbonyl]phenoxy}hexyl)oxy]phenyl 4-(hexyloxy)benzoate **i13(6,6)**

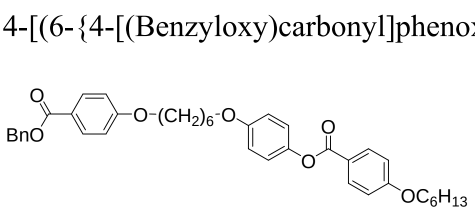

Formula: $C_{39}H_{44}O_7$, M = 624.76 g/mol
Synthesis: according to the general procedure 11.3.1 methode A
Reagents: 2.00 g (4.19 mmol) 4-[(6-bromohexyl)oxy]phenyl 4-(hexyloxy)benzoate **i12(6,6)**
0.79 g (3.49 mmol) benzyl 4-hydroxybenzoate
2.40 g (17.45 mmol) K_2CO_3

0.02 g (0.12 mmol) KI
100 ml butan-2-one

Purification: recrystallisation from EtOAc/EtOH (10/0.2)

Yield: 1.95 g (89 %), colorless solid

Transition temp.: Cr 102 [31.7] (SmA 76 [6.2] N 79 [2.8]) I

^{1}H-NMR: ($CDCl_3$, J/Hz, 400 MHz) δ 8.11 (d, J = 8.9 Hz, 2H, Ar-H), 8.00 (d, J = 8.9 Hz, 2H, Ar-H), 7.45 – 7.40 (m, 2H, Ar-H), 7.39 – 7.28 (m, 3H, Ar-H), 7.08 (d, J = 9.0 Hz, 2H, Ar-H), 6.94 (d, J = 8.9 Hz, 2H, Ar-H), 6.89 (dd, J = 9.0, 2.5 Hz, 4H, Ar-H), 5.32 (s, 2H, CH_2Ph), 4.01 (q, J = 6.4 Hz, 4H, OCH_2), 3.96 (t, J = 6.4 Hz, 2H, OCH_2), 1.87 – 1.77 (m, 6H, $OCH_2C\mathbf{H}_2$), 1.58 – 1.50 (m, 4H, CH_2), 1.50 – 1.42 (m, 2H, CH_2), 1.39 – 1.30 (m, 4H, CH_2), 0.90 (t, J = 7.1 Hz, 3H, CH_3).

4-{[6-(4-{[4-(Hexyloxy)phenyl]carbonyloxy}phenoxy)hexyl]oxy}benzoic acid **i14(6,6)**

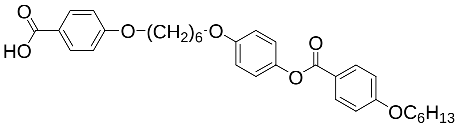

Formula: $C_{32}H_{38}O_7$, M = 534.64 g/mol

Synthesis: according to the general procedure 11.3.6 methode A

Reagents: 1.9 g (3.04 mmol) 4-[(6-{4-[(benzyloxy)carbonyl]phenoxy}hexyl)oxy]phenyl 4-(hexyloxy)-benzoate **i13(6,6)**
0.19 g Pd/C
40 ml ethyl acetate

Purification: recrystallisation from CH_3COOH

Yield: 1.24 g (77 %), colorless solid

Transition temp.: Cr 185 [38.4] N 205 [13.7] I

^{1}H-NMR: ($CDCl_3$, J/Hz, 400 MHz) δ 8.05 (d, J = 8.7 Hz, 2H, Ar-H), 7.97 (d, J = 8.7 Hz, 2H, Ar-H), 7.02 (d, J = 8.9 Hz, 2H, Ar-H), 6.88 (d, J = 8.8 Hz, 2H, Ar-H), 6.87 – 6.81 (m, 4H, Ar-H), 4.00 – 3.94 (m, 4H, OCH_2), 3.91 (t, J = 6.4 Hz, 2H), 1.82 – 1.70 (m, 6H, $OCH_2C\mathbf{H}_2$), 1.53 – 1.46 (m, 4H, CH_2), 1.45 – 1.37 (m, 2H, CH_2), 1.33 – 1.25 (m, 4H, CH_2), 0.85 (t, J = 6.9 Hz, 3H, CH_3).

4-[(6-Hydroxyhexyl)oxy]phenyl 4-(hexyloxy)benzoate **i15(6,6)**

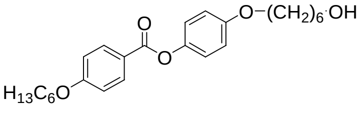

Formula: $C_{25}H_{34}O_5$, M = 414.53 g/mol

Synthesis: according to the general procedure 11.3.1 methode A

Reagents: 1.00 g (3.18 mmol) 4-hydroxyphenyl 4-(hexyloxy)benzoate **i11(6)**
0.69 g (3.81mmol) 6-bromohexan-1-ol
2.19 g (15.90 mmol) K_2CO_3
0.02 g (0.12 mmol) KI
50 ml dimethylformamide

Purification: column chromatography, eluent: $CHCl_3$/EtOAc (10/0.5 – 10/2) and further recrystallisation from EtOAc/PE (10/0.1)

Yield: 0.81 g (62 %), colorless solid

Transition temp.: Cr 84 [26.7] N 95 [1.6] I

^{1}H-NMR: ($CDCl_3$, J/Hz, 400 MHz) δ 8.10 (d, J = 9.0 Hz, 2H, Ar-H), 7.08 (d, J = 9.1 Hz, 2H, Ar-H), 6.94 (d, J = 9.0 Hz, 2H, Ar-H), 6.89 (d, J = 9.1 Hz, 2H, Ar-H), 4.02 (t, J = 6.6 Hz, 2H, OCH_2), 3.95 (t, J = 6.5 Hz, 2H, OCH_2), 3.65 (t, J = 6.5 Hz, 2H, $C\mathbf{H}_2OH$), 1.84 – 1.75 (m, 4H, $OCH_2C\mathbf{H}_2$), 1.64 – 1.56 (m, 2H, $HOCH_2C\mathbf{H}_2$), 1.53 – 1.40 (m, 6H, CH_2), 1.37 – 1.30 (m, 4H, CH_2), 0.90 (t, *J* = 7.1 Hz, 3H, CH_3).

4-({6-[(4-Formylphenyl)carbonyloxy]hexyl}oxy)phenyl 4-(hexyloxy)benzoate **i16(6,6)**

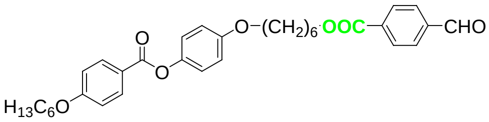

Formula:	$C_{33}H_{38}O_7$, M = 546.65 g/mol
Synthesis:	according to the general procedure 11.3.3
Reagents:	2.00 g (4.82 mmol) 4-[(6-hydroxyhexyl)oxy]phenyl 4-(hexyloxy)benzoate **i15(6,6)** 0.72 g (4.82 mmol) 4-formylbenzoic acid 1.09 g (5.30 mmol) DCC 0.05 g DMAP 50 ml dichloromethane
Purification:	recrystallisation from EtOH
Yield:	1.98 g (75 %), colorless solid
Transition temp.:	Cr 70 [45.5] I
^{1}H-NMR:	($CDCl_3$, *J*/Hz, 400 MHz) δ 10.08 (s, 1H, CHO), 8.18 (d, *J* = 8.2 Hz, 2H, Ar-H), 8.11 (d, *J* = 9.0 Hz, 2H, Ar-H), 7.93 (d, *J* = 8.5 Hz, 2H, Ar-H), 7.07 (d, *J* = 9.1 Hz, 2H, Ar-H), 6.94 (d, *J* = 9.0 Hz, 2H, Ar-H), 6.89 (d, *J* = 9.1 Hz, 2H, Ar-H), 4.37 (t, *J* = 6.6 Hz, 2H, $COOCH_2$), 4.02 (t, *J* = 6.6 Hz, 2H, OCH_2), 3.96 (t, *J* = 6.3 Hz, 2H, OCH_2), 1.87 – 1.76 (m, 6H, $OCH_2C\mathbf{H}_2$, $COOCH_2C\mathbf{H}_2$), 1.61 – 1.42 (m, 6H, CH_2), 1.38 – 1.30 (m, 4H, CH_2), 0.90 (t, *J* = 7.1 Hz, 3H, CH_3).

4-({[6-(4-{[4-(Hexyloxy)phenyl]carbonyloxy}phenoxy)hexyl]oxy}carbonyl)benzoic acid **i17(6,6)**

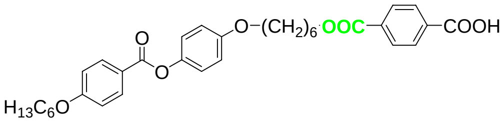

Formula:	$C_{33}H_{38}O_8$, M = 562.65 g/mol
Synthesis:	according to the general procedure 11.3.5
Reagents:	0.63 g (1.15 mmol) 4-({6-[(4-formylphenyl)carbonyloxy]hexyl}oxy)phenyl 4-(hexyloxy)-benzoate **i16(6,6)** 0.16 g (1.48 mmol) resorcinol 0.59 g (6.63 mmol) $NaClO_2$ 0.54 g (3.45 mmol) $NaH_2PO_4 \cdot 2H_2O$ 40 ml THF 30 ml water
Purification:	recrystallisation from CH_3COOH
Yield:	0.57 g (88 %), colorless solid
Transition temp.:	Cr 157 [57.6] I
^{1}H-NMR:	($CDCl_3$, *J*/Hz, 400 MHz) δ 8.19 – 8.07 (m, 6H, Ar-H), 7.08 (d, *J* = 9.0 Hz, 2H, Ar-H), 6.94 (d, *J* = 8.8 Hz, 2H, Ar-H), 6.89 (d, *J* = 9.0 Hz, 2H, Ar-H), 4.37 (t, *J* = 6.6 Hz, 2H, $COOCH_2$), 4.01 (t, *J* = 6.6 Hz, 2H, OCH_2), 3.96 (t, *J* = 6.3 Hz, 2H, OCH_2), 1.88 – 1.75 (m, 6H, $OCH_2C\mathbf{H}_2$, $COOCH_2C\mathbf{H}_2$), 1.60 – 1.41 (m, 6H, CH_2), 1.39 – 1.28 (m, 4H, CH_2), 0.90 (t, *J* = 7.0 Hz, 3H, CH_3).

Benzyl 4-[(6-bromohexanoyl)oxy]benzoate **i18(5)**

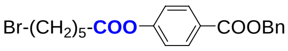

Formula: $C_{20}H_{21}O_4$, M = 405.28 g/mol
Synthesis: according to the general procedure 11.3.4 methode B
Reagents: 12.39 g (46.83 mmol) benzyl 4-hydroxybenzoate
10.00 g (46.83 mmol) 6-bromohexanoyl chloride
6.16 g (60.88 mmol) TEA
0.05 g DMAP
200 ml toluene
Purification: column chromatography, eluent: $CHCl_3$ and further recrystallisation from EtOAc/EtOH (10/0.2)
Yield: 12.52 g (66 %), oil at room temperature
Transition temp.: oil at room temperature
^{1}H-NMR: ($CDCl_3$, *J*/Hz, 400 MHz) δ 8.09 (d, *J* = 8.8 Hz, 2H, Ar-H), 7.45 – 7.30 (m, 5H, Ar-H), 7.15 (d, *J* = 8.8 Hz, 2H, Ar-H), 5.35 (s, 2H, OCH_2Ph), 3.42 (t, *J* = 6.7 Hz, 2H, $BrCH_2$), 2.59 (t, *J* = 7.4 Hz, 2H, CH_2COO), 1.96 – 1.87 (m, 2H, $BrCH_2C\mathbf{H}_2$), 1.82 – 1.73 (m, 2H, $C\mathbf{H}_2CH_2COO$), 1.62 – 1.51 (m, 2H, CH_2).

4-[(6-{4-[(Benzyloxy)carbonyl]phenoxy}-6-oxohexyl)oxy]phenyl 4-(hexyloxy)benzoate **i19(5,6)**

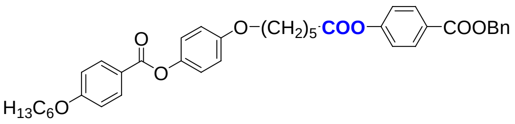

Formula: $C_{39}H_{42}O_8$, M = 638.75 g/mol
Synthesis: according to the general procedure 11.3.1 methode A
Reagents: 6.46 g (20.55 mmol) 4-hydroxyphenyl 4-(hexyloxy)benzoate **i11(6)**
9.99 g (24.66 mmol) benzyl 4-[(6-bromohexanoyl)oxy]benzoate **i18(5)**
14.19 g (102.74 mmol) K_2CO_3
0.05 g KI
100 ml butan-2-one
Purification: column chromatography, eluent: $CHCl_3$/EtOAc (10/0.2) and further recrystallisation from EtOAc/EtOH (10/0.2)
Yield: 7.22 g (55 %), colorless solid
Transition temp.: Cr 88 [64.6] (SmA 81 [6.1] N 85 [2.7]) I
^{1}H-NMR: ($CDCl_3$, *J*/Hz, 400 MHz) δ 8.11 (d, *J* = 9.0 Hz, 2H, Ar-H), 8.01 (d, *J* = 9.0 Hz, 2H, Ar-H), 7.45 – 7.40 (m, 2H, Ar-H), 7.40 – 7.28 (m, 3H, Ar-H), 7.19 (d, *J* = 9.1 Hz, 2H, Ar-H), 7.11 (d, *J* = 9.1 Hz, 2H, Ar-H), 6.95 (d, *J* = 9.0 Hz, 2H, Ar-H), 6.89 (d, *J* = 9.0 Hz, 2H, Ar-H), 5.32 (s, 2H OCH_2Ph), 4.03 (t, *J* = 6.5 Hz, 4H, OCH_2), 2.60 (t, *J* = 7.4 Hz, 2H, CH_2COO), 1.91 – 1.76 (m, 6H, $C\mathbf{H}_2CH_2COO$, $OCH_2C\mathbf{H}_2$), 1.66 – 1.56 (m, 2H, CH_2), 1.52 – 1.42 (m, 2H, CH_2), 1.39 – 1.30 (m, 4H, CH_2), 0.94 – 0.87 (m, 3H, CH_3).

4-{[6-(4-{[4-(Hexyloxy)phenyl]carbonyloxy}phenoxy)hexanoyl]oxy}benzoic acid **i20(5,6)**

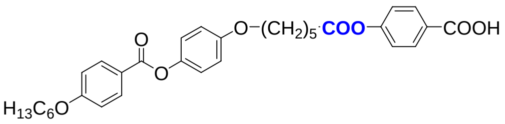

Formula: $C_{32}H_{36}O_8$, M = 548.62 g/mol

Synthesis:	according to the general procedure 11.3.6 methode A
Reagents:	4.44 g (6.95 mmol) 4-[(6-{4-[(benzyloxy)carbonyl]phenoxy}-6-oxohexyl)oxy]phenyl 4-(hexyloxy)benzoate **i19(5,6)** 0.44 g Pd/C 100 ml THF
Purification:	recrystallisation from CH_3COOH
Yield:	2.77 g (73 %), colorless solid
Transition temp.:	Cr 173 [31.1] N 212 [14.8] I
^{1}H-NMR:	($CDCl_3$, *J*/Hz, 400 MHz) δ 8.11 (d, *J* = 8.8 Hz, 2H, Ar-H), 8.02 (d, *J* = 8.8 Hz, 2H, Ar-H), 7.20 (d, *J* = 8.9 Hz, 2H, Ar-H), 7.11 (d, *J* = 8.9 Hz, 2H, Ar-H), 6.95 (d, *J* = 8.9 Hz, 2H, Ar-H), 6.92 (d, *J* = 8.9 Hz, 2H, Ar-H), 4.08 – 4.01 (m, 4H, OCH$_2$), 2.59 (t, *J* = 7.4 Hz, 2H, CH$_2$COO), 1.91 – 1.77 (m, 6H, $\mathbf{CH_2}$CH$_2$COO, OCH$_2$$\mathbf{CH_2}$), 1.66 – 1.58 (m, 2H, CH$_2$), 1.51 – 1.44 (m, 2H, CH$_2$), 1.38 – 1.32 (m, 4H, CH$_2$), 0.91 (t, *J* = 7.1 Hz, 3H, CH$_3$).

4-[(16-Bromohexadecanoyl)oxy]phenyl 4-(hexadecyloxy)benzoate **i21**

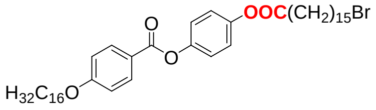

Formula:	$C_{45}H_{71}BrO_5$, M = 771.95 g/mol
Synthesis:	according to the general procedure 11.3.3
Reagents:	2.00 g (4.39 mmol) 4-hydroxyphenyl 4-(hexadecyloxy)benzoate **i11(16)** 1.47 g (4.39 mmol) 16-bromohexadecanoic acid 0.98 g (4.84 mmol) DCC 0.05 g DMAP 50 ml dichloromethane
Purification:	column chromatography, eluent: $CHCl_3$ and further recrystallisation from *n*-heptane
Yield:	2.64 g (78 %), colorless solid
Transition temp.:	Cr 85 [82.8] Cr 89 [23.9] I
^{1}H-NMR:	($CDCl_3$, *J*/Hz, 400 MHz) δ 8.11 (d, *J* = 8.9 Hz, 2H, Ar-H), 7.19 (d, *J* = 8.8 Hz, 2H, Ar-H), 7.11 (d, *J* = 8.9 Hz, 2H, Ar-H), 6.95 (d, *J* = 8.9 Hz, 2H, Ar-H), 4.02 (t, *J* = 6.6 Hz, 2H, OCH$_2$), 3.38 (t, *J* = 6.9 Hz, 2H, BrCH$_2$), 2.54 (t, *J* = 7.5 Hz, 2H, CH$_2$COO), 1.88 – 1.69 (m, 6H, $\mathbf{CH_2}$CH$_2$COO, OCH$_2$$\mathbf{CH_2}$), 1.50 – 1.20 (m, 48H, CH$_2$), 0.86 (t, *J* = 6.8 Hz, 3H, CH$_3$).

4-[(16-{4-[(Benzyloxy)carbonyl]phenoxy}hexadecanoyl)oxy]phenyl 4-(hexadecyloxy)-benzoate **i22**

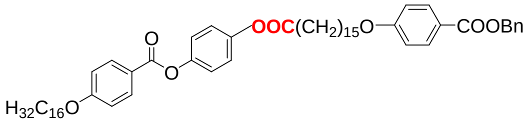

Formula:	$C_{59}H_{82}O_8$, M = 919.28 g/mol
Synthesis:	according to the general procedure 11.3.1 methode A
Reagents:	2.00 g (2.59 mmol) 4-[(16-bromohexadecanoyl)oxy]phenyl 4-(hexadecyloxy)benzoate **i21** 0.49 g (2.16 mmol) benzyl 4-hydroxybenzoate 1.49 g (12.49 mmol) K_2CO_3 0.02 g KI 50 ml butan-2-one
Purification:	column chromatography, eluent: $CHCl_3$/EtOAc (10/0.2) and further recrystallisation from EtOAc/EtOH (10/0.2)
Yield:	1.23 g (62 %), colorless solid
Transition temp.:	Cr 107 [98.6] I
^{1}H-NMR:	($CDCl_3$, *J*/Hz, 400 MHz δ 8.17 – 8.08 (m, 2H, Ar-H), 8.05 – 7.97 (m, 2H, Ar-H), 7.47 – 7.30

	(m, 5H, Ar-H), 7.23 – 7.17 (m, 2H, Ar-H), 7.15 – 7.05 (m, 2H, Ar-H), 7.01 – 6.93 (m, 2H, Ar-H), 6.92 – 6.85 (m 2H, Ar-H), 5.34 (s, 2H, OCH_2Ph), 4.08 – 3.95 (m, 4H, OCH_2), 2.59 – 2.49 (m, 2H, CH_2COO), 1.88 – 1.69 (m, 6H, $C\mathbf{H}_2CH_2COO$, $OCH_2C\mathbf{H}_2$), 1.51 – 1.20 (m, 48H, CH_2), 0.88 (t, *J* = 6.6 Hz, 3H, CH_3).

4-{[16-(4-{[4-(Hexadecyloxy)phenyl]carbonyloxy}phenoxy)-16-oxohexadecyl]oxy}benzoic acid **i23**

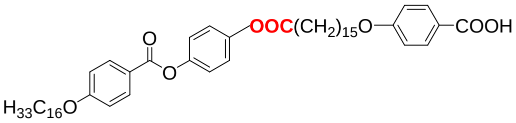

Formula:	$C_{52}H_{76}O_8$, M = 829.16 g/mol
Synthesis:	according to the general procedure 11.3.6 methode A
Reagents:	1.23 g (1.33 mmol) 4-[(16-{4-(benzyloxy)carbonyl]phenoxy}hexadecanoyl)oxy]phenyl 4-(hexadecyloxy)benzoate **i22** 0.12 g Pd/C 100 ml THF
Purification:	recrystallisation from CH_3COOH
Yield:	0.75 g (68 %), colorless solid
Transition temp.:	Cr 124 [78.0] N 137 [5.6] I
^{1}H-NMR:	($CDCl_3$, *J*/Hz, 400 MHz) δ 8.16 – 8.07 (m, 2H, Ar-H), 8.01 (d, *J* = 8.4 Hz, 2H, Ar-H), 7.21 – 7.17 (m, 2H, Ar-H), 7.13 – 7.04 (m, 2H), 6.98 – 6.88 (m, 4H), 4.03 (t, *J* = 6.5 Hz, 2H, OCH_2), 2.57 – 2.51 (m, 2H, CH_2COO), 1.85 – 1.70 (m, 6H, $C\mathbf{H}_2CH_2COO$, $OCH_2C\mathbf{H}_2$), 1.50 – 1.40 (m, 4H, CH_2), 1.39 – 1.19 (m, 44H, CH_2), 0.86 (t, *J* = 6.8 Hz, 4H, CH_3).

1-(Benzyloxy)-4-(dodecyloxy)benzene **i24**

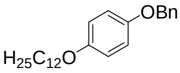

Formula:	$C_{25}H_{36}O_2$, M = 368.28 g/mol
Synthesis:	according to the general procedure 11.3.1 methode C
Reagents:	8.00 g (40.00 mmol) 4-(benzyloxy)phenol 12.66 g (44.00 mmol) 1-bromododecane 2.54 g (46.00 mmol) KOH 0.05 g KI 100 ml dimethylformamide
Purification:	recrystallisation from EtOH
Yield:	6.98 g (47 %), colorless solid
Transition temp.:	Cr 82 [21.5] I
^{1}H-NMR:	($CDCl_3$, *J*/Hz, 400 MHz) δ 7.43 – 7.39 (m, 2H, Ar-H), 7.39 – 7.33 (m, 2H, Ar-H), 7.32 – 7.27 (m, 1H, Ar-H), 6.88 (d, *J* = 9.2 Hz, 2H, Ar-H), 6.81 (d, *J* = 9.2 Hz, 2H, Ar-H), 5.00 (s, 2H, , OCH_2Ph), 3.88 (t, *J* = 6.6 Hz, 2H, OCH_2), 1.78 – 1.69 (m, 2H, $OCH_2C\mathbf{H}_2$), 1.46 – 1.38 (m, 2H, CH_2), 1.37 – 1.21 (m, 16H, CH_2), 0.87 (t, *J* = 6.9 Hz, 3H, CH_3).

4-(Dodecyloxy)phenol **i25**

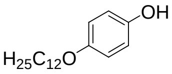

Formula:	$C_{18}H_{28}O_2$, M = 276.20 g/mol

Synthesis:	according to the general procedure 11.3.6 methode A
Reagents:	6.5 g (17.65 mmol) 1-(benzyloxy)-4-(dodecyloxy)benzene **i24** 0.65 g Pd/C 50 ml ethyl acetate
Purification:	recrystallisation from EtOH
Yield:	3.89 g (80 %), colorless solid
Transition temp.:	Cr 81 [12.1] I
^{1}H-NMR:	($CDCl_3$, J/Hz, 400 MHz) δ 6.79 – 6.70 (m, 4H, Ar-H), 3.87 (t, J = 6.6 Hz, 2H, OCH_2), 1.77 – 1.68 (m, 2H, OCH_2**CH_2**), 1.46 – 1.37 (m, 2H), 1.36 – 1.21 (m, 16H, CH_2), 0.86 (t, J = 6.9 Hz, 3H, CH_3).

4-(Dodecyloxy)phenyl 4-formylbenzoate **i26**

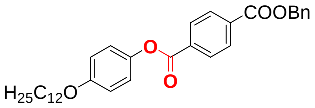

Formula:	$C_{33}H_{40}O_5$, M = 516.67 g/mol
Synthesis:	according to the general procedure 11.3.3
Reagents:	3.00 g (12.56 mmol) 4-(dodecyloxy)phenol **i25** 1.63 g (12.56 mmol) 4-(benzyloxycarbonyl)benzoic acid 2.46 g (11.95 mmol) DCC 0.02 g DMAP 50 ml dicloromethane
Purification:	recrystallisation from EtOH
Yield:	2.81g (63 %), colorless solid
Transition temp.:	Cr 102 [67.5] I
^{1}H-NMR:	($CDCl_3$, J/Hz, 400 MHz) δ 8.23 (d, J = 8.7 Hz, 2H, Ar-H), 8.18 (d, J = 8.7 Hz, 2H, Ar-H), 7.48 – 7.43 (m, 2H, Ar-H), 7.43 – 7.32 (m, 3H, Ar-H), 7.11 (d, J = 9.1 Hz, 2H, Ar-H), 6.92 (d, J = 9.1 Hz, 2H, Ar-H), 5.39 (s, 2H, OCH_2Ph), 3.94 (t, J = 6.6 Hz, 2H, OCH_2), 1.82 – 1.73 (m, 2H, OCH_2**CH_2**), 1.49 – 1.40 (m, 2H, CH_2), 1.39 – 1.22 (m, 16H, CH_2), 0.87 (t, J = 6.9 Hz, 3H, CH_3).

4-[4-(Dodecyloxy)phenoxycarbonyl]benzoic acid **i27**

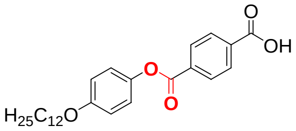

Formula:	$C_{26}H_{34}O_5$, M = 426.55 g/mol
Synthesis:	according to the general procedure 11.3.5
Reagents:	2.50 g (6.08 mmol) 4-(dodecyloxy)phenyl 4-formylbenzoate **i26** 0.86 g (7.84 mmol) resorcinol 5.13 g (34.65 mmol) $NaClO_2$ 2.85 g (18.24 mmol) $NaH_2PO_4 \cdot 2H_2O$ 100 ml THF 50 ml water
Purification:	recrystallisation from CH_3COOH
Yield:	2.07 g (80 %), colorless solid
Transition temp.:	Cr 167 [22.9] N 232 [14.1] I
^{1}H-NMR:	(DMSO, J/Hz, 400 MHz) δ 8.20 (d, J = 8.6 Hz, 2H, Ar-H), 8.12 (d, J = 8.6 Hz, 2H, Ar-H), 7.12 (d, J = 9.0 Hz, 2H, Ar-H), 6.93 (d, J = 9.1 Hz, 2H, Ar-H), 3.96 (t, J = 6.5 Hz, 2H, OCH_2), 1.81 – 1.72 (m, 2H, OCH_2**CH_2**), 1.50 – 1.41 (m, 2H, CH_2), 1.39 – 1.21 (m, 16H, CH_2), 0.87 (t, J = 6.9 Hz, 3H, CH_3).

1-[3-(Benzyloxy)phenyl] 4-[4-(dodecyloxy)phenyl]benzene-1,4-dicarboxylate **i28**

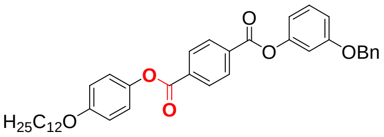

Formula: $C_{39}H_{44}O_6$, M = 608.76 g/mol

Synthesis: according to the general procedure 11.3.3

Reagents:
0.86 g (2.01 mmol) 4-[4-(dodecyloxy)phenoxycarbonyl]benzoic acid **i27**
0.40 g (2.01 mmol) 3-(benzyloxy)phenol **i5**
0.45 g (2.21 mmol) DCC
0.02 g DMAP
50 ml dichloromethane

Purification: recrystallisation from EtOAc/EtOH 10/0.1

Yield: 0.95 g (78 %), colorless solid

Transition temp.: Cr 109 [44.4] I

^{1}H-NMR: ($CDCl_3$, *J*/Hz, 400 MHz) δ 8.30 (s, 4H, Ar-H), 7.44 – 7.30 (m, 6H, Ar-H), 7.13 (d, *J* = 9.1 Hz, 2H, Ar-H), 6.93 (d, *J* = 9.1 Hz, 3H, Ar-H), 6.90 – 6.82 (m, 2H, Ar-H), 5.07 (s, 2H, OCH_2Ph), 3.95 (t, *J* = 6.6 Hz, 2H, OCH_2), 1.83 – 1.73 (m, 2H, $OCH_2C\mathbf{H}_2$), 1.50 – 1.40 (m, 2H, CH_2), 1.40 – 1.21 (m, 16H, CH_2), 0.87 (t, *J* = 6.9 Hz, 3H, CH_3).

1-[4-(Dodecyloxy)phenyl] 4-(3-hydroxyphenyl)benzene-1,4-dicarboxylate **i29**

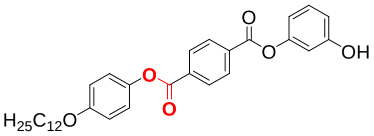

Formula: $C_{32}H_{38}O_6$, M = 518.64 g/mol

Synthesis: according to the general procedure 11.3.6 methode A

Reagents:
0.9 g (1.47 mmol) 1-[3-(benzyloxy)phenyl] 4-[4-dodecyloxy)phenyl]benzene-1,4-dicarboxylate **i28**
0.09 g Pd/C
100 ml THF

Purification: recrystallisation from EtOH

Yield: 0.51 g (67 %), colorless solid

Transition temp.: Cr 141 [38.9] I

^{1}H-NMR: ($CDCl_3$, *J*/Hz, 400 MHz) δ 8.21 (s, 4H, Ar-H), 7.14 (t, *J* = 8.1 Hz, 1H, Ar-H), 7.06 (d, *J* = 9.1 Hz, 2H, Ar-H), 6.86 (d, *J* = 9.1 Hz, 2H, Ar-H), 6.69 – 6.57 (m, 3H, Ar-H), 3.89 (t, *J* = 6.5 Hz, 2H, OCH_2), 1.75 – 1.65 (m, 2H, $OCH_2C\mathbf{H}_2$), 1.42 – 1.33 (m, 2H, CH_2), 1.32 – 1.14 (m, 16H, CH_2), 0.80 (t, *J* = 6.9 Hz, 3H, CH_3).

1-(3-{[4-(Benzyloxy)phenyl]carbonyloxy}phenyl) 4-[4-(dodecyloxy)phenyl]benzene-1,4-dicarboxylate **i30**

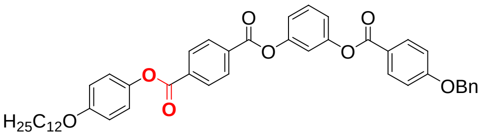

Formula: $C_{46}H_{48}O_8$, M = 728.87 g/mol

Synthesis: according to the general procedure 11.3.3

Reagents: 0.33 g (0.63 mmol) 1-[4-(dodecyloxy)phenyl] 4-(3-hydroxyphenyl)benzene-1,4-dicarboxylate

i29
0.14 g (0.63 mmol) 4-(benzyloxy)benzoic acid
0.14 g (0.69 mmol) DCC
0.02 g DMAP
50 ml dichloromethane

Purification: column chromatography, eluent: CHCl$_3$/EtOAc (10/0.2) and further recrystallisation from EtOAc/EtOH (10/0.2)
Yield: 0.39g (85 %), colorless solid
Transition temp.: Cr 112 [24.4] I
^{1}H-NMR: (CDCl$_3$, *J*/Hz, 400 MHz) δ 8.30 (s, 4H, Ar-H), 8.14 (d, *J* = 9.0 Hz, 2H, Ar-H), 7.50 – 7.31 (m, 6H, Ar-H), 7.21 – 7.10 (m, 5H, Ar-H), 7.05 (d, *J* = 9.0 Hz, 2H, Ar-H), 6.93 (d, *J* = 9.1 Hz, 2H, Ar-H), 5.15 (s, 2H, OCH$_2$Ph), 3.95 (t, *J* = 6.6 Hz, 2H, OCH$_2$), 1.82 – 1.73 (m, 2H, OCH$_2$**CH**$_2$), 1.51 – 1.40 (m, 2H, CH$_2$), 1.39 – 1.23 (m, 16H, CH$_2$), 0.87 (t, *J* = 6.9 Hz, 3H, CH$_3$).

1-[4-(Dodecyloxy)phenyl] 4-{3-[(4-hydroxyphenyl)carbonyloxy]phenyl}benzene-1,4-dicarboxylate **i31**

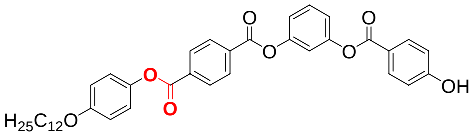

Formula: C$_{39}$H$_{42}$O$_8$, M = 638.75 g/mol
Synthesis: according to the general procedure 11.3.6 methode A
Reagents: 0.35 g (0.48 mmol) 1-(3-{[4-(benzyloxy)phenyl]carbonyloxy}phenyl) 4-[4-(dodecyloxy)-phenyl]benzene-1,4-dicarboxylate **i30**
0.035 g Pd/C
100 ml THF

Purification: recrystallisation from EtOH
Yield: 0.19 g (65 %), colorless solid
Transition temp.: Cr 159 [35.3] (N 147 [9.9]) I
^{1}H-NMR: (CDCl$_3$, *J*/Hz, 400 MHz) δ 8.30 (s, 4H, Ar-H), 8.08 (d, *J* = 8.8 Hz, 2H, Ar-H), 7.47 (t, *J* = 8.2 Hz, 1H, Ar-H), 7.21 – 7.09 (m, 5H, Ar-H), 6.93 (d, *J* = 9.1 Hz, 2H, Ar-H), 6.88 (d, *J* = 8.8 Hz, 2H, Ar-H), 3.95 (t, *J* = 6.6 Hz, 2H, OCH$_2$), 1.82 – 1.73 (m, 2H, OCH$_2$**CH**$_2$), 1.49 – 1.40 (m, 2H, CH$_2$), 1.39 – 1.21 (m, 16H, CH$_2$), 0.87 (t, *J* = 6.8 Hz, 3H, CH$_3$).

4-(Benzyloxy)phenyl 4-(dodecyloxy)benzoate **i32(12)**

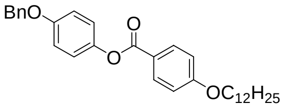

Formula: C$_{32}$H$_{40}$O$_4$, M = 488.66 g/mol
Synthesis: according to the general procedure 11.3.3
Reagents: 5.00 g (16.31 mmol) 4-(dodecyloxy)benzoic acid **i1(12)**
3.27 g (16.31 mmol) 4-(benzyloxy)phenol
4.19 g (20.49 mmol) DCC
0.05 g DMAP
150 ml dichloromethane

Purification: recrystallisation from EtOAc/EtOH
Yield: 6.81 g (86 %), colorless solid
Transition temp.: Cr 103 [60.3] (SmA 90 [1.3] N 96 [2.4]) I
^{1}H-NMR: (CDCl$_3$, *J*/Hz, 400 MHz) δ 8.11 (d, *J* = 9.0 Hz, 2H, Ar-H), 7.47 – 7.28 (m, 5H, Ar-H), 7.11 (d,

J = 9.1 Hz, 2H, Ar-H), 6.99 (d, *J* = 9.1 Hz, 2H, Ar-H), 6.95 (d, *J* = 9.0 Hz, 2H, Ar-H), 5.06 (s, 2H, CH_2Ph), 4.03 (t, *J* = 6.6 Hz, 2H, OCH_2), 1.86 – 1.77 (m, 2H, $OCH_2C\mathbf{H}_2$), 1.55 – 1.42 (m, 2H), 1.40 – 1.23 (m, 16H, CH_2), 0.89 (t, *J* = 6.9 Hz, 3H, CH_3).

4-Hydroxyphenyl 4-(dodecyloxy)benzoate **i33(12)**

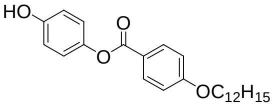

Formula:	$C_{25}H_{34}O_4$, M = 398.54 g/mol
Synthesis:	according to the general procedure 11.3.6 methode A
Reagents:	6.80 g (13.91 mmol) 4-(benzyloxy)phenyl 4-(dodecyloxy)benzoate **i32(12)** 0.68 g Pd/C 60 ml ethyl acetate
Purification:	recrystallisation from EtOH
Yield:	4.95 g (89 %), colorless solid
Transition temp.:	Cr 118 [53.5] I
^{1}H-NMR:	($CDCl_3$, *J*/Hz, 400 MHz) δ 8.10 (d, *J* = 8.9 Hz, 2H, Ar-H), 7.02 (d, *J* = 8.8 Hz, 2H, Ar-H), 6.94 (d, *J* = 8.8 Hz, 2H, Ar-H), 6.79 (d, *J* = 8.8 Hz, 2H, Ar-H), 4.03 (t, *J* = 6.5 Hz, 2H, OCH_2), 1.85 – 1.75 (m, 2H, $OCH_2C\mathbf{H}_2$), 1.51 – 1.41 (m, 2H, CH_2), 1.39 – 1.20 (m, 16H, CH_2), 0.87 (t, *J* = 6.3 Hz, 3H, CH_3).

3-Formylphenyl 4-(benzyloxy)benzoate **i34**

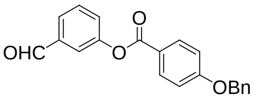

Formula:	$C_{21}H_{16}O_4$, M = 332.35 g/mol
Synthesis:	according to the general procedure 11.3.3
Reagents:	2.00 g (16.37 mmol) 3-hydroxybenzaldehyde 3.74 g (16.37 mmol) 4-(benzyloxy)benzoic acid 3.72 g (18.01 mmol) DCC 0.02 g DMAP 100 ml dichloromethane
Purification:	recrystallisation from DMF/EtOH and EtOAc/EtOH
Yield:	2.99 g (55 %), colorless solid
Transition temp.:	Cr 133 [41.9] I
^{1}H-NMR:	($CDCl_3$, *J*/Hz, 400 MHz) δ 9.94 (s, 1H, CHO), 8.06 (d, *J* = 8.8 Hz, 2H, Ar-H), 7.69 (d, *J* = 7.6 Hz, 1H, Ar-H), 7.66 – 7.63 (m, 1H, Ar-H), 7.50 (t, *J* = 7.8 Hz, 1H, Ar-H), 7.43 – 7.38 (m, 1H, Ar-H), 7.38 – 7.23 (m, 5H, Ar-H), 6.99 (d, *J* = 8.9 Hz, 2H, Ar-H), 5.09 (s, 2H, OCH_2Ph).

3-{[4-(Benzyloxy)phenyl]carbonyloxy}benzoic acid **i35**

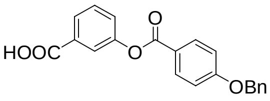

Formula:	$C_{21}H_{16}O_5$, M = 348.35 g/mol
Synthesis:	according to the general procedure 11.3.5
Reagents:	2.00 g (6.02 mmol) 3-formylphenyl 4-(benzyloxy)benzoate **i34** 0.86 g (7.76 mmol) resorcinol

	3.13 g (34.65 mmol) $NaClO_2$
	2.82 g (18.06 mmol) $NaH_2PO_4 \cdot 2H_2O$
	70 ml THF
	30 ml water
Purification:	recrystallisation from CH_3COOH
Yield:	1.93 g (92 %), colorless solid
Transition temp.:	Cr 197 [48.2] I
^{1}H-NMR:	($CDCl_3$, *J*/Hz, 400 MHz) δ 8.14 (d, *J* = 8.9 Hz, 2H, Ar-H), 7.99 (d, *J* = 7.5 Hz, 1H, Ar-H), 7.94 – 7.92 (m, 1H, Ar-H), 7.54 – 7.31 (m, 7H, Ar-H), 7.06 (d, *J* = 8.9 Hz, 2H, Ar-H), 5.16 (s, 2H, OCH_2Ph).

4-{[4-(Dodecyloxy)phenyl]carbonyloxy}phenyl 3-{[4-(benzyloxy)phenyl]carbonyloxy}-benzoate **i36(12)**

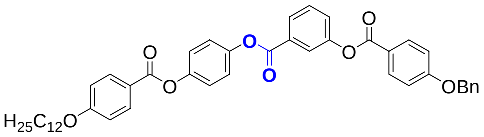

Formula:	$C_{46}H_{48}O_8$, M = 728.87 g/mol
Synthesis:	according to the general procedure 11.3.3
Reagents:	1.94 g (4.88 mmol) 4-hydroxyphenyl 4-(dodecyloxy)benzoate **i33(12)**
	1.70 g (4.88 mmol) 3-{[4-(benzyloxy)phenyl]carbonyloxy}benzoic acid **i35**
	1.11 g (5.37 mmol) DCC
	0.02 g DMAP
	50 ml dichloromethane
Purification:	recrystallisation from EtOAc7EtOH
Yield:	2.45 g (69 %), colorless solid
Transition temp.:	Cr 57 [59.1] N 74 [1.5] I
^{1}H-NMR:	($CDCl_3$, *J*/Hz, 400 MHz) δ 8.19 – 8.07 (m, 5H, Ar-H), 8.04 – 8.01 (m, 1H, Ar-H), 7.56 (t, *J* = 7.9 Hz, 1H, Ar-H), 7.52 – 7.46 (m, 1H, Ar-H), 7.46 – 7.31 (m, 5H, Ar-H), 7.27 – 7.24 (m, 4H, Ar-H), 7.06 (d, *J* = 9.0 Hz, 2H, Ar-H), 6.96 (d, *J* = 9.0 Hz, 2H, Ar-H), 5.16 (s, 2H, OCH_2Ph), 4.03 (t, *J* = 6.6 Hz, 2H, OCH_2), 1.86 – 1.76 (m, 2H, $OCH_2C\mathbf{H}_2$), 1.51 – 1.42 (m, 2H, CH_2), 1.39 – 1.20 (m, 16H, CH_2), 0.87 (t, *J* = 6.9 Hz, 3H, CH_3).

4-({3-[(4-Hydroxyphenyl)carbonyloxy]phenyl}carbonyloxy)phenyl 4-(dodecyloxy)benzoate **i37(12)**

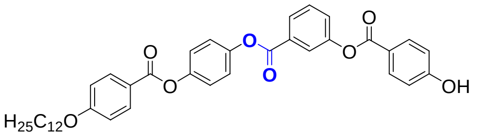

Formula:	$C_{39}H_{42}O_8$, M = 638.75 g/mol
Synthesis:	according to the general procedure 11.3.6 methode A
Reagents:	2.20 g (3.02 mmol) 4-{[4-(dodecyloxy)phenyl]carbonyloxy}phenyl 3-{[4-(benzyloxy)phenyl]-carbonyloxy}benzoate **i36(12)**
	0.22 g Pd/C
	100 ml THF
Purification:	recrystallisation from EtOAc/EtOH
Yield:	1.29 g (67 %), colorless solid
Transition temp.:	Cr 181 [42.8] I
^{1}H-NMR:	($CDCl_3$, *J*/Hz, 400 MHz) δ 8.15 – 8.07 (m, 5H, Ar-H), 8.03 – 8.00 (m, 1H, Ar-H), 7.55 (t, *J* =

7.9 Hz, 1H, Ar-H), 7.50 – 7.46 (m, 1H, Ar-H), 7.25 (s, 4H, Ar-H), 6.95 (d, J = 8.9 Hz, 2H, Ar-H), 6.90 (d, J = 8.8 Hz, 2H, Ar-H), 4.03 (t, J = 6.6 Hz, 2H, OCH_2), 1.85 – 1.76 (m, 2H, $OCH_2C\mathbf{H}_2$), 1.50 – 1.41 (m, 2H, CH_2), 1.25 (s, 16H, CH_2), 0.87 (t, J = 6.8 Hz, 3H, CH_3).

4-(3-Formylphenoxycarbonyl)phenyl 4-(dodecyloxy)benzoate **i38(12)**

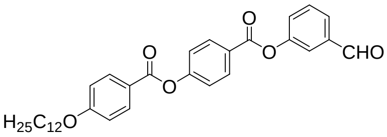

Formula: $C_{33}H_{38}O_6$, M = 530.65 g/mol
Synthesis: according to the general procedure 11.3.3
Reagents: 12.07 g (28.29 mmol) 4-{[4-(dodecyloxy)phenyl]carbonyloxy}benzoic acid **i3(12)**
3.46 g (28.29 mmol) 3-hydroxybenzaldehyde
6.42 g (31.13 mmol) DCC
0.02 g DMAP
200 ml dichloromethane
Purification: recrystallisation from EtOAc/EtOH
Yield: 13.29 g (89 %), colorless solid
Transition temp.: Cr 101 [49.3] SmA 123 [4.5] I
^{1}H-NMR: ($CDCl_3$, J/Hz, 400 MHz) δ 10.03 (s, 1H, CHO), 8.27 (d, J = 8.7 Hz, 2H, Ar-H), 8.14 (d, J = 8.9 Hz, 2H, Ar-H), 7.83 – 7.77 (m, 1H, Ar-H), 7.77 – 7.73 (m, 1H, Ar-H), 7.61 (t, J = 7.8 Hz, 1H, Ar-H), 7.52 – 7.47 (m, 1H, Ar-H), 7.37 (d, J = 8.7 Hz, 2H, Ar-H), 6.97 (d, J = 8.9 Hz, 2H, Ar-H), 4.04 (t, J = 6.6 Hz, 2H, OCH_2), 1.86 – 1.76 (m, 2H, $OCH_2C\mathbf{H}_2$), 1.51 – 1.41 (m, 2H, CH_2), 1.39 – 1.20 (m, 16H, CH_2), 0.86 (t, J = 6.8 Hz, 3H, CH_3).

3-[(4-{[4-(Dodecyloxy)phenyl]carbonyloxy}phenyl)carbonyloxy]benzoic acid **i39(12)**

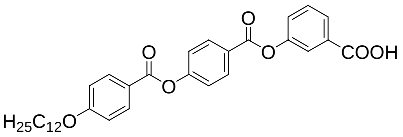

Formula: $C_{33}H_{38}O_7$, M = 546.65 g/mol
Synthesis: according to the general procedure 11.3.5
Reagents: 5.00 g (9.42 mmol) 4-(3-formylphenoxycarbonyl)phenyl 4-(dodecyloxy)benzoate **i38(12)**
1.34 g (12.17 mmol) resorcinol
4.9 g (54.23 mmol) $NaClO_2$
4.41 g (28.27 mmol) $NaH_2PO_4{\cdot}2H_2O$
150 ml THF
50 ml water
Purification: recrystallisation from CH_3COOH
Yield: 4.78 g (93 %), colorless solid
Transition temp.: Cr 169 [23.7] I
^{1}H-NMR: ($CDCl_3$, J/Hz, 400 MHz) δ 8.27 (d, J = 8.8 Hz, 2H, Ar-H), 8.14 (d, J = 8.9 Hz, 2H, Ar-H), 8.03 (d, J = 7.6 Hz, 1H, Ar-H), 7.98 – 7.95 (m, J = 1.8 Hz, 1H, Ar-H), 7.54 (t, J = 7.9 Hz, 1H, Ar-H), 7.51 – 7.47 (m, 1H, Ar-H), 7.37 (d, J = 8.8 Hz, 2H, Ar-H), 6.97 (d, J = 9.0 Hz, 2H, Ar-H), 4.04 (t, J = 6.5 Hz, 2H, OCH_2), 1.86 – 1.76 (m, 2H, $OCH_2C\mathbf{H}_2$), 1.51 – 1.41 (m, 2H, CH_2), 1.40 – 1.22 (m, 16H, CH_2), 0.87 (t, J = 6.8 Hz, 3H, CH_3).

4-{3-[4-(Benzyloxy)phenoxycarbonyl]phenoxycarbonyl}phenyl 4-(dodecyloxy)benzoate **i40(12)**

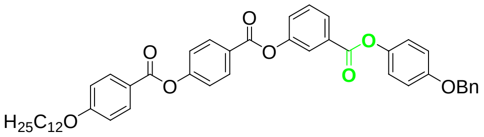

Formula:	$C_{46}H_{48}O_8$, M = 728.87 g/mol
Synthesis:	according to the general procedure 11.3.3
Reagents:	1.00 g (1.83 mmol) 3-[(4-{[4-(dodecyloxy)phenyl]carbonyloxy}phenyl)carbonyloxy]benzoic acid **i39(12)** 0.37 g (1.83 mmol) 4-(benzyloxy)phenol 0.42 g (2.01 mmol) DCC 0.02 g DMAP 50 ml dichloromethane
Purification:	recrystallisation from EtOAc/EtOH
Yield:	1.01 g (76 %), colorless solid
Transition temp.:	Cr 133 [55.2] I
^{1}H-NMR:	($CDCl_3$, *J*/Hz, 400 MHz) δ 8.27 (d, *J* = 8.9 Hz, 2H, Ar-H), 8.13 (d, *J* = 9.0 Hz, 2H, Ar-H), 8.12 – 8.08 (m, 1H, Ar-H), 8.05 – 8.02 (m, 1H, Ar-H), 7.57 (t, *J* = 8.0 Hz, 1H, Ar-H), 7.52 – 7.47 (m, 1H, Ar-H), 7.44 – 7.29 (m, 7H, Ar-H), 7.12 (d, *J* = 9.2 Hz, 2H, Ar-H), 7.02 – 6.95 (m, 4H, Ar-H), 5.06 (s, 2H, OCH_2Ph), 4.04 (t, *J* = 6.6 Hz, 2H, OCH_2), 1.86 – 1.77 (m, 2H, $OCH_2C\mathbf{H}_2$), 1.51 – 1.41 (m, 2H, CH_2), 1.40 – 1.22 (m, 16H, CH_2), 0.87 (t, *J* = 6.8 Hz, 3H, CH_3).

4-[3-(4-Hydroxyphenoxycarbonyl)phenoxycarbonyl]phenyl 4-(dodecyloxy)benzoate **i41(12)**

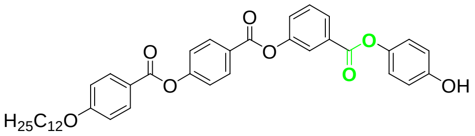

Formula:	$C_{39}H_{42}O_8$, M = 638.75 g/mol
Synthesis:	according to the general procedure 11.3.6 methode A
Reagents:	0.90 g (1.23 mmol) 4-{3-[4-benzyloxy)phenoxycarbonyl]phenoxycarbonyl}phenyl 4-(dodecyloxy)benzoate **i40(12)** 0.09 g Pd/C 100 ml THF
Purification:	recrystallisation from EtOH
Yield:	0.55 g (70 %), colorless solid
Transition temp.:	Cr 133 [48.4] I
^{1}H-NMR:	($CDCl_3$, *J*/Hz, 400 MHz) δ 8.28 (d, *J* = 8.8 Hz, 2H, Ar-H), 8.14 (d, *J* = 9.0 Hz, 2H, Ar-H), 8.10 (dt, *J* = 7.7, 1.4 Hz, 1H, Ar-H), 8.05 – 8.03 (m, 1H, Ar-H), 7.56 (t, *J* = 7.9 Hz, 1H, Ar-H), 7.52 – 7.49 (m, 1H, Ar-H), 7.38 (d, *J* = 8.9 Hz, 2H, Ar-H), 7.07 (d, *J* = 9.0 Hz, 2H, Ar-H), 6.98 (d, *J* = 9.0 Hz, 2H, Ar-H), 6.83 (d, *J* = 9.0 Hz, 2H, Ar-H), 4.05 (t, *J* = 6.6 Hz, 2H, OCH_2), 1.85 – 1.79 (m, 2H, $OCH_2C\mathbf{H}_2$), 1.50 – 1.44 (m, 2H, CH_2), 1.40 – 1.23 (m, 16H, CH_2), 0.88 (t, *J* = 7.0 Hz, 3H, CH_3).

4-{3-[(4-Formylphenyl)carbonyloxy]phenoxycarbonyl}phenyl 4-(dodecyloxy)benzoate **i42(12)**

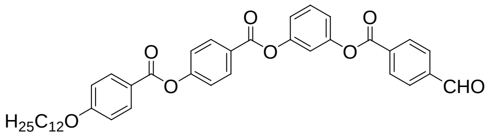

Formula: $C_{40}H_{42}O_8$, M = 650.76 g/mol
Synthesis: according to the general procedure 11.3.3
Reagents: 1.20 g (2.31 mmol) 4-(3-hydroxyphenoxycarbonyl)phenyl 4-(dodecyloxy)benzoate **i7(12)**
0.35 g (2.31 mmol) 4-formylbenzoic acid
0.53 g (2.54 mmol) DCC
0.02 g DMAP
50 ml dichloromethane
Purification: recrystallisation from EtOAc/EtOH
Yield: 0.97 g (65 %), colorless solid
Transition temp.: Cr 134 [55.5] I
^{1}H-NMR: ($CDCl_3$, *J*/Hz, 400 MHz) δ 12.12 (s, 1H, CHO), 8.37 (d, *J* = 8.2 Hz, 2H, Ar-H), 8.27 (d, *J* = 8.6 Hz, 2H, Ar-H), 8.15 (d, *J* = 8.8 Hz, 2H, Ar-H), 8.03 (d, *J* = 8.1 Hz, 2H, Ar-H), 7.51 (t, *J* = 8.1 Hz, 1H, Ar-H), 7.38 (d, *J* = 8.6 Hz, 2H, Ar-H), 7.24 – 7.18 (m, 3H, Ar-H), 6.99 (d, *J* = 8.8 Hz, 2H, Ar-H), 4.05 (t, *J* = 6.6 Hz, 2H, OCH_2), 1.87 – 1.78 (m, 2H, $OCH_2C\mathbf{H}_2$), 1.53 – 1.43 (m, 2H, CH_2), 1.42 – 1.23 (m, 16H, CH_2), 0.88 (t, *J* = 6.8 Hz, 3H, CH_3).

4-{3-[(4-{[4-(Dodecyloxy)phenyl]carbonyloxy}phenyl)carbonyloxy]phenoxycarbonyl}benzoic acid **i43(12)**

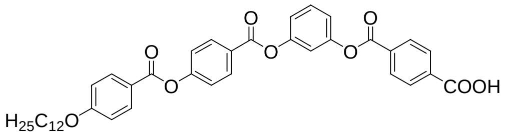

Formula: $C_{40}H_{42}O_9$, M = 666.76 g/mol
Synthesis: according to the general procedure 11.3.5
Reagents: 0.56 g (0.86 mmol) 4-{3-[(4-formylphenyl)carbonyloxy]phenoxycarbonyl}phenyl 4-(dodecyloxy)benzoate **i42(12)**
0.12 g (1.11 mmol) resorcinol
0.45 g (4.94 mmol) $NaClO_2$
0.40 g (2.57 mmol) $NaH_2PO_4{\cdot}2H_2O$
20 ml THF
10 ml water
Purification: recrystallisation from CH_3COOH
Yield: 0.52 g (90 %), colorless solid
Transition temp.: Cr 198 [52.9] I
^{1}H-NMR: (DMSO-d6, *J*/Hz, 400 MHz) δ 8.23 (t, *J* = 7.1 Hz, 4H, Ar-H), 8.13 (d, *J* = 8.2 Hz, 2H, Ar-H), 8.09 (d, *J* = 8.5 Hz, 2H, Ar-H), 7.58 (t, *J* = 8.1 Hz, 1H, Ar-H), 7.51 (d, *J* = 8.4 Hz, 2H, Ar-H), 7.39 (s, 1H, Ar-H), 7.31 (d, *J* = 7.1 Hz, 2H, Ar-H), 7.11 (d, *J* = 8.6 Hz, 2H, Ar-H), 4.08 (t, *J* = 6.3 Hz, 2H, OCH_2), 1.79 – 1.68 (m, 2H, $OCH_2C\mathbf{H}_2$),), 1.47 – 1.36 (m, 2H, CH_2), 1.36 – 1.16 (m, 16H, CH_2), 0.84 (t, *J* = 6.1 Hz, 3H, CH_3).

4-({6-[4-(Benzyloxy)phenoxy]hexyl}oxy)phenyl 4-(hexyloxy)benzoate **i44(6,6)**

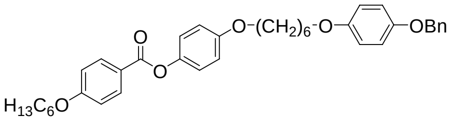

Formula:	$C_{38}H_{44}O_6$, M = 596.75 g/mol
Synthesis:	according to the general procedure 11.3.1 methode A
Reagents:	2.00 g (4.18 mmol) 4-[(6-bromohexyl)oxy]phenyl 4-(hexyloxy)benzoate **i12(6,6)** 0.49 g (2.46 mmol) 4-(benzyloxy)phenol 1.70 g (12.32 mmol) K_2CO_3 0.05 g KI 100 ml butan-2-one
Purification:	recrystallisation from EtOH/EtOAc (10/0.1)
Yield:	0.78 g (53 %), colorless solid
Transition temp.:	Cr 136 [65.4] (N 115 [5.8])I
^{1}H-NMR:	($CDCl_3$, *J*/Hz, 400 MHz) δ 8.11 (d, *J* = 8.9 Hz, 2H, Ar-H), 7.42 – 7.26 (m, 5H, Ar-H), 7.08 (d, *J* = 9.0 Hz, 2H, Ar-H), 6.94 (d, *J* = 8.9 Hz, 2H, Ar-H), 6.91 – 6.86 (m, 4H, Ar-H), 6.84 – 6.78 (m, 2H, Ar-H), 5.00 (s, 2H, OCH_2Ph), 4.02 (t, *J* = 6.6 Hz, 2H, OCH_2), 3.95 (t, *J* = 6.4 Hz, 2H, OCH_2), 3.91 (t, *J* = 6.5 Hz, 2H, OCH_2), 1.85 – 1.74 (m, 6H, $OCH_2C\mathbf{H}_2$), 1.56 – 1.42 (m, 6H, CH_2), 1.38 – 1.31 (m, 4H, CH_2), 0.90 (t, *J* = 7.0 Hz, 3H, CH_3).

4-{[6-(4-Hydroxyphenoxy)hexyl]oxy}phenyl 4-(hexyloxy)benzoate **i45(6,6)**

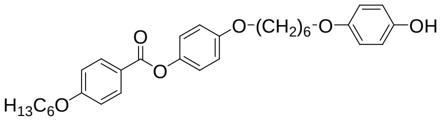

Formula:	$C_{31}H_{38}O_6$, M = 506.63 g/mol
Synthesis:	according to the general procedure 11.3.6 methode A
Reagents:	0.6 g (1.01 mmol) 4-({6-[4-(benzyloxy)phenoxy]hexyl}oxy)phenyl 4-(hexyloxy)benzoate **i44(6,6)** 0.06 g Pd/C 50 ml ethyl acetate
Purification:	recrystallisation from EtOH
Yield:	0.41 g (80 %), colorless solid
Transition temp.:	Cr 134 [54.0] I
^{1}H-NMR:	($CDCl_3$, *J*/Hz, 400 MHz) δ 8.11 (d, *J* = 9.0 Hz, 2H, Ar-H), 7.08 (d, *J* = 9.1 Hz, 2H, Ar-H), 6.94 (d, *J* = 9.0 Hz, 2H, Ar-H), 6.89 (d, *J* = 9.1 Hz, 2H, Ar-H), 6.75 (d, *J* = 9.1 Hz, 2H, Ar-H), 6.69 (d, *J* = 9.2 Hz, 2H, Ar-H), 4.02 (t, *J* = 6.6 Hz, 2H, OCH_2), 3.94 (t, *J* = 6.4 Hz, 2H, OCH_2), 3.91 (t, *J* = 6.4 Hz, 2H, OCH_2), 1.85 – 1.73 (m, 6H, $OCH_2C\mathbf{H}_2$), 1.57 – 1.43 (m, 6H, CH_2), 1.39 – 1.30 (m, 4H, CH_2), 0.91 (t, *J* = 7.1 Hz, 3H, CH_3).

4-(Benzyloxy)phenyl 4-cyanobenzoate **i46**

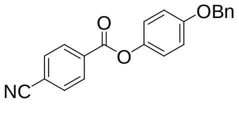

Formula:	$C_{21}H_{15}NO_3$, M = 329.35 g/mol
Synthesis:	according to the general procedure 11.3.3
Reagents:	12.50 g (84.95 mmol) 4-cyanobenzoic acid

17.01 g (84.95 mmol) 4-(benzyloxy)phenol
19.28 g (93.45 mmol) DCC
0.05 g DMAP
250 ml dichloromethane
Purification: recrystallisation fromEtOAc/EtOH
Yield: 24.20 g (86 %), colorless solid
Transition temp.: Cr 172 [43.7] I
^{1}H-NMR: ($CDCl_3$, *J*/Hz, 400 MHz) δ 8.27 (d, *J* = 8.2 Hz, 2H, Ar-H), 7.79 (d, *J* = 8.2 Hz, 2H, Ar-H), 7.45 – 7.29 (m, 5H, Ar-H), 7.12 (d, *J* = 8.9 Hz, 2H, Ar-H), 7.01 (d, *J* = 9.0 Hz, 2H, Ar-H), 5.07 (s, 2H, OCH_2Ph).

4-Hydroxyphenyl 4-cyanobenzoate **i47**

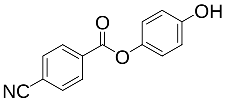

Formula: $C_{14}H_9NO_3$, M = 239.23 g/mol
Synthesis: according to the general procedure 11.3.6 methode A
Reagents: 22.00 g (66.79 mmol) 4-(benzyloxy)phenyl 4-cyanobenzoate **i46**
2.20 g Pd/C
250 ml THF
Purification: recrystallisation from EtOAc/EtOH (10/0.2)
Yield: 12.14 g (76 %), colorless solid
Transition temp.: Cr 158 [28.8] I
^{1}H-NMR: ($CDCl_3$, *J*/Hz, 400 MHz) δ 7.87 (d, *J* = 8.2 Hz, 2H, Ar-H), 7.12 (d, *J* = 8.0 Hz, 2H, Ar-H), 6.82 (d, *J* = 8.9 Hz, 2H, Ar-H), 6.69 (d, *J* = 8.9 Hz, 2H, Ar-H).

4-[(3-{[4-(Benzyloxy)phenyl]carbonyloxy}phenyl)carbonyloxy]phenyl 4-cyanobenzoate **i48**

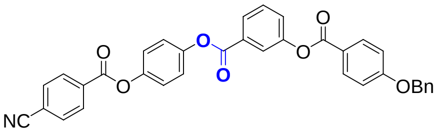

Formula: $C_{35}H_{23}NO_7$, M = 569.56 g/mol
Synthesis: according to the general procedure 11.3.3
Reagents: 0.73 g (2.09 mmol) 3-{[4-(benzyloxy)phenyl]carbonyloxy}benzoic acid **i35**
0.50 g (2.09 mmol) 4-hydroxyphenyl 4-cyanobenzoate **i47**
0.47 g (2.29 mmol) DCC
0.02 g DMAP
100 ml dichloromethane
Purification: recrystallisation from EtOAc/EtOH (10/0.2)
Yield: 0.67 g (56 %), colorless solid
Transition temp.: Cr 172 [54.3] I
^{1}H-NMR: ($CDCl_3$, *J*/Hz, 400 MHz) δ 8.16 (d, *J* = 8.9 Hz, 2H, Ar-H), 8.12 – 8.06 (m, 3H, Ar-H), 8.04 – 8.02 (m, 1H, Ar-H), 7.56 (t, *J* = 7.9 Hz, 1H, Ar-H), 7.51– 7.47 (m, 1H, Ar-H), 7.45 – 7.33 (m, 5H, Ar-H), 7.30 (d, *J* = 8.0 Hz, 2H, Ar-H), 7.26 (s, 4H, Ar-H), 7.06 (d, *J* = 8.9 Hz, 2H, Ar-H), 5.16 (s, 2H, OCH_2Ph).

4-({3-[(4-Hydroxyphenyl)carbonyloxy]phenyl}carbonyloxy)phenyl 4-cyanobenzoate **i49**

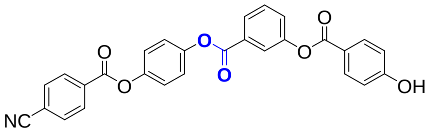

Formula: $C_{28}H_{17}NO_7$, M = 479.44 g/mol
Synthesis: according to the general procedure 11.3.6 methode A
Reagents: 0.60 g (1.05 mmol) 4-[(3-{[4-(benzyloxy)phenyl]carbonyloxy}phenyl)carbonyloxy]phenyl 4-cyanobenzoate **i48**
0.06 g Pd/C
100 ml THF
Purification: recrystallisation from EtOAc/EtOH (10/0.2)
Yield: 0.41g (82 %), colorless solid
Transition temp.: Cr 222 [49.8] I
^{1}H-NMR: (DMSO, *J*/Hz, 400 MHz) δ 8.02 – 7.91 (m, 6H, Ar-H), 7.50 (t, *J* = 7.9 Hz, 1H, Ar-H), 7.44 – 7.40 (m, 1H, Ar-H), 7.24 (d, *J* = 8.0 Hz, 2H, Ar-H), 7.19 (s, 4H, Ar-H), 6.85 (d, *J* = 8.8 Hz, 2H, Ar-H).

3-Chloro-4-(dodecyloxy)benzoic acid **i50**

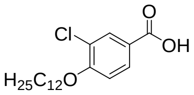

Formula: $C_{19}H_{29}ClO_3$, M = 340.88 g/mol
Synthesis: according to the general procedure 11.3.1 methode C
Reagents: 10.00 g (57.94 mmol) 3-chloro-4-hydroxybenzoic acid
15.88 g (63.73 mmol) 1-dodecylbromide
6.50 g (115.88 mmol) KOH
0.02 g KI
200 ml ethanol
Purification: recrystallisation from EtOH
Yield: 11.26 g (57 %), colorless solid
Transition temp.: Cr 106 [19.7] (SmC 85 [2.4] N 88 [0.9]) I
^{1}H-NMR: ($CDCl_3$, *J*/Hz, 400 MHz) δ 8.10 (d, *J* = 2.1 Hz, 1H, Ar-H), 7.96 (dd, *J* = 8.6, 2.1 Hz, 1H, Ar-H), 6.93 (d, *J* = 8.7 Hz, 1H, Ar-H), 4.09 (t, *J* = 6.5 Hz, 2H, OCH_2), 1.90 – 1.81 (m, 2H, $OCH_2C\mathbf{H}_2$), 1.53 – 1.44 (m, 2H, CH_2), 1.40 – 1.19 (m, 16H, CH_2), 0.87 (t, *J* = 6.8 Hz, 3H, CH_3).

4-[(Benzyloxy)carbonyl]phenyl 3-chloro-4-(dodecyloxy)benzoate **i51**

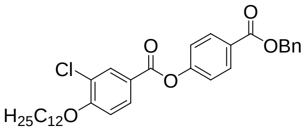

Formula: $C_{33}H_{39}ClO_5$, M = 551.11 g/mol
Synthesis: according to the general procedure 11.3.3
Reagents: 10.00 g (29.33 mmol) 3-chloro-4-(dodecyloxy)benzoic acid **i50**
6.76 g (29.62 mmol) benzyl 4-hydroxybenzoate
6.65 g (32.26 mmol) DCC
0.02 g DMAP

200 ml dichloromethane
Purification: recrystallisation from EtOH/EtOAc (10/0.1)
Yield: 12.37g (66 %), colorless solid
Transition temp.: Cr 71 [44.0] I
^{1}H-NMR: ($CDCl_3$, *J*/Hz, 400 MHz) δ 8.20 (d, *J* = 2.1 Hz, 1H, Ar-H), 8.16 (d, *J* = 8.8 Hz, 2H, Ar-H), 8.06 (dd, *J* = 8.7, 2.2 Hz, 1H, Ar-H), 7.48 – 7.32 (m, 5H, Ar-H), 7.29 (d, *J* = 8.8 Hz, 2H, Ar-H), 7.01 – 6.97 (m, 1H, Ar-H), 5.38 (s, 2H, OCH_2Ph), 4.12 (t, *J* = 6.5 Hz, 2H, OCH_2), 1.93 – 1.84 (m, 2H, $OCH_2C\mathbf{H_2}$), 1.56 – 1.47 (m, 2H, CH_2), 1.42 – 1.23 (m, 16H, CH_2), 0.89 (t, *J* = 6.8 Hz, 3H, CH_3).

4-{[3-Chloro-4-(dodecyloxy)phenyl]carbonyloxy}benzoic acid **i52**

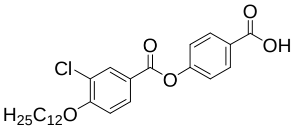

Formula: $C_{26}H_{33}ClO_5$, M = 460.99 g/mol
Synthesis: according to the general procedure 11.3.6 methode A
Reagents: 10.00 g (18.15 mmol) 4-[(benzyloxy)carbonyl]phenyl 3-chloro-4-(dodecyloxy)benzoate **i51**
1.00 g Pd/C
200 ml ethyl acetate
Purification: recrystallisation from CH_3COOH
Yield: 6.59 g (79 %), colorless solid
Transition temp.: Cr 96 [9.2] Sm 153 [7.4] N 208 I
^{1}H-NMR: ($CDCl_3$, *J*/Hz, 400 MHz) δ 8.20 (d, *J* = 2.1 Hz, 1H, Ar-H), 8.18 (d, *J* = 8.7 Hz, 2H, Ar-H), 8.06 (dd, *J* = 8.6, 2.2 Hz, 1H, Ar-H), 7.33 (d, *J* = 8.7 Hz, 2H, Ar-H), 6.99 (d, *J* = 8.8 Hz, 1H, Ar-H), 4.12 (t, *J* = 6.5 Hz, 2H, OCH_2), 1.91 – 1.84 (m, 2H, $OCH_2C\mathbf{H_2}$), 1.55 – 1.48 (m, 2H, CH_2), 1.42 – 1.35 (m, 2H, CH_2), 1.35 – 1.24 (m, 14H, CH_2), 0.88 (t, *J* = 6.9 Hz, 3H, CH_3).

4-[3-(Benzyloxy)phenoxycarbonyl]phenyl 3-chloro-4-(dodecyloxy)benzoate **i53**

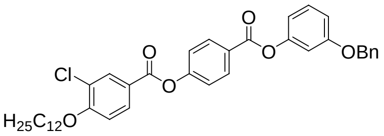

Formula: $C_{39}H_{43}ClO_6$, M = 643.21 g/mol
Synthesis: according to the general procedure 11.3.3
Reagents: 20 g (43.38 mmol) 4-{[3-chloro-4-(dodecyloxy)phenyl]carbonyloxy}benzoic acid **i52**
8.69 g (43.38 mmol) 3-(benzyloxy)phenol **i5**
9.85 g (47.72 mmol) DCC
0.05 g DMAP
200 ml dichloromethane
Purification: column chromatography, eluent: $CHCl_3$/EtOAc (10/0.2) and further recrystallisation from EtOH/EtOAc (10/0.2)
Yield: 18.69 g (67 %), colorless solid
Transition temp.: Cr 80 [35.8] I
^{1}H-NMR: ($CDCl_3$, *J*/Hz, 400 MHz) δ 8.26 (d, *J* = 8.9 Hz, 2H, Ar-H), 8.22 (d, *J* = 2.2 Hz, 1H, Ar-H), 8.07 (dd, *J* = 8.6, 2.2 Hz, 1H, Ar-H), 7.45 – 7.29 (m, 8H, Ar-H), 6.99 (d, *J* = 8.8 Hz, 1H, Ar-H), 6.92 – 6.87 (m, 2H, Ar-H), 6.86 – 6.82 (m, 1H, Ar-H), 5.07 (s, 2H, OCH_2Ph), 4.12 (t, *J* = 6.5 Hz, 2H, OCH_2), 1.93 – 1.84 (m, 2H, $OCH_2C\mathbf{H_2}$), 1.56 – 1.47 (m, 2H, CH_2), 1.43 – 1.22 (m, 16H, CH_2), 0.89 (t, *J* = 6.9 Hz, 3H, CH_3).

4-(3-Hydroxyphenoxycarbonyl)phenyl 3-chloro-4-(dodecyloxy)benzoate **i54**

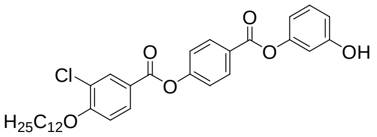

Formula:	$C_{32}H_{37}ClO_6$, M = 553.09 g/mol
Synthesis:	according to the general procedure 11.3.6 methode A
Reagents:	18.00 g (27.98 mmol) 4-[3-(benzyloxy)phenoxycarbonyl]phenyl 3-chloro-4-(dodecyloxy)-benzoate **i53** 1.8 g Pd/C 250 ml ethyl acetate
Purification:	recrystallisation from EtOH
Yield:	12.69 g (82 %), colorless solid
Transition temp.:	Cr 119 [31.7] I
^{1}H-NMR:	($CDCl_3$, *J*/Hz, 400 MHz) δ 8.24 (d, *J* = 8.8 Hz, 2H, Ar-H), 8.20 (d, *J* = 2.1 Hz, 1H, Ar-H), 8.06 (dd, *J* = 8.7, 2.2 Hz, 1H, Ar-H), 7.34 (d, *J* = 8.8 Hz, 2H, Ar-H), 7.24 (t, *J* = 8.5 Hz, 1H, Ar-H), 6.98 (d, *J* = 8.7 Hz, 1H, Ar-H), 6.78 – 6.74 (m, 1H, Ar-H), 6.71 – 6.66 (m, 2H, Ar-H), 4.11 (t, *J* = 6.5 Hz, 2H, OCH_2), 1.92 – 1.83 (m, 2H, $OCH_2C\mathbf{H}_2$), 1.55 – 1.45 (m, 2H, CH_2), 1.41 – 1.21 (m, 16H, CH_2), 0.87 (t, *J* = 6.8 Hz, 3H, CH_3).

4-(3-{[4-(Benzyloxy)phenyl]carbonyloxy}phenoxycarbonyl)phenyl 3-chloro-4-(dodecyloxy)-benzoate **i55**

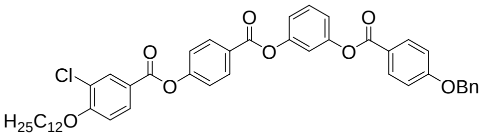

Formula:	$C_{46}H_{47}ClO_8$, M = 763.31 g/mol
Synthesis:	according to the general procedure 11.3.3
Reagents:	5.70 g (10.31 mmol) 4-(3-hydroxyphenoxycarbonyl)phenyl 3-chloro-4-(dodecyloxy)benzoate **i54** 2.35 g (10.31 mmol) 4-(benzyloxy)benzoic acid 2.34 g (11.30 mmol) DCC 0.02 g DMAP 100 ml dichloromethane
Purification:	recrystallisation from EtOAc/EtOH (10/0.2)
Yield:	5.35 g (68 %), colorless solid
Transition temp.:	Cr 99 [30.1] I
^{1}H-NMR:	($CDCl_3$, *J*/Hz, 400 MHz) δ 8.26 (d, *J* = 8.8 Hz, 2H, Ar-H), 8.21 (d, *J* = 2.1 Hz, 1H, Ar-H), 8.14 (d, *J* = 8.9 Hz, 2H, Ar-H), 8.07 (dd, *J* = 8.7, 2.2 Hz, 1H, Ar-H), 7.49 – 7.32 (m, 8H, Ar-H), 7.19 – 7.13 (m, 3H, Ar-H), 7.05 (d, *J* = 8.9 Hz, 2H, Ar-H), 6.99 (d, *J* = 8.8 Hz, 1H, Ar-H), 5.15 (s, 2H, OCH_2Ph), 4.12 (t, *J* = 6.5 Hz, 2H, OCH_2), 1.92 – 1.83 (m, 2H, $OCH_2C\mathbf{H}_2$), 1.55 – 1.45 (m, 2H, CH_2), 1.41 – 1.24 (m, 16H, CH_2), 0.88 (t, *J* = 6.8 Hz, 3H, CH_3).

4-{3-[(4-Hydroxyphenyl)carbonyloxy]phenoxycarbonyl}phenyl 3-chloro-4-(dodecyloxy)-benzoate **i56**

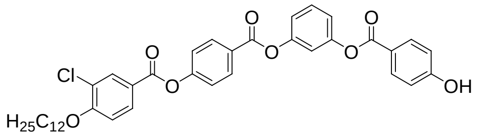

Formula:	$C_{39}H_{41}ClO_8$, M = 673.19 g/mol
Synthesis:	according to the general procedure 11.3.6 methode A
Reagents:	5.00 g (6.55 mmol) 4-(3-{[4-(benzyloxy)phenyl]carbonyloxy}phenoxycarbonyl)phenyl 3-chloro-4-(dodecyloxy)benzoate **i55** 0.5 g Pd/C 100 ml THF
Purification:	recrystallisation from EtOH
Yield:	3.75 g (85 %), colorless solid
Transition temp.:	Cr 186 [59.5] I
^{1}H-NMR:	(DMSO-d6, *J*/Hz, 400 MHz) δ 8.22 (dd, *J* = 8.9, 2.5 Hz, 2H, Ar-H), 8.13 (d, *J* = 2.2 Hz, 1H, Ar-H), 8.09 (d, *J* = 9.0 Hz, 2H, Ar-H), 7.99 (d, *J* = 8.8 Hz, 1H, Ar-H), 7.58 – 7.49 (m, 2H, Ar-H), 7.34 (d, *J* = 8.8 Hz, 1H, Ar-H), 7.30 (t, *J* = 2.2 Hz, 1H, Ar-H), 7.28 – 7.20 (m, 2H, Ar-H), 7.11 (d, *J* = 9.0 Hz, 1H, Ar-H), 6.93 (d, *J* = 8.8 Hz, 2H, Ar-H), 4.19 (t, *J* = 6.4 Hz, 2H, OCH$_2$), 1.82 – 1.69 (m, 2H, OCH$_2$C**H**$_2$), 1.49 – 1.37 (m, 2H, CH$_2$), 1.36 – 1.18 (m, 16H, CH$_2$), 0.84 (t, *J* = 6.8 Hz, 3H, CH$_3$).

4-(Carbonochloridoyl)phenyl 4-(dodecyloxy)benzoate **i57**

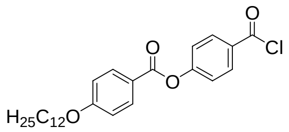

Formula:	$C_{26}H_{33}ClO_4$, M = 444.99 g/mol
Synthesis:	according to the general procedure 11.3.4 methode B
Reagents:	1.03 g (2.41mmol) 4-{[4-(dodecyloxy)phenyl]carbonyloxy}benzoic acid **i3** 3.59 ml (48.33 mmol) SOCl$_2$ 40 ml dicloromethane
Purification:	The crude compound **i57** was then used into the next reaction without further purification.

4-(3-Hydroxy-2-methylphenoxycarbonyl)phenyl 4-(dodecyloxy)benzoate **i58**

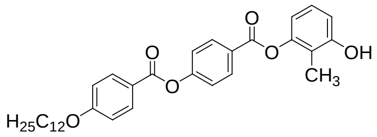

Formula:	$C_{33}H_{40}O_6$, M = 532.67 g/mol
Synthesis:	according to the general procedure 11.3.4 methode B
Reagents:	~ 1.00 g (~2.41mmol) 4-(carbonochloridoyl)phenyl 4-(dodecyloxy)benzoate **i57** (the crude product was used without further purification) 1.50 g (12.08 mmol) 2-methylresorcinol 10 ml pyridine 20 ml toluene
Purification:	column chromatography, eluent: CH$_2$Cl$_2$/MeOH (10/0.1) and further recrystallisation from EtOH/EtOAc (10/0.1)
Yield:	0.71g (55 %), colorless solid

Transition temp.:	Cr 123 [31.7] (N 101 [0.8]) I
^{1}H-NMR:	($CDCl_3$, *J*/Hz, 400 MHz) δ 8.28 (d, *J* = 8.8 Hz, 2H, Ar-H), 8.14 (d, *J* = 8.9 Hz, 2H, Ar-H), 7.35 (d, *J* = 8.6 Hz, 2H, Ar-H), 7.08 (t, *J* = 8.1 Hz, 1H, Ar-H), 6.97 (d, *J* = 8.9 Hz, 2H, Ar-H), 6.73 (d, *J* = 8.0 Hz, 1H, Ar-H), 6.67 (d, *J* = 7.8 Hz, 1H, Ar-H), 4.03 (t, *J* = 6.6 Hz, 2H, OCH_2), 2.09 (s, *J* = 2.7 Hz, 3H, $PhCH_3$), 1.86 – 1.76 (m, 2H, $OCH_2C\mathbf{H}_2$), 1.51 – 1.41 (m, 2H, CH_2), 1.39 – 1.20 (m, 16H, CH_2), 0.86 (t, *J* = 6.8 Hz, 3H, CH_3).

4-(3-{[4-(Benzyloxy)phenyl]carbonyloxy}-2-methylphenoxycarbonyl)phenyl 4-(dodecyloxy)-benzoate **i59**

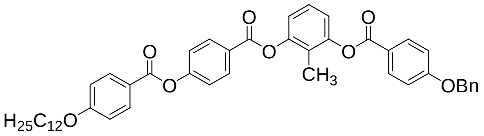

Formula:	$C_{47}H_{50}O_8$, M = 742.90 g/mol
Synthesis:	according to the general procedure 11.3.3
Reagents:	0.40 g (0.75 mmol) 4-(3-hydroxy-2-methylphenoxycarbonyl)phenyl 4-(dodecyloxy)benzoate **i58** 0.17 g (0.75 mmol) 4-(benzyloxy)benzoic acid 0.17 g (0.83 mmol) DCC 0.02 g DMAP 30 ml dichloromethane
Purification:	recrystallisation from EtOAc/EtOH (10/0.1)
Yield:	0.41 g (74 %), colorless solid
Transition temp.:	Cr 109 [37.2] I
^{1}H-NMR:	($CDCl_3$, *J*/Hz, 400 MHz) δ 8.30 (d, *J* = 8.8 Hz, 2H, Ar-H), 8.20 – 8.13 (m, 4H, Ar-H), 7.48 – 7.35 (m, 7H, Ar-H), 7.34 – 7.29 (m, 1H, Ar-H), 7.12 (d, *J* = 8.1 Hz, 2H, Ar-H), 7.08 (d, *J* = 8.9 Hz, 2H, Ar-H), 6.99 (d, *J* = 8.9 Hz, 2H, Ar-H), 5.17 (s, 2H), 4.06 (t, *J* = 6.6 Hz, 2H, OCH_2), 2.11 (s, 3H, $PhCH_3$), 1.87 – 1.78 (m, 2H, $OCH_2C\mathbf{H}_2$), 1.51 – 1.43 (m, 2H, CH_2), 1.42 – 1.24 (m, 16H, CH_2), 0.89 (t, *J* = 6.8 Hz, 3H, CH_3).

4-{3-[(4-Hydroxyphenyl)carbonyloxy]-2-methylphenoxycarbonyl}phenyl 4-(dodecyloxy)-benzoate **i60**

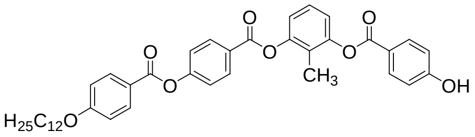

Formula:	$C_{40}H_{44}O_8$, M = 652.77 g/mol
Synthesis:	according to the general procedure 11.3.6 methode A
Reagents:	0.40 g (0.54 mmol) 4-(3-{[4-(benzyloxy)phenyl]carbonyloxy}-2-methylphenoxycarbonyl)-phenyl 4-(dodecyloxy)benzoate **i59** 0.04 g Pd/C 30 ml THF
Purification:	recrystallisation from EtOAc/EtOH (10/0.1)
Yield:	0.29 g (84 %), colorless solid
Transition temp.:	Cr 205 [40.9] I
^{1}H-NMR:	(DMSO-d6, *J*/Hz, 400 MHz) δ 8.26 (d, *J* = 8.5 Hz, 2H, Ar-H), 8.09 (d, *J* = 8.6 Hz, 2H, Ar-H), 8.02 (d, *J* = 8.7 Hz, 2H, Ar-H), 7.53 (d, *J* = 8.5 Hz, 2H, Ar-H), 7.37 (t, *J* = 8.0 Hz, 1H, Ar-H), 7.23 (d, *J* = 8.1 Hz, 1H, Ar-H), 7.19 (d, *J* = 8.2 Hz, 1H, Ar-H), 7.12 (d, *J* = 8.7 Hz, 2H, Ar-H), 6.94 (d, *J* = 8.5 Hz, 2H, Ar-H), 4.09 (t, *J* = 6.2 Hz, 2H, OCH_2) , 2.00 (s, 3H, $PhCH_3$), 1.79 –

1.68 (m, 2H, CH_2), 1.48 – 1.36 (m, 2H, CH_2), 1.36 – 1.15 (m, 16H, CH_2), 1.89 – 1.79 (m, 3H, CH_3).

4-{4-[(Benzyloxy)carbonyl]phenoxycarbonyl}phenyl 4-(dodecyloxy)benzoate **i61**

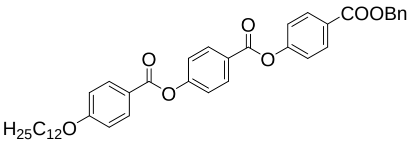

Formula:	$C_{40}H_{44}O_7$, M = 636.77 g/mol
Synthesis:	according to the general procedure 11.3.3
Reagents:	2.07 g (4.85 mmol) 4-{[4-(dodecyloxy)phenyl]carbonyloxy}benzoic acid **i3(12)** 1.11 g (4.85 mmol) benzyl 4-hydroxybenzoate 1.20 g (5.81 mmol) DCC 0.05 g DMAP 50 ml dichloromethane
Purification:	recrystallisation from DMF/EtOH (10/0.1)
Yield:	2.83 g (92 %), colorless solid
Transition temp.:	Cr 100 [50.1] (SmC 106) SmA 138 [5.2] I
^{1}H-NMR:	($CDCl_3$, *J*/Hz, 400 MHz) δ 8.25 (d, *J* = 8.6 Hz, 2H, Ar-H), 8.17 – 8.10 (m, 4H, Ar-H), 7.46 – 7.27 (m, 9H, Ar-H), 6.97 (d, *J* = 8.7 Hz, 2H, Ar-H), 5.36 (s, 2H, $COOCH_2$), 4.04 (t, *J* = 6.5 Hz, 2H, OCH_2), 1.85 – 1.76 (m, 2H, $OCH_2C\mathbf{H}_2$), 1.50 – 1.41 (m, 2H, CH_2), 1.26 (s, 16H, CH_2), 0.87 (t, *J* = 6.8 Hz, 3H, CH_3).

4-[(4-{[4-(Dodecyloxy)phenyl]carbonyloxy}phenyl)carbonyloxy]benzoic acid **i62**

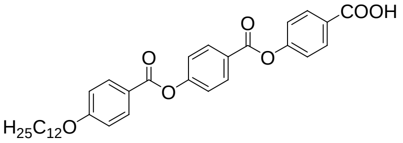

Formula:	$C_{33}H_{38}O_7$, M = 546.65 g/mol
Synthesis:	according to the general procedure 11.3.6 methode A
Reagents:	2.80 g (4.39 mmol) 4-{4-[(benzyloxy)carbonyl]phenoxycarbonyl}phenyl 4-(dodecyloxy)-benzoate **i61** 0.28 g Pd/C 50 ml THF
Purification:	recrystallisation from CH_3COOH
Yield:	2.08 g (87 %), colorless solid
Transition temp.:	Cr 186 [28.0] N 270 [7.1] N 288 [15.7] I
^{1}H-NMR:	($CDCl_3$, *J*/Hz, 400 MHz) δ 8.27 (d, *J* = 8.3 Hz, 2H, Ar-H), 8.18 (d, *J* = 8.4 Hz, 2H, Ar-H), 8.13 (d, *J* = 8.8 Hz, 2H, Ar-H), 7.41 – 7.31 (m, 4H, Ar-H), 6.97 (d, *J* = 8.3 Hz, 2H, Ar-H), 4.04 (t, *J* = 6.3 Hz, 2H, OCH_2), 1.87 – 1.75 (m, 2H, $OCH_2C\mathbf{H}_2$), 1.51 – 1.41 (m, 2H, CH_2), 1.39 – 1.18 (m, 16H, CH_2), 0.87 (t, *J* = 6.6 Hz, 3H, CH_3).

4-{4-[3-(Benzyloxy)phenoxycarbonyl]phenoxycarbonyl}phenyl 4-(dodecyloxy)benzoate **i63**

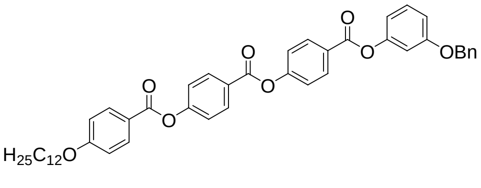

Formula:	$C_{46}H_{48}O_8$, M = 728.87 g/mol
Synthesis:	according to the general procedure 11.3.3
Reagents:	2.00 g (3.66 mmol) 4-[(4-{[4-(dodecyloxy)phenyl]carbonyloxy}phenyl)carbonyloxy]benzoic acid **i62** 0.73 g (3.66 mmol) 3-(benzyloxy)phenol 0.83 g (4.03 mmol) DCC 0.03 g DMAP 250 ml dichloromethane
Purification:	recrystallisation from EtOAc/EtOH (10/0.1)
Yield:	2.11 g (79 %), colorless solid
Transition temp.:	Cr 133 [48.7] SmA 158 [0.8] N 162 [0.6] I
^{1}H-NMR:	(DMSO, *J*/Hz, 400 MHz) δ 8.28 – 8.22 (m, 4H, Ar-H), 8.10 (d, *J* = 8.7 Hz, 2H, Ar-H), 7.44 – 7.28 (m, 10H, Ar-H), 6.99 (d, *J* = 8.5 Hz, 2H, Ar-H), 6.92 – 6.79 (m, 3H, Ar-H), 5.07 (s, 2H, OCH_2Ph), 4.05 (t, *J* = 6.5 Hz, 2H, OCH_2), 1.84 – 1.76 (m, 2H, $OCH_2C\mathbf{H_2}$), 1.51 – 1.41 (m, 2H, CH_2), 1.39 – 1.20 (m, 16H, CH_2), 0.86 (t, *J* = 6.6 Hz, 3H, CH_3).

4-[4-(3-Hydroxyphenoxycarbonyl)phenoxycarbonyl]phenyl 4-(dodecyloxy)benzoate **i64**

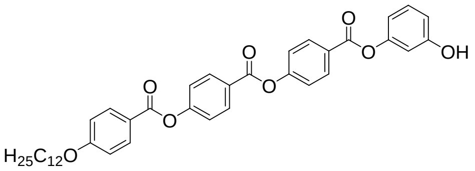

Formula:	$C_{39}H_{42}O_8$, M = 638.75 g/mol
Synthesis:	according to the general procedure 11.3.6 methode A
Reagents:	2.00 g (2.74 mmol) 4-{4-[3-benzyloxy)phenoxycarbonyl]phenoxycarbonyl}phenyl 4-(dodecyloxy)benzoate **i63** 0.2 g Pd/C 350 ml THF
Purification:	recrystallisation from EtOAc
Yield:	1.42 g (81 %), colorless solid
Transition temp.:	Cr 135 [13.5] SmA 195 [0.3] N 224 [0.5] I
^{1}H-NMR:	($CDCl_3$, *J*/Hz, 400 MHz) δ 8.30 – 8.23 (m, 4H, Ar-H), 8.14 (d, *J* = 8.8 Hz, 2H, Ar-H), 7.37 (dd, *J* = 8.8, 2.4 Hz, 4H, Ar-H), 7.26 (t, *J* = 7.4 Hz, 1H, Ar-H), 6.97 (d, *J* = 8.9 Hz, 2H, Ar-H), 6.78 (d, *J* = 8.2 Hz, 1H, Ar-H), 6.74 – 6.69 (m, 2H, Ar-H), 4.04 (t, *J* = 6.5 Hz, 2H, OCH_2), 1.87 – 1.77 (m, 2H, $OCH_2C\mathbf{H_2}$), 1.51 – 1.42 (m, 2H, CH_2), 1.40 – 1.20 (m, 16H, CH_2), 0.87 (t, *J* = 6.8 Hz, 3H, CH_3).

4-[4-(3-{[4-(Benzyloxy)phenyl]carbonyloxy}phenoxycarbonyl)phenoxycarbonyl]phenyl 4-(dodecyloxy)benzoate **i65**

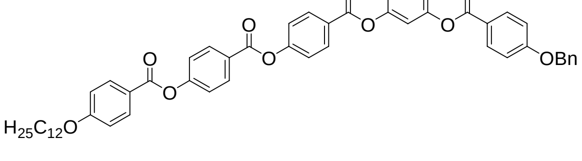

Formula:	$C_{53}H_{52}O_{10}$, M = 848.97 g/mol
Synthesis:	according to the general procedure 11.3.3
Reagents:	0.50 g (0.78 mmol) 4-[4-(3-ydroxyphenoxycarbonyl)phenoxycarbonyl]phenyl 4-(dodecyloxy)-benzoate **i64** 0.17 g (0.78 mmol) 4-(benzyloxy)benzoic acid 0.17 g (0.86 mmol) DCC

0.02 g DMAP
100 ml dichloromethane
Purification: column chromatography, eluent: $CHCl_3$/EtOAc (10/0.2 – 10/0.5) and further recrystallisation from EtOAc/EtOH (10/0.1)
Yield: 0.49 g (75 %), colorless solid
Transition temp.: Cr 148 [62.5] I
^{1}H-NMR: ($CDCl_3$, *J*/Hz, 400 MHz) δ 8.27 (d, *J* = 8.5 Hz, 4H, Ar-H), 8.14 (d, *J* = 8.9 Hz, 4H, Ar-H), 7.49 – 7.31 (m, 10H, Ar-H), 7.15 (d, *J* = 8.5 Hz, 3H, Ar-H), 7.05 (d, *J* = 8.9 Hz, 2H, Ar-H), 6.97 (d, *J* = 8.8 Hz, 2H, Ar-H), 5.15 (s, 2H, OCH_2Ph), 4.04 (t, *J* = 6.5 Hz, 2H, OCH_2), 1.86 – 1.77 (m, 2H, $OCH_2C\mathbf{H}_2$), 1.51 – 1.42 (m, 2H, CH_2), 1.40 – 1.22 (m, 16H, CH_2), 0.87 (t, *J* = 6.8 Hz, 3H, CH_3).

4-(4-{3-[(4-Hydroxyphenyl)carbonyloxy]phenoxycarbonyl}phenoxycarbonyl)phenyl 4-(dodecyloxy)benzoate **i66**

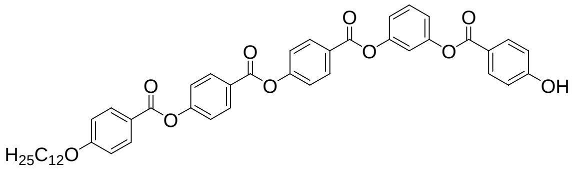

Formula: $C_{46}H_{46}O_{10}$, M = 758.85 g/mol
Synthesis: according to the general procedure 11.3.6 methode A
Reagents: 0.45 g (0.53 mmol) 4-[4-(3-{[4-(benzyloxy)phenyl]carbonyloxy}phenoxycarbonyl)phenoxycarbonyl]phenyl 4-(dodecyloxy)benzoate
i65
0.05 g Pd/C
200 ml THF
Purification: recrystallisation from EtOAc/EtOH (10/0.1)
Yield: 0.33 g (83 %), colorless solid
Transition temp.: Cr 208 [52.7] I
^{1}H-NMR: ($CDCl_3$, *J*/Hz, 400 MHz) δ 8.27 (d, *J* = 8.7 Hz, 4H, Ar-H), 8.14 (d, *J* = 8.9 Hz, 2H, Ar-H), 8.11 (d, *J* = 8.8 Hz, 2H, Ar-H), 7.46 (t, *J* = 8.2 Hz, 1H, Ar-H), 7.39 (d, *J* = 8.7 Hz, 4H, Ar-H), 7.20 – 7.13 (m, 3H, Ar-H), 6.98 (d, *J* = 8.9 Hz, 2H, Ar-H), 6.91 (d, *J* = 8.9 Hz, 2H, Ar-H), 4.05 (t, *J* = 6.6 Hz, 2H, OCH_2), 1.86 – 1.79 (m, 2H, $OCH_2C\mathbf{H}_2$), 1.51 – 1.42 (m, 2H, CH_2), 1.41 – 1.24 (m, 16H), 0.88 (t, *J* = 7.0 Hz, 3H, CH_3).

Benzyl 4-formylbenzoate **i67**

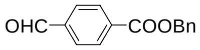

Formula: $C_{15}H_{12}O_3$, M = 240.25 g/mol
Synthesis: according to the general procedure 11.3.1 methode A
Reagents: 10.00 g (66.60 mmol) 4-formylbenzoic acid
12.9 g (73.26 mmol) K_2CO_3
11.96 g (69.93 mmol) benzyl bromide
0.05 g KI
100 ml DMF
Purification: The crude product was used without further purification
Yield: 13.60 g (85 %), colorless solid

4-[(Benzyloxy)carbonyl]benzoic acid **i68**

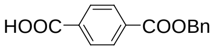

Formula:	$C_{15}H_{12}O_4$, M = 256.25 g/mol
Synthesis:	according to the general procedure 11.3.5
Reagents:	12.00 g (49.95 mmol) benzyl 4-formylbenzoate **i67**
	7.15 g (64.93 mmol) resorcinol
	25.97 g (287.21 mmol) $NaClO_2$
	23.37 g (149.85 mmol) $NaH_2PO_4 \cdot 2H_2O$
	100 ml THF
Purification:	recrystallisation from CH_3COOH
Yield:	11.93 g (93 %), colorless solid
Transition temp.:	Cr 183 [13.0] I
^{1}H-NMR:	($CDCl_3$, *J*/Hz, 400 MHz) δ 8.15 (s, 4H, Ar-H), 7.47 – 7.42 (m, 2H, Ar-H), 7.42 – 7.31 (m, 3H, Ar-H), 5.38 (s, 2H, OCH_2Ph).

1-Benzyl 4-(4-{3-[(4-{[4-(dodecyloxy)phenyl]carbonyloxy}phenyl)carbonyloxy]-phenoxycarbonyl}phenyl) benzene-1,4-dicarboxylate **i69**

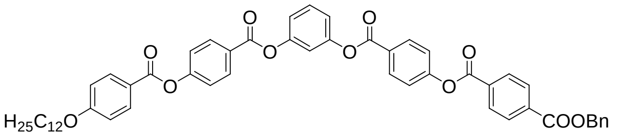

Formula:	$C_{54}H_{52}O_{11}$, M = 876.98 g/mol
Synthesis:	according to the general procedure 11.3.3
Reagents:	7.00 g (12.66 mmol) 4-{3-[(4-ydroxyphenyl)carbonyloxy]phenoxycarbonyl}phenyl 4-(dodecyloxy)benzoate **i9(12)**
	2.81 g (12.66 mmol) 4-[(benzyloxy)carbonyl]benzoic acid **i68**
	2.48 g (12.05 mmol) DCC
	0.02 g DMAP
	50 ml dichloromethane
Purification:	recrystallisation from DMF/EtOH (10/0.1) and EtOAc/EtOH (10/0.1)
Yield:	6.44 g (67 %), colorless solid
Transition temp.:	Cr 124 [36.6] I
^{1}H-NMR:	($CDCl_3$, *J*/Hz, 400 MHz) δ 8.33 – 8.26 (m, *J* = 9.0 Hz, 6H, Ar-H), 8.22 (d, *J* = 8.5 Hz, 2H, Ar-H), 8.15 (d, *J* = 8.9 Hz, 2H, Ar-H), 7.54 – 7.46 (m, 3H, Ar-H), 7.46 – 7.35 (m, 7H, Ar-H), 7.23 – 7.17 (m, 3H, Ar-H), 6.99 (d, *J* = 8.9 Hz, 2H, Ar-H), 5.42 (s, 2H, OCH_2Ph), 4.06 (t, *J* = 6.6 Hz, 2H, OCH_2), 1.88 – 1.78 (m, 2H, $OCH_2C\mathbf{H}_2$), 1.53 – 1.44 (m, 2H, CH_2), 1.42 – 1.23 (m, 16H, CH_2), 0.89 (t, *J* = 6.8 Hz, 3H, CH_3).

4-(4-{3-[(4-{[4-(Dodecyloxy)phenyl]carbonyloxy}phenyl)carbonyloxy]phenoxycarbonyl}-phenoxycarbonyl)benzoic acid **i70**

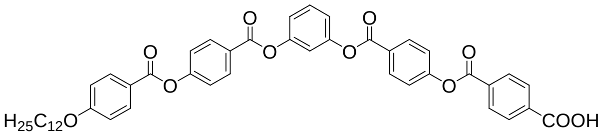

Formula:	$C_{47}H_{46}O_{11}$, M = 786.86 g/mol
Synthesis:	according to the general procedure 11.3.6 methode A

Reagents: 6.20 g (7.07 mmol) 1-benzyl 4-(4-{3-[(4-{[4-(dodecyloxy)phenyl]carbonyloxy}phenyl)-carbonyloxy]phenoxycarbonyl}phenyl)benzene-1,4-dicarboxylate **i69**
0.62 g Pd/C
300 ml THF

Purification: recrystallisation from CH_3COOH

Yield: 3.78 g (68 %), colorless solid

Transition temp.: Cr 221 [45.3] I

^{1}H-NMR: ($CDCl_3$, *J*/Hz, 400 MHz) δ 8.33 – 8.26 (m, 6H, Ar-H), 8.20 (d, *J* = 8.2 Hz, 2H, Ar-H), 8.15 (d, *J* = 8.5 Hz, 2H, Ar-H), 7.55 (t, *J* = 8.0 Hz, 1H, Ar-H), 7.47 (d, *J* = 8.4 Hz, 2H, Ar-H), 7.42 (d, *J* = 8.4 Hz, 2H, Ar-H), 7.23 (d, *J* = 8.4 Hz, 3H, Ar-H), 7.03 (d, *J* = 8.6 Hz, 2H, Ar-H), 4.09 (t, *J* = 6.4 Hz, 2H, OCH_2), 1.90 – 1.79 (m, 2H, $OCH_2C\mathbf{H}_2$), 1.56 – 1.46 (m, 2H, CH_2), 1.45 – 1.25 (m, 16H, CH_2), 0.90 (t, *J* = 6.5 Hz, 3H, CH_3).

Methyl 3,5-bis(benzyloxy)benzoate **i71**

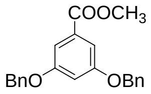

Formula: $C_{22}H_{20}O_4$, M = 348.39 g/mol

Synthesis: according to the general procedure 11.3.1 methode A

Reagents: 1.5 g (8.92 mmol) methyl 3,5-dihydroxybenzoate
4.58 g (27.00 mmol) benzylbromide
6.17 g (44.00 mmol) K_2CO_3
0.02 g Bu_4NI
50 ml butan-2-one

Purification: recrystallisation from EtOAc/EtOH (10/0.1)

Yield: 1.61 g (52 %), colorless solid

Transition temp.: Cr 69 [28.8] I

^{1}H-NMR: ($CDCl_3$, *J*/Hz, 400 MHz) δ 7.44 – 7.31 (m, 10H, Ar-H), 7.30 (d, *J* = 2.4 Hz, 2H, Ar-H), 6.80 (t, *J* = 2.4 Hz, 1H, Ar-H), 5.06 (s, 4H, OCH_2Ph), 3.90 (s, 3H, OCH_3).

3,5-Bis(benzyloxy)benzoic acid **i72**

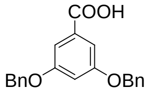

Formula: $C_{21}H_{18}O_4$, M = 334.37 g/mol

Synthesis: according to the general procedure 11.3.7

Reagents: 1.50 g (4.31 mmol) methyl 3,5-bis(benzyloxy)benzoate **i71**
1.21 g (21.53 mmol) KOH
50 ml ethanol
50 ml water

Purification: recrystallisation from EtOH/EtOAc (10/0.3)

Yield: 0.72 g (50 %), colorless solid

Transition temp.: Cr 218 [47.7] I

^{1}H-NMR: ($CDCl_3$, *J*/Hz, 400 MHz) δ 7.34 – 7.25 (m, 8H, Ar-H), 7.24 – 7.20 (m, 4H, Ar-H), 6.69 (t, *J* = 2.4 Hz, 1H, Ar-H), 4.97 (s, 4H, OCH_2Ph).

4-[(6-Hydroxyhexyl)oxy]phenyl 4-(hexyloxy)benzoate **i73(6,6)**

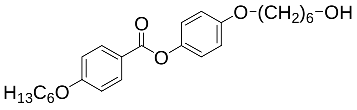

Formula: $C_{24}H_{32}O_5$, M = 400.51 g/mol
Synthesis: according to the general procedure 11.3.1 methode A
Reagents: 2.67 g (8.49 mmol 4-hydroxyphenyl 4-(hexyloxy)benzoate **i11(6)**
2.00 g (11.04 mmol) 6-bromohexanole
5.87 g (42.48 mmol) K_2CO_3
0.02 g KI
50 ml DMF
Purification: column chromatography, eluent: $CHCl_3$ and $CHCl_3$/EtOAc (10/0.2 – 10/2) and further recrystallisation from EtOAc/PE (10/0.1)
Yield: 1.80 g (53 %), colorless solid
Transition temp.: Cr 84 [25.8] N 95 [1.5] I
^{1}H-NMR: ($CDCl_3$, *J*/Hz, 400 MHz) δ 8.10 (d, *J* = 8.8 Hz, 2H, Ar-H), 7.08 (d, *J* = 8.9 Hz, 2H, Ar-H), 6.94 (d, *J* = 8.8 Hz, 2H, Ar-H), 6.89 (d, *J* = 9.0 Hz, 2H, Ar-H), 4.02 (t, *J* = 6.6 Hz, 2H, OCH_2), 3.95 (t, *J* = 6.4 Hz, 2H, OCH_2), 3.65 (t, *J* = 6.5 Hz, 2H, $HOCH_2$), 1.84 – 1.75 (m, 4H, $OCH_2C\mathbf{H_2}$), 1.64 – 1.56 (m, 2H, $HOCH_2C\mathbf{H_2}$), 1.54 – 1.29 (m, 8H, CH_2), 0.90 (t, *J* = 7.0 Hz, 3H, CH_3).

6-(4-{[4-(Hexyloxy)phenyl]carbonyloxy}phenoxy)hexyl 3,5-bis(benzyloxy)benzoate **i74(6,6)**

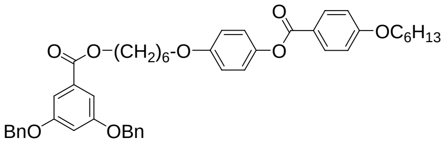

Formula: $C_{46}H_{50}O_8$, M = 730.88 g/mol
Synthesis: according to the general procedure 11.3.3
Reagents: 1.21 g (3.61 mmol) 3,5-bis(benzyloxy)benzoic acid **i72**
1.50 g (3.61 mmol) 4-[(6-hydroxyhexyl)oxy]phenyl 4-(hexyloxy)benzoate **i73(6,6)**
0.82 g (3.98 mmol) DCC
0.02 g DMAP
50 ml dichloromethane
Purification: column chromatography, eluent: $CHCl_3$/EtOAc (10/0.2) and further recrystallisation from EtOAc/EtOH (10/0.1)
Yield: 1.93 g (73 %), colorless solid
Transition temp.: Cr 103 [50.3] I
^{1}H-NMR: ($CDCl_3$, *J*/Hz, 400 MHz) δ 8.10 (d, *J* = 8.9 Hz, 2H, Ar-H), 7.44 – 7.26 (m, 10H, Ar-H), 7.06 (d, *J* = 9.0 Hz, 2H, Ar-H), 6.94 (d, *J* = 8.9 Hz, 2H, Ar-H), 6.88 (d, *J* = 9.0 Hz, 2H, Ar-H), 6.78 (t, *J* = 2.3 Hz, 1H, Ar-H), 6.71 (d, *J* = 2.2 Hz, 1H, Ar-H), 6.67-6.64 (m, 1H, Ar-H), 5.05 (s, 4H, OCH_2Ph), 4.30 (t, *J* = 6.6 Hz, 2H, $COOCH_2$), 4.02 (t, *J* = 6.6 Hz, 2H, OCH_2), 3.95 (t, *J* = 6.4 Hz, 2H, OCH_2), 1.85 – 1.71 (m, 6H, $OCH_2C\mathbf{H_2}$, $COOCH_2C\mathbf{H_2}$), 1.60 – 1.42 (m, 4H, CH_2), 1.39 – 1.30 (m, 6H, CH_2), 0.90 (t, *J* = 6.9 Hz, 3H, CH_3).

6-(4-{[4-(Hexyloxy)phenyl]carbonyloxy}phenoxy)hexyl 3,5-dihydroxybenzoate **i75(6,6)**

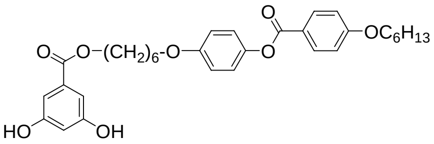

Formula:	$C_{32}H_{38}O_8$, M = 550.64 g/mol
Synthesis:	according to the general procedure 11.3.6 methode A
Reagents:	1.90 g (2.59 mmol) 6-(4-{[4-(hexyloxy)phenyl]carbonyloxy}phenoxy)hexyl 3,5-bis(benzyloxy)benzoate **i74(6,6)** 0.19 g Pd/C 100 ml THF
Purification:	recrystallisation from EtOH
Yield:	1.10 g (77 %), colorless solid
Transition temp.:	Cr 109 [23.1] I
^{1}H-NMR:	(CDCl$_3$, *J*/Hz, 400 MHz) δ 8.11 (d, *J* = 8.9 Hz, 2H, Ar-H), 7.08 – 7.01 (m, 4H, Ar-H), 6.94 (d, *J* = 8.9 Hz, 2H, Ar-H), 6.84 (d, *J* = 9.0 Hz, 2H, Ar-H), 6.50 – 6.45 (m, 1H, Ar-H), 4.30 (t, *J* = 6.4 Hz, 2H, COOCH$_2$), 4.02 (t, *J* = 6.6 Hz, 2H, OCH$_2$), 3.91 (t, *J* = 6.3 Hz, 2H, OCH$_2$), 1.86 – 1.70 (m, 6H, OCH$_2$C**H**$_2$, COOCH$_2$C**H**$_2$), 1.58 – 1.43 (m, 6H, CH$_2$), 1.39 – 1.29 (m, 4H, CH$_2$), 0.90 (t, *J* = 7.0 Hz, 3H, CH$_3$).

3-{[4-(Benzyloxy)phenyl]carbonyloxy}phenyl 4-(benzyloxy)benzoate **i76**

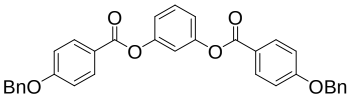

Formula:	$C_{34}H_{26}O_6$, M = 530.57 g/mol
Synthesis:	according to the general procedure 11.3.3
Reagents:	2.00 g (18.16 mmol) resorcinol 8.29 mg (35.92 mmol) 4-(benzyloxy)benzoic acid 8.24 mg (39.95 mmol) DCC 0.02 g DMAP 100 ml dichloromethane
Purification:	recrystallisation from EtAcO/EtOH
Yield:	7.99 g (83 %), colorless solid
Transition temp.:	Cr 196 [64.3] I
^{1}H-NMR:	(CDCl$_3$, *J*/Hz, 400 MHz) δ 8.12 (d, *J* = 9.0 Hz, 4H, Ar-H), 7.46 – 7.31 (m, 11H, Ar-H), 7.15 – 7.09 (m, 3H, Ar-H), 7.04 (d, *J* = 9.0 Hz, 4H, Ar-H), 5.14 (s, 4H, OCH$_2$Ph).

3-[(4-Hydroxyphenyl)carbonyloxy]phenyl 4-hydroxybenzoate **i77**

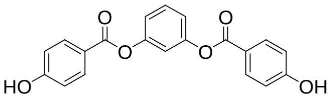

Formula:	$C_{20}H_{14}O_6$, M = 350.32 g/mol
Synthesis:	according to the general procedure 11.3.6 methode A
Reagents:	7.50 g (14.14 mmol) 3-{[4-(benzyloxy)phenyl]carbonyloxy}phenyl 4-(benzyloxy)benzoate **i76** 0.75 g Pd/C 400 ml THF
Purification:	recrystallisation from EtOAc

Yield:	3.91 g (79 %), colorless solid
Transition temp.:	Cr 230 [36.2] I
^{1}H-NMR:	(CDCl$_3$, *J*/Hz, 400 MHz) δ 7.74 (d, *J* = 8.6 Hz, 4H, Ar-H), 7.20 – 7.13 (m, 1H, Ar-H), 6.83 (d, *J* = 6.6 Hz, 3H, Ar-H), 6.65 (d, *J* = 8.6 Hz, 4H, Ar-H).

Bis[4-(benzyloxy)phenyl] isophthalate **i78**

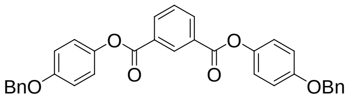

Formula:	$C_{34}H_{26}O_6$, M = 530.57 g/mol
Synthesis:	according to the general procedure 11.3.3
Reagents:	1.16 g (6.99 mmol) isophthalic acid 2.8 g (13.98 mmol) 4-(benzyloxy)phenol 3.17 g (15.38 mmol) DCC 0.02 g DMAP 300 ml dichloromethane
Purification:	recrystallisation from EtAcO/EtOH
Yield:	2.78 g (75 %), colorless solid
Transition temp.:	Cr 193 [67.9] I
^{1}H-NMR:	(CDCl$_3$, *J*/Hz, 400 MHz) δ 8.98 (t, *J* = 1.6 Hz, 1H, Ar-H), 8.42 (dd, *J* = 7.8, 1.7 Hz, 2H, Ar-H), 7.65 (t, *J* = 7.8 Hz, 1H, Ar-H), 7.45 – 7.29 (m, 10H, Ar-H), 7.14 (d, *J* = 9.1 Hz, 4H, Ar-H), 7.01 (d, *J* = 9.1 Hz, 4H, Ar-H), 5.07 (s, 4H, OCH$_2$Ph).

Bis(4-hydroxyphenyl) isophthalate **i79**

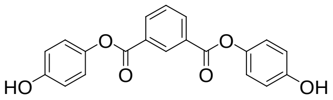

Formula:	$C_{20}H_{14}O_6$, M = 350.32 g/mol
Synthesis:	according to the general procedure 11.3.6 methode A
Reagents:	2.50 g (4.71 mmol) bis[4-(benzyloxy)phenyl]isophthalate **i78** 0.25 g Pd/C 450 ml THF
Purification:	recrystallisation from EtOAc
Yield:	1.14 g (69 %), colorless solid
Transition temp.:	Cr 223 [42.7] I
^{1}H-NMR:	(CDCl$_3$, *J*/Hz, 400 MHz) δ 8.98 (t, *J* = 1.6 Hz, 1H, Ar-H), 8.42 (dd, *J* = 7.8, 1.7 Hz, 2H, Ar-H), 7.65 (t, *J* = 7.8 Hz, 1H, Ar-H), 7.14 (d, *J* = 9.1 Hz, 4H, Ar-H), 7.01 (d, *J* = 9.1 Hz, 4H, Ar-H).

4-({6-[4-(4-Formylphenoxycarbonyl)phenoxy]hexyl}oxy)phenyl 4-(hexyloxy)benzoate **i80**

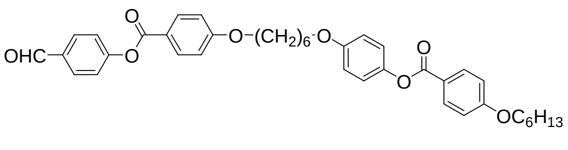

Formula:	$C_{39}H_{42}O_8$, M = 638.75 g/mol
Synthesis:	according to the general procedure 11.3.3
Reagents:	1.50 g (2.81 mmol) 4-{[6-(4-{[4-(hexyloxy)phenyl]carbonyloxy}phenoxy)hexyl]oxy}benzoic

acid **i14(6,6)**
0.34 g (2.81 mmol) 4-hydroxybenzaldehyde
0.64 g (3.09 mmol) DCC
0.02 g DMAP
150 ml dichloromethane

Purification: column chromatography, eluent: $CHCl_3$/EtOAc (10/0.2) and further recrystallisation from EtOAc

Yield: 1.57 g (88 %), colorless solid

Transition temp.: Cr 121 [54.8] N 180 [5.2] I

^{1}H-NMR: ($CDCl_3$, *J*/Hz, 400 MHz) δ 10.00 (s, 1H, CHO), 8.15 – 8.08 (m, 4H, Ar-H), 7.94 (d, *J* = 8.6 Hz, 2H, Ar-H), 7.38 (d, *J* = 8.5 Hz, 2H, Ar-H), 7.08 (d, *J* = 9.0 Hz, 2H, Ar-H), 7.00 – 6.87 (m, 6H, Ar-H), 4.06 (t, *J* = 6.4 Hz, 2H, OCH_2), 4.02 (t, *J* = 6.6 Hz, 2H, OCH_2), 3.97 (t, *J* = 6.4 Hz, 2H, OCH_2), 1.90 – 1.76 (m, 6H, $OCH_2C\mathbf{H}_2$), 1.60 – 1.42 (m, 6H, CH_2), 1.38 – 1.30 (m, 4H, CH_2), 0.90 (t, *J* = 7.1 Hz, 3H, CH_3).

4-[(4-{[6-(4-{[4-(Hexyloxy)phenyl]carbonyloxy}phenoxy)hexyl]oxy}phenyl)carbonyloxy]-benzoic acid **i81**

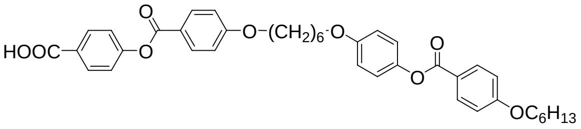

Formula: $C_{39}H_{42}O_9$, M = 654.75 g/mol

Synthesis: according to the general procedure 11.3.5

Reagents: 1.06 g (1.66 mmol) 4-({6-[4-(4-formylphenoxycarbonyl)phenoxy]hexyl}oxy)phenyl 4-(hexyloxy)benzoate **i80**
0.24 g (2.14 mmol) resorcinol
0.87 g (9.57 mmol) $NaClO_2$
0.77 g (4.8 mmol) $NaH_2PO_4\cdot 2H_2O$
10 ml THF
10 ml H_2O

Purification: recrystallisation from CH_3COOH

Yield: 0.99 g (92 %), colorless solid

Transition temp.: Cr 196 [40.2] N 244 [14.6] I

^{1}H-NMR: ($CDCl_3$, *J*/Hz, 400 MHz) δ 8.11 – 8.03 (m, 6H, Ar-H), 7.25 (d, *J* = 8.7 Hz, 2H, Ar-H), 7.06 (d, *J* = 9.0 Hz, 2H, Ar-H), 7.00 – 6.92 (m, 4H, Ar-H), 6.89 (d, *J* = 9.0 Hz, 2H, Ar-H), 4.07 (t, *J* = 6.4 Hz, 2H, OCH_2), 4.03 (t, *J* = 6.5 Hz, 2H, OCH_2), 3.97 (t, *J* = 6.4 Hz, 2H, OCH_2), 1.89 – 1.74 (m, 6H, $OCH_2C\mathbf{H}_2$), 1.59 – 1.52 (m, 4H, CH_2), 1.49 – 1.41 (m, 2H, CH_2), 1.36 – 1.29 (m, 4H, CH_2), 0.89 (t, *J* = 7.1 Hz, 3H, CH_3).

Acknowledgments

My first word of gratitude goes to my supervisor, Professor Wolfgang Weißflog, for his most valuable advice and encouragement in all stages of my Ph.D. studies. I am deeply grateful for his guidance, inspiration, patience, strong support and encouragement, and for fruitful discussions which we had during my Ph.D. studies.

I would like to express my sincere appreciation to Professor Gerhard Pelzl and Dr. Sigmar Diele for fruitful scientific discussions and the wholehearted support on the electro-optical and X-Ray measurements understanding at the beginning of my Ph.D. studies.

I sincerely thank to Dr. Ute Baumeister for introducing me to the world of XRD and for her support even from far distance.

Many thanks go to Professor Ralf Stannarius for his advice, his strong support and encouragement, for fruitful discussions and for permission of using different equipments in his working group during my measurements in Magdeburg. I enjoyed working during my time there together with Jana Heuer, Frank Müller and Alexandru Nemes.

My appreciation is also extended to all the colleagues of our research group for fruitful discussions and help. I enjoyed working together with Ulrike Bernasch, Kristin Brand, Sonja Findeisen, Laura Kovalenko, Karsten Pelz and Martin Schröder. I am thankful to my colleagues from Professor Blume group and Professor Tschierske group for the most beautiful barbeque evenings, football and movies watching and the best coffee time on the shore of Saale.

My special appreciation goes to Ms. Bettina Föhlting for the help with the DSC measurements, and not only. Special thanks are going to Ms. Beate Schramme which was there for me in difficult moments. I am grateful for technical support to Ms. Gottschlich, Ms. Kirkamm and Ms. Naumann.

Many thanks for the colleagues at the Institute of Organic Chemistry for performing the NMR, elemental analysis as well as mass spectroscopy measurements.

I would like to express my sincere and great appreciation to my Family and my friends that never ceased believing in me and they have been behind me all the way.

I simply thank to Dr. Marko Prehm because there is no way to express my gratitude in simple words. Thank you for everything!

The author wishes to express his sincere appreciation to Deutsche Forschungsgemeinschaft (DFG) for the financial support.

Finally, I would like to thank everyone else not mentioned yet that, in a way or another, helped me to reach this milestone in my life.

Maria Gabriela Tamba

PERSONAL INFORMATIONS

- Nationality: Romanian
- Date of Birth: 2nd August 1979
- Place of Birth: Bacau, Romania

EDUCATION

2012 – Present	**Research assistent** in the liquid crystals research at the Fakultät für Naturwissenschaften, Institut für Experimentelle Physik, Abteilung Nichtlineare Phänomene, Otto-von-Guericke-Universitaet, Magdeburg, Germany Supervisor: Prof. Dr. R. Stannarius (FNW/IEP/ANP, Otto-von-Guericke-Universitaet, Magdeburg, Germany)
2010 – 2012	**Research assistent** in the liquid crystals research at the Department of Chemistry, Hull University, UK, Supervisor: Prof. Dr. G.H. Mehl (Department of Chemistry, Hull University, UK)
2004 – 2009	**PhD student** in the liquid crystals research at the Institute of Physical Chemistry, Faculty of Chemistry, *Martin-Luther* University Halle-Wittenberg, Germany, with the project: "Linking of banana-shaped mesogens to incompatible fragments". Supervisors: Prof. Dr. W. Weissflog (*Martin-Luther* University, Germany) Prof. Dr. G. Pelzl (*Martin-Luther* University, Germany)
2002 – 2004	**Postgraduate studies** – Master equivalent (two years Master) at the Department of Organic Chemistry, Faculty of Chemistry, *Alexandru Ioan Cuza* University, Iasi, Romania. ***Master of Science in Chemistry***; Title of Master work: "Synthesis of novel materials with potential uses as insect repellents". Supervisors: Prof. Dr. I. Berdan (*Alexandru Ioan Cuza* University, Romania) Prof. Dr. Alex. Cecal (*Alexandru Ioan Cuza* University, Romania)
2002 – 2003	**Erasmus-Socrates Fellowship** at the Department of Organic and Bioorganic Chemistry, Faculty of Chemistry, *Martin-Luther* University Halle-Wittenberg, Germany, with the project: "Searching for novel materials with potential uses as insect repellents". Supervisors: Prof. Dr. R. Csuk (*Martin-Luther* University, Germany) Prof. Dr. Alex. Cecal (*Alexandru Ioan Cuza* University, Romania) Dr. R. Kluge (*Martin-Luther* University, Germany)
1998 – 2002	**Diploma research** at the Department of Inorganic Chemistry, Faculty of Chemistry, *Alexandru Ioan Cuza* University, Iasi, Romania. ***Licentiate in Chemistry*** **(Bachelor equivalent**) Title of Diploma work: "Structure-Property Relationships of oxoacids of transition metals". Supervisor: Prof. Dr. I. Berdan (*Alexandru Ioan Cuza* University, Romania)
1993 – 1997	High school *George Bacovia* in Bacau, Romania
1989 – 1993	Gymnasium in Oniscani, Romania
1985 – 1989	Elementary school in Oniscani, Romania

PROFESSIONAL EXPERIENCE

2012 – Present	**Research assistent** in the liquid crystals research at the Fakultät für Naturwissenschaften, Institut für Experimentelle Physik, Abteilung Nichtlineare Phänomene, Otto-von-Guericke-Universitaet, Magdeburg, Germany Liquid crystals research: synthesis of liquid crystal compounds and their characterization by NMR, IR, UV/Vis, POM, DSC, electro-optical and S.H.G. measurements and X-ray diffraction methods. Supervisor: Prof. Dr. R. Stannarius (FNW/IEP/ANP, Otto-von-Guericke-Universitaet, Magdeburg, Germany)
2010	**Guest Researcher** at the Department of Engineering Science, Oxford University, UK. Liquid crystals research: characterization of liquid crystal compounds by electro-optical measurements. Supervisors: Prof. S. J. Elston (Oxford University, UK) Prof. Dr. G.H. Mehl (Hull University, UK) Dr. P. W. Benzie (Oxford University, UK)
2010 – 2012	**Guest Researcher** at the Institute of Physical Chemistry, Faculty of Chemistry, *Martin-Luther* University Halle-Wittenberg, Germany, in different DFG projects. Liquid crystals research: synthesis of liquid crystal compounds and their characterization by NMR, IR, UV/Vis, POM, DSC, electro-optical measurements and X-ray diffraction methods. Supervisors: Prof. Dr. C. Tschierske (*Martin-Luther* University, Germany) Prof. Dr. G.H. Mehl (Hull University, UK) Dr. U. Baumeister (*Martin-Luther* University, Germany) Dr. M. Prehm (*Martin-Luther* University, Germany)
2010 – 2012	**Scientific Researcher** at the Department of Chemistry, Hull University, UK. Liquid crystals research: synthesis of liquid crystal compounds and their characterization by NMR, IR, UV/Vis, POM, DSC, electro-optical measurements and X-ray diffraction methods. Supervisor: Prof. Dr. G.H. Mehl (Hull University, UK)
2008	**Guest Researcher** at the European Synchrotron Radiation Facility (ESRF), Grenoble, France (EU-COST project). Investigation of an electric field induced phase transition in the nematic phases of bent core compounds by X-ray studies under a high electric field. Supervisors: Prof. Dr. R. Richardson (University of Bristol, United Kingdom) Prof. Dr. W. Weissflog (*Martin-Luther* University, Germany) Prof. Dr. G. Pelzl (*Martin-Luther* University, Germany)
2007 – 2009	**Scientific Researcher** at the Institute of Physical Chemistry, Faculty of Chemistry, *Martin-Luther* University Halle-Wittenberg, Germany, in different DFG projects. Liquid crystals research: synthesis of liquid crystal compounds and their characterization by NMR, IR, UV/Vis, POM, DSC, electro-optical measurements and X-ray diffraction methods. Supervisors: Prof. Dr. W. Weissflog (*Martin-Luther* University, Germany) Prof. Dr. G. Pelzl (*Martin-Luther* University, Germany)
2006	**Guest Researcher** for several weeks at the Institute of Experimental Physics, Department of Nonlinear Phenomena, *Otto-von-Guericke* University, Magdeburg, Germany. Nonlinear behaviour of liquid crystals: dynamics, pattern formation and self-organisation in soft condensed matter systems. Structure and dynamics of bent-core nematics. Supervisors: Prof. Dr. R. Stannarius (*Otto-von-Guericke* University, Germany) Dr. A. Eremin (*Otto-von-Guericke* University, Germany) Prof. Dr. W. Weissflog (*Martin-Luther* University, Germany) Prof. Dr. G. Pelzl (*Martin-Luther* University, Germany)

2003 – 2004	**Scientific Researcher** at the Department of Organic and Bioorganic Chemistry, Faculty of Chemistry, *Martin-Luther* University Halle-Wittenberg, Germany. Synthesis of organic compounds and their characterization by NMR, IR, UV/Vis, EA methods. Bioassay of novel materials with potential uses as insect–repellents. Supervisors: Prof. Dr. R. Csuk (*Martin-Luther* University, Germany) Dr. R. Kluge (*Martin-Luther* University, Germany)
2003	**Student Researcher** for six months at the Max Planck Institute of Microstructure Physics, Halle, Germany, with the subject “Preparation and investigation of nanoscale dielectric films and structures”. Synthesis of organic and inorganic compounds, preparation of nanoscale dielectric films and their characterization by SEM and high-resolution TEM. Supervisors: Prof. Dr. U. Gösele (Max Planck Institute of Microstructure Physics) Dr. M. Alexe (Max Planck Institute of Microstructure Physics)
2002 – 2004	**Student Researcher** at the Department of Organic Chemistry, Faculty of Chemistry, *Alexandru Ioan Cuza* University, Iasi, Romania. Supervisors: Prof. Dr. I. Berdan (*Alexandru Ioan Cuza* University, Romania) Prof. Dr. Alex. Cecal (*Alexandru Ioan Cuza* University, Romania)

SKILLS

- Organic and Inorganic synthesis;
- NMR spectroscopy (^{1}H, ^{19}F and ^{13}C-NMR) and EA analysis;
- UV-VIS and IR spectroscopy;
- MS and GC-MS spectrometry;
- Thin layer chromatography and column chromatography separation methods;
- Polarizing optical microscopy in characterization of liquid crystals;
- Calorimetric studies (differential scanning calorimetry in characterization of liquid crystals);
- Electro-optical measurements on liquid crystals samples;
- Second harmonic generation (S.H.G.) measurements on liquid crystals samples;
- X-ray diffraction techniques on non-oriented samples (Guinier film, oriented samples (two-dimensional detector) as well as high-resolution Synchrotron X-ray diffraction;
- Software and data analysis proficiency including Microsoft Office, CSC Chemdraw and Chemdraw 3D, Beilstein and ACS SciFinder, Core1 Draw, Adobe Photoshop, Adobe Illustrator, Adobe PageMaker, Irfan View, MathCad, Origin;
- Bioassay of novel materials with potential uses as insect –repellents: measurement of the pharmacological activity of new substances on *Myrmica rubra*;
- Preparation of nanoscale dielectric films;
- Driving Licence: clean.

LANGUAGES

- English – advanced
- German - advanced
- French – conversational level
- Romanian – mother tongue

PROFESSIONAL AFFILIATIONS

- 2008 Member of International Liquid Crystal Society

Maria Gabriela Tamba
29.05.2014

- 1. M.-G. Tamba, B. Kosata, K. Pelz, S. Diele, G. Pelzl, Z. Vakhovskaya, H. Kresse, W. Weissflog, *Mesogenic dimers composed of a calamitic and a bent-core mesogenic unit*, Soft Matter, **2006,** *2*, 60-65;
- 2. R. Stannarius, A. Eremin, M.-G. Tamba, G. Pelzl, W. Weissflog, *Induction of a biaxial nematic phase by means of an electric field*, e-Liq. Cryst. Comm., **2006**;
- 3. B. Kosata, M.-G. Tamba, U. Baumeister, K. Pelz, S. Diele, G. Pelzl, G. Galli, S. Samaritani, E. V. Agina, N. I. Boiko, V. P. Shibaev and W. Weissflog, *Liquid-crystalline dimers composed of bent-core mesogenic units*, Chem. Mater., **2006**, *18*, 691-701.
- 4. M.-G. Tamba, W. Weissflog, A. Eremin, J. Heuer, and R. Stannarius: *Electro-optic characterization of a nematic phase formed by bent core mesogens*, Eur. Phys. J. E, **2007**, *22*, 85 - 95;
- 5. R. Stannarius, A. Eremin, M.-G. Tamba, G. Pelzl, and W. Weissflog, *Field-induced texture transitions in a bent-core nematic liquid crystal*, Phys. Rev. E, **2007**, *76*, 061704;
- 6. J. Heuer, R. Stannarius, M.-G. Tamba, and W. Weissflog, *Longitudinal and normal electroconvection rolls in a nematic liquid crystal with positive dielectric and negative conductivity anisotropy*, Phys. Rev. E, **2008**, *77*, 056206.
- 7. G. Pelzl, M.-G. Tamba, S. Findeisen-Tandel, M. W. Schröder, U. Baumeister, S. Diele, W. Weissflog, *New bent-core mesogens with carbon-carbon multiple linkages in the terminal chains*, J. Mater. Chem., **2008**, *18*, 3017-3031;
- 8. W. Weissflog, U. Dunemann, S. Findeisen-Tandel, M.-G. Tamba, H. Kresse, G. Pelzl, S. Diele, U. Baumeister, A. Eremin, S. Stern, R. Stannarius, *At the boundary to banana-shaped liquid crystals: polar properties of phases formed by new asymmetric achiral four-ring bent-core mesogens*, Soft Matter, **2009,** *5*, 1840-1847;
- 9. S. Haddawi, M.-G. Tamba, G. Pelzl, W. Weissflog and U. Baumeister, *Induction of 'banana phases' in binary systems composed of bent-core and calamitic mesogen*, Soft Matter, **2010,** *6*, 1170-1181;
- 10. M.-G. Tamba, U. Baumeister, G. Pelzl, W. Weissflog, *Banana-calamitic dimers: unexpected mesophase behaviour by variation of the direction of ester linking groups in the bent-core unit,* Liq. Cryst., **2010**, Vol. *37*, Nos. 6-7, 853–874;
- 11. W. Weissflog, G. Pelzl, H. Kresse, U. Baumeister, K. Brand, M. W. Schröder, M.-G. Tamba, S. Findeisen-Tandel, U. Kornek, S. Stern, A. Eremin, R. Stannarius, J. Svoboda, *In search of a new design strategy for solid single-component organic ferroelectrics: Polar crystalline phases formed by bent-core molecules,* J. Mater. Chem., **2010**, *20*, 6057-6079;
- 12. G. Pelzl, S. Diele, M. W. Schröder, W. Weissflog, M.-G. Tamba & U. Baumeister, *Structural investigations on B_7 phases of new bent-core mesogens including a binary system,* Liq. Cryst., **2010**, Vol. *37*, Nos. 6-7, 839–852;
- 13. V. P. Panov, M. Nagaraj, J. K. Vij, A. Kohlmeier, M.-G. Tamba, R. A. Lewis, G. H. Mehl*, Spontaneous periodic deformations in nonchiral planar aligned bimesogens with a nematic-nematic transition and a negative elastic constant*, Phys Rev. Lett., **2010**, *105*, 167801;
- 14. M.-G. Tamba, A. Bobrovsky, V. Shibaev, G. Pelzl, U. Baumeister, W. Weissflog, *Photochromic azobenzene functionalised banana–calamitic dimers and trimers: mesophase behaviour and photo-orientational phenomena,* Liq. Cryst., **2011**, Vol. *38*, Nos. 11-12, 1531–1550;
- 15. A. Chakraborty, B. Das, M. K. Das, S. Findeisen-Tandel, M.-G. Tamba, U. Baumeister, H. Kresse & W. Weissflog, *New hockey stick compounds with a lateral methyl group showing nematic, synclinic and anticlinic smectic C phases,* Liq. Cryst., **2011**, Vol. *38*, No. 9, 1085–1097;
- 16. V. P. Panov, R. Balachandran, M. Nagaraj, J. K. Vij, M.-G. Tamba, A. Kohlmeier, G. H. Mehl, *Microsecond linear optical response in the unusual nematic phase of achiral bimesogens,* Appl. Phys. Lett, **2011**, *99*, 261903;
- 17. C. S. P. Tripati, P. Losada-Pérez, J. Leys, C. Glorieux, A. Kohlmeier, M.- G. Tamba, G. H. Mehl, and J. Leys, *Nematic-nematic phase transition in the liquid crystal dimer CBC9CB and its mixtures with 5CB: A high-resolution adiabatic scanning calorimetric study*, Phys. Rev. E, **2011**, *84*, 041707;
- 18. R. Csuk, M.-G. Tamba, R. Kluge, *Locking Out Ants - Synthesis and Biological Evaluation of Some Fluorinated Repellents*, ZEITSCHRIFT FUR NATURFORSCHUNG SECTION B-A JOURNAL OF CHEMICAL SCIENCES, **2011**, Vol. *66*, Issue *10*, 1069-1075;

- 19. W. Weissflog, U. Baumeister, M.-G. Tamba, G. Pelzl, H. Kresse, R. Friedemann, G. Hempel, R. Kurz, M. Roos, K. Merzweiler, A. Jákli, C. Zhang, N. Diorio, R. Stannarius, A. Eremin and U. Kornek, *Unexpected liquid crystalline behaviour of three-ring bent-core mesogens: bis(4-subst.-phenyl) 2-methyl-iso-phthalates,* Soft Matter, **2012**, *8*, 2671-2685;
- 20. C. H. Yu, C. P. J. Schubert, C. Welch, B. J. Tang, M.-G. Tamba and G. H. Mehl, *Design, Synthesis, and Characterization of Mesogenic Amine-Capped Nematic Gold Nanoparticles with Surface-Enhanced Plasmonic Resonances*, J. Am. Chem. Soc. **2012**, *134*, 5076−5079;
- 21. C. P. J. Schubert, M.-G. Tamba and G. H. Mehl, *Chiral nematic organo-siloxane oligopodes based on an axially chiral binaphthalene core*, Chem. Commun., **2012**, *48*, 6851-6853;
- 22. J. E. Halls, R. W. Bourne, K. J. Wright, L. I. Partington, M.-G. Tamba, Z. Yan, T. Ramakrishnappa, G. H. Mehl, S. M. Kelly, J. D. Wadhawan, *Electrochemistry of organometallic lyotropic chromonic liquid crystals*, Electrochemistry communications, ISSN 1388-2481, **2012**, *19*, 50-54;
- 23. R. Balachandran, P. Panov, J. K. Vij, A. Kocot, M. G. Tamba, G. H. Mehl, *Elastic properties of bimesogenic liquid crystals*, Liquid Crystals, **2013**, 40, 681–688;
- 24. V. P. Panov, R. Balachandran, J. K. Vij, M. G. Tamba, A. Kohlmeier, G. H. Mehl; *Field-induced periodic chiral pattern in the Nx phase of achiral bimesogens*, Appl Phys. Lett., **2012**, 101, 234106;
- 25. H.Aboubakr, M.-G. Tamba, A. K. Diallo, C. Videlot-Ackermann, L. Belec, O. Siri, J.-M. Raimundo, G. H. Mehl, H. Brisset**,** *Structure properties relationships of liquid crystal bent core organic semiconductors based on benzo[2,1-b:3,4-b']dithiophene-4,5-dion,* J. Mater. Chem*.,* **2012**, 22, 23159-23168;
- 26. E. Burnell, A. Kohlmeier, M. G. Tamba, G. H. Mehl, R. Dong, *Solute NMR study of a bimesogenic liquid crystal with two nematic phases*, Chem Phys. Lett., **2012**, 552, 44-48.
- 27. V. Borshch, Y.-K. Kim, J. Xiang, M. Gao, A. Jákli, V. P. Panov, J. K. Vij, C. T. Imrie, M. G. Tamba, G. H. Mehl, O.D. Lavrentovich, *Nematic twist-bend phase with nanoscale modulation of molecular orientation,* Nature Communications, **2013**, 4, 2635;
- 28. M.-G. Tamba, G. Pelzl, U. Baumeister and W. Weissflog, *Banana-calamitic dimers: Further variations of the bent-core mesogenic unit*, Ferroelectrics. **2014**, accepted;
- 29. S. Findeisen-Tandel, U. Baumeister, M.-G. Tamba, W. Weissflog*, Bent-core mesogens containing amide linking groups,* Ferroelectrics. **2014**, accepted;
- 30. M.-G. Tamba, C.H. Yu, B.J. Tang, C. Welch, A. Kohlmeier, C.P. Schubert, G. H. Mehl, *The Design and Investigation of Nanocomposites Containing Dimeric Nematogens and Liquid Crystal Gold Nanoparticles with Plasmonic Properties Showing a Nematic-Nematic Phase Transition (N_u-N_x/N_{tb})*, Materials, **2014**, *7*, 3494. doi:10.3390/ma7053494;
- 31. J.W. Emsley, M. Lelli, H. Joy, M.-G. Tamba, G.H. Mehl, J. Phys. Chem., **2014**, submitted;
- 32. H. Cachitas, J. L. Figueirinhas, C. Cruz, M. G. Tamba, A. Kohlmeier, and G. H. Mehl, *Elastic, Electric and Optical Properties of a Dimer Liquid Crystal with a NU-NX Phase TransitionLiq. Cryst*., **2014**, submitted.

LIST OF PRESENTATIONS

- 1 M.-G. Tamba, B. Kosata, G. Pelzl, S. Diele, W. Weissflog, *Twins containing banana-shaped mesogens*, *Oral presentation*, Workshop of Graduiertenkollegs 894 (*Self-organization by coordinative and non-covalent interactions.*), Kohren - Sahlis, Germany, 14th – 16th February **2005**;
- 2. M.-G. Tamba, B. Kosata, G. Pelzl, S. Diele, W. Weissflog, *Twins containing banana-shaped mesogens*, *Poster presentation* (P 46), 33. Topical Meeting on Liquid Crystals – Arbeitstagung Flüssigkristalle, Paderborn, Germany, 16th – 18th March **2005**;
- 3. M.-G. Tamba, B. Kosata, G. Pelzl, S. Diele, W. Weissflog, *Twins containing banana-shaped mesogens*, *Poster presentation* (P 109), 8th European Conference on Liquid Crystals, Sesto, Italy, 27th February – 4th March **2005**;
- 4. M.-G. Tamba, G. Pelzl, S. Diele, W. Weissflog, *Dimers composed of bent-core and calamitic mesogenic units*, *Oral presentation*, Workshop of Graduiertenkollegs 894 (*Self-organization by coordinative and non-covalent interactions.*), Freyburg (Unstrut), Germany, 21st – 24th February **2006**;
- 5. M.-G. Tamba, G. Pelzl, S. Diele, W. Weissflog, *Dimers composed of a bent-core and a calamitic mesogenic unit*, *Poster presentation* (P 40), 34. Topical Meeting on Liquid Crystals – Arbeitstagung Flüssigkristalle, Freiburg, Germany, 29th – 31st March **2006**;
- 6. M.-G. Tamba, G. Pelzl, S. Diele, U. Baumeister, W. Weissflog, *Liquid crystalline dimers composed of a bent-core and a calamitic mesogenic unit*, *Poster presentation* (D-PO-128), 1st European Chemistry Congress, Budapest, Hungary, 27 th – 31st August **2006**;
- 7. M.-G. Tamba, G. Pelzl, S. Diele, U. Baumeister, W. Weissflog, *Liquid crystalline dimers composed of a bent-core and a calamitic mesogenic unit*, *Poster presentation* (P 19), Triple Symposia Halle - Berlin - Göttingen, Freyburg (Unstrut), Germany, 8th - 10th October **2006**;
- 8. M.-G. Tamba, J. Heuer, A. Eremin, R. Stannarius, W. Weissflog, *Electro-optics and pattern formation of a nematic phase formed by bent-core mesogens*, *Poster presentation* (P 23), 35. Topical Meeting on Liquid Crystals – Arbeitstagung Flüssigkristalle, Bayreuth, Germany, 21st - 23 rd March **2007**;
- 9. A. Eremin, R. Stannarius, M.-G. Tamba, W. Weissflog, *Experimental evidence for an electrically induced transition into a biaxial nematic phase*, *Oral presentation* (L 09), 35. Topical Meeting on Liquid Crystals – Arbeitstagung Flüssigkristalle, Bayreuth, Germany, 21st - 23 rd March **2007**;
- 10. J. Heuer, M.-G. Tamba, A. Eremin, R. Stannarius, *Electro-optics and pattern formation of a bent-core nematic phase*, *Poster presentation* (DY 33), 35. DPG Frühjahrstagung 2007, Regensburg, Germany, 26th-29th March **2007**;
- 11. M.-G. Tamba, J. Heuer, A. Eremin, R. Stannarius, W. Weissflog, *New dimers and trimers composed of bent-core and calamitic mesogenic units*, *Poster presentation* (PA 26), 9th European Conference on Liquid Crystals, Lisbon, Portugal, 2nd – 6th July **2007**;
- 12. A. Eremin, J. Heuer, R. Stannarius, M.-G. Tamba, W. Weissflog, *Unusual electrooptic behaviour of a nematic phase formed by bent-core mesogens, Poster presentation* (PB 12), 9th European Conference on Liquid Crystals, Lisbon, Portugal, 2nd – 6th July **2007**;
- 13. M.-G. Tamba, G. Pelzl, U. Baumeister, J. Lagerwall, W. Weissflog, *Dimers and trimers composed of bent-core and calamitic mesogenic units containing azobenzene*, *Poster presentation* (P 23), 36th German Topical Meeting on Liquid Crystals – Arbeitstagung Flüssigkristalle, Magdeburg, Germany, 12th – 14th March **2008**;
- 14. J. Heuer, R. Stannarius, M.-G. Tamba, W. Weissflog, *Longitudinal and normal electroconvection rolls in a nematic liquid crystal with positive dielectric and negative conductivity anisotropy*, *Poster presentation* (P 4), 36th German Topical Meeting on Liquid Crystals – Arbeitstagung Flüssigkristalle, Magdeburg, Germany, 12th – 14th March **2008**;
- 15. M.-G. Tamba, G. Pelzl, U. Baumeister, W. Weissflog, *Liquid crystalline dimers and trimers composed of different bent-core and calamitic mesogenic unit*, *Poster presentation* (P 3-MA 111), 22nd International Liquid Crystal Conference, Jeju, Korea, 29th June – 4th July **2008**;
- 16. R. Stannarius, J. Heuer, A. Eremin, M.-G. Tamba, W. Weissflog, *Electrooptic behaviour of a bent-core nematic material*, *Poster presentation* (P 5-PHA 15), 22nd International Liquid Crystal Conference, Jeju, Korea, 29th June – 4th July **2008**;
- 17. M.-G. Tamba, G. Pelzl, U. Baumeister, W. Weissflog, *Dimers and trimers composed of bent-core and calamitic mesogenic units – mesomorphic and electro–optical properties*, *Poster presentation* (P 25), 37th German Topical Meeting on Liquid Crystals – Arbeitstagung Flüssigkristalle, Stuttgart, Germany, 1st – 3rd April **2009**;

- 18. W. Weissflog, H. Kresse, G. Pelzl, S. Findeisen-Tandel, M.-G. Tamba, S. Stern, A. Eremin, R. Stannarius, *In search for polar switchable crystalline materials derived from bent-core molecules*, *Poster presentation* (P 26), 37th German Topical Meeting on Liquid Crystals – Arbeitstagung Flüssigkristalle, Stuttgart, Germany, 1st – 3rd April **2009**;
- 19. A. Hoischen, H.-S. Kitzerow, M.-G. Tamba, W. Weissflog, *Dissipative structures in liquid crystals as a template for periodic patterns*, *Poster presentation* (P 12), 37th German Topical Meeting on Liquid Crystals – Arbeitstagung Flüssigkristalle, Stuttgart, Germany, 1st – 3rd April **2009**;
- 20. W. Weissflog, M.-G. Tamba, G. Pelzl, U. Baumeister, *At the boundary to banana-shaped liquid crystals*, *Oral presentation*, EU-COST project meeting, Stuttgart, Germany, 4th – 5th April **2009**;
- 21. R. Richardson, W. Weissflog, M.-G. Tamba, *Investigation of field-induced textures in bent-core mesogens by Synchrotron X-ray scattering*, *Oral presentation*, EU-COST project meeting, Stuttgart, Germany, 4th – 5th April **2009**;
- 22. M.-G. Tamba, U. Baumeister, G. Pelzl, W. Weissflog, *Mesomorphic and electro–optical properties of dimers and trimers composed of bent-core and calamitic mesogenic units*, *Poster presentation* (P 119), 10th European Conference on Liquid Crystals, Colmar, France, 19th - 24th April **2009**;
- 23. W. Weissflog, S. Findeisen-Tandel, G. Pelzl, U. Baumeister, H. Kresse, M.-G. Tamba, S. Stern, A. Eremin, R. Stannarius, *Polar crystalline materials derived from bent-core molecules*, *Poster presentation* (P 223), 10th European Conference on Liquid Crystals, Colmar, France, 19th - 24th April **2009**;
- 24. M.- G. Tamba, A. Kohlmeier, R. A. Lewis and G. H. Mehl, *Nematic - nematic phase transitions in dimers - the results of calorimetric, optical and structural investigations*, *Poster presentation* (P-3.20), 23rd International Liquid Crystal Conference ILCC 2010, Krakow, Poland, 11th – 16th July **2010**;
- 25. M.- G. Tamba, A. Kohlmeier, G. H. Mehl, *Nematic – nematic phase transitions in binary systems containing liquid crystal dimers with a positive dielectric anisotropy*, *Poster presentation* (P-3.57), 23rd International Liquid Crystal Conference ILCC 2010, Krakow, Poland, 11th – 16th July **2010**;
- 26. M.- G. Tamba, A. Kohlmeier, R. A. Lewis and G. H. Mehl, *Nematic - nematic phase transitions in liquid crystal dimers with a negative dielectric anisotropy*, *Poster presentation* (P-3.54), 23rd International Liquid Crystal Conference ILCC 2010, Krakow, Poland, 11th – 16th July **2010**;
- 27. A. Kohlmeier, M.- G. Tamba, G. H. Mehl, *Synthesis* and *characterization* of a *novel nematic three-ring tripod system*, *Poster presentation* (P-1.77), 23rd International Liquid Crystal Conference ILCC 2010, Krakow, Poland, 11th – 16th July **2010**;
- 28. C. S. P. Tripati, P. Losada-Pérez, J. Leys, C. Glorieux, A. Kohlmeier, M. G. Tamba, G. H. Mehl, and J. Thoen, *Phase transitions study of a cyanobiphenyl dimer exhibiting a nematic-nematic phase transition by means of high-resolution adiabatic scanning calorimetry*, 23rd International Liquid Crystal Conference ILCC 2010, Krakow, Poland, 11th – 16th July **2010**;
- 29. I. Miglioli, A. Arcioni, C. Bacchiocchi, R. Berardi, L. Muccioli, A. Pizzirusso, D. Summa, A. Kohlmeier, M.-G. Tamba, G. H. Mehl and C. Zannoni, *An ESR characterization of α,ω-bis(4'-cyanobiphenyl-4-yl)undecane symmetric dimer mesophases*, 23rd International Liquid Crystal Conference ILCC 2010, Krakow, Poland, 11th – 16th July **2010**;
- 30. M.- G. Tamba, A. Kohlmeier, G. H. Mehl, *Detailed investigations of the nematic – nematic phase transition in binary systems containing liquid crystal dimers*, *Poster presentation* (P2-26), 11th European Conference on Liquid Crystals, Maribor, Slovenia, 6th - 11th February **2011**;
- 31. M.- G. Tamba, A. Kohlmeier, G. H. Mehl, *Synthesis and investigation of the structure-properties relationships of new symmetric and non-symmetric dimeric molecules which exhibit nematic – nematic phase transitions*, *Oral presentation* (O17), 11th European Conference on Liquid Crystals, Maribor, Slovenia, 6th - 11th February **2011**;
- 32. C. S. P. Tripathi, P. Losada-Pérez, J. Leys, A. Kohlmeier, M. G. Tamba, G. H. Mehl, and C. Glorieux, *Investigations of the nematic-nematic phase transition in mixtures of the cyanobiphenyl dimer CB_C9_CB and 5CB by means of high resolution adiabatic scanning calorimetry*, 11th European Conference on Liquid Crystals, Maribor, Slovenia, 6th - 11th February **2011**;
- 33. I. Miglioli, A. Arcioni, C. Bacchiocchi, A. Kohlmeier, M.-G. Tamba, G. H. Mehl and C. Zannoni, *An ESR characterization of α,ω-bis(4'-cyanobiphenyl-4-yl)nonane symmetric*

dimer mesophases, 11th European Conference on Liquid Crystals, Maribor, Slovenia, 6th - 11th February **2011**;

- 34. M.- G. Tamba, A. Kohlmeier and G. H. Mehl, *The structure-properties relationships of dimeric molecules which exhibit nematic–nematic phase transitions*, *Oral presentation* (O8), *BLCS* **2011**, Nottingham, UK;
- 35. M.- G. Tamba, R. A. Lewis, A. Kohlmeier and G. H. Mehl, *Nematic – nematic phase transitions in dimers with a negative dielectric anisotropy*, *Poster presentation* (P25), *BLCS* **2011**, Nottingham, UK;
- 36. M.-G. Tamba, A. Kohlmeier, C. H. Yu, B. J. Tang and G. H. Mehl, *Nematic–nematic phase transitions of binary mixtures containing gold nanoparticles and symmetric dimeric molecules*, *Poster presentation* (P20), *BLCS* **2012**, Glasgow, UK;
- 37. M.- G. Tamba, H. Joy, A. Kohlmeier and G. H. Mehl, *Effect of molecular symmetry and dielectric anisotropy on formation of multiple nematic – nematic phase transitions*, *Poster presentation* (PII-60), 24th International Liquid Crystal Conference ILCC 2012, 19th – 24th August **2012**, Mainz, Germany;
- 38. M.-G. Tamba, A. Kohlmeier, C. H. Yu, B. J. Tang and G. H. Mehl, *Nematic–nematic phase transitions of binary mixtures containing gold nanoparticles and symmetric dimeric molecules*, *Poster presentation* (PIII-124), 24th International Liquid Crystal Conference ILCC 2012, 19th – 24th August **2012**, Mainz, Germany;
- 39. H.C. Yu, B. J. Tang, C. Welch, C. J. Schubert, M.G. Tamba, G. H. Mehl, *Synthesis and investigations of mesogen encapsulated gold nanoparticles,* American Physical Society Meeting, 27.02-02.03.**2012**, Boston, USA;
- 40. C. Cruz, P. J. Sabastao, F. Vaca Chavez, M. G. Tamba, A. Kohlmeier, G. H. Mehl, *Proton NMR Study of the Nu-Nx phase transition in a CB-C9-CB liquid crystal*, A. Alucelesei, 7-11.05.**2012**, NANAX5, Fuengirola, Spain;
- 41. C.H. Yu, B.J. Tang, C. Schubert, C. Welch, M. G. Tamba X. B. Mang, X. B. Zeng, G. Ungar, G. H. Mehl, *The design and the control of the self-assembly behaviour of liquid crystal gold nanoparticles with plasmonic properties and controlled 1D, 2D and 3D self assembly behaviour* International Cnference on Metamaterials, 3-4. 06. **2012** Jena, Germany;
- 42. G. H. Mehl, C. H. Yu, B. J. Tang, C. Schubert, M.-G. Tamba, C. Welch, X. B. Zeng, X. Mang, F.Liu, G. Ungar, *Designing liquid crystal superlattice forming gold nanoparticles and controlling the self-assembly behaviour*, *Oral presentation*, 24th International Liquid Crystal Conference ILCC 2012, 19th – 24th August **2012**, Mainz, Germany;
- 43. F. Lodato, M. Wright, M.-G. Tamba, M. ONeill, S. M. Kelly, G. H. Mehl, *Controlling the phase behaviour and the semiconducting properties of extended aromatic systems*, *Oral presentation*, 24th International Liquid Crystal Conference ILCC 2012, 19th – 24th August **2012**, Mainz, Germany;
- 44. J. K. Vij, V. P. Panov, M. Nagaraj, R. Balachandran, M.-G. Tamba, G. H. Mehl, *Spontaneous periodic deformations and linear optical response in nonchiral bimesogens with nematic-nematic transition*, *Oral presentation*, 24th International Liquid Crystal Conference ILCC 2012, 19th – 24th August **2012**, Mainz, Germany;
- 45. V. P. Panov, J. K. Vij, M.-G. Tamba, A. Kohlmeier, G. H. Mehl, *Field-induced linear optical response domains in the* N_x *phase of achiral bimesogens*, *Oral presentation*, 24th International Liquid Crystal Conference ILCC 2012, 19th – 24th August **2012**, Mainz, Germany;
- 46. M.-G. Tamba, H. Joy, A. Kohlmeier, G. H. Mehl, *Effect of molecular symmetry and dielectric anisotropy on formation of multiple nematic-nematic phase transitions*, *Oral presentation*, British Liquid Crystal Society Conference, 25-27.03. **2013**, Cambridge, UK;
- 47. C. H. Yu, B. J. Tang, C. Schubert, M. G. Tamba, C. Welch, X. B. Zeng, X. Mang, F. Liu, G. Ungar, J. Dintinger, T. Scharf, T. Kienzler, C. Rockstuhl, G. H. Mehl, *Design and control of liquid crystal superlattice forming gold nanoparticles – a route to plasmonic metamaterials*, *Oral presentation*, British Liquid Crystal Society Conference, 25-27.03. **2013**, Cambridge, UK;
- 48. F. Lodato, M. Wright, M. G. Tamba, M. O’Neill, S. M. Kelly, G. H. Mehl, *Controlling the phase behaviour and semi-conductiong properties of bent-core and linear extended aromatic systems*, *Oral presentation*, British Liquid Crystal Society Conference, 25-27.03. **2013**, Cambridge, UK;
- 49. M. G. Tamba, A. Kohlmeier, A. Balachandran, V. P. Panov, J. K. Vij, G. H. Mehl, *The investigation of dimeric liquid crystals with a nematic –nematic* (N-N_x) *phase transition, Oral presentation*, 11th Meeting - Novel Optical Materials and Applications (NOMA) 10-15. 06. **2013**, Cetraro, Italy;

- 50. M.-G. Tamba, A. Kohlmeier, G. H. Mehl, *The investigation of dimeric materials with a nematic – nematic phase transition, Oral presentation (O 12)*, 12th European Conference on Liquid Crystals, 22.- 27. 09.**2013**, Rhodos, Greece;
- 51. H. Cachitas, J. L. Figueirinhas, C. Cruz, M. G. Tamba, A. Kohlmeier, G. H. Mehl, *Capacitance and optical studies of elastic, dielectric and optical properties in the dimer system CB-C9-CB, Poster presentation (P II.14)*, 12th European Conference on Liquid Crystals, 22.- 27. 09.**2013**, Rhodos, Greece;
- 52. J. K. Vij, V. P. Panov, M. G. Tamba and G. H. Mehl, *Spontaneous Periodic deformations and linear optical response in nonchiral bimesogens with a nematic-nematic transition, Oral presentation (I 15),* 12th European Conference on Liquid Crystals, 22.- 27. 09.**2013**, Rhodos, Greece;
- 53. A. Aluculesei, C. Cruz, F. Vaca Chávez, P. J. Sebastião, D. M. Sousa, M. G. Tamba, A. Kohlmeier, G. H. Mehl, *NMR relaxometry study of the CB-C9-CB liquid crystal dimer, Oral presentation (O 24),* 12th European Conference on Liquid Crystals, 22.- 27. 09.**2013**, Rhodos, Greece;
- 54. M.-G. Tamba, G. Pelzl, U. Baumeister and W. Weissflog, *Dimers and trimers composed of bent - core and calamitic mesogenic units – mesomorphic and electro – optical properties, Poster presentation (P 37)*, 14th International Conference on Ferroelectric Liquid Crystals, 01.-06.09.**2013**, Magdeburg, Germany;
- 55. M.-G. Tamba, A. Kohlmeier, G. H. Mehl, *Investigation of dimeric systems with a nematic – nematic phase transition, Oral presentation (O 19)*, 41st German Liquid Crystal Conference, 25.-27.03.**2014**, Magdeburg, Germany;
- 56. M.-G. Tamba, G. Pelzl, U. Baumeister and W. Weissflog, *Oligomeric materials composed of bent - core and calamitic mesogenic units – mesomorphic and electro – optical properties, Poster presentation (P 42)*, 41st German Liquid Crystal Conference, 25.-27.03.**2014**, Magdeburg, Germany.

Eidesstattliche Erklärung

Hiermit erkläre ich an Eides statt, dass ich die vorliegende Arbeit selbstständig und nur unter Verwendung der angegebenen Quellen und Hilfsmittel angefertigt habe.

Diese Arbeit wurde bisher an keiner anderen Universität oder Hochschule vorgelegt. Auch habe ich nicht anderweitig eine Promotion zur Erlangung des Doktorgrades (Dr. rer. nat) eingereicht.

Halle (Saale), den 29.05.2014

Maria Gabriela Tamba